INSTITUTE
FOR
AEROSPACE STUDIES

UNIVERSITY OF TORONTO

TP 7560E

INVESTIGATIONS OF THE DYNAMICS OF LARGE AIR CUSHIONS

by

P. A. Sullivan, M. J. Hinchey, T. A. Graham, J. E. Byrne,
A. Dupuis, N. Milligan and C. Walsh

Prepared for

Transportation Development Centre
Transport Canada

August, 1986

TP 7560E

INVESTIGATIONS OF THE DYNAMICS OF LARGE AIR CUSHIONS

by

P. A. Sullivan, M. J. Hinchey, T. A. Graham, J. E. Byrne,
A. Dupuis, N. Milligan and C. Walsh

Prepared for

Transportation Development Centre
Transport Canada

August, 1986

Libr [illegible]
[illegible] 987
[illegible] Canada

"Experience does not ever err, it is only your judgement that errs in promising itself results which are not caused by your experiments."

Attributed to Leonardo da Vinci

by Daniel Boorstein in "The Discoverers" (1983)

The contents of this report reflect the views of the authors and not necessarily the official views or policies of the Transportation Development Centre.

Un sommaire en français de ce rapport est inclus avant la Table des matières.

Transport Canada Transports Canada

Development Développement

REPORT DOCUMENTATION FORM

1. Transport Canada Report No.
TP 7560 E

2. TDC Project No.
4481

3. Recipient's Catalogue No.

4. Title and Subtitle
Investigations of the Dynamics of
Large Air Cushion Vehicles

5. Report Date
August 1986

6. Performing Organization Report No

7. Author(s) P.A. Sullivan, M.J. Hinchey, T.A. Graham,
J.E. Byrne, A. Dupuis, N. Milligan, C.E. Walsh

8. Transport Canada File No.
D 1460-125-2

9. Performing Organization Name and Address
University of Toronto Institute for Aerospace Studies
4925 Dufferin St.
Downsview, Ontario
M3H 5T6

10. DSS File No.
T8200-1-1532

11. DSS or Transport Canada Contract No
0SU81-00441

12. Sponsoring Agency Name and Address
Transportation Development Centre (TDC)
200 Dorchester Blvd. West
Suite 601, West Tower
Montreal, Quebec H2Z 1X4

13. Type of Report and Period Covered

14. Sponsoring Agency Code
4481

15. Supplementary Notes
Sponsored by Energy R&D Program of Energy, Mines
and Resources, Canada.

16. TDC Project Officer
J.E. Laframboise

17. Abstract

Investigations of aspects of the dynamics of air cushions are described. There were two main objectives: exploration of those problems thought to be of special significance for large platform cushions, and the development of model testing methodologies. However an emphasis is placed on exploring the effect of viscoelastic properties of flexible skirts on dynamics. The following six completed projects are described. (1) Analysis and experiment showing that, for some skirt geometries, small skirt deformations caused by cushion pressure fluctuations can have major effects. (2) Modulation of the escaping cushion air caused by periodic skirt-groung contact is shown to have large non-linear effects on the dynamics. (3) Analysis of heave dynamics of large cushions shows that they may be inadequately damped in general, and that acoustic wave propagation effects can be destabilizing. (4) Analysis of the heave stability when hovering over water shows that pumping of the water surface can have a major destabilizing effect. (5) A method of scaling cushion capacitance is proposed. (6) A computer model of the pitch-heave dynamics of an uncompartmented, segmented skirt is developed, which shows that the skirt is subject to dynamic instability. Finally, preliminary investigations into stress relaxation effects on skirt-ground contact forces and into a technique for measuring unsteady fan response to fluctuating cushion pressure are described.

18. Key Words
Air cushion vehicles, flexible, large
platform, ACV, hovercraft, skirt,
model testing.

19. Distribution Statement
Limited number of copies available
from the Transportation Development
Centre on request.

20. Security Classification (of this report)
Unclassified

21. Security Classification (of this page)
Unclassified

22. No. of Pages
358

23. Price
–

Canada

Transports Canada Transport Canada

Développement Development

FORMULE DOCUMENTAIRE DU RAPPORT

1. N° du rapport Transports Canada

TP 7560 E

2. N° de l'étude — CDT

4481

3. N° de catalogue du destinataire

4. Titre et sous-titre

Investigations of the Dynamics of
Large Air Cushion Vehicles

5. Date du rapport

Août 1986

6. N° du rapport de l'organisme exécutant

7. Auteur(s) P.A. Sullivan, M.J. Hinchey, T.A. Graham, J.E. Byrne, A. Dupuis, N. Milligan, C.E. Walsh

8. N° de dossier Transports Canada

D 1460-125-2

9. Nom et adresse de l'organisme exécutant

University of Toronto Institute for Aerospace Studies
4925 Dufferin St.
Downsview, Ontario
M3H 5T6

10. N° de dossier — ASC

T8200-1-1532

11. N° de contrat — ASC ou Transports Canada

OSU81-00441

12. Nom et adresse de l'organisme parrain

Centre de développement des transports (CDT)
200 ouest, boul. Dorchester
Suite 601, tour ouest
Montréal, Québec H2Z 1X4

13. Genre de rapport et période visée

14. Code de l'organisme parrain

4481

15. Remarques additionnelles

Parrainé par le programme de R&D énergétique de Energie, Mines et Ressources, Canada.

16. Agent de projet — CDT

J.E. Laframboise

17. Résumé

Ce rapport décrit des études sur divers aspects de la dynamique du coussin d'air ayant comme objectifs principaux i) l'étude de problèmes intéressant les plates-formes à coussin d'air lourdes et ii) le développement de méthodes d'essai de maquettes. L'effet des propriétés visco-élastiques des jupes flexibles sur la dynamique a été spécialement approfondi. Les six projets suivants ont été complétés: (1) Démonstration analytique et expérimentale des effets considérables produits, pour certains types de jupes, par de petites déformations causées par les variations de pression. (2) Identification de non-linéarités dans le comportement dynamique du coussin d'air dues à la modulation de l'échappement d'air par les contacts périodiques de la jupe sur le sol. (3) Démonstration analytique que le pilonnement des coussins lourds est généralement sous-amorti et peut être déstabilisé par l'effet de propagation d'ondes acoustiques. (4) Analyse de la stabilité en pilonnement au-dessus de l'eau démontrant que le pompage de la surface d'eau est déstabilisant. (5) Méthodologie pour la reproduction de la capacitance du coussin d'air sur maquettes. (6) Modélisation par ordinateur des oscillations en tangage et pilonnement d'un coussin unicellulaire à jupe segmentée démontrant que ce type de coussin est sujet à des instabilités. Finalement, le rapport décrit des études préliminaires sur l'effet de la relaxation des tensions sur les forces de contact jupe-sol et sur une technique de mesure des débits non stationnaires des ventilateurs créés par des variations de pression du coussin d'air.

18. Mots-clés

Véhicule à coussin d'air, grande surface, aéroglisseur, jupe souple, essais sur modèles réduits.

19. Diffusion

Le Centre de développement des transports dispose d'un nombre limité d'exemplaires.

20. Classification de sécurité (de ce rapport)

non classifié

21. Classification de sécurité (de cette page)

non classifiée

22. Nombre de pages

358

23. Prix

—

CDT/TDC 79-005
Rev 86

Canada

SUMMARY

This report describes the results of a research programme on selected aspects of the dynamics of flexible skirt air cushion vehicles (ACV) at the Institute for Aerospace Studies, University of Toronto (UTIAS) during the period November 1981 to December 1986. The work has two major purposes:

(i) development and experimental validation of mathematical models of cushion dynamics which can be used as aids to design, and

(ii) development of a facility for model testing together with identification of associated scaling and data analysis procedures.

Particular emphasis has been placed on exploring the effects of flexible skirt systems on cushion dynamics.

Crucial to understanding the approach adopted in the present work is the distinction that must be made between investigations of configurations of immediate design interest, and those selected to obtain what has been described as an "unequivocal confrontation between theory and experiment". The dynamics of a flexible skirt air cushion can be complex, so that an analysis of a complete vehicle, in order to be at all tractable, invariably introduces many simplifying assumptions, the applicability of which can be very uncertain. Consequently experimental data obtained from a complete vehicle is usually unsuited to exploration of the validity of these assumptions. This problem is usually not appreciated by those faced with the day-to-day pressures of vehicle development, but it has been noted elsewhere that development of ACV's has actually been hampered by lack of experiments designed to gain insight. A key part of the research at the authors' Institute has been to seek opportunities for unequivocal confrontations.

The work has however been focussed on investigation of an uncompartmented, segmented cushion system developed in Canada for large low speed platform cushions and used on a 270 tonne Icebreaker Bow (ACIB). Previous investigations of models of this skirt at the authors' Institute have shown that its dynamical behaviour can be strongly dependent on the material used to make the skirts. Specifically, with one material it is subject to a nonlinear pitch-heave instability which would be dangerous in a full scale vehicle. With another material, which causes large hysteresis in static stiffness tests, the motion is always heavily damped. Hence a key part of the present investigation is the investigation of the origin of this instability and the role played by skirt material properties, both at model scale and full scale. The work done towards the various objectives is described in three groups:

(A) Basic studies,
(B) Development of the UTIAS 43 metre Circular Track for model testing,
(C) Investigations of the dynamics of large platform cushions. These are described in turn.

(A) Basic Studies

The first basic study was the development of a method for measuring lift-fan response to the unsteady cushion pressures that are generated by vehicle motion. Analyses of dynamics almost invariably assume quasisteady response, yet evidence is accumulating that this may not be adequate. The report describes a simple technique based on plenum chamber cushion concepts and use of a servohydraulically driven heave table. Development of the concept was initially hampered by data acquisition problems, but these are now solved and preliminary results are very encouraging. This technique could be used to test models of full scale fan installations.

The effect of the viscoelastic properties of skirt materials on cushion dynamics appears to fall into two groups: (i) for some skirt geometries, skirt deformations caused by cushion pressure variations can significantly modify both the effective hovergap and cushion capacitance, and (ii) the creep or stress-relaxation properties of some skirt materials can generate contact forces in those parts of a skirt being forced towards the surface, which are absent or greatly diminished when the movement is away from the ground. The latter phenomenon appears to be the most important contribution to stiffness hysteresis. A theoretical and experimental investigation using a slightly tapered cone shows very large effects on both hovergap and cushion capacitance for one material which we have used in our segmented skirt models. We have frequently observed the second effect in our model tests and, if the static hysteresis all appears in the dynamics, it is a major source of damping. However, evidence of its existence at full scale is sketchy. Consequently, some exploratory measurements were obtained from the ACIB. These suggested that, when the cushion segments were being forced towards the ground, up to 4% of the total weight might be supported directly by contact forces. This result prompted us to develop a more detailed investigation of both its significance for dynamics and its origin. Owing to both conceptual and data acquisition problems two prelimnary investigations proved unsuccessful; however, initial results from our third try have yielded promising results. This has clearly demonstrated that the static hysteresis can have major effects on the dynamics, and has provided some useful insights into the mechanisms involved.

The last basic project is a theoretical and experimental investigation of the amplitudes and frequencies of the limit cycle oscillations that occur when a cushion is dynamically unstable. While such phenomena are of no direct practical interest, because they are highly nonlinear, they provide a severe test of the assumptions typically used in such analyses. The results of this work have played a key role in building confidence in various key assumptions used in the other analyses described here.

(B) Facility Development

The work towards development of a model test facility and procedures involved three projects. The first was development of a new lift fan system for the UTIAS Circular Track test vehicle. The system originally installed did not produce enough air flow to correctly scale some vehicle test conditions, introduced gyroscopic torques which greatly complicated data interpretation, and made modelling of response to unsteady cushion pressures very difficult. The new system, which provides a great improvement in all three aspects, is based on a high efficiency two-stage counterrotating axial geometry. This is now operational.

The second project was development of techniques for analysis of flight test data. Currently we use response matching system identification procedures similar to those used to interpret aircraft flight tests, and our initial attempts used programmes based on a linear dynamics model and actually developed for aircraft tests. However, these were basically unsuccessful. This has been attributed to the presence of nonlinearities peculiar to ACV dynamics and to the uncertainty about the significance of the air compressibility in the cushion volume for our model tests. Inclusion of air compressibility in the model in the linearized form as a pneumatic capacitance almost always caused the analysis to diverge. This is consistent with other experience at UTIAS. Hence it became clear that special methods appropriate to ACV dynamics were required. The work planned falls into two stages: (i) development of a mathematical model of the skirt system currently being tested to allow generation of simulated flight test data and (ii) development of the new identification procedure itself. Use of simulated instead of experimental data has a crucial advantage: the coefficients to be identified are known precisely, so that the effects of various approximations on the accuracy of prediction can be tested. To date, stage (i) has been completed as described below.

The third model testing project is the development of rules for scaling. We have considered two aspects: the roles of the viscoelastic properties of skirt material, and of the cushion capacitance. Both present difficulties; solutions to the first will follow from the results of our investigations described above, and these are not yet complete. The second depends on ascertaining the conditions under which it must be included, and this is still not completely established. One of the functions of the detailed modelling of the uncompartmented segmented cushion described below is to provide further insight into this question. However, a possible method of scaling the air compressibility for a model of a full scale vehicle on the UTIAS track is described.

(C) Investigations of Large Platform Cushion Dynamics

The work oriented towards the dynamics of large platform cushions included three projects, two of which were exploratory. The first of these investigated the effect on dynamics and stability of the time delays introduced by acoustic wave propagation in the interior of very large plenum chambers. To make the analysis tractable, an axisymmetric geometry was used. The results indicated that for cushions weighing about 3000 tonnes or more, acoustic wave propagation might have significant destabilizing effects. However, they also demonstrated the existence of another effect, one not intrinsically related to acoustic propagation. If no additional damping is present, large cushions may have unacceptably low stability margins, typically the phase margin, the angle by which the cushion force leads the motion, may only be a few degrees at most. The second investigation explored the stability of cushions hovering over water. Some field trials at the National Research Council of Canada indicated that, under some circumstances, an uncompartmented, segmented cushion that is stable over land can be very unstable when hovering without forward motion over water. The analyses and a limited amount of experiment indicate two possibilities. First, the heaving of a cushion can generate standing waves in the cushion interior which modulate both the effective cushion volume and the effective hovergap. Both of these can be destabilizing, with the latter effect possibly being the more important. The second effect is an instability in the air escape process from the cushion which involves an interaction between the air flow, the water surface and the segment motion itself. Surprisingly, this occurs at a frequency which is low enough to couple with the heave motion of the basic vehicle. The report describes an exploratory investigation using a highly simplified geometry.

The third project is the development of a mathematical model of the pitch-heave dynamics of the uncompartmented segmented cushion. A feature of this work is accurate modelling of both cushion footprint and air escape areas, and of the cushion volume as they are affected by cushion motion. Hysteretic skirt contact forces can also be included. The computer programme is now developed and is yielding useful results. For example, it predicts the pitch-heave instability observed in our model tests, and suggests that the hysteretic skirt contact forces may play a crucial role in suppressing the instability in full scale vehicles. It also shows that the predicted properties of the cushion are surprisingly dependent on such factors as the details of the shape of the footprint area, and has provided insights into the importance of cushion capacitance.

In conclusion, the work described here has made a significant contribution to the task of laying a sound foundation for the analysis of the dynamics of practical configurations. However, two key areas requiring urgent attention are: the determination of unsteady fan response and its inclusion in dynamics models, and the understanding of skirt material hysteresis and its implications both for scale model testing and analysis.

SOMMAIRE

Ce rapport décrit les résultats d'un programme de recherche sur certains aspects de la dynamique des véhicules à coussin d'air à jupe flexible. Ces recherches, qui ont été effectuées de novembre 1981 à décembre 1986, avaient deux objectifs principaux:

(i) l'élaboration et la vérification expérimentale de modèles mathématiques de la dynamique du coussin d'air, que l'on pourrait utiliser comme outils de conception,

(ii) l'élaboration d'une installation pour l'essai de maquettes et l'établissement de procédures connexes d'analyse dimensionnelle et d'analyse des données.

Les effets des jupes flexibles sur la dynamique du coussin d'air ont fait l'objet d'une attention particulière.

Afin de bien comprendre l'approche adoptée dans ce programme, il est essentiel de bien distinguer les études sur les configurations d'intérêt immédiat pour la conception de celles sur des configurations choisies pour obtenir "une comparaison sans ambiguïté entre la théorie et l'expérience". La dynamique d'un coussin d'air retenu par une jupe flexible peut être complexe, de sorte que, pour analyser la dynamique d'un véhicule complet, il faut invariablement faire plusieurs hypothèses simplificatrices dont la justesse est très incertaine. Par conséquent, les données expérimentales obtenues avec un véhicule complet sont généralement inappropriées pour déterminer la validité de ces hypothèses. L'importance de ce problème échappe généralement aux concepteurs de véhicules, mais il a par ailleurs été constaté que la mise au point de véhicules à coussin d'air a été entravée par l'absence d'expériences pouvant éclaircir ce problème. Une partie importante de la recherche effectuée à l'Institute for Aerospace Studies de l'Université de Toronto (UTIAS) a porté sur l'obtention de telles comparaisons sans ambiguïté.

Les travaux ont toutefois été concentrés sur l'étude d'un système à coussin d'air unicellulaire à jupe segmentée mis au point au Canada pour les grandes plates-formes à coussin d'air et utilisée, en particulier, sur une proue brise-glace à coussin d'air (ACIB) de 270 tonnes. Des études effectuées précédemment à l'UTIAS sur ce type de jupe ont démontré que son comportement dynamique peut dépendre fortement du matériau utilisé pour sa fabrication. Plus spécifiquement, on a observé qu'avec un certain matériau on retrouve des instabilités de tangage et de pilonnement non linéaires qui seraient dangereuses pour un véhicule vraie grandeur. Avec un autre matériau, pour lequel on a constaté une forte hystérésis lors des essais de rigidité statique, les mouvements sont toujours fortement amortis. Par conséquent, une partie importante de l'étude a porté sur l'origine des instabilités et le rôle joué par les propriétés du matériau de la jupe, et ce, sur maquette ou sur véhicule vraie grandeur.

Les travaux sur les objectifs visés peuvent être classés en trois groupes:

(A) les études de base,

(B) la mise au point de la piste circulaire de 43 m de l'UTIAS pour essais sur maquettes,

(C) l'étude de la dynamique des grandes plates-formes à coussin d'air.

(A)

La première étude de base a été l'élaboration d'une méthode de mesure de la réaction du ventilateur de sustentation aux variations irrégulières de la pression du coussin d'air engendrées par le mouvement du véhicule. Dans les analyses de dynamique, on suppose presque invariablement que cette variation est quasi stationnaire, cependant il semblerait d'après diverses observations que cette hypothèse n'est peut-être pas adéquate. Ce rapport décrit une méthode simple, basée sur le concept de jupe rigide pour le coussin d'air et sur l'utilisation d'une table à pilonnement à entraînement servohydraulique. Le développement de la méthode de mesure a, au début, été entravé par des problèmes de saisie de données, mais ceux-ci ont été résolus et les résultats préliminaires sont très encourageants. On pourrait utiliser cette méthode pour l'essai de ventilateurs grandeur nature.

La viscoélasticité du matériau de la jupe affecte la dynamique du coussin d'air de deux manières. En premier lieu, pour certaines géométries de jupe, les déformations de cette dernière, provoquées par les variations de la pression du coussin d'air, peuvent faire varier sensiblement la hauteur de fuite et le volume du coussin d'air. Une étude théorique et expérimentale utilisant une jupe circulaire à faible conicité et un matériau utilisé par ailleurs pour nos modèles de jupes segmentées a fait ressortir des effets très marqués. Cependant les implications pour d'autres géométries restent à clarifier. En second lieu, le phénomène du fluage peut modifier les forces de contact entre le sol et la jupe, en fonction de l'historique des déformations précédentes. Ainsi, lorsqu'une partie de la jupe s'éloigne du sol, les forces observées sont inférieures à celles observées lors du mouvement contraire. Cet effet a été observé fréquemment, donnant lieu à une hystérésis lors d'essais de rigidité statique; si cette hystérésis apparaît dynamiquement, ce serait une source majeure d'amortissement. Cependant, son existence en vraie grandeur n'est pas démontrée. Certaines mesures préliminaires effectuées sur le ACIB semblent indiquer que, lorsque les segments de la jupe sont poussés vers le sol, jusqu'à 4% du poids total peut être supporté directement par les forces de contact. Ce résultat nous a amenés à examiner de façon plus détaillée son importance pour la dynamique ainsi que son origine. Par suite de problèmes conceptuels et de problèmes de saisie de données, les deux premières études sur cette question ont échoué; toutefois, la troisième a donné des résultats prometteurs. Elle a démontré indubitablement que l'hystérésis statique peut avoir des effets importants sur la dynamique et a jeté une certaine lumière sur les mécanismes en cause.

Le dernier projet de base a été une étude théorique et expérimentale des amplitudes et des fréquences des oscillations, stabilisées en un cycle limite, obtenues lorsqu'un coussin d'air est dynamiquement instable. Bien que ces phénomènes n'aient aucun intérêt pratique immédiat, en raison de leur non-linéarité marquée, ils permettent de vérifier sans ambiguïté les hypothèses habituellement formulées dans ces analyses. Les résultats de ces travaux ont contribué grandement à confirmer la validité de diverses hypothèses clé utilisées dans les autres analyses décrites ici.

(B)

L'élaboration d'une installation d'essai de maquettes ainsi que la définition des procédures d'essais se divisaient en trois projets. Le premier était la mise au point d'un nouveau ventilateur de sustentation destiné au véhicule d'essai. Le système original avait un débit insuffisant pour reproduire à l'échelle certaines conditions d'essai; il introduisait des couples gyroscopiques qui compliquaient considérablement l'interprétation des données et rendaient très difficile la modélisation de la réaction aux instabilités de pression du coussin d'air. Le nouveau ventilateur est maintenant opérationnel; sa conception contra rotative à deux étages et son rendement supérieur apportent une amélioration considérable sous tous les aspects.

Le deuxième projet était l'élaboration de méthodes d'analyse de données similaires à celles utilisées pour les essais en vol. L'UTIAS utilise présentement une technique d'identification par comparaison de réactions semblable à celle utilisée pour interpréter les données d'essais de vol d'avion; les premiers programmes utilisés par l'UTIAS étaient basés sur un modèle dynamique linéaire mis au point pour les essais d'avion. Leur utilisation a été un échec attribué à la présence de non-linéarités particulières à la dynamique des véhicules à coussin d'air et à l'incertitude quant à l'importance de la capacitance (terme exprimant la variation de la masse d'air du coussin en fonction de celle de la pression) du coussin d'air dans les essais sur maquettes. L'inclusion de la capacitance dans le modèle menait presque invariablement à des résultats divergents et confirmait les résultats obtenus d'autres façons. Il est donc devenu évident que l'étude de la dynamique des véhicules à coussin d'air nécessitait des méthodes spéciales. Les travaux ont alors été entrepris sur deux fronts:

(a) l'élaboration et l'essai d'un modèle mathématique de la jupe pouvant engendrer des données d'essai de vol simulé,

(b) l'élaboration d'une nouvelle procédure d'identification.

L'utilisation de données simulées présente un avantage capital: les coefficients à identifier sont connus exactement, de sorte qu'il est possible de vérifier les effets des diverses approximations sur la précision des calculs. Le premier objectif a été atteint et les résultats obtenus sont décrits ci-dessous.

Le troisième projet touchant les maquettes était l'élaboration de règles de dimensionnement. Deux aspects ont été examinés: le rôle des propriétés viscoélastiques de la jupe et celui de la capacité du coussin. Toutefois les deux aspects entraînent des difficultés; pour résoudre le premier, il faudra utiliser les résultats des études décrites plus haut, lesquelles ne sont pas encore terminées. Pour résoudre le second, il faudra déterminer les conditions dans lesquelles il faudra en tenir compte; celles-ci ne sont pas tout à fait établies. Un des objectifs de la modélisation du coussin d'air unicellulaire à jupe segmentée décrit ci-après était d'éclairer un peu plus ces deux aspects touchant l'essai de maquettes. Néammoins, nous avons supposé que, pour certains essais, la capacité du coussin devra être à l'échelle; à cet effet, une méthode a été étudiée pour le véhicule d'essai utilisé sur la piste circulaire de l'UTIAS.

(C)

Les travaux sur la dynamique des grandes plates-formes à coussin d'air comportaient trois projets, dont deux de nature exploratoire:

Le premier examinait l'effet sur la dynamique et la stabilité du temps de propagation des ondes acoustiques à l'intérieur des chambres de coussin de très grandes dimensions. Il a fallu utiliser une géométrie axisymétrique pour le coussin afin de permettre la solution du problème. D'après les résultats obtenus, la propagation des ondes acoustiques pourrait avoir des effets déstabilisateurs importants sur les plates-formes de 3 000 tonnes et plus. Toutefois, les résultats ont aussi démontré l'existence d'un autre phénomène non relié à la propagation des ondes acoustiques. S'il n'y a aucune autre source d'amortissement présente, les coussins d'air de grandes dimensions peuvent avoir une marge de stabilité beaucoup trop faible, la marge de phase (l'angle par lequel la force de pression précède le mouvement) étant au plus de quelques degrés.

Le deuxième projet portait sur la stabilité des coussins d'air au-dessus de l'eau. Certains essais effectués par le Conseil national de recherches sur un petit véhicule d'essai équipé d'un coussin unicellulaire à jupe segmentée ont indiqué que, sous certaines conditions, un système très stable au-dessus du sol pouvait avoir un comportement instable lorsqu'il est immobile au-dessus de l'eau. Des analyses ainsi que des expériences limitées suggèrent deux explications possibles. La première: le pilonnement du coussin peut créer sur l'eau des ondes stationnaires qui modifient le volume du coussin et la hauteur de fuite; ces deux variations peuvent avoir un effet déstabilisateur, la dernière étant probablement la plus importante. La seconde explication: une instabilité dans l'échappement d'air sous la jupe, ce qui suppose une interaction entre l'écoulement d'air, la surface de l'eau et le mouvement des segments de la jupe. Résultat inattendu, ceci se produirait à une fréquence suffisamment basse pour permettre un couplage avec le mouvement de pilonnement du véhicule. Le rapport décrit une étude exploratoire utilisant une géométrie très simplifiée.

Le troisième projet, orienté vers les grands coussins d'air, a porté sur l'élaboration d'un modèle mathématique de pilonnement et tangage du coussin unicellulaire à jupe segmentée. Ce modèle se caractérise par une représentation précise de l'effet du mouvement du coussin sur les aires de l'empreinte du coussin et de la zone de fuite des jupes ainsi que sur le volume du coussin. Les forces de contacts hystérétiques de la jupe peuvent aussi être incluses dans ce modèle, qui a par ailleurs donné des résultats utiles. Il explique par exemple les instabilités de tangage et de pilonnement observées dans nos essais sur maquettes. Les résultats obtenus semblent indiquer que les forces de contact hystérétiques jouent peut-être un rôle capital dans la suppression des instabilités de tangage et de pilonnement dans les véhicules grandeur nature. Autre résultat inattendu, le comportement du coussin dépendrait fortement de la forme exacte de l'empreinte. Le modèle a également permis de mieux comprendre l'importance de la capacitance du coussin.

En conclusion, le programme de recherche décrit ici a apporté une importante contribution à l'établissement d'une fondation solide pour analyser la dynamique des configurations pratiques. Toutefois, deux questions nécessitent une attention urgente:

(i) la description du comportement non stationnaire du ventilateur et son incorporation au modèle dynamique,

(ii) la compréhension de l'hystérésis de la jupe et ses conséquences pour les essais et les analyses sur maquettes à échelle réduite.

TABLE OF CONTENTS

Page

1. INTRODUCTION 1
   - 1.1 Objectives 1
   - 1.2 Discussion of Research Philosophy 1
   - 1.3 General Assessment of Progress 3

2. BASIC INVESTIGATIONS IN ACV DYNAMICS 4
   - 2.1 Measurement of Lift Fan Response to Unsteady Cushion Pressure 4
   - 2.2 Skirt Material Effects in ACV Dynamics 6
   - 2.3 Nonlinearities in ACV Dynamics 9

3. DEVELOPMENT OF THE UTIAS CIRCULAR TRACK FOR ACV MODEL TESTING 10
   - 3.1 Introduction 10
   - 3.2 Scaling of Model Tests 11
   - 3.3 Development of a High Performance Lift Fan System for Vampire 1 12
   - 3.4 Procedures for the Acquisition and Analysis of Test Data 14

4. INVESTIGATIONS OF THE DYNAMICS OF LARGE PLATFORM CUSHIONS 16
   - 4.1 Acoustic Wave Propagation Effects on the Dynamics and Stability of Large Cushions 16
   - 4.2 Dynamical Problems Arising from Hovering Over Water 17
   - 4.3 A Model of the Dynamics of a Large Platform Cushion Equipped with an Uncompartmented Segmented Skirt. 18

5. CONCLUSIONS 19

APPENDIX A TECHNICAL PORTIONS OF CONTRACT WORK STATEMENT 21
   - A.1 Introduction 21
   - A.2 Overall Objective 21
   - A.3 Specific Objective 21
   - A.4 Description of Work 21

APPENDIX B SKIRT MATERIAL EFFECTS ON AIR CUSHION DYNAMIC HEAVE STABILITY 23
   - B.1 Introduction 26
   - B.2 Comments on the Properties of Skirt Materials 27
   - B.3 Dynamic Stability Analysis 29
   - B.4 Measurements of Skirt Material Properties 32
   - B.5 Predicted Effects of Skirt Material Properties on Stability 36
   - B.6 Stability Experiments: Apparatus and Method 41
   - B.7 Results of Experiments and Discussion 42
   - B.8 Conclusions 44

REFERENCES - APPENDIX B 50

APPENDIX C NONLINEAR OSCILLATIONS OF A SINGLE FLEXIBLE SKIRT AIR CUSHION 53
C.1 Introduction 55
C.2 Mathematical Model 56
C.3 Experiment 59
C.4 Results and Discussion 63
C.5 Conclusions 77

REFERENCES - APPENDIX C 79

APPENDIX D ON THE HEAVE DYNAMICS OF LARGE AIR CUSHION PLATFORMS 81
D.1 Introduction 83
D.2 Mathematical Model 87
D.3 Impedance Analysis 88
D.4 Method of Characteristics Analysis 91
D.5 Dynamic Stability Results 95
D.6 Discussion 99
D.7 Conclusions 108

REFERENCES - APPENDIX D 111

APPENDIX E HEAVE STIFFNESS HYSTERESIS MEASUREMENTS ON A LARGE SCALE AIR CUSHION 113
E.1 Introduction 115
E.2 Model Scale Hysteresis 115
E.3 Effect of Static Hysteresis on Dynamics 126
E.4 Full Scale Hyteresis: ACIB Measurements 134
E.5 Conclusions 137

REFERENCES - APPENDIX E 140

APPENDIX F ON THE DYNAMIC STABILITY OF AIR CUSHIONS HOVERING OVER WATER 141
F.1 Introduction 143
F.2 Pressure-Water Surface Interaction 145
  F.2.1 Basic Theory 145
  F.2.2 Spatially Averaged Deflection of Water Surface in Plenum 148
  F.2.3 Deflection of Water Surface at Lip 149
F.3 Heave Stability Analysis 152
  F.3.1 Lumped Capacitance Model 152
  F.3.2 Lip Flow Model 154
  F.3.3 Stability Criterion 156
F.4 Results for HEX-5 159
  F.4.1 Effect of Cavity Pumping 159
  F.4.2 Effect of Flow Modulation at Lip 160
  F.4.3 Spatially Averaged Deflection and Lip Flow Modulation 164
F.5 Results for ACIB 167
  F.5.1 Cavity Pumping 167
  F.5.2 Flow Modulation and Cavity Pumping 167
F.6 Conclusions 167

REFERENCES - APPENDIX F 174

APPENDIX G PREDICTION OF HOVERCRAFT HEAVE STABILITY 175
G.1 Introduction 178
G.2 Air Cushion Model 178
G.3 Stability Concepts 182
G.4 Insights from Linear Theory 185
  G.4.1 System Characteristic Equation 185
  G.4.2 Routh-Hurwitz Stability Criteria 186
  G.4.3 Nyquist Stability Concept 192
G.5 Nonlinear Phenomena 198
G.6 Experiment 201
G.7 Conclusion 206

REFERENCES - APPENDIX G 208

APPENDIX H MEASUREMENT OF FAN RESPONSE TO UNSTEADY PRESSURE 211
H.1 Introduction 212
H.2 Data Acquisition and Analysis Problems 212
H.3 Quasisteady Lip Flow Assumption 214
H.4 Preliminary Results 214
H.5 Concluding Remarks 220

REFERENCES - APPENDIX H 224

APPENDIX I NONLINEAR DYNAMICS OF SEGMENTED SKIRT AIR CUSHION 225
I.1 Introduction 227
I.2 Equations of Motion 230
I.3 Geometric Function Approximations 233
I.4 Simulation Results and Discussion 237
I.5 Conclusions 244

REFERENCES - APPENDIX I 247

APPENDIX J GEOMETRIC FUNCTIONS USED IN ANALYSIS OF SEGMENTED SKIRT DYNAMICS 249
J.1 Introduction 255
J.2 The Dynamic Skirt Model 255
J.3 Leak Area 260
  J.3.1 General Comments on Leak Area 260
  J.3.2 Case 1 260
  J.3.3 Case 2 261
    J.3.3.1 Case 2: Perimeter Considerations 261
    J.3.3.2 Leak Area 264
    J.3.3.3 Heave Derivatives 265
    J.3.3.4 Pitch Derivatives 266
    J.3.3.5 Pressure Derivatives 267
  J.3.4 Case 3 269
  J.3.5 Symmetry Conditions 270
J.4 Footprint Area 270
  J.4.1 General Comments on Footprint Area 270
  J.4.2 Case 1 270
  J.4.3 Case 2 271

J.4.3.1 Footprint Area 271
J.4.3.2 Heave Derivatives 271
J.4.3.3 Pitch Derivatives 272
J.4.3.4 Pressure Derivatives 273
J.4.4 Case 3 274
J.4.4.1 Footprint Area 274
J.4.4.2 Heave Derivatives 275
J.4.4.3 Pitch Derivatives 276
J.4.4.4 Pressure Derivatives 277
J.5 Restoring Moment 279
J.5.1 General Comments on Restoring Moment 279
J.5.2 Case 1 279
J.5.3 Case 2 280
J.5.3.1 Moment Arms and Moment 280
J.5.3.2 Heave Derivatives 281
J.5.3.3 Pitch Derivatives 282
J.5.3.4 Pressure Derivatives 283
J.5.4 Case 3 284
J.5.4.1 Moment Arms and Moment 284
J.5.4.2 Heave Derivatives 285
J.5.4.3 Pitch Derivatives 286
J.5.4.4 Pressure Derivatives 287
J.6 Cushion Volume 288
J.6.1 Assumptions to Calculate Cushion Volume 288
J.6.2 "Dead" Volu;me 291
J.6.3 Total Volume Including "Active" and "Dead" Volumes 292
J.6.3.1 Case 1 292
J.6.3.2 Case 2 292
J.6.3.3 Case 3 293
J.6.4 Symmetry Conditions 294
J.7 Skirt Hysteresis 294

REFERENCES - APPENDIX J 295

APPENDIX K MEASUREMENT OF SKIRT CONTACT FORCES IN A SINGLE CELL 297
K.1 Introduction 297
K.2 Initial Test Proposal 297
K.3 Apparatus Developed for Measuring Contact Forces 298
K.4 Preliminary Results 301
K.5 Discussion and Conclusion 301

REFERENCES - APPENDIX K 308

APPENDIX L DEVELOPMENT OF SYSTEM IDENTIFICATION TECHNIQUES FOR THE ANALYSIS OF ACV FLIGHT TEST DATA 309
L.1 Introduction 309
L.2 Approach Adopted in Present Work 309

REFERENCES - APPENDIX L 313

APPENDIX M ON THE ROLE OF PNEUMATIC CAPACITANCE IN ACV DYNAMICS AND ITS MODELLING 315
M.1 Introduction 317
M.2 Conditions for Scaling Pneumatic Capacitance 318
M.3 Implications for Model Testing 322
M.4 Concluding Remarks 324

REFERENCES - APPENDIX M 325

APPENDIX N RESPONSE FUNCTIONS IN THE LIMIT OF ZERO FREQUENCY FOR OVERWATER STABILITY ANALYSIS 327
N.1 Introduction 327
N.2 Spatially Averaged Deflection 327
N.3 Deflection at Lip 328
N.4 Sine and Cosine Integral Functions of Ref. N.1 329

REFERENCES - APPENDIX N 330

APPENDIX O PRESSURE-WATER SURFACE INTERACTION COMPUTED BY LAMB 331
O.1 Pressure-Water Surface Interaction 331
O.2 Spatially Averaged Deflection 331
O.3 Water Deflection at Lip 332
O.4 Quasi-Static Limiting Cases: Spatially Averaged Deflection 332
O.5 Water Deflection at Lip 333

APPENDIX P PRELIMINARY INVESTIGATION OF SEGMENT-WATER SURFACE INTERACTIONS 335
P.1 Introduction 336
P.2 Analysis 336
P.3 Experimental Models 344
P.4 Results and Discussion 346

REFERENCES - APPENDIX P 349

APPENDIX Q EFFECT OF SEGMENT GEOMETRY ON HEAVE DYNAMICS AND STABILITY 351
Q.1 Introduction 352
Q.2 Determination of Segment Flow Function 352
Q.3 Investigations of the Dynamics 354
Q.4 Discussion and Conclusion 354

REFERENCES - APPENDIX Q 359

1. INTRODUCTION

1.1 Objectives

This report describes the results of a research programme on selected aspects of the dynamics of flexible skirt air cushion vehicles (ACV), undertaken at the Institute for Aerospace Studies, University of Toronto, to fulfill a contract with the Transportation Development Centre (TDC). The work described here covers the period November 1981 to December 1985, and builds on previous work on ACV dynamics undertaken for TDC [B.10]. The Contract Work Statement, given in Appendix A, specifies an overall or long term objective, and specific or short-term objectives. The overall objective has been essentially that of previous UTIAS work for TDC, namely development of a basic understanding of the dynamics of ACV's, with special reference to the role of the flexible skirt systems that are now universally used on these vehicles. The intention is to provide TDC with a source of technical expertise for the assessment of projects of interest to the Centre. However, as for previous contracts, an application of current interest has been identified, and this has provided a focus for the specific objectives. This application is the large platform cushions that can be used either for the movement of heavy loads over land, sea and ice in the Arctic, or as icebreaking platforms propelled by a ship.

The overall objective has been achieved through the continuation of the two main activities of the previous contract:

(i) Formulation of mathematical models of aspects of cushion dynamics believed to be of current or potential design interest, together with appropriate experimental validations,

(ii) Development of a facility for model testing, and identification of associated scaling and data analysis procedures.

Some specific tasks identified for the short-term objectives are:

(a) Preparation of a report for use by the industry to predict the onset of dynamic instabilities,

(b) Development of a methodology for ACV model testing,

(c) Investigation of various damping mechanisms inherent in air cushions,

(d) Investigation of passive stabilizing devices,

(e) Investigation of active stabilizing devices.

It was also envisaged that two skirt systems would be tested on the UTIAS 43m diameter enclosed Circular Test Track. One was to be the uncompartmented-segmented system then in use on TDC's 24.7m × 24.7m, 270 tonne Air Cushion Ice Breaker (ACIB), and the second was to be specified.

1.2 Discussion of Research Philosophy

The first UTIAS contract for TDC, undertaken in 1974, attempted to evaluate a Canadian-designed skirt system intended for use on low-speed overland vehicles. This system was at that time undergoing field trials. The evaluation was intended to be achieved by comparative testing of models of this skirt and a French-designed system. Also, a long-term UTIAS goal has always been, where appropriate, the fostering of direct contacts with the industry, and our first effort in this direction was a collaboration with a small firm in an investigation of the factors that affect the onset of self-excited oscillations, or "vehicle bounce". Although efforts such as these were to a certain extent successful, they revealed the existence of many areas of uncertainty; for example the rules for scaling of laboratory models were not clearly understood, and the factors that should be included in a simple but realistic analysis of the "vehicle bounce" problem had only been tentatively explored.

In parallel with this difficulty, early attempts at UTIAS and elsewhere to mathematically analyze complete cushion systems revealed that ACV dynamics can be very complex. It involves consideration of the fluid mechanical processes, the basic vehicle dynamics, and the structural and dynamical aspects of the skirt with the interaction of all three processes. Furthermore, skirt geometry can be complex, and certain aspects of the dynamics, such as that associated with skirt-ground contact can be highly nonlinear. Consequently, to analyze problems of engineering interest it has been, and continues to be, necessary to make many ad hoc assumptions, the validity of which can often be open to question. In particular it gradually became clear to us that experiments on complete cushion systems, while possibly producing data of immediate design interest, were unsuited to validation of the assumptions typically used in an analysis. There was a clear need for experiments on simplified configurations which, while not being intrinsically useful, were nevertheless contrived to facilitate testing of at most a few assumptions.

Although the ultimate test of a research programme of the present type must be its value to the industry, the tension between needs for experimental data of design interest and data suitable for validating a theory should not perhaps be unexpected. In an analysis of the development of the pure sciences, a well known historian of science has noted that "there are seldom many areas in which a scientific theory, particularly if it is cast in a predominantly mathematical form, can be directly compared with nature" [C.22], and that many manipulations of theory reported in the journal literature are undertaken "not because the predictions in which they result are intrinsically valuable, but because they can be confronted directly with experiment".

This crucial distinction between the two types of experiment that occur in engineering research is often not appreciated by those faced with the day-to-day task of vehicle development. In fact research of the present type frequently appears to pass through three distinct phases:

(i) an initial exploratory phase, perhaps involving trial and error experimentaion on the complete configuration,

(ii) basic investigations in which, where possible, theoretical ideas are tested against experiments on simplified configurations,

(iii) investigations of complete configurations of practical interest.

Much of UTIAS ACV research, including work reported here, has involved phase (ii) projects, and these have given many important insights. However, mindful of the need to produce results of demonstrable practical significance, we have sought ways to expedite transition to phase (iii) projects. In this respect a project started during our previous TDC contract [B.10] provided an excellent opportunity; this was an investigation of the dynamics of an uncompartmented segmented skirt system developed in Canada for use on such low-speed vehicles as an icebreaker platform. This is also known as the HSL skirt. Of all of the practical cushion systems developed to date, its geometry is the simplest, and thus it is amenable to the development of a mathematical model which has a minimum of ad hoc assumptions. Furthermore, it is an appropriate geometry for the type of large platform cushion that is the focus for the research of the present contract. Thus it has provided a useful conjunction of UTIAS and TDC interests, so that the present work has consisted largely of investigation of problems related to this geometry.

In concluding this brief perspective on our approach ACV research, it is worth noting that a recent review of ACV research in Britain [C.23] observed that development in that country has been impeded by lack of phase (ii) type research:

> "Several analytical models have been proposed in the last ten years, but in many respects these have proven unsatisfactory owing to the absence of adequate experimental data on some of the mechanisms present."

1.3 General Assessment of Progress

Considerable effort has been expended on phase (ii) type projects, some of which were not identified by the specific objectives. These projects were included in the contract work plan, and undertaken because in our judgement they had the potential to provide needed insights into certain questions basic to the development of dynamical models of large platform cushions or into the scaling of skirt material. Some have been completed, these include: a theoretical investigation on the effects of the viscoelastic properties of two model skirt materials on the dynamics and stability of a single conical cell (see Section 2.2 and Appendix B), an analytical investigation of acoustic effects on the stability of large platform cushions (Section 4.1 and Appendix D), an explanation of an instability of cushions hovering over water, first observed by Fowler [F.1] (Section 4.2 and Appendices F and P), and exploitation of an opportunity to validate analytical models involving skirt-ground contact (Section 2.3 and Appendix C). All four projects have yielded key insights into the tasks specified for the present contract; furthermore, they have also played a key role in building our confidence in modelling those ACV dynamic problems for which unequivocal experimental confirmation will not be possible.

Progress on one key project has been hampered by the lack of availability of suitable personnel, and by equipment limitations. This is the significance and mechanism of the hysteresis repeatedly observed in static pitch, roll and heave stiffness model tests at UTIAS. Previous work

[B.10, E.5] has indicated that this phenomenon can be caused by sliding friction between skirt and ground, but is more usually related to local buckling phenomena induced by skirt-ground contact. However, we have postponed aggressive investigation of the phenomenon until we obtained an indication of its practical significance for full scale vehicles. Measurements of its magnitude on TDC's ACIB were obtained during the tenure of the present contract. These are discussed in Section 2.2 and Appendix E. They indicated that at full scale the hysteresis could be comparable to that observed in some tests at UTIAS, and they highlighted the need for a systematic investigation of the phenomenon. For a variety of reasons our initial steps in this direction proved unsatisfactory, but very recently equipment and personnel problems were solved and we have made rapid progress. This is discussed in Section 2.2 and Appendix K.

A major part of the project has been the completion of the development of the UTIAS 43 metre diameter enclosed Circular Test Track, and the testing of two skirt systems, the Canadian uncompartmented segmented system noted above, and a second unspecified system. Successful execution of the project hinged on application of the system identification procedures now widely used to analyse the results of experiments on complex dynamical systems [B.10]. One of the ideas was to ascertain if the hysteretic damping observed in static pitch and roll stiffness characteristics was appearing in the dynamics. Our first attempt in this direction was to apply a programme developed for aircraft flight testing. However we eventually concluded that certain aspects of ACV dynamics, such as nonlinearities associated with skirt-ground contact, prohibited direct application of the aircraft-oriented programmes, since they are usually based on linear dynamical models.

This forced a decision to reorient the project. We decided to proceed with the development from first principles of a complete theory for the pitch-heave dynamics of the uncompartmented segmented skirt system, and then to validate the theory in simple experiments. The initial motivation was to use this theory to generate simulated experimental data for use in the development of system identification programmes. This theory has been developed (see Section 4.3 and Appendix I), and even though we have not yet been able to experimentally validate it, intriguing insights into the dynamical properties of the skirt system have been obtained. For example this theory has provided an explanation of the pitch-heave instability previously observed on the system [B.10], and highlighted the key role that material hysteresis plays in suppressing it.

The development of this theory implies that we have made a transition to a phase (iii) type project. Furthermore, our confidence in our ability to mathematically model skirt systems has enabled us to successfully execute two other phase (iii) projects, not part of the present contract.

2. BASIC INVESTIGATIONS IN ACV DYNAMICS

2.1 Measurement of Lift Fan Response to Unsteady Cushion Pressure

It has been known for some time that the response of the lift fan to unsteady cushion pressures induced by vehicle motion can deviate considerably from that measured in a steady state test [H.2]. Consequently, computation of vehicle response may, in many applications, require development of a suitable dynamic model. However, unless the fan geometry is especially simple, development of an accurate model from theoretical considerations is believed to be difficult. This appears to be particularly the case for the scroll or volute-enclosed centrifugal fan commonly used in the laboratory and on some vehicles. In fact, the uncertainty introduced into analysis by dynamic fan behaviour was the reason why the UTIAS Sphere Facility has been used for many of our experiments, including those described in Appendices B and C. This facility uses a 1000 m^3 sphere as a large pneumatic capacitance to completely uncouple the fan dynamics from that of the cushion system under test.

Nevertheless, all vehicles use fans, so that an experimental technique has to be found to characterize their dynamic behaviour. The challenge is to find a way of measuring the history of the unsteady flow at the fan exit. For a centrifugal fan enclosed by a volute, it is apparent that this is a difficult task, since even the steady flow is known to be highly nonuniform across the volute exit. Hence, although the response of hot wire anemometers is adequate to frequencies well above those required for ACV dynamics, the nonuniformity across the fan outlet implies that the unsteady exit velocities would have to be measured at many points. Obviously the task of data recording and analysis is associated with such an approach is likely to be prohibitively large.

A simplified approach suitable for testing laboratory models has been suggested by M. Hinchey; it is an extension of the ideas of ACV dynamics analyses. The concept is depicted in Figure H.1 [p. 213], which shows a plenum chamber cushion fed by a centrifugal fan and mounted over the UTIAS Heave Dynamics Table. In the usual ACV experiment, the aim would be to determine the heave frequency response of the plenum chamber to the table oscillations, and the results would be compared with a theory used assumed a model of the fan behaviour. In the present experiment the model is fixed, and the hovergap and cushion pressures are measured and their histories recorded. The quasisteady orifice flow law is applied to these measurements to compute the history of the flow leaving the cushion, and the conservation of mass principle for the cushion volume is then used to compute the history of the flow being delivered by the fan.

Success in the method depends on two crucial assumptions: (i) the validity of the quasisteady orifice law used in ACV dynamics analyses to calculate the flow leaving the cushion, and (ii) the availability of suitable data acquisition equipment. Now investigations of ACV dynamics such as those described in Appendices B and C have indicated that, for the conditions of interest in UTIAS ACV experiments, the quasisteady assumption is probably sufficiently accurate. Nevertheless a special calibrating experiment has been set up. This is described in Appendix H, along with some preliminary results which tend to confirm our supposition. The idea is to use it to establish the errors involved for the conditions actually used in the fan experiment.

Progress on this work has however been inhibited by lack of suitable data acquisition equipment. Preliminary experiments attempted to use analog recording devices. Data analysis involved digitizing the strip-chart records manually, an approach which makes the labour involved prohibitively time consuming. However, towards the end of the present contract period we acquired a microcomputer-based digital data acquisition system. This system has been applied to the experiment, and data analysis procedures have been developed. Appendix H describes preliminary measurements which indicate that the method can give useful results, and thus merits further detailed investigation.

Now while the technique obviously cannot be applied to the testing of full scale fan installations, nevertheless the data in Appendix H suggests an interesting possibility. This is to test on a facility such as the heave table scale models of full size systems, including inlet housings and neighbouring vehicle geometry, and then use scaling laws to predict full scale unsteady response. The laws for scaling steady fan behaviour are well known and very accurate. As suggested in Appendix H, simply esting at an appropriate reduced frequency should permit the scaling of the unsteady case.

2.2 Skirt Material Effects in ACV Dynamics

From the earliest days of UTIAS work for TDC, model tests both on the Cushion Dynamics Table and the Circular Track have revealed significant dynamical effects attributable to the viscoelastic and other properties of the typical elastomer-fabric ACV skirt material. UTIAS research in this direction has been aimed at (i) ascertaining the mechanisms involved, and (ii) establishing their significance at full scale. We believe this has important implications for both mathematical analysis of dynamics and the rules of scaling for laboratory model tests.

The work undertaken to date at UTIAS suggests that skirt material effects on laboratory models can be divided into two distinct groups:

(a) for some geometries, skirt deformations under the action of the cushion pressure, although small, are nonetheless significant enough to modify the pneumatic capacitance and the effective hovergap,

(b) hysteresis in static heave, pitch and roll stiffness characteristics, which is apparently related to stress-relaxation phenomena triggered by the local buckling associated with skirt-ground contact.

Appendix B describes a theoretical and experimental investigation of the first effect. The skirt geometry was a slightly tapered cone, and the UTIAS sphere facility was used for the tests. The conical skirt geometry was chosen because it is the simplest that retains the features of a flexible skirt, namely, inflation and structural stabilization by the pressure of the cushion air, and a flexible lower edge or lip suitable for passing over obstacles. It is relatively easy to compute the skirt deformations caused by the cushion pressure whereas, in contrast, computation from first principles of the deformations of a segment of the uncompartmented, segmented skirt is, owing to its geometry and the complicated structural properties of elastomer-fabrics, much more difficult.

Two materials were used in the tests: an 0.01 mm urethane-coated nylon fabric and an 0.12 mm thick extruded polyethylene film. Both materials have been used on UTIAS models, and both have produced different effects on the dynamics of these models; for example, the pitch stiffness of a 2.4m × 1.22m planform uncompartmented segmented skirt model displayed substantial hysteresis when equipped with polyethylene segments, and negligible hysteresis when equipped with the nylon-urethane segments. Correspondingly, when oscillating in pitch, the polyethylene segments generated much more damping [B.10]. The viscoelastic properties of the two materials were obtained by using the UTIAS servohydraulically driven heave table to perform oscillating uniaxial tension tests, and the stress-strain data thus obtained was used to determine phenomenological material models. Both materials displayed significant viscoelastic effects, including, at the frequencies used in the tests, stiffnesses substantially higher than those measured in stress- relaxation tests. Also, as is typical of materials which use woven fabrics as the main structural element, the nylon-urethane material stiffens considerably as stresses increase.

The linear stability analysis used the material models to predict skirt deformations and its effect on the dyamics. These deformations interacted with the dynamics in two ways: hoop deformation of the cone increased the effective pneumatic capacitance of the cushion volume, and longitudinal contraction increased the effective hovergap. Although these deformations are small relative to the basic cone diameter, nevertheless the calculations predicted large effects on the dynamic stability properties of the model. Furthermore, whereas the hoop deformation is destabilizing, the analysis predicts that the longitudinal contraction tends to stabilize the cushion. Tests to confirm the theoretical predictions were conducted in the Sphere Facility, and they included a special test in which hoop deformation was allowed, but by using a special clamp, longitudinal contraction could be prevented. This test clearly demonstrated the predicted opposing effects of hoop extension and longitudinal contraction on stability.

The second effect, static hysteresis, has been observed in UTIAS model tests from the earliest stages of our work for TDC, but until recently, its practical significance has not been established. In the model tests four sources have been identified:

(i) For one skirt geometry, a multicell system, buckling of the skirt material caused a loss of the cushion seal, and the resultant loss of lift caused collapse of the cushion,

(ii) sliding friction between skirt and ground,

(iii) the ability of the skirts to sustain small but nevertheless significant lift forces at the region of skirt-ground contact which are present when the material is being forced towards the ground but which, owing to creep or stress-relaxation phenomena, are reduced or absent when being moved away.

(iv) material creep phenomena may cause the effective hovergap to be larger when the skirt is moving away from the surface than when moving towards it.

Appendix E summarizes the evidence which leads us to believe that, of these three, some combination of the third and fourth is perhaps the most frequently encountered in both model testing and at full scale.

We have generally avoided detailed investigation of the phenomenon until its significance at full scale could be assessed. However during the tenure of the present contract we were presented with an opportunity to make measurements on TDC's Icebreaker Bow and these measurements are described in Appendix E. Although very limited in extent, they nevertheless indicated that for this 250 tonne platform, depending on heave height, between 1% and 4% of the vehicle weight could be carried directly on the segments. Some simple calculations are presented to show that forces of this magnitude could generate pitch and roll moments which are significant when comapred with that of the basic cushion.

This result provided the rationale for a more systematic laboratory investigation of the phenomena, and the work completed to date is described in Appendix K. At the beginning of the present contract, the work plan called for the testing of a special configuration in the Sphere Facility. This choice reflected the then held perception that, in the absence of a suitable dynamical model for the Heave Table fan, experiments on the Heave Table risked being inconclusive. The concept originally proposed, and first tested, is depicted in Figure K.1 (p. 299). The idea was to use a single conical cell, again for geometric simplicity, but to maximise the hysteresis effect, remaining completely in contact with the ground during cushion motion. The air cushion effect was simulated by using the special valve depicted in Figure K.1. The experiment consisted of measuring the static hysteresis force for this single cell by the technique used for the Icebreaker Bow, and then using this measured value in a nonlinear theory of the heave dynamics. The cushion was to be made unstable in the linear sense, so that the aim was to observe heave response to an initial disturbance, and by comparing predicted and observed responses, ascertain the extent to which the static hysteresis is present in the dynamics.

However initial attempts to measure the static contact forces did not succeed for several reasons, the principal one being that in these tests the forces showed a significant level of time dependence. Consequently a different approach had to be developed. In the meantime, the arrival of the microprocessor-based digital data acquisition system (DDAS) mentioned in Section 2.1 and the prospect of obtaining realistic dynamic characteristics for the Heave Table fan enabled us to contemplate an experiment based on that facility.

The apparatus now used for measuring contact forces is described in Appendix K, and is depicted in Figures K.2 and K.3 (pp. 300 and 302). As for the preliminary experiments, to obtain both geometric simplicity and maximum hysteresis force, a conical cell continuously in contact with the ground is used. The cell is fixed over the heave table and, with the table oscillating at a known frequency, the cell pressure, total cell force and table displacement histories are recorded by the DDAS shown in Figure K.3. Subsequently the skirt contact force that existed at each instant in time is determined by subtracting from the total force the cushion pressure force, with the latter being determined from the measured pressure, and the computed footprint area. The data obtained in this way is correlated with flexural rigidity measurements on samples of the skirt material obtained by using in the Heave Table the apparatus shown in Figure K.4, and with the uniaxial tension tests described in Appendix C.

This experiment has encountered several development difficulties, some of which are described in Appendix K. However it is now working satisfactorily, and the data indicates the presence of significant hysteresis in the contact forces even at frequencies as low as 0.01 Hz. Furthermore it clearly shows a tendency to increase with increase in frequency. We have also conducted flexural rigidity tests using the apparatus depicted in Figure K.4 (p. 303), and the preliminary data confirms the trends. In particular these indicate that the increase in contact force with increase in frequency is large. This frequency dependence is an important aspect that would not have been adequately explored by the approach first used.

The ultimate goal of this work is to use simple material tests, such as the dynamic uniaxial tension tests described in Appendix B, to predict the magnitude of the skirt contact forces for practical skirt geometries and materials. For skirt geometries such as the segmented system which is the focus of this report, and for the typical orthotropic nonlinear ACV skirt material, it can be readily appreciated that this is a very difficult task. However, as a first step, a theory for the cone and for isotropic materials is currently being developed. Even a simple theory can be expected to reduce the level of empiricism involved.

2.3 Nonlinearities in ACV Dynamics

Certain aspects of ACV dynamics, such as the cushion air escape area modulation caused by skirt-ground contact, and the orifice-like nature of the flow process from cushion to atmosphere, can be highly nonlinear. Yet work such as that described in Appendix B tests only the validity of the linearized theory. Appendix C describes the results of an experimental project which was suggested by a theoretical analysis of an aspect of ACV dynamics which apparently has no practical significance. However, it provided an excellent opportunity for a critical test of the nonlinear aspects of the dynamics. It has been observed that when an air cushion becomes unstable, the growing oscillation that is characteristic of linear dynamic instability frequently becomes a stable finite amplitude oscillation. This is called a limit cycle, since it is the end result of the oscillations of a linearly unstable system and is independent of the initial conditions. Limit cycles are an inherently nonlinear phenomena, so that prediction of such features of the motion as the amplitudes and frequency is completely beyond the scope of a linear theory.

For this work, the duct-plenum system described in Section 2.2 and Appendix B was used, and the analysis and experiment are described in Appendix C. The work is conceptually the same as the linear stability investigation of the duct-plenum system of the previous TDC contract [1] except that now the nonlinear aspects of the mathematical model have been tested. The principal assumptions being tested are the lumped capacitance model of the plenum volume, the lumped inertance model of the duct flow, the quasisteady orifice flow assumption for the duct inlet and cushion exit flows, and the effects of skirt-ground contact. The agreement between theory and experiment was good enough to conclude that, even in the presence of flow shut-off and reversal induced by skirt-ground contact, these assumptions are very accurate. These results have given us considerable confidence in our modelling of nonlinear dynamics, and this applies especially to the modelling of the segmented skirt system described in Appendix J and Section 4.3.

For the segmented skirt investigated here the flow shut-off nonlinearity arising from skirt-ground contact is not as abrupt as that investigated in Appendix C. Since, at equilibrium, the botton tips of the segments contact the ground, in pure heave motion and for a certain range of cushion heights, the cushion air escapes through approximately triangular regions between adjacent segments. The investigation of the effects of this behaviour on heave dynamics is described in Appendix Q. Using the 2.44 m × 1.22 m planform model air flow rates were measured as a function of cushion pressure for selected skirt heights. By assuming that the air escapes according to the usual Bernoulli orifice law, an effective orifice area and equivalent hovergap were calculated. This data is presented as a function of cushion pressure in Figure Q.1 (p. 352), and as a function of skirt height in Figure Q.2 (p. 353). It shows a weak dependence of equivalent hovergap on cushion pressure, owing apparently to skirt deformation as a function of p_c. Figure Q.2 gives the dependence of effective hovergap on skirt height; as expected, in the region where the air escapes through the triangular regions between segments, the dependence is highly nonlinear.

This data was incorporated into an analysis of the heave dynamics by assuming that the air escape process remains quasisteady. Since it was originally intended to test a model in the Sphere Facility, the analysis was used to predict the linear stability properties. These showed very large deviations of the stability from those for a rigid skirt operating at the same cushion pressure and cushion flow. An experimental programme was started but, owing to a lack of suitable personnel, it has not been completed.

3. DEVELOPMENT OF THE UTIAS CIRCULAR TRACK FOR ACT MODEL TESTING

3.1 Introduction

One of the major tasks identified for the present Contract is the development of model testing methodologies. The approach to this objective taken for the present Contract has been continued development of the UTIAS 43 m diameter enclosed Circular Test Track. The effect of this approach is twofold: (i) the Facility itself is prepared for testing of the models of interest to TDC, and (ii) it provides a clear focus for the identification of problem areas. Three areas have been investigated in the tenure of the present Contract:

(i) Problems of dynamic scaling and, particularly, of skirt material effects.

(ii) Development of a test vehicle having well understood dynamics, so that its peculiarities do not become an issue in the interpretation of experiments.

(iii) Development of procedures for the analysis of test data.

These three areas are discussed in turn.

As noted in Section 1.1, initial plans called for testing of two skirt systems on the Circular Track. This proposal was contingent on completion of both development of the facility, and the data analysis procedures. Owing to a number of technical, development, and financial problems, completion has been delayed considerably, so that the skirt system tests originally envisaged have not been done. At the time of writing, the Track development is essentially complete, but much remains to be done to complete development of data analysis procedures.

3.2 Scaling of Model Tests

A crucial part of the development of any model testing methodology is the identification of the appropriate scaling laws. Although discussions of scaling laws are available (see for example Ref. M.1, pp. 61-65), the literature has little to say on two features of ACV dynamics that work at this Institute has suggested may be important. These are: (i) the effect of the compressibility of the air in basic cushion volume, and (ii) the role of skirt materials. The air compressibility question has two, in turn, aspects. Although some published analyses include it, and others leave it out, there appears to be no consensus in the literature on the conditions under which it is important. The second is that, in a scale model the compressibility of the air in the cushion volume does not scale correctly. Consider these points in turn.

The fundamental role that air compressibility (or its equivalent-skirt flexibility) in generating dynamic instability has been long established [M.1]. However, for stable cushion systems, the picture is not so clear. It has been suggested that it is important only for high cushion pressures [M.2], disturbances having wavelengths which are short compared to the vehicle length [M.4] or for very small effective hovergaps [M.3]. It is expected that the analytical model for the uncompartmented segmented skirt developed in Appendix I will provide additional insights into this question. However, it is worth noting that some recent calculations at UTIAS of the linear frequency response in heave for a rigid cushion indicate that for cushion sizes, weights and flow rates representative of the Bell Aerospace Voyageur, including the capacitance made little difference, whereas for parameters representative of TDC's ACIB a large difference occurred. Our current judgement is that this difference is attributable to the much higher cushion flow coefficients — or nondimensional equivalent air gaps — used on vehicles such as Voyageur. Although more work on this question is obviously required, one preliminary conclusion relevant to model testing can be made: cushion flow rates should be scaled correctly.

Lavis et al [M.5] were the first to note the problem of scaling cushion capacitance; they noted that if λ is the ratio of model scale to full scale, then capacitance must be scaled in proportion to λ^2, and this is impossible if the basic cushion volume is used, since the latter scales in proportion to λ^3. In Appendix M the Pi-theorem of dimensional analysis is used to demonstrate this problem and to suggest ways of compensating for it. Two suggestions have been made in the literature, one is to test in a wind-tunnel in which atmospheric pressure can be controlled [M.5], and the second is to use a whirling arm facility to alter the effective gravity constant [M.6]. However, the dimensional analysis of Appendix M indicates that the first proposal will not work. The whirling arm approach, proposed by Richardson [M.6] does enable capacitance to be scaled correctly, but at a penalty which makes its use impractical. It turns out that the Froude number is given by $Fr = \phi^{-1/2}$ where ϕ is the angle subtended by the model at the whirling arm centre. If, following the suggestion of [M.6], one assumes that models should be no larger than $\phi = 30°$, then scale speeds are limited to no less than the highest speeds that might be used by high speed aerodynamically propelled vehicles.

The approach to scaling capacitance suggested in Appendix M is to incorporate pressure-dependent flexible volume in the unoccupied super-structure of the model. Ways of achieving this for the UTIAS Circular Track Test Vehicle are discussed in Appendix M. One of the main conclusions is that only a facility of the type and size of the UTIAS track has a realistic prospect of scaling capacitance.

Final resolution of the role of skirt materials in model testing must await completion of both the work described in Appendix K, and the experiments to validate the theory for the uncompartmented-segmented skirt developed in Appendix I. However, our current belief is that significant contact force hysteresis exists for all practical skirts operating over land or over water at planing speeds. Some recent analytical work at UTIAS on the bag and finger skirt not included in the present report has suggested that the large effects of the viscoelastic properties of skirt materials on the dynamics observed for the conical cells investigated in Appendix C may be peculiar to that geometry.

3.3 Development of a High Performance Lift Fan for the Circular Track Test Vehicle

The major test vehicle development undertaken during the tenure of the present Contract has been the design, construction and development of a new lift fan package for the Circular Track Test Vehicle, Vampire I. The decision to embark on this project was made for several reasons, all related to the central objective specified in Section 3.1 above. The original fan, installed in 1975, used a single stage axial unit, and was chosen for reasons of economy. Experience since that time has revealed several serious deficiencies. First it was inefficient and did not generate enough flow to correctly scale full scale behaviour, especially for high speed amphibious vehicles. Second, the single vertical axis rotor generated gyroscopic torques during vehicle motion that, for some certain skirt geometries, were large enough to create rolling motion in response to pitch disturbances; this complicated an already difficult task of interpretation of the experiments. Third, the fan geometry was chosen in the absence of an appreciation of the way fans can respond to fluctuating cushion pressures generated by cushion motion. As noted in Section 2.1 and Appendix K evidence now available indicates that even at the low frequencies involved in vehicle-dominated motion, fan response can differ greatly from that determined in a steady state test. We believe that at low frequencies provided that the pressure fluctuations are not so large as to cause flow reversal, the deviation is caused by unsteady air inertia effects in the fan housing.

The configuration chosen to resolve these various difficulties is shown in Figure 1. It is based on an 0.762 m diameter two-stage contra-rotating geometry which, reducing to a minimum the kinetic energy lost in swirl, generates high pressure at high efficiency. It also keeps gyroscopic torques to a minimum. The associated ducting has been kept to the absolute minimum in order to reduce unsteady inertia effects and thus make the

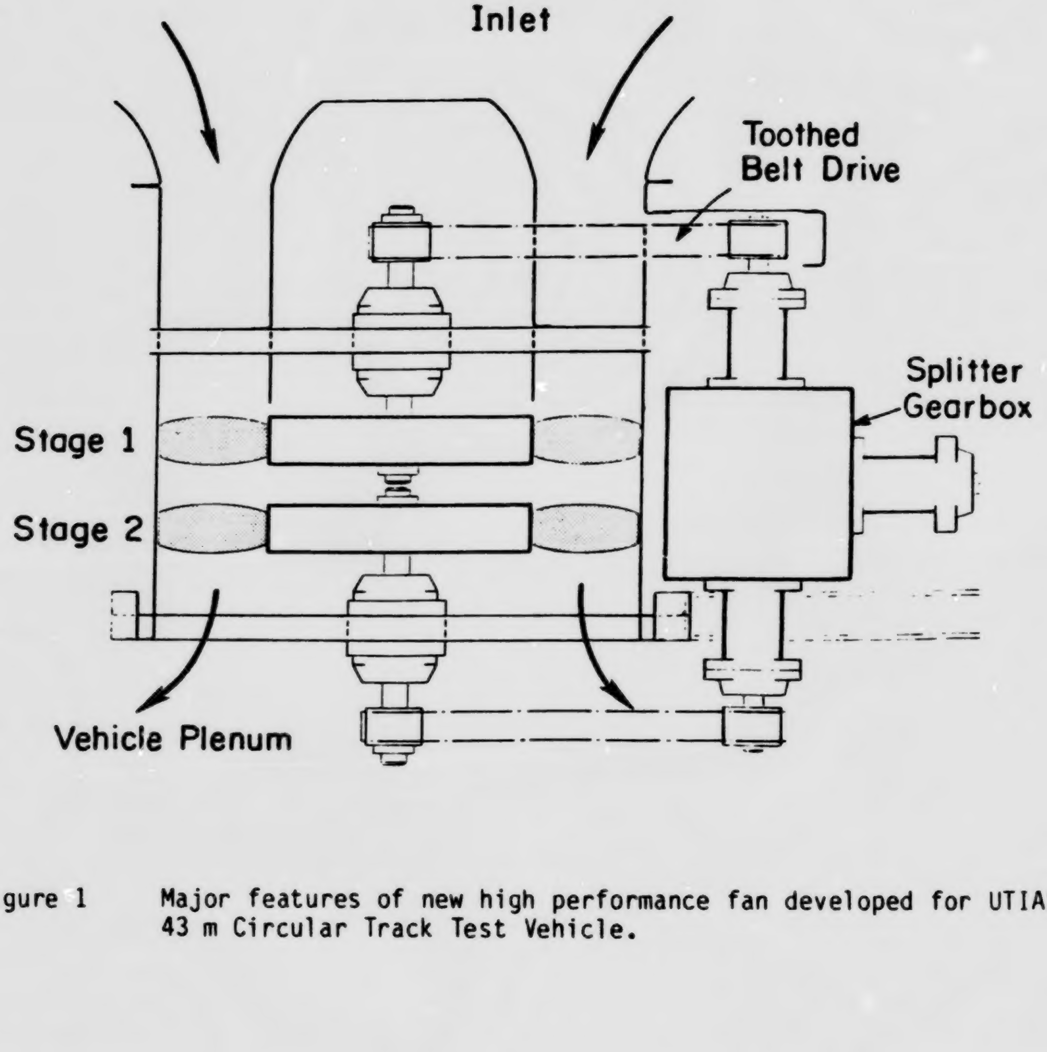
Inlet
Toothed
Belt Drive
Splitter
Gearbox
Stage 1
Stage 2
Vehicle Plenum

Figure 1 Major features of new high performance fan developed for UTIAS 43 m Circular Track Test Vehicle.

response quasisteady to the highest frequency possible. In the event that test conditions occur in which the flow does become unsteady, we believe that for moderate flow fluctuations this geometry is much more amenable to the development of a reasonably rigorous theory, than that of a centrifugal fan.

The fan is driven by a 24 kW two-cylinder two-stroke gasoline engine through a toothed belt speed reduction and a splitter gearbox. The steady state characteristic is given in Figure 2. It is anticipated that its unsteady behaviour will be examined by using the technique described in Appendix H to test a model.

3.4 Procedures for the Acquisition and Analysis of Test Data

As noted above, the data retrieved from the experiments on the Circular Track consists of digitized histories of the oututs of twelve or more transducers. It was decided that the most satisfactory way to interpret such large amounts of data is to use system identification techniques similar to those developed for the analysis of aircraft flight-test data. The concept is depicted in Figure L.1 of Appendix L (p. 310). Initial attempts, started during our previous TDC Contract [L.1], used an existing aircraft-oriented programme which assumed a linear model [L.2]. However, we only met with indifferent success; convergence was obtained only with great difficulty and, in many cases, not at all.

During the tenure of the present Contract efforts to use this programme continued. This included recompiling by a second computer programmer to eliminate obscurities in the first compilation, and even using a third compilation by the UTIAS flight-test group. However it was found that, while these programmes would converge when applied to aircraft flight test data, no success could be obtained with Circular Track data. At this stage it was decided to test the programme on simulated ACV data for simplified configurations. Simulated data is generated on a computer by solving the differential equations of interest to generate histories of outputs and then adding computer generated random noise to the solutions. The advantages of using simulated data are that the coefficients to be identified are known, and that any desired noise level can be used. The simplified cushions were a two-conical-cell system and an adaptation of the uncompartmented-segmented cushion. Again convergence could be obtained only under very restricted conditions, in particular the procedure failed if the nonlinearities were excited to any significant extent, or if cushion capacitance was included. We thus concluded that special programmes based on nonlinear models would have to be developed, and that the role of cushion capacitance in the Circular Track experiments would have to be clearly established. In this respect, two well-known workers in the field of parameter identification have noted that success is contingent upon including in the model only those features which are important and no more [L.3].

Hence we decided to halt further development of system identification procedures for the Circular Track experiments until the mathematical model of the dynamics of the uncompartmented-segmented skirt cushion was available to generate the requisite simulated data.

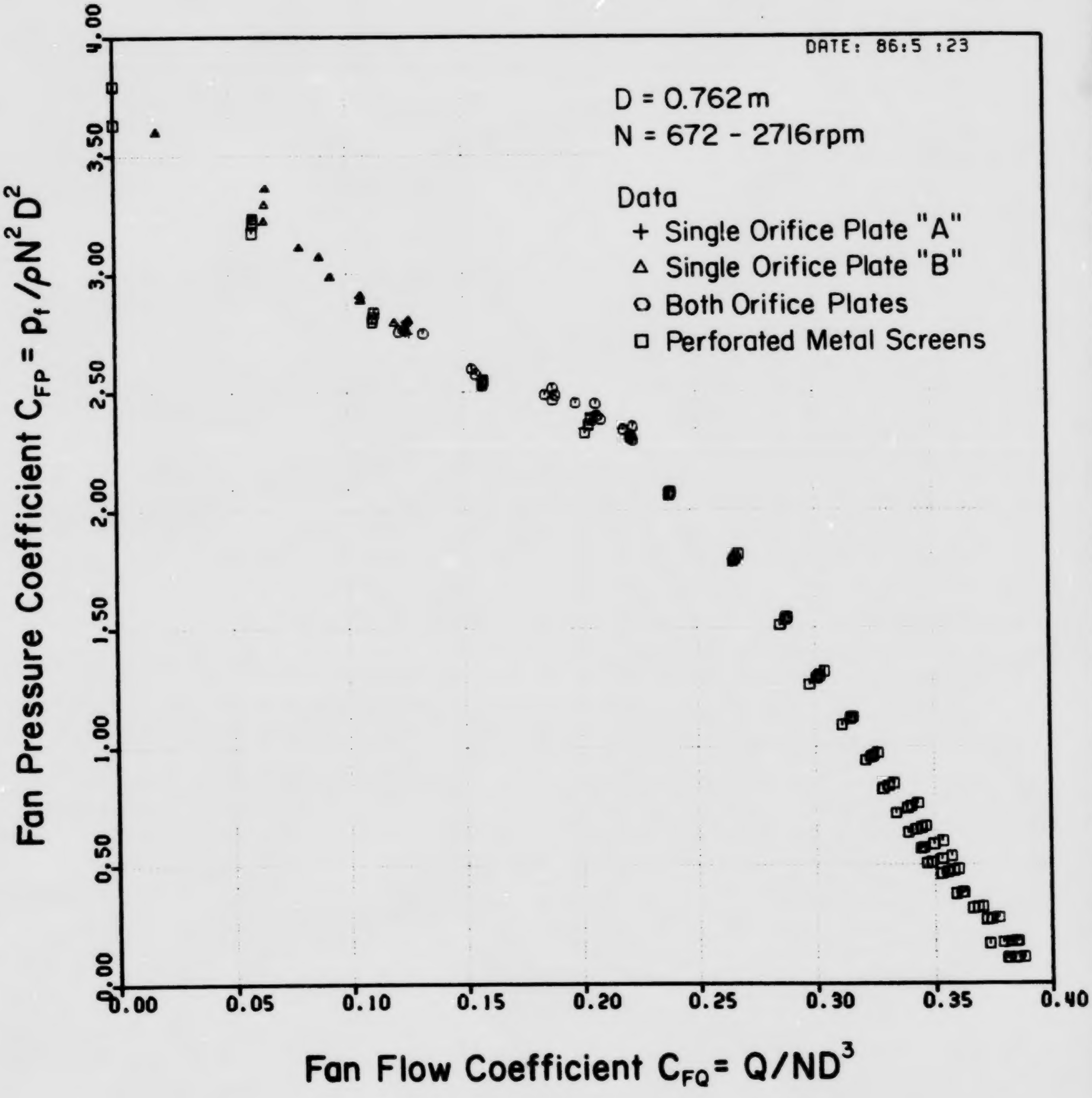

Figure 2 Measured steady state pressure-volume flow characteristic of new fan. The original method of measuring volume flux was to block off the vehicle base and pass all air through two standard 12 in. orifice plate installations. This could not cope with the high volume flux generated by the new fan, so that the vehicle was mounted on a special box, the walls of which included sections of perforated metal screen. These were calibrated individually by the orifice plate installations.

4. INVESTIGATIONS OF THE DYNAMICS OF LARGE PLATFORM CUSHIONS

4.1 Acoustic Wave Propagation Effects on the Dynamics and Stability of Large Cushions

Analyses of cushion dynamics, including work at UTIAS, generally assume that, when important, the air compression-expansion process in the cushion volume can be modelled as a lumped pneumatic capacitance. For this assumption to be valid, pressure disturbances at any point within the cushion must propagate acoustically throughout the cushion volume in a time which is very short relative to the period of an oscillation or any time characterizing the vehicle motion. Only then can the pressure at any instant in time be assumed uniform throughout the cushion volume. As the size of cushions increase, one might expect this approximation to become increasingly poor, but since it would seem that as size increases, the characteristic times of vehicle motion also increase, at first thought it would seem that, with one obvious exception, the lumped capacitance approximation should still be useful for large vehicles. The exception is high speed passage over short wavelength disturbances. This can lead to ride comfort problems.

There is however another exception which is directly relevant to the present work. For the heave stability problem it can be shown that, as planform size increases, the natural frequency of heave oscillations decreases to a limit which is determined mostly by the cushion pressure and depth, and is typically 1 to 2 Hz. Hence as size increases, it is inevitable that acoustic propagation effects become significant, and the only question is: How large must the cushion be?

Appendix D describes an exploratory investigation of the phenomenon. To make this analysis tractable only a very simple case is considered; this is an axially symmetric rigid plenum chamber subject to axisymmetric disturbances. Two cushion air feed cases are investigated, a single central feed and a peripheral feed. The equations are based on the one-dimensional equations of radial acoustics, and two methods of analysis are presented. The first uses separation of variables and classical impedance techniques to solve the linearized equations and the second uses numerical techniques based on the method of characteristics. The latter method was included because it provides a check on the first, and because typical ACV nonlinear aspects can be easily incorporated. The latter feature proves to be important.

The results indicate the presence of significant acoustic effects for large cushions. Typically for a diameter of 91.4m, corresponding to a cushion weight of 3344 tons at a cushion pressure of 5 kPa, significant acoustic destabilizing effects occur at small hovergaps for the centrally fed case. However if the cushion is fed peripherally these effects largely disappear.

The results also show the presence of another disturbing feature, one that is not specifically an acoustic effect. Even when large cushions are operating at pressures well away from a linear stability boundary their phase margin can be very low, a few degrees at most. Thus, in the absence of other forces these cushions are very lightly damped. A typical desired minimum damping corresponds to a phase margin of 30°. Thus even for stable cushions some additional form of damping is required. The method of characteristics analysis has been modified to show that the hysteresis in skirt-ground contact forces might be used effectively for this purpose.

4.2 Dynamical Problems Associated with Hovering Over Water

Fowler [F.1], while pursuing field trials of a small test vehicle, observed an instability that we believe to be of major interest to the present Contract. Whereas this vehicle was found to be dynamically stable over land, when hovering without forward motion over water, it was subject to a violent heave instability. Fowler attributed this to the pumping or wave-making action of the heaving cushion on the water beneath it, and to a resonance between the cushion motion and the oscillations of the water. This oscillation was found to be suppressed as soon as the vehicle moved forward at any but the smallest speeds, thus indicating that it has little practical significance except for vehicles that would be expected to hover without forward motion for extensive periods. We considered that this could occur for the type of large platform cushion that is the focus of the present Contract, hence we continued an extended investigation of it that was started under the previous TDC contract [F.8, see Section 6].

The previous work adapted an analysis developed for a two-dimensional pneumatic wave-maker [F.5]. This uses classical linearized water wave theory to predict the motion of the water surface caused by a spatially uniform pressure acting over a finite width and at a known frequency. The spatially averaged motion in the interior of the pressurized section of the water surface was used to compute an "equivalent piston" pumping of the cavity by the water surface. This analysis predicted trends opposite to that reported by Fowler [F.1].

During the tenure of the present Contract some exploratory experiments were conducted. This included the construction of a small water tank in which the water surface in the interior of the cushion could be observed while it is heaving; this is shown in Figure F.1 (p. 144). This showed that a standing wave is set up in the cushion interior, so that the cushion volume and the hovergap are modulated by the water motion in different ways. A second experiment, set up to measure the effective discharge coefficient for air escaping under segments partially immersed in water, led to a surprising result which suggested the existence of a second source of heave instability for segmented skirts hovering over water. The segments were observed to oscillate at a frequency low enough to couple with the model heave motion. Observation of the process with a motion picture camera indicate that this instability is related to a dynamic instability of the interface between the water and the air escaping under the cushion.

During the tenure of the present Contract the analyses described in [F.8] was extended, for the two-dimensional case, to include the effect of lip-flow modulation. The results show that it could be both stabilizing and destabilizing but in general it dominated the air cavity pumping effect. An investigation of the air-water interface instability has been started. This is not complete but progress to date is described in Appendix P.

4.3 A Model of the Dynamics of the Uncompartmented Segmented Cushion

This project, described in Appendix I is - in a sense - the culmination of the present Contract, and much of the other work is a necessary prelude to it. The aim is the development of a theory of the pitch-heave dynamics for the uncompartmented-segmented cushion from first principles, and with a minimum of empirical data. It includes provision for a dynamical model of the cushion fan response, skirt-ground contact hysteresis forces and the elastic deformation of the skirt under cushion pressure and the resultant effect on cushion volume, footprint area and restoring moment.

However the major part of the work required in this development has been the formulation of mathematical expressions for the area and centroid location of the cushion footprint and for the cushion volume as functions of pitch angle and centre of gravity height. These are described in Appendix J, and are required to compute cushion lift and restoring moment, and for the cushion volume conservation law. Observation of vehicle motion on the Track has shown that three cases have to be considered; these are depicted in Figure I.3 (p. 235), and are: (1) the skirt system is completely clear of the ground, (2) contact of part of the bottom perimeter with the ground, and (3) contact of the entire perimeter. Three approximations to the shape of the cushion footprint are considered; these are: a rectangle, and two more detailed shapes. The analysis in Appendix J also gives the derivatives of the three cushion geometry functions with respect to pitch angle and heave height to enable computation of the linear system matrix at any condition.

The programme is now working and is giving intriguing results. For example the computed pitch stiffness shows a surprising sensitivity to the details of the shape of the cushion footprint. Typically Figure I.5 (p. 238) shows that a rectangular footprint predicts a static pitch moment which is only 72% of the measured value. Corresponding differences are observed in the dynamics; some typical results are shown in Figure I.7 (p. 240). One difficulty is that the major parameter controlling skirt behaviour is the segment angle β defined in Figure J.1 (p. 256), and deviations from a nominal design value caused by manufacturing error or skirt deformation under cushion pressure can introduce large errors. For the 0.10 mm thick nylon-urethane segments on the 2.44m × 1.22m planform model, when pressurized the segment angle at their tips was found to be about 32.5°, when compared with a nominal value of 40°. This measured value gave good agreement between predicted and measured values of pitch moment. However, measurements of footprint area suggested an effective angle of about 38°; this is shown in Figure I.6 (p. 239).

Two important dynamics results have already been obtained. The first is that, for the 2.44m long cushion, the pneumatic capacitance has only a negligible effect on the dynamics, whereas for a cushion twenty times larger it has a major effect. Apart from the significance for the model testing problem discussed in Appendix M, it is a welcome result for the system identification development, since including capacitance seems to have been a major source of convergence failure. The second major result is the reproduction of the pitch-heave dynamic instability observed on both the 2.44m × 1.22m model and the Circular Track test vehicle when equipped with the 0.10 mm thick nylon-urethane segments. It is a nonlinear or finite stability problem in the sense that the linear state matrix indicates that the cushion is linearly dynamically stable at zero pitch angle, but becomes unstable at a small but finite pitch angle. This occurs without the presence of cushion capacitance, and it also suggests that for the cushions currently in use on full scale vehicles the instability is suppressed by an unspecified mechanism. One possibility is hysteresis in the skirt contact forces, another is hysteretic modulation of flow area.

5. CONCLUSIONS

Although some of the detailed objectives specified in the Work Statement for the present Contract have not been achieved, nevertheless we have made considerable progress towards the two major goals: understanding the elements required for a realistic model of the dynamics of large platform cushions, and developing a facility and procedures for scale model testing. Indeed, for the first of these goals, we are confident of the basic validity of the mathematical model developed for the uncompartmented-segmented skirt system and, although the experimental validation has only just begun, the analysis has already yielded a major result; this is the prediction of an inherent pitch-heave dynamic instability that in practical systems is apparently suppressed only by the hysteresis in skirt-ground contact forces. In relation to the second major goal considerable progress towards identifying the scaling laws for model testing has been made and, in particular, insights into the possible role that the viscoelastic properties of ACV skirt materials may play.

However, work is required in two key areas before it can be said that all the essential elements are in place. These are (i) the measurement and modelling of unsteady fan response, and (ii) the elucidation of the mechanism of skirt contact force hysteresis. In any future work they should be given a high priority.

In two areas progress has been markedly less than envisaged. The first is in the development of system identification procedures for analysis of ACV flight test data. Considerable development work is required, but at least the reasons for the failure of the computer programmes used to date have been identified. In the second, development of devices for stabilization of cushions, owing to a lack of suitable personnel, only some preliminary work has been undertaken. However, we believe that this is a relatively straightforward task, and in any case some of the work described here is an important, even necessary, preliminary.

APPENDIX A. TECHNICAL PORTIONS OF CONTRACT WORK STATEMENT

A.1 Introduction

In the early 1970's a group was formed within the University of Toronto Institute for Aerospace Studies (UTIAS) to specialize on research in air cushion technology. This group has developed into a centre of excellence, having highly skilled personnel and test facilities for air cushion vehicle (ACV) research which are not available elsewhere in Canada. The air cushion dynamic stability work carried out by the group in recent years has led to international recognition of their ACV research achievements. This project will build upon the expertise which has been established at UTIAS, and provide a valuable technical resource for use by Transport Canada, other federal government departments and Canadian industry.

The work of this project is directed to the solution of the problem of dynamic instability inherent to the large air cushion platforms which will be needed for forthcoming Arctic exploration and development projects. The methodologies, analytical techniques, and modelling experiments to be carried will also be applicable to other ACV developments such as the Arctic air cushion ice-breaking bow.

A.2 Overall Objective

To sustain a centre of excellence in air cushion technology which can investigate problems related to the application of this technology to Canadian transportation.

A.3 Specific Objective

To investigate damping mechanisms, either passive or active, to forestall the pneumatic heave instability incipient in very large air cushion vehicles (ACV) such as Arctic air cushion ice-breakers.

A.4 Description of Work

The work will comprise theoretical and experimental analysis of damping mechanisms for heave instability in large air cushion vehicles. The objectives will be met by mathematical analysis of the phenomenon, with confirmation of the analysis by scale model tests. The models are to be of two types: models reproducing pneumatic characteristics (but not necessarily to geometric scale), and models reproducing dynamic characteristics of full size vehicles. Based upon the results obtained, the project will define damping mechanisms that could be installed in large air cushion vehicles. The specific tasks to be addressed by the contractor shall include:

A.4.1 Present a technical work plan and schedule through contract completion, identifying material and personnel requirement, and outlining a control procedure for proper allocation and monitoring of resources. The work plan shall describe in detail the activities for the current year, and describe in more general terms the activities for future years. It shall be submitted to TDC for review and approval within three (3) weeks of the contract award. This technical work plan shall be revised and resubmitted for review and approval by TDC on an annual basis.

A.4.2 The work to be addressed by the contractor shall consist of the following principal tasks:

(a) Review preceding work on ACV stability and prepare a separate report on heave prediction methodologies, describing the lumped characteristic method, and outlining useful but simple procedures for use by ACV designers.

(b) Address ACV model methodology, developing test systems as a means of varifying analytical approaches. A fully developed sub-proposal is to be presented, at a date to be specified in the work plan, to cover model technology.

(c) Investigate inherent damping mechanisms in various air cushion systems, particularly the ones pertaining to skirt interaction, between skirt segments and between skirt and ground, or skirt and water. As part of this task measurements on existing air cushion devices shall be carried out on an opportunity basis.

(d) Investigate passive damping systems in air cushion vehicles such as resonator chambers and flexible capsules.

(e) Investigate active damping mechanisms in air cushion vehicles.

APPENDIX B. SKIRT MATERIAL EFFECTS ON AIR CUSHION DYNAMIC HEAVE STABILITY

(T. A. Graham, P. A. Sullivan, and M. J. Hinchey)

NOMENCLATURE

Roman

a	atmospheric sound speed
A_b	area of vehicle planform used as reference in calculating C_{QC} and C_{SW}, for conical cell, $A_b = (\pi/4)D_{st}^2$
A_d	cross sectional area of duct
C_c	cushion capacitance = $V_{ce}/\rho a^2$
C_m	discharge coefficient in cushion air escape law
C_{mi}	flow coefficient for duct inlet
C_{PC}	cushion pressure coefficient = p_{ce}/P_a
C_{QC}	cushion flow coefficient, $C_{QC} = Q_e(\rho/2WA_{base})^{1/2}$
C_{SW}	$C_{SW} = w_s A_b/W$
D_{in}	cushion inlet diameter
d_r	D_{sb}/D_{sm}
D_{sb}	diameter of conical skirt at lip
D_{sm}	mean diameter of conical skirt
D_{st}	diameter of skirt at top
E_1, E_2	storage and loss modulus characterizing response of material to oscillating strains
E, E_g, E_v	spring coefficients in phenomenological material models, E = Young's modulus, E_g = spring element in series with Voigt element to make standard linear model, E_v = spring element of Voigt model
g	acceleration due to gravity
h	hovergap
h_s	height of skirt, see Fig. B.2
ℓ_ℓ	length of perimeter of skirt at lip

ℓ_s	mean length of skirt perimeter
L_d	duct length
p_a	absolute atmospheric pressure
p_c	cushion gauge pressure
p_{df}	pressure in the duct at conical inlet
p_f	equivalent fan or source pressure
Q_a	volume flux past cushion lip to atmosphere
Q_d	volume flux through duct
r_c	radius of curved region at top of skirt
s	slant length of skirt
S_a	cushion support area
t	time
t_s	thickness of skirt material
V_a	cushion "active" volume = $S_a h$
V_c	total cushion volume
V_d	cushion "dead" volume
W	gross weight supported by cushion
w_s	weight per unit area of skirt material
x	height of cushion base above ground

Greek

γ	isentropic exponent
δ	material loss angle, $\tan\delta = E_1/E_2$
ε	strain
η	material damping coefficient
θ	skirt taper angle
ν	Poisson's ratio
ν_e	skirt contraction coefficient

ρ	air density
σ	stress
ω	angular frequency

Subscripts

e	equilibrium value
h	hoop direction
o	undeformed quantities

B.1 Introduction

The success of all modern air cushion vehicles (ACV) depends largely on the use of flexible skirts to permit negotiation of obstacles or waves while retaining relatively low levitation power or hovergap. A skirt is a collapsible structure inflated and stabilized by the pressure of the cushion air and is usually made from a woven fabric coated with an elastomer. Such composite materials can possess nonlinear, viscoelastic and anisotropic properties, and it is of fundamental interest to ascertain the effect of these properties on the dynamics of the vehicle, both at full scale and for test models. Although detailed analyses of ACV cushion and skirt dynamics are now appearing in the open literature (see, for example, Refs. B.1, B.2 and B.3) they generally assume an "ideal" skirt material behaviour [B.2, B.3, B.4]. This ideal is an inelastic massless membrane incapable of sustaining any compressive stress. There is, however, very little available on the effect of skirt material properties on dynamics, both for full scale vehicles and in terms of scaling requirements for models. The work described here shows that the viscoelastic properties of two materials used in the writers' laboratory to build model skirts have major effects on the dynamics. This occurs because small deformations of the skirt can interact strongly with the dynamics by causing large changes in both the hovergap and the effective pneumatic capacitance of the cushion volume. This raises fundamental questions about the scaling of model skirts, as well as about the significance of skirt material properties at full scale.

The role of skirt extensibility in ACV dynamics was first considered by Ribich and Richardson [B.5] in 1967, who undertook an analytical investigation of a guided ground vehicle configuration. They also identified the key role played by the compressibility of the air in the cushion volume; it is the basic source of dynamic instability. However, they used a purely elastic model, and indications that this may be insufficient have come from several sources. Sullivan [B.6] described uniaxial tension tests of typical skirt materials, which showed that the stiffness depends strongly on strain rates, and Hinchey [B.7] and Cox [B.8] noted that predicted test model behavior can be very underdamped relative to that experimentally observed.

Large differences in the dynamics of model skirts attributable directly to material properties have been observed at the writers' laboratory [B.4, B.9-B.11]. For example, a 2.44m × 1.22m planform model of an uncompartmented, segmented skirt was found to be subject to a combined pitch-heave dynamic instability when equipped with segments made from an 0.10 mm thick urethane coated nylon fabric, for which $w_s = 0.076$ kg/m^2 and $C_{SW} = 0.0054$. For segments made from 0.13 mm thick extruded polyethylene film, with $w_s = 0.118$ kg/m^2 and $C_{SW} = 0.0083$, the motion was always heavily damped. Measurements of static pitch and roll stiffness for this model with the nylon-urethane segments installed agreed closely with a theory based on the ideal model material concept [B.10, B.11]. In contrast, the polyethylene segments generate large hysteresis of a type observed by the authors for other geometries [B.4, B.9]. This hysteresis has been attributed to sliding friction between the segments and the ground [B.13], and to localized buckling generated by skirt-ground contact [B.12]. Experiments by the authors indicate that both mechanisms can occur [B.4, B.9]. Corresponding skirt material effects on both dynamic stability and hysteresis in roll and pitch stiffness have been observed on a 4.08m × 2.06m 850 kg test model at the authors' laboratory [B.10, B.11].

The marked differences in dynamics caused by these model materials emphasized the need for an investigation of their effect on the dynamics of a simple cushion configuration which was already well understood. The configuration chosen for this investigation is depicted in Figure B.1; it is a single plenum chamber free to move in heave only with its air supplied from a large pressurized spherical reservoir by a moderately long duct. This apparatus completely uncouples the dynamics of the air supply system from that of the model being tested, and provides an ideal constant pressure source of air. Information on the dynamical properties of a cushion system is obtained by observing the effect of various parameters such as cushion weight and cushion volume flow on dynamic stability. Although cushion dynamics can be highly nonlinear, particularly when skirt-ground contact occurs [B.3, B.14, B.15], it has been found that this configuration accurately reproduces the stability predictions of a linear analysis for a rigid plenum chamber [B.14, B.16].

The present work extends the analysis of Ref. B.16 to include the effects of the viscoelastic properties of the two materials discussed above on the dynamics of a flexible skirt installed in the apparatus depicted in Figure B.1. The geometry chosen for the skirt is an inverted slightly tapered cone; it is perhaps the simplest that retains the essential properties of an amphibious flexible skirt, these are: a geometry stabilized by the cushion pressure and a flexible bottom edge or lip. Oscillatory uniaxial tension and stress relaxation tests were used to obtain data on the viscoelastic properties of the 0.10 mm nylon-urethane and 0.13 mm polyethylene materials, and this data was in turn used to specify phenomenological material models for prediction of the effect of cushion pressure on cushion volume and hovergap. The extended stability analysis was then used to demonstrate the effects of material properties on stability for ranges of the material parameters that might be expected in model skirts, and to predict the effect of the two materials discussed above on the stability of the duct-plenum system shown in Figure B.1. The second set of predictions is compared with results of experiments.

B.2 Comments on the Properties of Skirt Materials

Both components of ACV skirt material, the woven fabric and its elastomer coating, are usually manufactured from polymers. These substances can have complicated structural properties; typically they exhibit highly nonlinear stress-strain relationships which can depend strongly on temperature, stress histories and, in the case of oscillatory loading, strain rates or excitation frequencies. They can also be subject to substantial creep and stress relaxation [B.17, B.18]. One phenomenon of direct interest here is the existence of a range of excitation frequencies, below which the material can have a very low elastic modulus and is said to be "rubbery", and above which the elastic modulus may be much higher, and the material is said to be "glassy". In the transition regime the material may be highly viscoelastic, whereas in both the rubbery and glassy regimes the elastic modulus is independent of frequency and viscous effects are usually small. For structural analysis this behaviour is modelled by series and parallel combinations of

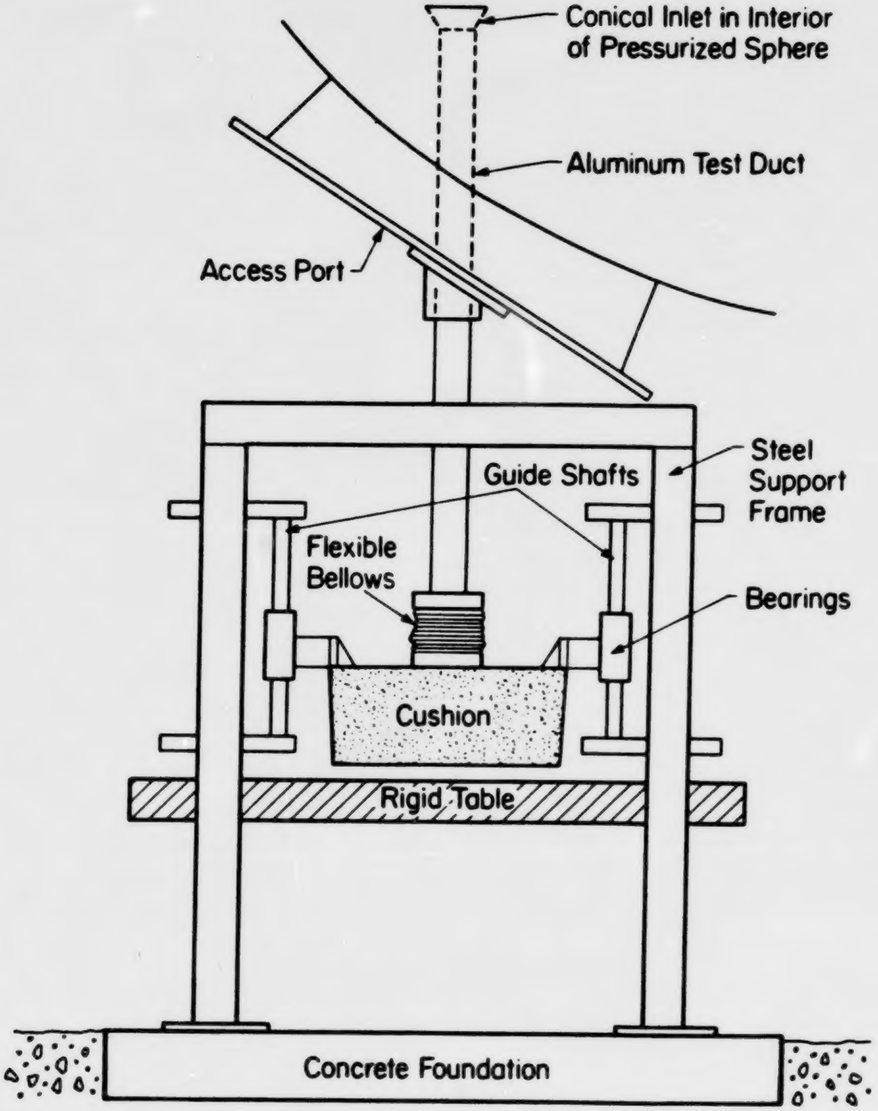
Conical Inlet in Interior of Pressurized Sphere
Aluminum Test Duct
Access Port
Steel Support Frame
Guide Shafts
Flexible Bellows
Bearings
Cushion
Rigid Table
Concrete Foundation

Figure B.1 Dynamic stability experiment used in the present investigation.

equivalent springs and dashpots [B.17, B.18]. The choice of combination depends on both the aspect to be modelled and the accuracy required. Samples taken from full scale vehicles have shown a single transition [B.6] which can be reproduced, qualitatively at least, by the standard linear model. This model and the Voigt model were used in the calculations described below.

An additional problem in characterizing ACV skirt material is that, since the major structural element is a woven fabric, properties peculiar to this type of construction have to be considered. The weaving process can bend the individual fibres considerably, so that the basic stiffness of a fabric is initially low but increases as the fibres straighten under load [B.19]. Also, the initial stiffness in the warp fibre direction is usually much higher than in the fill fibre direction. Furthermore, the effective stiffness in directions not close to either fabric direction may be very low. These orthotropic properties together with viscoelastic effects make the task of analysis of loads and deformation of practical skirt geometries very difficult, and the basic reason for the choice of a slightly tapered cone for the present work is that many of these difficulties are minimized.

B.3 Dynamic Stability Analysis

The principal geometric quantities used in the analysis are depicted in Figures B.1 and B.2. The elements of the theory are as follows. The sphere provides a source of air at constant pressure p_f. The flow through the conical inlet from the sphere to the duct entrance is assumed to be quasisteady and governed by Bernoulli's law:

$$Q_d = C_{mi} A_d [2(p_f - p_{df})/\rho]^{1/2} \qquad (B.1)$$

Pressure gradients along the duct are assumed to arise only from the unsteady inertia of the air [B.14], in which case

$$dQ_d/dt = (A_d/\rho \ell_d)(p_{df} - p_c) \qquad (B.2)$$

The compression process in the cushion volume V_c is assumed to be isentropic so that for low p_c, application of the continuity principle to the cushion volume leads to the equation

$$C_c(dp_c/dt) + dV_c/dt = Q_d - Q_a \qquad (B.3)$$

The air escape process from the cushion volume is also assumed to be governed by the same law as for the inlet:

$$Q_a = C_m \ell_s h (2p_c/\rho)^{1/2} \qquad (B.4)$$

The heave dynamics is assumed to be governed by Newton's law for a single rigid mass:

$$(W/g)d^2x/dt^2 = S_a p_c - W \qquad (B.5)$$

For a rigid skirt, $x = h_s + h$, $V_c = V_d + S_a h$, and the formulation is complete.

The formulation for a flexible skirt requires description of the effects

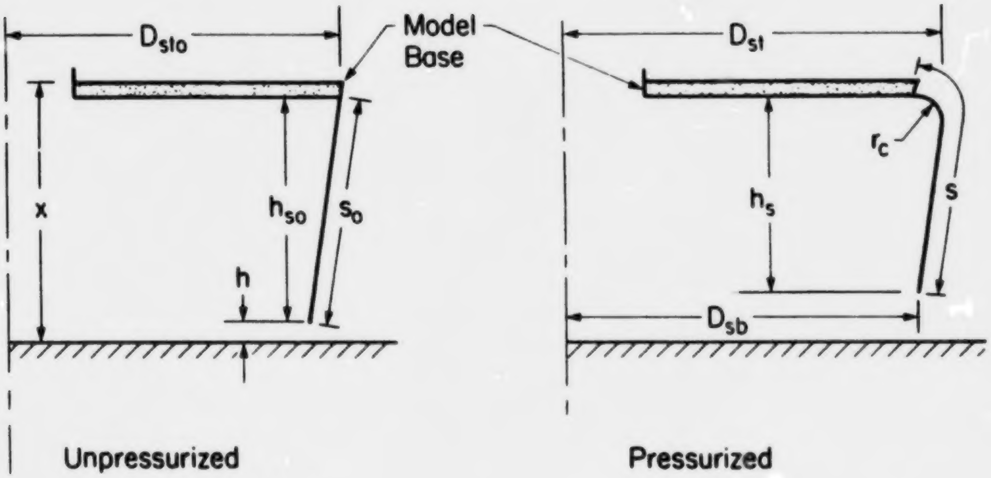
D_{sto}
Model Base
x
h_{so}
s_o
h
Unpressurized
D_{st}
r_c
h_s
s
D_{sb}
Pressurized

Figure B.2 Undeformed and deformed geometry of conical cells. In all cases $D_{sto} = 0.508$m, $D_{in} = 0.127$m and $h_{so} = 0.213$m. For the rigid skirt $D_{sbo} = 0.467$m, for the polyethylene $D_{sbo} = 0.469$ and for the nylon-urethane $D_{sbo} = 0.473$.

of skirt deformation on S_a, ℓ_s, V_c and h_s under the action of $p_c(t)$ as depicted in Figure B.2. To calculate these quantities it is assumed that except for a small region in the neighbourhood of the top the deformed skirt remains conical. To calculate h_s it is assumed that the top of the conical portion, which has diameter D_{st}, is connected to the base of the model by a segment of material which has a circular cross section of radius $r_c = (D_{st} - D_{sto})/2$. This shape change causes a shortening of the skirt

$$\Delta h_{s1} = (\pi/2 - 1)r_c \tag{B.6}$$

In the conical portion the longitudinal stress varies from zero at the bottom to a maximum of twice the mean stress

$$\sigma_{\ell m} = p_c(D_{st} - D_{sb})/4t_s \tag{B.7}$$

For values of the skirt taper angle θ used in the present work, $\sigma_{\ell m}$ is usually less than 5% of σ_h, so that its effect on the hoop deformation of the conical portion is ignored. The overall effect of p_c in shortening the skirt by an amount $\Delta h_s = h_{so} - h_s$ can be expressed as a contraction ratio $\nu_e = (\Delta h_s \ell_{so})/(\Delta \ell_s h_{so})$ which is taken to be the sum of three terms. With $\varepsilon^* = (\ell_s - \ell_{so})/\ell_{so}$,

$$\nu_e = \nu_h + (\Delta h_{s1} - \Delta h_{s2})/(h_{so}\varepsilon^*) \tag{B.8}$$

In this expression ν_h is Poisson's ratio associated with hoop deformation, Δh_{s1} is given by Eq. (B.6), and Δh_{s2} is the extension caused by longitudinal stresses. The quantity ν_e may be considered as an equivalent Poisson's ratio and, for the values of θ used here, the third term is very small compared to the other two.

The final forms of the expressions for S_a, ℓ_s, V_c and h depend on the viscoelastic material model adopted. For the standard linear model, after some algebra, one obtains

$$S_a = \ell_s^2 d_r^2/4\pi - A_d \tag{B.9}$$

$$\eta \frac{d}{dt}\left[\frac{p_c \ell_s}{2\pi t_s E_g} - \varepsilon^*\right] = E_v \varepsilon^* - \left[1 + \frac{E_v}{E_g}\right]\frac{p_c \ell_s}{2\pi t_s} \tag{B.10}$$

$$V_c = \frac{h \ell_s^2 d_r^2}{4\pi} + \frac{h_{so}}{12\pi}[1 - \nu_e \varepsilon^*]\ell_s^2(d_r^2 - 2d_r + 4) \tag{B.11}$$

$$h = x - [1 - \nu_e \varepsilon^*]h_{so} \tag{B.12}$$

To determine the stability of this system of equations, standard linear analysis procedures are used. When these equations are linearized about a given equilibrium operating point, p_{ce} and Q_e, the linearized system is grouped in the matrix form $\underline{\underline{A}}\ \underline{\dot{x}} = \underline{\underline{B}}\ \underline{x}$ where, for a standard linear material model, the system is of sixth order, and $\underline{x} = [\Delta p, \Delta h, \Delta \dot{h}, \Delta \Omega_d, \Delta \ell_s, \Delta \ell_s]^T$. Stability is determined by direct examination of the system eigenvalues which, for given p_{ce} and Q_e, are determined numerically [B.20]. For the materials used in the tests and in the comparative studies, the analysis showed that oscillation frequencies lay in a narrow range of about 12 Hz to 16 Hz. This simplified the task of characterization of the materials.

B.4 Measurements of Skirt Material Properties

In the oscillatory tension tests a servo-controlled hydraulic ram was used to impose small amplitude deformation oscillations at several levels of mean deformation on the samples for frequencies in the range 2 Hz to 17 Hz [B.20]. The load response of the sample was obtained by a piezoelectric load cell, and the resultant data was expressed in terms of the complex modulus concepts of storage modulus E_1 and loss angle δ [B.17]. The same apparatus was used to impose step deformations for the stress relaxation data. The principal results are given in Figures B.3 and B.4 and in Table B.1. Data was obtained for material samples taken at 0° and 90° to the extrusion direction in the polyethylene material, and at 0° and 90° to the warp direction of the nylon-urethane material.

Figure B.3 gives E_1 as a function of frequency for polyethylene at the 90^0 orientation for three stress levels, and the corresponding stress relaxation data for four initial strains. A stress σ_h = 2.5 MPa corresponds to a cushion pressure of about 1kPa for the present cell geometry, and is representative of that used in the experiments. The most noticeable feature is that at frequencies of 2 Hz and above E_1 is larger than the stress relaxation values by a factor of about 2-1/2. It is also independent of the stress and is a slowly increasing function of frequency. The stress relaxation data also shows significant decreases of modulus with time, and for the data at each time point there is a small but consistent trend of decreasing modulus with increasing strain. Thus the value of the static modulus quoted in Table B.1 is an average and is based on the load at 20 minutes elapsed time. This interval was chosen because it was representative of the times involved in the experiment. The data for the 0° orientation is essentially the same as for the 90° orientation.

Figure B.4 gives data on E_1 for nylon-urethane samples oriented at 90° to the warp direction; this was the orientation of the hoop direction in the model tests. E_1 is effectively independent of frequency, but it increases substantially with increases in σ. E_1 is also substantially above the values of E determined in the stress relaxation tests. It was found that the stress relaxation properties of this material are critically dependent on the recent stress history. In a series of measurements in which the initial strain was increased in steps monotonically, the resultant force histories usually differed greatly from those obtained by allowing the sample to recover at zero stress between strain increments for a period equal to the test period. The data given in Figure B.4 was obtained from monotonically increasing strains, since this corresponds to the way in which the stability experiments were performed. Table B.1 gives estimates of the 20 minute value of E for the data plotted in Figure B.4, in which no resting or recovery was allowed, and values of E with recovery. The latter values of E were much more stress dependent and

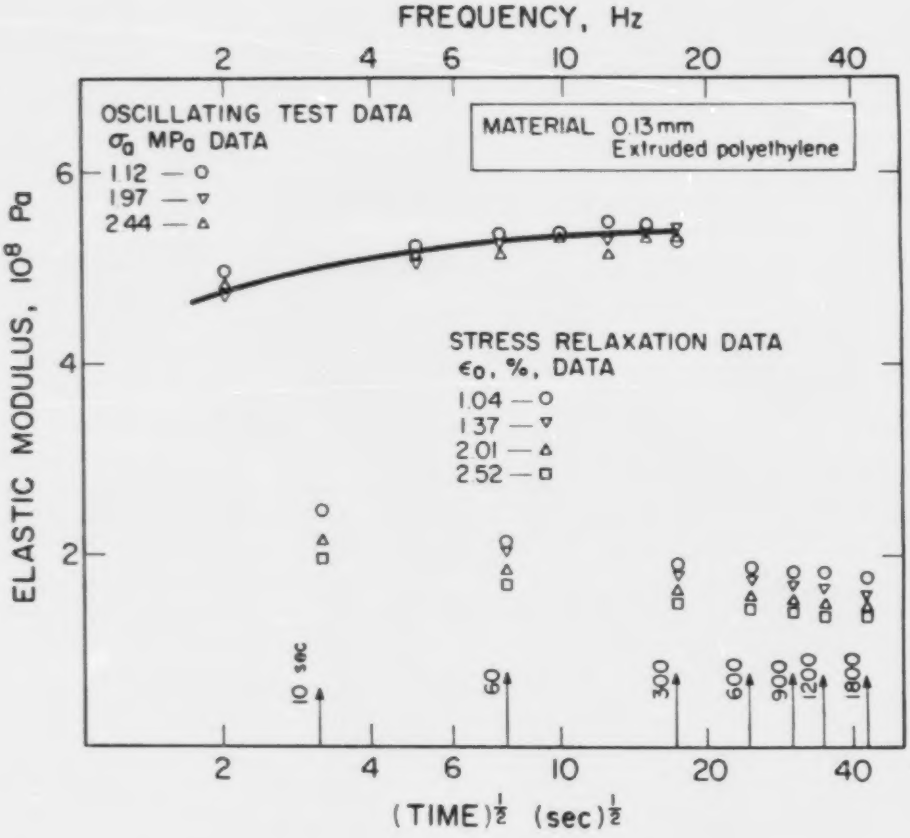

Figure B.3 Dynamic stiffness and stress relaxation data for polyethylene.

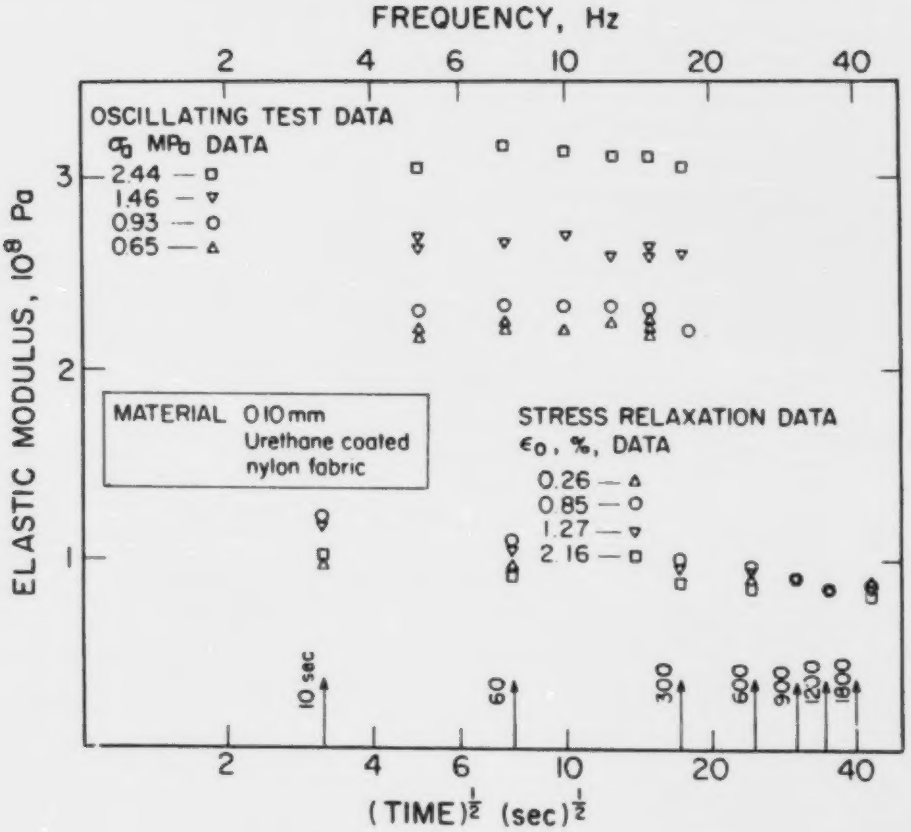

Figure B.4 Dynamic stiffness and stress relaxation data for nylon-urethane fabric at 90° to warp direction.

Table B.1

Material	Thickness mm	Static Modulus E, Pa	Dynamic Properties		Poisson's Ratio
			Storage Modulus E_1 (1)	Loss Angle δ (1)	
Aluminum	1.58	6.9×10^{10}	-	-	0.33
Polyethylene at 0° and 90°	0.127	1.5×10^{8}	5.4×10^{8}	2°	0.3
Nylon-Urethane 0° to warp	0.102	6.25×10^{8}	$6.52\times10^{8}+49.4\sigma$	<0.5°	-
Nylon-Urethane 90° to warp		No recovery: 0.87×10^{8} Recovery: $1.60\times10^{8}\times(1+10^{-7}\sigma+10^{-14}\sigma^2)$	$1.84\times10^{8}+51.8\sigma$	<0.5°	0.75

Notes: (1) Values of E_1 and δ are quoted for a frequency of 15 Hz, which is the average of measured frequencies in test model.

close to the value of E_1. Also, as shown in Table B.1, the values of E and E_1 for a sample cut parallel to the warp direction, although higher than those for the 90° sample, are roughly equal.

Loss angles for both materials are small and for the nylon-urethane are negligible. However, those of the polyethylene decrease almost linearly with increase in frequency changing from about 7.5° at 2 Hz to 2° at 17 Hz; this behaviour and that for E_1 in Figure B.3 are consistent with that of a standard linear model at frequencies approaching a glassy region.

Estimates of the static Poisson's ratio for the two materials were obtained by placing sharp-edged grid patterns on the samples, and then photographing them in the stressed and unstressed state. The changes in grid length were obtained by examining the negatives in a universal measuring projector. The results are given in Table B.1, however it should be noted that these measurements are subject to large errors, possibly 50% and higher, and ultimately an improved technique will have to be developed.

B.5 Predicted Effects of Skirt Material Properties on Stability

The stability characteristics of the duct-plenum model are presented in the form of stability boundaries, and these are plotted in terms of nondimensional equivalents of the two quantities of basic design interest, p_{ce} and Q_e. These are:

$$C_{PC} = p_{ce}/P_a, \qquad C_{QC} = Q_e(\rho/2WA_b)^{1/2} \qquad (B.13)$$

The quantity C_{QC} scales cushion flow rates for model tests, and the range $0.001 < C_{QC} < 0.02$ is representative of full scale values [B.21]. The dimensions of the model used in the calculations are those used in the experiment which utilizes a 0.0779m diameter supply duct with a friction factor of 0.017 and cushions of the geometry given in Figure B.2. Hinchey has shown that, for a family of directly fed geometrically similar cells, the effect of cell size on the value of C_{PC} at instability enters only through C_{QC} [B.7]. If a duct is present this similitude is preserved approximately. Hence, qualitatively at least, the results apply to larger geometries.

Predictions of the effect of material parameter changes on stability are given in Figures B.5, B.6 and B.7, and stability boundaries for the two skirt materials used in the experiments are given in Figure B.8. In each case the stability boundary corresponding to an inelastic skirt is used as a reference condition. Figure B.5 shows typical elastic modulus effects, and a Voigt material model was used to obtain them because $E_1 = E_v$ and is thus independent of frequency [B.17]. Also both η and ν_e were given very small values to eliminate both material loss and contraction effects on V_c and h_s. The results show that materials having E_v = 500 MPa and less, which is representative of those used in the experiments, cause large departures from the corresponding boundary for an inelastic skirt. Since the curves in Figure B.5 are unstable to the left, the elasticity thus has a large destabilizing effect. The effect of the material damping was also examined by using a Voigt model, with the quantities E_v and t_s assigned representative values and ν_e kept small. The results in Figure B.6 show a stabilizing effect, in fact for large enough values of δ, the inelastic boundary is crossed. Values of δ = 25° and higher can be expected for materials operating at frequencies in the transition

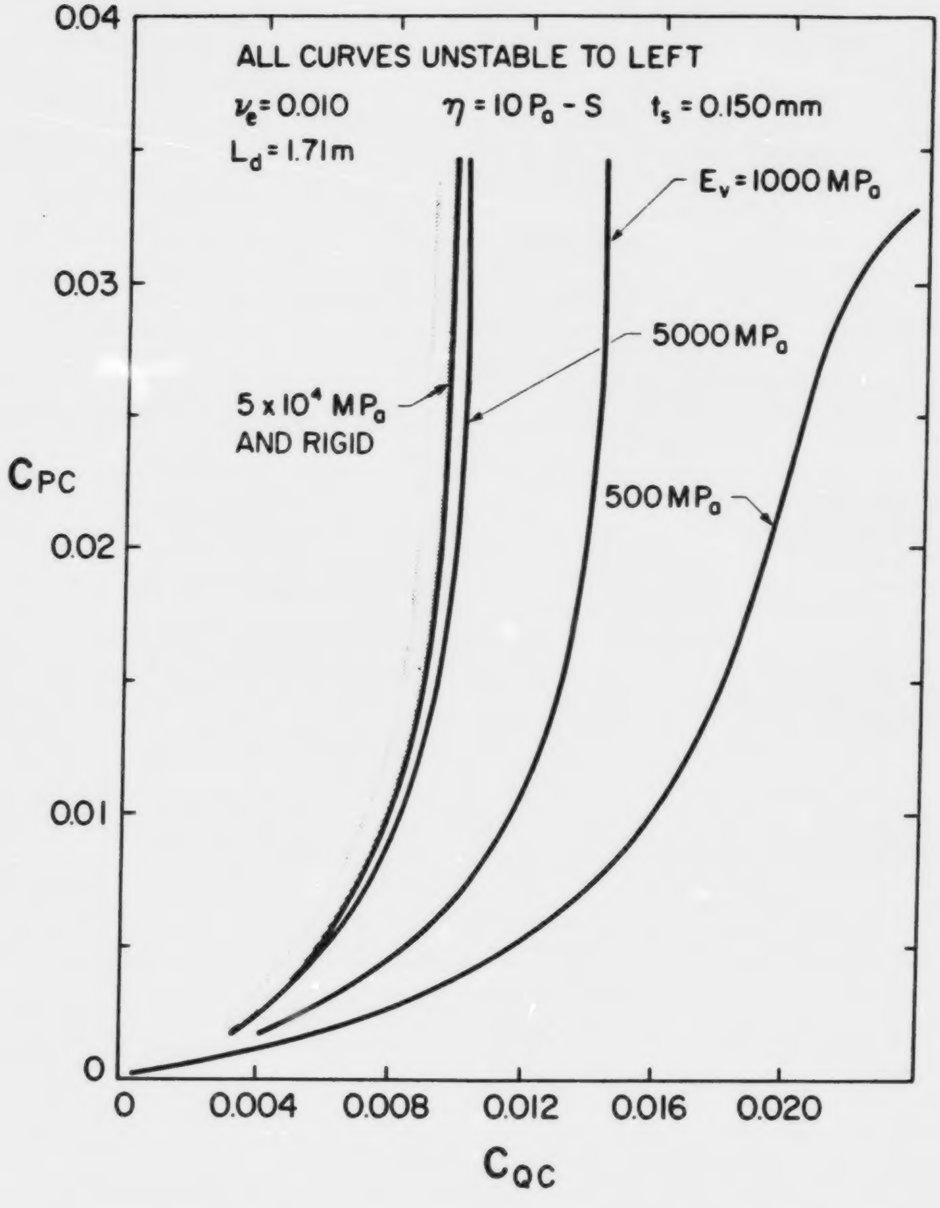

Figure B.5 Predicted effect of elastic modulus on dynamic stability.

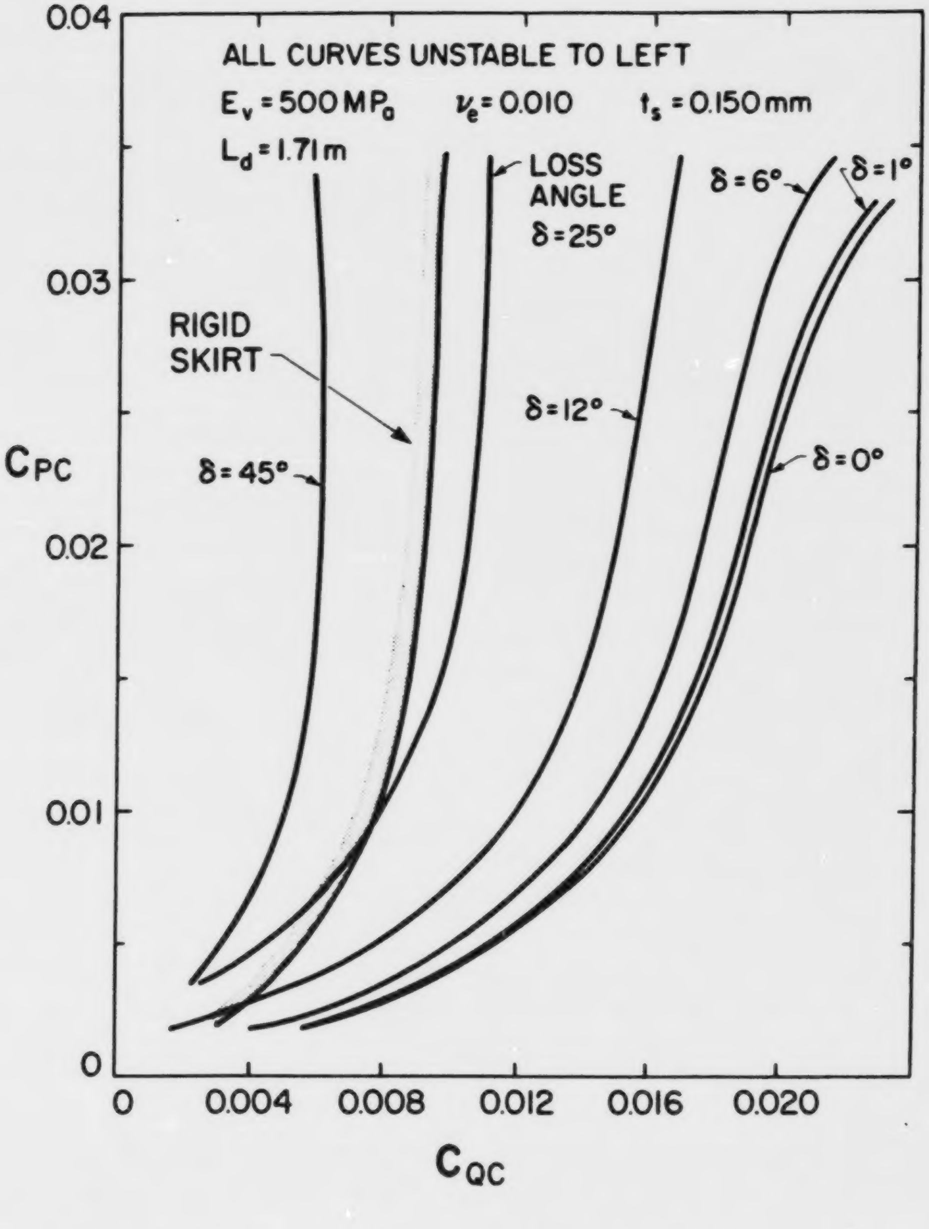

Figure B.6 Effect of loss angle on dynamic stability.

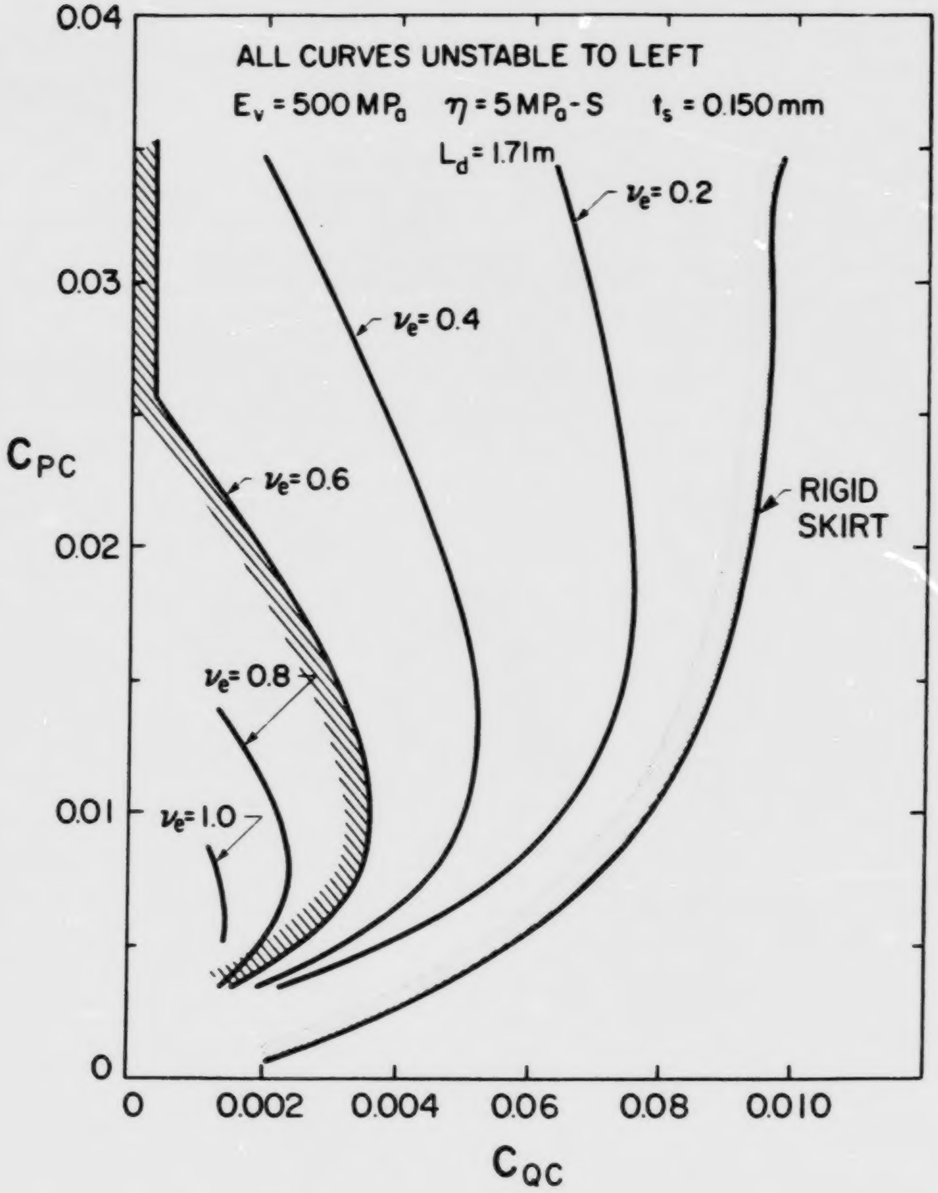

Figure B.7 Effect of skirt contraction on dynamic stability.

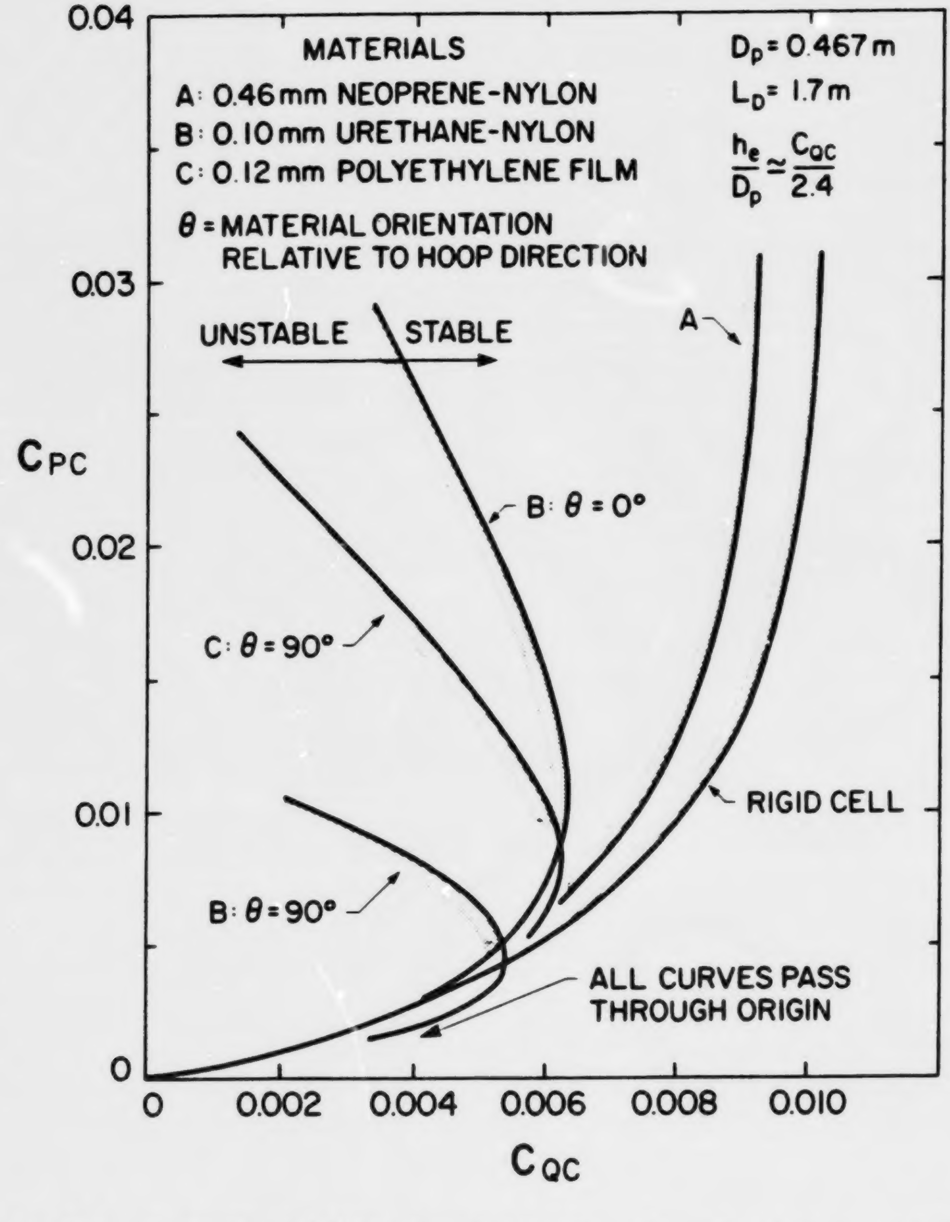

Figure B.8 Dynamic stability boundaries for the polyethylene and nylon-urethane materials.

between rubbery and glassy regimes [B.17]. Variation of skirt thickness also affects stability through equation (B.10). The increase in t_s usually increases stability, but at large loss angles a destabilization can occur.

Figure B.7 shows the predicted effect of skirt contraction ratio; a Voigt material model was again used. The effect of increasing ν_e is twofold, it both increases h and reduces V_c. For a cylinder the perturbation in volume owing to a hoop strain ε_h is $\delta V_c/V_c = (2-\nu_e)\varepsilon_h$ to first order, so that for values of $\nu_e < 2$, there is still an increase in V_c associated with hoop deformation. In general the effect of increasing skirt contraction is stabilizing, since the curves are moved to the left, and this must be associated with the modulation of the hovergap, since the effect occurs for values of $\nu_e < 2$. The curves also display a feature not present in the results for an inelastic skirt, or those for an elastic skirt undergoing changes only in V_c. For a given stability boundary and for large enough ν_e, as p_{ce} increases from zero, the slope dQ_e/dp_{ce} of the boundary is at first positive and then becomes negative and finally crosses $Q_e = C_{QC} = 0$. This is shown for $\nu_e = 0.6$ in Fig. B.7. This implies that, in the absence of contraction effects on hovergap for any given W or p_{ce}, there is always a value of Q_e below which the system is dynamically unstable. However, for $\nu_e > 0$, above a certain critical p_{ce} the system can be dynamically stable for all Q_e. Clearly the presence of such an effect in the experimental results provides a critical test of the present theory. Of course at $Q_e = 0$, the system becomes statically unstable, since a plenum chamber cushion requires $Q_e > 0$ to have a positive stiffness. The presence of this static instability is illustrated for $\nu_e = 0.6$ in Figure B.7 by the cross hatching along the C_{PC} axis.

Predicted results with mean values for static and dynamic stiffnesses, loss angles and contraction coefficients of skirt materials used in the experiments are given in Figure B.8. In all cases a standard linear model was used for the stability calculations. The results show large deviations from the inelastic boundary for both materials, especially for values of p_{ce} above 1 kPa. Also, for the nylon-urethane material oriented at 90°, the intersection of the stability boundary with $Q_e = 0$ occurs at values of p_{ce} well within the range attainable in the experiments.

B.6 Stability Experiments, Apparatus and Method

Since the hoop direction of a conical surface becomes a circular arc when developed, it cannot be aligned with one of the fibre directions of a fabric. The impact of this problem was minimized by building the cells from four sectors of fabric, so that for $\theta = 5.5°$, the hoop direction deviated from the fabric direction at a maximum of 4°. An estimate of the reduction in the mean hoop stiffness, made by counting the fraction of fibres that were not continuous from one side of the sector to the other, indicated that the effect should be less than 1%.

In a given experiment, the required p_{ce} is obtained by attaching calibrated weights to the top of the cushion, and the required Q_e is set by using a blow-off valve to adjust the pressure in the sphere. The value of Q_e is measured by the conical inlet, which was calibrated in situ by an ASME standard orifice plate meter [B.22] inserted prior to final installation of the model cushion. A baffle plate is located in the cushion to break up the flow from the duct, and static pressure is measured by two taps in the cushion base plate located to the sides of this baffle plate. A Shaevitz model 5000HR displacement transducer is used to measure the cushion height above the table.

For the materials used in these experiments, it proved to be very difficult to trim the bottom edge of the cell to obtain a visually uniform hovergap. This problem was circumvented as follows. For any flexible skirt installed in the apparatus, including one in which parts of the periphery are touching the table, the flow is still expected to be orifice-like, but there may be an irregular orifice area and a discharge coefficient which are functions of x, and of p_{ce} if skirt deformation is significant. Hence dimensional considerations imply that

$$C_{QC} = f_{\ell}[x/D_{st}, (p_{ce}D_{st}/Et_s)] \qquad (B.14)$$

and, if the flow is governed by Bernoulli's law, the "flow function" f_{ℓ} should be independent of p_{ce} in the absence of skirt deformation. In general, this function can be linearized and incorporated in the stability analysis; however, if the dependence on x is linear then it can be used to obtain an equivalent hovergap. This was shown to be the case for the results described below.

Finally the dynamic stability at a given p_{ce} and Q_e is determined by the simple expedient of manually disturbing the cushion and observing the subsequent motion be it growth to limit cycle oscillations [B.3, B.15], or decay to equilibrium. This experimental configuration was tested with an inelastic skirt and it was shown [B.15] that the test method, although potentially subject to considerable error, yielded highly repeatable boundaries in close agreement with the linear theory predictions. Moreover, the ±4% accuracy obtained in C_{QC} was as good as that from a technique based on the determination of oscillation damping at various Q_e in the stable region, and finding the critical value of Q_e by extrapolating this data to zero damping. Furthermore location of predicted stability boundaries using the numerical solution of the nonlinear equations with finite initial displacements of up to 100% of h_e yielded results in close agreement with the linear theory [B.16]. Hinchey [B.7] has suggested that this occurs because at the stability boundaries the real parts of the eigenvalues of the linear system matrix are rapidly varying functions of p_{ce} and Q_e, a situation which is not the case for all ACV configurations [B.23].

B.7 Results of Experiments and Discussion

A typical flow function for the nylon-urethane skirt is given in Fig. B.9. It shows a strong dependence on W; in contrast, the polyethylene skirt displayed no detectable dependence on W. Linear regression was applied to the data in Figure B.9 to obtain an estimate of C_m as a function of p_{ce}, and this was used in the theoretical predictions. The measured values of C_m for both skirts are quoted with the appropriate figures. The data in Figure B.9 was used to obtain an estimate of ν_e for the static case; and for a representative value of C_{QC}, $\nu_e = 1.9$, which compares with the value 1.4 determined from Eq. (B.8).

It was found that, apparently owing to creep, the position of the stability boundary depended on the previous stress history and the amount of time the cushion was loaded with the particular weight being tested. This effect was most pronounced for the nylon-urethane skirt; it produced changes of up to ±17% in the value of C_{QC} at a stability boundary as shown by the data at

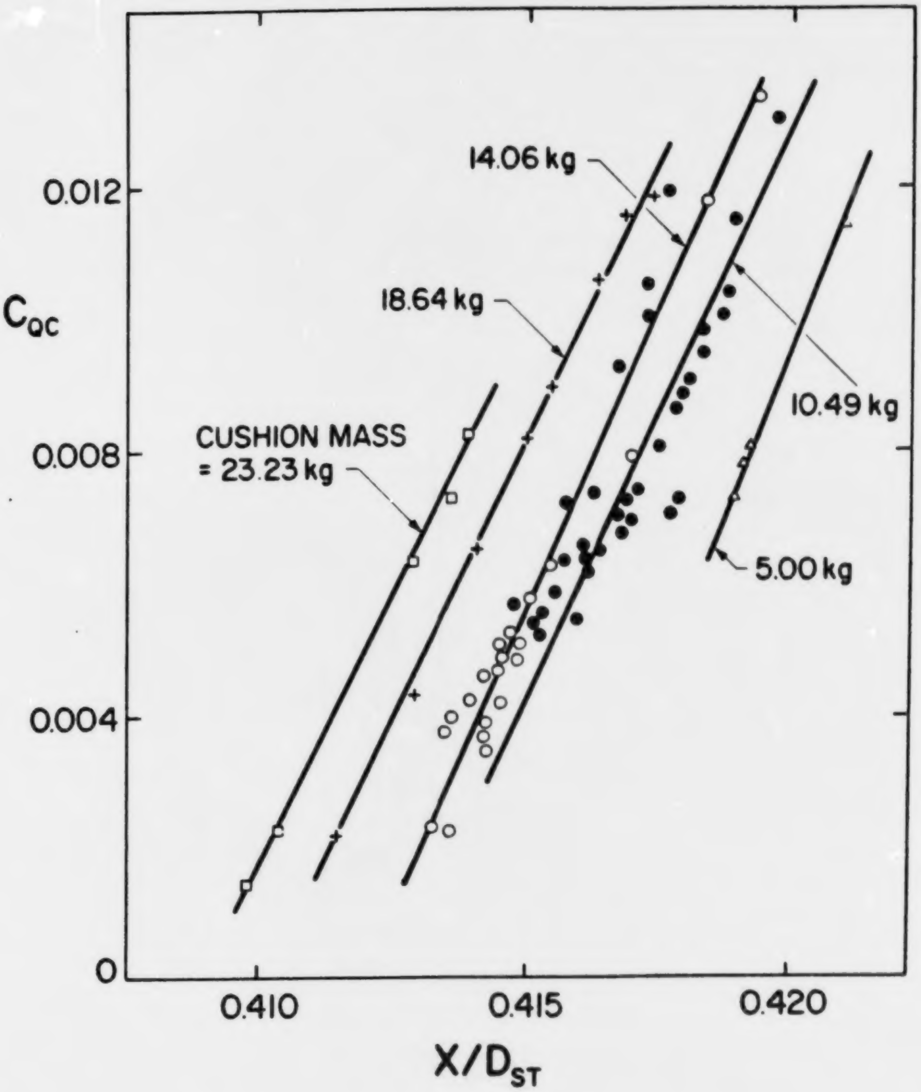

Figure B.9 Cushion flow function for nylon-urethane material.

C_{PC} near 0.006 in Figure B.10. To counter this effect in the subsequent stability boundary tests, the cushion was allowed to condition at the test pressure approximately 15 minutes.

The stability boundaries for the two skirt materials are compared with theory in Figures B.10 and B.11. The theory and experiment for the rigid skirt with $L_d = 1.71$m[14] are included in Figure B.10. For the nylon-urethane skirt, the theory incorporated its nonlinear stress-strain relationship; at a given p_{ce} the hoop stress was calculated, and the formulae given in Table B.1 were used to compute the equilibrium strain and to estimate a local elastic modulus for small deviations in strain about equilibrium. This local modulus was used in a Voigt model of the material for the stability analysis. Considering the various difficulties discussed above, good qualitative agreement between theory and experiment for both materials has been obtained; in particular, both the marked shift from the rigid skirt data and the slope reversal associated with skirt contraction are present for the nylon-urethane data at the two duct lengths. Furthermore, the experimental data for $L_d = 1.71$m showed clear evidence of the intersection of the dynamic stability boundary with $C_{QC} = 0$ at about $C_{PC} = 0.009$. For the three points labelled "A" in Figure B.10, which correspond to values of C_{QC} less than about 0.0002, the cushion simply collapsed under its own weight, as is characteristic of a static instability [B.24]. The major source of the discrepancy between theory and experiment for the nylon-urethane skirt probably lies in measurements of Poisson's ratio ν and the estimation of ν_e.

Finally a demonstration of the opposing effects on stability of skirt contraction and hoop extension was obtained by a simple modification of the experiment. A clamp which prevented skirt contraction while still permitting hoop deformation was installed. It was a ring of outer diameter D_{sb} supported at the bottom of the skirt by rods attached to and extending downwards from the model base. The lip of the flexible skirt was clamped to this ring, and a substitute rigid lip was attached to the bottom of the ring. The arrangement is shown in Figure B.12. According to the theory, the use of such a clamp should eliminate the critical C_{PC} above which the system becomes dynamically stable near $Q_e = 0$, and should shift the dynamic stability boundary to the right of the inelastic boundary. The data obtained by using this clamp is given in Figure B.13; it clearly confirms these predictions. Note however that the boundaries for the clamped skirt do not have the shape predicted in Figure B.5. Instead they approach the inelastic boundary as C_{PC} increases. Presumably this is a result of the tendency of a fabric to stiffen as it is loaded.

B.8 Conclusions

The large departure of the dynamic stability characteristics of a model air cushion skirt from those for an ideal skirt material, predicted for two laboratory model materials, have been confirmed by the experiments. An interesting feature of the results is the way in which the urethane-coated nylon fabric, which for static pitch and roll stiffness was effectively ideal, caused the largest departures from this ideal in the dynamic experiments. It occurred because small deformations of skirt material, which may not be very significant in vehicle static behavior, have large effects on the cushion hovergap history and pneumatic capacitance. In contrast, the extruded polyethylene material, which in static pitch and roll experiments generated

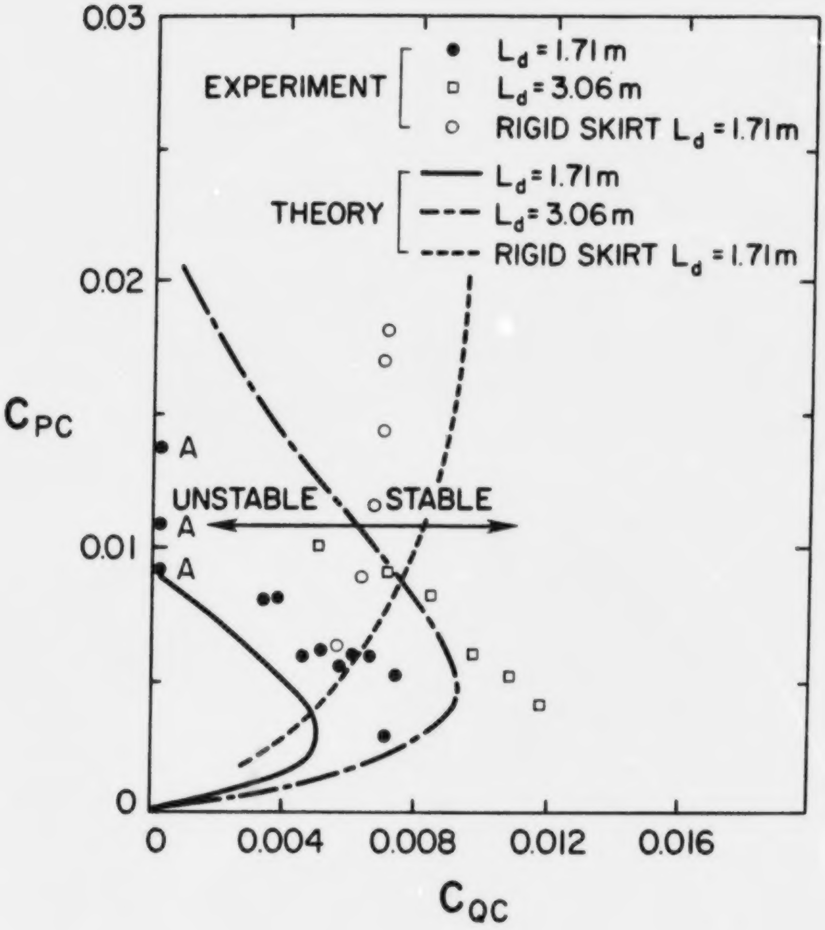

Figure B.10 Comparison of theory and experimental results for nylon-urethane skirt and two duct lengths. For rigid skirt $C_m = 0.60$ and for nylon-urethane $C_m = 0.591 - 0.147 \times 10^{-3} p_c$.

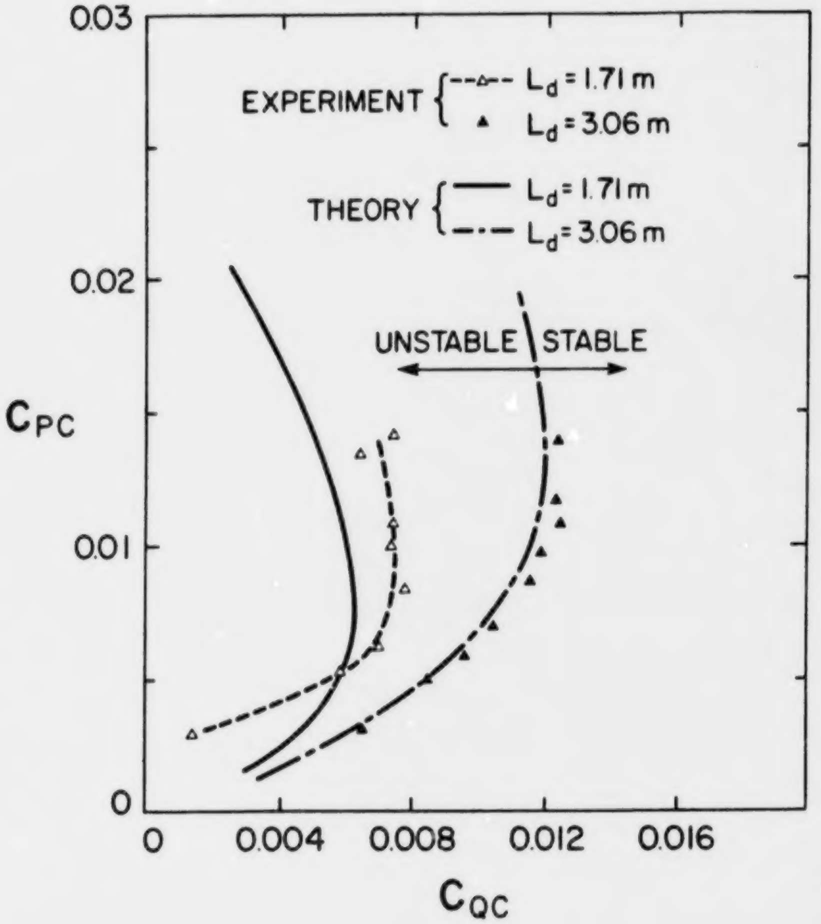

Figure B.11 Comparison of theory and experimental results for polyethylene skirt and two duct lengths, C_m = 0.53.

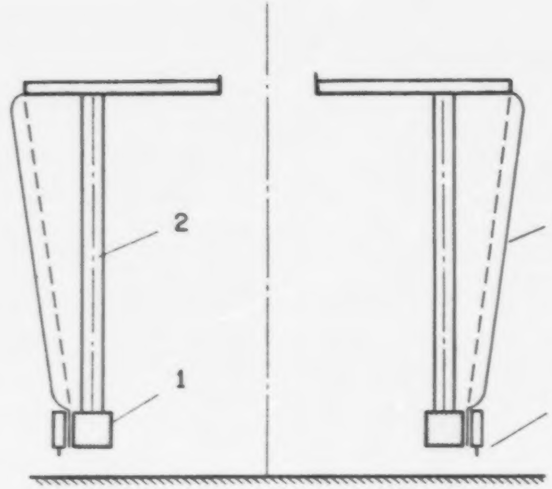

Figure B.12 Skirt clamping device used to demonstrate the opposing effects of skirt contraction and volume modulation on stability. A rigid ring (1) was supported by four rods (2). The skirt (3) was fixed to the ring (1) by a clamp which contained a substitute lip (4).

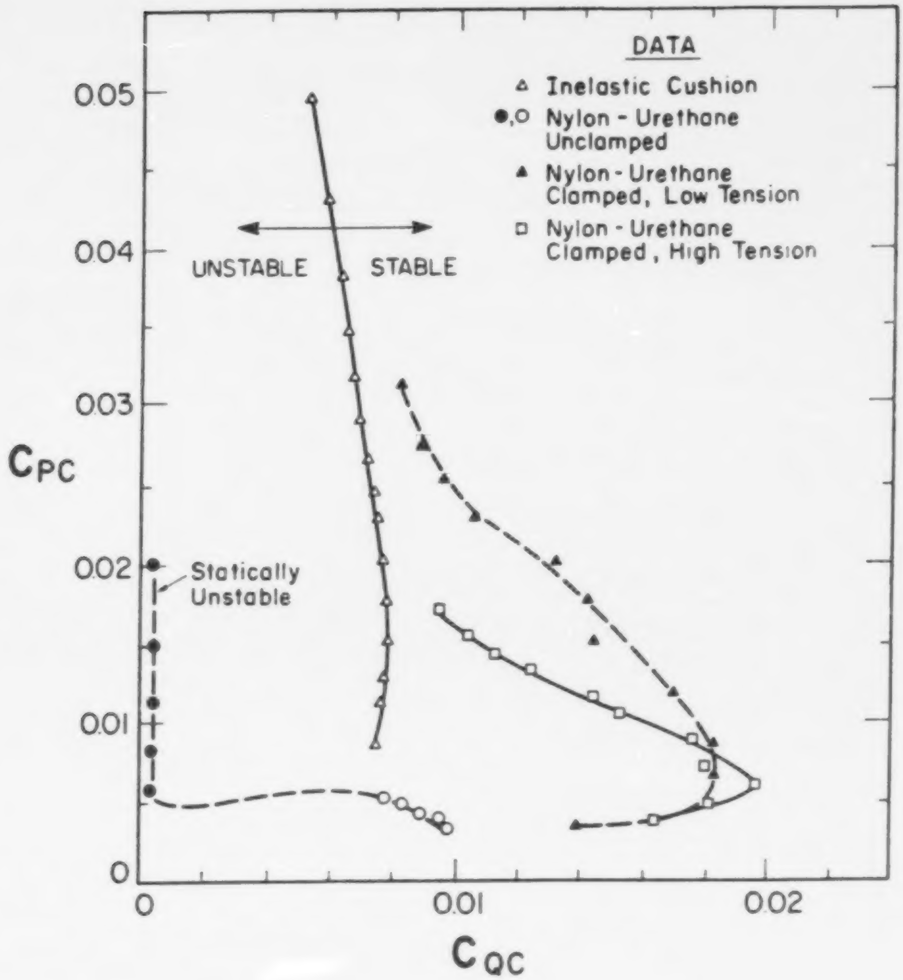

Figure B.13 Effect on stability using clamp to prevent skirt contraction. All curves are unstable to the left.

large hysteresis, was closer to ideal in its dynamic behavior. This tends to reinforce an earlier conclusion that the hysteresis is associated with local buckling phenomena, triggered by skirt-ground contact.

Finally, it should be reaffirmed that, since dynamic stability is but one manifestation of the dynamical properties of a cushion system, the conclusions drawn here are relevant to other dynamics problems. For example, the implication for testing of physical models of practical configurations is that great care may have to be exercised in the choice of model material, otherwise spurious results may be obtained.

REFERENCES - APPENDIX B

B.1 Doctors, L. J., "Nonlinear Motion of an Air Cushion Vehicle over Waves", Journal of Hydronautics, Vol. 9, No. 2, April 1975, pp. 49-57.

B.2 Carrier, R., Magnuson, A. H., and Swift, M. R., "Seakeeping Dynamics of a Single Cushion Peripheral Cell-Stabilized Air Cushion Vehicle", Journal of Hydronautics, Vol. 12, No. 2, April 1978, pp. 49-54.

B.3 Hinchey, M. J., and Sullivan, P. A., "A Theoretical Study of Limit Cycle Oscillations of Plenum Air Cushions", Journal of Sound and Vibration, Vol. 79, No. 1, Nov. 1981, pp. 61-77.

B.4 Sullivan, P. A., Hinchey, M. J., and Delaney, R. G., "Static Roll Stiffness Characteristics of Two Multicell Type Air Cushion Systems", Journal of Terramechanics, Vol. 15, No. 1, March 1978, pp. 15-41.

B.5 Ribich, W. A. and Richardson, H. H., "Dynamic Analysis of Heave Motion for a Transport Vehicle Fluid Suspension", Dept. of Mechanical Engineering, Massachusetts Institute of Technology, Boston, Mass., DSR-76110-3, Jan. 1967.

B.6 Sullivan, P. A., "The Air Cushion Technology Program at the University of Toronto", Canadian Aeronautics and Space Journal, Vol. 20, No. 6, June 1974, pp. 269-286.

B.7 Hinchey, M. J., "Heave Instabilities of Amphibious Air Cushion Suspension Systems", Institute for Aerospace Studies, University of Toronto, Canada, Report No. 246, Nov. 1980.

B.8 Cox, R. J., "Measurements of the Dynamic Response of a Hovercraft Model to Waves of Various Lengths Using the Whirling Arm Facility", College of Aeronautics, Cranfield Institute of Technology, Bedford, England, Aero Report No. 7803, Nov. 1977.

B.9 Sullivan, P. A., Hinchey, M. J., Murra, I., and Parravano, G. J., "Research on the Stability of Air Cushion Systems", Institute for Aerospace Studies, University of Toronto, Canada, Report No. 238, Nov. 1979, Section 3: "Roll Hysteresis of a Two Cell Cushion System".

B.10 Sullivan, P. A., Hinchey, M. J., Hartmann, P. V., Dupuis, A., Green, G. M., and Graham, T. A., "Research Into Air Cushion Stability, 1979 Report", Transportation Development Centre, Montreal Canada, Report TP3109E, Jan. 1982, Section 3, "Static Pitch and Roll Stiffness Characteristics of a Segmented Skirt Cushion".

B.11 Sullivan, P. A., Hartmann, P. V., and Graham, T. A., "Application of System Identification Flight Analysis Techniques to the Pitch-Heave Dynamics of an Air Cushion Vehicle", Canadian Aeronautics and Space Journal, Transactions, Vol. 29, No. 4, Dec. 1983.

B.12 ——————,"Stability and Control of Hovercraft: Notes for Commanders", United Kingdom Department of Industry, Ship and Marine Technology Requirements Board Report, 1980.

B.13 Lee, E. G. S., et al, "Experimental and Analytical Studies of Advanced Air Cushion Landing Systems", National Aeronautics and Space Administration, Langley Research Center, Hampton, VA, Contractor Report NAS-7723.5-3, Aug. 1981.

B.14 Sullivan, P. A., Hinchey, M. J., and Green, G. M., "A Review and Assessment of Methods for the Prediction of the Dynamic Stability of Air Cushions", Journal of Sound and Vibration, Vol. 54, No. 3, Oct. 1982, pp. 337-358.

B.15 Sullivan, P. A., Byrne, J. E., and Hinchey, M. J., "Nonlinear Oscillations of a Simple Flexible Skirt Air Cushion", Journal of Sound and Vibration, Vol. 102, No. 2, 1985, pp. 269-283.

B.16 Hinchey, M. J., and Sullivan, P. A., "Duct Effects on the Heave Stability of Plenum Air Cushions", Journal of Sound and Vibration, Vol. 60, No. 1, Sept. 1978, pp. 87-99.

B.17 Ward, I. M., Mechanical Properties of Polymers, Wiley, New York, 1971, p. 95.

B.18 Aklonis, J. J., MacNight, W. J., and Shen, M. C., Introduction to Polymer Elasticity, Wiley Interscience, New York, 1972.

B.19 Minami, H., and Hakahara, Y., "An Application of the Finite Element Method to the Deformation Analysis of Coated Plain Weave Fabrics", Journal of Coated Fabrics, Vol. 11, April 1981, pp. 310-327.

B.20 Graham, T. A., "The Effects of Skirt Material Choice on the Heave Stability of an Air Cushion", Institute for Aerospace Studies, University of Toronto, Canada, M.A.Sc. Thesis, Nov. 1980.

B.21 Fowler, H. S., "On the Lift-Air Requirement of Air Cushion Vehicles and Its Relation to the Terrain and Operational Mode", Division of Mechanical Engineering, National Research Council of Canada, Rept. ME-246, May 1979.

B.22 ———, Flow Meter Computation Handbook, American Society of Mechanical Engineers, New York, 1961.

B.23 Hinchey, M. J., Sullivan, P. A., and Dupuis, A. D., "Heave Dynamics of Large Air Cushion Platforms", Journal of Sound and Vibration, Vol. 96, No. 4, 1984, pp. 469-484.

B.24 Huseyin, K., Vibrations and Stability of Multiple Parameter Systems, Noordhoff, Alphen Aan Den Rijn, Holland, 1978, p. 50.

APPENDIX C. NONLINEAR OSCILLATIONS OF A SIMPLE FLEXIBLE SKIRT AIR CUSHION

(P. A. Sullivan, J. E. Byrne and M. J. Hinchey)

NOMENCLATURE

Roman

a	atmospheric sound speed
A_{base}	area of vehicle planform used as reference in calculating C_{QC}, $= \frac{\pi}{4} D_p{}^2$
A_d	cross sectional area of duct
C_c	cushion capacitance $= V_{ce}/\rho a^2$
C_D	cushion exit flow discharge coefficient
C_m	flow coefficient for duct inlet
C_{PC}	cushion pressure coefficient $= p_{ce}/P_a$
C_{QC}	cushion flow coefficient, $C_{QC} = Q_e(\rho/2WA_{base})^{1/2}$
D_p	plenum chamber diameter
f	friction factor in duct
f_L	linear natural frequency, see Eq. C.12
f_Q	cushion flow function defined by Eq. C.9
g	acceleration due to gravity
h	hovergap
I_d	inertance of duct air $= \rho L_d/A_d$
L_d	duct length
L_p	perimetral length of cushion
L_s	length of skirt, or plenum chamber height
M	mass of cushion
p_a	absolute atmospheric pressure
p_c	cushion gauge pressure
p_{df}	pressure in the duct at conical inlet
p_f	equivalent fan or source pressure

Q_a	volume flux past cushion lip to atmosphere
Q_d	volume flux through duct
S_a	cushion support area
t	time
V	velocity of air in duct, $V = V(x,t)$
V_c	total cushion volume $= V_d + S_a h$
V_d	cushion "dead" volume $= \frac{\pi}{4} D_p{}^2 L_s$
x	distance along duct
y	height of base of cushion above ground plane, $y_e = h_e + L_s$
z	$y - L_s$

Greek

γ	isentropic exponent
ρ	air density

Subscripts

dc	cushion end of duct
df	fan or inlet end of duct
e	equilibrium

C.1· Introduction

There is widespread interest in the use of air cushion vehicles (ACV) for a variety of transportation tasks, including aerodynamically propelled high speed marine ferries used in civilian and military roles, landing systems for aircraft, and large platforms for moving oil drilling machinery over land and arctic ice. A key to the success of these vehicles is the use of a flexible skirt, which is attached to the base of the vehicle and which contains the air cushion. A skirt is essentially a collapsible elastomer-fabric structure, which is inflated and stabilized by the pressure of the cushion air, and which enables the vehicle to negotiate large obstacles or waves while keeping the cushion air flow rate low. As might be expected, the geometry of the skirt system depends on the application, and several different configurations have evolved. There is a growing body of literature on the analysis of the dynamics of various configurations [C.1-C.21], and work on the experimental validation of these analyses [C.3, C.4, C.10, C.12, C.13, C.15, C.17, C.19-C.21]. However, much of this experimental work has a very unsatisfactory aspect.

A well-known science historian, in a study of the development of the pure sciences, has observed that

> "there are seldom many areas in which a scientific theory, particularly if it is cast in a predominantly mathematical form, can be directly compared with nature" [C.22].

The authors believe that a corresponding problem exists in the development of mathematical models of the dynamics of flexible skirt cushions. ACV dynamics can be very complex; it involves consideration of the dynamic behaviour of the skirt structure, the fluid mechanical processes in the cushion and the air supply system, and the vehicle dynamics, together with the interaction of all three. Furthermore, the geometry of the typical practical cushion can be complex, and certain aspects, such as the effect of skirt-ground contact on air flow from the cushion, can be highly nonlinear. In our opinion, this complexity is such that analyses of complete vehicles such as those described in References C.1-C.13, C.16, C.17 and C.21 invariably make many ad hoc assumptions, the applicability of which may be unclear. Consequently, such analyses, although of direct practical interest, are usually unsuited to an unequivocal confrontation between theory and experiment. There remains a clear need for carefully defined experiments in which only a few assumptions are tested. A recent survey of ACV research in Britain reaches a similar conclusion:

> "Several analytical models have been proposed in the past 10 years, but in many respects these have proven unsatisfactory owing to the absence of adequate experimental data on some of the mechanisms present" [C.23].

The work described here is one result of a search for a confrontation, and particular emphasis is placed on those nonlinear aspects that appear to be most frequently encountered in flexible skirt cushions. The phenomenon exploited is the susceptibility of air cushions to generate stable limit cycle oscillations when they are dynamically unstable in the linear sense [C.18]. While practical interest in such limit cycles probably exists only insofar as it is necessary to suppress them, they provide a simple and convenient way of obtaining experimental data on some of the intrinsically nonlinear aspects of cushion dynamics. This Appendix describes measurements of frequencies, amplitude and waveform characteristics of these oscillations, and compares them with the theory developed by Hinchey and Sullivan [C.18].

The configuration used in the experiments is depicted in Figure C.1. A very large (950 m^3) spherical volume uncouples the cushion dynamics from that of the fan system, and thus provides a source of constant pressure air. The cushion air enters an 0.078 m diameter, 1.71 m long duct through a conical inlet which also provides static stability for the cushion. The duct is in turn connected to the cushion by a short flexible bellows; and the cushion, which has a top diameter $D_p = 0.508$ m and height $L_s = 0.213$ m, is constrained to move in heave by a linear ball bushing assembly. The skirt geometry is an inverted slightly tapered truncated cone; it is believed that this is the simplest geometry that retains the essential features of an amphibious skirt: structural stabilization by the pressure of the cushion air, and a flexible lower edge or lip suitable for skirt-ground contact. The apparatus was originally used to demonstrate the effects of ducting and skirt material flexibility on the linear dynamic stability of a plenum chamber cushion [C.19, C.20]. Hinchey and Sullivan [C.18] suggest that it incorporates the nonlinear phenomena universally characteristic of air cushions, namely the orifice flow processes and the air flow shut-off caused by skirt-ground contact.

C.2 Mathematical Model

The equations used in the analysis are given below; a detailed discussion of the underlying assumptions have been given by Hinchey and Sullivan [C.18].

For the configuration depicted in Figure C.1, the air in the sphere has a known constant gauge pressure p_f. The air flow through the inlet is assumed to obey the usual quasisteady model; if Q_{df} is the volume flux into the duct and p_{df} is the pressure at the junction of duct and inlet, then

$$Q_{df} = C_m A_d [2(p_f - p_{df})/\rho]^{1/2}, \qquad Q_{df} \geqq 0 \qquad \text{(C.1a)}$$

and

$$p_{df} = p_f, \qquad Q_{df} < 0 \qquad \text{(C.1b)}$$

Here C_m is the usual inlet coefficient, A_d is the cross-sectional area of the duct and ρ is the atmospheric density. Equation (C.1b) applies when the flow is reversed.

The flow in the duct is modelled by the equations of one-dimensional unsteady turbulent hydraulic transients [C.24], which are

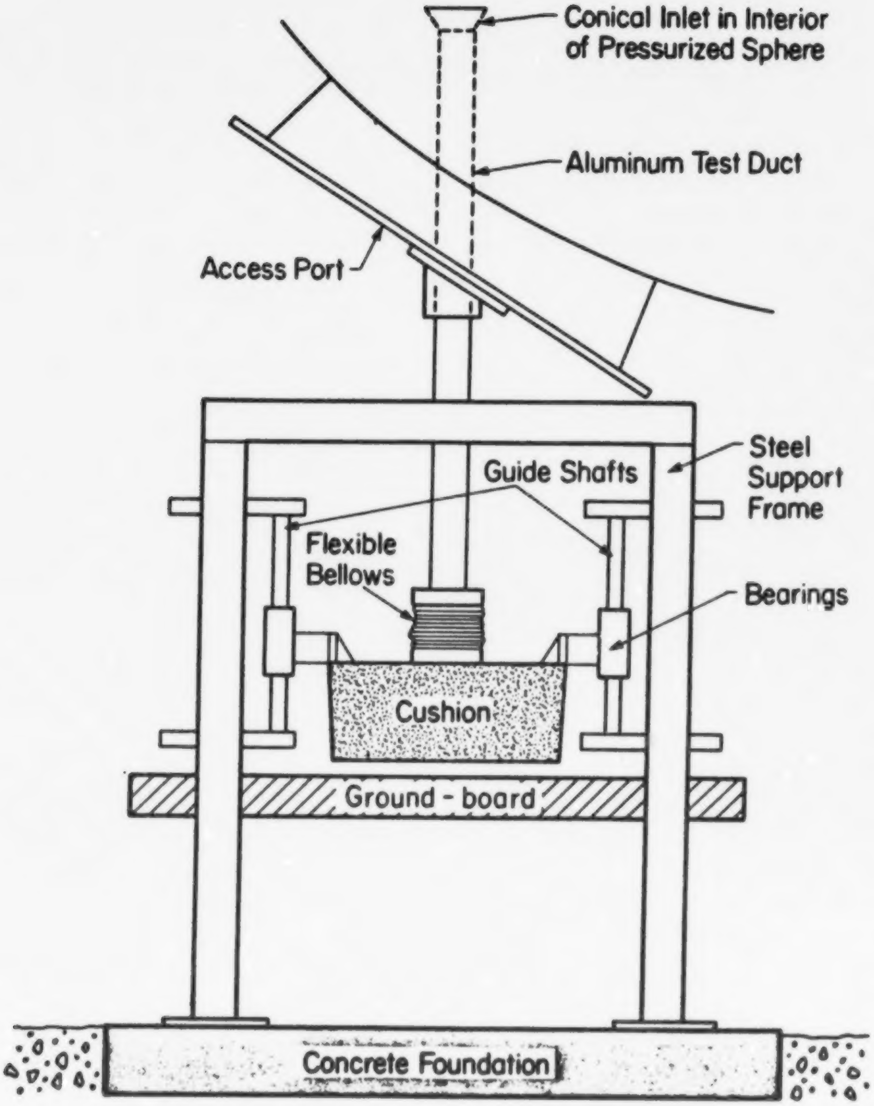
Conical Inlet in Interior of Pressurized Sphere
Aluminum Test Duct
Access Port
Steel Support Frame
Guide Shafts
Flexible Bellows
Bearings
Cushion
Ground - board
Concrete Foundation

Figure C.1 Apparatus used in the experiments. The cushion pressure transducer was mounted with its sensitive surface level with the top of the ground-board, and under a baffle plate which eliminated dynamic effects by the air entering the cushion from the duct.

Momentum:

$$\frac{1}{\rho}\frac{\partial p}{\partial x} + V\frac{\partial V}{\partial x} + \frac{\partial V}{\partial t} + \frac{f}{2D}V|V| = 0 \qquad (C.2)$$

Continuity:

$$\frac{\partial V}{\partial x} + \frac{1}{\rho a^2}\left(V\frac{\partial p}{\partial x} + \frac{\partial p}{\partial t}\right) = 0 \qquad (C.3)$$

Here p(x,t) and V(x,t) are the pressure and mean velocity distributions in the duct, which are functions of both distance x along the duct and time t; f is the usual friction factor, and a is the sound speed. The two boundary conditions for equations (C.2) and (C.3) are equation (C.1), which relates Q_{df} and p_{df}, and the requirement that the pressure at the cushion end of the duct, p_{dc}, be equal to the pressure p_c in the cushion volume.

The lumped capacitance model of the cushion volume is assumed to apply [C.2]:

$$C_c dp_c dt + S_a dh/dt = Q_c - Q_a \qquad (C.4)$$

Here C_c is the pneumatic capacitance of the cushion volume, Q is the flow into the cushion volume from the duct, Q_a is the flux that escapes to atmosphere under the cushion lip, S_a is the footprint area of the cushion and h is the hovergap, or lip height relative to the ground plane. Negative values of Q_c and Q_a correspond to flow from the cushion volume into the duct, and from atmosphere into the cushion, respectively. The capacitance $C_c = V_{ce}/\rho a^2$, where V_{ce} is the volume enclosed by the cushion at equilibrium, and $Q_c = A_d V_{dc}$ where $A_d = \pi D_d{}^2/4$ and V_{dc} is the velocity of the air at the cushion end of the duct.

The heave dynamics of the cushion is assumed to be governed by Newton's law for a single rigid mass, that is

$$Md^2y/dt^2 = S_a p_c - Mg \qquad (C.5)$$

in which M is the total mass of the cushion, y is the height of the base of the cushion above the ground plane, the hoverheight, and g is the acceleration due to gravity. When the cushion is hovering at equilibrium height y_e, the cushion pressure is p_{ce}, and $Q_d = Q_c = Q_a \triangleq Q_e$. The two variables p_{ce} and Q_e are the quantities of basic design interest, and are specified for a given application.

The cushion air escape process is modelled as a quasisteady orifice flow:

$$Q_a = C_D L_p h\left[|p_c/\rho|\right]^{1/2}\mathrm{sgn}(p_c - p_a) \qquad (C.6)$$

In this equation C_D is the usual discharge coefficient, $L_p = \pi D_p$, and the formulation allows for flow reversal. The skirt is assumed to behave like an inelastic but perfectly collapsible massless membrane, which is the so-called ideal skirt material [C.18, C.20]. It follows that the hovergap is assumed to be related to the hoverheight by

$$z \triangleq y - L_s = h \quad \text{for} \quad z > 0; \qquad h = 0 \quad \text{for} \quad z < 0 \qquad (C.7)$$

This is the shut-off relationship; it assumes the skirt makes a perfect seal when it contacts the ground plane. Note also that this formulation assumes that the skirt does not collapse when $p_c < p_a$.

For certain cases, a lumped inertance model of the duct flow process is also used. According to this model, compressibility and fluid friction effects are ignored, so that $Q_{df} = Q_{dc} = Q_d$ and, for a duct having a constant cross-sectional area A_d, only unsteady inertia terms are important, in which case [C.19]

$$I_d dQ_d/dt = p_{df} - p_c \tag{C.8}$$

where I_d is the duct air inertance. Although far simpler than the hydraulic transient model, for ducts of the length used here its use is believed to be appropriate. It has been shown to reproduce the major linear stability properties for this system [C.19].

Solutions to the system of equations (C.1) to (C.7) were obtained by converting equations (C.2) and (C.3) to ordinary differential equations along the characteristic lines $dx/dt = V \pm a$, and then using a Runge-Kutta numerical procedure to integrate the system in time. This followed the approach suggested by Wylie and Streeter [C.24]. For the lumped inertance model of the duct flow, equations (C.1) and (C.4) to (C.8) were also solved by a Runge-Kutta procedure. The predictions obtained from these computations are discussed in conjunction with the experimental results.

The Galerkin method first used to investigate the problem [C.18] was not employed, because its associated computational burden was not much less than that of the numerical procedure, and it gave much less detail about the shapes of motion and cushion pressure waveforms, and nothing on limit cycle stability. Furthermore, for certain equilibrium values of p_{ce} and Q_e, the numerical simulations suggested that not one, but two stable limit cycles could exist. The Galerkin method as originally formulated was not able to predict this result.

C.3 Experiment

Care was taken to ensure that the skirt behaviour corresponded closely to that assumed in the analysis, and in this regard the only materials that could approach the concept of ideal-model material were certain elastomer-coated fabrics having a thickness of less than about 0.15 mm. However, even at the relatively low values of p_c used here, small deformations of such materials can have a major effect on cushion dynamics. Graham, Sullivan and Hinchey [C.20] have shown that, for the conical cell depicted in Figure C.1 and for the materials typically used to model skirts, the deformation is large enough to significantly increase both C_c and h. Consequently, for the present experiments, most of the tapered cone was replaced by a rigid metal cylinder, onto which a 2.50 cm flexible extension was attached. This also minimized the possible effect of skirt collapse on the dynamics. We have observed that, when models using the full conical skirt limit cycled at an amplitude large enough to cause skirt contact and flow shut off, skirt collapse would occur for part of the cycle.

However, even the shortened skirt sometimes proved to be unsatisfactory, because it was found to be very difficult to trim the bottom edge parallel to the ground-board and to maintain the slightly tapered conical geometry. Indeed, to ensure structural stability when pressurized, it was found necessary to include a substantial taper, which usually varied significantly around the periphery owing, apparently, to the orthotropic properties of the fabric. Furthermore, in some cases these extensions exhibited visually detectable deformation under the action of the cushion pressure. To circumvent these difficulties, the following approach was adopted. For systems for which the air gap and skirt taper is not uniform around the periphery, the flow should nevertheless be orifice-like, in which case one would expect the expression for Q_e to have the form

$$Q_e = L_p f_Q(x, p_{ce})[2p_{ce}/\rho]^{1/2} \tag{C.9}$$

Here $x = y + c$ is the height of a rigid part of the model above the ground-board. The cushion "flow function" $f_Q(x, p_c)$ has the dimensions of a length, and is independent of p_{ce} if no skirt deformation occurs. Furthermore, if $f_Q(x, p_{ce})$ is linear in x it is appropriate to employ the concept of a hovergap and a discharge coeficient, in which case $f_Q = C_D h$. In the present tests, Q_e was measured by the conical inlet, which had been calibrated by an ASME orifice plate flowmeter installed prior to final installation of the cushion. Hence, from equation (1) for a given x and p_c,

$$f_Q(x, p_{ce}) = K[(p_f - p_{df})/(p_{ce})]^{1/2}, \qquad K = C_m A_d/L_p \tag{C.10}$$

Figure C.2 shows typical data obtained for one extension; there is no detectable dependence of f_Q on p_{ce}, and it is linear in x. This justified the use of an equivalent h. Two extensions were used in the experiments, and for the first, "A", $C_D = 0.576$, whereas for the second, "B", $C_D = 0.506$. In both cases the value of x corresponding to $h = 0$ was obtained by extrapolating the curve for f_Q to zero.

Figure C.3 shows predicted linear stability characteristics for the two extensions, together with those for the corresponding rigid lip cushion, for which $C_D = 0.61$. These characteristics are presented in the form of stability boundaries, which are plotted in terms of nondimensional equivalents of p_{ce} and Q_e, defined by

$$C_{PC} = \frac{p_{ce}}{P_a}, \qquad C_{QC} \triangleq Q_e(\rho/2WA_{base})^{1/2}. \tag{C.11}$$

Here P_a is the absolute atmospheric pressure, $W = Mg$ and $A_{base} = \pi/4 D_p{}^2$. The quantity C_{QC} scales cushion flow rates for model tests. In fact, for a uniform hovergap, equation (C.6) shows that $C_{QC} = 4C_D h_e/D_p$. On full scale vehicles usually $0.001 \leq C_{QC} \leq 0.015$ [C.25]. The experimentally determined boundary for extension A is also given in Figure C.3; this data was obtained by an observed motion method [C.19]. The main point to be noted is the sensitivity of the location of the boundaries to C_D.

The pressure waveforms in the cushion volume were measured by a Kistler Model 206 piezoelectric transducer, which had a quoted resolution of 0.006 kPa and a rise time of 3 μsec. The transducer was mounted on the

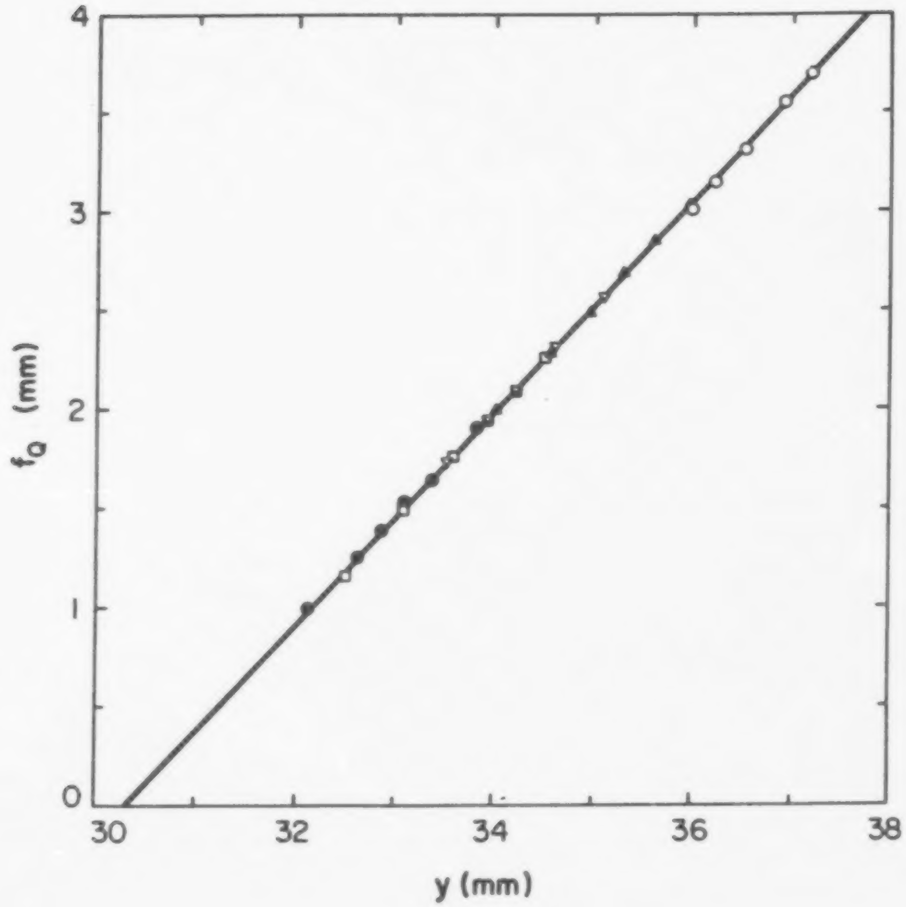

Figure C.2 Typical data used to determine the flow function $F_Q(x,p_{ce})$ for flexible skirt. Data points, p_{ce}: ○ , 0.434 kPa; Δ, 0.580 kPa; ∇,0.725 kPa: □ , 0.818 kPa; ● , 0.942 kPa.

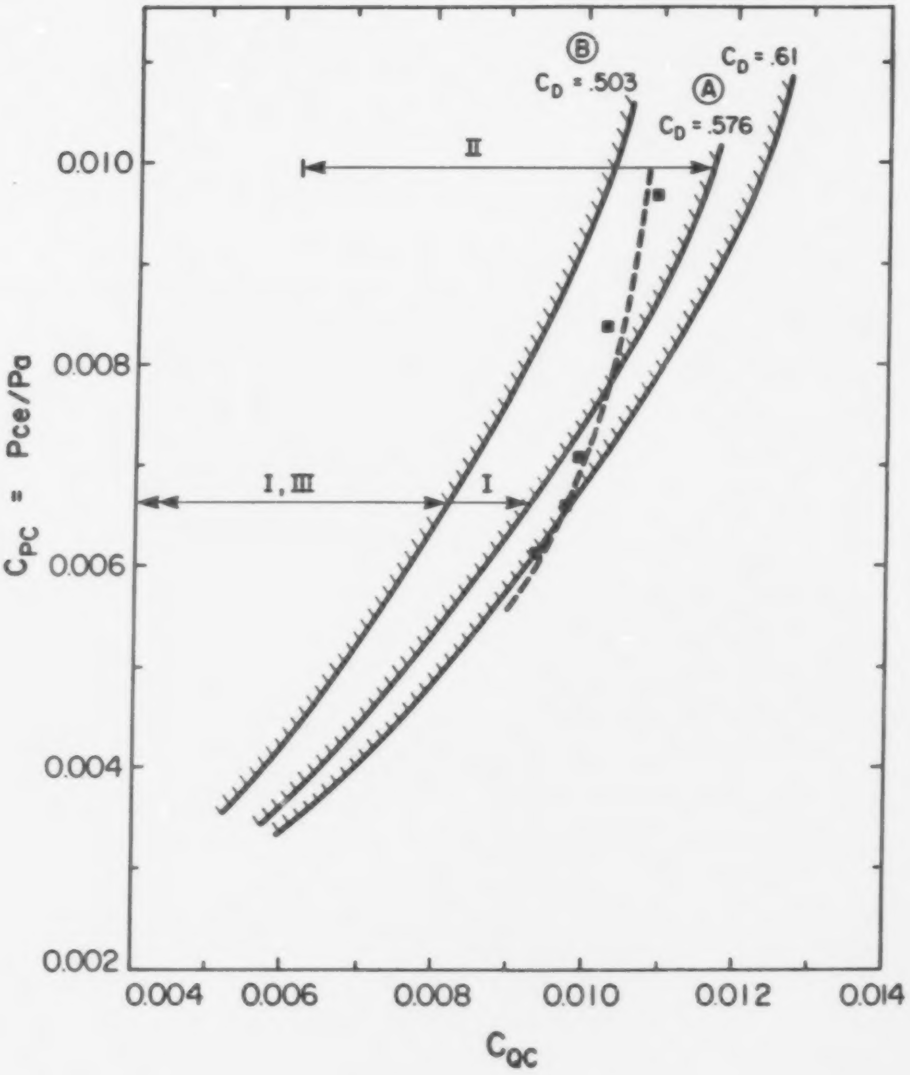

Figure C.3 Linear stability boundaries for the duct plenum system used in the experiments. Theory, with hatched side unstable, ////// Computed boundaries are given for rigid lip (C_D = 0.61), and the extension A, C_D = 0.576 and extension B, C_D = 0.503. Ranges of equilibrium operating points for limit cycle measurements: |↔|; Cases I and III, C_{PC} = 0.00;66, Case II, C_{PC} = 0.0097. Measured stability data for extension A only, ■ -----.

ground-board directly under a baffle plate with its sensitive surface level with that of the ground-board. The baffle plate, which was located under the duct entrance to the cushion, was intended to eliminate any possible flow structure effects [C.19]. The heave motion was measured by a Shaevitz Model 5000HR linear variable differential transformer (LVDT) displacement transducer which had previously been calibrated against a standard workshop vernier micrometer. The steady state calibrations of these types of transducers have proved to be very stable, and the frequency response was adequate, since the "3 dB down" frequency was 250 Hz.

To determine the frequencies of the oscillations and to examine the harmonic content of the displacement oscillations, the output of the LDVT was recorded on a Bruel and Kjaer Model 7001 frequency modulated tape recorder. At the tape speed used in the experiments, this instrument had a frequency response which was flat from DC to 500 Hz. Three samples were obtained for each of the two cushion weights and various Q_e. A Spectral Dynamics Model 360 Fast Fourier Transform Digital Signal Processor was then used to obtain the power spectra of these signals.

C.4 Results and Discussion

Measurements of amplitude and frequency were obtained for extension A at two model weights, corresponding to $C_{PC} = 0.0066$ (Case I) and 0.0097 (Case II) respectively, and for extension B at $C_{PC} = 0.0066$ (Case III), as shown in Figure C.3. Figures C.4, C.5 and C.6 give predicted and measured frequencies for the three cases as a function of distance from the stability boundary measured in increments of nondimensional volume flux ΔC_{QC}. Note that the stability curves in Figure C.3 show that increases in ΔC_{QC} correspond to reductions in Q_e. Also, in an attempt to minimize the effects of errors in the estimation of C_D and in the location of the linear stability boundaries, in the experiments the reference value of Q_e used to compute ΔC_{QC} was the experimentally determined value corresponding to the onset of instability.

The predicted values of frequency f given in Figures C.4, C.5 and C.6 were obtained by using the distributed property model of the duct process, and the most prominent feature of these results is the existence of two stable limit cycles for values of ΔC_{QC} less than about 0.002. The higher frequency oscillation was obtained by starting the computations with a disturbance δh of about 90% of h_e, whereas the lower frequency oscillation developed when $\delta h \approx 4h_e$ or greater. Note that in Figure C.4 the numerically computed frequencies are given in the form of data points for 15 discrete values of ΔC_{QC}, and that the shape of the predicted curve has been inferred from this data. Also, the low frequency oscillations are associated with skirt-ground contact, and the first point on the high frequency branch at which skirt-ground contact occurs is marked.

Figures C.7, C.8 and C.9 give the predicted and measured values of the amplitudes for the three cases. In Figure C.7 an equivalent h_e, computed from the known C_{QC}, is also given. As expected, the amplitude of the high frequency branch of the curves approaches zero as $\Delta C_{QC} \rightarrow 0$. Note that the data in Figure C.7 shows that at the onset of skirt-ground contact the mean value of $h(t)$ is considerably larger than h_e. Also the simulations show that under some circumstances it is possible to initiate large amplitude

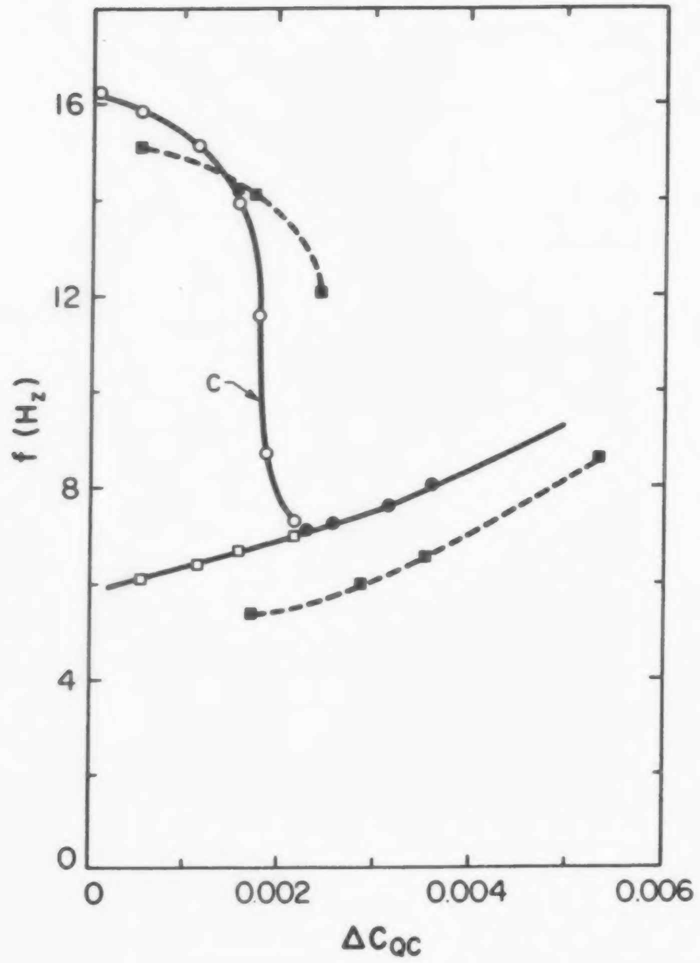

Figure C.4 Predicted and measured frequencies of limit cycles for Case I, C_{PC} = 0.00;66 and C_D = 0.576 Predictions, ——; $\delta h/h_e$ = 0.9, ○; $\delta h/h_e$ = 4, □ ; $\delta h/h_e$ = 0.9 and 4.0, ● . Measured data, ■ - - - - -. The point "C" denotes the frequency at which skirt contact first occurs. The scatter in the measurements of frequency was usually less than ± 0.5 Hz and in ΔC_{QC}, $\pm 0.1\times 10^{-3}$.

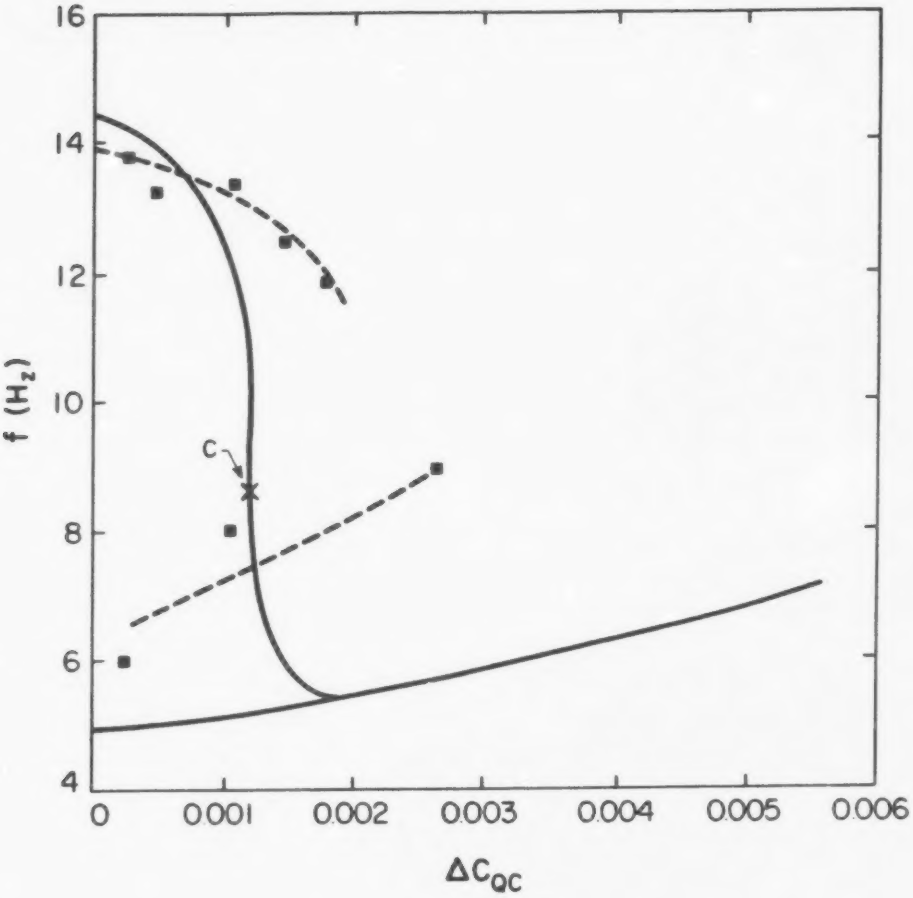

Figure C.5 Predicted and measured frequencies of limit cycles for Case II, C_{PC} = 0.0097 and C_D = 0.576. Predictions, ——; measured data, ■ - - - - - -.

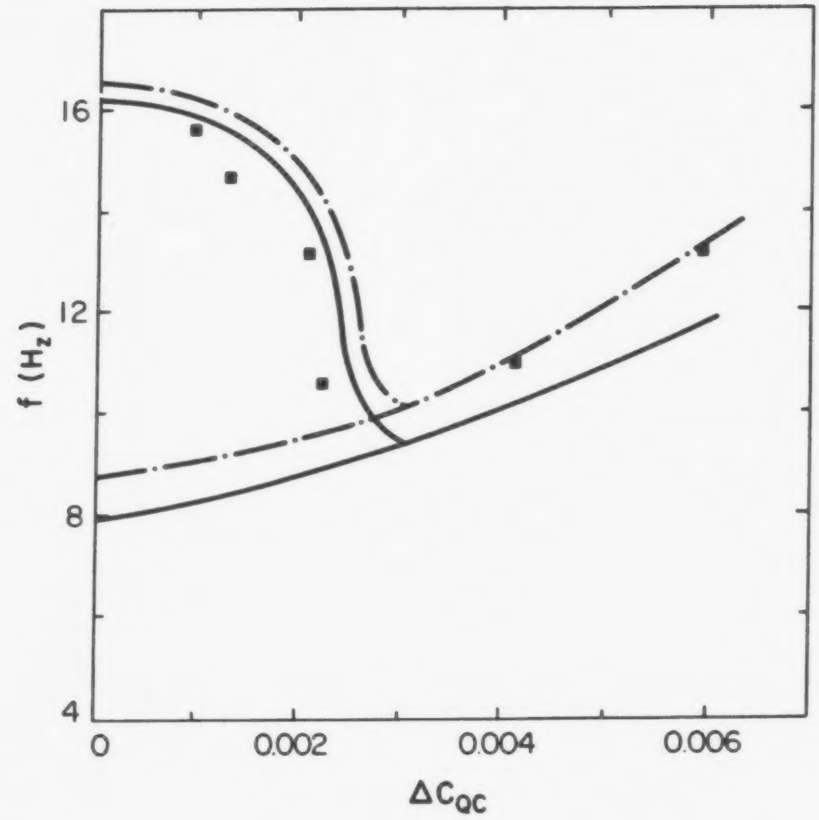

Figure C.6 Predicted and measured frequencies of limit cycles for Case III, C_{PC} = 0.0066 and C_D = 0.503. Predictions with distributed property duct model, ——; with lumped inertance duct model, — • — • —; measured data, ■ .

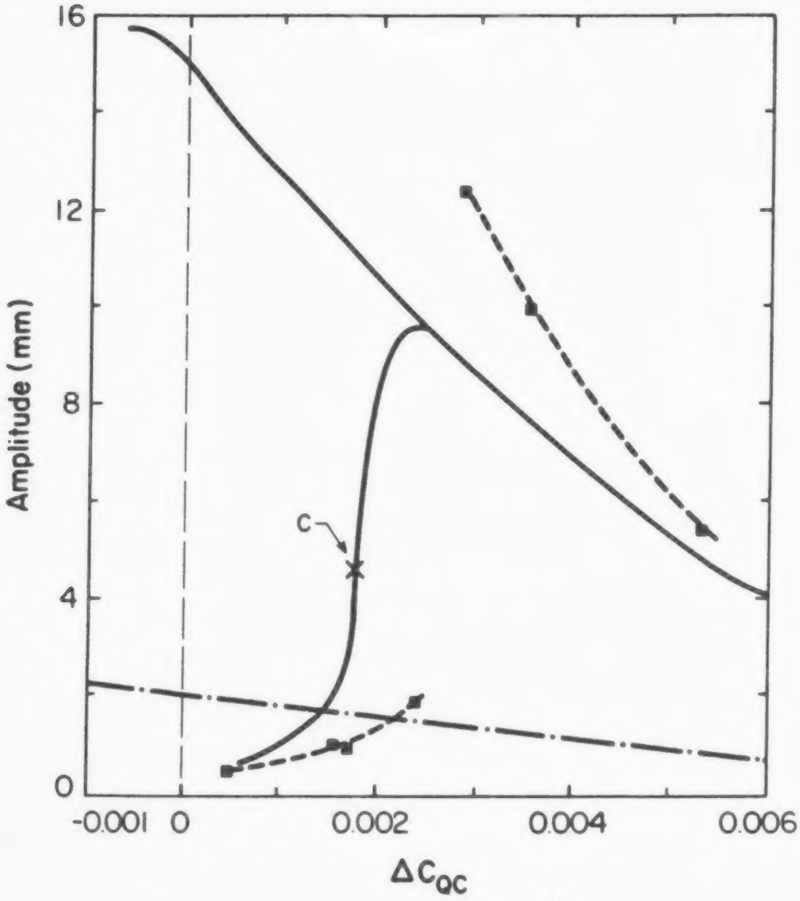

Figure C.7 Predicted and measured amplitudes of limit cycles for Case I, C_{PC} = 0.0066 and C_D = 0.576. Predictions, —; computed value of h_e, — • — • —, measured data, ■ - - - - -.

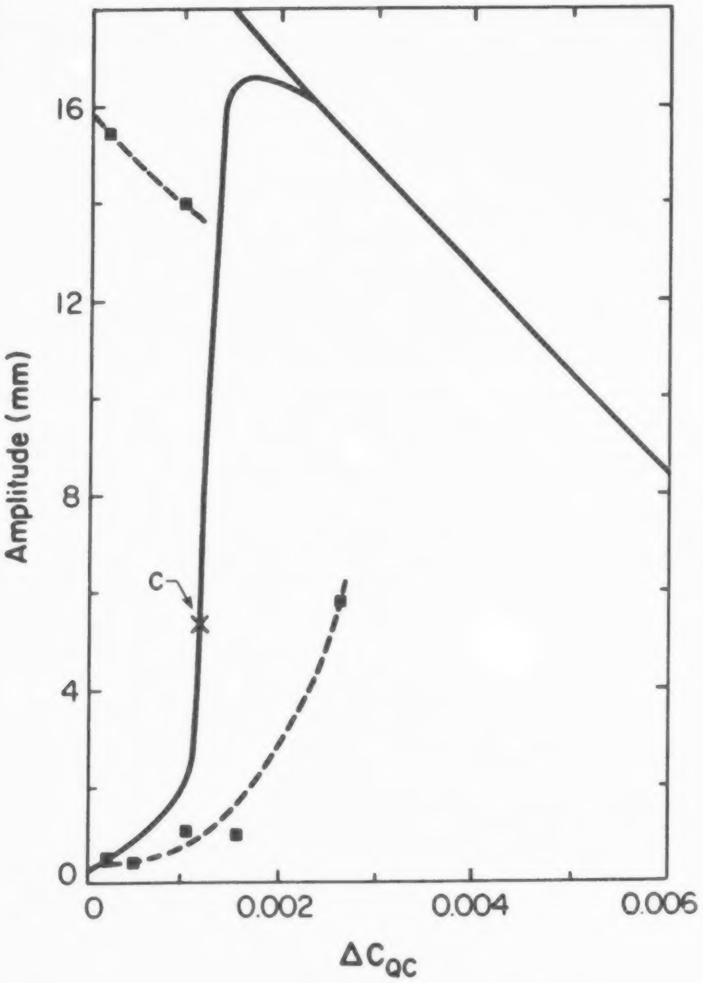

Figure C.8 Predicted and measured amplitudes of limit cycles for Case II, $C_{PC} = 0.0097$ and $C_D = 0.576$. Predictions, ——; measured data, ■ - - - - - -.

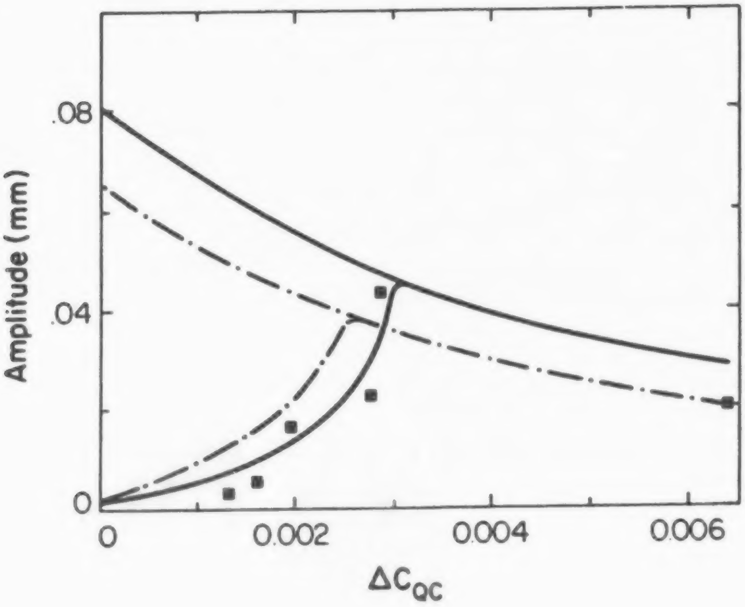

Figure C.9 Predicted and measured amplitudes of limit cycles for Case III, C_{PC} = 0.0066 and C_D = 0.503. Predictions with distributed property duct model, ——; lumped inertance duct model, — • — • —; measured data, ■ .

oscillations for values of C_{QC} at which the system is linearly stable.

Figures C.6 and C.9 give the predictions of frequency and amplitude obtained for Case III by using a lumped inertance model of the duct process. This model gives good qualitative agreement with those obtained by using the distributed property model, and this includes the prediction of the existence of two stable limit cycles for $\Delta C_{QC} < 0.002$. In fact the lumped inertance model can be used to provide another check of the consistency of the present calculations. In an analysis of the linear stability characteristics of the present system [C.14], this model of the duct flow was used to show that, at the onset of instability, the frequency should be given approximately by

$$f_L = (1/2\pi)\left[(A_d a^2)/(L_d V_c) + S_a{}^2/(MC_c)\right]^{1/2} \qquad \text{(C.12)}$$

When $C_{PC} = 0.0066$ (Cases I and III) this formula predicts $f_L = 16.8$ Hz; and for $C_{PC} = 0.0097$ (Case II), $f = 14.4$ Hz. These may be compared with the values obtained from the distributed property duct model, which are 16.3 Hz and 14.4 Hz respectively.

The experimentally measured values of frequency and amplitude are given in Figures C.4 to C.9. Each data point gives the average of three measurements. In general it was not possible to obtain all parts of the predicted curves at any one of the three cases. For example, as the data in Figures C.6 and C.9 for Case III shows, the low frequency mode could not be produced for extension B no matter how large an initial disturbance was imparted to the model. Furthermore, the low frequency oscillations that were observed with extension A installed could only be obtained for initial disturbances considerably in excess of the value $\delta h_0/h_e \approx 4$ used in the simulations. Typically, at $h_e \approx 2$ mm, the cushion had to be lifted to about 10 cm above the ground-board and then dropped. It is also worth noting that, in the simulations, an input $\delta h/h_e = 8$ or larger was required to initiate low frequency oscillations for Case III. However, these difficulties notwithstanding, taken as a whole, the data generally confirms the predictions of the theory.

Typical histories of z, p_c, Q_d and Q_a for oscillations involving skirt-ground contact, computed using the lumped inertance model, are given in Figures C.10, C.11 and C.12; those for oscillations without skirt contact were essentially single sinusoids. Typical spectral analyses of measured z for oscillations with and without shut-off are given in Figures C.13 and C.14 respectively; they confirm the observation that oscillations involving skirt-ground contact generates considerable second and higher order harmonic content, as suggested in the original analysis [C.18]. However, the most striking feature of the results is the pressure waveform that occurs during oscillations; $p_c < 0$ for a short interval, and there is an associated reversal in Q_a. An experimentally observed pressure waveform is given in Figure C.15.

The discrepancies between the theoretical and experimental results given in Figures C.4 to C.9, which take the form of consistent shifts, suggest the influence of factors not included in the analysis. One possibility is that the materials used to make the extensions are subject to creep, and, some permanent deformation was observed over the period of the testing. Changes of C_D associated with this deformation could cause such

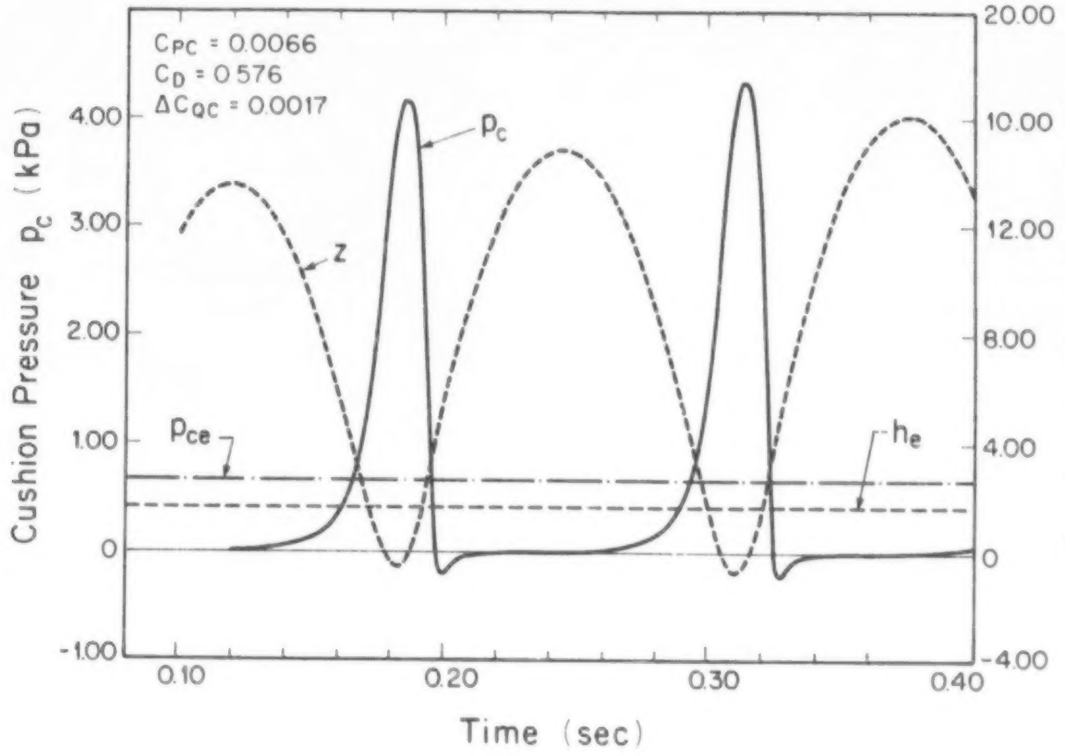

Figure C.10 Typical predicted displacement and cushion pressure waveforms for oscillations involving skirt-ground contact, showing growth to a limit cycle, obtained by using a lumped inertance model of the duct process. Note the long time scale of the growth process. The equilibrium values of cushion pressure and hovergap for this condition are marked for comparisons. Note that the peak pressure and hovergap are in excess of six and nine times their respective equilibrium values.

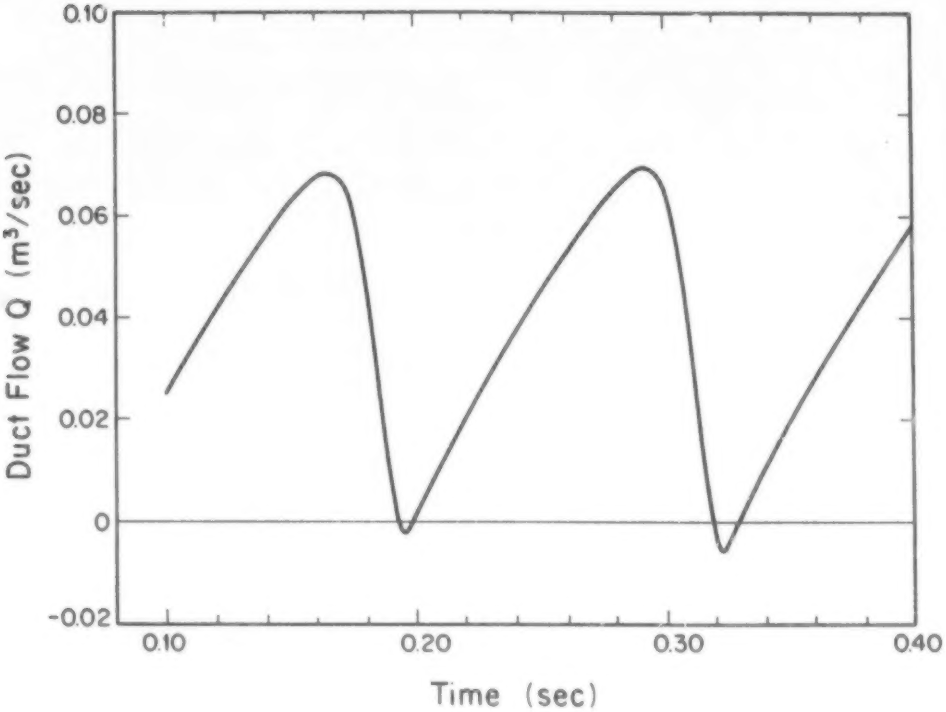

Figure C.11 Typical predicted duct flow wave-form for oscillations involving skirt-ground contact showing growth to a limit cycle, obtained by using a lumped inertance model for the duct process. $C_{PC} = 0.0066$, $C_D = 0.576$, $\Delta C_{QC} = 0.00171$.

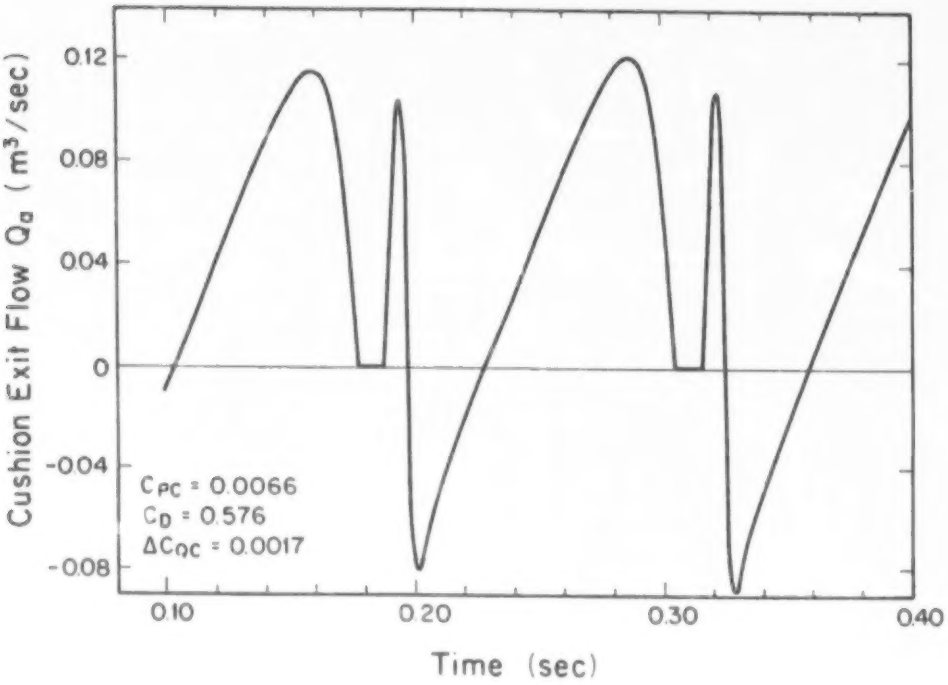

Figure C.12 Typical predicted cushion air escape flow wave-form for oscillations involving skirt-ground contact showing growth to a limit cycle, obtained by using a lumped inertance model for the duct process. $C_{PC} = 0.0066$, $C_D = 0.576$ and $\Delta C_{QC} = 0.00171$.

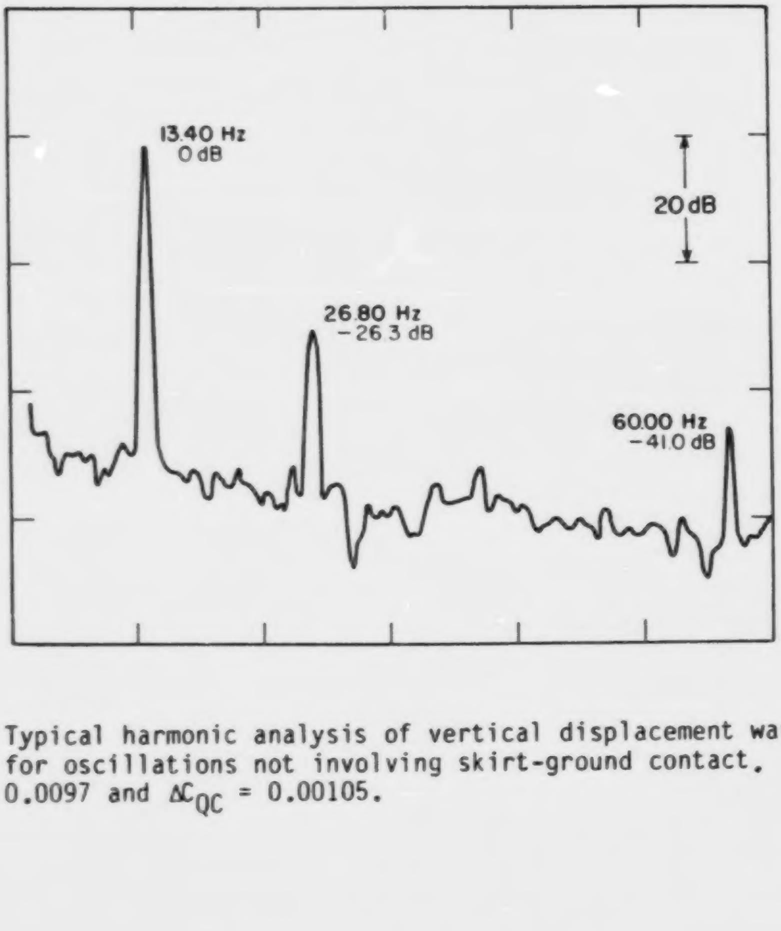

Figure C.13 Typical harmonic analysis of vertical displacement wave-form for oscillations not involving skirt-ground contact. C_{PC} = 0.0097 and ΔC_{QC} = 0.00105.

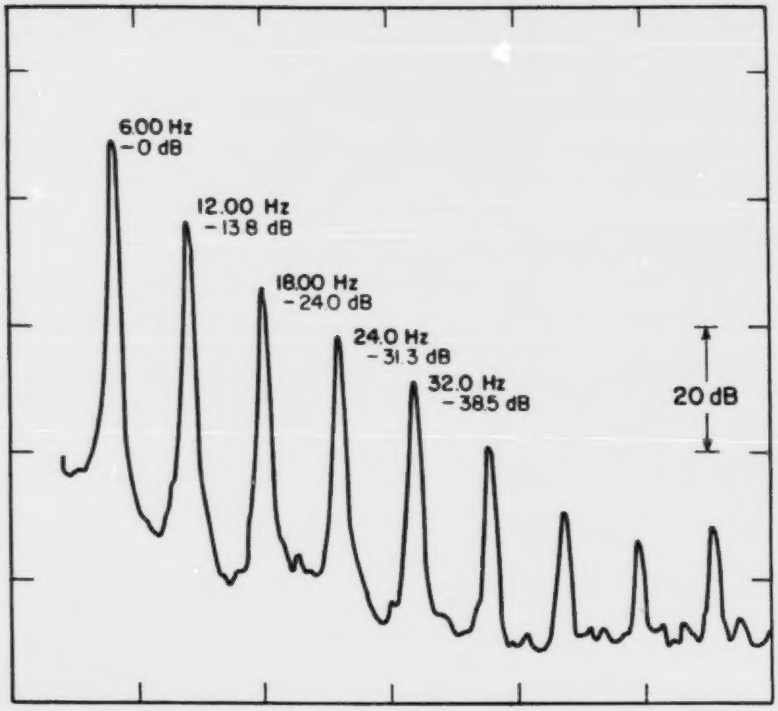

Figure C.14 Typical harmonic analysis of vertical displacement wave-form for oscillations involving skirt-ground contact. $C_{PC} = 0.0097$ and $\Delta C_{AC} = 0.00025$.

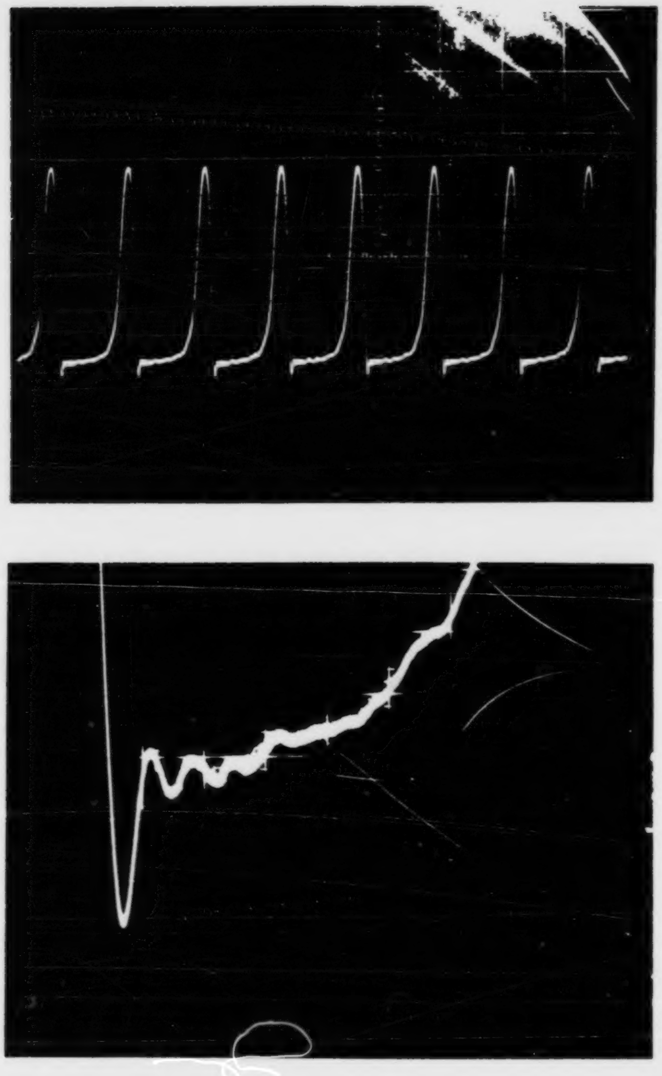

Figure C.15 Photographs of observed pressure oscillations involving skirt-ground contact. The upper photograph gives the complete signal, while the lower trace shows the details of the transient oscillation that occurs after the minimum pressure is reached. The frequency of the overall oscillation is 8.0 Hz, and that of the transient is about 160 Hz.

shifts. For example, although the frequency at the onset of instability predicted by both the linear analysis (Equation C.12) and the numerical simulations is independent of C_D, the other features of the curves are sensitive to this parameter. Typically, for Cases I and III the skirt contact is predicted to occur at amplitudes of 4.60 and 2.95 mm respectively. Another potential source of error is the location of the linear stability boundary. Although the value of C_{QC} corresponding to marginal stability was measured with an error of less than 2%, skirt deformation due to creep and the consequent effect on C_D could cause the boundary to shift substantially. A third factor not included in the analysis is the effect of any inherent material damping and any frictional forces generated by skirt-ground contact. The latter type of damping might explain why initiation of the low frequency mode required a much greater initial perturbation than that suggested by the analysis.

A simple check that the large amplitude oscillations are associated with shut-off was obtained from the simulations by linearizing the shut-off relationshp, that is, by setting $h = z$ for $z < 0$. This forces $Q_e < 0$ when $h < 0$. When this was done the pressure waveforms were still found to be clipped, but the large amplitude limit cycle did not occur.

For the oscillations involving skirt-ground contact, the superposition of the predicted pressure and hovergap histories in Figure C.10 shows that the peak of the pressure spike occurs at the lowest point of the oscillation and when Q_a is shut off. In the neighbourhood of this point the cushion is subjected to very high acceleration, whereas for values of h greater than about h_e, the cushion is very nearly in free fall. Hence the overall motion has the character of a relaxation oscillation in which the cushion acts as a very stiff spring for a small fraction of the period.

An interesting feature of the pressure waveform in Figure C.15 is the presence of a transient of about 160 Hz that begins at the point of minimum p_c. This frequency is well below the resonant frequency of the transducer, which is above 50 kHz. The numerical simulations suggest that most of this oscillation occurs in the period when p_c is very close to zero, and when flow reversal occurs. This in turn suggests that the high frequency oscillation may be a Helmholtz resonator effect, in which the cushion cavity provides the stiffness element and the air in the neighbourhood of the lip provides the equivalent mass element. An estimate of the frequency can be obtained by the usual argument [C.26], in which h is the equivalent of the radius of a circular opening. This yields an equivalent mass of $1.5\ \rho D_p h^2$ and a frequency $f_H{}^2 = 2a^2/(3\pi^2 D_p L)$. This is independent of h, which, in contrast to the usual resonator geometry, for which the volume of the mass element is proportional to the cube of the radius. This independence is significant here, since the simulations show that h is varying very rapidly when this oscillation occurs. For the present experiments, $f_H \sim 274$ Hz. The lowest frequency corresponding to standing waves in the duct is about 203 Hz.

C.5 Conclusions

The analytical model of limit cycle oscillations of air cushions proposed by Hinchey and Sullivan [C.18] is confirmed experimentally. In particular it shows that the quasisteady Bernoulli model describes the major features of the flow phenomena even in the presence of the highly nonlinear behaviour induced by skirt-ground contact. Both the Bernoulli law nonlinearity and flow shut-off caused by skirt-ground contact are shown to generate limit cycles, and this occurs even when the duct flow can be modelled by a lumped inertance. Also the experiments suggest that, even when flow reversal occurs, the flow is effectively quasisteady except possibly for the very low flow rates in the immediate neighbourhood of the reversal itself.

One area that needs further exploration is the possible effect of skirt collapse. Originally we thought it to be peculiar to the skirt geometry used here, but it has been observed for other geometries [C.23]. It seems likely that for the present geometry the effect should be small, since the cushion pressure is negative for only a very small fraction of the time, and when negative, its magnitude is also very small. Unfortunately, owing to the large effects of skirt material flexibility [C.20], this cannot be checked in the present experiments by simply replacing the metal cylinder by the full conical skirt. One would however like to generalize to practical skirt systems the observations about its significance for the present geometry, otherwise analysis might be greatly complicated.

REFERENCES - APPENDIX C

C.1 Casey, B. L., "Static and Dynamic Behaviour of a Flexible Base Fluid Suspension", Massachusetts Institute of Technology, Department of Mechanical Engineering Report DSR-76110-5, 1966.

C.2 Ribich, W. A. and Richardson, H. H., "Dynamic Analysis of Heave motion for a Transport Vehicle Fluid Suspension, Massachusetts Institute of Technology, Department of Mechanical Engineering Report DSR-76110-3, 1967.

C.3 Bickford, L. L., and Olson, G. K., "Dynamics of a Multiple Skirt Air-Cushion Vehicle", Journal of Aircraft, Vol. 6, No. 6, 1969, pp. 564-565.

C.4 Captain, K. M. and Richardson, H. H., "Heave Dynamics of Flexible-Base Fluid Suspensions", Massachusetts Institute of Technology, Department of Mechanical Engineering Report DSR-76110-9, 1969.

C.5 Leatherwood, J. D., "Analog Analysis of the Heave Response and Control of a Plenum Type Air Cushion Vehicle, National Aeronautics and Space Administration, Washington, Technical Note TN D-6257, 1971.

C.6 Reynolds, A. J., West, R. P. and Brooks, B. E., "Heaving and Pitching Response of a Hovercraft Moving Over Regular Waves, Journal of Mechanical Engineering Science, Vol. 14, No. 5, 1972, pp. 340-352.

C.7 Captain, K. M., Boghani, A. B. and Wormley, D. N., "Dynamic Heave-Pitch Analysis of Air Cushion Landing Systems", National Aeronautics and Space Administration, Washington, Contractor Report CR 2530 1975.

C.8 Reynolds, A. J., "A Nonlinear Theory for a Hovercraft Moving Over Regular Waves", Journal of Mechanical Engineering Science, Vol. 16, No. 5, 1974, pp. 310-316.

C.9 Doctors, L. J., "Nonlinear Motion of an Air Cushion Vehicle Over Waves", Journal of Hydronautics, Vol. 9, No. 2, 1975, pp. 49-57.

C.10 Parravano, G. J. and Sullivan, P. A., "A Theoretical and Experimental Investigation of a Hinged Lip Tracked Air Cushion Vehicle Suspension System", Transport Canada Research and Development Centre, Montreal, Contract Report D-500-210, 1977.

C.11 Sullivan, P. A. and Parravano, G. J., "Analysis of a Loop-Type Flexible Skirt Air Cushion", Canadian Aeronautics and Space Journal, Vol. 23, No. 6, 1977, pp. 346-358.

C.12 Boghani, A. B., Captain, K. M. and Wormley, D. N., "Heave-Pitch-Roll Analysis and Testing of Air Cushion Landing Systems", National Aeronautics and Space Administration, Washington, Contractor Report CR 2917, 1978.

C.13 Carrier, R., Magnuson, A. H. and Swift, M. R., "Seakeeping Dynamics of a Single Cushion Peripheral Cell-Stabilized Air Cushion Vehicle", Journal of Hydronautics, Vol. 12, No. 2, 1978, pp. 49-54.

C.14 Hinchey, M. J. and Sullivan, P. A., "Duct Effects on the Heave Stability of Plenum Air Cushions", Journal of Sound and Vibration, Vol. 60, No. 1, 1978, pp. 87-99.

C.15 Sullivan, P. A., Hinchey, M. J. and Delaney, R. G., "Static Roll Stiffness Characteristics of Two Multicell Type Air Cushions", Journal of Terramechanics, Vol. 15, No. 1, 1978, pp. 15-49.

C.16 Wormley, D. N., Garg, D. P. and Boghani, A. B., "Nonlinear and Finite Pad Length Performance of Vehicle Air Cushion Suspensions", Massachusetts Institute of Technology, Department of Mechanical Engineering Report EPL 72-72966-1, 1978.

C.17 Boghani, A. B. et al, "Experimental and Analytical Studies of Advanced Air Cushion Landing Systems", National Aeronautics and Space Administration, Washington, Contract Report, Contract Number NASL 15051, 1980.

C.18 Hinchey, M. J. and Sullivan, P. A., "A Theoretical Study of Limit Cycle Oscillations of Plenum Air Cushions", Journal of Sound and Vibration, Vol. 79, No. 1, 1981, pp. 61-77.

C.19 Sullivan, P. A., Hinchey, M. J. and Green, G. M., "A Review and Assessment of Methods for the Prediction of the Dynamic Stability of Air Cushions", Journal of Sound and Vibration, Vol. 84, No. 3, 1982, pp. 337-358.

C.20 Graham, T. A., Sullivan, P. A. and Hinchey, M. J., "Skirt Material Effects on Air Cushion Dynamic Heave Stability", Journal of Aircraft, Vol. 22, No. 2, Feb. 1985, pp. 101-108.

C.21 Sullivan, P. A., Hartmann, P. V. and Graham, T. A., "Application of System Identification Flight Analysis Techniques to the Pitch-Heave Dynamics of an Air Cushion Vehicle", Canadian Aeronautics and Space Journal, Vol. 29, No. 4, 1983, pp. 348-370.

C.22 Kuhn, T. S., The Structure of Scientific Revolutions. University of Chicago Press, Chicago, 1970. See p. 26.

C.23 Clayton, B. R. and Tuckey, P. R., "Recent Hovercraft Research in the United Kingdom. Part 2. Analytical Work Related to Hovercraft Dynamics", High Speed Surface Craft, Vol. 23, No. 1, 1984, pp. 24-30.

C.24 Wylie, E. B. and Streeter, V. L., Fluid Transients. McGraw-Hill, New York, 1978. See p. 27.

C.25 Fowler, H. S., "On the Lift Air Requirement of Air Cushion Vehicles and Its Relation to the Terrain and Operational Mode, National Research Council of Canada, Division of Mechanical Engineering, Ottawa, Report ME-246, 1979.

C.26 Kinsler, L. and Frey, A., Fundamentals of Acoustics. John Wiley and Sons, New York, second edition, 1962. See p. 193.

APPENDIX D. ON THE HEAVE DYNAMICS OF LARGE AIR CUSHION PLATFORMS (M. J. Hinchey, P. A. Sullivan and A. D. Dupuis)

NOMENCLATURE

Roman

A_f	effective area of stabilizing orifice, $A_f = \pi r_f^2$
a	atmospheric sound speed
$C_{d\ell}$	cushion discharge coefficient at lip
C_f	overall resistance coefficient for flow from fan to radius r_f
C_h, C_u	defined in Eq. D.49
$C_{h\ell}$, $C_{u\ell}$	defined in Eq. D.8
C_{PQ}	slope of fan characteristic = $dp_f/dQ_f\|_e$
g	acceleration due to gravity
h	effective hovergap
h_s	cushion height
L_p	length of cushion perimeter = $2\pi r_\ell$
m	mass of cushion
p_c	cushion pressure
p^*	defined in Eq. D.13
Q	volume flux
r	radial distance
r_f	radial distance at which air from fan is completely turned and flowing radially
s	Laplace variable, $s = \sigma + i\omega$
t	time
u	radial velocity, $u = u(r,t)$

Greek

Δ	small perturbation
η	sr/a, dimensionless Laplace variable
ρ	air density
σ	real part of Laplace variable
ω	imaginary part of Laplace variable, radian frequency

Subscripts

e	equilibrium
f	properties defined at $r = r_f$
ℓ	properties defined at lip

Superscripts

$(\bar{\ })$	denotes Laplace transform

D.1 Introduction

Large air cushion platforms are being considered in Canada and elsewhere for use in the Arctic to support and transport oil drilling rigs and other structures. These platforms would have to be moved over land, open water and pack-ice, and they could weigh as much as 10^4 tonnes. They might be expected to traverse obstacles such as ridges in pack ice [D.1]. Concern has been expressed about the possibility that such large platforms may be particularly susceptible to a dynamic instability which can lead to self excited oscillations [D.2]. This problem generally manifests itself as a motion in vertical translation, or heave, although other motions have been observed.

Like all modern air cushion vehicle (ACV) applications, platform cushions will use a flexible skirt to obtain the requisite obstacle clearance ability. A flexible skirt is essentially a collapsible structure, constructed from an elastomer-fabric composite material, which is inflated and stabilized by the cushion air pressure, and which enables the cushion to be sustained by very low air flow requirements. The lift air requirement can be expressed in terms of an equivalent uniform hovergap or 'daylight clearance': Fowler [D.3] reports that a 150 tonne craft, which was built in Canada and which has a 'hard structure clearance' of about 1.5 m, operates at equivalent air gaps less than 2 cm.

Cushion systems for large platforms are expected to have several distinctive features. One is that the equilibrium cushion footprint pressure p_{ce} is determined by the nature of the surface over which it is expected to operate. For operation over Arctic tundra the upper limit is about 7 kPa. A recent design study for a self-propelled platform weighing up to 800 tonnes specifies a pressure of 0.85 psi (5.9 kPa) [D.4]. The pressure limitation, together with payload and structural requirements, determines the basic vehicle planform dimensions. Typically, for an 800 tonne platform the planform may be about 30 by 45 m. Furthermore, since such vehicles are usually moved only very slowly, pitch and roll attitude changes associated with vehicle motion are usually very small, and the skirt depth is determined largely by the size of the largest obstacle it is expected to encounter. Thus even for large cushions, the skirt depth will probably be no more than about 2.5 m. Finally, the modest pitch and roll static stiffness requirements will allow the use of flexible skirt designs such as the segmented system shown in Figure D.1; these do not rely on interior compartmentation to generate restoring moments [D.5]. Hence the cushion will likely consist of a single large volume, usually with its depth very much less than its length or width.

Analyses of the dynamics of ACV's generally assume that the process in the cushion and other volumes is an isentropic compression-expansion which, for the low cushion pressures typical of most applications, can be modelled by a lumped pneumatic capacitance. The fundamental role played by the compressibility of the air in the cushion in causing dynamic instability was first pointed out by Ribich and Richardson in 1967 [D.6]. It adversely modifies the phase relationship between the cushion pressure oscillations

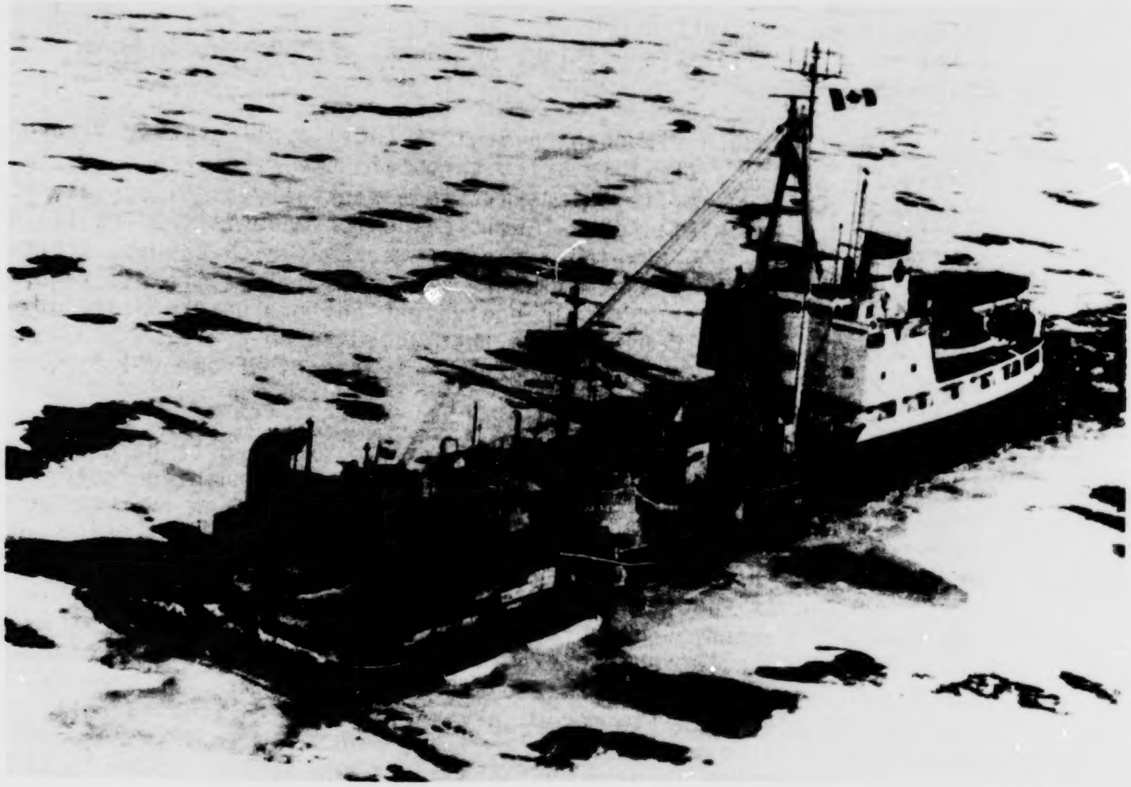

Figure D.1 The first platform cushion used to demonstrate icebreaking was the 250 ton platform ACT-100 originally designed as an Arctic heavy load transporter, shown here being pushed by the Canadian Coast-Guard icebreaker Alexander Henry. This vehicle used an uncompartmented loop and segment skirt.

and the motion oscillations that are generated in response to small disturbances. It is also known that the viscoelastic properties of the skirt material can play a similar role in destabilizing the cushion [D.7].

The lumped capacitance cushion model assumes that the pressure in the cushion volume is uniform throughout that volume at each instant in time. The primary purpose of the analysis described here is an exploratory investigation into the effects of acoustic wave propagation in the interior of a very large cushion volume on the dynamics, with special reference to the heave stability aspect. Now one might at first expect that acoustic wave phenomena would not have a significant effect on such a low frequency phenomenon as self excited oscillations of the basic vehicle, since it might be expected that the frequency of such oscillations decreases as the vehicle size increases. However, it turns out that the geometry and operating conditions of large platform cushions are such that the oscillation frequency decreases with increase in size to a limit of about 1 Hz. It is shown below that the natural frequency of heaving motion of a large platform cushion can be calculated quite accurately by assuming that it is a single mass supported by the pneumatic stiffness of the air in the cushion volume, with the latter computed by ignoring the effect of flow into and out of the volume. For small amplitude oscillations the radian frequency ω is then given by

$$\omega^2 = (\rho a^2 g)/(h_s p_{ce}) \tag{D.1}$$

where ρ and a are the atmospheric density and sound speed respectively, g is the acceleration due to gravity and h_s is the effective skirt height. Hence ω is controlled entirely by h_s and p_{ce}, and is independent of the basic planform dimensions. For $h_s \doteq 2$ m and $p_{ce} = 6$ kPa, the frequency $f = \omega/2\pi \equiv 1.5$ Hz. One concludes that significant acoustic wave propagation effects must inevitably occur as cushion size increases beyond a certain level. Also, because ω increases when p_{ce} is lowered, one would expect to see such effects at low cushion pressures.

The analysis herein considers the axisymmetric geometry depicted in Figure D.2, and assumes that the platform is subject to axisymmetric disturbances, for which the resultant motion is pure heave. Non-axisymmetric disturbances, which would also excite pitch and roll, are not considered. We consider these major simplifications to be appropriate at this stage because in practice the dynamic instability is usually observed to be a pure heave motion. This observation suggests that for the axisymmetric cushion the axisymmetric disturbance might be the most unstable. Such a result would be the equivalent of Squire's theorem for the stability of parallel shear flows, which states that infinitesimally small disturbances propagating in the basic flow direction are more destabilizing than those travelling at a non-zero angle [D.8]. This question is not explored here.

Two methods of analysis are used [D.10]. The first is based on separation of variables, and uses impedance concepts. The second uses the method of characteristics for hyperbolic partial differential equations together with numerical integration procedures. Apart from the fact that the latter provides a check on the consistency of the first method, the main advantage of the second is that it can easily treat convective inertia effects and the nonlinearities that are important in ACV heave dynamics

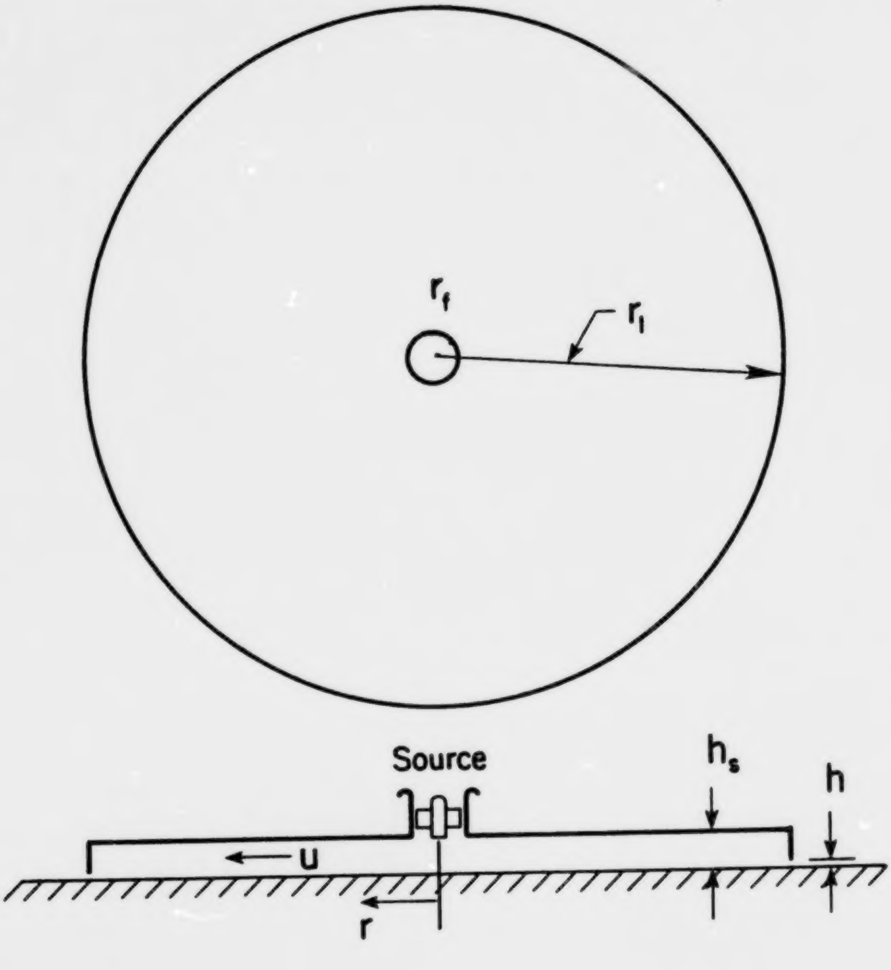
r_f
r_1
Source
h_s
h
u
r

Figure D.2 Large axisymmetric air cushion platform.

[D.9]. Hence it can provide an insight into practical stability. In connection with this point, the present linear calculations have shown that the typical large cushion can have very low damping, even though it may be operating at a value of p_{ce} well below that corresponding to the onset of instability; typically the phase margin may only be a few degrees at most, in contrast with the usual practical requirement of 30° or more. Although this problem was brought into focus by the acoustic model presented here, it is also implicit in the lumped capacitance model of the cushion. The reasons for this phenomenon and its practical implications are discussed below. The calculations are described in greater detail in Reference [D.10].

D.2 Mathematical Model

The axisymmetric cushion depicted in Figure D.2 has a uniform cushion height h_s, outer radius r_ℓ and hovergap h. Two cushion air supply cases are considered; one is the centrally located fan depicted in Figure D.2, and the second is an annular feed duct located at the periphery and just inside the cushion. All flow processes in the cushion volume are assumed to be axisymmetric; that is, functions of the radial distance r from the centre and time t alone. Since for the geometries of present interest $h_s \ll r_\ell$, it is assumed that, except in a small region of radius r_f surrounding the origin and a corresponding region near $r = r_\ell$, velocity perturbations in the vertical direction arising from motion of the vehicle are small compared to those in the radial direction. This is consistent with the usual long-wave approximation in which the wavelength of disturbances is assumed to be much greater than h_s. With the above assumptions, the governing equations are the equivalent of those used to model hydraulic transients in elastically deforming pipes [D.11]. In linearized form these are

Continuity

$$\partial\Delta p/\partial t + (\rho a^2/r)\partial(r\Delta u)/\partial r + (\rho a^2/h_s)\partial\Delta h/\partial t = 0 \qquad (D.2)$$

Momentum

$$\partial\Delta u/\partial t + (1/\rho)\partial\Delta p/\partial r = 0 \qquad (D.3)$$

where Δp is the static pressure perturbation, Δu is the perturbation in radial flow velocity and Δh is the hovergap perturbation. Note that the continuity equation couples the wave propagation in the cushion volume to the heave dynamics of the vehicle and, in the momentum equation, the convective inertia contributions are assumed to be negligible. The latter requirement would be satisfied if $u \ll a$ everywhere.

The boundary conditions for these equations are determined by the flow processes in the cushion air feed system and by the cushion air escape process, and these are assumed to be incompressible and quasisteady [D.12]. Consider first the centrally fed case, since the annular feed duct case can be obtained by a simple modification. The fan has a known steady characteristic for air delivery pressure p_f as a function of volume flow Q_f. The linearized approximation to this is

$$\Delta p_f(t) = C_{pQ}\Delta Q_f(t) \qquad (D.4)$$

where $C_{pQ} = (dp_f/dQ_f)|e$ is the local slope of the fan characteristic. As depicted in Figure D.2, the air is delivered vertically to the cushion volume. It is assumed that at $r = r_f$ the air turns into the horizontal direction and $u(r_f) = u_f$ is uniform across the height of the cushion volume. With the assumption that this turning process is quasisteady, and if $p_{cf} = p(u_f)$, then the linearized equivalent is a resistance across which

$$\Delta p_f(t) - \Delta p_{cf}(t) = C_{uf}\ \Delta u_f(t) \qquad \text{(D.5a)}$$

In this equation Δu_f is the velocity perturbation at $r = r_f$ corresponding to the inlet volume flux perturbation ΔQ_f, that is,

$$\Delta u_f = \Delta Q_f/(2\pi r_f h_s) \qquad \text{(D.5b)}$$

Note that momentum balance considerations indicate that for steady flow $p_{cf} < p_f$. Also, the term C_{uf} is assumed to include the effects of any resistance orifice included for static stabilization purposes. The boundary conditions (D.4) and D.5) can be combined to give

$$\Delta p_{cf} = C_f\ \Delta u_f(t) \qquad \text{(D.6)}$$

The condition at the lip is obtained from the usual quasisteady orifice flow law

$$Q_\ell(t) = 2\pi C_{d\ell} r_\ell h(t)\{2p_{c\ell}(t)/\rho\}^{1/2} \qquad \text{(D.7)}$$

in which Q_1 is the volume flux out of the cushion, $p_{c\ell}$ is the pressure in the cushion at $r = r_\ell$, and $C_{d\ell}$ is the discharge coefficient. Upon linearization, this reduces to

$$\Delta p_{c\ell}(t) = C_{u\ell}\Delta u_\ell(t) + C_{h\ell}\Delta h(t) \qquad \text{(D.8)}$$

where

$$C_{u\ell} = (2p_{ce}/Q_e)(2\pi r_\ell h_s), \qquad C_{h\ell} = -2p_{ce}/h_e \qquad \text{(D.9)}$$

The formulation is completed by applying Newton's second law for the vehicle heave motion. In linearized form, this is, with m = mass of the cushion,

$$m\ddot{h} = 2\pi \int_{r_f}^{r_\ell} r\Delta p_c(r,t)dr \qquad \text{(D.10)}$$

For the peripherally fed cushion, the boundary condition at $r = r_f$ becomes simply $u_f = 0$. At $r = r_\ell$ the inflow and outflow conditions are combined to give an equation similar in form to that of Eq. (D.8).

D.3 Impedance Analysis

Differentiation of Eqs. (D.2) and (D.3) with respect to t and x together with appropriate manipulation yields the two wave equations

$$\partial^2\Delta p/\partial t^2 + (\rho a^2/h_s)\partial^2\Delta h/\partial t^2 = (a^2/r)\partial(r\partial\Delta p/\partial r)/\partial r \qquad \text{(D.11)}$$

$$\partial^2\Delta u/\partial t^2 = (a^2/r^2)[r^2\partial^2\Delta u/\partial r^2 + r\partial\Delta u/\partial r - \Delta u] \tag{D.12}$$

Define

$$\Delta p^* = \Delta p + (\rho a^2/h_s)\Delta h \tag{D.13}$$

and substitute into Eq. (4) to obtain

$$\partial^2\Delta p^*/\partial t^2 = (a^2/r)\partial(r\partial\Delta p^*/\partial r)/\partial r \tag{D.14}$$

Let $s = \sigma + i\omega$ be the Laplace transform variable and $\Delta\bar{p}^*(s,r)$ and $\Delta\bar{u}(s,r)$ be the transforms of Δp^* and Δu respectively. Also, define the nondimensional radial distance $\eta = (sr/a)$. Then apply the Laplace transform to Eqs. (D.12) and (D.14) and rearrange to obtain the standard forms [D.13]

$$r^2\partial^2\Delta\bar{u}/\partial r^2 + r\partial\Delta\bar{u}/\partial r - (\eta^2 + 1)\Delta\bar{u} = 0 \tag{D.15}$$

$$r^2\partial^2\Delta\bar{p}^*/\partial r^2 + r\partial\Delta\bar{p}^*/\partial r - \eta^2\Delta\bar{p}^* = 0 \tag{D.16}$$

The solution to Eqs. (D.15) and (D.16) can be expressed in terms of modified Bessel functions [D.14] as follows:

$$\Delta\bar{p}^* = A_1(s)I_0(\eta) + A_2(s)K_0(\eta) \tag{D.17a}$$

and

$$\Delta\bar{u} = -[A_1(s)/(\rho a)]I_1(\eta) + [A_2(s)/(\rho a)]K_1(\eta) \tag{D.17b}$$

where I_0, I_1, K_0 and K_1 are the modified Bessel functions. The functions of integration, $A_1(s)$ and $A_2(s)$, are uniquely determined by the boundary conditions.

Equations (D.17a) and (D.17b) can be applied to the boundary conditions to obtain

$$-(\rho a^2/h_s)\Delta\bar{h}(s) + A_1(s)I_0(\eta_f) + A_2(s)K_0(\eta_f)$$

$$= -[C_f A_1(s)/(\rho a)]I_1(\eta_f) + [C_f A_2(s)/(\rho a)]K_1(\eta_f) \tag{D.18}$$

$$-(\rho a^2/h_s)\Delta\bar{h}(s) + A_1(s)I_0(\eta_\ell) + A_2(s)K_0(\eta_\ell)$$

$$= -[C_{u\ell}A_1(s)/(\rho a)]I_1(\eta_\ell) + [C_{u\ell}A_2(s)/(\rho a)]K_1(\eta_\ell) + C_{h\ell}\Delta\bar{h}(s) \tag{D.19}$$

The latter can be rewritten in the matrix form

$$\begin{vmatrix} G_{11} & G_{12} \\ G_{21} & G_{22} \end{vmatrix} \begin{vmatrix} A_1(s) \\ A_2(s) \end{vmatrix} \begin{matrix} = \\ = \end{matrix} \begin{vmatrix} L_1 \\ L_2 \end{vmatrix} \overline{\Delta h}(s) \qquad (D.20)$$

where

$$G_{11} = I_0(\eta_f) + [C_f/(\rho a)]I_1(\eta_f); \qquad G_{12} = K_0(\eta_f) - [C_f/(\rho a)]K_1(\eta_f)$$

$$G_{21} = I_0(\eta_\ell) + [C_{u\ell}/(\rho a)]I_1(\eta_\ell); \qquad G_{22} = K_0(\eta_\ell) - [C_{u\ell}/(\rho a)]K_1(\eta_\ell)$$

$$L_1 = \rho a^2/h_s; \qquad L_2 = L_1 + C_{h\ell} \qquad (D.21)$$

Solving for $A_1(s)$ and $A_2(s)$ gives

$$A_1(s) = B_1\overline{\Delta h}(s); \qquad A_2(s) = B_2\overline{\Delta h}(s) \qquad (D.22)$$

where

$$\begin{aligned} B_1 &= (G_{22}L_1 - G_{12}L_2)/(G_{11}G_{22} - G_{12}G_{21}) \\ B_2 &= (-G_{21}L_1 + G_{11}L_2)/(G_{11}G_{22} - G_{12}G_{21}) \end{aligned} \qquad (D.23)$$

Thus one obtains the following relationship between the pressure distribution under the craft and its heaving motion

$$\overline{\Delta p}(s,r) = [-(\rho a^2/h_s) + B_1 I_0(\eta) + B_2 K_0(\eta)]\overline{\Delta h}(s) \qquad (D.24)$$

The Laplace transform of the equation for the heave motion is

$$\overline{\Delta F}(s) = ms^2\overline{\Delta h}(s) = 2\pi \int_{r_f}^{r_\ell} \overline{\Delta p}(s,r)r\,dr \qquad (D.25)$$

so that

$$\overline{\Delta F}(s) = (\zeta_1 B_1 + \zeta_2 B_2)\overline{\Delta h}(s) - (\rho a^2/h_s)(\pi r_\ell^2 - \pi r_f^2)\overline{\Delta h}(s) \qquad (D.26)$$

where

$$\zeta_1(s) = 2\pi \int_{r_f}^{r_\ell} rI_0(\eta)dr \quad \text{and} \quad \zeta_2(s) = 2\pi \int_{r_f}^{r_\ell} rK_0(\eta)dr \qquad (D.27)$$

During heave motion of an air cushion platform the generated pressure force can either lag or lead the motion. When the force lags, the net work done on the platform mass during a cycle of oscillation is positive, whereas when the force leads the work done is negative. This implies that when the force lags, the platform mass gains kinetic energy whereas when the force leads, it loses kinetic energy. An energy gain implies oscillation amplitude growth or instability while an energy loss implies amplitude decay, or stability. Critical stability occurs when the generated pressure force is exactly in phase with heave motion so that energy is neither gained nor lost [D.15]. Using D'Alembert's principle, we can rewrite Eq. (D.25) to obtain

$$\overline{\Delta F}_P(s) + \overline{\Delta F}_I(s) = 0 \qquad (D.28)$$

where

$$\overline{\Delta F}_P(s) = [\zeta_1 B_1 + \zeta_2 B_2 - (\rho a^2/h_s)(\pi r_\ell^2 - \pi r_f^2)]\overline{\Delta h}(s) = N(s)\overline{\Delta h}(s) \qquad (D.29)$$

and

$$\overline{\Delta F}_I(s) = -ms^2\overline{\Delta h}(s) = \frac{\overline{\Delta h}(s)}{M(s)} \qquad (D.30)$$

Further manipulation yields

$$\frac{\overline{\Delta F}_P(s)}{\overline{\Delta F}_I(s)} = N(s)M(s) = -1 \qquad (D.31)$$

At the onset of instability, where $s = i\omega^*$, this reduces to

$$N(i\omega^*)\ M(i\omega^*) = -1 \qquad (D.32)$$

where ω^* is the so-called Nyquist frequency. If one plots the Nyquist function, $N(i\omega)M(i\omega)$, in a real-imaginary plane, then the critical pressure for a given gap is that which causes the plot to pass through the minus one point in the plane as ω is varied from zero to infinity. A Nyquist plot illustrating this is shown schematically in Figure D.3. To ascertain from a Nyquist plot the nature of stability immediately next to a stability boundary, one can use the fact that, because $M(i\omega)$ is real and positive, the lead-lag characteristics of the Nyquist function, $N(i\omega)M(i\omega)$, are identical to those of $N(i\omega)$, which is the transfer function relating generated pressure force to heave motion. It turns out that when the force lags the heave motion the phase of $N(i\omega)M(i\omega)$ at $|N(i\omega)M(i\omega)| = 1$ is more negative than (-180°) and when the force leads, the phase is less negative. These situations are also shown schematically in Figure D.3. Recall that force lead implies stability while force lag implies instability.

D.4 Method of Characteristics Analysis

Because of their hyperbolic nature, the partial differential equations (D.2) and (D.3) can be reduced to ordinary differential equations by the method of characteristics [D.11]. Along characteristic lines in the r-t plane given by

$$dr/dt = a, \qquad (D.33)$$

the partial differential equations reduce to

$$d\Delta p^*/dt + (\rho a)d\Delta u/dt = 0 \qquad (D.34)$$

while along lines given by

$$dr/dt = -a \qquad (D.35)$$

they reduce to

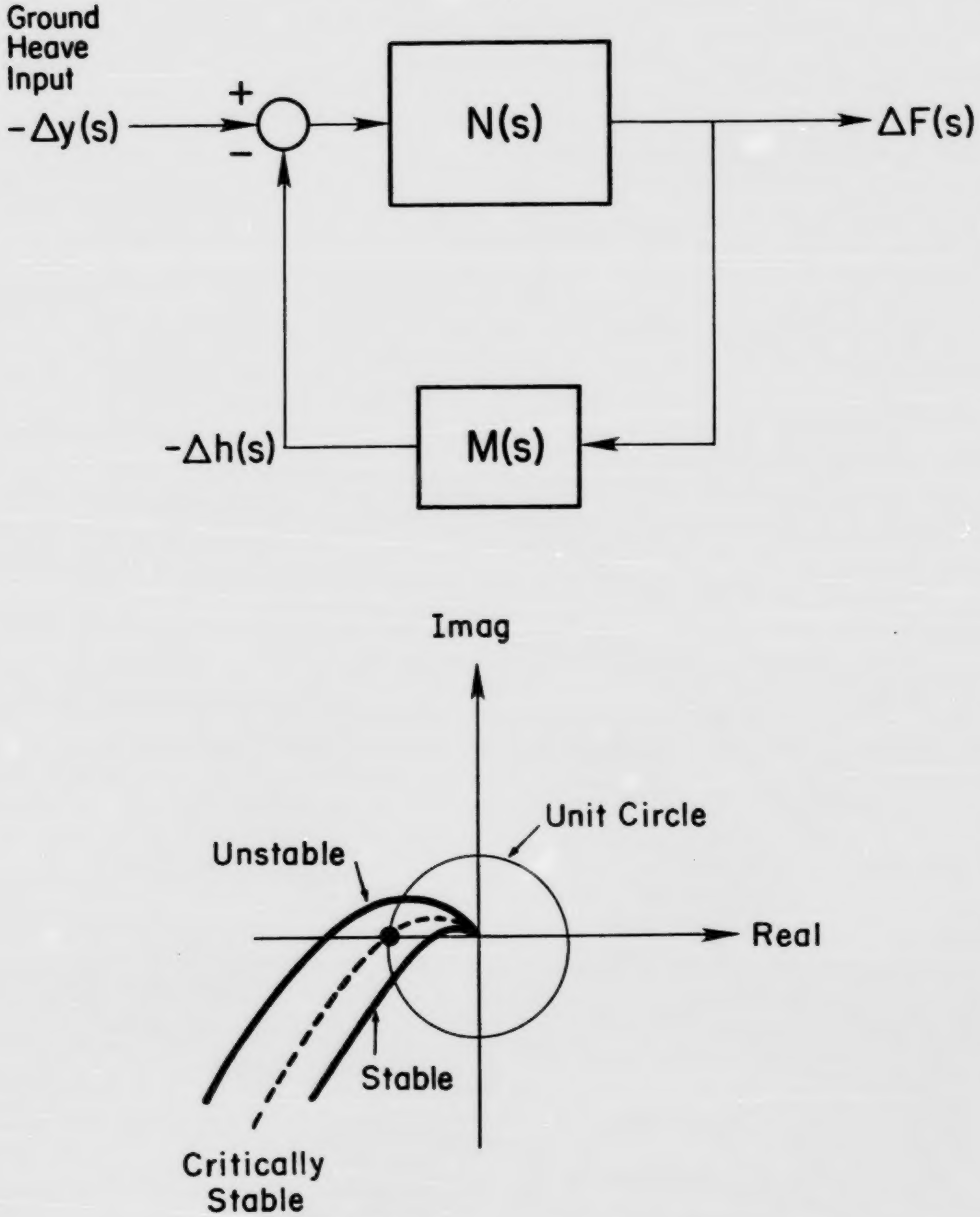
Ground Heave Input
$-\Delta y(s)$
+
−
N(s)
$\Delta F(s)$
M(s)
$-\Delta h(s)$
Imag
Unit Circle
Unstable
Real
Stable
Critically Stable

Figure D.3 Illustration of the Nyquist criteria.

$$d\Delta p^*/dt - (\rho a)d\Delta u/dt = 0 \qquad \text{(D.36)}$$

Numerical integration applied to the ordinary differential equations can be used to relate flow velocities and pressures at a particular time to known values at a preceding time. From the two characteristic lines passing through an interior point P such as that shown in Figure D.4, one obtains [D.11]

$$\Delta u_p = 0.5[\Delta u_R + \Delta u_S + (\Delta p_R^* - \Delta p_S^*)/(\rho a)] \qquad \text{(D.37)}$$

$$\Delta p_P^* = 0.5[\Delta p_R^* + \Delta p_S^* + (\rho a)(\Delta u_R - \Delta u_S)] \qquad \text{(D.38)}$$

At the fan, one has

$$\Delta p_{cf} = C_f \Delta u_f \qquad \text{(D.6)}$$

With Δh known, this equation together with the characteristic equation

$$\Delta u_f - \Delta u_S - (\Delta p_{cf}^* - \Delta p_S^*)/(\rho a) = 0 \qquad \text{(D.39)}$$

allows one to solve for Δu_f and Δp_{cf}. Similarly, at the cushion lip, one has

$$\Delta p_{c\ell} = C_{u\ell}\Delta u_\ell + C_{h\ell}\Delta h \qquad \text{(D.8)}$$

This equation together with

$$\Delta u_\ell - \Delta u_R + (\Delta p_{c\ell}^* - \Delta p_R^*)/(\rho a) = 0 \qquad \text{(D.40)}$$

allows one to solve for Δu_ℓ and $\Delta p_{c\ell}$.

Newton's second law for the air supported mass is given approximately by

$$md^2\Delta h/dt^2 = \sum_{i=1}^{n-1} \pi(r_i + r_{i+1})\Delta r(\Delta p_i + \Delta p_{i+1})/2 \qquad \text{(D.41)}$$

A fourth order Runge-Kutta procedure applied to this was used to obtain Δh step by step in time.

To determine the stability of a particular operating state of the system, the above can be used to obtain the system response following a small disturbance. The logarithmic decrement (see Figure D.5)

$$\delta = \mathrm{Ln}(x_1/x_2) \qquad \text{(D.42)}$$

can then be used to determine the amount of damping present in the system [D.16].

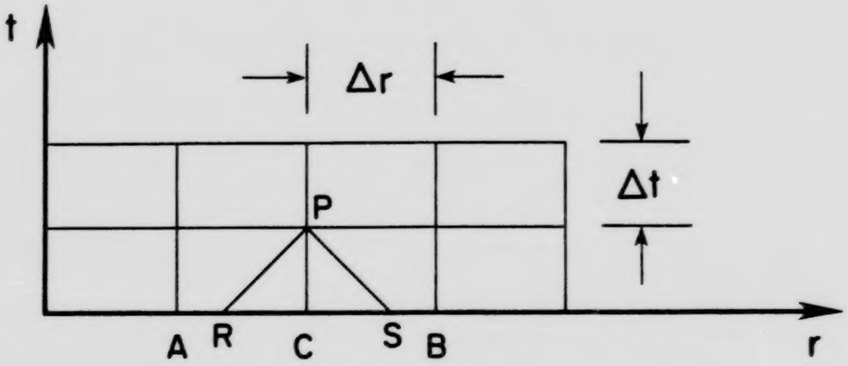
t
Δr
Δt
P
A
R
C
S
B
r

Figure D.4 Characteristic lines in r-t plane

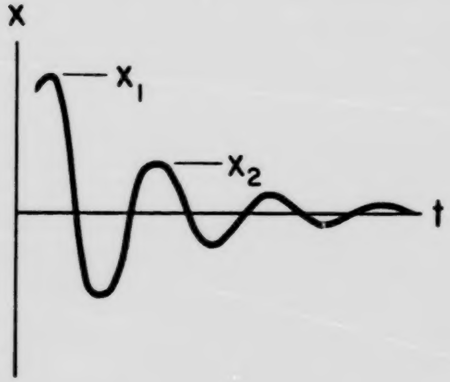

Figure D.5 Schematic of a typical heave response.

D.5 Dynamic Stability Results

To illustrate the effects of acoustic phenomena on dynamic stability characteristics, heave stability boundaries are presented below in terms of the two variables of basic design interest, p_{ce} and h_e. In the plots the boundaries corresponding to a lumped capacitance cushion model and two limiting forms of air supply behaviour are used as reference conditions. The two limiting forms are: a constant pressure source or flat pressure-flow characteristic, for which $C_{pQ} = 0$, and a constant volume flux source or steep characteristic, for which $C_{pQ} = -\infty$. Both of these source models show that, for a given h_e, increasing p_{ce} eventually causes the system to become unstable, and they predict that the pressure at the onset of instability is [D.12]:

$$p_{ce} = (\rho a^2/h_s)\left[1 + (C_{df}^2 A_f^2)/(C_{d\ell}^2 L_p^2 h_e^2)\right](h_e/2) \qquad (D.43)$$

for $C_{pQ} = 0$, and

$$p_{ce} = (\rho a^2/h_s)(h_e/2) \qquad (D.44)$$

for $C_{pQ} = -\infty$. In Equation (D.43), A_f is the area of the feed orifice included to obtain static stability. For all computations the region immediately downstream of the fan was modelled as an orifice with

$$A_f = \pi r_f^2 \qquad (D.45)$$

as its effective area.

Typical results showing an acoustic effect obtained by the method of characteristics are given in Figure D.6. For these $r_\ell = 45.7$ m, $r_f = 1.52$ m, $C_{pQ} = 0$, $h_s = 1.53$ m, $C_{df} = 0.5$ and $C_{d\ell} = 0.61$, the value corresponding to a uniform h_e. The comparison shows that for this geometry acoustic wave propagation has a significant destabilizing effect.

Typical Nyquist plots obtained for $h_e = 15.5$ mm are given in Figure D.7, where the letters "a" and "b" refer to equilibrium points in Figure D.6. The agreement with the characteristics results is qualitatively very good. Note that in the Nyquist plots the vertical scale is greatly exaggerated relative to the horizontal scale; it follows that the phase margin [D.17] for stability is very low. In other words, the system is typically either very lightly damped or very lightly undamped.

Figure D.8 plots the effect of p_{ce} on phase margin, again for $h_e = 15.5$ mm. Note that, even well into the stable region, the phase margin is limited to about 2°. Ideally, for safe operation, the phase margin should be at least 30° [D.17]. Note that for a disturbance to decay to 50% of its initial level, a system with a phase margin of 1° would pass through about 12 cycles of oscillation. Phase margin results for a skirt

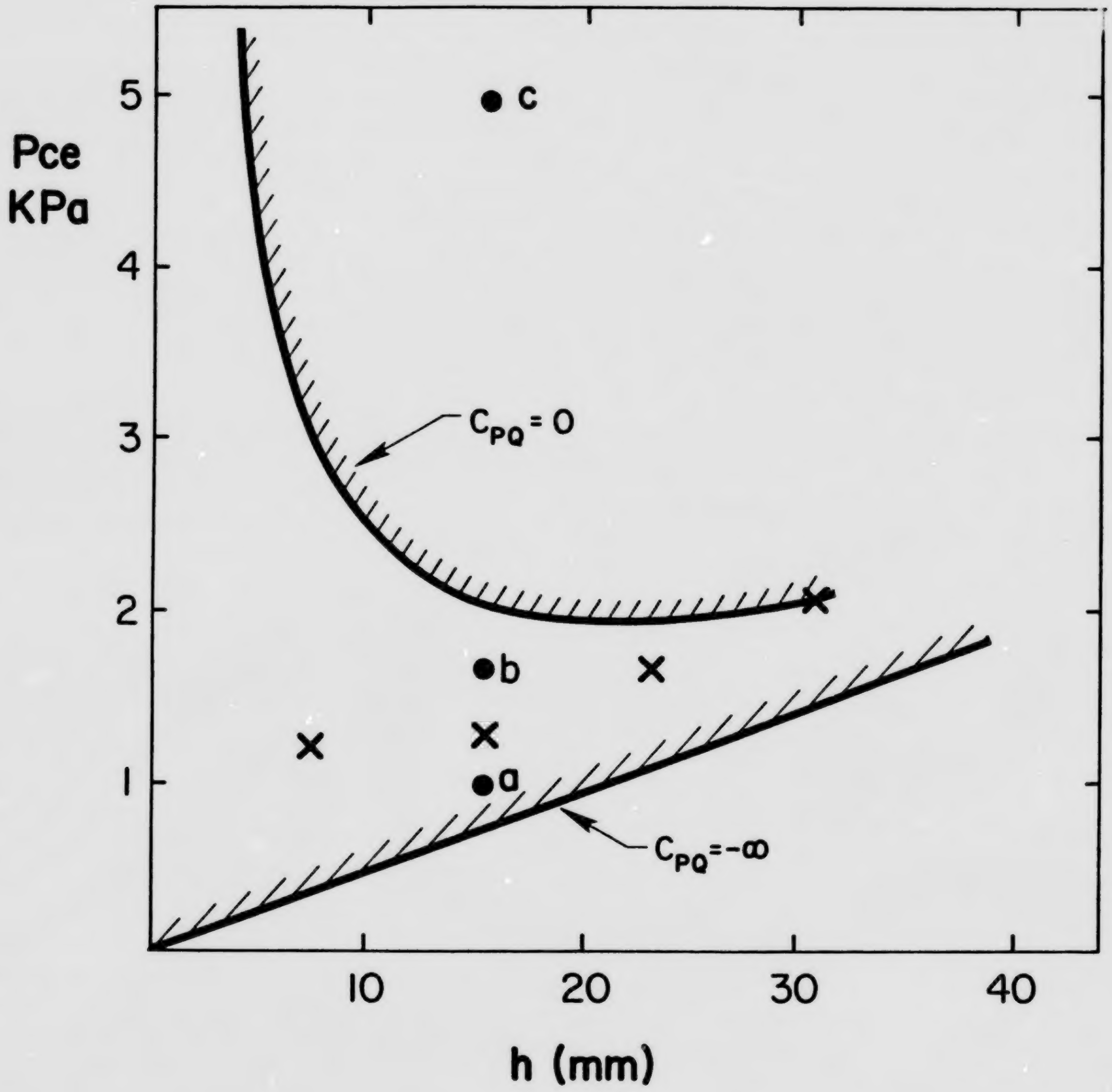

Figure D.6 Typical heave stability results showing an acoustic effect. The feed hole is located centrally. The full line curves were obtained using a lumped capacitance cushion model: Upper curve, $C_{PQ} = 0$; lower curve, $C_{PQ} = -\infty$. The hatched side of the curves are unstable. The acoustic results ($C_{PQ} = 0$) are denoted by the symbol x. They were obtained by applying the log decrement technique to individual responses obtained from the characteristic numerical simulation.

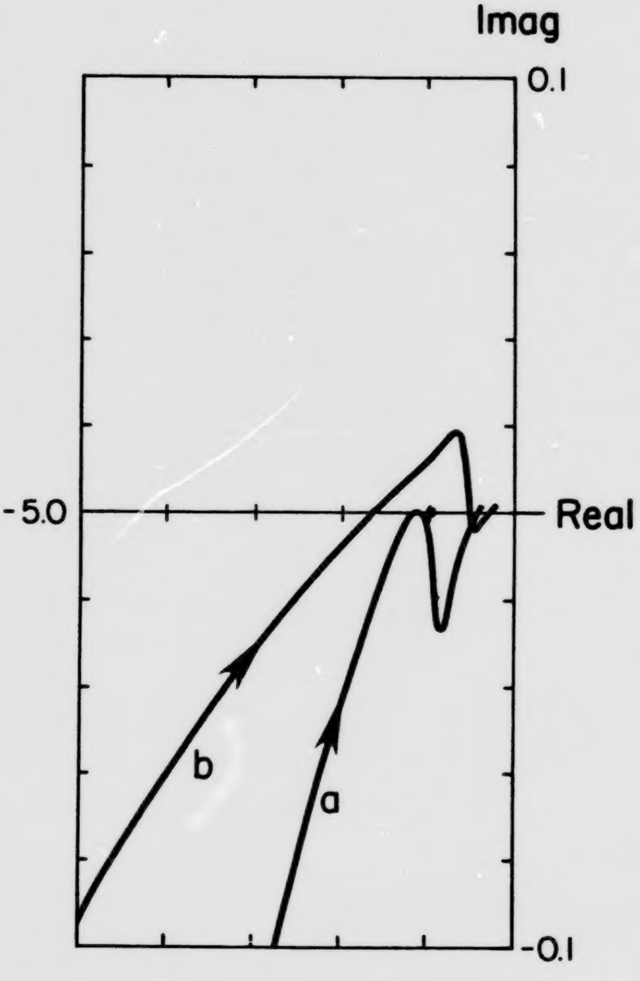

Figure D.7 Nyquist plots for points a and b in Figure D.6. Curve a: P_{ce} = 0.96 kPa; curve b: P_{ce} = 1.68 kPa.

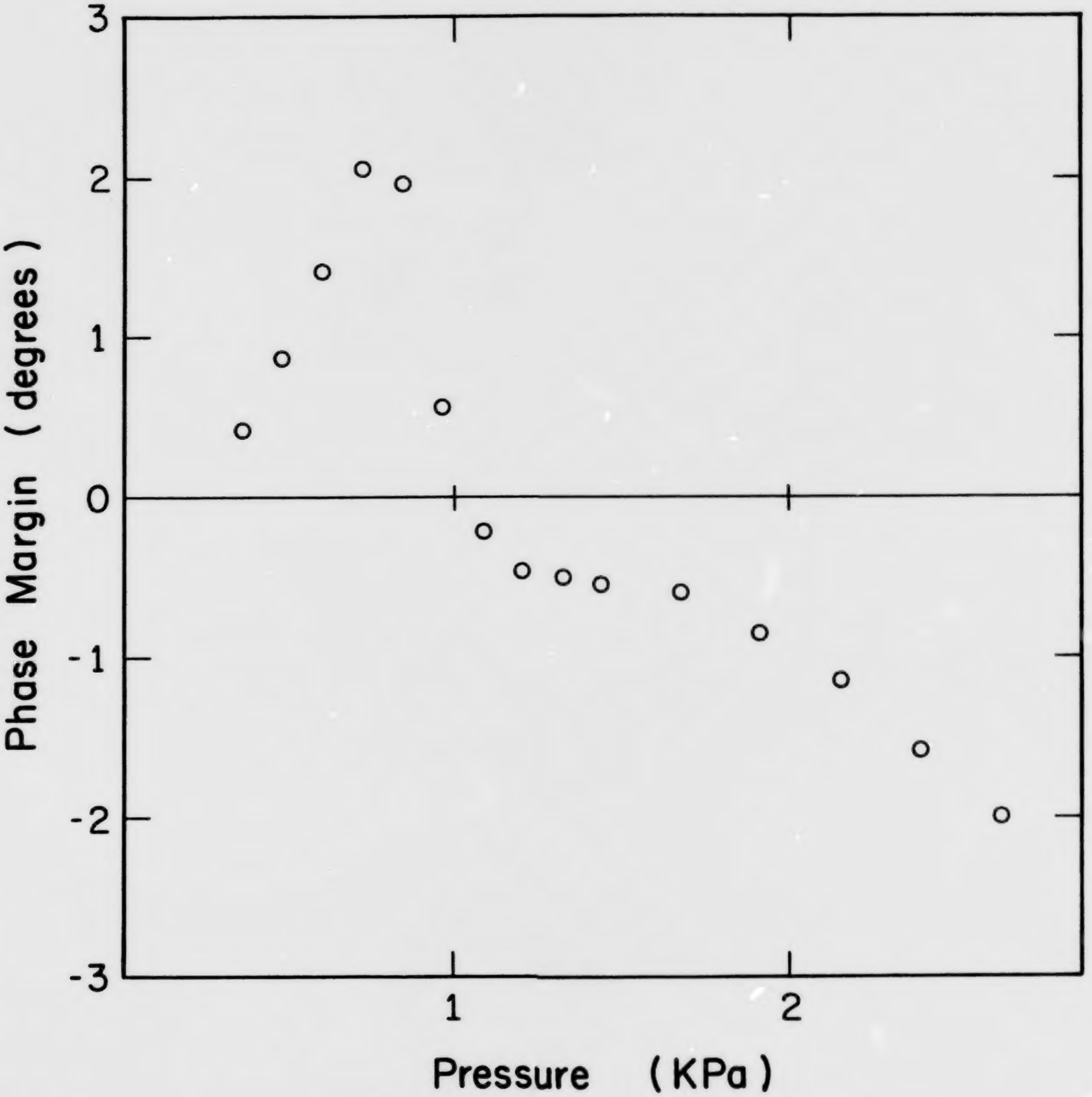

Figure D.8 Phase margin versus P_{ce} for h_e = 15.5 mm in Figure D.6.

which has $C_{d\ell} = 0.20$, which is typical for a segmented skirt in contact with the ground, are presented in Figure D.9. For this case, the lumped capacitance critical pressures are much higher and the acoustic effect is less significant. However, the phase margin is still very low.

The Nyquist plots presented in Figures D.10 and D.11 illustrate the effects of selected geometrical changes. Those in Figure D.10 show that, when the inlet orifice area is quadrupled by doubling r_f with all other dimensions are left unchanged, the acoustic effect is greatly attenuated. When A_f is quadrupled, the lumped capacitance critical pressures are much higher. Thus, for a given pressure in the stable operating regions, the basic phase margin is much higher. Apparently acoustic phenomena cannot counteract this. A similar effect occurs when r_ℓ is reduced. The plots in Figure D.11 show that, when h_e, r_ℓ, and r_f are each increased three-fold while h_s is kept fixed, the acoustic effect becomes more prominent.

The lumped capacitance model predicts that geometrically similar platforms operating at a geometrically similar hovergap would become unstable above the same equilibrium cushion pressure. Figure D.12 shows that this is not necessarily the case when acoustic effects are present. In Figure D.12, 'SF' is a geometric scaling factor.

Finally, Figure D.13 shows that the acoustic effect is greatly attenuated when the air supply is located peripherally instead of centrally. If the cushion air is incompressible, peripheral feed, unlike central feed, would effectively rule out the possibility of an unsteady radial motion of the cushion air mass; this could be the source of the attenuation. Something like this was observed in previous work by two of the present authors [D.12] on the heave stability of a duct plenum system. The incompressible or lumped inertance motion of the slug of fluid in the duct when coupled to the basic cushion, caused an Helmholtz resonator type effect and a large reduction in critical pressure at low hover-gaps. Phase margin results for the annular feed case, given in Figure D.14 for $h_e = 15.5$ mm, show that the phase margin is again very low.

D.6 Discussion

Locating the air supply peripherally instead of centrally appears to attenuate the acoustic phenomena. The impedance analysis for the peripheral case gives

$$\Delta\bar{F}_p(s) = [-(\rho a^2/h_s)(\pi r_\ell^2) + B\zeta(s)]\Delta\bar{h}(s) \tag{D.46}$$

where

$$B = (\rho a^2/h_s + C_h)/[I_o(\eta_\ell) + (C_u/(\rho a))I_1(\eta_\ell)] \tag{D.47}$$

and

$$\zeta(s) = 2\pi \int_0^{r_\ell} r I_o(\eta)\,dr \tag{D.48}$$

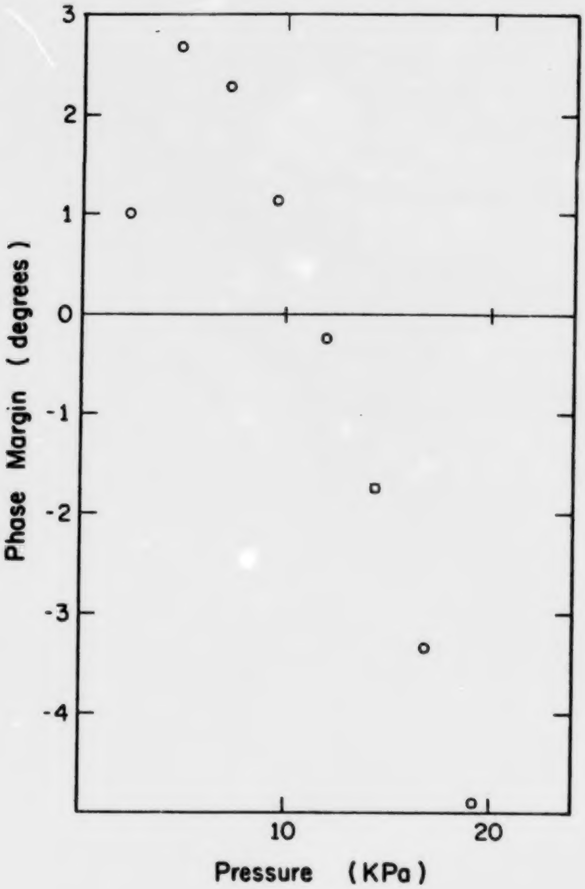

Figure D.9a Phase margin results for a lower lip discharge coefficient, $C_{d\ell} = 0.203$. Hovergap h = 15.0mm, and lumped capacitance critical p_{ce} = 12.6 kPa.

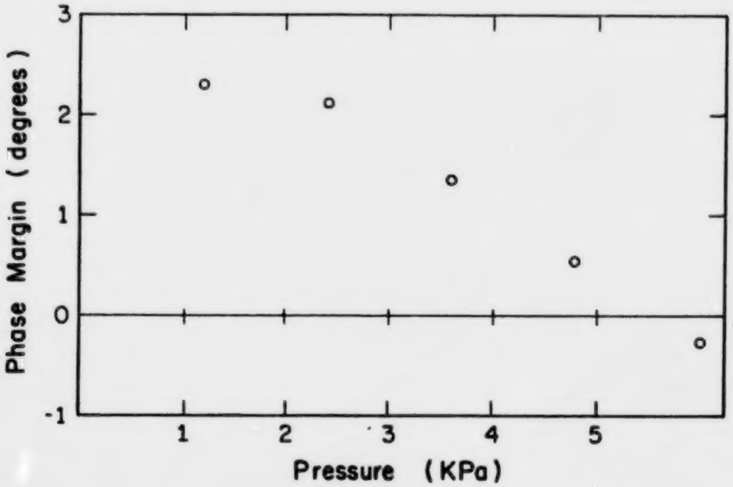

Figure D.9b Phase margin results for $C_{d\ell} = 0.203$ and h = 62.0mm, for which lumped capacitance critical p_{ce} = 5.8 kPa.

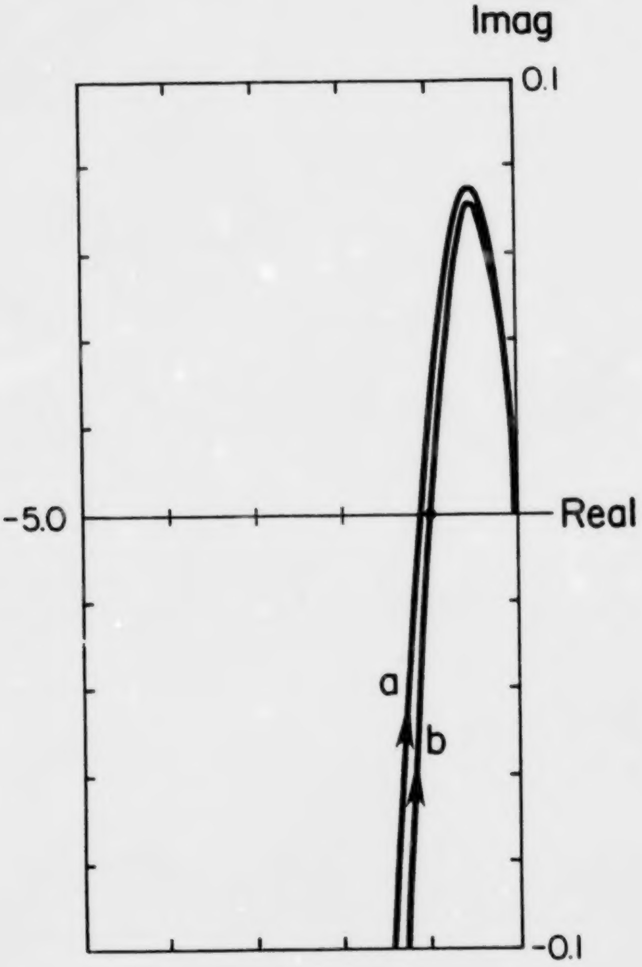

Figure D.10 Nyquist plots for h_e = 15.5 mm showing the effect of quadrupling A_f while holding r_ℓ and h_s fixed. Curve a: P_{ce} = 21.0 kPa; curve b: P_{ce} = 18.9 kPa. The lumped capacitance critical pressure is P_{ce} = 21.0 kPa.

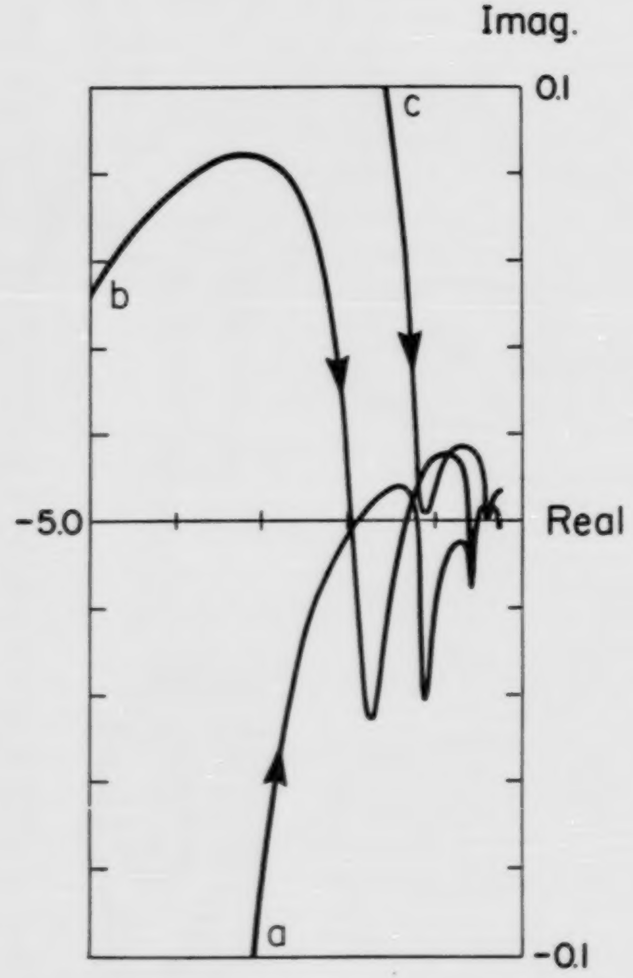

Figure D.11 Nyquist plots for h_e = 46.5 mm showing the effect of tripling r_f and r_ℓ while holding h_s fixed. Curve a: P_{ce} = 6.0 kPa; curve b: p_{ce} = 4.0 kPa; curve c: p_{ce} = 6.0 kPa. The lumped capacitance critical pressure is P_{ce} = 6.0 kPa.

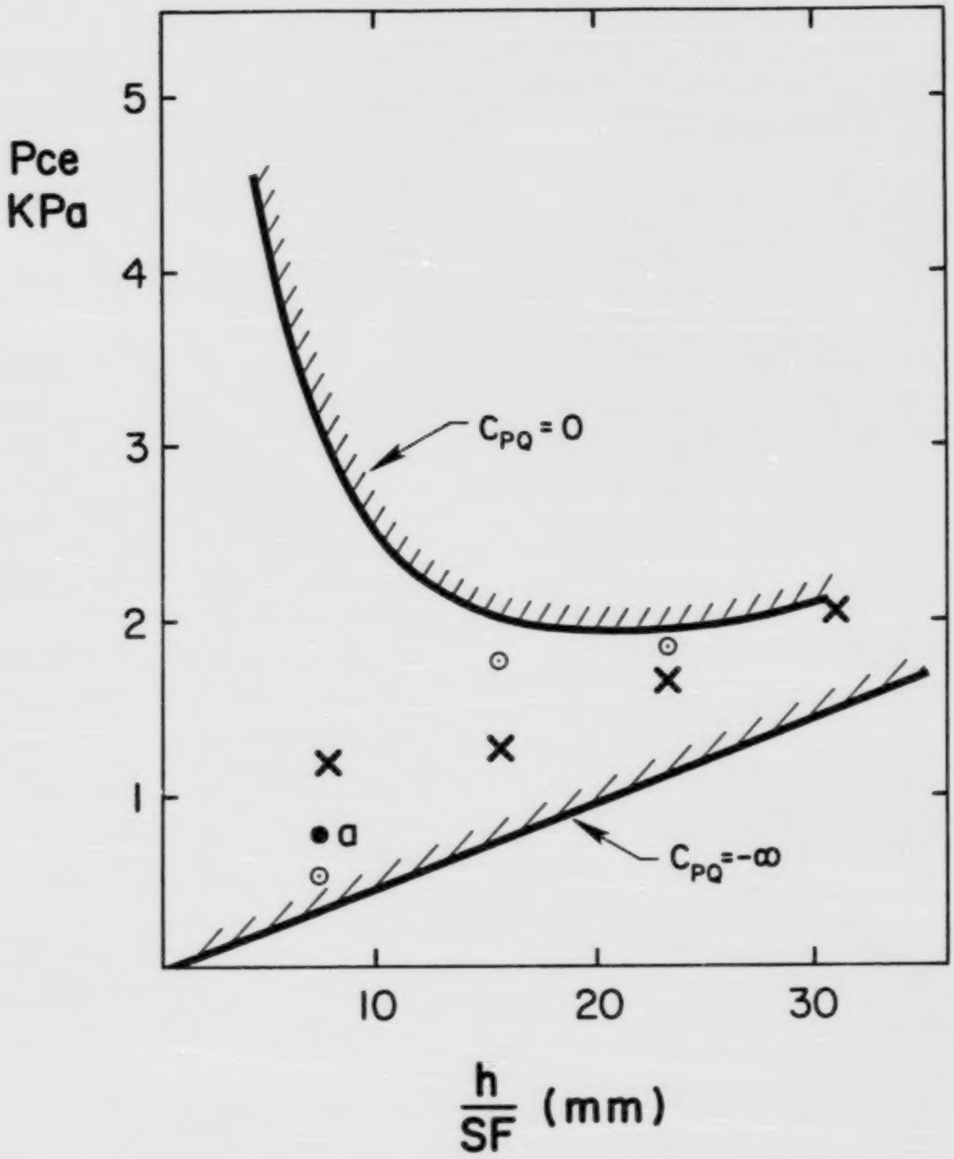

Figure D.12a Acoustic results showing lack of scaling. As for previous results, the full line curves were obtained using a lumped capacitance cushion model. The acoustic results ($C_{PQ} = 0$) are denoted by x for SF = 1 and by 0 for SF = 2.

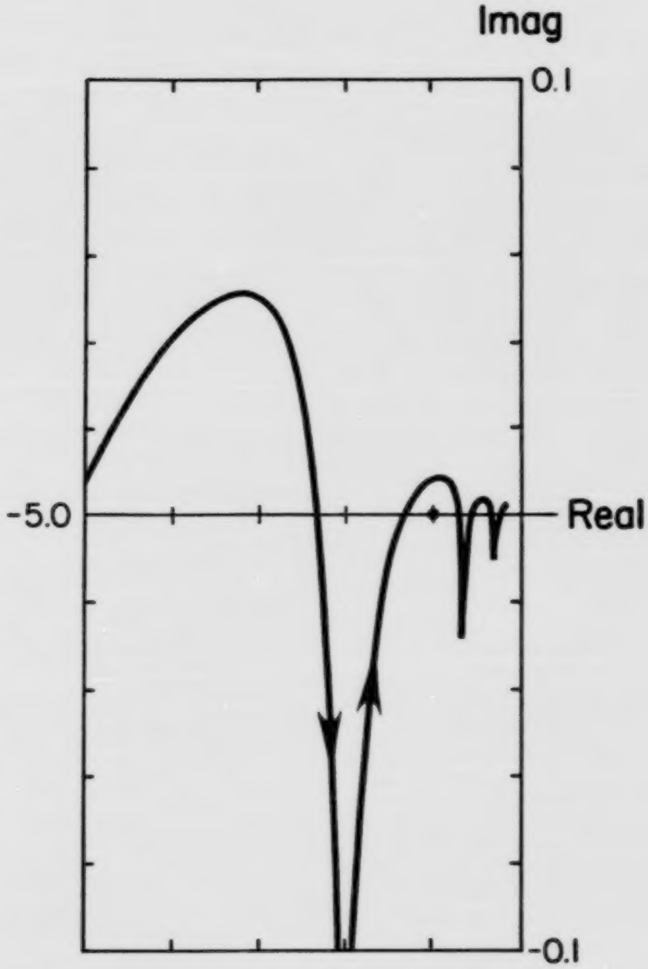

Figure D.12b Nyquist plot for SF = 2 geometry for operating point "a" in Figure D.12a.

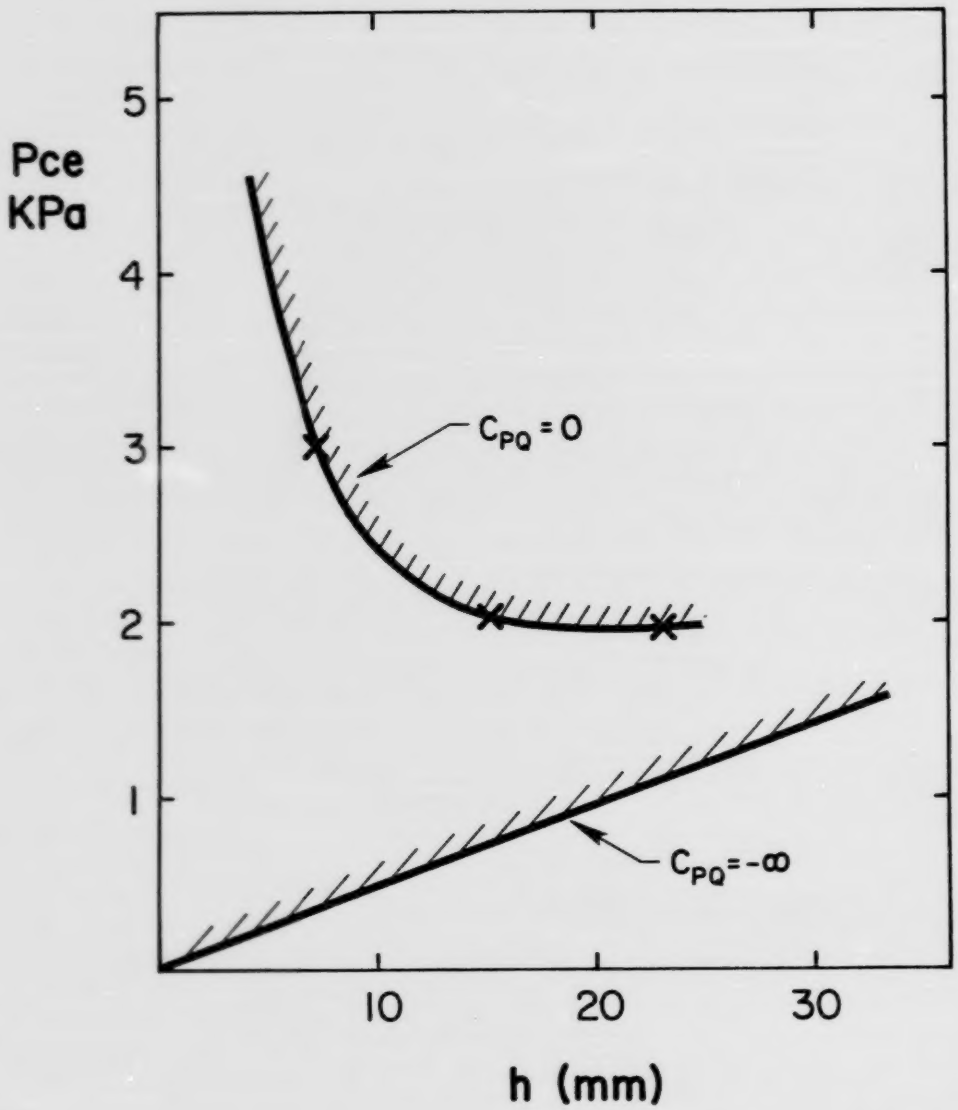

Figure D.13 Typical stability results for annular air supply duct located peripherally. As before the full line curves were obtained using a lumped capacitance cushion model. The acoustic results (C_{PQ} = 0) are denoted by the symbol x.

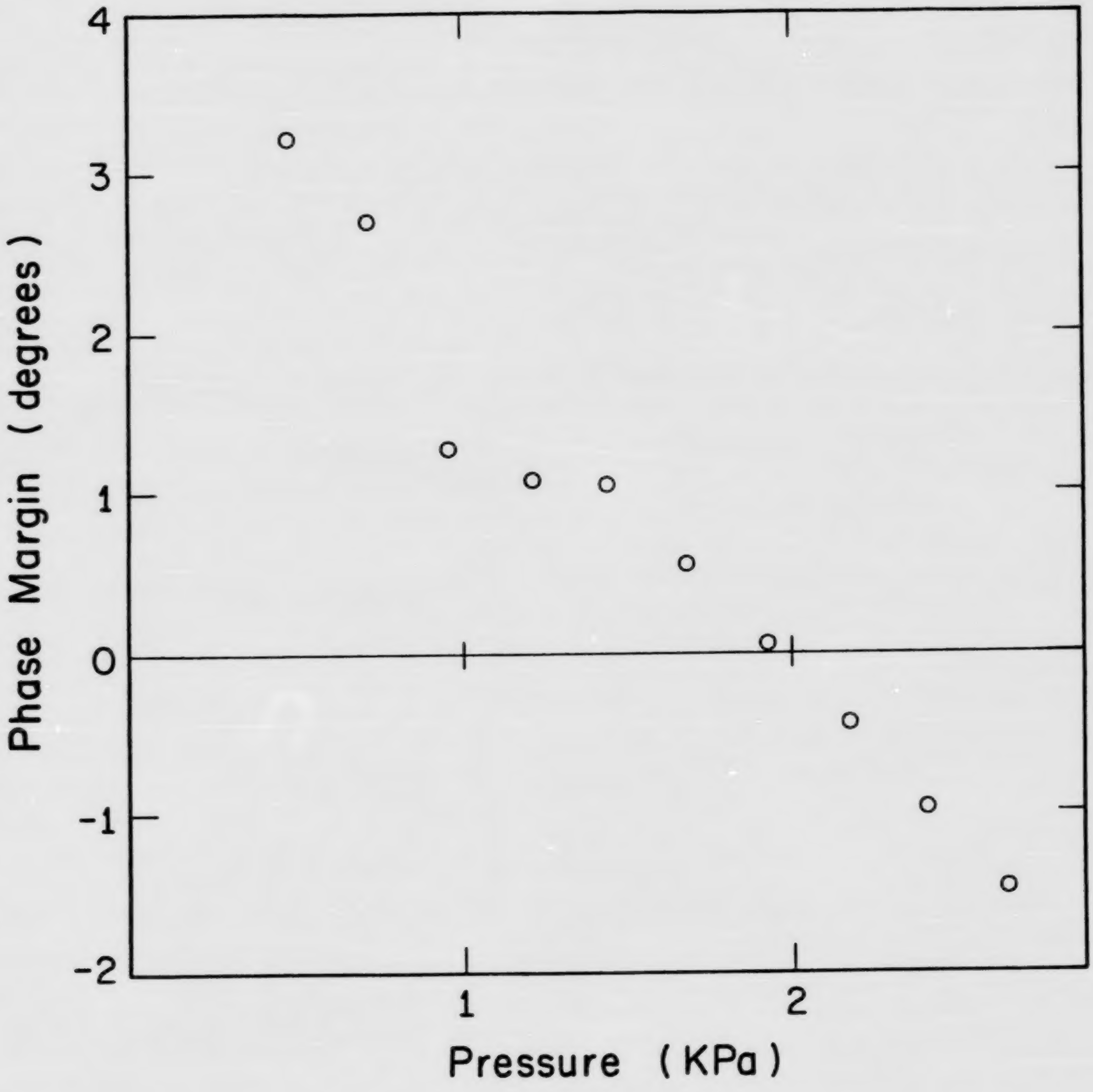

Figure D.14 Phase margin versus p_{ce} for h_e = 15.5 mm in Figure D.13.

where in terms of the usual orifice flow resistances

$$C_u = [R_\ell R_f/(R_\ell + R_f)](2\pi r_\ell h_s)$$

$$C_h = -[R_\ell R_f/(R_\ell + R_f)]/\alpha_h \tag{D.49}$$

where

$$R_\ell = 2p_{ce}/Q_e, \qquad R_f = 2(p_f - p_{ce})/Q_e \tag{D.50}$$

and

$$\alpha_h = h_e/Q_e \tag{D.51}$$

Upon performing the integration in (D.48), one obtains

$$\zeta(s) = 2\pi(a^2/s^2)\eta_\ell I_1(\eta_\ell) \tag{D.52}$$

and the product $B\zeta(s)$ reduces to

$$B\zeta(s) = \frac{(\rho a^2/h_s + C_h)\ 2\pi(a^2/s^2)\ \eta_\ell I_1(\eta_\ell)}{I_0(\eta_\ell) + (C_u/(\rho a))I_1(\eta_\ell)} \tag{D.53}$$

The lead-lag characteristics of $\Delta\bar{F}_p(s)$ are controlled by those of the imaginary part of the product $B\zeta(s)$. Letting $s = i\omega$ in this product shows that acoustic phenomena only modulate phase characteristics. They do not for example cause a lag to become a lead or vice versa. This is because with $s = i\omega$, $I_0(\eta_\ell)$ is purely real while $I_1(\eta_\ell)$ is purely imaginary, and manipulation shows that the Bessel function terms only scale the imaginary part of $B\zeta(s)$ by a factor which never changes sign. However, at certain pressures, where the heave oscillation frequency is such that $I_1(\eta_\ell) = 0$, they would cause the system to become critically stable. The lead-lag characteritics are determined by the sign of the factor

$$\frac{\rho a^2}{h_s} + C_h \tag{D.54}$$

This is the same factor that controls the lead-lag characteristics in a lumped capacitance model. Thus, it is not surprising that acoustic effects appear attenuated.

Low phase margin implies that nonlinear phenomenon could dominate. For example, nonlinearities could limit the amplitude of limit cycle oscillations in a linearly unstable operating region to such an extent that the system operation is not adversely affected by their presence: the system in this case is said to be practically stable. One major nonlinearity considered previously by two of the present authors is the square root dependence of the outflow on cushion pressure coupled to a varying gap [D.9]. Another is the abrupt flow shut-off which occurs when the flexible skirt makes contact with the ground. In [D.9], these were shown to generate limit cycles in linearly unstable operating regions. The low phase margin could make stability boundaries very difficult to define experimentally. Also, it could make phenomena such as skirt-ground contact hysteresis very important. This would be especially true for segmented systems because they rely on ground contact to maintain pitch and roll static stability. Observations sugget that hysteresis results from the ability of the skirt material to sustain small compression loads when being pushed onto the ground, and no load when moving away from the ground [D.19]. Some preliminary results from a nonlinear version of the characteristics program are given in Figure D.15. These are for the operating point marked "c" in Figure D.6. They show that a modest amount of skirt hysteresis can be quite beneficial. When moving downward, the skirt was allowed to support 5.0% of the vehicle weight.

Finally, the natural frequency in heave can be estimated by ignoring the flow into and out of the cushion. By using a lumped pneumatic capacitance cushion model with $s = i\omega$, one obtains from Newton's second law

$$-m\omega^2 \Delta h = S_a \Delta p_c \tag{D.55}$$

and, since the mass in the cushion is assumed fixed

$$(S_a h_s)/(\rho a^2) \Delta p_c = -S_a \Delta h \tag{D.56}$$

Manipulation of these equations yields the following equation for frequency

$$\omega^2 = (\rho a^2/h_s)(g/p_{ce}) \tag{D.57}$$

For the geometry of Figure D.6 this formula gives for the typical operating point, h_e = 15.5 mm with p_{ce} = 1.42 kPa, $f = \omega/2\pi$ = 4.04 Hz. The oscillation frequency obtained from the method of characteristics numerical simulation applied to this state is approximately 4 Hz and this is independent of the air supply configuration. Thus the system is apparently just a mass on a simple air spring; the boundary conditions have little effect on the oscillation frequency. This could be the source of the low phase margin.

D.7 Conclusions

The results presented have shown that acoustic phenomena can destabilize large air cushion platforms. Also, even when stable, large cushions have typically very low phase margin. The nonlinear simulation suggests that the latter might be avoided if there is sufficient static hysteresis in the skirt. In fact, hysteresis can stabilize the system. An important point to note is that the lumped capacitance model also predicts low phase margin. Thus low phase margin is not an acoustic phenomenon, and the shape of the planform is not a controlling factor. In practice, some

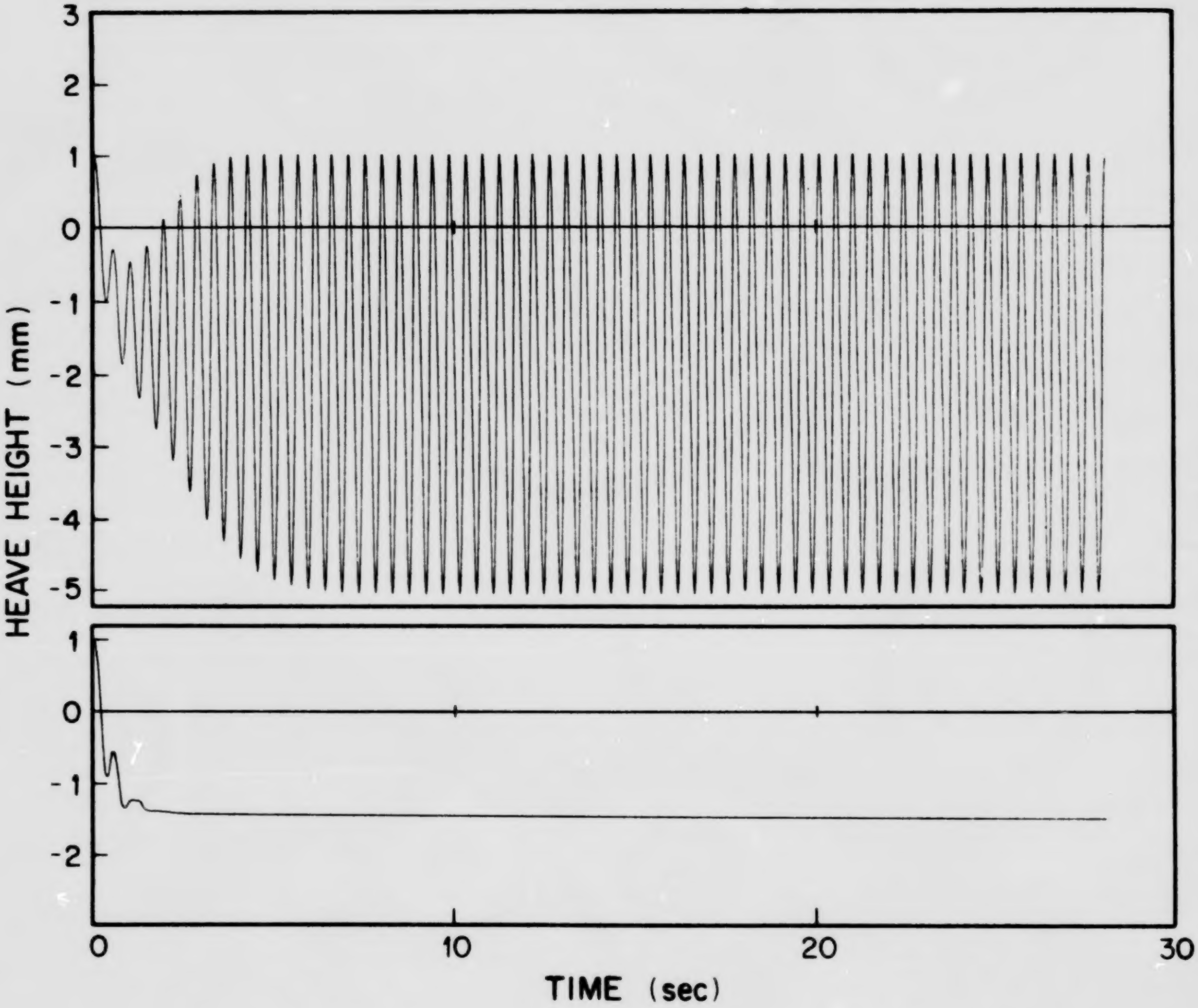

Figure D.15 Nonlinear simulation results for point "c" in Figure D.6. Upper curve, no hysteresis; lower curve, 5.0% hysteresis.

form of secondary suspension might have to be added to overcome this problem if skirt hysteresis is not sufficient.

Although the work has so far been limited to axisymmetric geometries subject to axisymmetric disturbances, the conclusions generated have much broader implications. Besides the removal of these limitations, one might, in any future work, also want to consider the effects of skirt flexibility, supply ducting, and the details of the flow immediately downstream of the fan.

REFERENCES - APPENDIX D

D.1 Wade, R., Canadian Coast Guard: Air Cushion Technology Group, Private Communication, 1982.

D.2 Laframboise, J., Transport Canada, Transportation Development Centre, Montreal, Private Communication, 1982.

D.3 Fowler, H. S., "On the Lift-Air Requirement of Air Cushion Vehicles and Its Relation to the Terrain and Operational Mode", National Research Council of Canada, Division of Mechanical Engineering, Report ME 246, 1979.

D.4 "Sohio Petroleum Examining Hover Platforms", Bulletin of the Hovercraft Society, London, August Issue, 1982.

D.5 Sullivan, P. A., Hinchey, M. J., Hartmann, P. V., Dupuis, A., Green, G. M., and Graham, T. A., "Research Into Air Cushion Stability: 1979 Report", Transport Canada, Montreal, Report TP3109E, Jan. 1982.

D.6 Ribich, W. A. and Richardson, H. H., "Dynamic Analysis of Heave Motion for a Transport Vehicle Fluid Suspension", Massachusetts Institute of Technology, Report DSR 76110-3, 1967.

D.7 Graham, T. A., Sullivan, P. A. and Hinchey, M. J., "Skirt Material Effects on Air Cushion Dynamic Heave Stability", Journal of Aircraft, Vol. 22, No. 2, Feb. 1985, pp. 101-108.

D.8 Drazin, P. G. and Reid, W. H., Hydrodynamic Stability, Cambridge University Press, Cambridge, 1981, see p. 155.

D.9 Hinchey, M. J. and Sullivan, P. A., "A Theoretical Study of Limit Cycle Oscillations of Plenum Air Cushions", Journal of Sound and Vibration, Vol. 79, No. 1, 1981, pp. 61-77.

D.10 Hinchey, M. J., Sullivan, P. A. and Dupuis, A. D., "Wave Propagation Effects on the Heave Dynamics of Large Air Cushion Platforms", University of Toronto, Institute for Aerospace Studies, Technical Note No. 234, 1981.

D.11 Wylie, E. B. and Streeter, V. L., Fluid Transients, McGraw-Hill, New York, 1978, see p. 31.

D.12 Sullivan, P. A., Hinchey, M. J. and Green, G. M., "A Review and Assessment of Methods for the Prediction of the Dymamic Stability of Air Cushions", Journal of Sound and Vibration, Vol. 84, No. 3, 1982, pp. 337-358.

D.13 Hilderbrand, F. B., Advanced Calculus for Applications, Prentice Hall, Englewood Cliffs, New Jersey, 1962, see p. 465.

D.14 Kinsler, L. E. and Frey, A. R., Fundamentals of Acoustics, John Wiley & Sons, New York, 1962, see pp. 86-97.

D.15 Fung, Y. C., An Introduction to the Theory of Aeroelasticity, Dover Publications, New York, 1964, see p. 168.

D.16 Thomson, W., Vibration Theory and Applications, Prentice Hall, Englewood Cliffs, New Jersey, 1965.

D.17 Harrison, H. L. and Bollinger, J. G., Introduction to Automatic Controls, International Textbook, Scranton, Pennsylvania, 1969, see pp. 217-219.

D.18 Davis, S. A., Feedback and Control Systems, Simon and Schuster, New York, 1974.

D.19 See Appendix E.

APPENDIX E. HEAVE STIFFNESS HYSTERESIS MEASUREMENTS ON A LARGE SCALE AIR CUSHION (T. A. Graham, P. A. Sullivan and M. J. Hinchey)

Roman

A_{base}	craft hard structure base area
B	craft hard structure width
C_M	roll moment coefficient = $M/W_{eq}B$
C_{MP}	pitch moment coefficient = $N/W_{eq}L$
C_{QC}	cushion flow coefficient = $Q_c\{\rho/(2W_{eq}A_{base})\}^{1/2}$
C_{PC}	cushion pressure coefficient = p_c/P_{atm}
C_{SC}	local fan slope coefficient
C_{ST}	skirt thickness coefficient = t/B for roll, = t/L for pitch
C_{SW}	skirt weight coefficient = $\sigma_s A_{base}/W_{eq}$
E	Young's modulus of elasticity
g	gravitational acceleration
h	height of vehicle centre of mass
L	vehicle base length
m	vehicle mass
M	roll moment
N	pitch moment
P_{atm}	atmospheric pressure
p_c	cushion pressure (gauge)
Q_c	cushion flow
t_s	skirt thickness
w_s	skirt surface density (kg/m^2)
W_{eq}	vehicle weight = mg

Greek

α	roll angle
σ	skirt weight per unit area
ρ	cushion air density
θ	pitch angle

Abbreviations

BHC	British Hovercraft Corporation
HSC	Hard Surface Contact
HSL	Hovercraft Systems Limited
UTIAS	University of Toronto, Institute for Aerospace Studies

E.1 Introduction

Model scale ACV testing at UTIAS has revealed that commonly used types of skirt systems exhibit hysteresis in their roll and pitch stiffness curves [E.1-E.5]. The hysteresis is associated with skirt-ground contact and can be caused by sliding friction, venting effects, and the ability of the skirt material to sustain small compression loads. Cushion pressure measurements described in [E.4], together with analytic computations of footprint area indicate that the load carried by multicell skirts ranges from 2.5 to 6% for roll angles from 0.5° to 4.5°. This was estimated to alter the roll moment C_M by about 1.5%. For segmented skirt designs, roll and pitch hysteresis associated with skirt load carrying has been found to be typically in the order of 1% to 3%, although it is effectively zero in some cases. In addition, it has been found to make a significant contribution to system damping in model tests [E.3]. An obvious question is, "Does significant hysteresis occur at full scale?" If it does, it represents an important source of damping that should be exploited. If it does not, then it suggests that skirt systems have not been scaled properly. This appendix presents and discusses results of model tests on multicell and segmented skirt systems as well as some full scale measurements of heave hysteresis in an air cushion ice breaker bow platform (ACIB) (shown in Figure E.1), currently being developed in Canada.

E.2 Model Scale Hysteresis

Measurements of pitch and roll stiffness characteristics made on models at UTIAS indicate that hysteresis is present in both the segmented and multicell types of skirt design [E.1-E.5], shown in Figures E.2 and E.3 respectively. Most of the tests were performed on multicell and Hovercraft Systems Ltd. (HSL) segmented skirt systems which were fitted to a 1.22 m × 1.44 m plenum base. In addition a 0.63 m × 1.25 m "two cell" cushion consisting of two cells from a multicell cushion was studied. The air supply and other aspects of the laboratory test facilities are given in [E.4 and E.5]. The tests themselves consisted of simply moving calibrated weights from one side or end of the model to the other. With the moment thus applied it and the resulting angle were recorded. Data were taken for both the roll-down and the return cycle, and in general the aforementioned hysteresis was observed.

Hysteresis is clearly associated with skirt-ground contact. This is demonstrated by the data shown in Figures E.4 and E.5, which give measured roll stiffnesses for a multicell cushion at two different equilibrium flow rates. On the roll-moment increasing portion of the cycle, the curves display the characteristic "two-slope" behaviour of multicell systems hovering over a solid surface. That is, for small roll angles and before skirt-ground contact occurs, owing to modulation of the pressure in the cell, the cushion is very stiff. At a certain roll angle, after skirt-ground contact first occurs the flow is effectively shut-off, and no further pressure modulation occurs. The stiffness is then greatly decreased since it is associated purely with the cell taper. For the data in Figure E.5, in which the flow at zero roll angle is 62% higher than that in Figure E.4, as one would expect, transition to the second slope occurs at much

Figure E.1 Transportation Development Centre's 24.7 m × 24.7 m 270 tonne icebreaker bow.

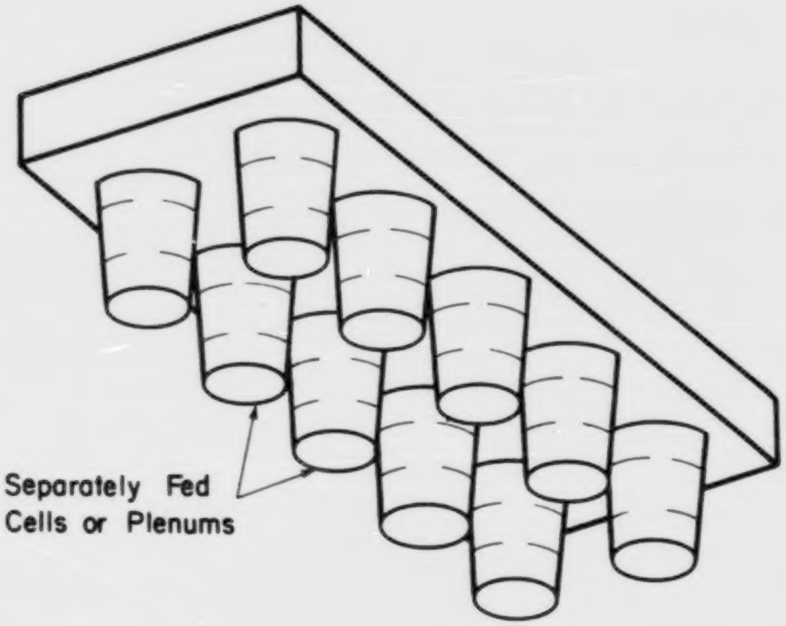
Separately Fed
Cells or Plenums

Figure E.2 Multicell cushion - schematic.

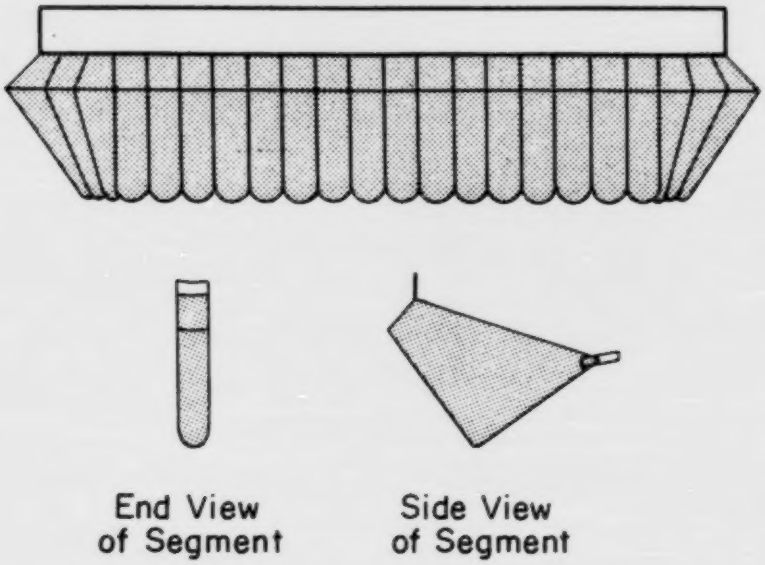

End View
of Segment

Side View
of Segment

Figure E.3 Segmented-skirt cushion - schematic.

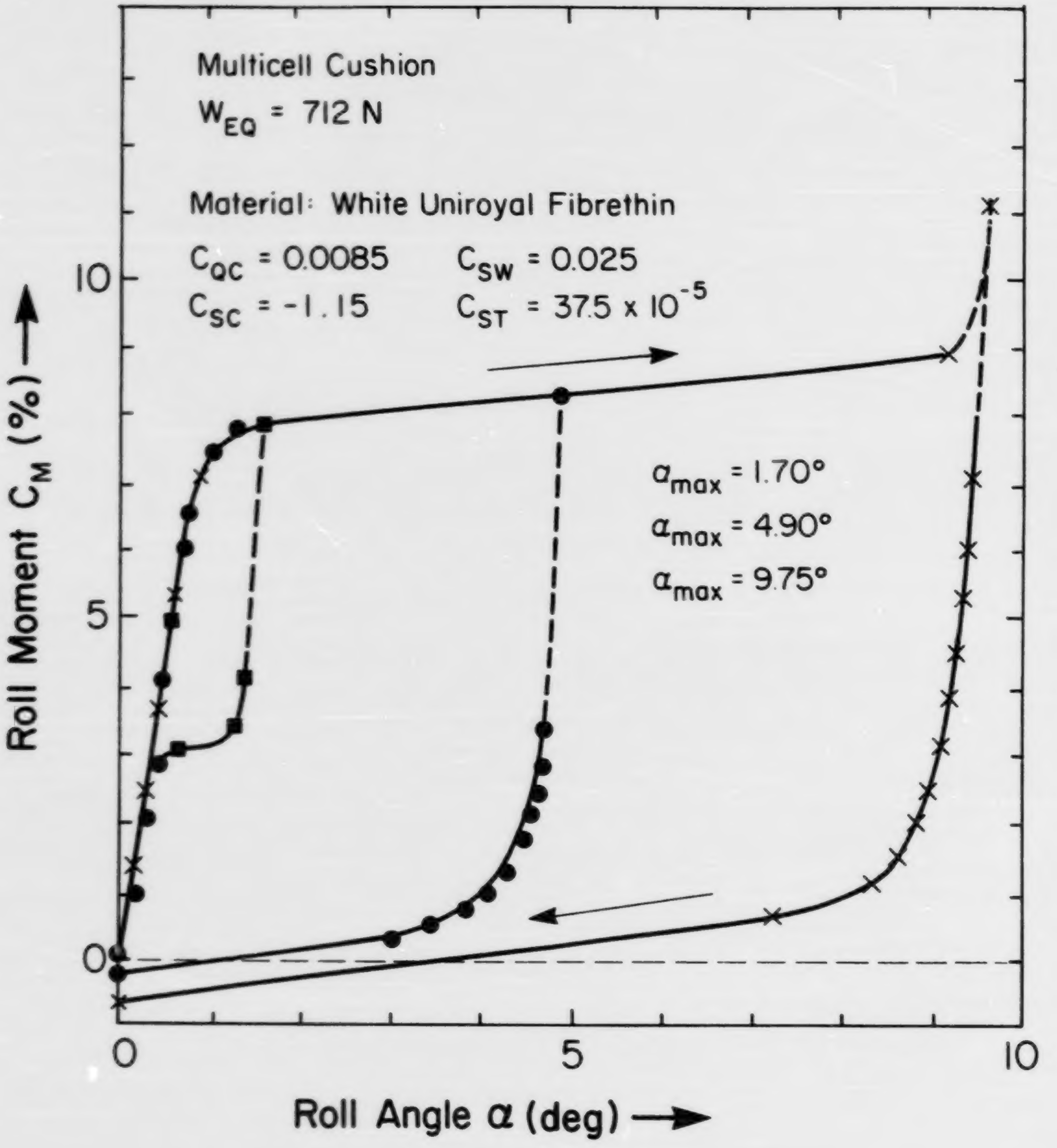

Figure E.4 Roll hysteresis for multicell cushion at various values of maximum roll angle.

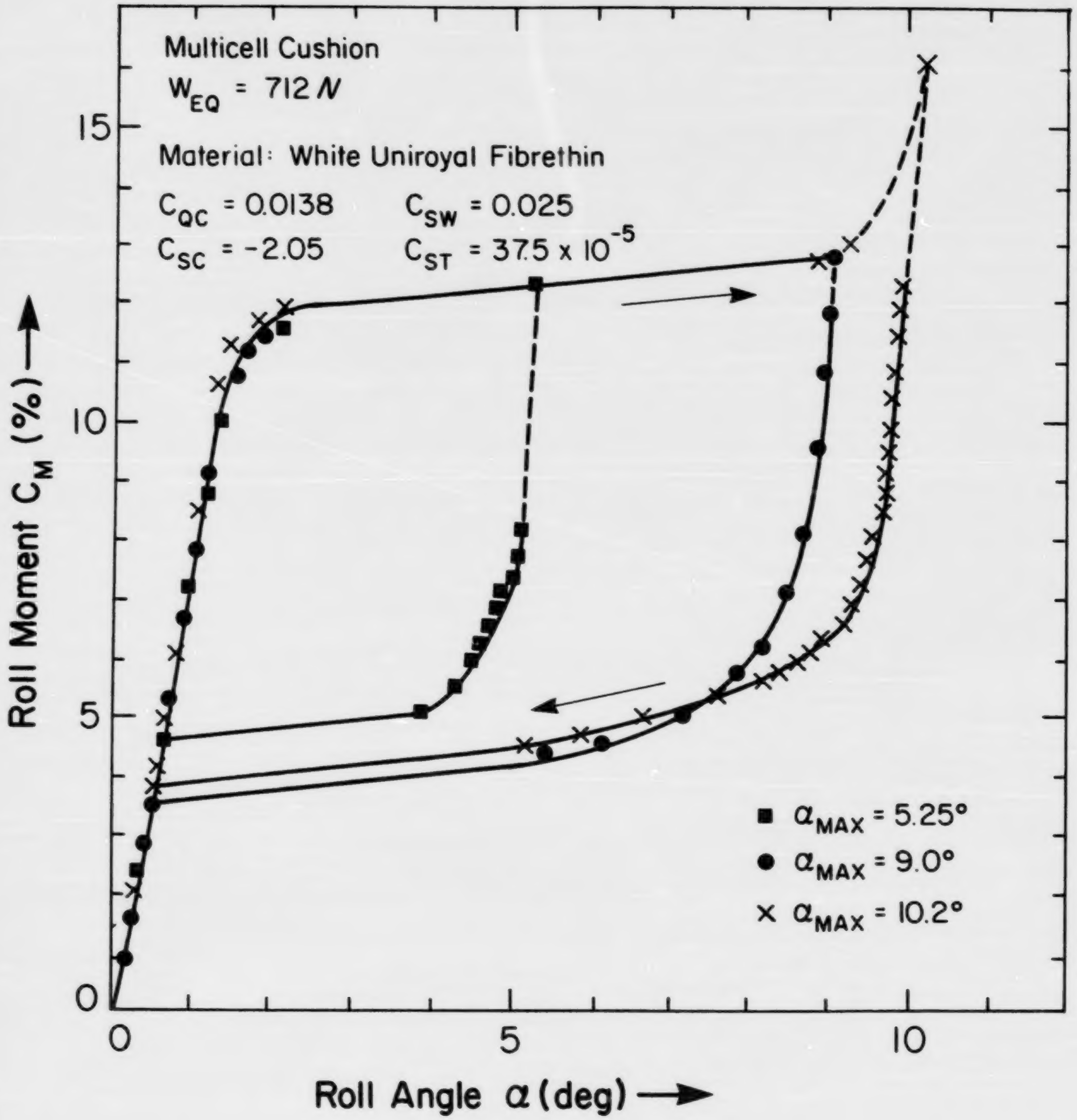

Figure E.5 Roll stiffness for a multicell cushion at various values of maximum roll angle, and for Q_c 62% higher than that in Figure E.4.

higher value of C_M and α. For the return portion of the cycle the loss in C_M is roughly the same in both cases so that in Figure E.5 the cessation of hysteresis occurs at higher values of C_M and α. Similar results have been obtained on other cushion systems [E.4, E.5].

Sliding friction between the skirt and ground can be a source of hysteresis. Figures E.6 and E.7 show results for the cushion consisting of just two conical cells and the segmented skirt. In these tests the ground surface was supported on a compliant surface air bearing system which could be activated to allow motion of the ground board. Thus the ground board would move with the model, providing greatly reduced friction resistance. The results of Figure E.6 show that sliding friction with the normal surface roughness has little or no effect on the roll characteristic. They do, however, show an increase in hysteresis when the fixed ground is made abrasive by the attachment of garnet paper to the ground surface. Figure E.7 shows that the segmented skirt system exhibits hysteresis due to friction when the skirt material is polyethylene, but the corresponding result for the nylon-urethane skirt, shown in cross hatching, shows no difference due to friction in the roll characteristic. The effect of the friction on the polyethylene is to increase both the mean slope and the amount of hysteresis. In fact almost 40% of the hysteresis for the polyethylene skirt with the ground fixed is due to friction. Thus friction can contribute to the amount of hysteresis but does not account for it all, since significant hysteresis remains for all of the results in Figures E.5, E.6 and E.7.

Table E.1

Model Skirt Materials

	Reference Name	Description
1.	Nylon-urethane	Woven nylon fabric coated one side with urethane; t_s = 0.102 mm; w_s = 0.075 kg/m^2
2.	Polyethylene	Extruded polyethylene sheet; t_s = 0.127 mm; w_s = 0.12 kg/m^2
3.	"White"	Uniroyal Fiberthin woven fabric coated with rubber on both sides. t_s = 0.457 mm; w_s = 0.061 kg/m^2
4.	"Blue"	Woven fabric coated with rubber on one side, t_s = 0.229 mm; w_s = 0.245 kg/m^2

The ability of the skirt structure to sustain small compressive loads is another important cause of hysteresis. Figures E.7, E.8 and E.9 give comparative test results for several materials which are described in Table E.1. In all cases the amount of hysteresis is reduced with thinner, lighter materials. The structural forces depend on both the modulus and the thickness of a material so that for a given modulus thinner materials should

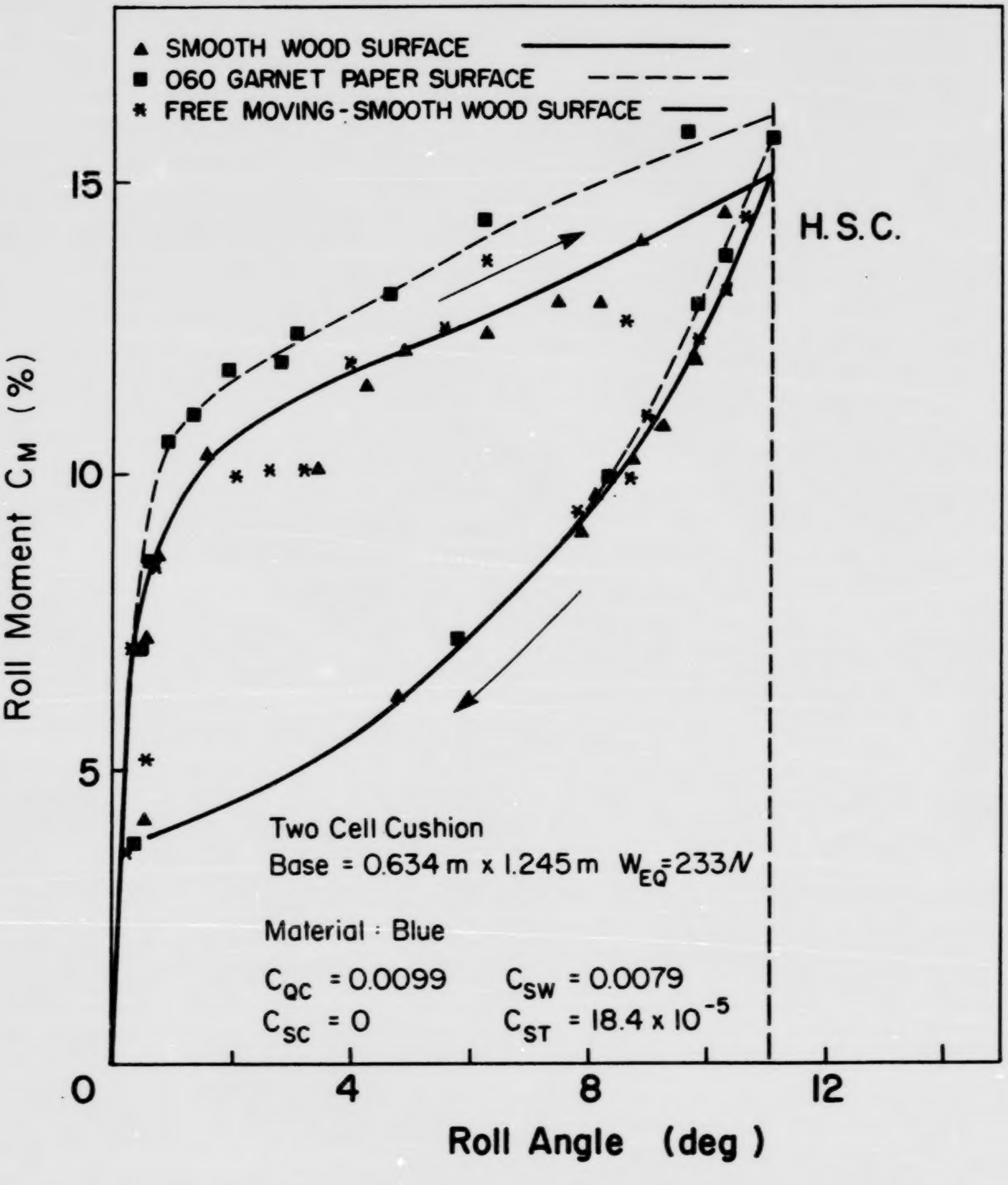

Figure E.6 Friction effect on hysteresis with blue skirt.

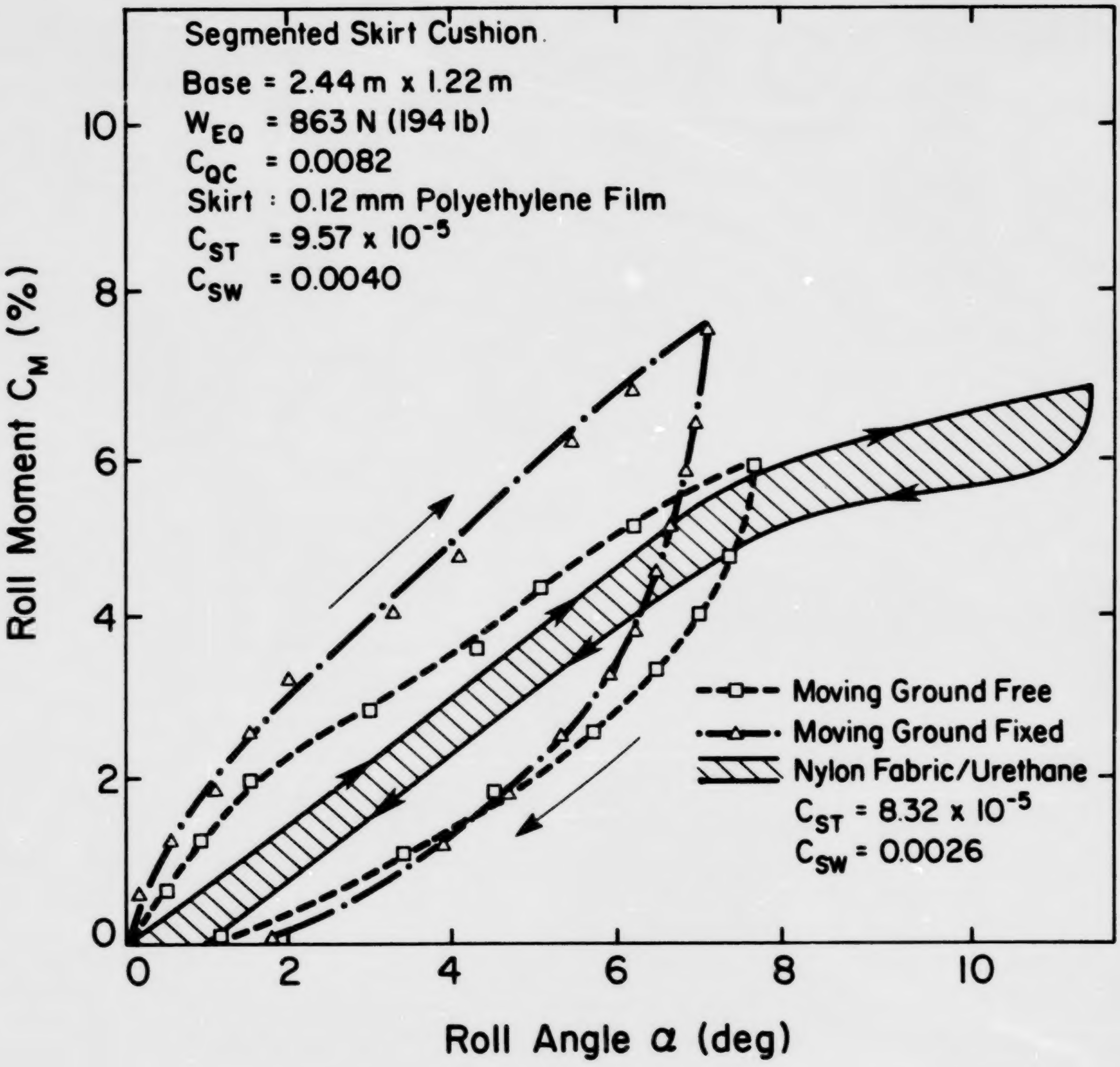

Figure E.7 Roll stiffness characteristic of cushion dynamics model equipped with HSL skirt including the effect of skirt-ground friction. Skirt material is polyethylene film.

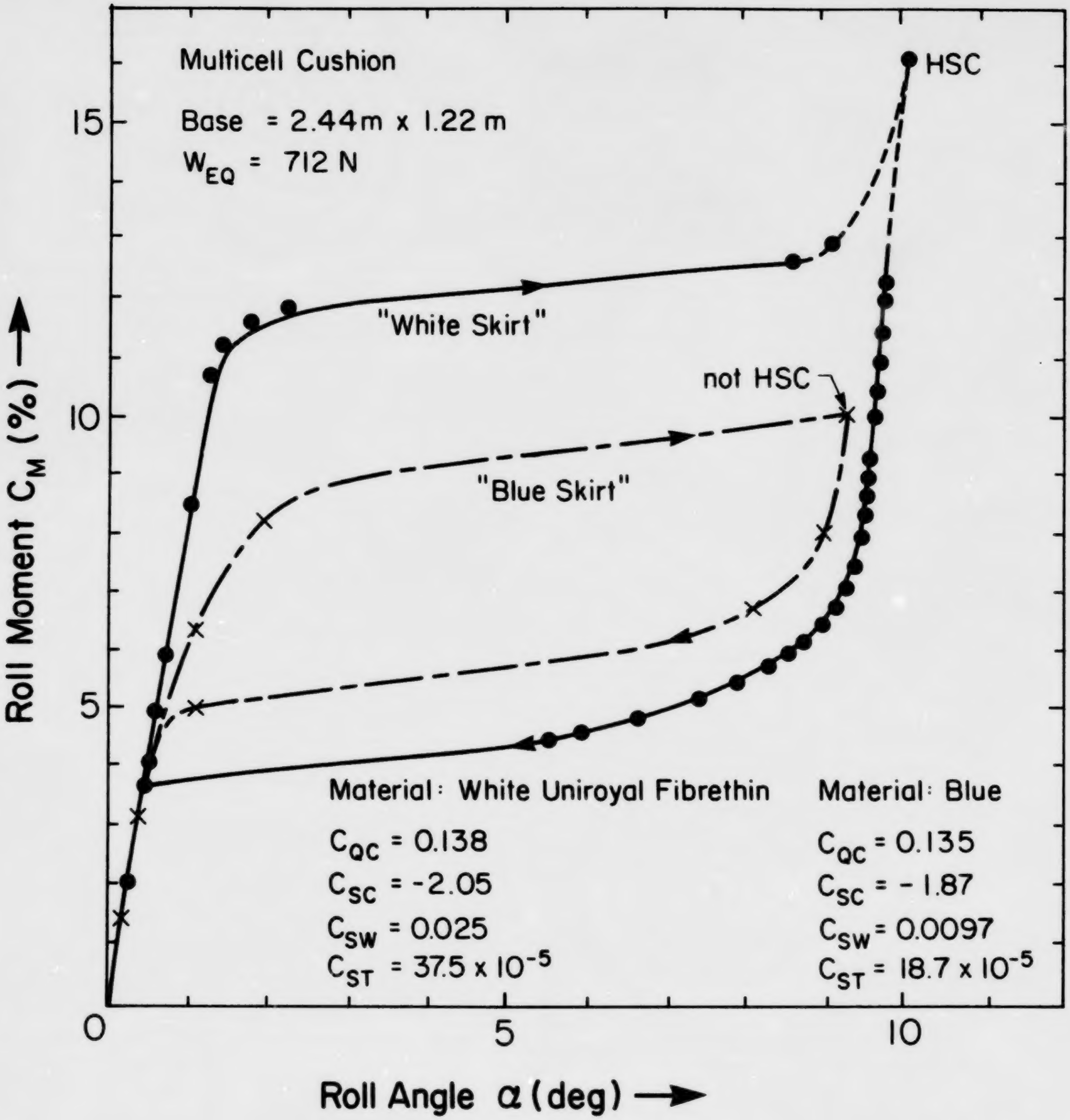

Figure E.8 Effect of material change on cushion roll stiffness characteristic at $C_{PC} = 0.0268$.

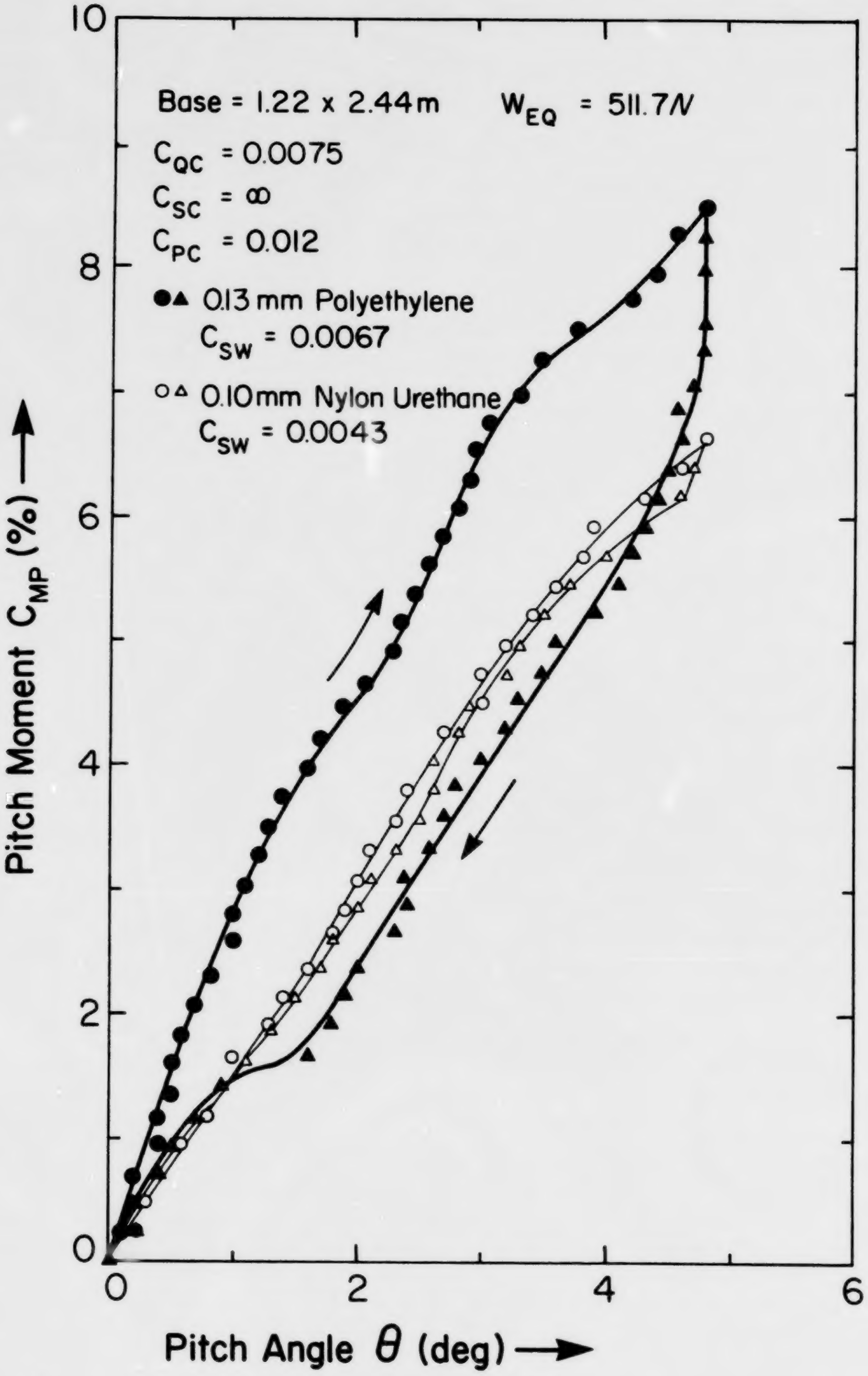

Figure E.9 Experimental pitch cycles for polyethylene and polyurethane-coated nylon segmented skirt systems.

support less force. If these forces are produced by deformations of the overall skirt system, then bending stiffness should be negligible, and the hysteresis should be governed by membrane stiffness and thus proportional to Et_s. In contrast, if they arise from the localized deformation in the neighbourhood of the region of skirt-ground contact then bending stiffness effects might be important, in which case the hysteresis should be proportional to Et_s^3. Unfortunately, adequate material stiffness data is not available to permit a proper comparison. Further evidence of the importance of structural forces comes from measurements of stiffness curves at various cushion weights and from measurement of cushion pressures during a pitch cycle. Figures E.10 and E.11 show that for both the multicell and segmented skirt the amount of hysteresis is reduced at larger weights. Friction forces scale with the cushion weight because the normal force producing them is proportional to the cushion pressure times the area of material lying on the ground surface. The area in question is determined by the relative positions of the ground and the skirt system and is not altered by the weight, but the cushion pressure is proportional to the weight. Thus the friction forces are proportional to the craft weight and their contribution to the nondimensional moment coefficient, C_M, is independent of weight. Therefore the reduction in hysteresis is unaffected by friction and is due to effects less dependent on cushion pressure; the structural load carrying ability is an example of this. Figure E.12 gives nondimensional pressure data as a function of pitch angle for the polyethylene segmented skirt. The hysteresis present in this data is a result of the load carrying capability of the skirt because the cushion pressure is determined by the footprint area, the vehicle weight, and the amount of load carried in the skirt and does not depend on friction.

The multicell skirt system also exhibited a third cause of hysteresis, venting failure. Here the downgoing cells at either end of the vehicle would become shut off by contact with the ground and would fail by buckling as shown in Figure E.13. This caused the cells to vent to atmosphere and the cushion to drop to the point of hard structure contact before recovering lift. This effect occurs only at high values of flow. Figure E.14 shows data from the two cell cushion in such a collapse with theoretical values for the reaction moments obtained as described in References E.4 and E.5. Non-venting hysteresis for the same skirt is shown in Figure E.6. Note the large increase in hysteresis when this phenomenon occurs.

Tests performed on the UTIAS Circular Track vehicle with the segmented skirt have shown that hysteresis similar to that of Figures E.7 and E.9 also occurs on larger scale vehicles [E.6].

E.3 Effect of Static Hysteresis on Dynamics

Static hysteresis can be an important form of damping if it appears in the dynamics. Figures E.15 and E.16 give experimentally obtained dynamic pitch angle response traces from the 2.44 m × 1.22 m test facility equipped with the segmented skirt systems whose static pitch characteristics are given in Figure E.9. Note the increased damping in the case of the polyethylene skirt and that, whereas the nylon-urethane skirt exhibited a limit cycle behaviour for the combined pitch-heave motion, the resulting oscillation for the polyethylene skirt remained well damped. Similar behaviour has also been found at larger scale on the UTIAS Circular Track

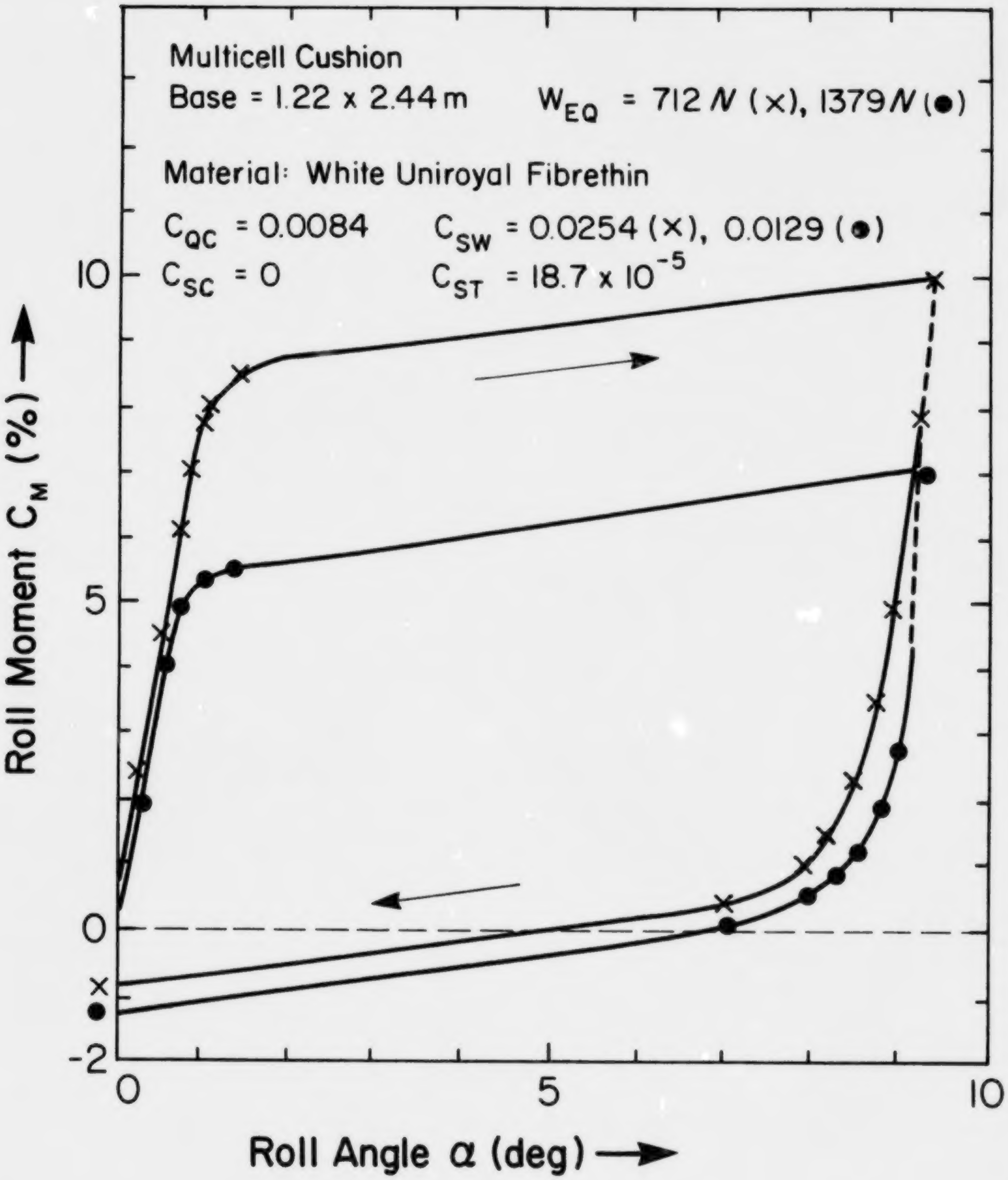

Figure E.10 Effect of model weight on roll stiffness characteristic - multicell cushion, neoprene-nylon material.

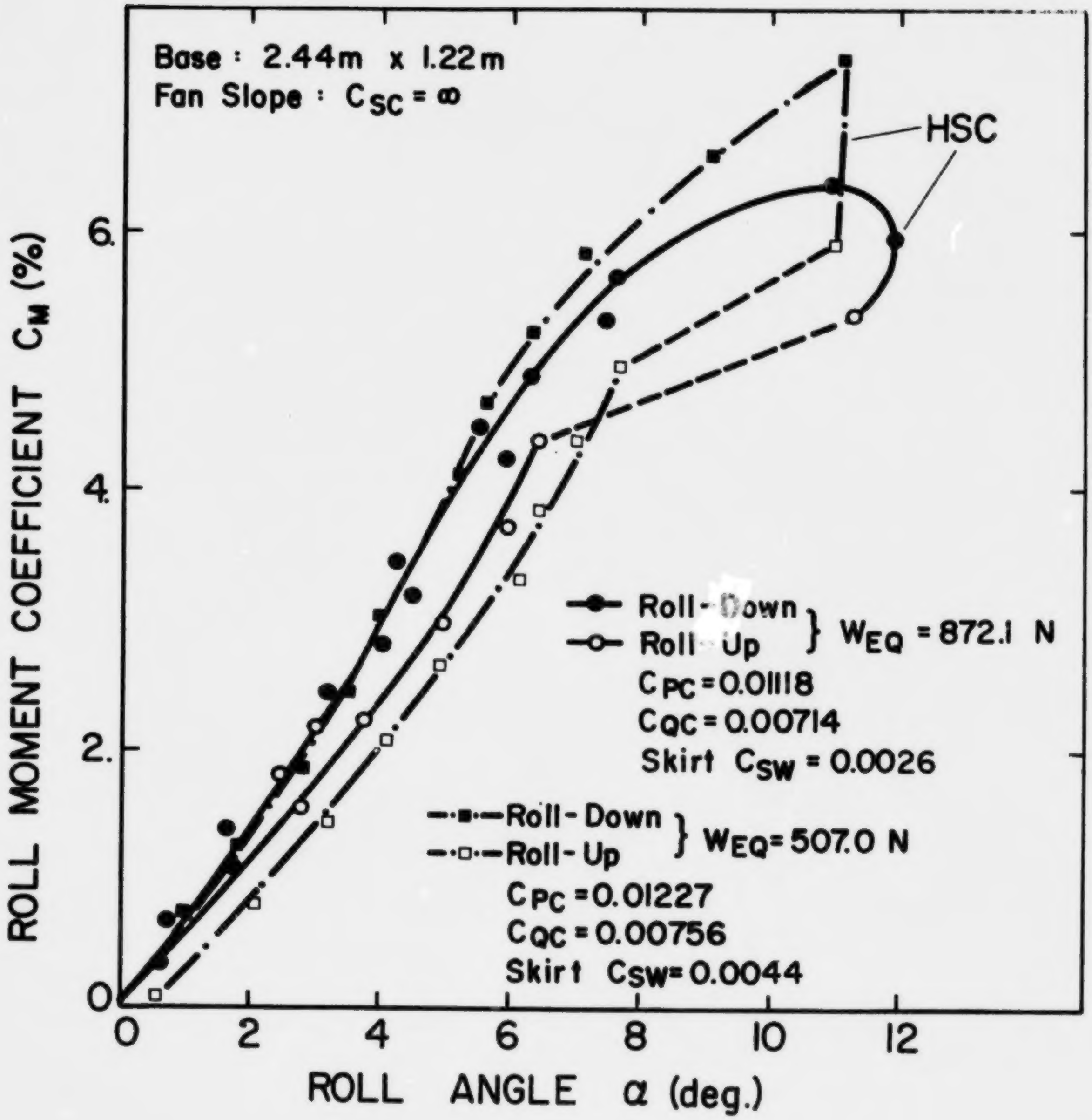

Figure E.11 Effect of gross model weight on the roll stiffness characteristic of the cushion dynamics facility with HSL skirt. Skirt material is urethane-coated nylon.

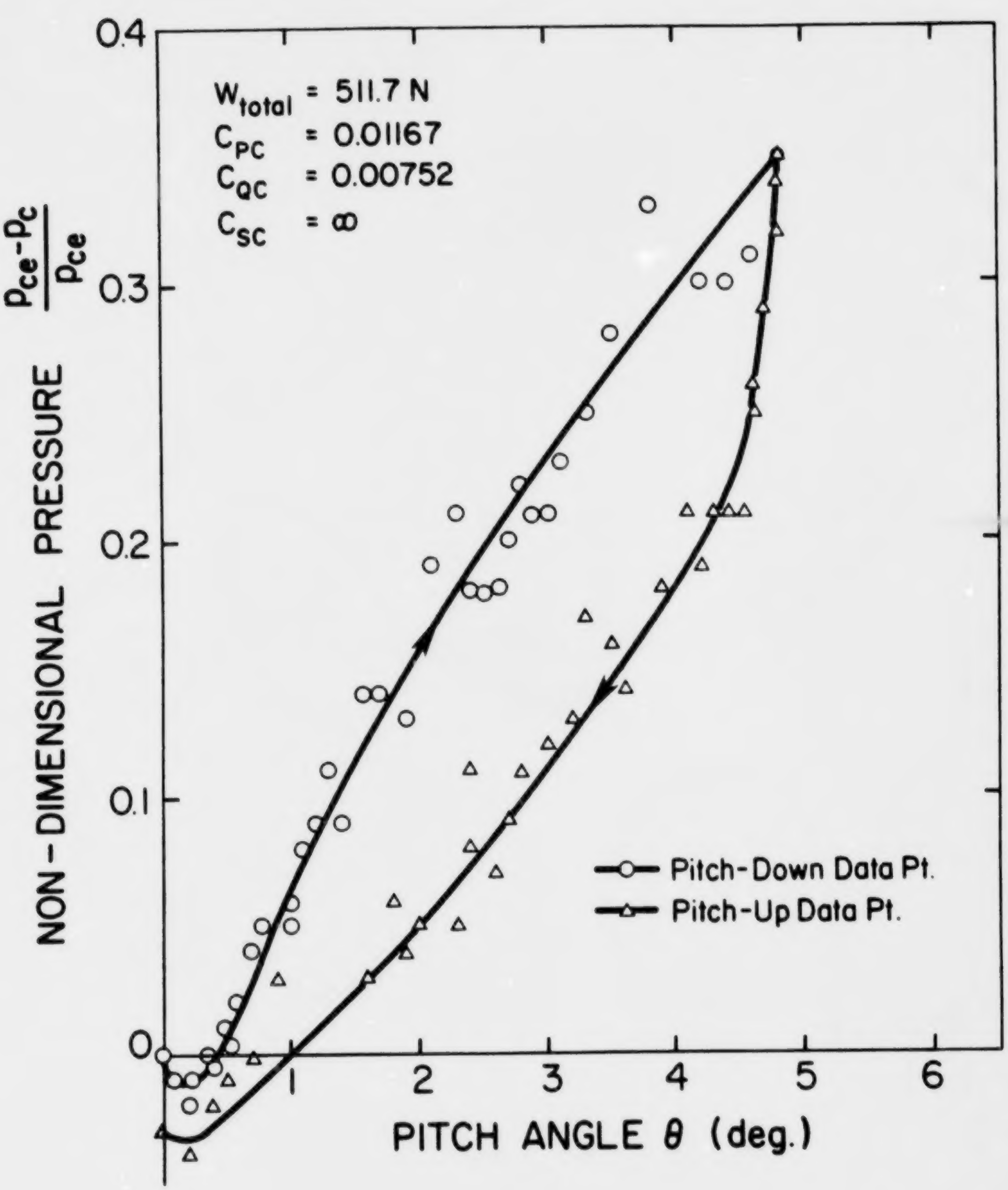

Figure E.12 Nondimensional pressure versus pitch angle θ, for the cushion dynamics model equipped with the polyethylene HSL skirt.

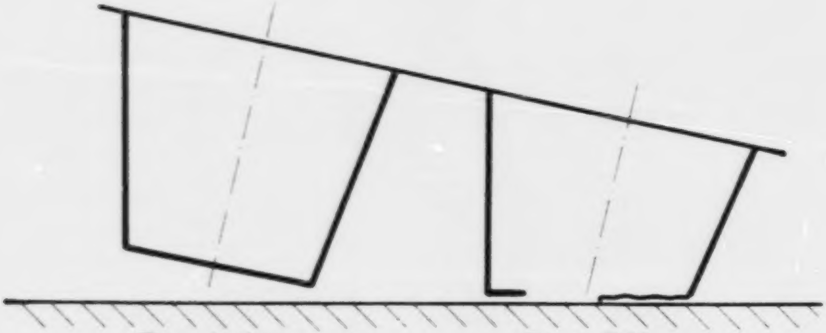

Regulating Shut Off

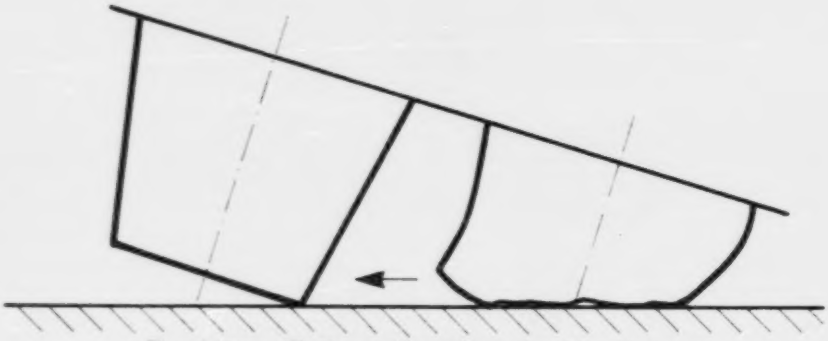

Buckling Failure Leading to Venting and Lift Loss

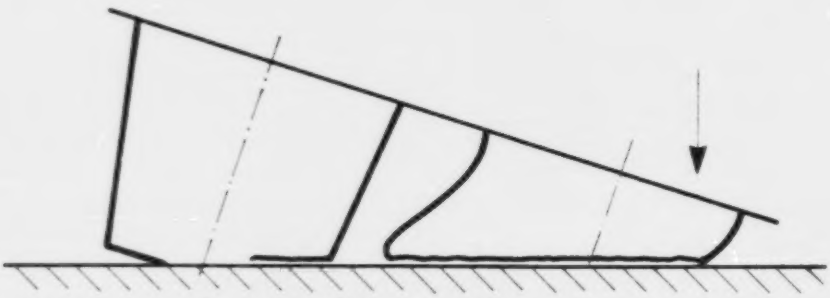

Cushion Drops to Recover Lift

Figure E.13 Venting effects in multicell cushions.

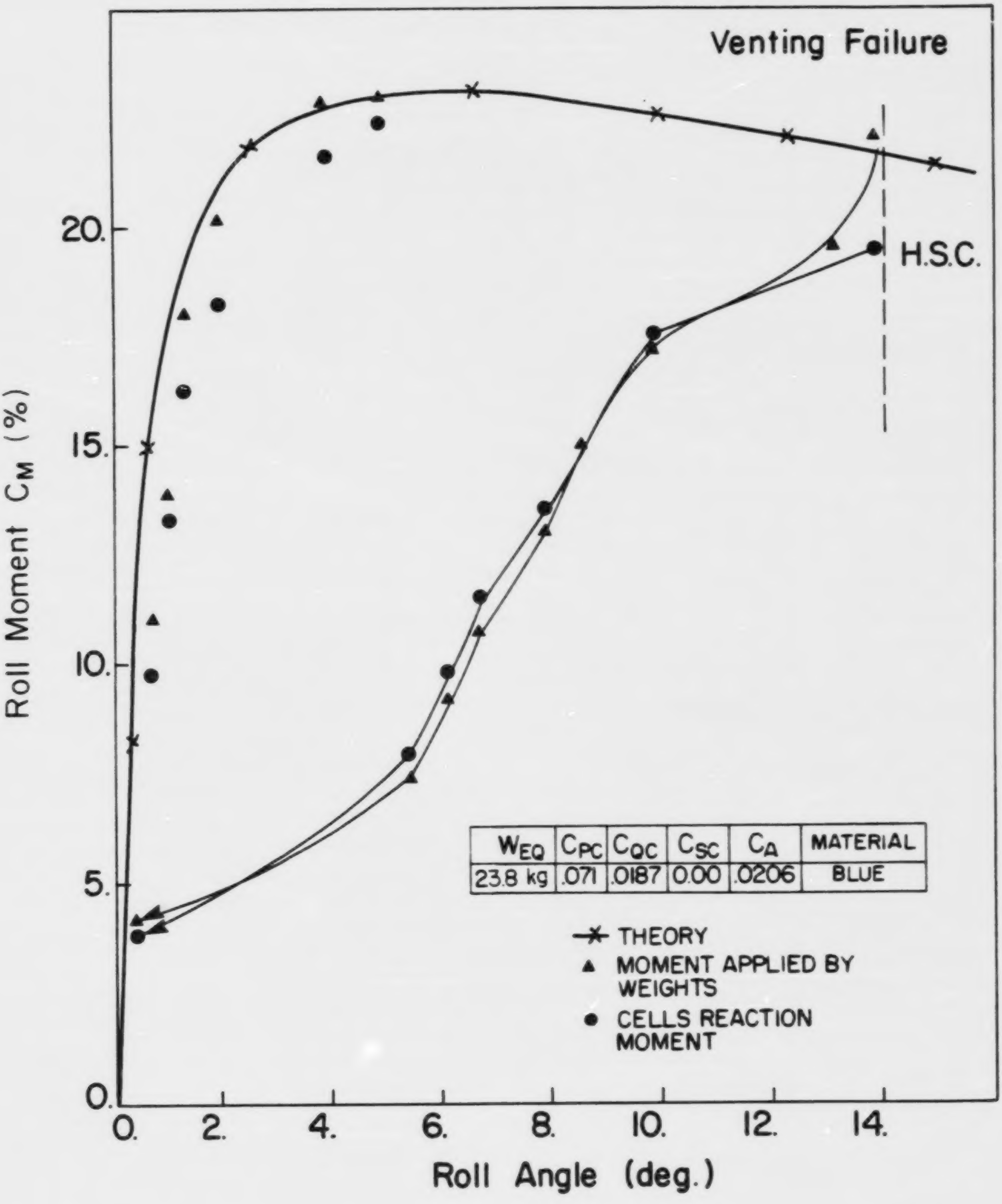

Figure E.14 Venting failure hysteresis.

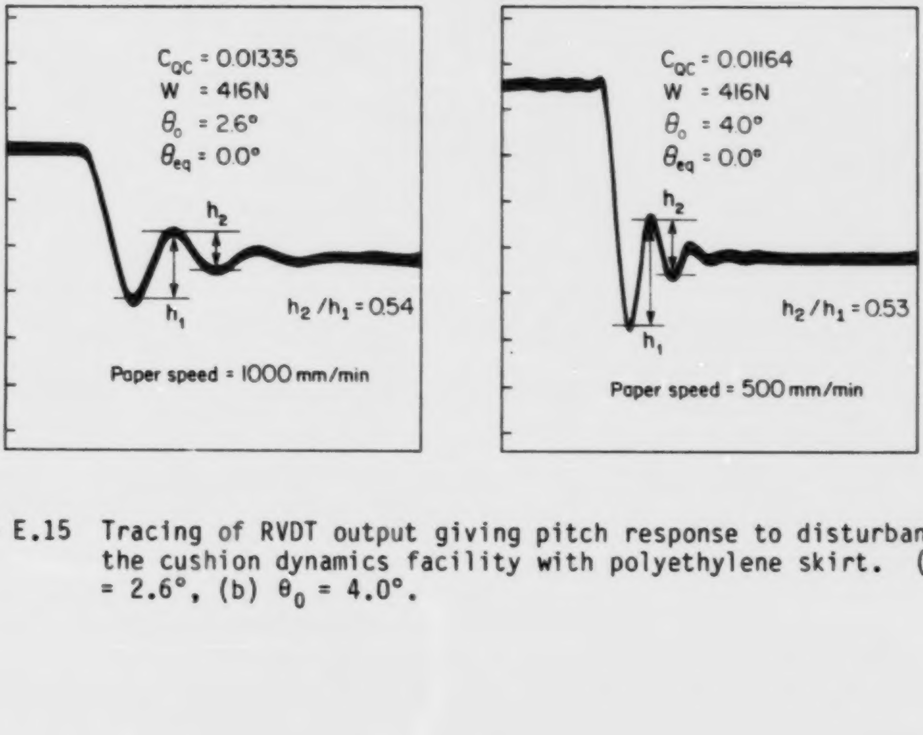

Figure E.15 Tracing of RVDT output giving pitch response to disturbance of the cushion dynamics facility with polyethylene skirt. (a) θ_0 = 2.6°, (b) θ_0 = 4.0°.

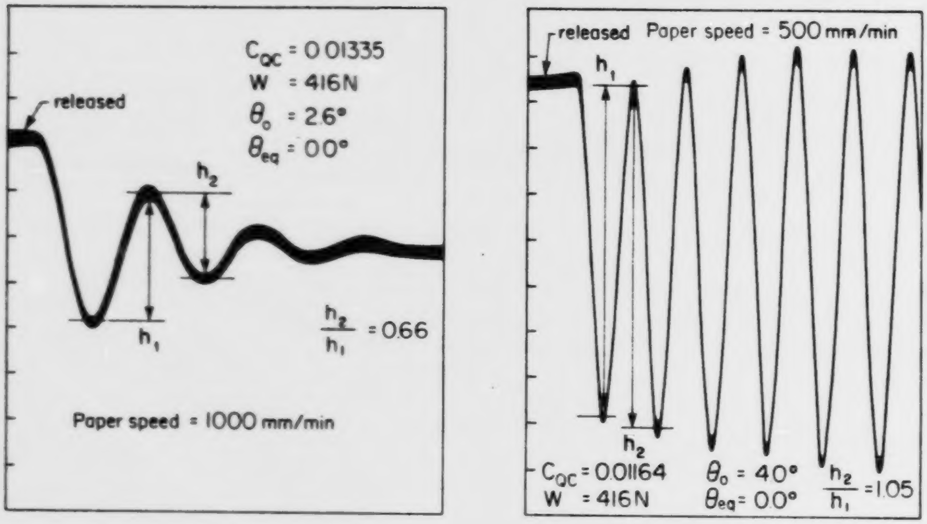

Figure E.16 Tracing of RVDT output giving pitch response to disturbance of the cushion dynamics facility with nylon-urethane skirt. (a) θ_0 = 2.6°, h_2/h_1 = 0.66, (b) θ_0 = 4.0°, h_2/h_1 = 1.05.

Test Vehicle, Vampire 1, with the segmented skirt system installed. Here, roll motion was induced as a result of gyroscopic coupling from the fan system, and a combined pitch-heave-roll limit cycle type oscillation was obtained under certain conditions when the same lightweight nylon-urethane material was used for skirt construction. In [E.6] curves were presented which showed that the hysteresis measured in roll for a heavier skirt material used on the UTIAS circular track vehicle produced significant damping.

The traces given in Figures E.15 and E.16 are also subject to flexibility effects which are discussed in detail for a conical skirt geometry in Appendix B. Here it is shown that, in the absence of air escape area modulation with cushion pressure, increasing flexibility modulated the pneumatic capacitance, and tended to make the system more unstable in heave. Stiffness measurements on the two materials showed that the nylon-urethane material was stiffer in the warp direction but less stiff in the fill direction than the polyethylene, which was isotropic. Owing to the complex geometry of the segments and the material, the combined effect of this on the cushion capacitance relative to the polyethylene has not been determined. It is expected that there is some increase in capacitance, and this plays a role in determining the onset of the limit cycle behaviour, but that the improved damping with the polyethylene is mainly a result of the increased static hysteresis. This is because attempts to create an unstable oscillation with the polyethylene skirt failed even though it was operated well into the unstable regime for the nylon-urethane skirt. In addition no deformation of the skirt system due to pressure action was noted, whereas the large material change effects on cushion stability noted in [E.7] were accompanied by visible skirt deformation.

E.4 Full Scale Hysteresis: ACIB Measurements

The measurements were made on February 25, 1983 at the Canadian Coast Guard terminal in Thunder Bay, Ontario. Only pure heave measurements over land could be made. The vehicle operating point was altered by varying fan engine speed in small steps. After each speed change the vertical position and cushion pressure were allowed to stabilize. The vertical position was then measured using a surveyor's level which sighted on three 1.3m graduated rods mounted on the deck in the positions shown in Figure E.17. The corresponding cushion pressure was measured in two ways, once using a water manometer and once using a pressure gauge, both of which were mounted in the control room. The height of the geometric centre of the deck was found by fitting a plane through the vertical positions of the three measurement stations. The test results are given in Figure E.18. Data from two down-up cycles are plotted in this figure and as can be seen, there is very little scatter. Also, the pressure versus height data are linear both downgoing and upgoing. The data show that the skirt supports about 4% of the gross weight when the vehicle hard structure is almost in contact with the ground, but it supports about 1% during normal operation.

For segmented skirt systems, the roll stiffness caused by the geometrical shift in the centroid of the pressurized support area, is typically about 1-1.5% per degree roll. An estimate of the hysteresis one

---

*Roll is meant to mean rotation about axis w in Figure E.17.

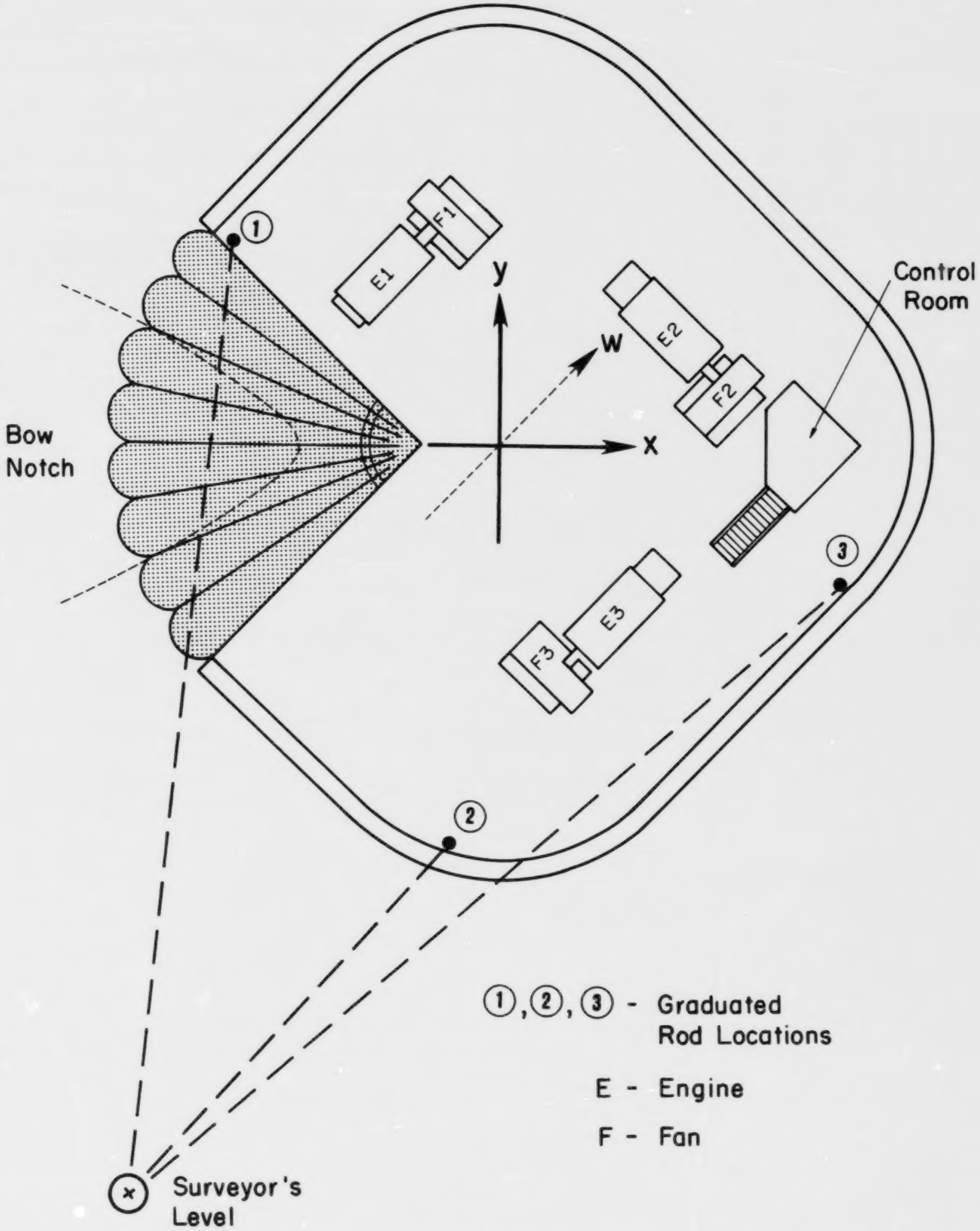
①
Bow Notch
y
W
x
E1
F1
E2
F2
E3
F3
Control Room
③
②
①,②,③ - Graduated Rod Locations
E - Engine
F - Fan
Surveyor's Level

Figure E.17 ACIB layout showing location of graduated rods and surveyor's level.

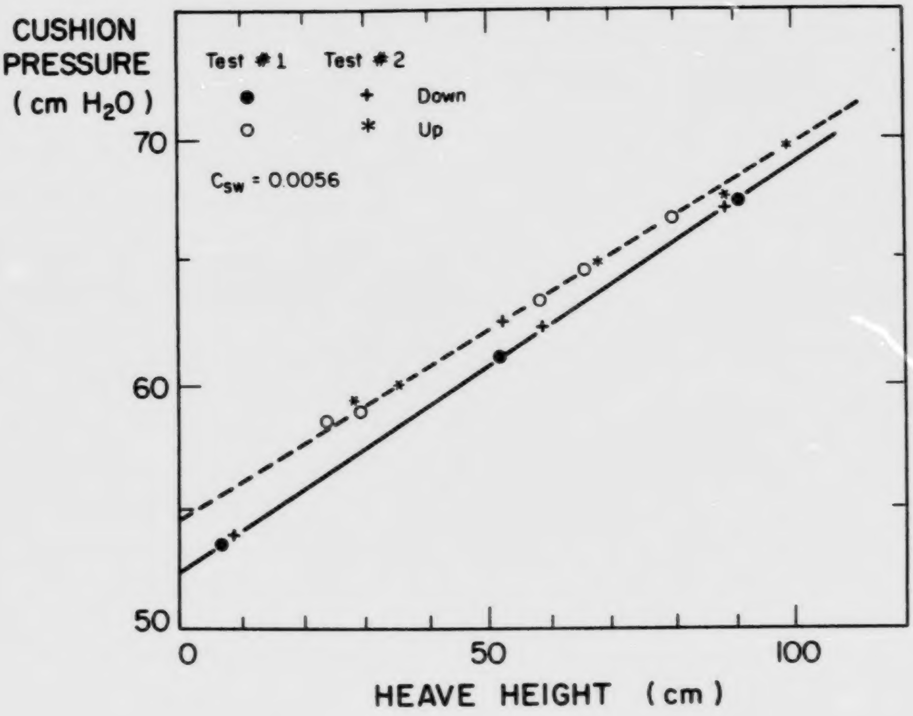

Figure E.18 Experimental data from heave cycle tests on ACIB.

example, when the pure heave skirt load is taken to be 2%, the roll would expect in roll* due to skirt loads can be obtained from the heave data by using it to calculate typical skirt loads per unit perimeter. For hysteresis due to skirt load carrying capability can be roughly estimated as follows. Assume that the vehicle rotates about a centre of mass located at the geometric centre of the craft and that the hysteresis mechanism operates only during downgoing motion. The hysteresis moment contributed by the edges of the craft is then $\approx (b/2)\times(0.02/4)W$ where b is the beam and W the craft weight. For the other sides of the craft the moment arm varies from 0 to b/2 so the average moment contribution is $\approx(2/3)\times(b/2)\times(0.02/4)W$. The total roll moment hystereis is then $\approx$0.42% of Wb. This method gives a conservative estimate of the hysteresis, since any contribution due to the rising side is neglected. This amount of roll hysteresis is shown schematically in Figure E.19.

As noted earlier, roll and pitch hysteresis measured in models with a segmented skirt system ranges from near zero to about 3%, so that this conservative estimate places full-scale hysteresis at the lower end of the range, but it is still significant. Also the amount of hysteresis measured in heave, 1-4%, is of the same order as load carried in the skirt material by a multicell cushion at various non-zero roll angles, $\approx$ 2.5-6%.

An estimate of the heave damping associated with hysteresis can be obtained by noting that the work done by hysteresis during an oscillation cycle must show up as a change in the kinetic energy of the air-supported mass. If the change in amplitude is small relative to the amplitude itself, this balance reduces to

$$2h_0F_s = Mh_0\Delta h\,\omega^2$$

where F_s is the skirt force, M is the air supported mass, h_0 is the oscillation amplitude, Δh is the change in amplitude over one cycle, and ω is the oscillation frequency. Solving for Δh gives

$$\Delta h = \frac{F_s}{M}\,\frac{2}{\omega^2}$$

This shows that the change in amplitude over one cycle is independent of the amplitude. For F_s = 2% Mg and $\omega = 2\pi$ rad/sec, one obtains Δh = 1 cm.

E.5 Conclusions

The measurements of hysteresis in the heave characteristic of the ACIB have shown that model and full scale hysteresis are of similar magnitude. In addition, other information [E.8, E.9] recently made available has shown that similar roll hysteresis is present in the BHC bag and finger skirt system and a new Canadian hybrid design currently being tested.

The importance of this hysteresis is indicated in some recent work done at UTIAS on the dynamics of large air cushion platforms [Appendix C]. This work has shown that these cushions typically operate with very low phase margin or damping. Even well into the stable pressure-flow operating region, disturbance generated motions are only lightly damped. It is

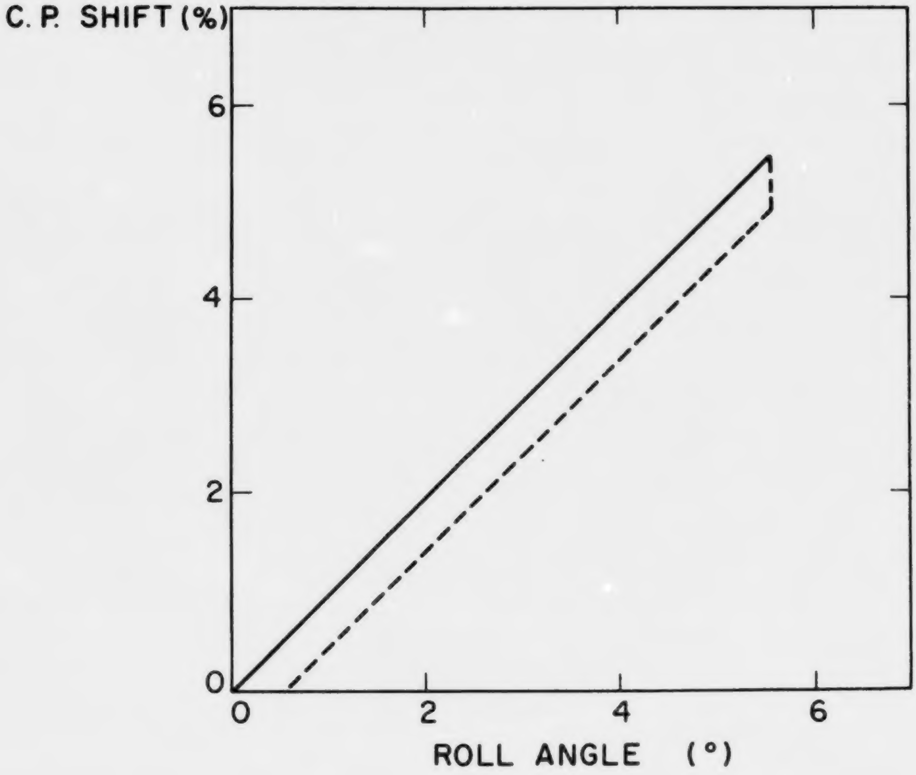

Figure E.19 Prediction of roll hysteresis from heave hysteresis measurements. Stiffness set nominally at 1% per degree for illustration purposes.

possible that, if properly exploited, skirt hysteresis could improve this situation.

The existence of hysteresis at full scale and its role in producing damping forces coupled with the lack of a detailed explanation of the physical mechanisms involved points out the need for in-depth study of the phenomenon. A complete exploitation of the hysteresis and scaling of materials between model and full scale can only be achieved when the mechanisms are understood. Hysteresis, however, is only one of several factors to be considered when scaling skirt systems for dynamic experiments [E.3]. Depending on the system, skirt thickness, weight per unit area, elastic constants and/or viscoelastic constants must be scaled as well. This can be quite difficult, since many contradictory constraints are introduced when dimensional analysis is performed in consideration of these factors. The importance of hysteresis at full scale thus adds another factor to an already difficult scaling problem.

REFERENCES - APPENDIX E

E.1 Sullivan, P. A., Hinchey, M. J., and Delaney, R. G., "Static Roll Stiffness Characteristics of Two Multicell Type Air Cushion Systems", Journal of Terramechanics, Vol. 15, No. 1, 1978, pp. 15-41.

E.2 Sullivan, P. A., Hinchey, M. J., Hartmann, P. V., and Dupuis, A., "Research Into Air Cushion Stability: 1978 Report", Transportation Development Centre, Transport Canada, Montreal, Report TP-1760, Jan. 1981.

E.3 Sullivan, P. A., Hinchey, M. J., Hartmann, P. V., Dupuis, A., Green, G., and Graham, T., "Research Into Air Cushion Stability: 1979 Report", Transportation Development Centre, Transport Canada, Montreal, Report TP-3109-E, Jan. 1982.

E.4 Sullivan, P. A., Hinchey, M. J., and Delaney, R. G., "An Investigation of the Roll Stiffness Characteristics of Three Flexible Skirted Cushion Systems", UTIAS Report No. 213, March 1977.

E.5 Sullivan, P. A., Hinchey, M., Murra, I., Parravano, J., "Research on the Stability of Air Cushion Systems", University of Toronto, Institute for Aerospace Studies Report No. 238, Nov. 1979.

E.6 Sullivan, P. A., Hartmann, P. V., and Graham, T. A., "Application of System Identification Flight Analysis Techniques to the Pitch-Heave Dynamics of an Air Cushion Vehicle", Canadian Aeronautics and Space Journal, Vol. 29, No. 4, Dec. 1983, pp. 348-370.

E.7 Graham, T. A., Sullivan, P. A., and Hinchey, M. J., "Skirt Material Effects on Air Cushion Dynamic Heave Stability", Journal of Aircraft, Vol. 22, No. 2, Feb. 1985, pp. 101-108.

E.8 ————, "Stability and Control of Hovercraft: Notes for Commanders", United Kingdom Department of Industry Ship and Marine Technology Requirements Board BHC SP 4432, 1980.

E.9 Jones, D., Private Communication, 1983.

E.10 See Appendix D.

APPENDIX F. ON THE DYNAMIC STABILITY OF AIR CUSHIONS HOVERING OVER WATER
(M. J. Hinchey and P. A. Sullivan)

NOMENCLATURE

Roman

a	sound speed in air
b	vehicle semi-width
C_c	lumped pneumatic capacitance
C_i	cosine integral function
C_m	discharge coefficient
C_{PQ}	slope of fan pressure-flow characteristic
$f(z)$, $g(z)$	auxiliary exponential integral functions
g	gravitational acceleration
$G(i\omega)$, $H(i\omega)$	transfer function in Nyquist block diagram
h	hovergap
i	$\sqrt{-1}$
ℓ	cushion perimeter
m	suspension mass
M	transfer function relating the motion of the water surface at the lip of the cushion to the cushion pressure
N	transfer function relating the averaged motion of the water surface inside the plenum to the cushion pressure
p	pressure
Q	volumetric flow
R_a	outlet orifice resistance
R_c	inlet orifice resistance
si	sine integral function
t	time

$V\!\!\!{-}$	volume
x	horizontal coordinate
y	vertical coordinate
z	$x + iy$

Greek

α_a	hovergap flow parameter
γ	polytropic coefficient = 1.4 (isentropic)
Δ	perturbation
η	deflection of wave free surface
μ_a, μ_w	dynamic viscosity of air and water respectively
λ	wave length
ν	wave number
π	3.14159
ρ	density
χ	heave displacement
ω	angular frequency

Subscripts

a	air
c	cushion
e	equilibrium
f	fan
t	partial derivative w.r.t. time
w	water
y	partial derivative w.r.t. vertical coordinate

F.1 Introduction

All of the investigations of dynamic stability conducted by UTIAS for TDC have thus far considered only cushions hovering over a smooth, flat surface. During field trials of a small test vehicle known as HEX-5, which was equipped with the uncompartmented segmented skirt system that is the focus of the present contract, Fowler [F.1] observed that, whereas the vehicle was very stable when operated over land, it was subject to a severe heave instability when hovering without forward motion over water. A certain minimum air flow was required to initiate the instability, and beyond this minimum, the amplitude of the oscillation increased linearly with cushion flow. The frequency of the observed motion was found to be about 4.5 Hz and independent of both cushion flow and craft weight, which ranged from 7120N to 10680N. Fowler suggested that the water under the cushion acted as a combined piston and spring, in addition to that of the basic air cushion, and that resonance between the two systems could excite the instability.

For an ACV in forward motion at any but the lowest speeds, one would not expect this "water pumping" mechanism to be excited. Fowler found this to be the case; even speeds as low as 0.2 m/sec were sufficient to suppress the most severe oscillation. However, for large platform cushions which are expected to hover without forward motion for significant periods during their operation, the water pumping phenomenon could present a problem. Furthermore, although aspects of the dynamics of air cushion vehicles hovering over water have been investigated (see for example [F.2 to F.4]), these have been directed towards problems associated with forward motion such as the prediction of wavemaking drag. Hence we concluded that an exploratory investigation of this problem fell within the mandate of the present contract.

We conducted two preliminary experiments. In the first, a two-dimensional section of a rigid plenum chamber was mounted in a tank which incorporated transparent sides to permit observation of the motion of the water surface. To ensure that the excited wave motion was predominantly two-dimensional, the sides of the cushion adjacent to the viewing windows, which were also transparent, extended well below the water surface. Furthermore, the width of the tank was only slightly wider than that of the plenum chamber. Finally to ensure that only outgoing waves were present, the tank included suitable wave absorbers at both ends. This is shown in Figure F1. The main result was the observation that, when instability had generated a stable oscillation, contrary to the suggestion by Fowler [F.1], motion of the water surface was not piston-like but took the form of a standing wave. Thus any theory of the water motion has to predict the history of the shape of this surface in order to compute both an average or "equivalent piston" deflection for the modulation of the plenum chamber volume, and the effective "hovergap" at the cushion lip for the modulation of the air flow to atmosphere. The work described in Appendix B shows that both of these quantities can have a very large effect on dynamics and stability.

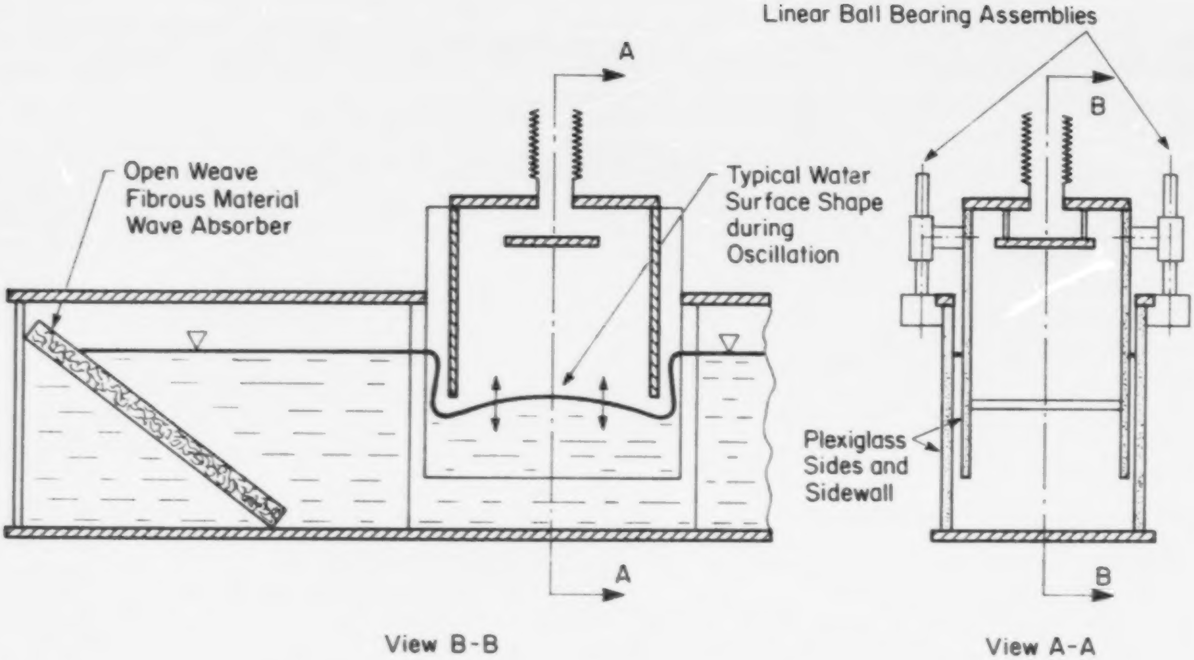
Linear Ball Bearing Assemblies
A
B
Open Weave Fibrous Material Wave Absorber
Typical Water Surface Shape during Oscillation
Plexiglass Sides and Sidewall
A
B
View B-B
View A-A

Figure F.1 Two-dimensional test tank used to observe motion of water surface inside oscillating cushion.

In the second experiment we attempted to measure the effective discharge coefficient for air escaping under skirt segments partially immersed in water. These segments had the same geometry as those used by Fowler and for the present contract. We were however confronted with an unexpected result: the segments almost always oscillated at a frequency of about 5 Hz, and this appeared to be associated with a corresponding motion of the water in the small tank used to make the measurements. This made measurements of effective discharge coefficient very difficult, but it also suggested the existence of a second mechanism for the instability observed by Fowler [F.1]. This is explored in Appendix P.

The only available work on water surface pumping directly applicable to the ACV problem appears to be an analysis by Ogilvie [F.5]. He used classical linearized deep water wave theory, as developed by Lamb [F.6] and Stoker [F.7] to derive a frequency response function relating the deflection of the free surface of the water directly beneath the vehicle to a sinusoidal cushion pressure variation. He used a two-dimensional geometry with no inflow from the lift fan or outflow from the cushion. However, he included the compressibility of the air in the cushion volume and allowed for lip immersion in the water. Thus his model corresponds to a very long sidewall vehicle. He computed equivalent mass, stiffness and damping terms, but did not address the stability aspect.

The present analysis extends Ogilvie's model by including simple models of the air inflow and outflow processes, and applies this extended model to the stability question. A preliminary version of this analysis was presented in the previous Contract report [F.8]. This included the modulation of the cushion volume by the water motion, but used the average deflection of the water surface to compute the effective hovergap. Thus it did not allow for the separate modulation of the escaping air flow, and it predicted trends which were opposite to those observed by Fowler [F.1]. It was suggested that the modelling of the lip flow modulation could be the source of the discrepancy.

F.2 Pressure-Water Surface Interaction

F.2.1 Basic Theory

For the present work, the air cushion vehicle is approximated by the two-dimensional inverted box configuration shown schematically in Figure F.2.

The frequency response function developed by Ogilvie [F.5] for the case where the lip is not immersed in the water is used here to examine the heave stability of an air cushion vehicle hovering over water. This function is based on classical linearized water wave theory which is in turn based on potential flow theory for an incompressible ideal fluid where one is interested in finding a velocity potential ϕ which satisfies Laplace's equation

$$\nabla^2\phi = 0 \quad \text{for } y < 0 \qquad \text{(F.1)}$$

subject to the dynamical free surface or pressure condition,

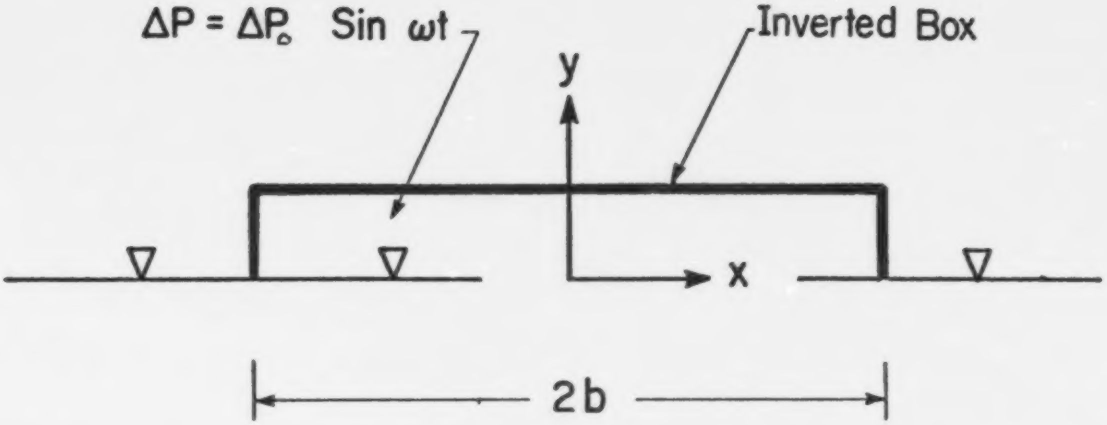
$\Delta P = \Delta P_o$ Sin ωt
Inverted Box
y
x
2b

Figure F.2 Two-dimensional inverted box configuration used in analysis.

$$\Delta\eta = -\frac{1}{g}\phi_t - \frac{\Delta p}{\rho_w g} \qquad (F.2)$$

and to the kinematic free surface or displacement condition,

$$\Delta\eta_t = \phi_y \qquad (F.3)$$

where

$$\begin{aligned} \Delta p &= \Delta p_0 \sin\omega t \qquad |x| < b \\ &= 0 \qquad\qquad\quad |x| > b \end{aligned} \qquad (F.4)$$

Here $\Delta\eta$ is the deflection of the water surface from its reference ($y = 0$) position, b is the vehicle semi-width, Δp_0 is the amplitude of the cushion pressure oscillation, g is the acceleration due to gravity, and ρ_w is the density of water. The subscripts "t" and "y" indicate partial derivatives with respect to time and the vertical coordinate respectively. Substituting Equation (F.2) into Equation (F.3) gives

$$-\frac{1}{g}\phi_{tt} - \frac{\Delta p_t}{\rho_w g} = \phi_y \qquad (F.5)$$

By letting

$$\phi(x,y,t) = \phi_1(x,y)\sin\omega t + \phi_2(x,y)\cos\omega t \qquad (F.6)$$

and substituting into Equation (F.5), one obtains

$$\phi_{1y} - \nu\phi_1 = 0 \qquad -\infty < x < \infty, \quad y = 0 \qquad (F.7.1)$$

$$\begin{aligned} \phi_{2y} - \nu\phi_2 &= \frac{-\omega\Delta p_0}{\rho_w g} \qquad |x| < b, \quad y = 0 \\ &= 0 \qquad\qquad\quad |x| > b, \quad y = 0 \end{aligned} \qquad (F.7.2)$$

where

$$\nu = \frac{\omega^2}{g} \qquad (F.8)$$

is the wave number of generated waves. The latter is related to the wavelength λ by

$$\lambda = \frac{2\pi}{\nu} \qquad (F.9)$$

To obtain a unique solution, Ogilvie [F.5], following Stoker's work [F.6], assumed the water to be initially at rest and enforced the condition that there be only outgoing waves at $|x| = \infty$. This is in contrast to Lamb [F.7] who used fictitious damping forces to suppress free oscillations and thus achieve a unique solution. The $|x| = \infty$ conditions together with the requirement that the fluid velocity vanish in the limit as y tends to minus ∞ gives [F.5]

$$\phi_1(x,y) = \frac{-2\Delta p_o}{\rho_w \omega} e^{\nu y} \sin \nu b \cos \nu x \tag{F.10.1}$$

$$\phi_2(x,y) = \mathrm{Re}[f(z)] - \frac{2\Delta p_o}{\rho_w \omega} e^{\nu y} \sin \nu b \sin \nu x \tag{F.10.2}$$

where

$$f(z) = \frac{-\omega \Delta p_o}{\pi \rho_w g} e^{-i\nu z} \oint_{i\infty}^{z} e^{i\nu t} \mathrm{Ln} \frac{t-b}{t+b} \, dt \tag{F.11}$$

and

$$z = x + iy \tag{F.12}$$

Substitution into the dynamical condition gives for $|x| < b$ the water surface deflection [F.6]

$$\Delta\eta(x,t) = \left[\frac{-\Delta p_o}{\rho_w g} (1 + 2\sin \nu b \sin \nu x) + \frac{\omega}{g} \mathrm{Re}[f(x-i0)] \right] \sin \omega t + \left[\frac{2\Delta p_o}{\rho_w g} \sin \nu b \cos \nu x \right] \cos \omega t \tag{F.13}$$

F.2.2 Spatially Averaged Deflection of Water Surface in Plenum

Ogilvie [F.5] showed how for the air cushion problem one could integrate over x to obtain an average or "equivalent piston" deflection

$$\overline{\Delta\eta}(t) = \frac{1}{2b} \int_{-b}^{b} \Delta\eta(x,t)dx = \frac{2\Delta p_o}{\rho_w g \nu b} \left[\sin^2 \nu b \cos \omega t + \frac{1}{2\pi} \{ C_e + \mathrm{Ln}(2\nu b) + g(2\nu b) \} \sin \omega t - \sin \nu b \cos \nu b \sin \omega t \right] \tag{F.14}$$

where C_e = Euler's constant = 0.577216 and

$$g(x) = \int_{o}^{\infty} \frac{u e^{-xu}}{u^2 + 1} du \tag{F.15}$$

Equation (F.14) can be rewritten in the complex form

$$\frac{\overline{\Delta\eta(i\omega)}}{\Delta p(i\omega)} = N(i\omega) \tag{F.16}$$

and

$$N(i\omega) = A + Bi \tag{F.17}$$

where

$$A = \frac{2}{\rho_w g \nu b}\left[\frac{1}{2\pi}\{C_e + \mathrm{Ln}(2\nu b) + g(2\nu b)\} - \sin\nu b \cos\nu b\right]$$

$$B = \frac{2}{\rho_w g \nu b}\sin^2\nu b \tag{F.18}$$

This is presented as a Bode Plot in Figure F.3. Note that in the limit as ω tends to zero, B tends to zero and A tends to $-(1/\rho_w g)$. In other words, the water surface responds quasi-statically to cushion pressure variations, as expected (see Appendix N).

F.2.3 Deflection of Water Surface at Lip

Equation (F.13) is singular at $|x| = b$. However, as noted by Ogilvie [F.5], the singularity is very weak and any error should be local in scope. If it can be assumed that Eq. (F.13) is approximately correct at each of the lips, then the total deflection of the water-free surface at $|x| = b$ is

$$\Delta\eta_{lip}(t) = \Delta\eta(b,t) + \Delta\eta(-b,t)$$

$$= \left[\frac{\omega}{g}\,\{\mathrm{Re}[f(b - i0) + f(-b - i0)] - \frac{2\Delta p_o}{\rho_w g}\right]\sin\omega t$$

$$+ \left[\frac{2\Delta p_o}{\rho_w g}\sin 2\nu b\right]\cos\omega t \tag{F.19}$$

Now

$$f(b\text{-}i0) = -\frac{\omega\Delta p_o}{\pi\rho_w g}\,I_1, \qquad f(-b\text{-}i0) = -\frac{\omega\Delta p_o}{\pi\rho_w g}\,I_2 \tag{F.20}$$

where

$$I_1 = e^{-i\nu b}\int_{i\infty}^{b-i0} dt\; e^{i\nu t}\;\mathrm{Ln}\;\frac{t-b}{t+b}$$

$$I_2 = e^{i\nu b}\int_{i\infty}^{-b-i0} dt\; e^{i\nu t}\;\mathrm{Ln}\;\frac{t-b}{t+b} \tag{F.21}$$

Upon evaluating the integrals one obtains [F.5]

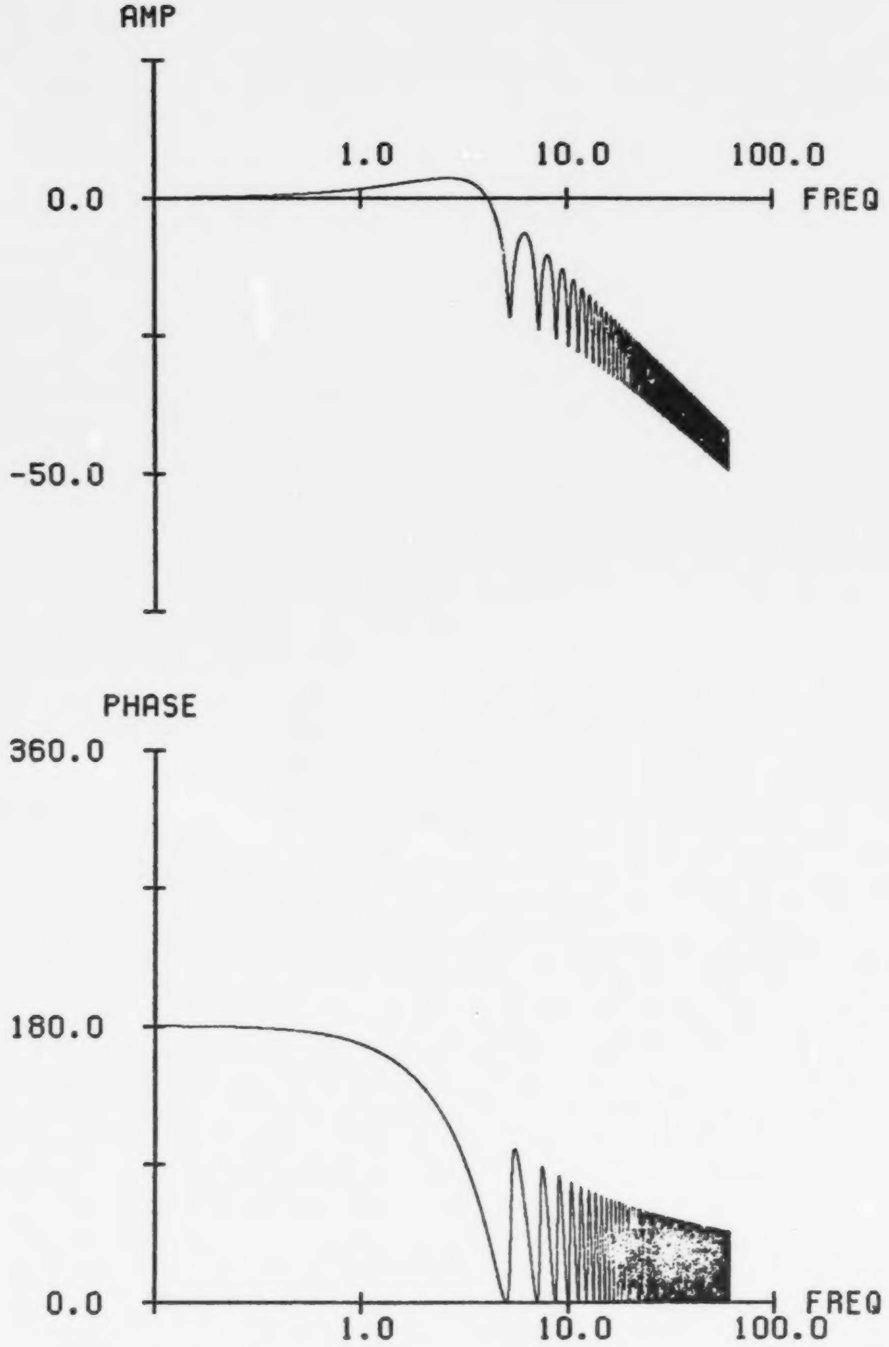

Figure F.3 Bode plot of frequency response to cushion pressure oscillations of average water surface deflection in interior of cushion.

$$I_1 = \frac{1}{\nu}\Big[\frac{\pi}{2} - si(\nu b) - iCi(\nu b) + i[C_e + Ln(2\nu b)] - e^{-i\nu b}[2f(\nu b) + 4\pi i \sin \nu b]$$

$$- e^{-2i\nu b}[Ci(2\nu b) - Ci(\nu b) + isi(2\nu b) - isi(\nu b)] \Big] \qquad (F.22)$$

$$I_2 = \frac{1}{\nu}\Big[\frac{\pi}{2} - si(\nu b) + iCi(\nu b) - e^{i\nu b}2f(\nu b) - i[C_e + Ln(2\nu b)]$$

$$+ ie^{2i\nu b}[Ci(2\nu b) - Ci(\nu b) - isi(2\nu b) + isi(\nu b)] \Big]$$

where

$$si(z) = -f(z)\cos z - g(z)\sin z, \qquad Ci(z) = f(z)\sin z - g(z)\cos z \qquad (F.23)$$

and

$$f(z) = \int_o^\infty \frac{e^{-zt}}{t^2+1}\,dt, \qquad g(z) = \int_o^\infty \frac{te^{-zt}}{t^2+1}\,dt \qquad (F.24)$$

Substitution back in Equation (F.19) gives

$$\Delta\eta_{ip}(t) = -\frac{2\Delta p_o}{\rho_w g}\sin\omega t - \frac{\Delta p_o}{\pi\rho_w g}\{\pi - 2si(\nu b) - 4f(\nu b)\cos(\nu b)$$

$$- 4\pi\sin^2(\nu b) - 2\sin(2\nu b)[Ci(2\nu b) - Ci(\nu b)] + 2\cos(2\nu b)[si(2\nu b)$$

$$- si(\nu b)]]\}\sin\omega t + \frac{4\Delta p_o}{\rho_w g}\sin(\nu b)\cos(\nu b)\cos\omega t \qquad (F.25)$$

Equation (F.25) can be rewritten in the complex form

$$\frac{\Delta\eta_{ip}(i\omega)}{\Delta p(i\omega)} = M(i\omega) \qquad (F.26)$$

where

$$M(i\omega) = X + Yi \qquad (F.27)$$

where

$$X = \frac{-1}{\pi\rho_w g}\{3\pi - 2si(\nu b) - 4f(\nu b)\cos(\nu b) - 4\pi\sin^2(\nu b)$$

$$- 2\sin(2\nu b)[Ci(2\nu b) - Ci(\nu b)] + 2\cos(2\nu b)[si(2\nu b) - si(\nu b)]\} \quad (F.28)$$

and

$$Y = \frac{2}{\rho_w g}\sin(2\nu b)$$

The Bode plot of Equation (F.27) is given in Figure F.4. Note that in the limit as ω tends to zero Y tends to zero and X tends to $-(2/\rho_w g)$. In other words, the water surface at the cushion lip responds quasi-statically to cushion pressure variations, again as expected (see Appendix N).

F.3 Heave Stability Analysis

F.3.1 Lumped Capacitance Model

The lumped capacitance model for a unit length of an infinite length vehicle is used. For this model the thermodynamic processes within the air cavity are assumed to behave isentropically, and the flows into and out of the cavity are assumed to be governed by quasisteady incompressible orifice flow laws. In the model used below the lift fan delivers air to a plenum box at pressure p_f, which in turn feeds the cushion through an orifice. In linearized form the governing equations are: (i) conservation of volume flux for the basic cushion volume

$$C_c \frac{d\Delta p_c}{dt^2} = \Delta Q_c - \Delta Q_a - 2b\left(\frac{d\Delta x}{dt} - \frac{\overline{d\Delta\eta}}{dt}\right) \quad (F.29)$$

and (ii) Newton's law for the heave motion of the cushion

$$m\frac{d^2\Delta x}{dt^2} = 2b\ \Delta p_c + F_d \quad (F.30)$$

In these equations $C_c = V_{ce}/(\rho a_a{}^2))$ is the lumped capacitance of the cushion volume, $a = (\gamma RT)^{1/2}$ is the atmospheric sound speed, ΔQ_c is the flow perturbation into the cushion, ΔQ_a is the flow perturbation to atmosphere, Δx is the perturbation in heave, and F_d includes additional damping forces possibly due to spray formation or skirt material hysteresis. We have

$$\Delta Q_c = \Delta p_c/(R_c - C_{PQ}) \quad (F.31)$$

where

$$R_c = \frac{2(p_{fe} - p_{ce})}{Q_e}, \qquad C_{PQ} = \left.\frac{dp_f}{dQ}\right|_e \quad (F.32)$$

and Q_e is the equilibrium flow. Although in practice the damping forces in

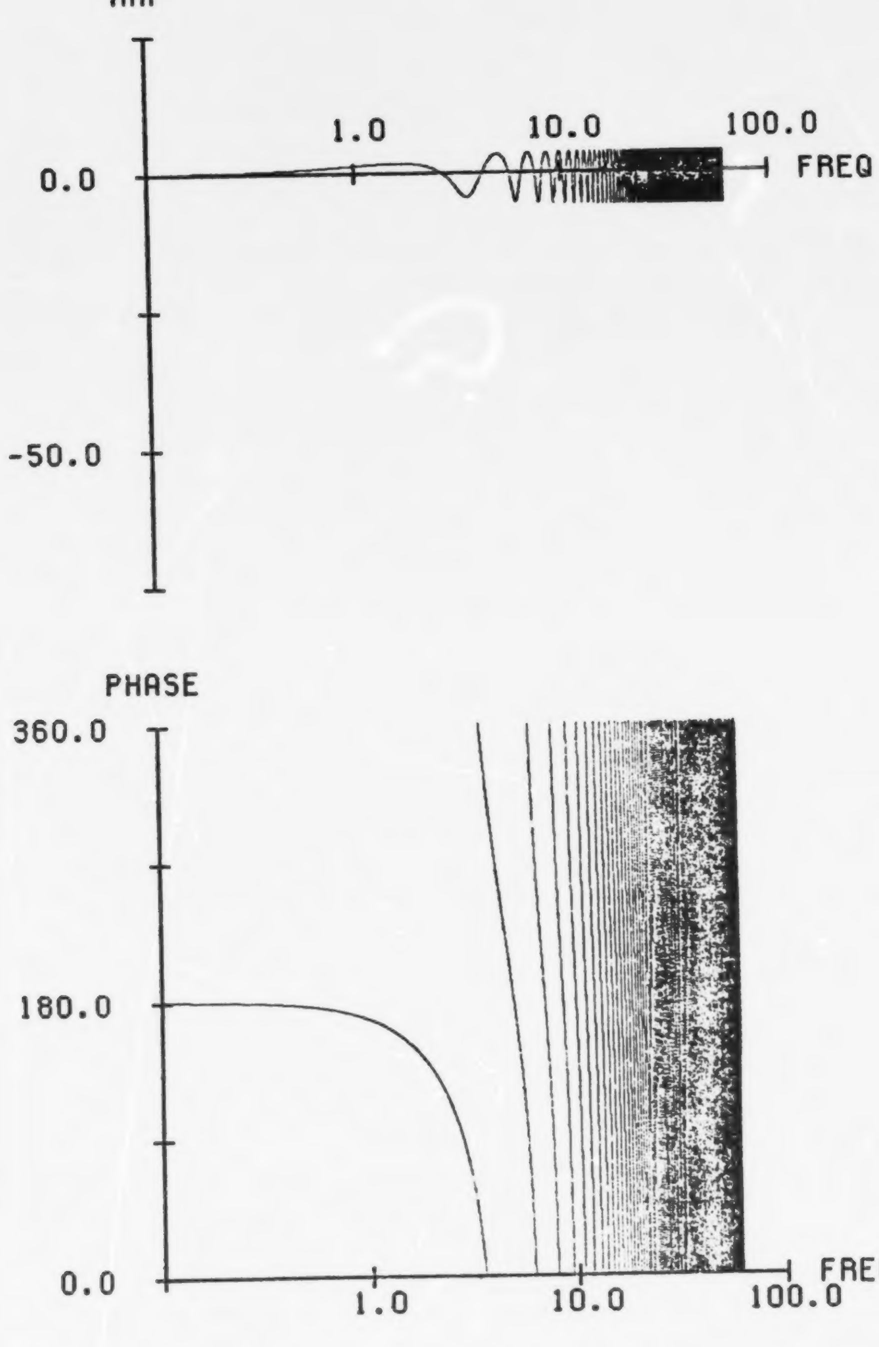

Figure F.4 Bode plot of frequency response to cushion pressure oscillations of water surface deflection at cushion lip.

(F.30) may be quite significant, for the present work they are assumed to be negligible.

F.3.2 Lip Flow Model

Observations of the flow under the lip of an air cushion vehicle hovering over water such as those shown in the photograph of Figure F.5 how that the air-water interface is almost always unstable, so that the flow degenerates into an unsteady air-water spray. Nevertheless, when the cushion is not heaving, the photographs also suggest that the flow from the interior of the cushion up to just beyond the lip is steady, so that the flow escaping from the cushion is steady. If this is the case, consideration of the equations of incompressible viscous flow of air and water suggest that for a given geometry

$$Q_a = f(\ell,\ h,\ p_c,\ g,\ \rho_a,\ \rho_w,\ \mu_a,\ \mu_w,\ \sigma) \qquad \text{(F.33.1)}$$

In this grouping the air-water surface tension σ is included since one would expect this quantity to control the rate of spray formation and thus the process of transfer of momentum from the air to the water, and thus in turn affect Q_a. Apply the Pi-theorem of dimensional analysis, using h, p_c and ρ_a as reference quantities to rewrite equation (F.33.1) in the form of an orifice flow law

$$Q = C_d \ell h (2p_c/\rho_a)^{1/2} \qquad \text{(F.33.2)}$$

where the discharge coefficient C_d has the following functional dependence:

$$C_d = f_1\left(\frac{\rho g h}{p_c},\ \frac{\rho_w}{\rho_a},\ \frac{\mu_a}{h(p_c\rho)^{1/2}},\ \frac{\mu_w}{h(p_c\rho)^{1/2}},\ \frac{\sigma}{p_c h}\right) \qquad \text{(F.33.3)}$$

Now set $p_c = \rho g H$ where H is the depth of the cushion interior water surface below the unpressurized surface, and since the dimensional analysis holds for any product of the above nondimensional groups, then we also have

$$C_d = f_2\left(\frac{h}{H},\ \frac{\rho_w}{\rho_a},\ \frac{\mu_a}{\rho g^{1/2} H^{3/2}},\ \frac{\mu_w}{\mu_a},\ \frac{\sigma}{\rho g H^2}\right) \qquad \text{(F.33.4)}$$

For a given combination of fluids this becomes

$$C_d = f_3\left(\frac{h}{H},\ \frac{\mu_a}{\rho g^{1/2} H^{3/2}},\ \frac{\sigma}{\rho g H^2}\right) \qquad \text{(F.33.5)}$$

Since $\mu_a/\rho g^{1/2}H^{3/2} \ll 1$ and $\sigma/\rho g H^2 \ll 1$ one might expect that to a first approximation C_d is thus a function of h/H only. Some preliminary measurements show a strong dependence of C_d on h/H. Typically C_d decreases from the rigid surface value of 0.61 to about 0.3 as H/h increases from zero to 2.0.

With the assumption that during heaving motion the lip flow remains quasisteady and obeys a law of the form of equation (F.33.5), the linearized form of the equation governing air escape becomes

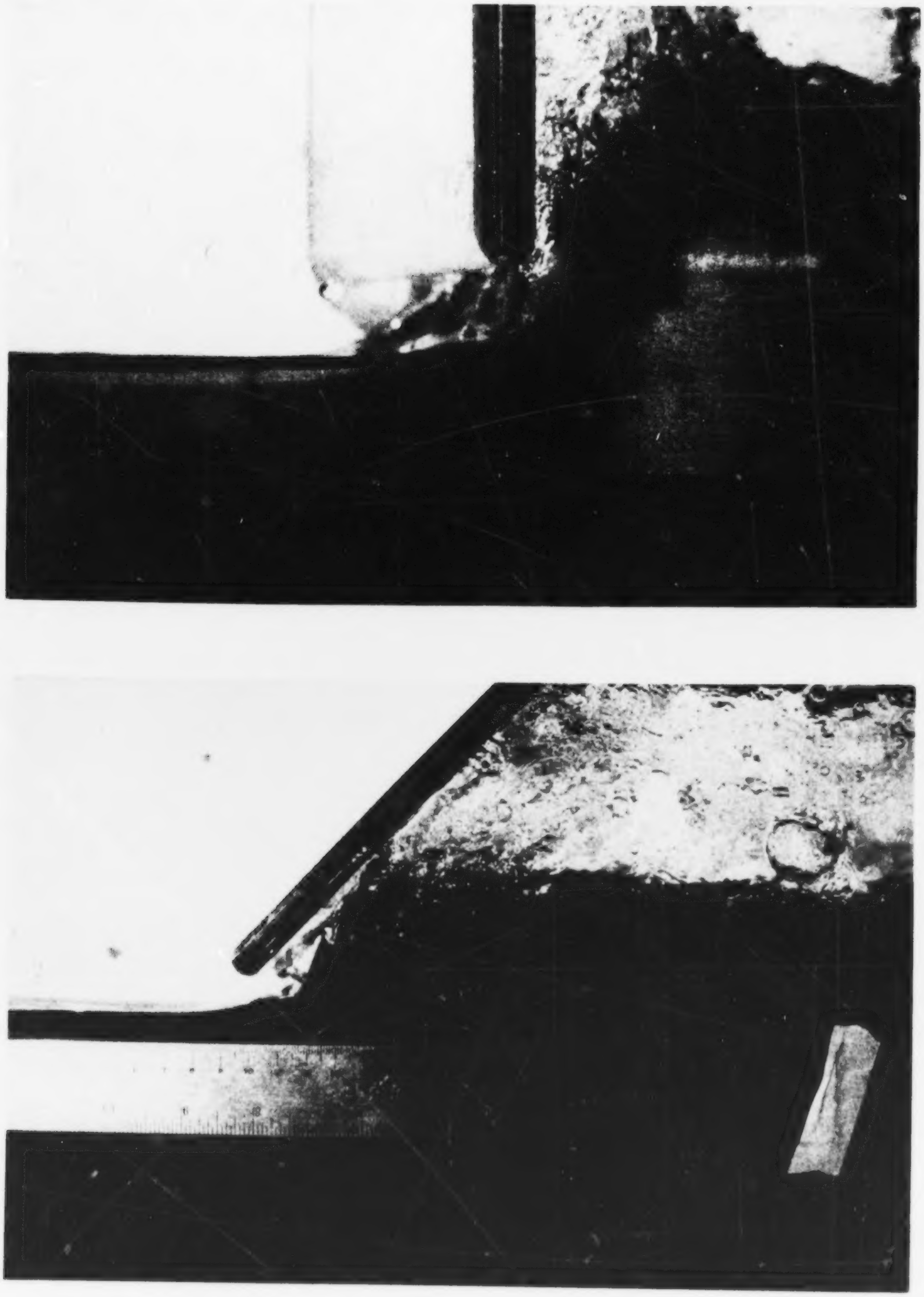

Figure F.5 Photographs of air escape process for a cushion hovering over water. The air-water interface is unstable; this instability appears to interact with the segments of a skirt, causing the latter to oscillate.

$$\Delta Q_a = \frac{\Delta p_c}{R_a} + \frac{\Delta h}{\alpha_a} \tag{F.34}$$

where

$$R_a = \frac{2p_{ce}}{Q_a} \tag{F.35}$$

and

$$\Delta h = \Delta\chi - \frac{\Delta\eta_{lip}}{2} \tag{F.36}$$

In [F.8] the flow modulation produced by deflection of the water-free surface at the lip of the plenum was ignored and $\Delta\eta$ was set equal to $\Delta\chi$.

F.3.3 Stability Criterion

By introducing the Laplace variable "s" and noting that at a stability boundary $s = i\omega$, one obtains

$$\begin{aligned} C_c i\omega\Delta p_c(i\omega) = &- \frac{\Delta p_c(i\omega)}{R_c - C_{PQ}} - \frac{\Delta p_c(i\omega)}{R_a} - \frac{\Delta\chi(i\omega)}{\alpha_a} + \frac{\Delta\eta_{lip}(i\omega)}{2\alpha_a} \\ &- 2bi\omega[\Delta\chi(i\omega) - \overline{\Delta\eta}(i\omega)] \end{aligned} \tag{F.37}$$

and

$$-m\omega^2\Delta\chi(i\omega) = 2b\Delta p_c(i\omega) \tag{F.38}$$

where

$$\Delta\eta_{lip}(i\omega) = (X + Yi)\Delta p_c(i\omega), \qquad \overline{\Delta\eta}(i\omega) = (A + Bi)\Delta p_c(i\omega) \tag{F.39}$$

Substitution of Eqs. (F.38) and (F.39) into (F.37) gives

$$(\Delta_R + \Delta_I i)\Delta p_c(i\omega) = 0 \tag{F.40}$$

where

$$\begin{aligned} \Delta_R &= \frac{1}{R_c - C_{PQ}} + \frac{1}{R_a} - \frac{2b}{m\omega^2}\frac{1}{\alpha_a} + 2Bb\omega - \frac{X}{2\alpha_a} \\ \Delta_I &= -2Ab\omega - \frac{(2b)^2}{m\omega} + C_c\omega - \frac{Y}{2\alpha_a} \end{aligned} \tag{F.41}$$

where

$$\Delta_R + i\Delta_I = 0 \tag{F.42}$$

is the system characteristic equation with $s = i\omega$. For a nontrivial solution to exist, both the real and imaginary parts of the characteristic equation must separately vanish [F.9]. Thus

$$\Delta_R = 0, \qquad \Delta_I = 0 \tag{F.43}$$

When the equilibrium gap h_e is specified, the remaining unknowns in Equations (F.43) are the equilibrium cushion pressure p_{ce} and the oscillation frequency ω. A numerical search of the (p_{ce}-ω) plane could be used to obtain a solution. Unfortunately, the technique of setting $s = i\omega$ to find a stability boundary has the limitation that a solution of Eqs. (F.43) is not necessarily associated with critical stability. This is because Equations (F.43) are satisfied when any root of the system characteristic equation lies on the imaginary axis in the s-plane. Thus the system could already be asymptotically unstable because there could already be one or more roots in the right half of the s-plane. The problem could be circumvented by multiplying the coefficients in the water compliance transfer functions by a factor β. With $\beta = 0$, the water compliance effect is effectively removed, and one should be left with the case of an air cushion vehicle hovering over a rigid surface. The value of p_{ce} for critical stability for this case as obtained by the rigid surface lumped capacitance Routh-Hurwitz criteria should agree with the prediction of Equations (F.43). As β is increased from zero to one, a continuous change in the values of p_{ce} and ω at which Equations (F.43) are satisfied should occur which would indicate that the values obtained are associated with critical stability. This was found to be the case here when the piston effect was studied.

The stability question can also be dealt with the aid of the Nyquist plot concepts and the block diagram representation given in Figure F.6. The open-loop frequency response function of the system is $G(i\omega)H(i\omega)$ where

$$G(i\omega) = \frac{-\dfrac{1}{\alpha_a} - 2bi\omega}{C_c i\omega + \dfrac{1}{R_c - C_{PQ}} + \dfrac{1}{R_a} - \dfrac{X + Yi}{2\alpha_a} - 2bi\omega(A + Bi)}, \qquad H(i\omega) = \frac{2b}{m\omega^2} \tag{F.44}$$

A Nyquist plot is a plot of $G(i\omega)H(i\omega)$ in a real-imaginary plane. Theory shows that $s = i\omega$ when $|G(i\omega)H(i\omega)| = 1$ and the phase angle of $G(i\omega)H(i\omega)$ is -180°. In other words, it occurs when the $G(i\omega)H(i\omega)$ plot passes through the $s = -1$ point in the complex plane. When the phase of $G(i\omega)H(i\omega)$ at $|G(i\omega)H(i\omega)| = 1$ is less negative than -180°, the force acting on the suspension mass leads the negative of $\Delta\chi$ whereas when the phase is more negative than -180° it lags. Simple arguments based on the work done on the suspension mass during an oscillation cycle show the lead case is stable whereas the lag case is unstable.

Note that it has been implicitly assumed that the water response functions $N(i\omega)$ and $M(i\omega)$ are unaffected by transients in the basic air cushion. Thus one has a characteristic equation with complex coefficients

$$C_3 s^3 + C_2 s^2 + C_1 s + C_0 = 0 \tag{F.45}$$

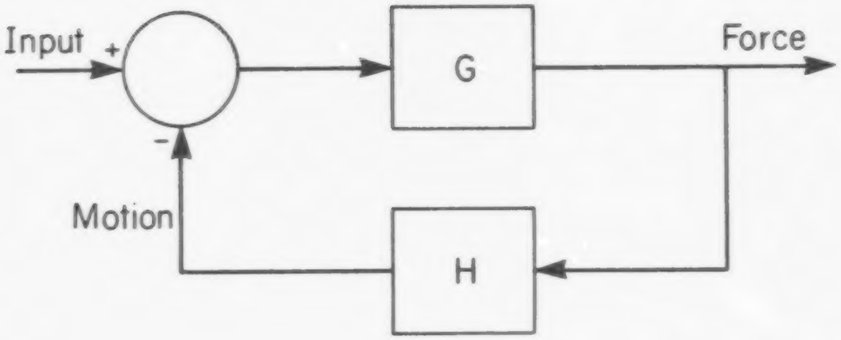
Input
+
G
Force
-
Motion
H

Figure F.6 Canonical block diagram used in Nyquist stability analysis.

where

$$C_3 = m\left(C_c/(2b) - N(i\omega)\right), \quad C_2 = \frac{m}{2b}\left\{\left(\frac{1}{R_c - C_{PQ}} + \frac{1}{R_a}\right) - \frac{M(i\omega)}{2\alpha_a}\right\}$$

$$C_1 = 2b, \qquad C_0 = \alpha_a^{-1} \qquad \text{(F.46)}$$

If the coefficient of the imaginary part of any root of this equation is equal to the frequency used to evaluate $N(i\omega)$ and $M(i\omega)$, then that particular root is valid provided that its real part is close to zero; otherwise the roots have no physical significance. This fact is used in the following sections to determine the nature of stability immediately next to a particular stability boundary.

F.4 Results for HEX-5

F.4.1 Effect of Spatially Averaged Deflection

The theory was applied to the HEX-5 research craft. Its dimensions are given in Table F.1.

Table F.1

Data for the Two Vehicles Used in Calculations

Parameter	Vehicle HEX-5	Large Platform
Length (m)	3.75	15
Beam width (m)	2.5	15
Cushion depth (m)	0.2	1.4
Maximum weight (tonnes)	1.27	270
Fan slope (kPa m^{-3} sec)	-1.875/metre at 1 kPa	-0.15 at 5 kPa
Discharge coefficient of equivalent fan orifice	0.61	0.61
Discharge coefficient at lip	0.8	0.40

For a typical operating gap of $h_e = 4.57$ mm[1] rigid surface lumped capacitance calculations indicate that the system would be unstable for cushion pressures p_{ce} greater than 6.84 kPa; note in Table F.1 that a typical operating pressure is 1 kPa. So the HEX-5 should be very stable over land, which in fact it is. The theory of Section F.3 indicates that the spatially averaged deflection acting by itself would cause an approximately 5-fold increase in critical stability pressure. The behaviour at other gaps is similar. Figures F.8 to F.11 give Nyquist plots for selected values of equilibrium cushion pressure showing the piston effect. Rigid surface Nyquist plots are given for reference in Figure F.7. To obtain these and the following plots the theory of Ogilvie-Stoker has been used unless specifically stated to the contrary, in which case Lamb's theory, as described in Appendix O has been used.

---

[1] For a cushion pressure of 1 kPa, this gap gives a typical operating flow.

The major reason for the large stabilizing tendency is that the oscillation frequency at the critical stability pressure is typically well beyond the break frequency associated with the cushion pressure-water surface interaction. In fact, the water piston motion is typically close to being in phase with the cushion pressure. This is similar to a skirt flexibility which causes the cushion volume to decrease when the cushion pressure increases. As has been shown elsewhere [F.11, F.12], such a flexibility is stabilizing because it counteracts the destabilizing lag effect of cushion air compressibility.

The Routh-Hurwitz stability criterion for the rigid surface case is

$$\frac{Q_e}{2(p_{fe} - p_{ce})} + \frac{Q_e}{2p_{ce}} > \frac{C_c}{2b}\frac{1}{\alpha_a} \qquad (F.47)$$

The criterion with quasi-static piston-like water motion is

$$\frac{Q_e}{2(p_{fe} - p_{ce})} + \frac{Q_e}{2p_{ce}} > \frac{C_c}{2b}\frac{1}{\alpha_a} + \frac{1}{\rho_w g}\frac{1}{\alpha_a}$$

$$> \left(\frac{h_s}{\rho_a a^2} + \frac{1}{\rho_w g}\right)\frac{1}{\alpha_a} \qquad (F.48)$$

In this case the water compliance piston term would dominate the air compressibility term and cause a large decrease in critical stability pressure. So at very low frequencies the piston-like water motion would reduce stability. It would add to the destabilizing lag effect of cushion air compressibility.

F.4.2 Effect of Flow Modulation Produced by Deflection at Lip

The theory of Section F.3 indicates that the flow modulation produced by deflection of the water surface at the lip acting alone causes unstable behaviour at low cushion pressures but greatly improved stability at high cushion pressures.

The Routh-Hurwitz criterion with quasi-static lip flow modulation is

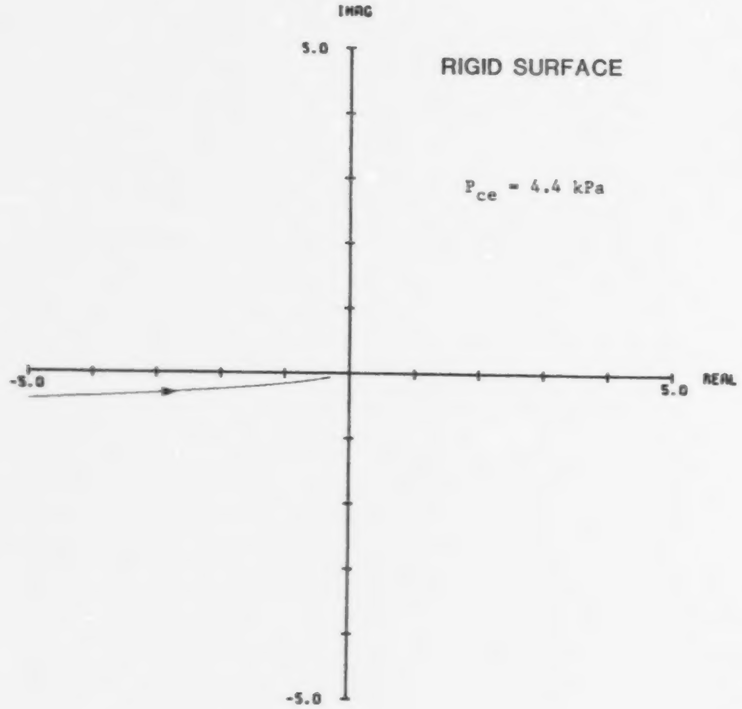

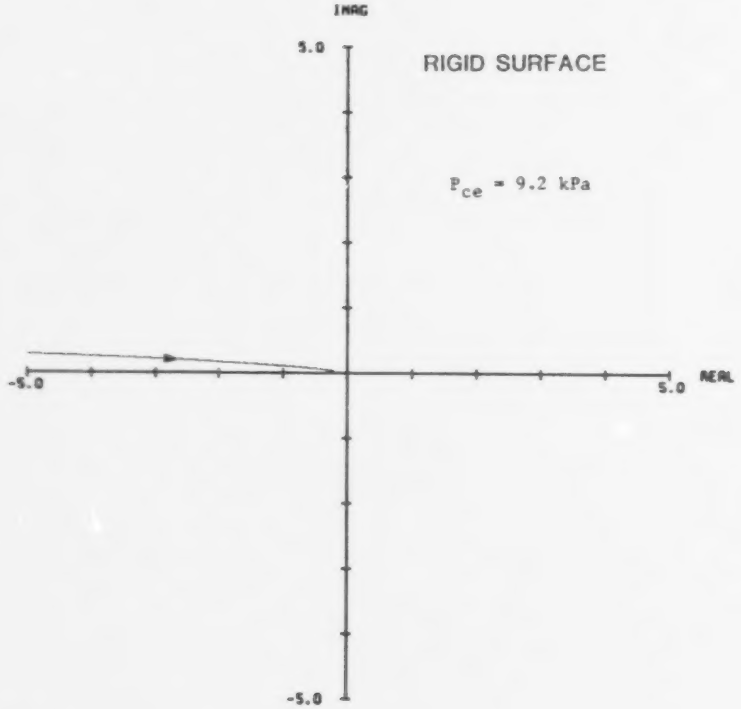

Figure F.7 Typical Nyquist plots for overland operation of HEX-5, for p_{ce} = 4.4 kPa and p_{ce} = 9.2 kPa. For the latter case the system is unstable.

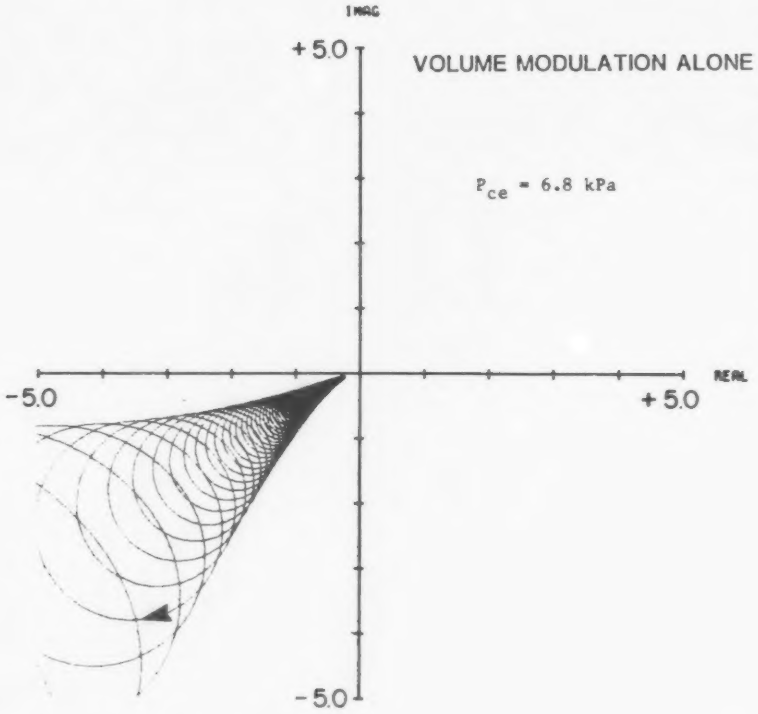

Figure F.8 Nyquist plot for HEX-5 showing cavity pumping effect at P_{ce} = 6.84 kPa. The cushion is stable.

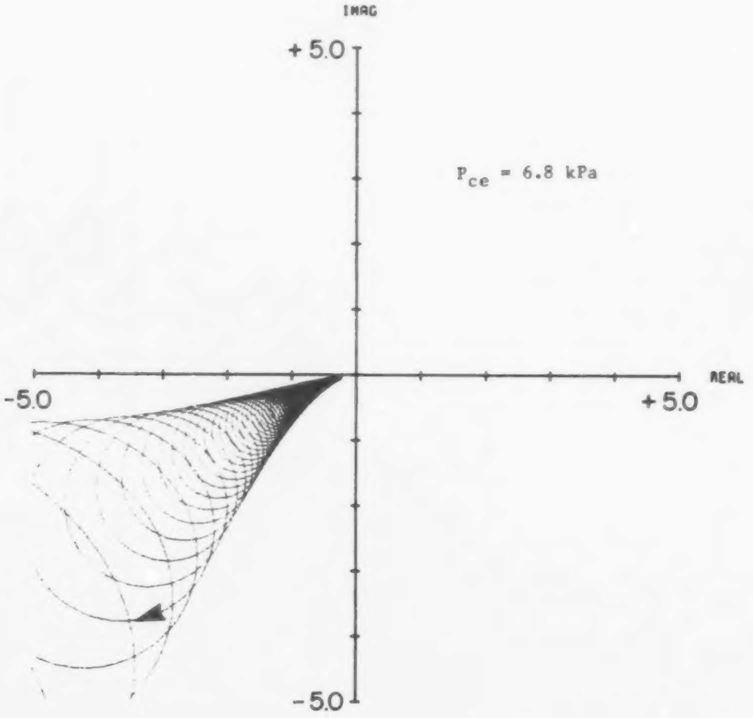

Figure F.9 Nyquist plot for HEX-5 showing cavity pumping effect at P_{ce} = 6.84 kPa according to theory of Lamb.

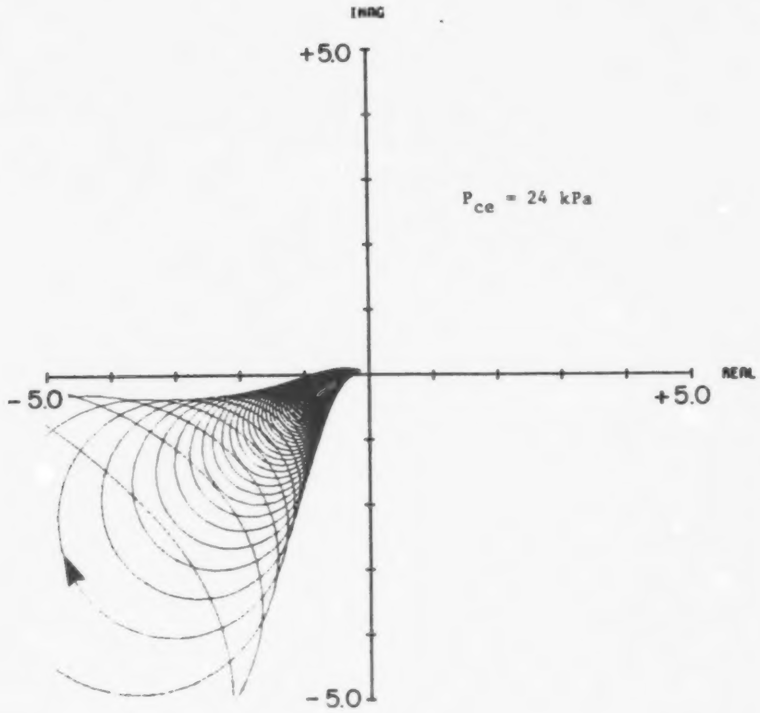

Figure F.10. Nyquist plot for HEX-5 showing the cavity pumping effect at P_{ce}=24.0 kPa. The cushion is stable.

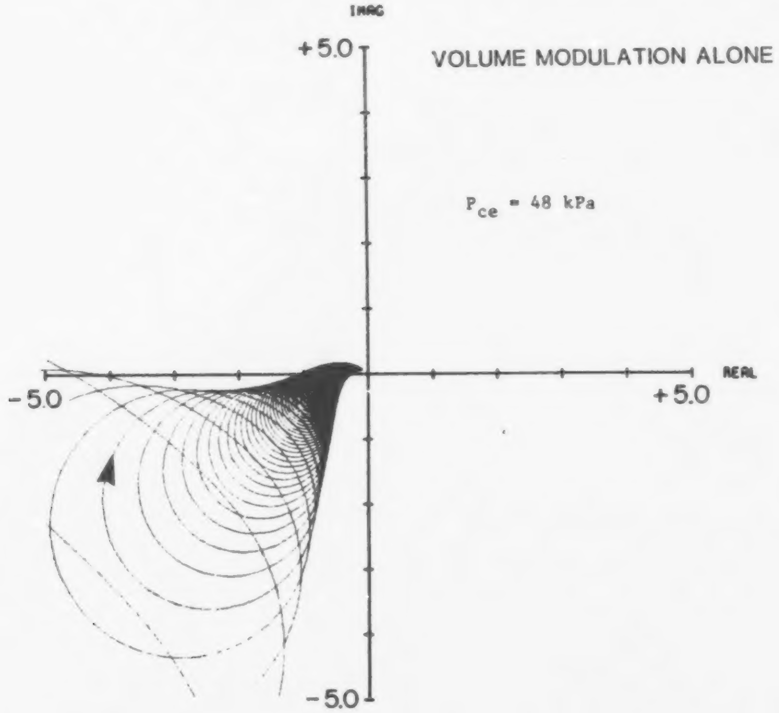

Figure F.11 Nyquist plots for HEX-5 showing cavity pumping effect at P_{ce} = 48.0 kPa. The cushion is unstable.

$$\frac{Q_e}{2(p_{fe} - p_{ce})} + \frac{Q_e}{2p_{ce}} > \left(\frac{C_c}{2b} - \frac{2}{\rho_w g}\right) \frac{1}{\alpha_a}$$

$$> \left(\frac{h_s}{\rho_a a^2} - \frac{2}{\rho_w g}\right) \frac{1}{\alpha_a} \tag{F.49}$$

In this case the lip flow modulation term would again dominate the air compressibility term but unlike the water compliance piston term it would cause a very large increase in critical stability pressure. This suggests that the improved stability at high cushion pressures is due to the water surface responding approximately quasi-statically.

F.4.3 Spatially Averaged Deflection and Lip Flow Modulation

When both flow modulation and spatially averaged deflection are considered together it is found that in general flow modulation dominates. Figures F.12 to F.15 show Nyquist plots for this case. These show improved stability at high cushion pressures and unstable behaviour at low cushion pressures.

Equation (F.45) shows that for p_{ce} slightly greater than the critical pressure at approximately 3.0 kPa the system is unstable whereas for pressures slightly less the system is stable. The work done argument also suggests this. However the work done argument also predicts that the system is very stable at high cushion pressures. This means that there must be a stability boundary at some pressure greater than 3.0 kPa where the system passes into the stable region at high cushion pressures. Using equation (F.45), it was found that at this boundary $s \neq i\omega$. In other words, the boundary is not one at which the damping associated with a particlar root changes sign. It was found that this boundary occurred at a cushion pressure where the frequency associated with the potentially unstable root failed to match the frequency used to evaluate $N(i\omega)$ and $M(i\omega)$, no matter what value of ω was used, while at slightly lower pressures the frequencies did match. In other words as the cushion pressure is increased beyond this value instability would suddenly disappear. This behaviour is a consequence of having a characteristic equation with complex coefficients.

F.5 Results for a Large Platform

F.5.1 Cavity Pumping

The basic data assumed for a large platform cushion is given in Table F.1. For this vehicle, when cavity pumping is considered on its own, one obtains Nyquist plots such as those shown in Figures F.16 and F.17. Those in Figure F.16 are for a range of hovergaps; for each hovergap the cushion pressure is equal to the overland critical pressure. They show that cavity pumping on its own improves stability but only slightly. A small increase in pressure causes the Nyquist plots to move up and pass through the minus one point. Two examples of this shift with pressure are given in Figure F.17.

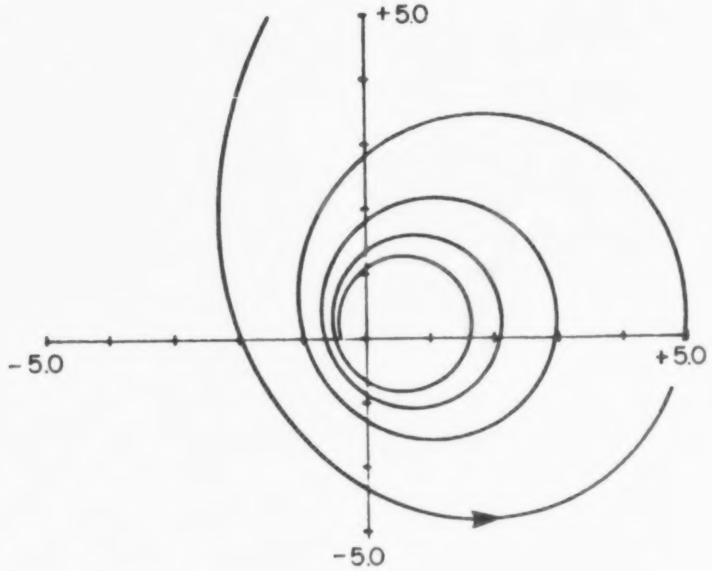

Figure F.12. Nyquist plot for HEX-5 showing combined lip flow modulation and cavity pumping effect at p_{ce}=1.5 kPa. The cushion is stable.

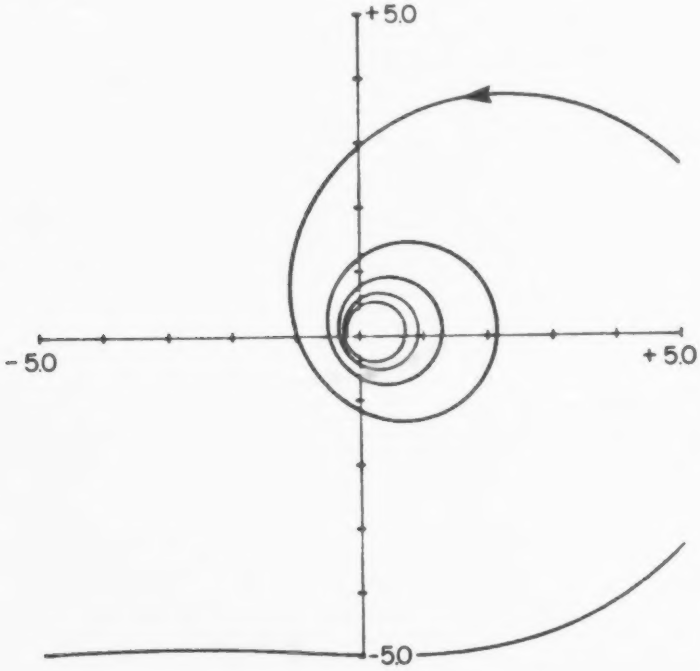

Figure F.13. Nyquist plot for HEX-5 showing combined lip flow modulation and cavity pumping effect at p_{ce}=3.0 kPa. The cushion is unstable.

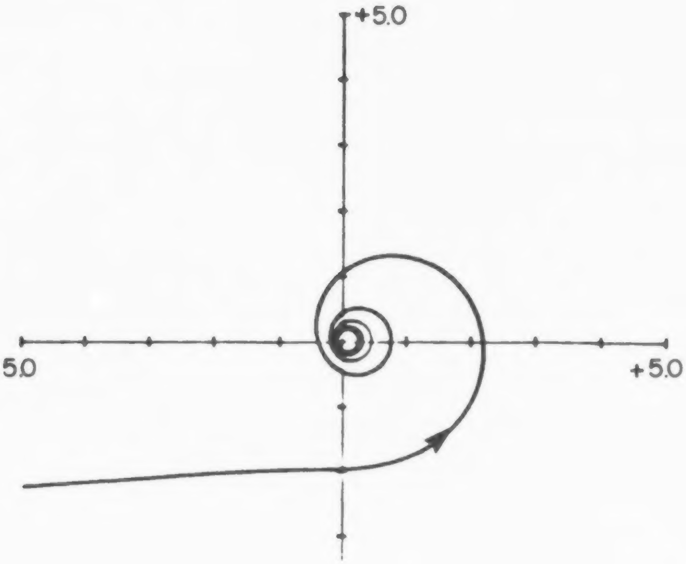

Figure F.14. Nyquist plot for HEX-5 showing a combined flip flow modulation and cavity pumping effect at p_{ce}=6.8 kPa. The cushion is unstable.

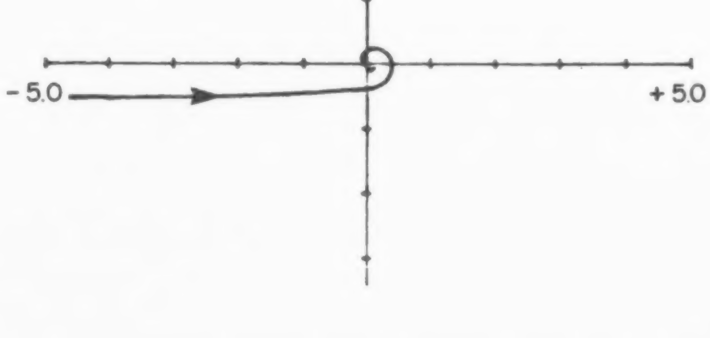

Figure F.15. Nyquist plot for HEX-5 showing a combined lip flow modulation and cavity pumping effect at p_{ce}=35 kPa. The cushion is stable.

F.5.2 Flow Modulation and Cavity Pumping

As for HEX-5, when flow modulation and cavity pumping are considered together, flow modulation generally dominates. Typical plots with both effects included are given in Figures F.18 to F.21. Compared to those accounting for cavity pumping on its own, these can be seen to have a fundamentally different structure. Those in Figure F.18 show that the effect is not prominent at low pressures. Also, passage through the minus one point for a given gap can be seen to occur for an infinite sequence of critical pressures. Figures F.19 to F.21 show respectively the trends associated with changes in gap, leakage discharge coefficient and fan slope. They are for the highest pressure in the sequence of critical pressures associated with passage through the minus one point. Although these parameters have a large effect over land, they apparently have much less of an effect over water. It is interesting to note that a quasi-static water response model predicts that volume modulation would greatly reduce stability relative to over land and flow modulation would greatly increase it. These predictions contrast sharply with those of the dynamic water response model.

F.6 Conclusions

The computed results indicate that, of the two effects of a heaving cushion on the motion of the water under it considered here, namely cushion cavity pumping and lip flow modulation, the latter is more important in affecting vehicle stability. Furthermore no simple rule can be given, other than that it appears to have a large effect. It should also be noted that since the present theory has been developed for an infinitely long two-dimensional cross-section air cushion, it can at best give qualitative insights. Two important extensions to this work that should be pursued are (i) the equivalent linear axisymmetric geometry analysis, and (ii) nonlinear effects. The axisymmetric analysis could be expected to give results which are more physically realistic.

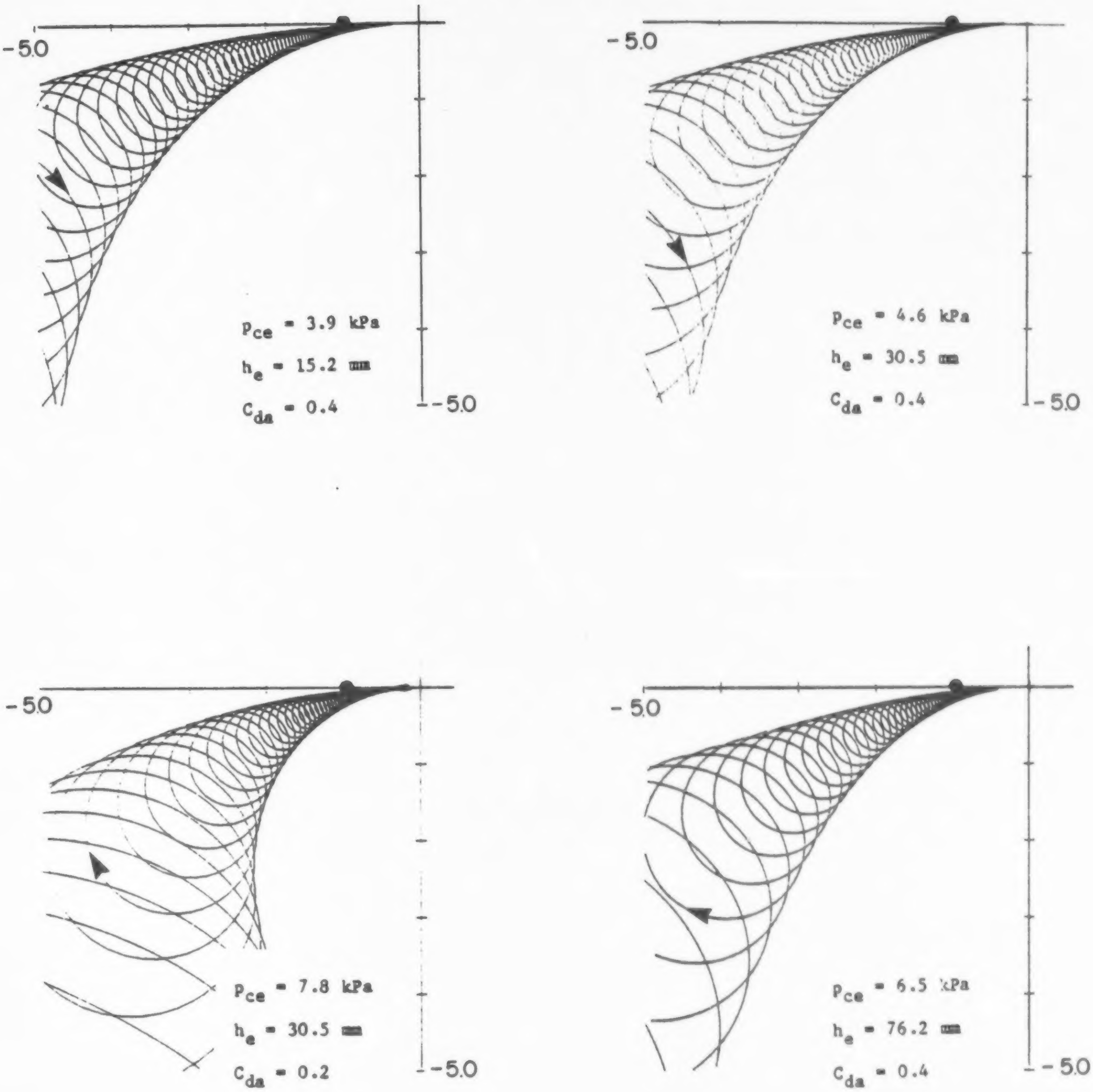

Figure F.16. Nyquist plots for the large platform showing cavity pumping effect for a range of hovergaps with p_{ce} set equal to the critical stability value for overland operation.

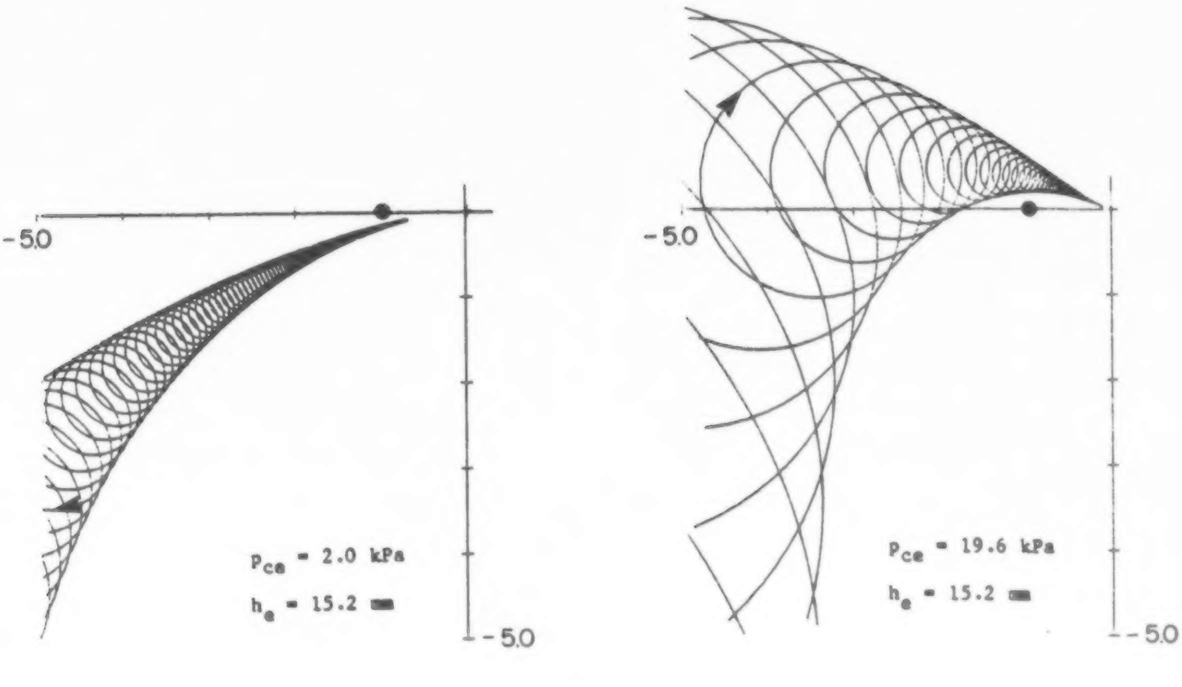

Overland 3.9 kPa

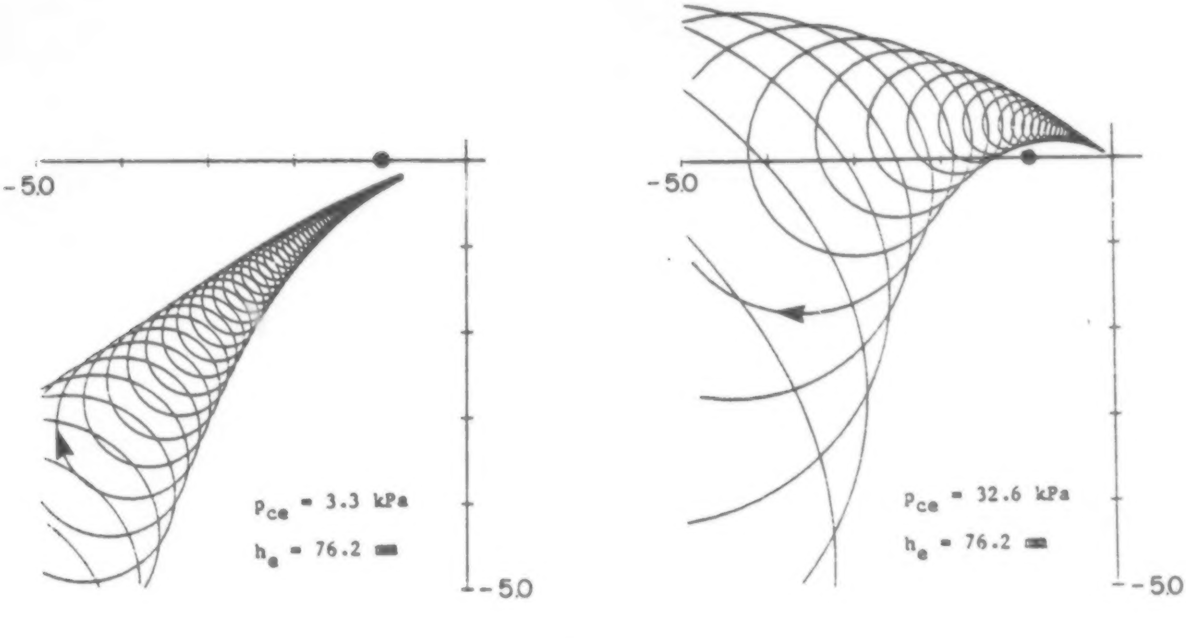

Overland 6.5 kPa

C_{da} = 0.4

Figure F.17. Nyquist plots for the large platform showing cavity pumping effect and the effect of a change of pressure for two hovergaps, (a) 15.2 mm, and (b) 76.2 mm. The lip discharge coefficient is 0.4.

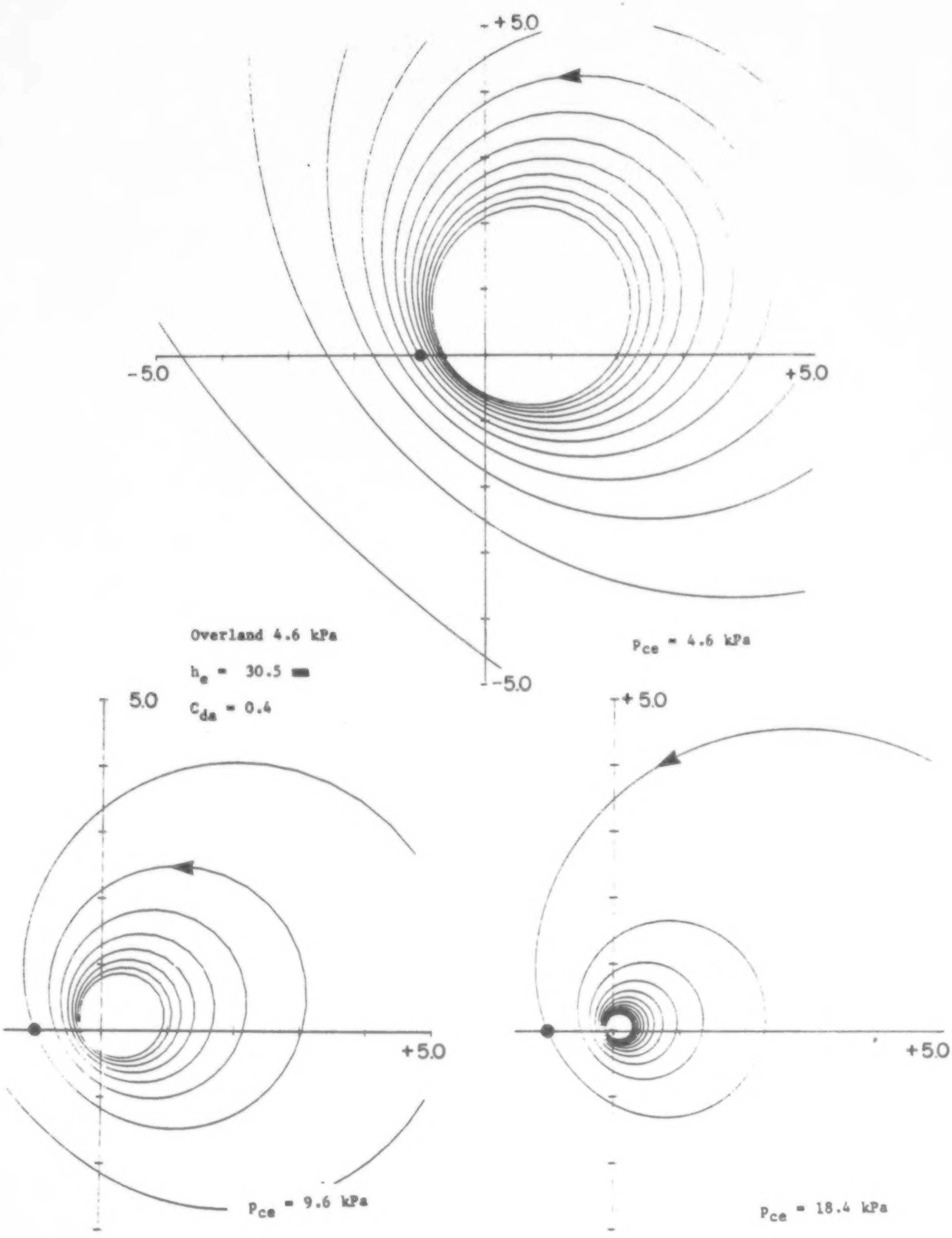

Figure F.18. Nyquist plots for the large platform showing lip flow modulation effect for hovergap = 30.5 mm. Lip discharge coefficient = 0.4 and overland critical p_{ce}=4.6 kPa.

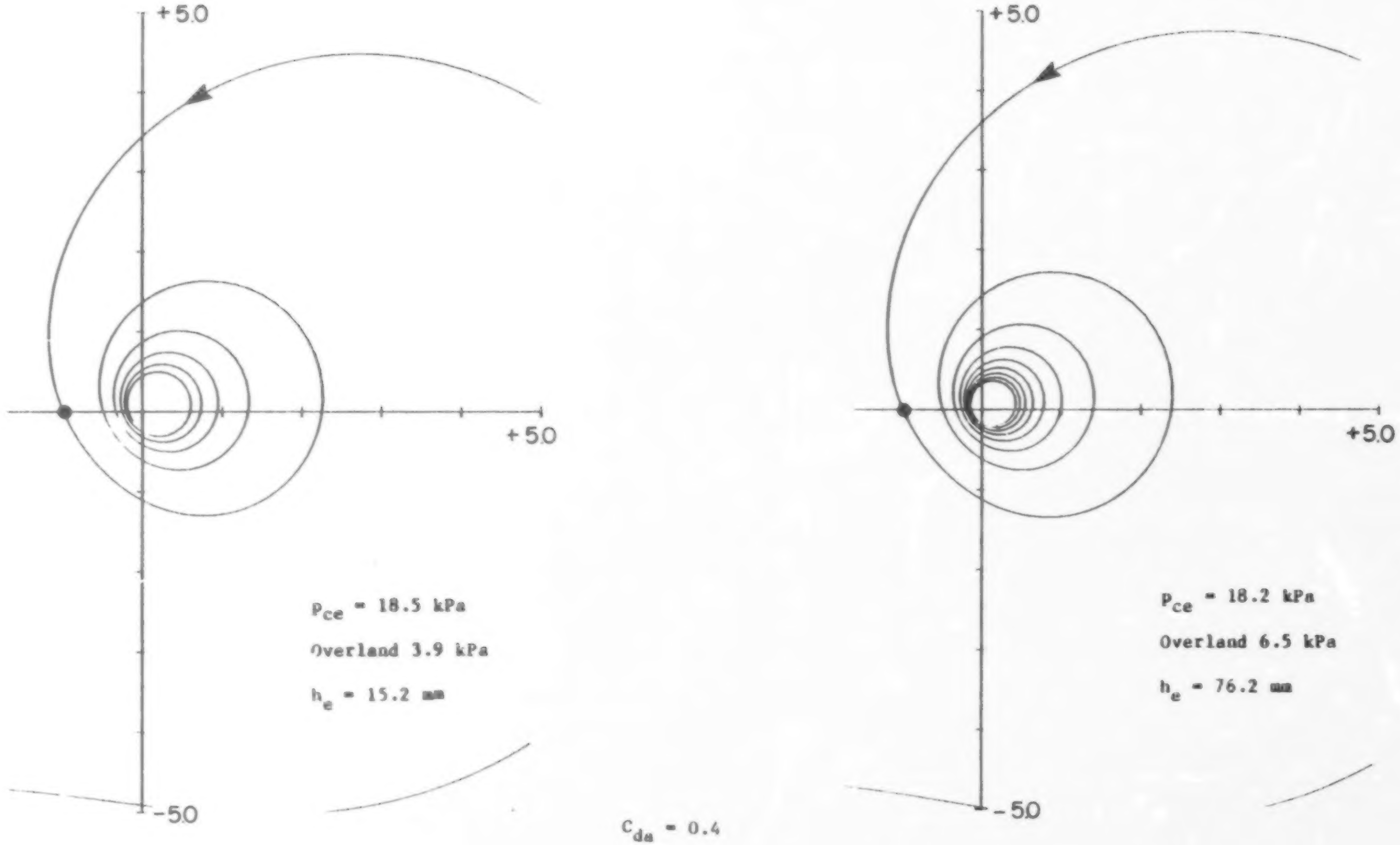

Figure F.19. Nyquist plots for the large platform showing effect of changing hovergap. Lip discharge coefficient = 0.4.

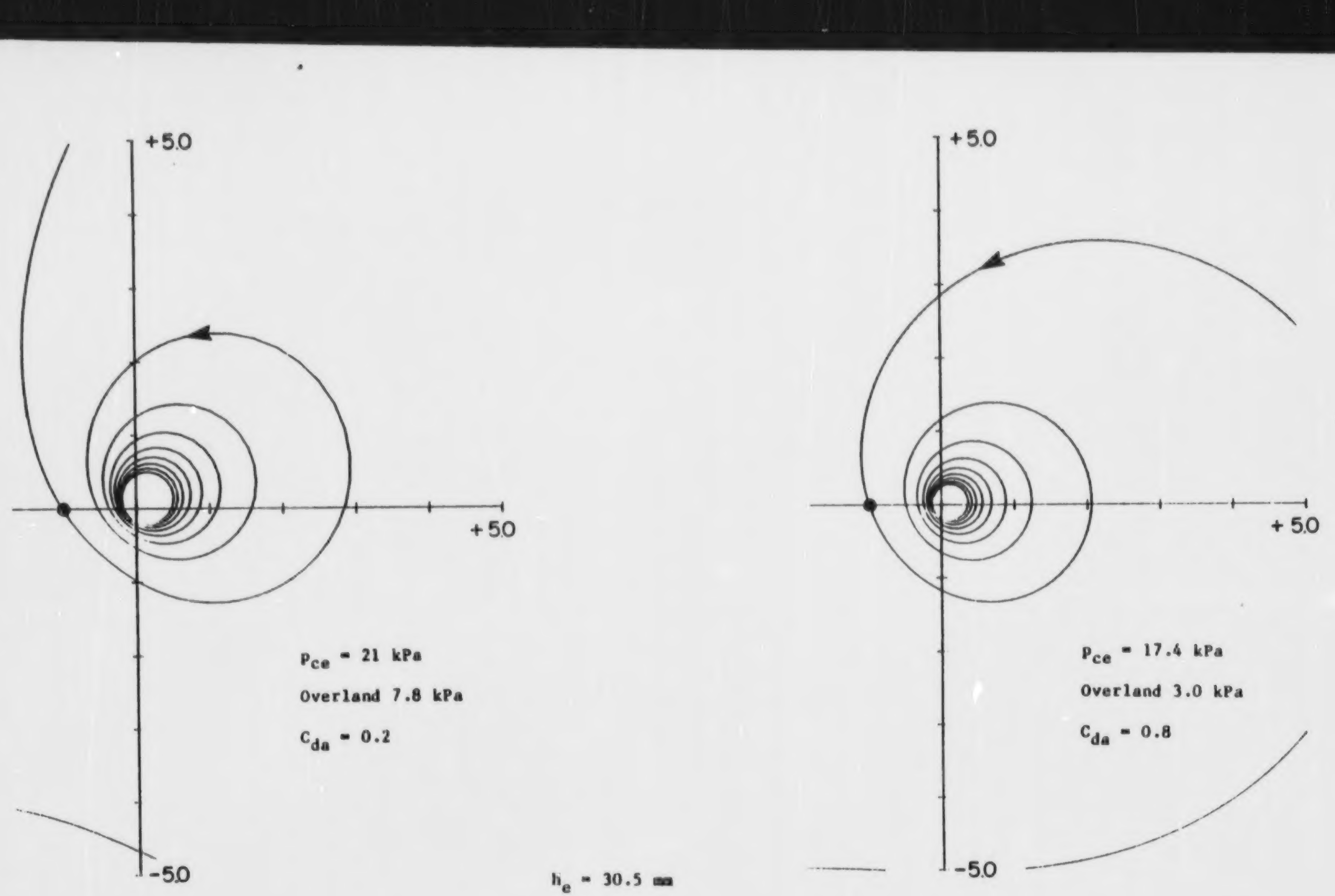

Figure F.20. Nyquist plots for the large platform showing effect of changing discharge coefficient at a hovergap h_e = 30.5 mm.

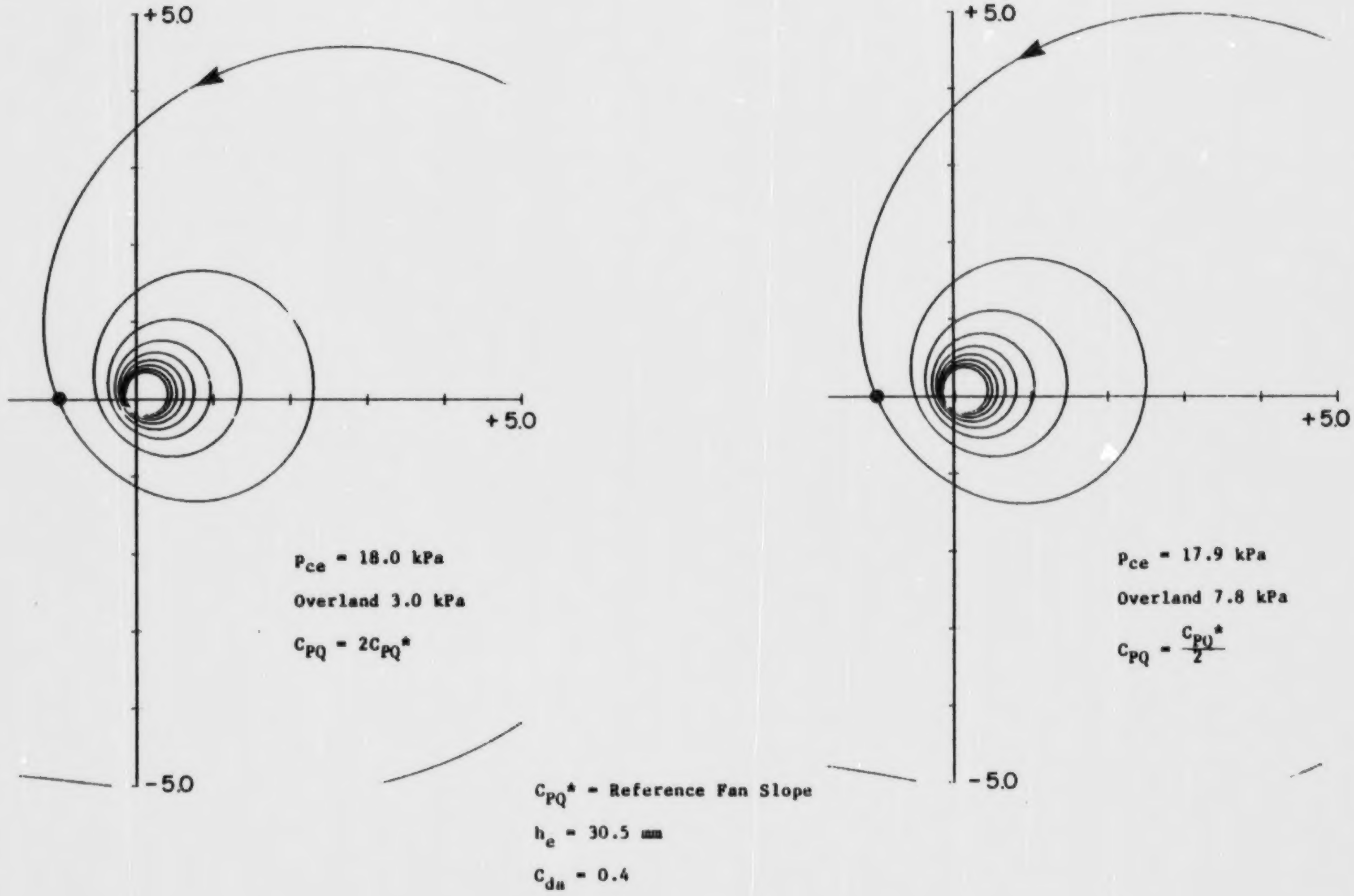

Figure F.21. Nyquist plots for the large platform showing effect of changing lift fan characteristic slope at a hovergap of 30.5 mm and for discharge coefficient = 0.4. Here C_{PQ}^* is the reference value given in Table F.1.

REFERENCES - APPENDIX F

F.1 Fowler, H. S., "An Experiment on the Heave Oscillation of a Light Air Cushion Vehicle Over Water", Canadian Aeronautics and Space Journal, Vol. 26, No. 2, 1980, pp. 92-96.

F.2 Barratt, M. J., "The Wave Drag of a Hovercraft", Journal of Fluid Mechanics, Vol. 22, No. 1, 1965, pp. 39-47.

F.3 Hogben, N., "Hovering Craft Over Water", Advances in Hydroscience, Vol. 14, Academic Press, New York, 1967, see pp. 1-72.

F.4 Doctors, L. J., "The Experimental Wave Resistance of an Accelerating Two-Dimensional Pressure Distribution", Journal of Fluid Mechanics, Vol. 72, No. 3, 1975, pp. 513-527.

F.5 Ogilvie, T. F., "Oscillating Pressure Fields on a Free Surface", University of Michigan, Department of Naval Architecture and Marine Engineering, Ann Arbor, Michigan, Report No. 030, Sept. 1969.

F.6 Stoker, J. J., Water Waves, Interscience, new York, 1957, see pp. 58-66.

F.7 Lamb, H., "On Deep Water Waves", Proceedings of the London Mathematical Society, Series 2, Vol. 2, Nov. 1904, pp. 371-400.

F.8 Sullivan, P. A., et al, "Research into Air Cushion Stability - 1979 Report", Transportation Development Centre, Transport Canada, Montreal, Quebec, TP3109E, Jan. 1982. See Sect. 6.

F.9 Hahn, W., Stability of Motion, Springer-Verlag, Berlin, 1967.

F.10 Fung, Y. C., An Introduction to the Theory of Elasticity, Dover, New York, 1964.

F.11 Ribich, W. A., and Richardson H. H., "Dynamic Analysis of Heave Motion for a Transport Vehicle Fluid Suspension", Massachusetts Institute of Technology, Cambridge, Mass., Department of Mechanical Engineering Report DSR-76110-3, 1967.

F.12 Hinchey, M. J., "Heave Instabilities of Amphibious Air Cushion Suspension Systems", University of Toronto, Institute for Aerospace Studies Report No. 246, 1979.

APPENDIX G. PREDICTION OF HOVERCRAFT HEAVE STABILITY (M. J. Hinchey and P. A. Sullivan)

NOMENCLATURE

Roman

A	orifice area
$\underline{A}$	system matrix, $\dot{\underline{x}} = \underline{A}\,\underline{x}$
a	sound speed, $(\gamma RT)^{1/2}$
C_A	inlet area/cushion pressure coefficient, $\left.\frac{dA_f}{d\dot{p}_c}\right\|_e$
C_c	cushion pneumatic capacitance, $V_{ce}/\rho a^2$
C_d	discharge coefficient
C_{PQ}	fan slope, $dp_f/dQ_f\|_e$
C_{QC}	flow coefficient, Q_e/Q_{ref}
C_V	cushion volume/cushion pressure coefficient, $dV_c/dp_c\|e$
C_0, C_1, C_2, C_2	coefficients in characteristic equation
C_s	skirt damping coefficient
D	diameter
F	flexibility contribution to cushion volume
G	flexibility contribution to skirt height
GH	open loop transfer function
g	gravitational acceleration
h	hovergap
$\underline{I}$	identity matrix
i	imaginary number, $(-1)^{1/2}$
K_0, K_1, K_2, K_3	coefficients in non-linear fan characteristic
k_s	skirt spring coefficient
L_s	perimeter

L_d	duct length
L_o	characteristic length
$\dot{M}$	mass flow rate
m	supported mass
n	polytropic exponent
p	pressure
Q	volumetric flow rate
R	gas constant
R_j	residual
S	support area
T	temperature
t	time
U	flow velocity
V	volume
W_k	weighting function
W	weight or work
x	state variable

Greek

α_n	gap flow parameter
γ	isentropic exponent
Δ	perturbation
κ	static air spring stiffness
λ	eigenvalue
ρ	air density
τ_1	lead time constant
τ_2	lag time constant
χ	heave displacement
ω	frequency

Subscripts

c	cushion
d	duct
e	equilibrium
eff	effective
f	fan
h	hovergap
m	model
o	outlet or orifice
p	prototype
ref	reference
s	skirt or streamline

G.1 Introduction

An air cushion vehicle or hovercraft is an amphibious vehicle which floats on a cushion of pressurized air supplied by one or more fans and contained by a flexible skirt. The skirt is essentially a collapsible structure constructed from an elastomer coated fabric. It is inflated and stabilized by the cushion pressure, and it enables the vehicle to negotiate large obstacles or waves while maintaining low cushion airflow requirements. The success of the hovercraft concept is in large part due to skirt development.

Since the early sixties hovercraft have been developed in Canada for a number of specialized uses. For example, they are now being used on a regular basis by the Canadian Coast Guard for search and rescue operations and also for icebreaking and flood control. They are being considered for use in the Arctic to support and transport oil drilling rigs and other structures. However, one problem frequently encountered during operation is the tendency of the systems to be unstable, usually in heave. This tendency often leads to steady state oscillations known as limit cycles. For some applications these are of only a nuisance value, and a nominal change in operating conditions is often sufficient to suppress them. However, they can cause operational difficulties and, in extreme cases, lead to destruction of the vehicle. Such oscillations were encountered during the field trials of the ACT-100 in the early seventies and more recently during the field trials of an icebreaker bow platform or ACIB currently being developed in Canada.

The present report reviews the mathematical procedures that have been developed for studying the heave instability. The emphasis throughout is on establishing physical insights. For this work, only simple air cushion models such as that shown in Figure G.1 are used. Also, attention is restricted to heave motion only. The governing equations and their inherent assumptions are presented first. This is followed by a brief review of basic stability concepts. Insights from linear theory are presented next, followed by a discussion of some inherently non-linear phenomena. The report ends with a review of the available experimental data.

G.2 Air Cushion Model

The equations used to study stability and dynamics of air cushions employ many assumptions. The implications of these assumptions are dealt with in detail in references G.3 and G.4. Here, for the geometry of Figure G.1, they are summarized briefly.

First, the air in the cushion volume is assumed to be compressible, and at any instant in time the pressure is assumed to be uniform throughout the volume. Thus, one can write the lumped volume conservation of mass equation

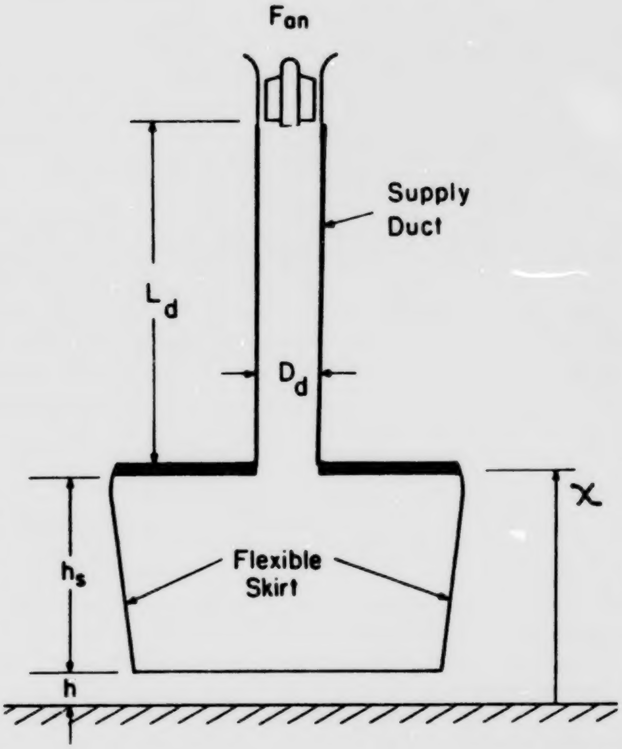
Fan
Supply Duct
L_d
D_d
x
h_s
Flexible Skirt
h

Figure G.1 Air cushion model used in the analysis.

$$\frac{d}{dt}(\rho V_c) = \dot{M}_{in} - \dot{M}_{out} \qquad (G.1)$$

where ρ is the cushion air density, V_c is the total cushion volume, and $\dot{M}_{in}$ and $\dot{M}_{out}$ are the air mass flow rates into and out of the volume respectively. The effects of internal flow such as jets and vortices are usually ignored. References G.3 and G.4 show that the latter are rarely significant. It is further assumed that cushion air pressure and density changes are related by a polytropic equation of state

$$\frac{P}{\rho^n} = \text{constant} \qquad (G.2)$$

where n is taken to be equal to γ, the ratio of specific heats. In other words, the process is assumed to be isentropic. This and the ideal gas law $P = \rho RT$ allow one to write

$$\dot{P} = \gamma RT\dot{\rho} \qquad (G.3)$$

For pressure and temperature perturbations which are small relative to atmospheric conditions, this reduces to

$$\dot{P} = \dot{p} = a^2\dot{\rho} \qquad (G.4)$$

where $a = \sqrt{\gamma RT}$ is the speed of sound in air. The conservation equation then reduces to

$$\frac{V_c}{\rho a^2}\frac{dp_c}{dt} + \frac{dV_c}{dt} = Q_{in} - Q_{out} \qquad (G.5)$$

where Q_{in} and Q_{out} are volumetric flow rates. The first term in Equation (G.5) is due solely to cushion air compressibility and is a major source of instability. The second term accounts for changes in cushion volume due to heave motion and skirt flexibility; the former provides a stabilizing effect whereas the latter is generally destabilizing.

The volumetric flows are assumed to be governed by steady inviscid orifice flow laws applied quasi-steadily in time. For gauge pressures low relative to atmospheric pressure, the flows can be assumed incompressible in which case

$$Q_{in} = C_{df}A_f[2(p_f - p_c)/\rho]^{1/2} \qquad (G.6)$$

$$Q_{out} = C_{dh}L_s h\,(2p_c/\rho)^{1/2} \qquad (G.7)$$

where p_c is the gauge cushion pressure, p_f is the gauge fan pressure, A_f is the inlet orifice area, L_s is the perimeter of the skirt at ground level, h is the effective hovergap or leakage gap, and C_{df} and C_{dh} are orifice flow discharge coefficients. The quasi-static law is based on

Euler's equation for flow along an orifice streamline

$$\underset{\text{local acceleration}}{\frac{\partial U_s}{\partial t}} + \underset{\text{convective acceleration}}{U_s \frac{\partial U_s}{\partial s}} + \frac{1}{\rho}\frac{\partial p_s}{\partial s} = 0 \qquad (G.8)$$

By assuming the flow to be steady and ρ to be constant, Euler's equation reduces to

$$U_s \frac{dU_s}{ds} + \frac{1}{\rho}\frac{dp_s}{ds} = 0 \qquad (G.9)$$

Integration wth respect to s gives

$$\frac{1}{2}\rho U_s^2 + p_s = \text{constant}$$

For orifice flow, both

$$U_o = (2p_o/\rho)^{1/2} \qquad (G.10)$$

and

$$Q_o = C_{do} A_o U_o \qquad (G.11)$$

follow directly. Use of the quasi-static law is only justified when peak to peak variations in the local acceleration during an oscillation cycle are much smaller than corresponding variations in the convective acceleration. Simple order-of-magnitude arguments give

$$\omega_r = \frac{\Delta\left(\frac{\partial U_s}{\partial t}\right)}{\Delta\left(U_s \frac{\partial U_s}{\partial s}\right)} = \alpha \frac{L_o \omega}{U_{oe}} \qquad (G.12)$$

where α is of the order of unity [G.4], L_o is the characteristic dimension of the orifice, ω is the oscillation frequency, and U_{oe} is the mean flow velocity at the orifice vena contracta. Ideally the reduced frequency ω_r should be much less than unity. One would expect this to be the case at the cushion lip because there $L_o = h$.

The pressure-flow operating point of the fan is assumed to move along its static characteristic quasi-statically in time where, in general the static characteristic is a non-linear relationship usually expressed in the form

$$p_f = K_0 + K_1 Q_f + K_2 Q_f^2 + --- + K_n Q_f^n \qquad (G.13)$$

where $Q_f = Q_{in}$. Unsteady blade aerodynamics and oscillatory volute flow are seldom considered. For both, fluid inertia plays a dominant role. References G.3 and G.4 show that oscillatory volute flow can cause an unstable region to appear at low volumetric flows in the vehicle pressure-flow operating plane, and this becomes larger as the volute or effective duct length is increased. The system behaves as an Helmholtz resonator: the fluid in the duct oscillates as a lumped mass on the cushion air spring. Reference G.6 presents a theory for unsteady blade aerodynamics which predicts that unsteady effects would occur if the time for a typical air particle to travel one blade chord length was reduced until it became of the same order as the period of a typical vehicle oscillation. This would tend to occur at low Q_f, where surge is also a possibility. During the 1983 winter field trials of TDC's ACIB at Thunder Bay, Ontario, the latter did in fact occur. The operators called the phenomenon "breathing".

The cushion volume V_c is assumed to be made up of three components as follows:

$$V_c = V_d + Sh + F(p_c) \tag{G.14}$$

where S is the pressurized support area, V_d is a fixed or dead volume component, Sh is an active component produced by the vehicle heave motion, and $F(p_c)$ is a flexibility component for which it is assumed that the skirt deforms quasi-statically in time to temporal variations in cushion pressure. Inertial and hysteretic behaviour are generally ignored. The active component helps provide a stabilizing influence whereas the fixed volume and flexibility components are generally destabilizing. To account for a flexibility effect on the skirt height h_s one assumes that

$$h_s = h_o + G(p_c) \tag{G.15}$$

where h_o is the static skirt height and $G(p_c)$ is a quasi-static flexibility component. Reference G.7 shows that there is usually a marked improvement in stability relative to a rigid skirt case when an increase in cushion pressure causes a skirt contraction vertically.

Finally, Newton's second law gives for the heave displacement χ

$$m \frac{d^2\chi}{dt^2} = Sp_c - mg \tag{G.16}$$

where

$$\chi = h + h_s \tag{G.17}$$

and m is the air supported mass, and g is the acceleration due to gravity.

G.3 Stability Concepts

Using matrix notation the governing equations can, with substitution of the algebraic equations into the differential equations, be rewritten in the compact form

$$\dot{\underline{x}} = \underline{f}(x) \tag{G.18}$$

for which the most useful definition of stability is that due to Liapunov (Reference G.8). By this, an equililbrium state of the system is considered locally asymptotically stable if the system gradually returns to this state after being perturbed slightly from it. The equilibrium is said to be critically stable if the response neither grows nor decays (see Figure G.2). A locally stable equilibrium is said to be globally stable is there is no limit on the initial disturbance.

One can linearize the governing equations locally about an equilibrium state to obtain

$$\Delta\underline{\dot{x}} = \underline{A}\ \Delta\underline{x} \tag{G.19}$$

where

$$\Delta\underline{x} = \underline{x} - \underline{x}_e \tag{G.20}$$

provided that in the vicinity of the equilibrium state $\underline{x}_c$ the non-linear terms $\underline{n}(\Delta\underline{x})$ in

$$\underline{f}(\underline{x}) = \underline{A}\ \Delta\underline{x} + \underline{n}(\Delta\underline{x}) \tag{G.21}$$

are small relative to the linear terms $\underline{A}\ \Delta\underline{x}$. For a particular equilibrium to be locally asymptotically stable, the real part of each eigenvalue λ of the $\underline{A}$ matrix must be negative. Consider a system governed by only one first order ordinary differential equation

$$\Delta\dot{x} = A\ \Delta x \tag{G.19*}$$

The general solution is

$$\Delta x = \Delta x_0 e^{\lambda t} \qquad t > 0 \tag{G.22}$$

where λ is the eigenvalue and Δx_0 is an initial disturbance. Substitution into the governing equation gives

$$\Delta x_0 \lambda e^{\lambda t} = A\ \Delta x_0 e^{\lambda t} \tag{G.23}$$

or

$$(A - \lambda)\Delta x_0 e^{\lambda t} = 0 \tag{G.24}$$

which implies $\lambda = A$ for non-zero Δx_0. So if A is positive, the eigenvalue λ is also positive, and an initial disturbance Δx_0 will grow in time whereas if A is negative it will decay. When a coupled set of differential equations describes the system, the eigenvalues are often complex but the real parts still determine stability. The imaginary parts given information on the oscillation frequencies.

If a system is linear, local stability implies global stability. If a system is non-linear this is not necessarily the case, and one must consider the notion of practical stability. For example, a system which is unstable in the linear sense discussed above could enter a limited amplitude non-linear oscillation or 'limit cycle' which is of sufficiently small amplitude that the basic operation of the system is not adversely affected by its presence; the system is said to be practically stable. Similarly, non-linearities could make a system which is stable in the linear sense practically unstable.

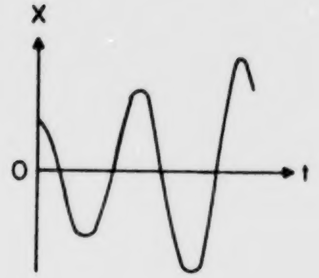

Unstable

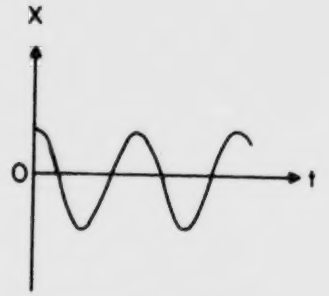

Critically Stable

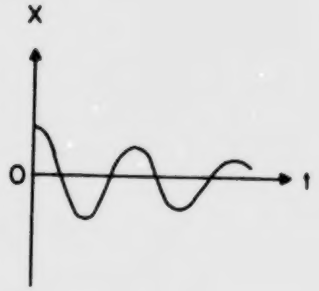

Stable

Practically Unstable

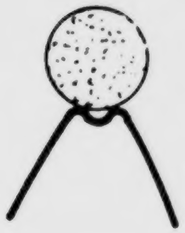

Practically Stable

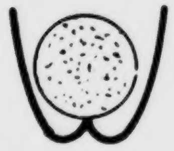

Figure G.2 Stability concepts.

G.4 Insights from Linear Theory

G.4.1 System Characteristic Equation

For a linearized single cell system one can expand the determinant

$$|\underline{A} - \lambda \underline{I}| = 0, \qquad \underline{I} = \text{unit matrix} \tag{G.25}$$

to obtain the system characteristic equation

$$\underset{[\text{mass-dashpot-spring}]}{C_0\lambda^3 + [C_1\lambda^2 + C_2\lambda + C_3] = 0} \tag{G.26}$$

where for a rigid skirted cushion

$$C_0 = \frac{C_c m}{\dfrac{1}{R_f - C_{PQ}} + \dfrac{1}{R_c}} \tag{G.27.1}$$

$$C_1 = m \tag{G.27.2}$$

$$C_2 = \frac{S^2}{\dfrac{1}{R_f - C_{PQ}} + \dfrac{1}{R_c}} \tag{G.27.3}$$

$$C_3 = \frac{S}{\alpha_h\left(\dfrac{1}{R_f - C_{PQ}} + \dfrac{1}{R_c}\right)} \tag{G.27.4}$$

and

$$C_c = \frac{V_{ce}}{\rho a^2} \approx \frac{S h_s}{\rho a^2} \tag{G.28.1}$$

is the cushion pneumatic capacitance. Also

$$R_f = \frac{2(p_{fe} - p_{ce})}{Q_e} \tag{G.28.2}$$

and

$$R_c = \frac{2p_{ce}}{Q_e} \tag{G.28.3}$$

are orifice flow resistances,

$$C_{PQ} = \left.\frac{dp_f}{dQ_f}\right|_e \tag{G.28.4}$$

is the local slope of the fan characteristic, and

$$\alpha_h = \frac{h_e}{Q_e} \qquad (G.28.5)$$

is a gap flow parameter. The three roots of Equation (G.26) are the eigenvalues of the system. Note that matrix notation is not essential for the present work. Equation (G.26) could be obtained directly by linearization together with substitutions into Equation (G.5).

The linearized system can also be manipulated into the block diagram form [G.8, G.9] of Figure G.3. For a single cell cushion this manipulation gives

$$G(\lambda) = \frac{-\kappa}{S} \, \frac{\tau_1 \lambda + 1}{\tau_2 \lambda + 1} \qquad (G.29.1)$$

and

$$H(\lambda) = \frac{-S}{m\lambda^2} \qquad (G.29.2)$$

where τ_1 amd τ_2 are lead and lag time constants, and κ is the static air spring stiffness. The characteristic equation in terms of these functions is

$$1 + G(\lambda) \, H(\lambda) = 0 \qquad (G.30)$$

One could solve the characteristic equation directly for its roots. Stability information could then be ascertained simply by inspection of the results. However, greater insight can be obtained if either the Routh-Hurwitz ideas or the Nyquist concepts are employed.

G.4.2 Routh-Hurwitz Stability Criteria

The Routh-Hurwitz criteria work with the coefficients in the characteristic equation. For stability of a third order system they require

$$C_1 C_2 - C_0 C_3 > 0 \qquad (G.31)$$

This can be manipulated into a stabiity boundary equation of the form

$$p_{ce} = f(h_e) \qquad (G.32)$$

where p_{ce}, the equilibrium cushion pressure, is directly proportional to the gross weight supported by the cushion; while; h_e, the equilibrium gap, is a measure for a given operating terrain of the lift air needs [G.3]. For a contant pressure source or flat pressure-flow characteristic one obtains, for a rigid skirt case, the stability requirement

$$p_{ce} < \frac{\rho a^2}{2} \left(1 + \frac{C_{df}^2 \, A_f^2}{C_{dh}^2 \, L_s^2 \, h_e^2}\right) \frac{h_e}{h_s} \qquad (G.33)$$

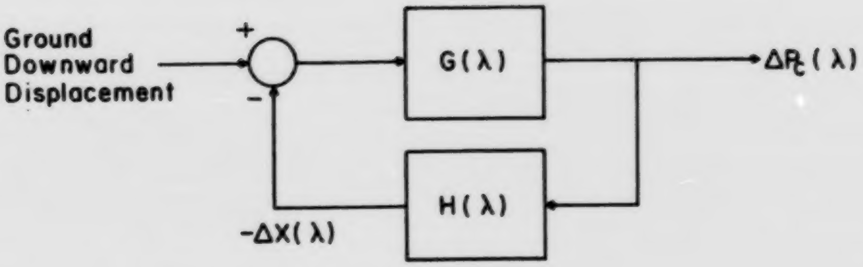
Ground
Downward
Displacement
+
−
G(λ)
H(λ)
ΔP_c(λ)
−ΔX(λ)

Figure G.3 System block diagram.

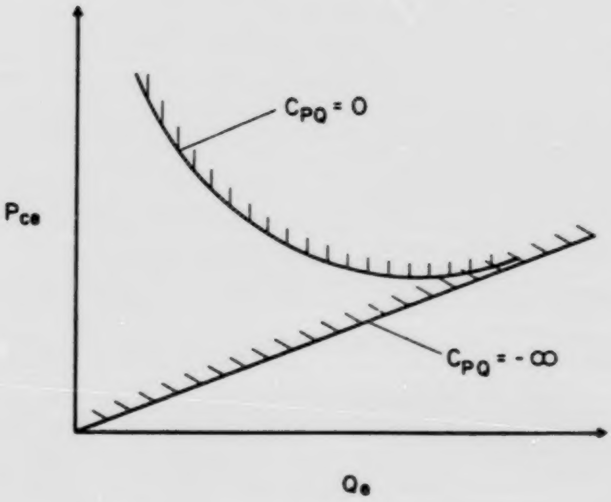

Figure G.4 Fan slope effect on heave stability.

while for a constant flow source or very steep pressure-flow characteristic one obtains

$$p_{ce} < \frac{\rho a^2}{2} \frac{h_e}{h_s} \qquad (G.34)$$

Characteristics in between these two limits can be represented by an effective orifice A_0 in series with A_f. Recall that for an incompressible fluid $a = \infty$. The above equations show that with such a working fluid the system would be stable for any finite operating pressure. Unfortunately, air is not incompressible.

Notice how geometrically similar cushions such as a model and its prototype operating at a geometrically similar gap

$$\left(\frac{h_e}{h_s}\bigg|_m = \frac{h_e}{h_s}\bigg|_p\right) \qquad \left(\frac{A_f}{L_s h_e}\bigg|_m = \frac{A_f}{L_s h_e}\bigg|_p\right) \qquad (G.35)$$

would be unstable above the same cushion pressure. This presents a problem for scaling up to large sizes because it means that the critical stability pressure would not scale up. Note also that for stability the skirt height h_s should be made as small as possible.

The two stability boundaries associated with equations (G.33) and (G.34) are shown schematically in Figure G.4, where the hatched side of each curve indicates an unstable region. The figure shows how the constant pressure source gives a much larger stable pressure-flow region than the constant flow source. The minimum which occurs for the constant pressure source case is given by

$$p_{ce} = \rho a^2 \frac{h_e}{h_s} \qquad (G.36)$$

where

$$h_e = \frac{C_{df} A_f}{C_{dh} L_s} \qquad (G.37)$$

This shows how one should try to make A_f as large as possible by dumping air directly into the cushion. It also shows that a segment-skirted cushion which has an effective lip discharge coefficient C_{dh} of approximately 0.2 would be much more stable than a tapered cone multicell which has a discharge coefficient of approximately 0.6.

Some results for TDC's ACIB, based on provisional data provided by HoverLift Systems Limited and rigid skirt theory, are given in Table G.1. Note how as one moves up the fan characteristic (Figure G.5) by increasing the craft weight, stability improves. A similar trend was observed during the 1982 field trials. it implies that an active or passive control device designed to make the fan behave dynamically as a constant pressure source would be very useful. The control would have to be fast acting relative to the basic vehicle period, otherwise on its own it could cause a hunting-like vehicle motion.

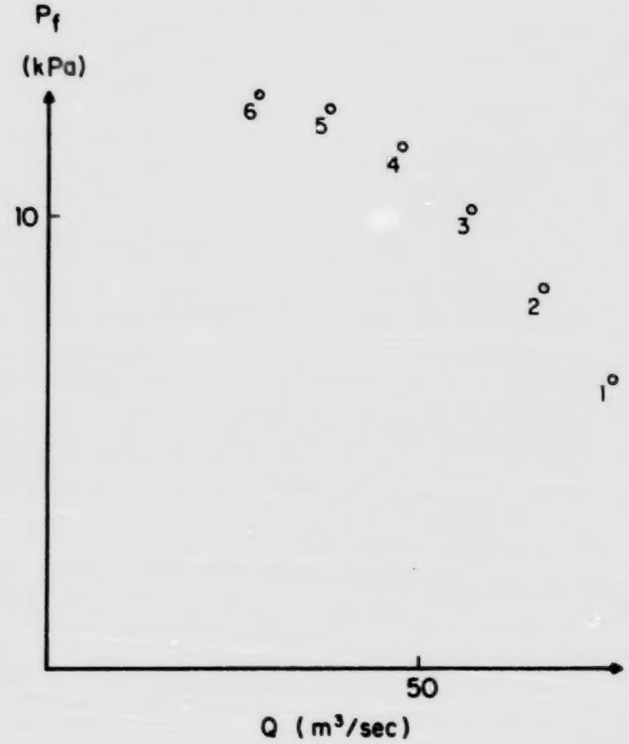

Figure G.5 ACIB fan characteristic.

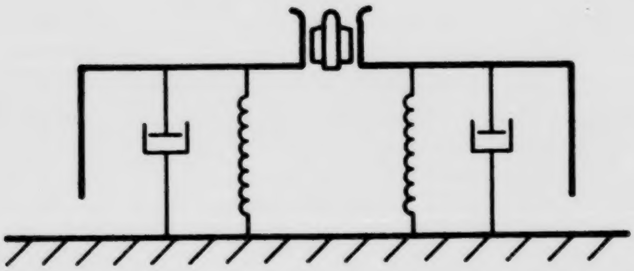

Figure G.6 Spring-dashpot skirt model.

Table G.1

ACIB Heave Stability Geometry

Length	21.5 m
Beam	16.5 m
Perimeter	70.0 m
Support area	350 m^2
Cushion volume	1150 m^3
Cushion lip discharge coefficient	0.2

Three centrifugal fans dump air directly into cushion

Heave Stability

Point	$\frac{C_1C_2}{C_0C_3}$	Stable
1	0.75	No
2	0.30	No
3	0.50	No
4	0.60	No
5	1.20	Yes
6	3.60	Yes

At a stability boundary $\lambda = i\omega$, where $i = \sqrt{-1}$ and ω is the oscillation frequency. With $\lambda = i\omega$, the characteristic equation reduces to

$$\underset{\text{I}}{-C_0\omega^2 i\omega} - \underset{\text{II}}{C_1\omega^2} + \underset{\text{III}}{C_2 i\omega} + \underset{\text{IV}}{C_3} = 0 \qquad \text{(G.38)}$$

The first term in this equation can be thought of as a contributing negative damping. Instability occurs when the magnitude of this term is greater than the third term which is the positive damping term associated with the underlying mass-dashpot-spring system, see Equation (G.26). In other words, instability occurs when

$$C_0\omega^2 > C_2 \qquad \text{(G.39)}$$

The real terms (II and IV) give

$$\omega^2 = \frac{C_3}{C_1} \qquad \text{(G.40)}$$

Equation (G.27) shows that the fan slope C_{PQ} appears in Equation (G.39) only indirectly through the ω^2 factor. Equation (G.40) shows that ω decreases when the fan slope is made less steep. This helps explain the fan slope effect noted above.

Substitution of Equation (G.40) into Equation (G.39) yields

$$\frac{C_1C_2}{C_0C_3} > 1 \tag{G.41}$$

or

$$C_1C_2 - C_0C_3 > 0 \tag{G.42}$$

which, not surprisingly, is identical to that obtained using the Routh-Hurwitz criteria, see Equation (G.31). If the cushion air was incompressible, the negative damping term would be zero. Note that it might be possible to manipulate skirt flexibility to counteract the destabilizing effect of air compressibility. The effective capacitance of the cushion with flexibility included is given by

$$C_{eff} = C_c + C_v \tag{G.43}$$

where [see Equations (G.5) and (G.14)]

$$C_v = \left.\frac{dV_c}{dP_c}\right|_e = \left.\frac{dF(p_c)}{dp_c}\right|_e \tag{G.44}$$

is based on the quasi-static skirt model. For C_v to have a stabilizing effect, it would have to be negative. This is not the natural situation, and a negative C_v may be very difficult to achieve in practice. One other possibility is to use derivative control on the fan inlet area

$$\Delta A_f = C_A \frac{d\Delta p_c}{dt} \tag{G.45.1}$$

$$C_{eff} = C_c - C_A \frac{Q_c}{A_f} \tag{G.45.2}$$

With C_A positive, the effective capacitance would be reduced.

If skirt-ground contact forces could be modelled as a spring-dashpot auxiliary suspension system (see Figure G.6), then the coefficients in the characteristic equation would become

$$C_0 = m + \frac{C_c m}{\frac{1}{R_f - C_{PQ}} + \frac{1}{R_c}} \tag{G.46.1}$$

$$C_1 = m + \frac{C_c C_s}{\frac{1}{R_f - C_{PQ}} + \frac{1}{R_c}} \tag{G.46.2}$$

$$C_2 = C_s + \frac{S^2}{\frac{1}{R_f - C_{PQ}} + \frac{1}{R_c}} + \frac{C_c k_s}{\frac{1}{R_f - C_{PQ}} + \frac{1}{R_c}} \tag{G.46.3}$$

$$C_3 = k_s + \frac{S}{\alpha_h\left(\frac{1}{R_f - C_{PQ}} + \frac{1}{R_c}\right)} \qquad (G.46.4)$$

where C_s and k_s are respectively the dashpot and spring coefficients of the skirt-ground auxiliary suspension. Using the negative damping stability arguments, one can show that the addition of a spring by itself would not affect stability. The addition of a dashpot, on the other hand, would improve stability as expected. It does this in two ways: first, it adds to the positive damping term C_2; and second it reduces the frequency ω, and thus the negative damping term $C_0\omega^3$. If the skirt load-deflection cycle exhibits static or rate independent hysteresis (see Figure G.7), one would expect the damping associated with it to show up during an oscillation cycle as a change in kinetic energy of the air supported mass. In other words, the negative work done by hysteresis should be balanced by an appropriate amplitude decay.

G.4.3 Nyquist Stability Concept

The single-cell equations can be manipulated into a force-displacement transfer function of the form

$$\frac{\Delta f(\lambda)}{-\Delta\chi(\lambda)} = \kappa\,\frac{\tau_1\lambda + 1}{\tau_2\lambda + 1} = -m\lambda^2 \qquad (G.47)$$

where the parameters are as defined previously. For a rigid skirted cushion

$$\tau_1 = S\alpha_h \qquad (G.48)$$

$$\tau_2 = \frac{C_c}{\frac{1}{R_c - C_{PQ}} + \frac{1}{R_a}} \qquad (G.49)$$

and

$$\kappa = \frac{S/\alpha_h}{\frac{1}{R_c - C_{PQ}} + \frac{1}{R_a}} \qquad (G.50)$$

In terms of these parameters, the characteristic equation can be written as

$$m\tau_2\lambda^3 + m\lambda^2 + \kappa\tau_1\lambda + \kappa = 0 \qquad (G.51)$$

The Routh-Hurwitz criteria applied to this yields the stability requirement

$$\kappa(\tau_1 - \tau_2) > 0 \qquad (G.52)$$

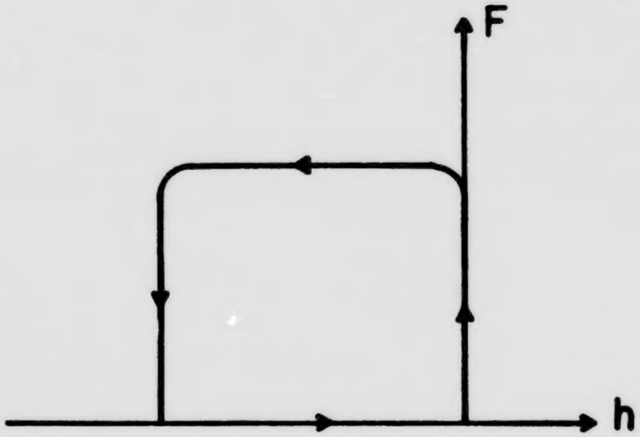

Figure G.7 Static hysteresis in skirt load deflection cycle.

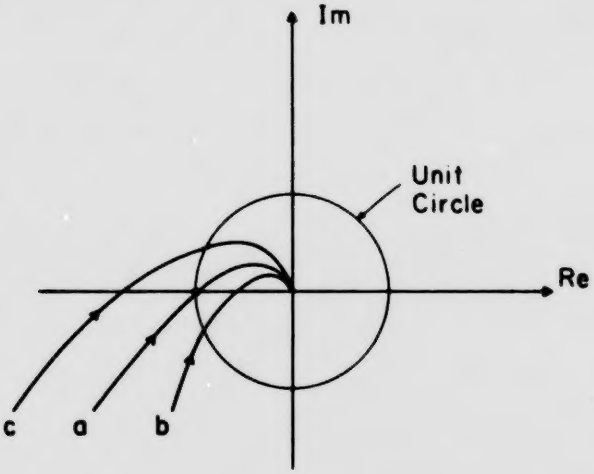
Im
Unit
Circle
Re
c
a
b

Figure G.8 Illustrations of Nyquist concept; behaviour of GH for (a) critically stable, (b) stable, (c) unstable

where $\kappa > 0$ implies static stability, while $\tau_1 > \tau_2$ implies dynamic stability. Now, over one cycle of an oscillation, the work done by the lift force on the supported mass is

$$W = \int_0^{2\pi/\omega} \mathrm{Re}\left[\Delta F(i\omega)\right] \cdot \mathrm{Re}\left[\Delta \dot{x}(i\omega)\right] dt \qquad (G.53)$$

Evaluation of this integral [G.3] shows that when $\tau_1 > \tau_2$ the work done is negative, whereas when $\tau_1 < \tau_2$ it is positive. In other words, when the lift force lags the heave motion, the supported mass extracts energy from the pressurized air, and this shows up as an increase in its kinetic energy.

The Nyquist procedure can be thought of as an extension of the work-done concept. It is graphical in nature and based on the block diagram representation given in Figure G.3. Its theoretical development for a general system is beyond the scope of the present work. Stability information is ascertained from a plot of the function $G(i\omega)H(i\omega)$ in a real-imaginary plane as ω is varied from 0 to ∞. At a stability boundary $\lambda = i\omega$ and the characteristic equation reduces to

$$1 + G(i\omega)\,H(i\omega) = 0, \qquad G(i\omega)\,H(i\omega) = -1 \qquad (G.54)$$

So the critical pressure for a given hovergap is that which causes the Nyquist plot to pass through the minus one oint in the real-imaginary plane as shown in Figure G.8a. When the phase of $G(i\omega)H(i\omega)$ at $|G(i\omega)H(i\omega)| = 1$ is less negative than minus 180°, as shown in Figure G.8b, the force acting on the air supported mass leads the heave displacement whereas when the phase is more negative than minus 180°, as in Figure G.8c, the force lags. The work-done concept shows that force lead implies negative work done on the supported mass during an oscillation cycle. In other words, the supported mass loses energy and its motion is damped. On the other hand, force lag implies positive work done and thus energy gain or instability.

One advantage of this graphical procedure is that it can handle very complicated $G(i\omega)H(i\omega)$ functions. Examples of these are given in [G.10 to G.13]. Figure G.9, taken from [G.10 and G.11], shows a Nyquist plot for a large air cushion platform (see Table G.2). Here the $G(i\omega)H(i\omega)$ function is complicated by the presence of acoustic waves in the cushion volume. Results show that the damping of large vehicles is generally very low, even well into the stable pressure-flow operating region. Figure G.10 is based on the theory developed in [G.12 and G.13] and shows plots for overwater operation (see Table G.3). Here stability is affected by cushion volume modulation and lip airflow modulation resulting from the generated water surface motion. For the small Canadian research craft HEX-5, shown schematically in Figure G.11, results show that volume modulation is generally stabilizing whereas flow modulation is destablizing at low cushion pressures. Similar trends were observed for the ACIB. More recently, water tank experiments at UTIAS showed that the airflow directly beneath the segments of a segment skirt can lead to another quite different instability in which the high-speed airflow causes the water surface to become unstable.

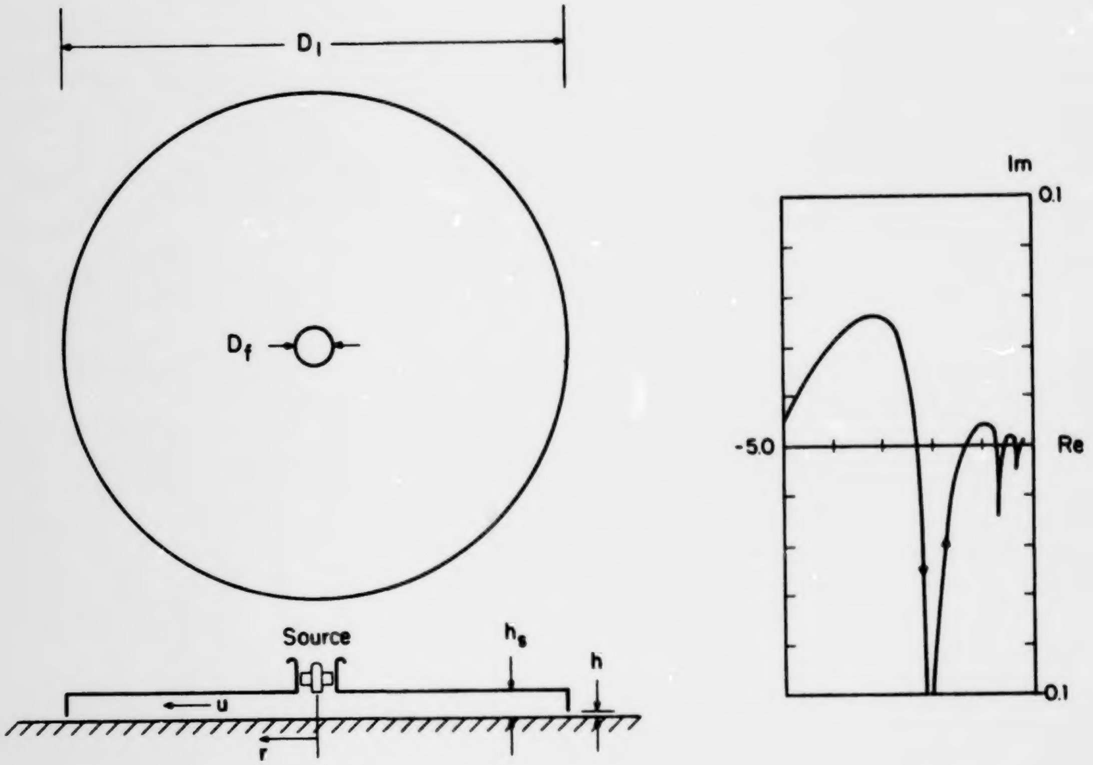

Figure G.9 Nyquist plot for large air cushion platform.

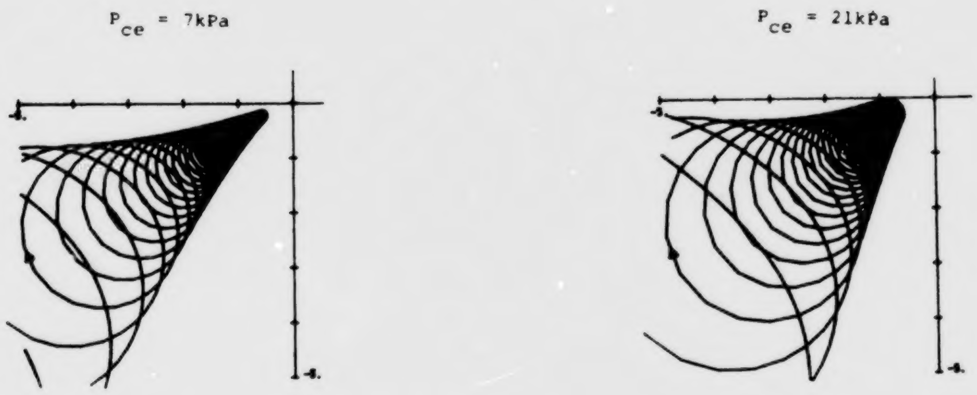

Cushion volume pumping effect

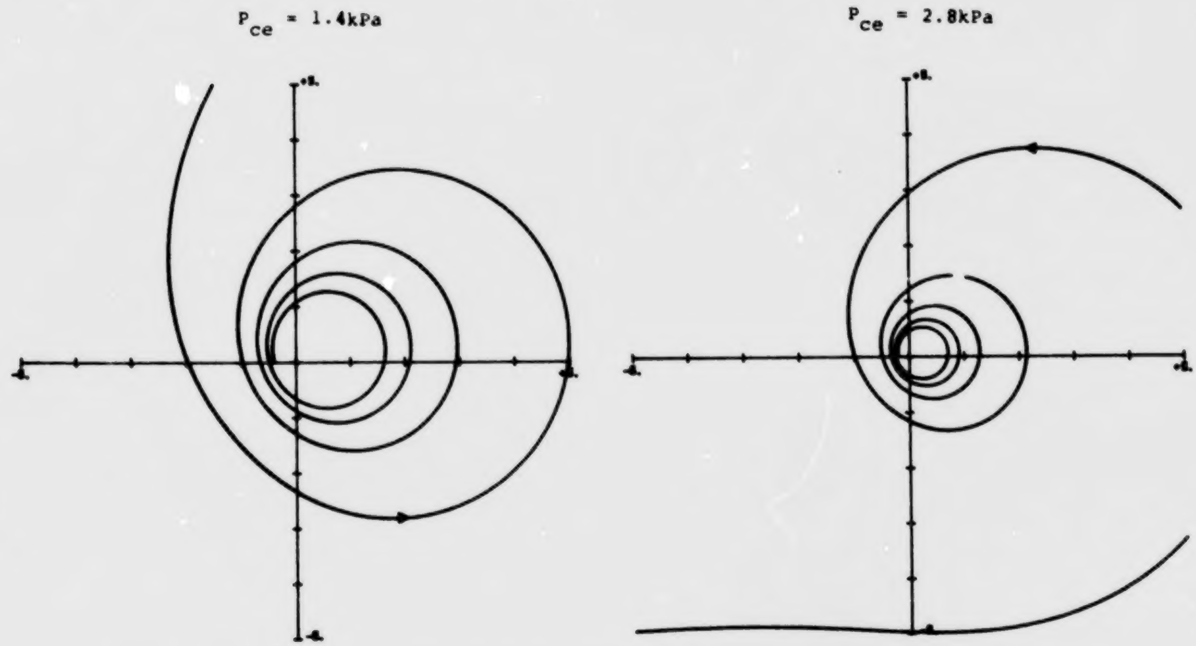

Lip airflow modulation effect

Figure G.10 Nyquist plots for overwater operation (overland critical pressure 7 kPa).

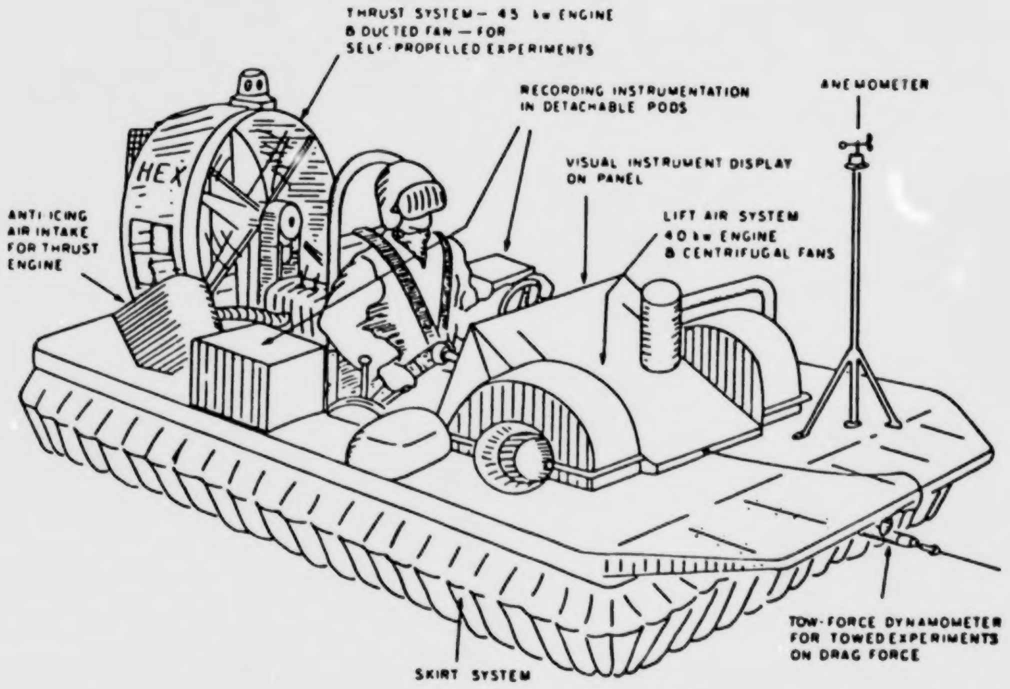
THRUST SYSTEM – 45 kw ENGINE
& DUCTED FAN — FOR
SELF-PROPELLED EXPERIMENTS
RECORDING INSTRUMENTATION
IN DETACHABLE PODS
ANEMOMETER
HEX
VISUAL INSTRUMENT DISPLAY
ON PANEL
ANTI-ICING
AIR INTAKE
FOR THRUST
ENGINE
LIFT AIR SYSTEM
40 kw ENGINE
& CENTRIFUGAL FANS
TOW-FORCE DYNAMOMETER
FOR TOWED EXPERIMENTS
ON DRAG FORCE
SKIRT SYSTEM

Figure G.11 Canadian research craft HEX-5.

This instability was observed in HEX-5 [G.14] and more recently in the ACIB [G.15].

Table G.2

Large Air Cushion Platform

Geometry: axisymmetric
Air supply: centrally located feed hole

Cushion depth: h_s = 3 m
Feed hole radius: r_f = 3 m
Skirt radius: r_1 = 90 m
Hover gap: h_e = 1.5 cm
Cushion pressure: p_{ce} = 0.8 kPa

Table G.3

HEX-5 Data

Cushion Dimensions

Length:	3.75 m
Width:	2.5 m
Depth:	0.2 m

Typical Operating Conditions

Cushion pressure: p_{ce} = 1 kPa
Hovergap: h_e = 4.5 mm

G.5 Non-Linear Phenomena

Non-linearities in air cushion systems arise from several sources. Some of these have already been mentioned. For example, the source of cushion air often has a non-linear quasi-static pressure-flow characeristic (Equation G.13). Also, the unsteady air escape process from the cushion to atmosphere is assumed to be quasi-static and orifice-flow-like (Equation G.11). This has two associated non-linearities. One is the square-root dependence of the volume flux on the cushion pressure coupled to a varying leakage gap area. The second is the shut-off process associated with skirt-ground contact. Finally, the skirts themselves are known to display significant hysteretic behaviour, both static and dynamic.

There are a number of approaches available for studying non-linear behaviour. One is analog computer simulation where an electronic analog of the non-linear equations governing air cushion motion is patched together using standard analog functions. Another is digital computer simulation. A more analytic approach is that based on the Galerkin describing function concept.

For a Galerkin analysis, one assumes limit cycle solutions of the form

$$\phi_i = \phi_{ib} + \sum_{n=1}^{N} \phi_{in}{}^{s} \sin n\,\omega t + \sum_{m=1}^{M} \phi_{in}{}^{c} \cos m\,\omega t \qquad (G.55)$$

where the ϕ_i for the duct-plenum system moving in pure heave are χ, $\dot{\chi}$, Q_d, and p_c. The $\phi_{i1}{}^{c}$ coefficient for one of these assumed forms is set to zero. This is because limit cycles exist for relative phase only. When the solution forms are substituted into the governing non-linear ordinary differential equations, one obtains the generally non-zero residuals $R_j(\phi_i)$. The Galerkin technique forces these residuals to be zero in a weighted average sense over an oscillation cycle by making them orthogonal to weighting functions as shown below.

$$\int_{0}^{2\pi/\omega} W_j R_j(\phi_{ib}, \phi_{in}{}^{s}, \phi_{im}{}^{c}, \omega, t)dt = 0 \qquad (G.56)$$

where the weighting functions W_k are taken to be 1, sin n ωt, and cos m ωt. The integrations give a set of non-linear algebraic equations for the coefficients ϕ_{ib}, $\phi_{in}{}^{s}$, $\phi_{im}{}^{c}$, and for the frequency ω. Results [G.16] show that the motion on the unstable side of a linear stability boundary is usually a stable limit cycle. Also, the systems are often practically as well as linearly unstable. Recently it has been found that the stability of predicted limit cycles can be ascertained using the work-done concept.

Limit cycle results for a duct-plenum system (see Table G.4), obtained from a numerical simulation, are shown in Figure G.12, where the letters e to h denote points in the linearly unstable operating region in Figure G.13. Table G.5 presents first-order Galerkin results for these points together with Fourier decompositions of the numerical simualtions for e and g. As can be seen, the Galerkin results are in close agreement with those of the numerical simulation. The computational burden required to obtain the Galerkin results is usually much less than that of the numerical simulation. However, it is not insignificant, and a computer must be used to evaluate the integrals and solve the resultant non-linear equations. This detracts from the usefulness of the method.

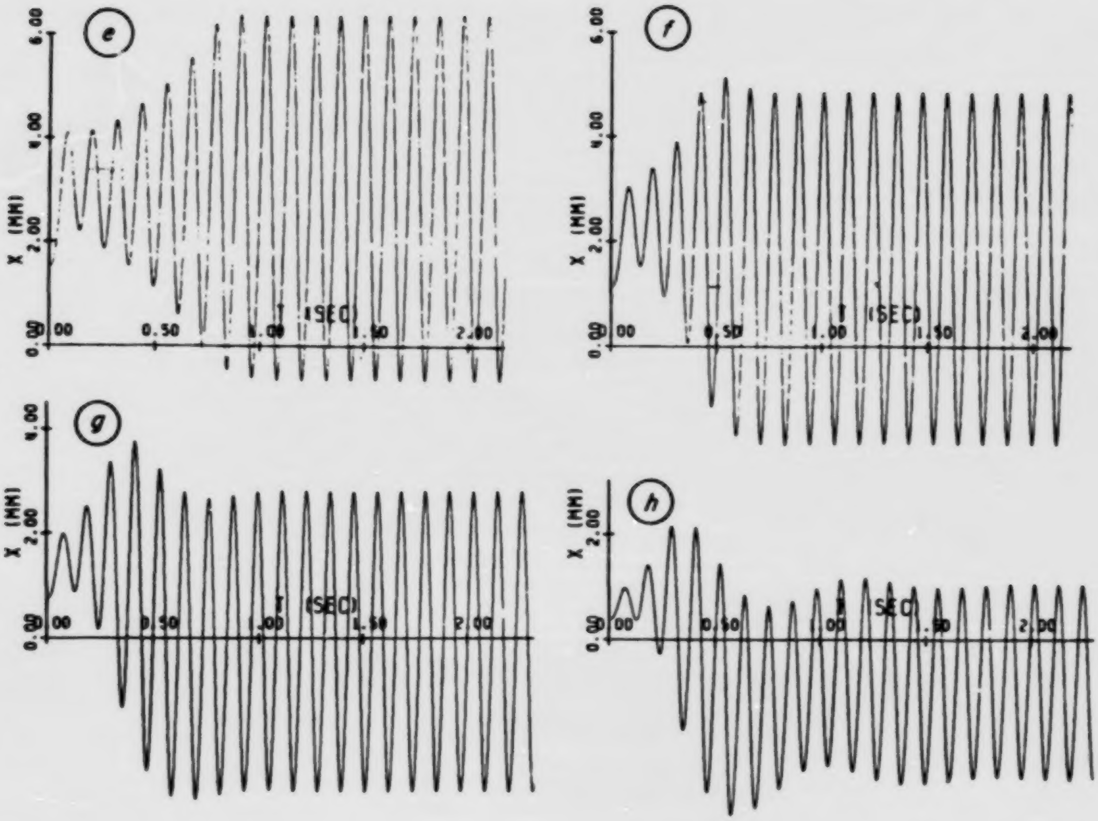

Figure G.12 Non-linear numerical simulation of a duct-plenum system.

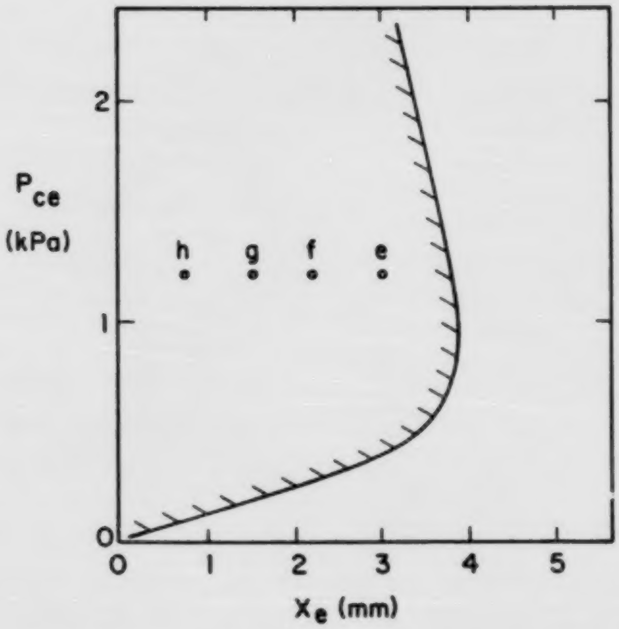

Figure G.13 linear heave stability boundary for duct-plenum system.

Table G.4

Dimensions of Duct-Plenum System

Duct Length:	6.1 m
Duct diameter:	0.544 m
Cell diameter:	1.83 m
Cell height:	0.914 m
Fan slope	zero
Orifice Data	
Diameters:	0.3 m
Discharge coefficients:	0.61

G.6 Experimentation

Very little data is available suitable for critically testing air cushion mathematical models and their inherent assumptions. However some has been generated at UTIAS. The goal of the UTIAS experiments was to verify the Helmholtz resonator of supply duct effect mentioned earlier. For this, the critical experiment shown schematically in Figure G.14 (Table G.6) was devised. The hollow sphere, because of its large size relative to the scale of the experiment, acted as a pneumatic filter. It filtered out fan static and dynamic effects; the former hard to control and the latter largely unknown. A standard industrial fan supplied pressurized air to the sphere which in turn supplied air to a rigid test duct and tapered cell cushion. The airflow rate to the cushion was controlled by bypassing some sphere air directly to atmosphere through exhaust ports. The cushion was constrained by a linear recirculating ball bearing assembly to move vertically in heave over a rigid flat table. It was coupled to the test duct by a short length of flexible ducting. The steel support structure was bolted to a concrete foundation. A conical inlet, calibrated in situ by an ASME standard orifice plate, was used to measure the equilibrium cushion flow rate. A detachable baffle plate, mounted on the table directly below the inlet to the cushion, was used in an attempt to minimize internal flow effects. Two skirts were used, one rigid and one flexible. The lip discharge coefficient C_{dh} for each was measured experimentaly after the cushion was assembled and installed in the guidance mechanism.

A typical result is shown in Figure G.15 for a rigid skirt case with duct length 1.71 m. The theoretical results for both isothermal and isentropic cushion thermodynamic processes are given. Figure G.16 gives some demonstrations of data repeatability. The good agreement between theory and experiment implies that the geometry tested can be regarded as a base line to which other factors can be added one at a time. in this vein, the original experiment has since been modified to study in greater detail skirt damping and limit cycle phenomena. Figure G.17 gives tyical results from the skirt damping study [G.7]. These show that the effective hoop Poisson's Ratio of the skirt has a stabilizing influence. It causes a skirt contraction vertically when there is an increase in cushion pressure, and

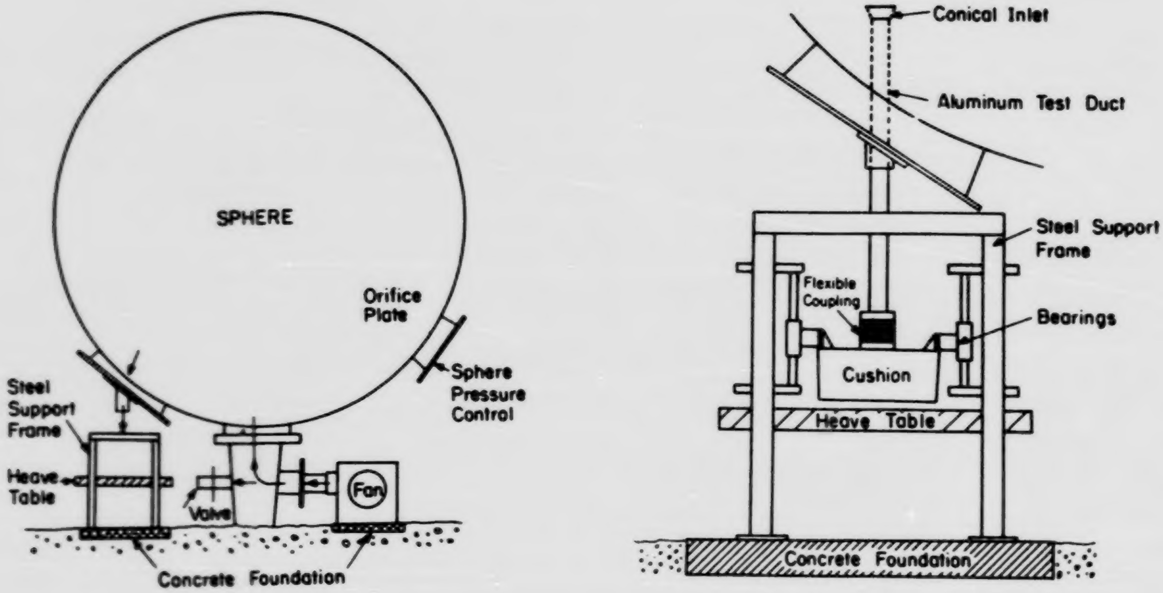
SPHERE
Orifice Plate
Steel Support Frame
Sphere Pressure Control
Heave Table
Valve
Fan
Concrete Foundation
Conical Inlet
Aluminum Test Duct
Steel Support Frame
Flexible Coupling
Bearings
Cushion
Heave Table
Concrete Foundation

Figure G.14 Schematics of sphere facility.

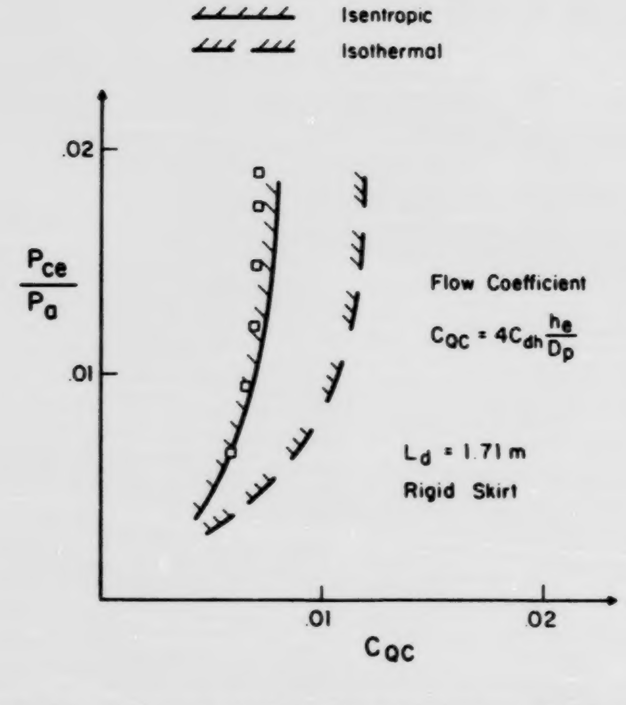

Figure G.15 Heave stability boundaries: rigid skirt case.

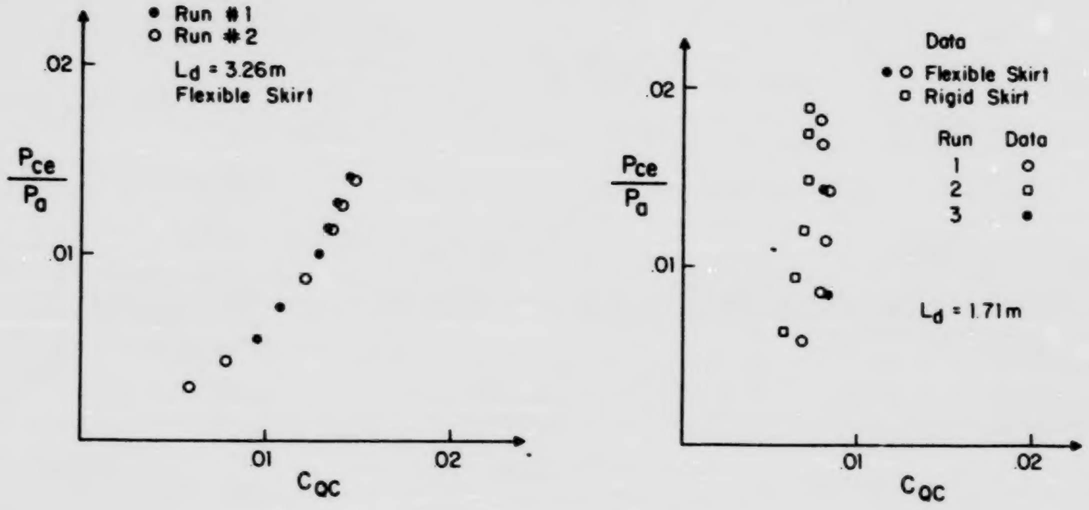

Figure G.16 Data repeatability.

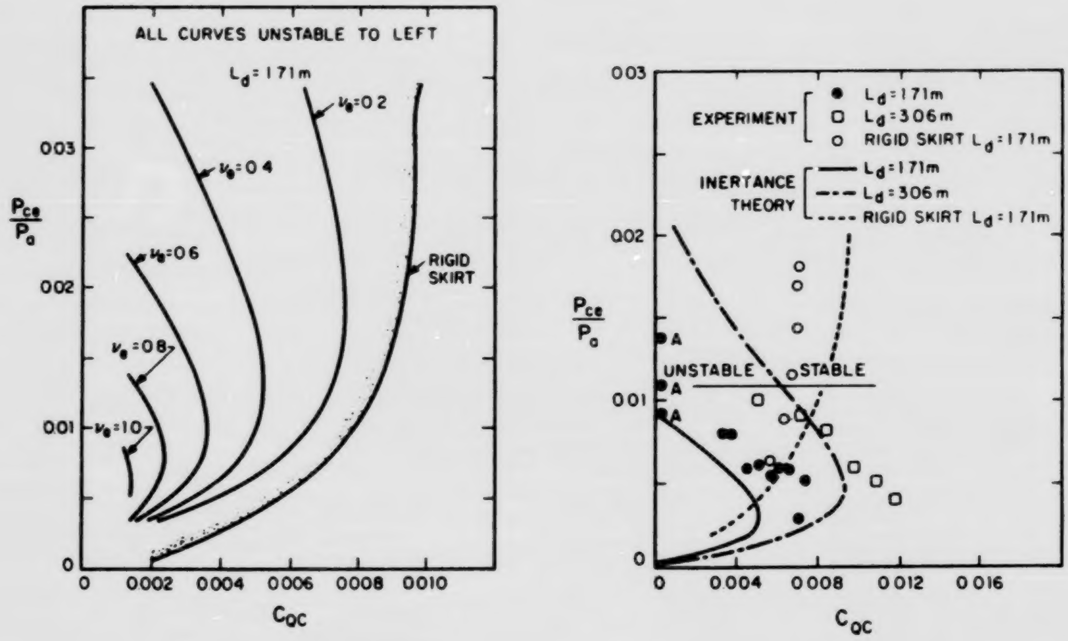

Poisson's Ratio effect

Theory-experiment comparison

Figure G.17 Heave stability boundaries: flexible skirt case.

Table G.5

Limit Cycles for Duct-Plenum System

Typical Galerkin results for duct supply model with first order harmoncs only; p_{ce} = 1.197 kPa

			Coefficients in expansion		
				First harmonic	
Operating point	Variable	Frequency ω	Constant	Amplitude	Phase
e	χ		2.77	3.32	0
h_e = 3.05	p_c	54.0	1.197	1.178	180°
	Q_d		0.2595	0.6797	-75.9
f	χ		1.44	3.29	0
h_e = 2.29	p_c	54.3	1.197	1.183	180°
	Q_d		0.1480	0.6810	-77.5
g	χ		-0.05	2.86	0
h_e = 1.52	p_c	54.5	1.197	1.039	180°
	Q_d		0.0750	0.6014	-79.5
h	χ		-0.81	1.90	0
h_e = 0.76	p_c	54.9	1.197	0.694	180°
	Q_d		0.0279	0.4048	-83.1

Fourier decomposition of numerical simulation for duct supply model; p_{ce} = 1.197 kPa

			Coefficients in expansion				
				First harmonic		Second harmonic	
Operating point	Variable	Frequency ω	Constant	Amplitude	Phase	Amplitude	Phase
e	χ		2.84	3.51	0	0.1275	-165
h_e = 3.05	p_c	52.8	1.197	1.190	180	0.153	16
	Q_d		0.2663	0.7023	-75.8	0.0586	91.9
g	χ		-0.07	2.85	0.0	0.0036	47.8
h_e = 1.52	p_c	54.6	1.197	1.030	180	0.013	-160
	Q_d		0.0747	0.6003	-79.7	0.0070	-4.6

Table G.6

Sphere Facility

Dimensions of sphere facility

Sphere diameter = 12.2 m (40 ft)

Skirt diameter - top = 0.508 m (1.67 ft)
- bottom = 0.467 m (1.53 ft)

Skirt height = 0.213 m (0.70 ft)

Duct length - long = 3.26 m (10.7 ft)
- short = 1.71 m (5.6 ft)

Duct diameter = 0.0779 m (0.256 ft)

Basic model weight - flexible = 49.35 N (11.09 lb)
- rigid = 58.96 N (13.25 lb)

Duct flow friction factor = 0.01656

Lip discharge coefficient - flexible = 0.567
- rigid = 0.60

Duct discharges directly into the cushion

Skirts for sphere experiment

Flexible skirt:

Material = Uniroyal Fiberthin 131
(rubber coated fabric)

Thickness = 0.51 mm

Weight = 6.97 Pa

Rigid skirt:

Material = aluminum

Thickness = 1.25 mm

this favourably modulates the exit flow. Figure G.18 gives typical results from the limit cycle experiment [G.17]. As can be seen, pressure wave forms, both measured and calculated, exhibit higher harmonics.

G.7 Conclusion

Under suitably controlled experimental conditions the models developed for air cushion dynamics can predict the onset of instability to engineering accuracy. However, for a practical vehicle, the models, because of the many hard-to-control factors involved, may only provide qualitative trends. The models show that the compressibility of the air enclosed by the skirt is the major cause of instability. They also show that the inertia of the air in the cushion air supply ducts can cause an Helmholtz resonance effect at low volumetric flows. Finally, fan slope and skirt flexibility are two other factors having significant effects. One area mentioned requiring further study is stabilization. Because of the dominance of cushion air compressibility, one should probably first attempt to counteract it.

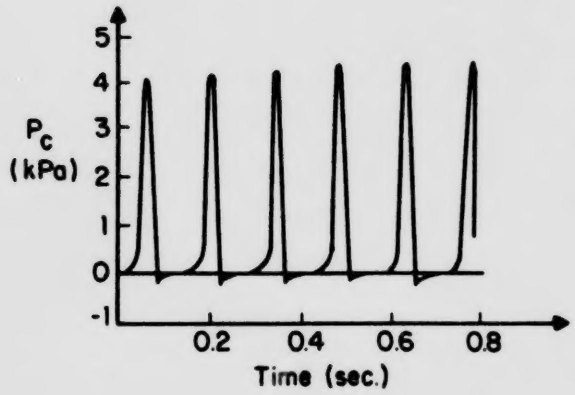

Numerical Simulation

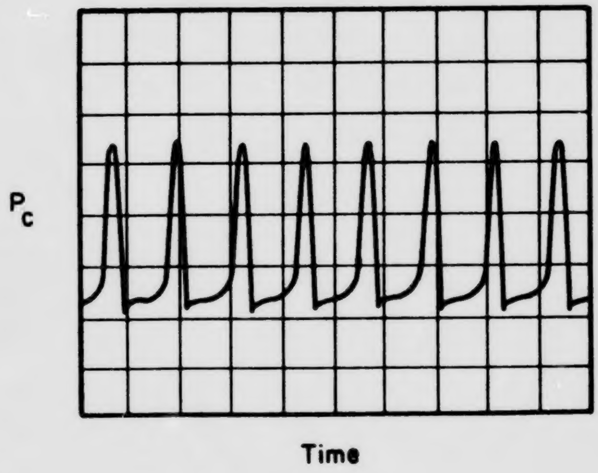

Sphere Experiment

Figure G.18 Limit cycles in duct-plenum system.

REFERENCES - APPENDIX G

G.1 Tulin, M. P., "On the Vertical Motions of Edge Jet Vehicles", presented at a Symposium on Ground Effect Phenomena, Princeton University, NJ, October 1959.

G.2 Ribich, W. A. and Richardson, H. H., "Dynamic Analysis of Heave Motion for a Transport Vehicle Fluid Suspension", Massachusetts Institute of Technology, Department of Mechanical Engineering, Boston, Report DSR-76110-3, 1967.

G.3 Hinchey, M. J., "Heave Instabilities of Amphibious Air Cushion Suspension Systems", University of Toronto, Institute for Aerospace Studies, Toronto, Report No. 246, November 1980.

G.4 Sullivan, P. A., Hinchey, M. J. and Green, G. M., "A Review and Assessment of Methods for Prediction of the Dynamic Stability of Air Cushions", Journal of Sound and Vibration, Vol. 84, No. 3, Oct. 1982, pp. 337-358, ~~October 1982.~~

G.5 Wylie, E. B. and Streeter, V. L., Hydraulic Transients, McGraw-Hill, New York, 1978.

G.6 Ohashi, H., "Analytical and Experimental Study of the Dynamic Characteristics of Turbopumps", NASA TN D-8413, 1968.

G.7 Graham, T. A., Sullivan, P. A. and Hinchey, J. J., "Skirt Material Effects on Air Cushion Dynamic Heave Stability", Journal of Aircraft, Vol. 22, No. 2, Feb. 1985, pp. 101-108.

G.8 Hahn, W., Stability of Motion, Springer-Verlag, 1967.

G.9 Fung, Y. C., An Introduction to the Theory of Elasticity, Dover PUblications, 1969.

G.10 Hinchey, M. J., Sullivan, P. A. and Dupuis, A., "Wave Propagation Effects on the Heave Dynamics of Large Air Cushion Platforms", University of Toronto, Institute for Aerospace Studies, Toronto, Technical Note No. 234, August 1982.

G.11 Hinchey, M. J., Sullivan, P. A. and Dupuis, A., "On the Heave Dynamics of Large Air Cushion Platforms", Journal of Sound and Vibration, Vol. 96, No. 4, 1984, pp. 469-484.

G.12 Hinchey, M. J., "Heave Stability of Air Cushion Vehicles Hovering Over Deep Water", University of Toronto, Institute for Aerospace Studies, Toronto, Technical Note No. 236, August 1982.

G.13 See Appendix F.

G.14 Fowler, H., "An Experiment on the Heave Oscillation of a Light Air Cushion Vehicle", Canadian Aeronautics and Space Journal, Vol. 2, No. 2, Second Quarter, 1980.

G.15 Laframboise, J., Private Communication.

G.16 Hinchey, M. J. and Sullivan, P. A., "A Theoretical Study of Limit Cycle Oscillations of Plenum Air Cushions", *Journal of Sound and Vibration,* Vol. 79, No. 1, Nov. 1981, pp. 61-77.

G.17 Sullivan, P. A., Byrne, J. and Hinchey, M. J., "Nonlinear Oscillations of a Simple Flexible Skirt Air Cushion", *Journal of Sound and Vibration*, Vol. 102, No. 2, Sept. 1985, pp. 269-283.

APPENDIX H. MEASUREMENT OF FAN RESPONSE TO UNSTEADY PRESSURE (P. A. Sullivan and N. H. Milligan)

NOMENCLATURE

Roman

C_c	capacitance of cushion volume
$C_{d\ell}$	discharge coefficient at lip
f	frequency of table oscillation
h	hovergap
L_p	peripheral length of hovergap
p_c	cushion or plenum chamber pressure
p_f	fan delivery pressure, assumed equal to p_c
Q_a	air flow to atmosphere from cushion
Q_f	air flow delivered by fan
S_a	support area of cushion
t	time

Greek

ρ	atmospheric air density

H.1 Introduction

The idea for measurement of the history of fan response to unsteady cushion pressures, suggested by M. Hinchey, is depicted in Figure H.1. The fan under test (1) delivers air to a cylindrical plenum chamber (2) which is mounted over the UTIAS servohydraulic Heave Table (4). Although in Figure H.1 the plenum chamber is shown constrained by the linear ball bushings (3) to move vertically, for the present investigation it is fixed. With the fan running the table is set to oscillate at a known frequency. The pressure in the plenum chamber and the hovergap are measured by the pressure transducer (6) and the displacement transducer (5) respectively. The histories of the electrical outputs of these transducers are recorded. If the flow out of the chamber through the relatively narrow hovergap can be treated as quasisteady, then the usual air cushion mass conservation law and orifice flow formulae can be used to compute the flow from the fan using the equation

$$Q_f = C_c \dot{p}_c + S_a \dot{h} + Q_a \tag{H.1a}$$

$$Q_a = C_{d\ell} L_p h(t) \{2p_c(t)/\rho\}^{1/2} \tag{H.1b}$$

where the symbols have their usual meaning.

Success in this technique then depends on two key conditions:

(i) the adequacy of data acquisition and analysis procedures,

(ii) the accuracy of the quasisteady assumption implicit in the use of Equation (H.1b) to compute Q_a.

Consider these in turn.

H.2 Data Acquisition and Analysis Problems

When the experiment was initially proposed, the only available equipment was a Honeywell 2202 Visicorder. This had adequate frequency response, but the data was recorded in analog form on a strip-chart. Although preliminary experiments had indicated that the concept was feasible, nevertheless the task of analysis remained onerous. As originally conceived, this required manual digitization of the oscillatory cushion pressure and hovergap signals for computation of Q_f together with Fourier analysis of p_c and Q_f. Also lack of availability of suitable personnel prevented any progress until recently.

Initially, we planned to circumvent the data acquisition difficulty by using an available Spectral Dynamics Model 360 Fast Fourier Transform Digital Signal Processor, and this was used for some preliminary experiments on the model set up to investigate the limitations of the quasisteady flow

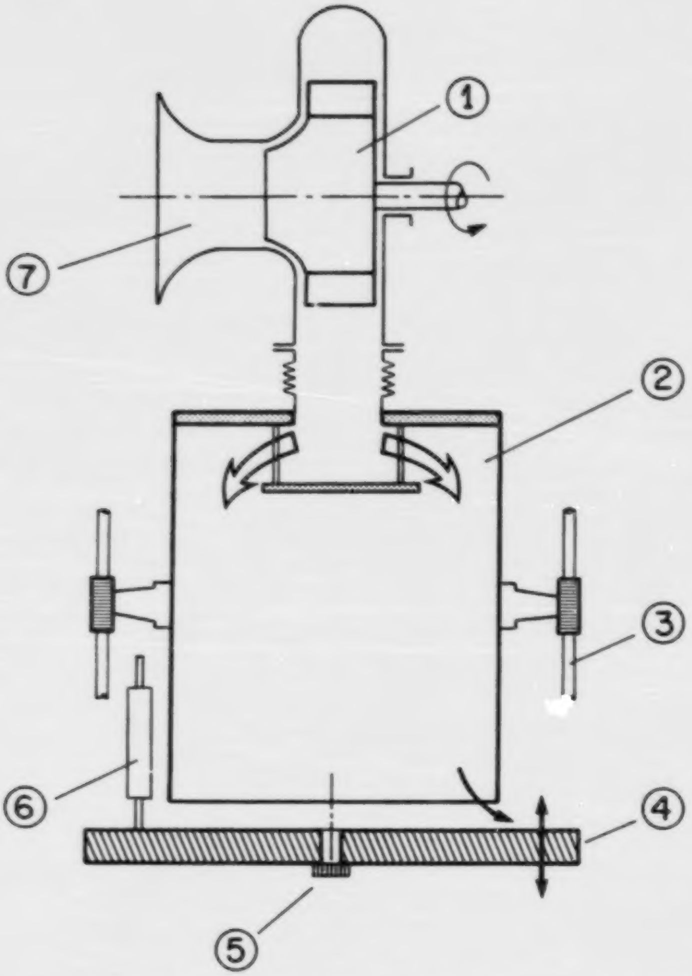

Figure H.1 Apparatus used in unsteady fan calibrations. The fan under test (1) pumps air into a rigid plenum chamber (2), which in an experiment on the cushion dynamics is constrained to move in pure heave by the linear ball bushing assembly. Oscillating ground inputs are imposed by the servohydraulically driven heave table (4). The cushion pressure and hovergap histories are measured by the transducers (5) and (6).

assumption. However we recently acquired a Keithly-DAS Series 500 Digital Data Acquisition system which which uses an IBM PC-XT microcomputer. Now completely operational, this made the entire task of data acquisition and processing very straightforward. Figure K.3, Appendix K, is a configurational diagram of the system.

H.3 Quasisteady Lip Flow Assumption

Previous UTIAS work on ACV dynamics, such as that described in Ref H.1 and Appendix C has demonstrated that for the frequencies and sizes of hovergap encountered in UTIAS ACV experiments, the quasisteady assumption is usually very accurate. Reference H.1 gives a criterion which suggests that the error may typically be less than 1%. Nevertheless, because of its pivotal role, we considered it necessary to ascertain the limits of its validity through a suitable calibrating experiment. The experiment that has been set up for this purpose is depicted in Figure H.2. Air is drawn from atmosphere by a fan through a narrow slot orifice (1) into a chamber (2). The orifice flow is made unsteady by means of a rotating butterfly valve diaphragm (3). The magnitude and frequency of the unsteadiness are controlled by changing the size of the diaphragm and its speed of rotation respectively. The true unsteady velocity of the flow just downstream of the slot is measured by a standard hot-wire anemometer, and the pressure in the chamber is measured by a piezo-resistive pressure transducer.

For the preliminary results shown in Figure H.3 the diaphragm size is 100% of the pipe diameter, and the imposed frequency is 15.2 Hz. The Spectral Dynamics Digital Signal Processor was used to analyse the signals. The curves in Figure H.3 give the experimentally measured pressure, and the pressure predicted by applying the steady state Bernoulli law to the hot wire measurements of velocity. In both cases the signal processor's fast Fourier Transform routine was applied to the experimental signals, and the curves in Figure H.3 were reconstructed from the harmonics. This is a severe test, since the frequency is well above those usually encountered in our experiments, the flow is almost completely shut off at one point of the cycle, and errors in computing velocity histories from given pressure histories should be much smaller than in the reverse computation that was done here.

These results are encouraging, but further progress has been delayed, owing to lack of suitable personnel.

H.4 Preliminary Results

Figure H.4 gives the steady state fan curve obtained simply by oscillating the table at a very low frequency, typically 0.01 Hz. The data was obtained for fan speeds N in the range $2000 < N < 3000$ rpm, and is presented in the standard form of pressure coefficient $C_{FP} = p_f/\rho N^2 D^2$ as a function of flow coefficient $C_{FQ} = Q/ND^3$. The scatter in the data at high C_{FQ} is currently attributed to turbulence impinging on the pressure transducer. Figures H.5 and H.6 give typical dynamic data obtained at N = 2000 rpm and f = 3.16 Hz and 5.77 Hz respectively. The data give the instantaneous pressure and computed instantaneous fan flow, and presented in the usual steady state format. For these and all subsequent results the

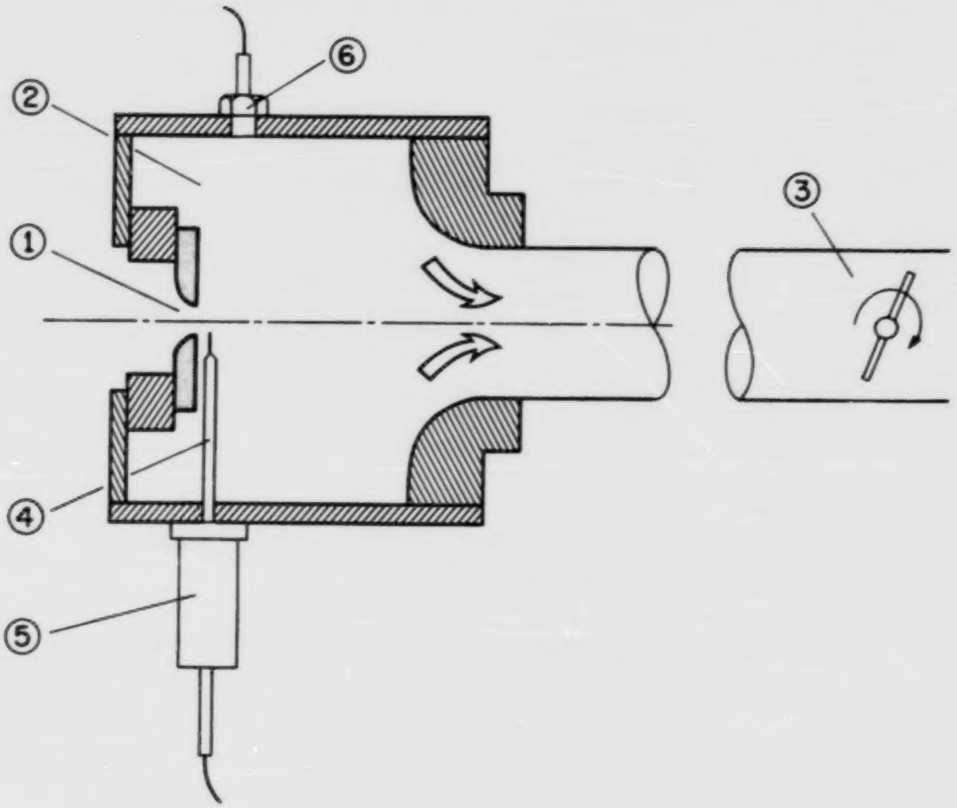

Figure H.2 Concept of unsteady slot orifice calibration experiment. Air is drawn through the slot orifice, 1, into the chamber, 2, by a fan downstream of the rotating butterfly valve, 3. The size of the butterfly valve and its speed of rotation can be changed to control the magnitude and frequency of the pressure fluctuations in 2. The true unsteady flow is measured by the hot wire anemometer, 4, and compared with the predicted value obtained from the pressure measured by the transducer, 6.

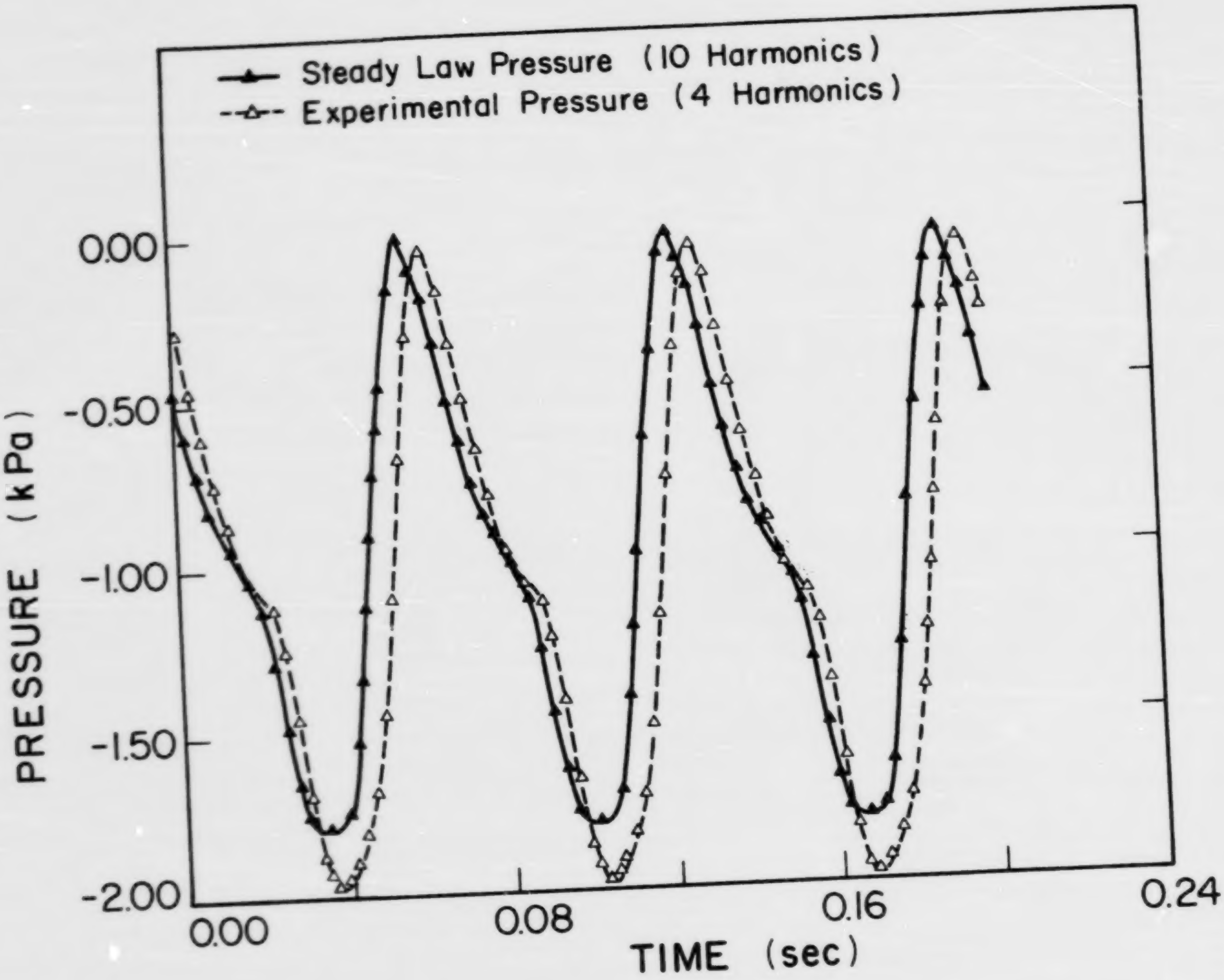

Figure H.3 Preliminary results from the unsteady slot flow calibration experiment. The frequency of valve rotation is 15.2 Hz and the reduced frequency fL/V, based on the mean velocity, is about 0.0052.

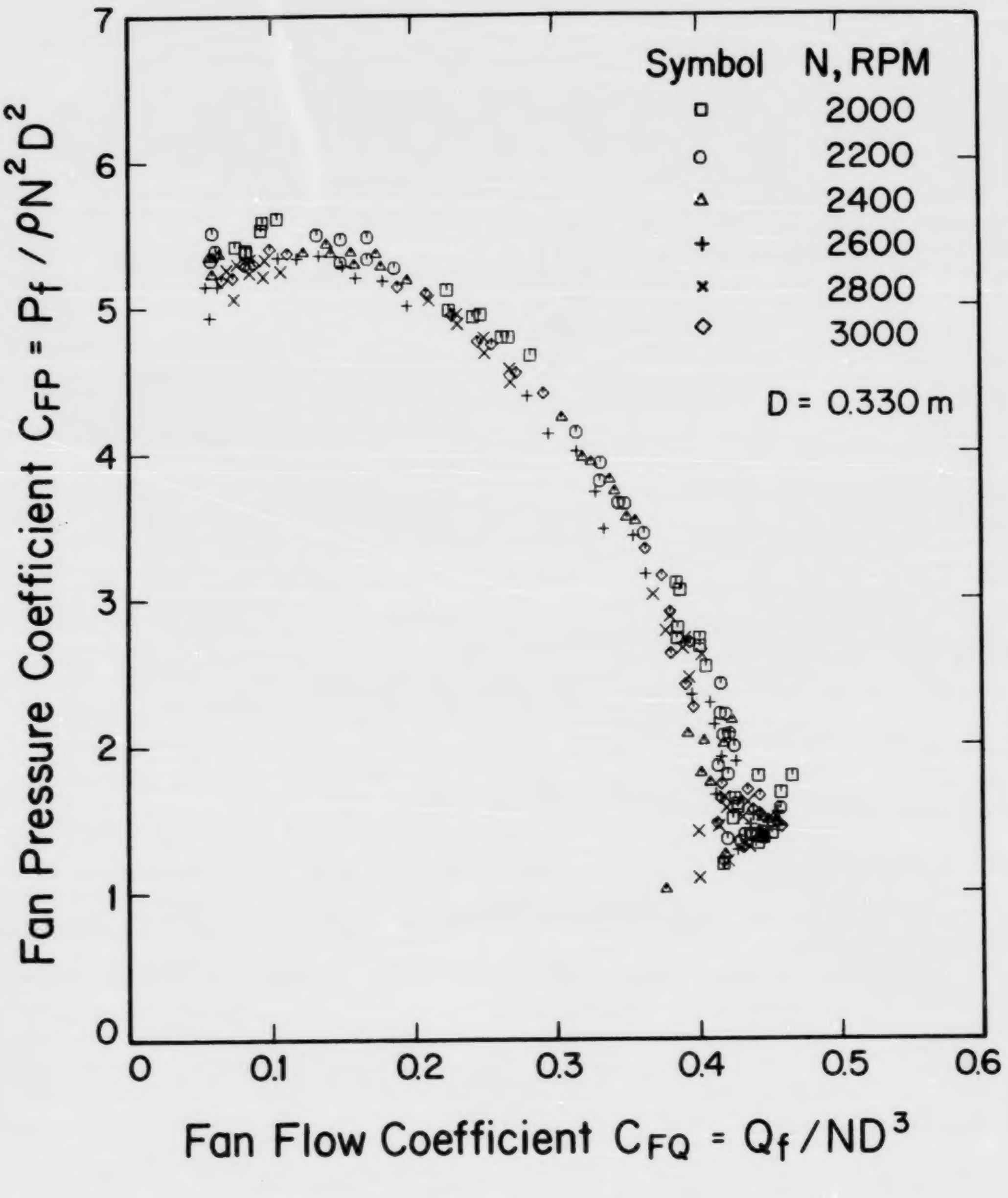

Figure H.4 Steady state pressure-flow characteristic of fan used in dynamic tests.

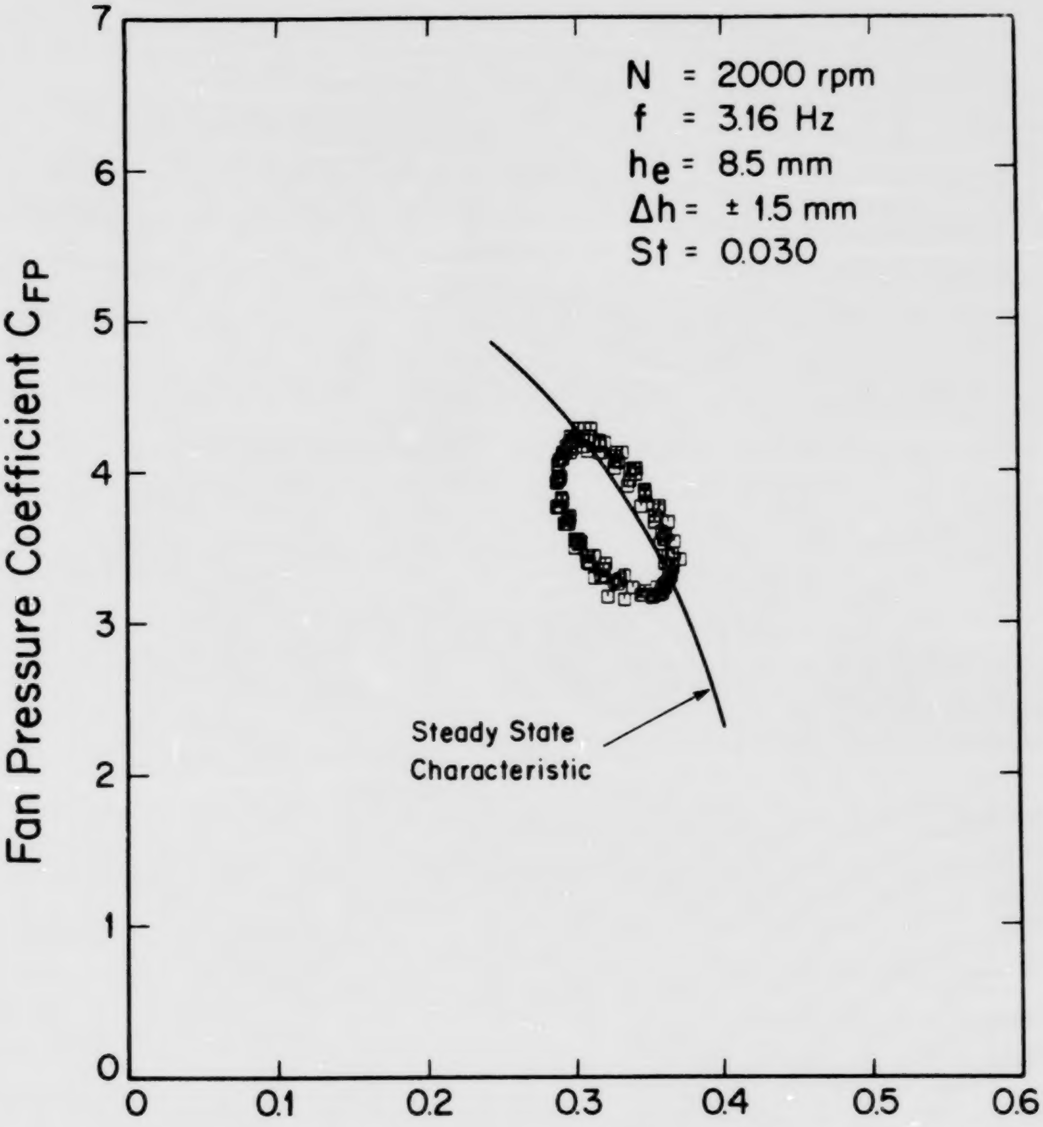

Figure H.5 Dynamic characteristic obtained at a frequency of 3.16 Hz. The offset of the long axis of the oval from the steady state curve may be caused by phase shifts in the anti-aliasing filters of the data acquisition system of Figure K.2

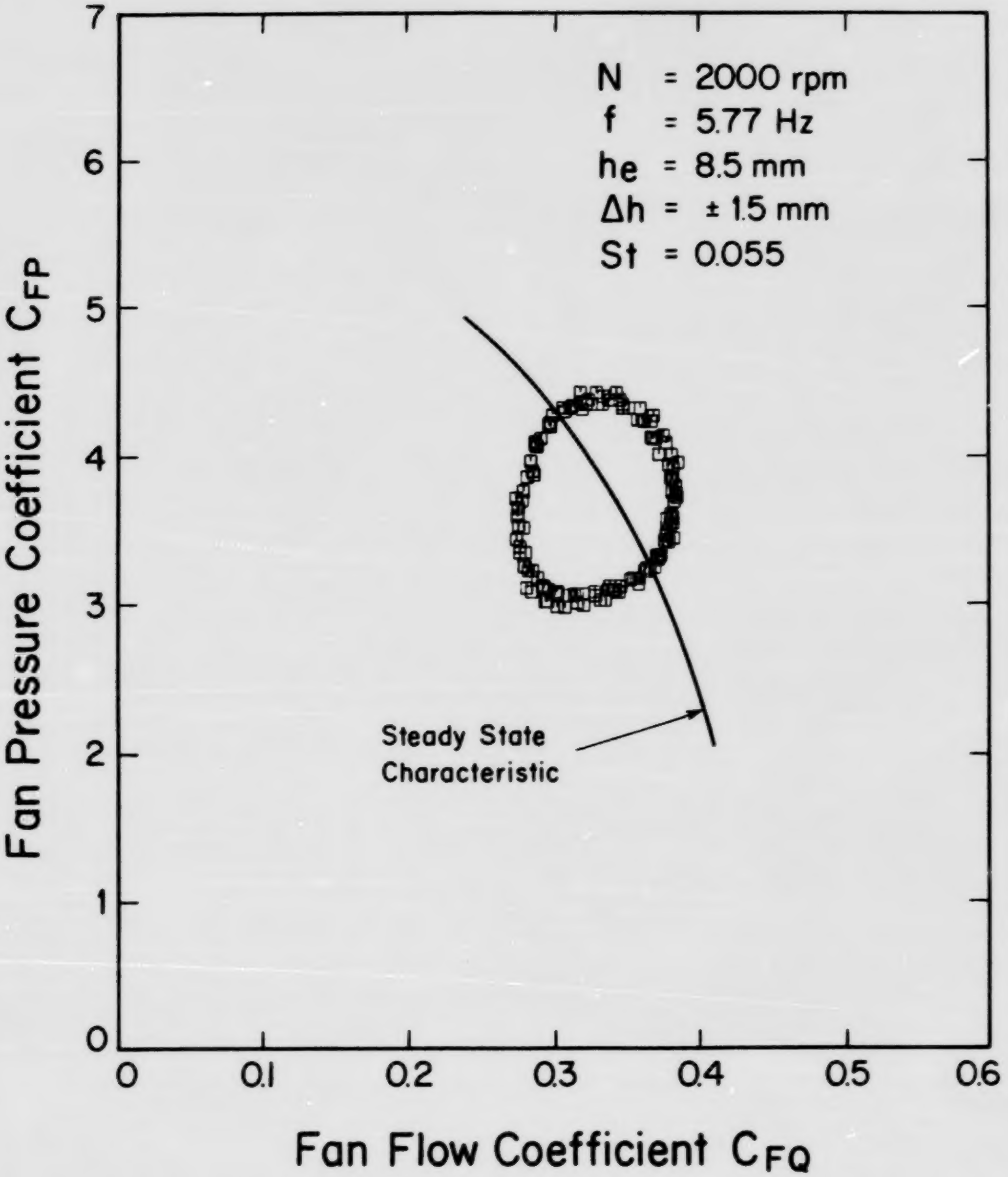

Figure H.6 Dynamic characteristic obtained at a frequency of 5.77 Hz.

mean hovergap is 8.5 mm and the amplitude of the imposed table oscillation is 1.5 mm. The steady state curve is included for reference.

To obtain these curves, data was sampled at the rate of 100 points per cycle over two to three cycles. Now to compute the instantaneous Q_f, both dp_c/dt and dh/dt are required. For the firt tests, the $p_c(t)$ and $h(t)$ data was smoothed by using a narrow band digital filter routine, the derivatives were then computed using a three point central difference formula, and finally Equation (H.1) was used to compute Q_f. It was howver found that the digital filtering was unnecessary. Typically about half of the computed data points are presented.

The data in Figure H.5 shows that for the Heave Table fan, at frequencies as low as 3 Hz there is already significant deviation from the steady state behaviour. Figure H.6 shows that at 5.77 Hz, which is typical of the natural frequencies of air cushion models tested in this facility, the dynamic response cleanly bears little relationship to the steady state response. Figure H.7 is a superposition of the dynamic characteristics obtained at N = 2000 rpm at selected frequencies up to 13.53 Hz. For clarity, the data points have been omitted. This shows that, for a hovergap oscillation which has a fixed mean and amplitude, as the frequency increases, the amplitude of both the pressure and flow fluctuations increase. Now if the unsteady effects were purely due to the inertia of the air in the fan, at high enough f, the amplitude of the volume flow oscillations should decrease as the frequency increases. This suggests that unsteady blade aerodynamics or the capacitance effect of the fan volute may play a role. However, owing to the preliminary nature of these experiments, the existence of artifacts in the experiment or in the data analysis cannot be ruled out. Recent work has indicated that the anti-aliasing analog filters (see Figure K.3) may be introducing significant errors at the higher frequencies.

H.5 Concluding Remarks

The recently obtained preliminary results described here indicate that the technique has the potential to yield high quality data on unsteady fan behaviour, and should therefore be actively developed. Although it obviously cannot be applied directly to full scale installations, nevertheless it could be applied to scale models of such installations, and through appropriate scaling laws, be used to predict full scale unsteady behaviour. The relevant scaling parameter is a reduced frequency or Strouhal number, defined by

$$St = \frac{fL_{ref}}{V_{ref}} = \frac{60f}{\pi N} \tag{H.2}$$

where $L_{ref} = D$ and $V_{ref} = \pi ND/60$.

Figure H.8 compares data obtained in the tests at N = 2000 and 3000 rpm for selected f. This shows that the data obtained at N = 2000 and f = 7.78 Hz, corresponding to St = 0.074, is close to that obtained at N = 3000 with f = 10.48 Hz and 13.53 Hz, corresponding to St = 0.067 and 0.086 respectively; this supports the idea that St is the appropriate scaling parameter.

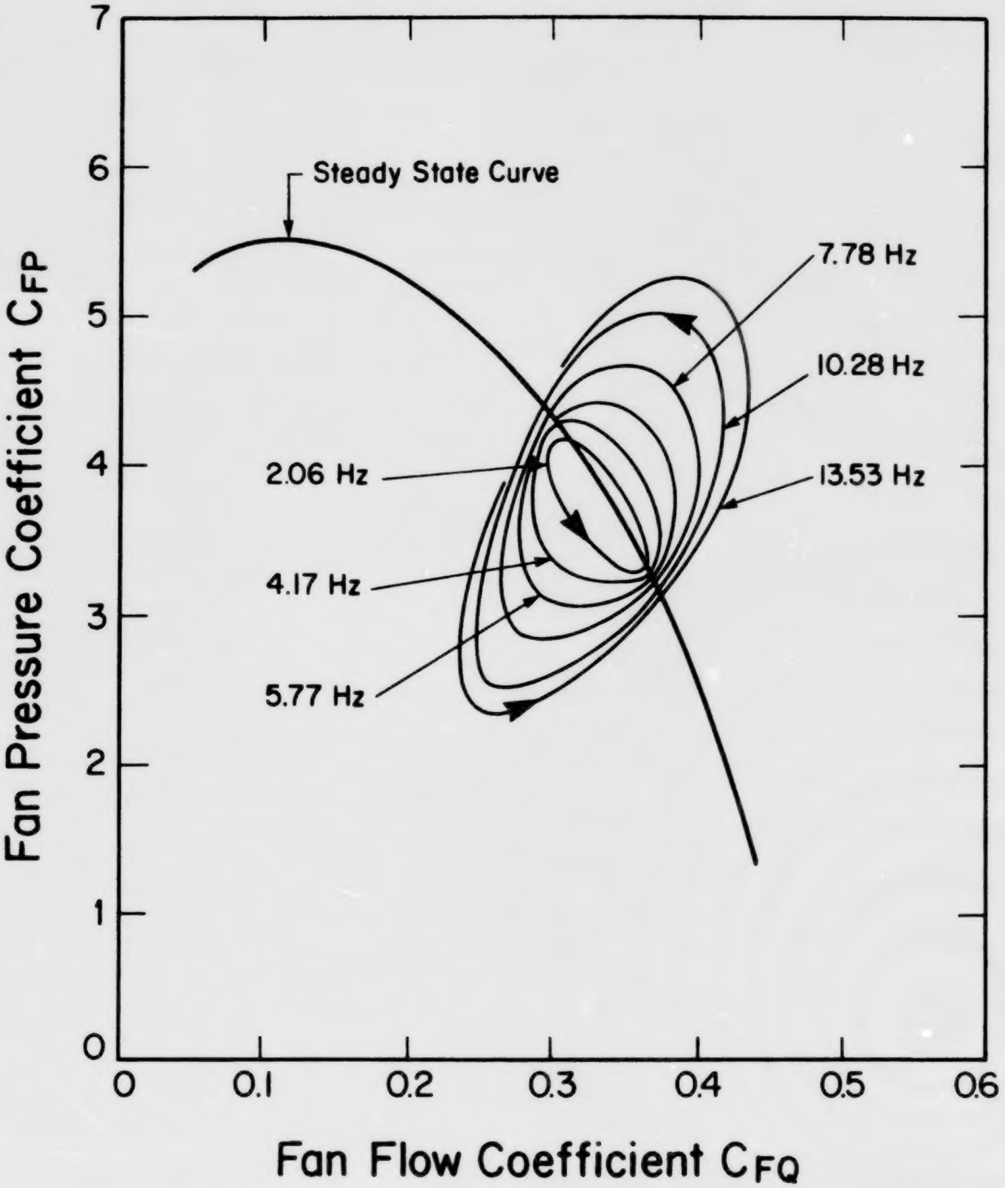

Figure H.7 Evolution of the dynamic characteristics as frequency increases from 2.06 Hz to 13.53 Hz. The amplitude and the mean value of the oscillating hovergap is the same for all cases and equal to the values in Figures H.5 and H.6.

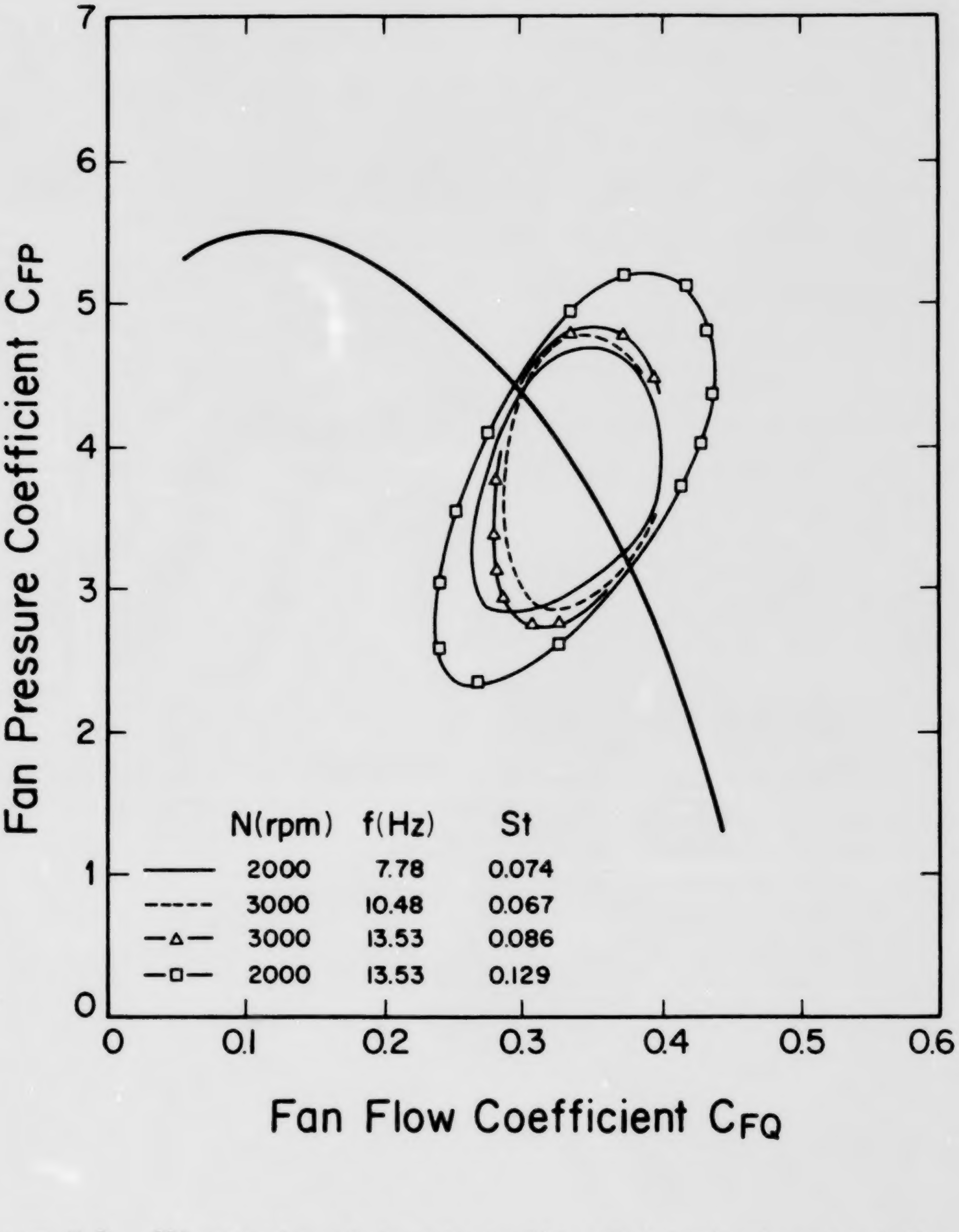

Figure H.8 Illustration of dynamic scaling of dynamic characteristics at different frequencies and fan speeds.

As a final comment, these results support the importance of using the Sphere Facility in the absence of an adequate model of the Heave Table Facility's dynamic fan behaviour.

REFERENCES - APPENDIX H

H.1 Sullivan, P. A., Hinchey, M. J., and Green, G. M., "A Review and Assessment of Methods for the Prediction of Dynamic Stability of Air Cushions", Journal of Sound and Vibration, Vol. 84, No. 3, 1982, pp. 337-358.

APPENDIX I: NONLINEAR DYNAMICS OF A SEGMENTED SKIRT AIR CUSHION (T. A. Graham and P. A. Sullivan)

NOMENCLATURE

a	speed of sound in air
a_f	cushion footprint area
a_ℓ	cushion air escape or leakage area
A_d	duct cross-sectional area
Bs	cushion width at bottom of skirt
C	viscous damping coefficient
C_c	cushion pneumatic capaciance
C_D	discharge coefficient
C_{MP}	pitch moment coefficient
d	duct diameter or equivalent diameter
f	friction factor
f	frequency
g	gravitational acceleration
h	height of centre of mass above datum
H_h	heave hysteresis force
H_p	pitch hysteresis moment
I_{yy}	moment of inertia in pitch
k	stiffness
L	length in general, length of craft hard structure
L_d	duct length
Ls	cushion length at bottom of skirt
m	mass, mass of cushion
M_P	total restoring moment
M_{P_f}	portion of restoring moment due to momentum flux of air from cushion

p_c	cushion pressure
Δp_f	static pressure rise across fan
Q_c	exit air flow from the cushion
Q_d	volume flow of air in the duct
R_s	radius of cushion corners at skirt bottom
t	time
V_c	cushion volume
W	craft all-up weight
x	variable
$\bar{x}$	moment arm of centre of pressure
β	segment angle with ground when $\theta = 0$
ζ	damping factor
θ	pitch angle
π	3.14159...
ρ	air density
ω_n	natural frequency (rad/s)

I.1 Introduction

One of the objectives of the Air Cushion Vehicle (ACV) research program at the University of Toronto Institute for Aerospace Studies (UTIAS) is to study the dynamics of ACV's equipped with the uncompartmented segmented skirt system shown in Figure I.1. This skirt has been used in icebreaking, low speed barges, and ferry applications. Typical craft using this skirt are the air cushion icebreaking bow (ACIB), the Hoverlift Systems HL101, and the Air Trek 140. Initial UTIAS studies of this skirt resulted in an experimentally validated theory for the static pitch and roll stiffness of this skirt system which was presented in [I.1, I.2]. This theory has been extended and incorporated into a dynamics model. This paper presents some preliminary results from this model.

A dynamic theory for the cushion must describe the method of generating restoring forces, predict cushion pressure and flow, and model the vehicle motion. The restoring forces, cushion pressure and centre of gravity motion are intrinsically coupled. For example, in order to apply Newton's laws of mechanics, the movement of the centre of mass that occurs during a pitching manoeuvre must be known to reasonable accuracy. Also, application of the basic cushion mass flux conservation law requires information about the mass flux of air from the cushion. This must be calculated and requires knowledge of both the cushion pressure and the effective air escape area generated by the cushion as a result of its motion. Thus, as a minimum, the air escape area geometry during motion and a description of the duct-fan flow characteristics are necessary.

Force and moment measurements made on full scale and laboratory vehicles have shown that static hysteresis can exist in the heave stiffness [I.1] and pitch stiffness [I.2] curves, see Figure I.2. This hysteresis represents damping in the dynamics and tests on the UTIAS circular track vehicle [I.3] indicate that all the static hysteresis contributes to the vehicle's damping. Although studies are currently in progress at UTIAS the nature and cause of this hysteresis is not adequately understood. The forces are, however, generated during skirt ground contact and current thinking is that they arise from stress relaxation and internal friction induced by local buckling which occurs as a result of this contact.

The geometry of an amphibious air cushion skirt system also plays an important role in determining the system stiffness and damping parameters. Some systems, such as the British Hovercraft (BHC) bag and finger skirt, the Bertin multicell, and the peripheral cell cushion achieve pitch and roll stiffness primarily through cushion compartmentation; others such as the Hovercraft Development Ltd. (HDL) loop and segment skirt allow the skirt to shift laterally relative to the vehicle centre of mass to obtain pitch and roll stiffness. The uncompartmented segmented skirt system differs from these in that it obtains pitch and roll stiffness through centre of pressure shifts resulting only from the deformation of the skirt which occurs during surface contact. The details of the contact area are thus crucial for a good qualitative and quantitative study of segmented skirt system dynamics.

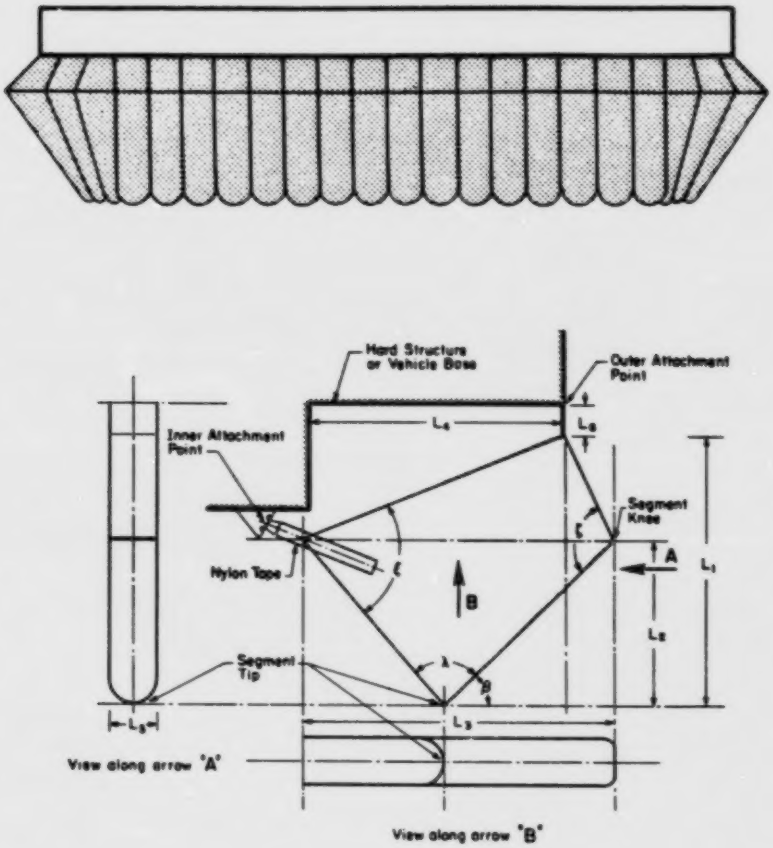
Hard Structure or Vehicle Base
Outer Attachment Point
Inner Attachment Point
L_4
L_6
Segment Knee
ζ
A
L_1
ε
Nylon Tape
B
L_2
Segment Tip
λ
β
L_5
L_3
View along arrow 'A'
View along arrow 'B'

End View
of Segment

Side View
of Segment

Figure I.1: Segmented Skirt System

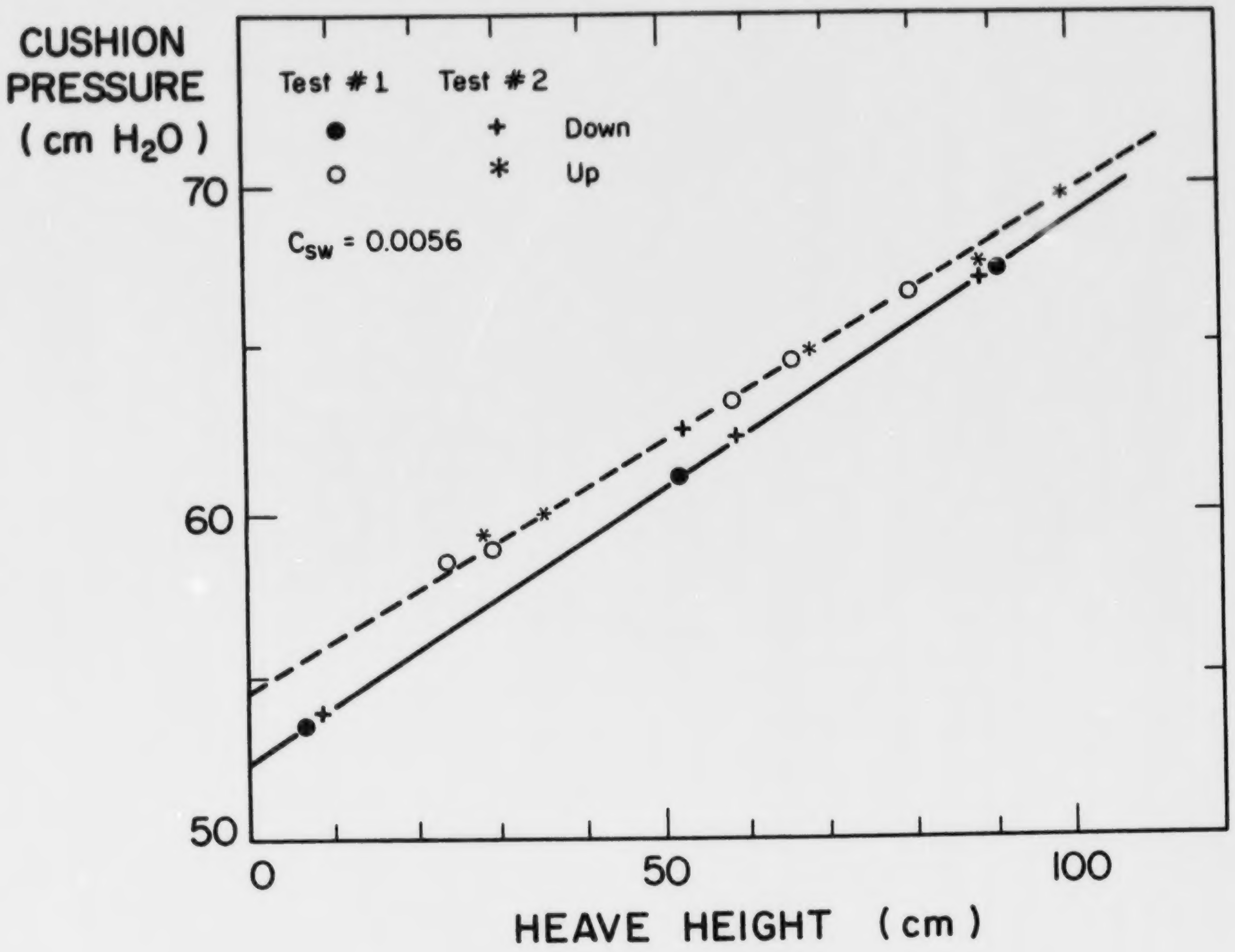

Figure I.2: Experimental Data Showing Hysteresis in Heave Cycle Tests on the Air Cushion Icebreaker Bow (ACIB)

Several approximations to the footprint geometry are presented here to demonstrate its effect on predicted cushion response.

The duct-fan flow model for the system requires the both steady fan characteristic and terms to account for dynamic effects When the blade aerodynamics is steady, the fan and duct dynamics be handled by the method of characteristics [I.2, I.4], transmission line techniques [I.2, I.4], or a lumped parameter model, depending on the accuracy required, the system geometry, and the frequency range of interest. For the laboratory craft under study, frequencies of vehicle dominated motion are low and dimensions are small enough so that the lumped parameter model assumptions are valid. Therfore a lumped parameter approach which utilizes an inertance for the duct and a capacitance for the plenum, has been chosen for this investigation.

The lumped parameter models permit direct comparison of different system models. Thus it can be determined if the added inertance and capacitive orders represent significant differences in vehicle response. It has been shown by Sweet, Richardson,and Wormley [I.5] that inclusion of capacitance is required to predict dynamic heave stability. Hinchey [I.6] has shown that even relatively short duct feeding systems can radically shift heave stability boundaries. Captain, Boghani, et al [I.7] have also indicated that duct inertia and plenum capacitance are of fundamental importance for air cushion response prediction. Doctors has shown [I.8] that at higher frequencies, the cushion capacitance causes large deviations in response amplitude and phase characteristics. However, many authors ignore the capacitance, citing reasons such as "likely to be less important at lower frequencies" [I.9], or "Because of the large leakage of ACV's the effects of compressibility and hence absolute pressure may be neglected" [I.10]. Simply put, criteria for the inclusion of orders for capacitance and/or inertance have not been adequately delineated so that a complete dynamics investigation should assess the effects of both.

I.2 Equations of Motion

The equations of pitch-heave motion include Newton's law for the heave motion, Euler's equation for pitch motion, the lumped capacitance equation for the combined plenum box cushion volume, and the lumped inertance equation for the fan-duct system. The resulting sixth order dynamics mode is based on the following assumptions:

i) the vehicle is moving at zero forward speed and is disturbed in pitch and heave only.

ii) gyroscopic effects from rotating subassemblies such as fans and propellers are negligible.

iii) the skirt system is massless and inelastic and on contact with the ground deforms according to a geometric theory.

iv) the skirt material damping forces can be represented by a static hysteresis model in which forces are proportional to the perimeter of skirt in contact. These skirt forces act only when the material is being compressed, that is that no force acts when the amount of compression is being reduced.

v) the frequencies of excitation and oscillation are low enough that the lumped parameter models apply to the flow processes. A conservative empirical criterion for this is that

$$f < 0.04a/L \qquad (I.1)$$

where a is the speed of sound and L is the longest dimension of the flow element, [I.4].

vi) the fan blade aerodynamics are quasi-steady.

vii) cushion exit flow is governed by the quasisteady orifice flow law.

viii) vehicle pitch motion is about the centre of mass which lies on the longitudinal and lateral axes of symmetry of the craft.

ix) ground friction is negligible.

x) cushion internal flow effects are small.

The resulting system equations are given as follows:

The heave force balance:

$$m\ddot{h} = p_c a_f(h,\theta) - mg + H_h(h,\theta,\dot{h},\dot{\theta}) \qquad (I.2)$$

where m is the cushion mass
h is the cushion centre of mass height above datum
θ is the pitch angle
p_c is the cushion plenum pressure
a_f is the cushion footprint area
g is gravitational acceleration
H_h is the magnitude of the heave hysteresis force
and $(\dot{\ }) = d(\ )/dt$.

The pitch moment balance:

$$I_{yy}\ddot{\theta} = M_p(h,\theta,p_c) + H_p(h,\theta,\dot{h},\dot{\theta}) \qquad (I.3)$$

where I_{yy} is the pitch moment of inertia,
M_p is the cushion restoring moment given by

$$M_p = -p_c a_f(h,\theta)\bar{x}(h,\theta) + M_{pf}(h,\theta,p_c), \qquad (I.4)$$

$\bar{x}$ is the moment arm of the centre of pressure from the centre of mass,
M_{pf} is a minor contribution due to momentum of fluid exiting from the cushion,
and H_p is the pitch hysteresis term.

Conservation of mass for the cushion requires:

$$C_c\dot{p}_c = Q_d - Q_c - V_{c_h}(h,\theta)\dot{h} - V_{c_\theta}(h,\theta)\dot{\theta}, \qquad (I.5)$$

where C_c is the cushion capacitance given by

$$C_c = V_c(h,\theta)/\rho a^2 \qquad (I.6)$$

V_c is the cushion volume,
ρ is the air density,
Q_d is the volume flow of air in the duct,
Q_c is the cushion exit flow,
and V_{c_h} and V_{c_θ} are the partial derivatives of V_c with respect to h and θ respectively.

The lumped inertance equation for the duct:

$$\left(\frac{\rho L_d}{A_d}\right)\dot{Q}_d = \Delta p_f - p_c - \left(\frac{4fL_d}{d}\right)\left(\frac{\rho Q|Q|}{2A_d^2}\right) \qquad (I.7)$$

where L_d is the duct length,
A_d is the duct cross-sectional area,
Δp_f is the static pressure rise across the fan,
d is the duct diameter or equivalent diameter,
and f is the usual duct friction factor.

The description is completed with the steady fan law,

$$\Delta p_f = p_o + pQ_d + p_2Q_d^{\,2} + p_3Q_d^{\,3} + p_4Q_d^{\,4} \qquad (I.8)$$

and the exit flow law,

$$Q_c = C_D a_\ell(h,\theta)\left(\frac{2p_c}{\rho}\right)^{1/2} \qquad (I.9)$$

where C_D is the exit discharge coefficient, and a_ℓ is the cushion leak or air escape area. Equations I.8 and I.9 apply at each instant of time.

When the capacitance and inertance are negligible the system is fourth order and the lumped capacitance and inertance equations become

$$Q_c = Q_d - V_{c_h}(h,\theta)\dot{h} - V_{c_\theta}(h,\theta)\dot{\theta} \qquad (I.10)$$

and

$$\Delta p_f = p_c + \left(\frac{4fL_d}{d}\right)\left(\frac{\rho Q_d|Q_d|}{2A_d^2}\right) \qquad (I.11)$$

respectively. With the exit flow equation, I.9, these provide the boundary conditions for equations I.1 and I.2.

I.3 Geometric Function Approximations

Four terms in the above equations are geometry dependent; these are the geometric functions $a_\ell(h,\theta)$, $a_f(h,\theta)$, $V_c(h,\theta)$, and $\bar{x}(h,\theta)$. The calculation of these functions is facilitated by making two initial approximations. First, the curved edges at the lip of the skirt are replaced with a simple mean perimeter line. Second, the flow area associated with the rounded tips of the segments is modelled as an equivalent leak height which is calculated using the above perimeter, the measured flow, and the cushion pressure when all the segment lower tips are just touching the ground. This leak height is indicated as H_L in Figure I.3, which also shows the three geometry cases for which each of the functions must be calculated. The three cases are:

i) the skirt is totally out of contact with the ground,

ii) the skirt is in partial contact with the ground, that is, the plane formed and bounded by the undeformed skirt lip perimeter and the ground plane intersect,

and

iii) the skirt is in contact with the ground throughout its entire perimeter.

The details of the geometry are given in Appendix J. Some discussion is appropriate since the nature of assumptions made about the shape of the footprint will be shown to have a significant effect on cushion operation.

The detailed footprint area used in the three cases is shown in Figure I.4 and has the dimensions given in the first column of Table I.1. These dimensions are those of the UTIAS laboratory test facility, hereafter referred to as the Labrig. Another approximation, referred to here as the "alternate" footprint, has been constructed. This footprint is the same as the detailed area except that the corner radius, Rs, is assumed to be zero so that the case 1 footprint is a rectangle. Column 2 of Table I.1 gives the appropriate dimensions. A simpler footprint is obtained by assuming $R_S = 0$, and that the footprint does not expand laterally as a result of ground contact during pitch motion. Thus the side triangles and curved section of cases 2 and 3 are ignored and a rectangular footprint is obtained. Of the three footprints the detailed footprint most closely duplicates tracings made of the footprint periphery of the Labrig test cushion.

In the results that follow all of the geometry functions are affected by the changes in footprint except the cushion volume. $V_c(h,\theta)$ is calculated assuming that Rs=0 and is similar to the alternate footprint except that the lower corner areas are formed by extension of the side triangle perimeter lines to meet the line formed by the outer edge of the skirt ground contact area at the lower end. Thus the lower ellipsoidal corners are replaced with trapezoids. The hysteresis functions, $H_h(h,\theta,\dot{h},\dot{\theta})$, and $H_p(h,\theta,\dot{h},\dot{\theta})$, are altered by the change in Rs. The associated forces are larger for a given (h,θ) when Rs=0 since the cushion perimeter length is increased over the detailed perimeter. The change in footprint area couples with associated changes in $\bar{x}(h,\theta)$ to produce changes in the restoring moment. The air leakage area, $a_\ell(h,\theta)$, is larger for a given (h,θ) when Rs=0. The geometry function differences are summarized in Table I.2 where geometry functions which are identical for different footprints have been marked in the appropriate column.

TABLE I.1

Footprint Details

	Detailed Footprint	Alternate Footprint	Rectangular Footprint	x20 Scaled Vehicle
Ls (m)	2.214	2.214	2.214	44.280
Bs (m)	0.991	0.991	0.991	19.820
Rs (m)	0.326	0.000	0.000	6.520
β (deg)	32.5	32.5	32.5	32.5
m (kg)	97.7	97.7	97.7	780000

TABLE I.2

Correspondence of Cushion Geometry Functions

Geometry Function	Detailed Area	Alternate Area	Rectangular Area	Comments
$a_\ell(h,\theta)$		Function is the same for alternate and rectangular footprints.		Modified by change in Rs
$a_f(h,\rho)$				
$M_p(h,\theta)$				
$V_c(h,\theta)$	Function is the same for all footprints.			Obtained in separate unaffected calculation.
$H_h(h,\theta,\dot{h},\dot{\theta})$		Function is the same for alternate and rectangular footprints.		Modified by change in Rs
$H_p(h,\theta,\dot{h},\dot{\theta})$		Function is the same for alternate and rectangular footprints.		Modified by change in Rs

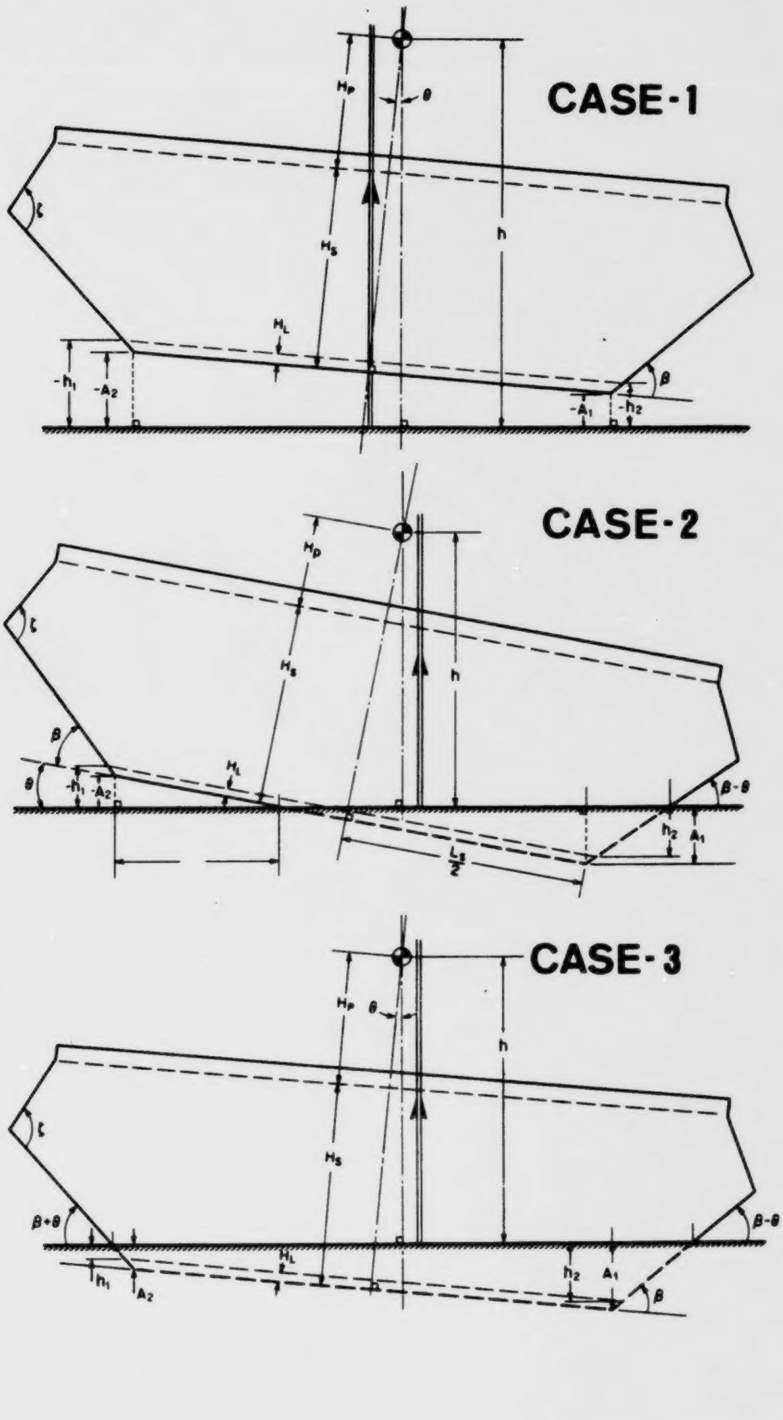
CASE-1
H_P
θ
h
H_S
H_L
ζ
-h_1
-A_2
-A_1
-h_2
β
CASE-2
H_p
h
H_s
ζ
β
θ
-h_1
-A_2
H_L
β-θ
h_2
A_1
L_s/2
CASE-3
H_P
θ
h
H_S
ζ
β+θ
β-θ
h_1
A_2
H_L
h_2
A_1
β

Figure I.3: Side View of Cushion for the Three Geometry Cases

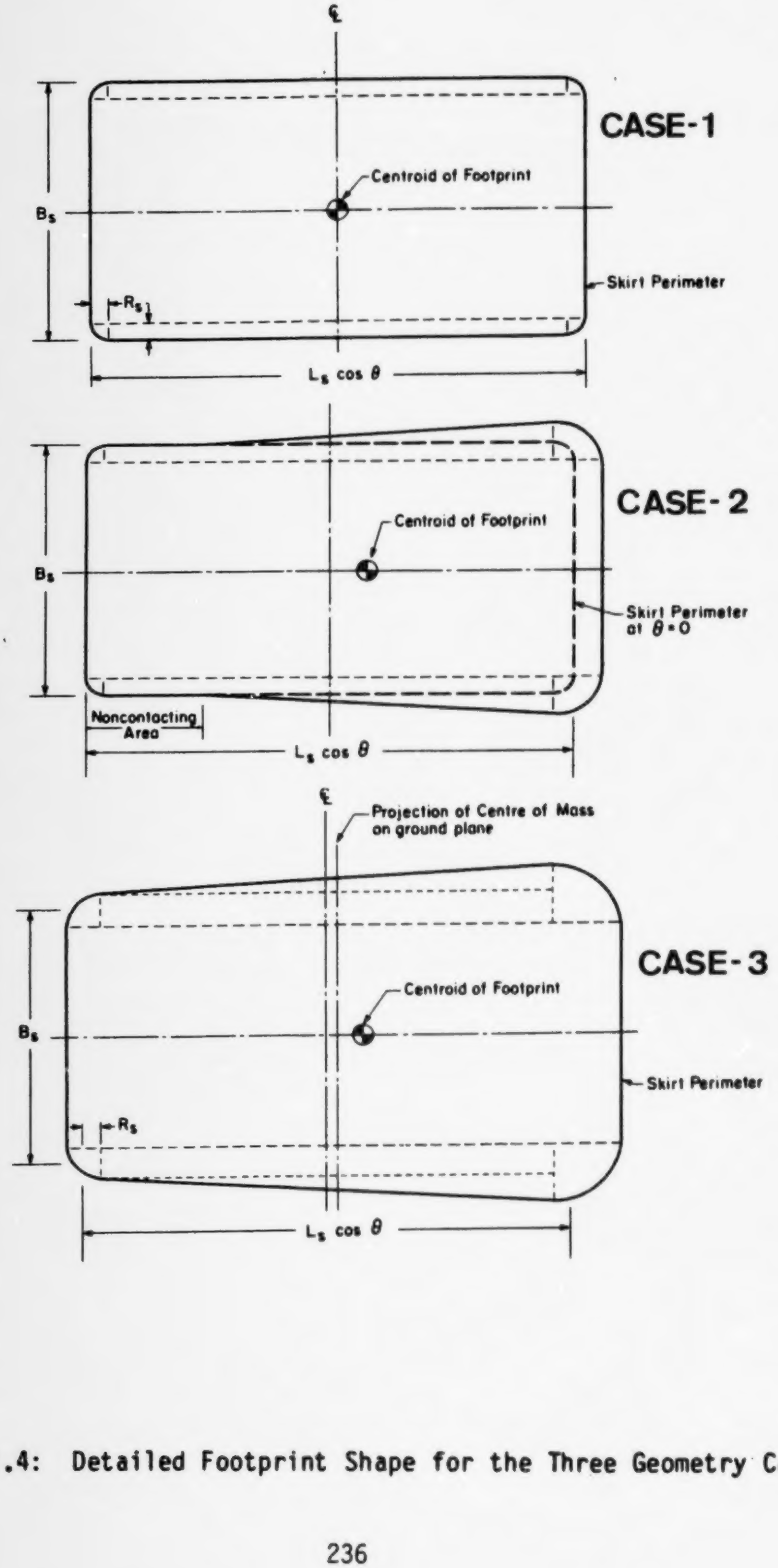
℄
CASE-1
Centroid of Footprint
B_s
Skirt Perimeter
R_s
$L_s \cos\theta$
CASE-2
Centroid of Footprint
B_s
Skirt Perimeter at $\theta = 0$
Noncontacting Area
$L_s \cos\theta$
℄
Projection of Centre of Mass on ground plane
CASE-3
Centroid of Footprint
B_s
Skirt Perimeter
R_s
$L_s \cos\theta$

Figure I.4: Detailed Footprint Shape for the Three Geometry Cases

I.4 Simulation Results and Discussion

Static simulation results were obtained with the skirt hysteresis set to zero. Figure I.5 gives experimental static pitch stiffness results along with theory for the three different footprint approximations of the Labrig test model. When compared to the measured values, the rectangular footprint underestimates the stiffness by 27%, the alternate footprint overestimates the stiffness by 24%, while the detailed area overestimates by 2.5%. Measured values of footprint area are presented with predictions of the three footprint approximations are shown in Figure I.6. Note that when Rs=0, the footprint areas at $\theta = 0$ are overestimated by about 5.5% compared to 1.8% for the detailed area. At larger pitch angles, above 2.5 degrees, the rectangular area underestimates the measured area. The alternate and detailed footprints continue to overestimate the area, at θ=3.2° the alternate is 16% over and the detailed is 7.0% over. The slope of the footprint area curve is important since it influences the dynamics through the pitch stiffness. Thus, although the rectangular footprint gives a closer fit to the footprint area on average the detailed area gives a preferable representation of these geometry related parameters.

Both the footprint area and restoring moment functions depend on the segment angle, β, shown in Figure I.1. The angle used in all theory presented here is 32.5°; this value was obtained from direct measurements of the angle between the tangent to the outer edge of the segment near its tip, and the ground plane. This was necessary because cushion pressure caused significant curvature of the segment outer surface between the knee and tip. Measurements of the distances from the segment knee to ground and from the segment tip to the perpendicular from the ground to the knee gave the design value of 40° for β. Still another estimate of β was obtained by determining the angle for which the detailed area gave the best fit to the area data: this value was 38°. If 38 or 40° is used in the theory the following changes occur in the results. The pitch stiffness is reduced in all cases so that the alternate area curve now agrees closely with the measured values, and the detailed area stiffness curve lies closer to the rectangular curve of Figure I.5. The footprint area predicted by the detailed geometry agrees with the footprint data closely while the alternate footprint still overestimates at all angles. The results for the rectangular area greatly underestimate the pitch stiffness and show only a very small footprint area change during pitch motion. The discrepancy between the moment and area suggests that there are forces which produce moment on the cushion not included in the analysis. Current speculation is that these forces are produced by the air supply ducts and/or an elastic force resulting from skirt ground contact.

All dynamics simulation results are presented for cushions with β of 32.5° and are the response to a simple initial disturbance test. The model is clamped in equlibrium at 2° pitch until t=0 when the vehicle is released and the response is plotted. The fourth order system model is used with the three footprint area approximations to obtain the comparative results shown in Figure I.7. The pitch and heave responses are given for each approximation. Of the three, the rectangular skirt is much more highly damped.

This increase in damping may be interpreted by loose analogy with a second order system with viscous damping as follows. Make the gross - and

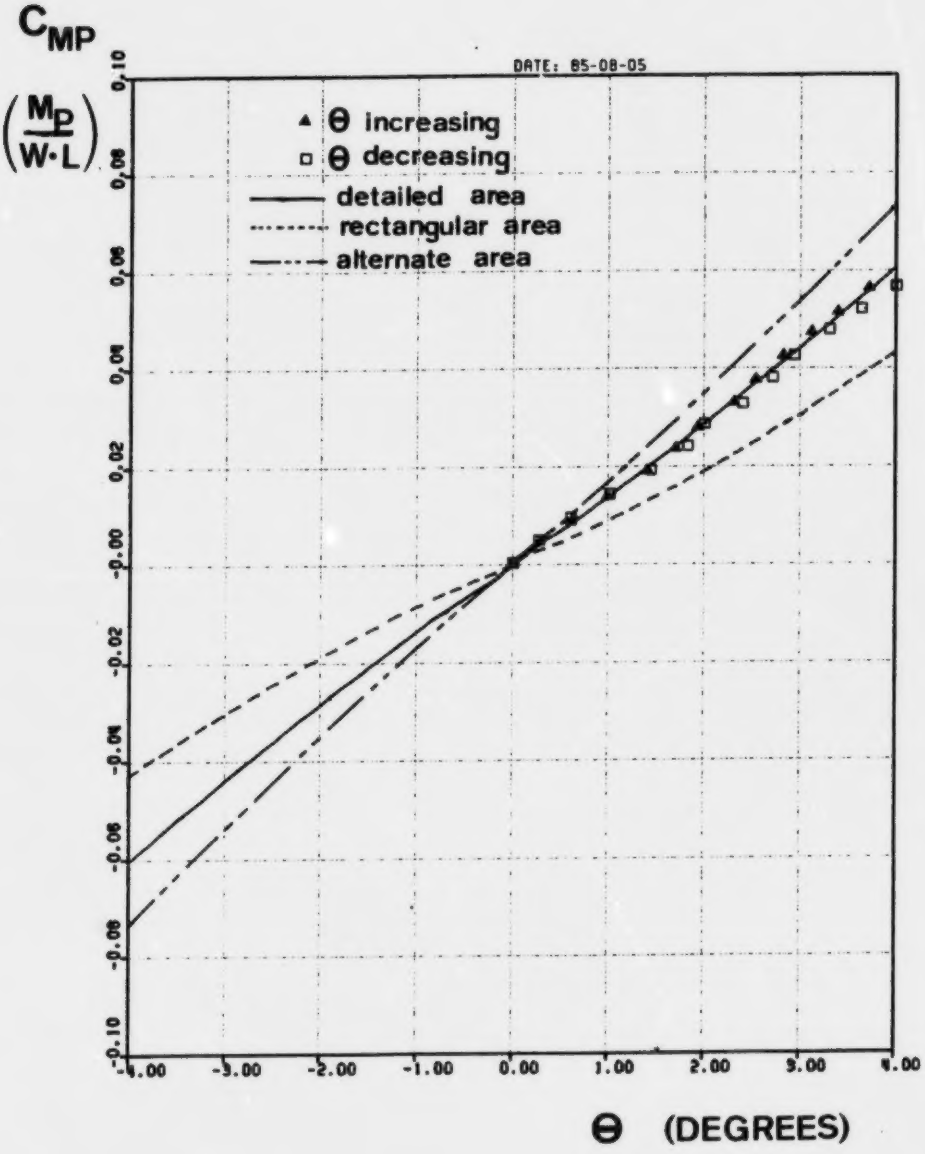

Figure I.5: Pitch Stiffness - Experimental Results and Theory for Three Footprint Area Approximations
a) Detailed Area
b) Rectangular Area
c) Alternate Area

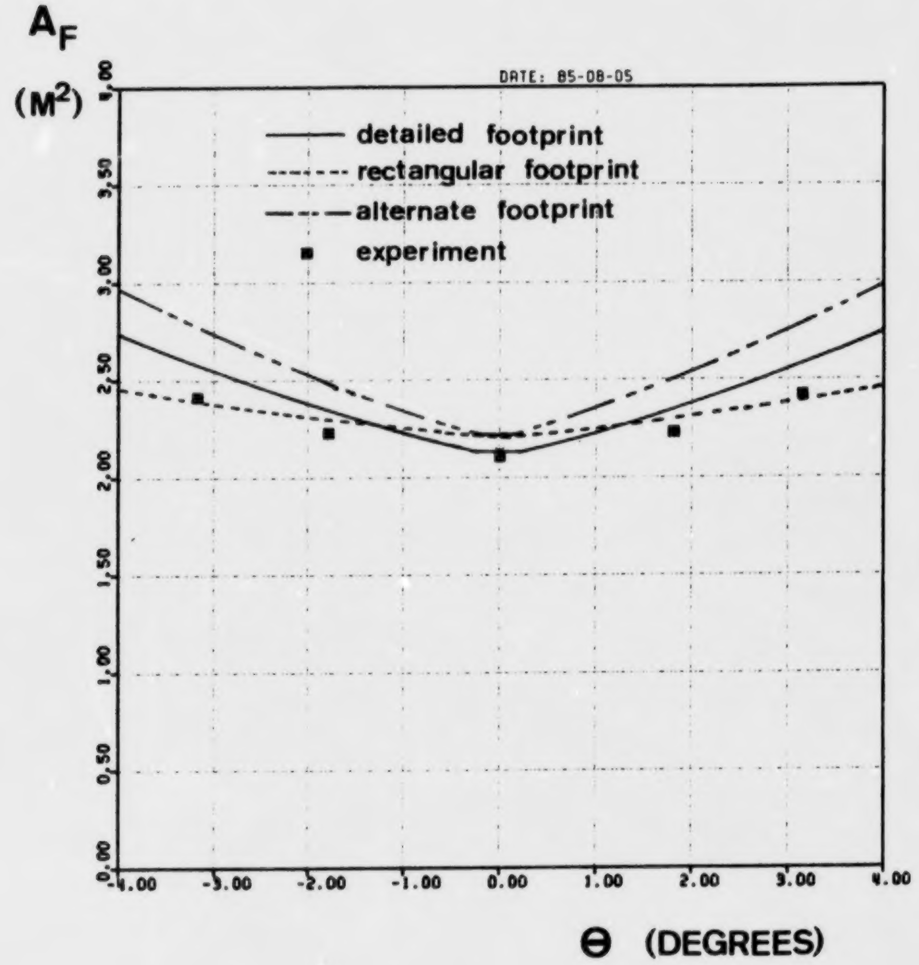

Figure I.6: Footprint Area - Experimental Results and Theoretical Results for Different Footprint Approximations
a) Detailed Area
b) Rectangular Area
c) Alternate Area

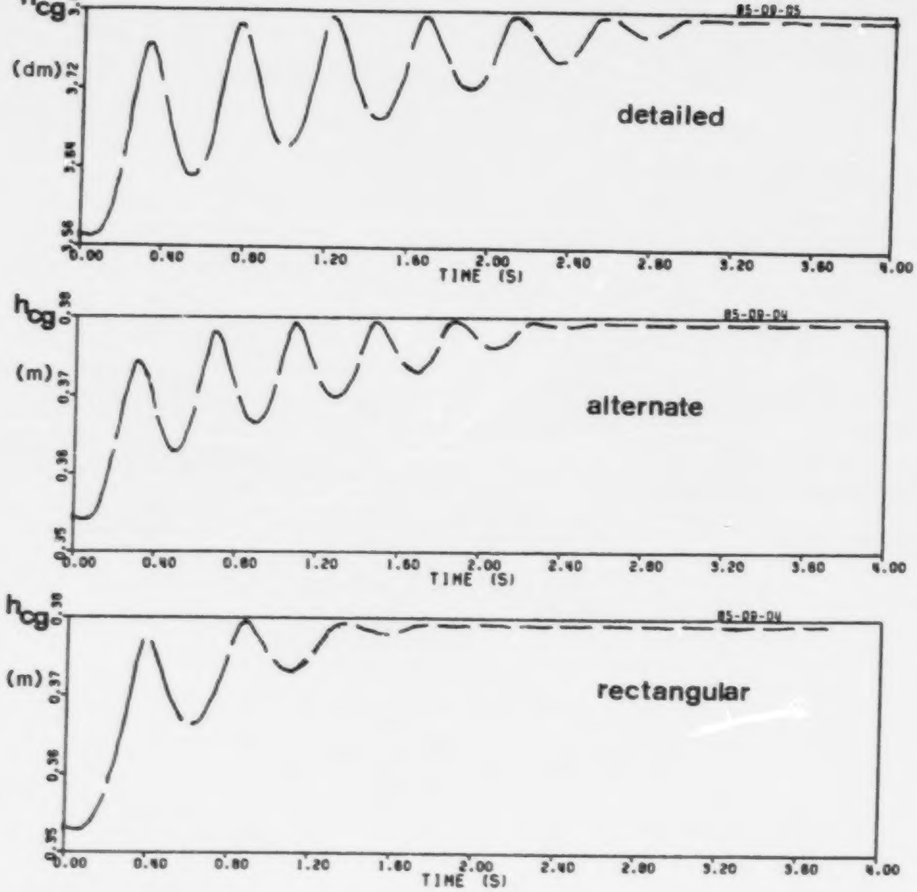

Figure I.7: Initial Disturbance Response for Three Footprint Approximations
a) Detailed Area
b) Rectangular Area
c) Alternate Area

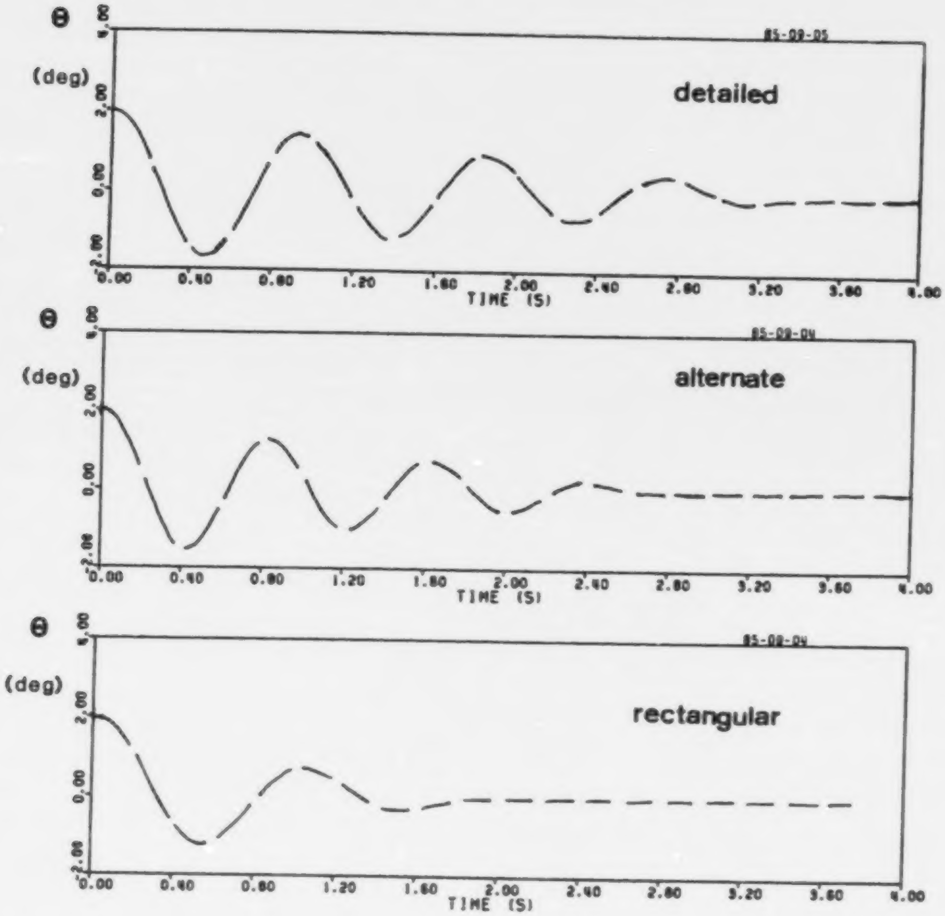

Figure I.7: Continued.

for pitch angles over 0.25 to 0.5° unrealistic - assumption that the pitch and heave motions are uncoupled, so that each is represented by an equation of the form

$$\ddot{z} + 2\zeta\omega_n\dot{z} + \omega_n^2 z = 0 \tag{I.12}$$

where ζ is the damping ratio $=0.5C/(mk)^{1/2}$
C is the viscous damping coefficient
m is the mass or pitch moment of inertia
k is the heave or pitch stiffness
and ω_n is the natural frequency $= (k/m)^{1/2}$.

The geometry details of Table I.1 and the function comparisons of Table I.2 indicate that near $\theta = 0$ where the footprint areas, leak areas, and heave heights will be close, the main difference between the rectangular and alternate footprints is the slope of the moment curve indicated in Figure I.5. The hysteretic damping energy loss per cycle can be represented by an equivalent viscous dashpot. The value of this dashpot will be close for the alternate and rectangular footprints since the hysteresis forces are determined by the same function of h and θ and near $\theta = 0$ the heave height will be close. Thus the decrease in stiffness seen with the rectangular footprint leads to an increased damping ratio, ζ. This stiffness change is further evidenced by the reduction in pitch frequency which can be seen by comparing the number of cycles complete at t = 1.2s on the lower two curves of Figure I.7. Similarly the rate of change of footprint area with respect to heave height is smaller in magnitude at non-zero pitch angles so that the heave stiffness of the rectangular footprint is reduced and that ζ is increased in heave as well. Further evidence of this is again shown by the decrease in frequency of the rectangular footprint heave motion from that of the alternate footprint. Differences between the detailed geometry and the alternate geometry are more subtle. Although the frequency change follows from the differences in the two stiffnesses the damping factor is seen to be only slightly different. This results from the coincident reduction of damping and stiffness of the detailed area compared to the alternate area.

Figure I.8 shows the responses predicted under the detailed area assumptions for the fourth and sixth order models of craft dynamics. As can be seen there is virtually no difference in the response. Similar simulations are shown in Figure I.9 for a craft geometrically scaled to 20 times the size of Labrig. The importance of the additional orders is indicated by the large difference in the response predicted by the two models. This is especially significant since the frequencies involved are low, about 0.65 Hz in heave and 0.33 Hz in pitch. The large difference in response is mainly due to capacitance, since the fan characteristic closely follows the steady fan characteristic. Although the dimensions of this craft place it slightly outside the range of lumped parameter applicability given in Equation I.1 the assumption is expected to be quite good. This is because the inertance effects are small and Hinchey [I.12] has shown that wave propagation effects are small in cushions of this size if feed holes are located peripherally, as is commonly the case with ACV's.

The amount of hysteresis used in the simulations was chosen in an ad hoc fashion since no reliable measurements are currently available. In particular, the hysteresis force per unit length chosen for the scaled up

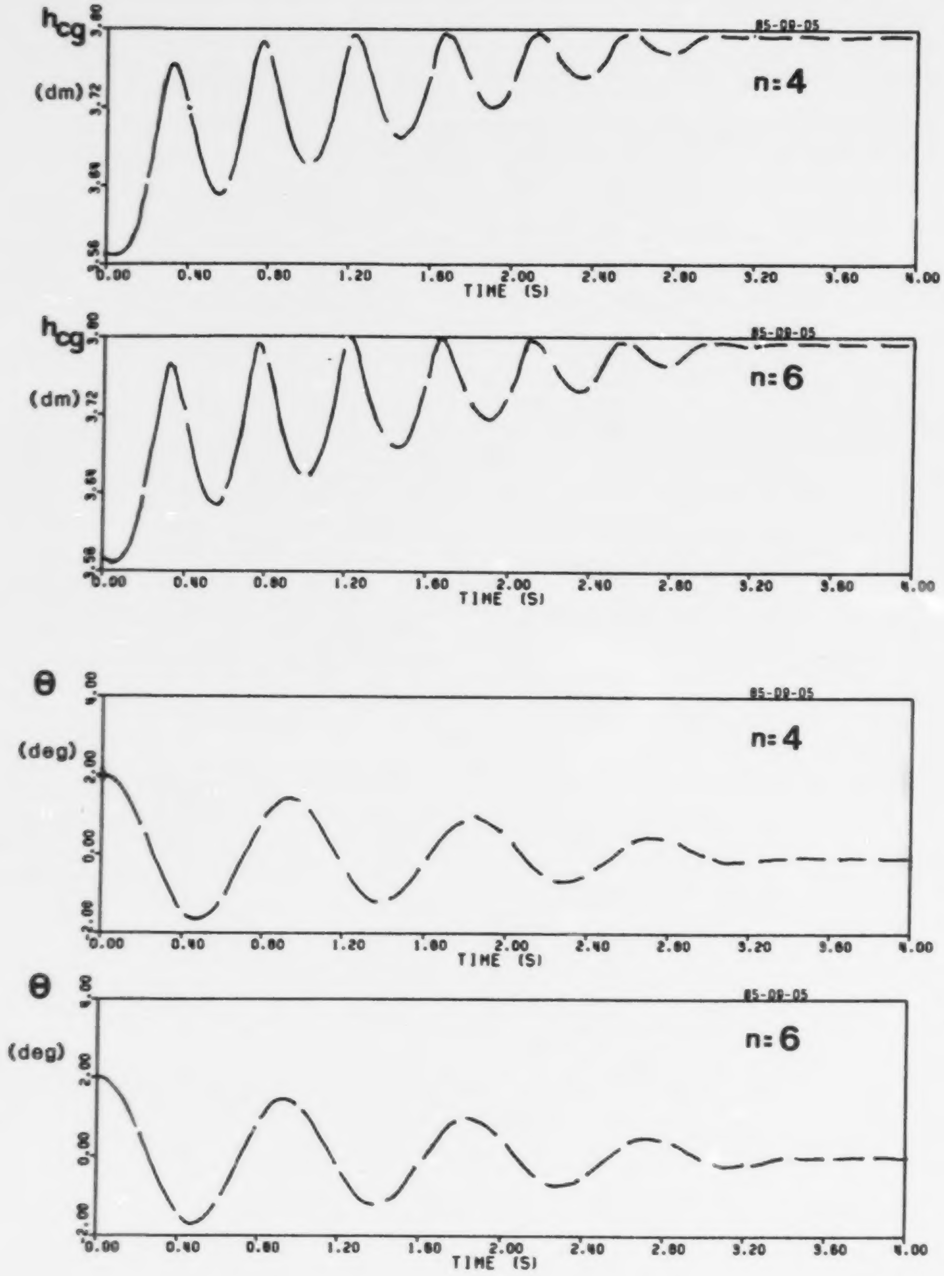

Figure I.8: Response of the Fourth and Sixth Order Models To a Two Degree Initial Condition Disturbance in Pitch - Labrig Model

version was selected so that a lightly damped oscillation was produced when the sixth order model was used. With the fourth order model this amount of hysteresis gives the well damped response shown in Figure I.9. Similarly when hysteresis was scaled to the Labrig model of the well damped response of Figure I.10 was obtained. Note the close correspondence of this response to that of the fourth order model of the ×20 scaled-up vehicle. Also this scaled hysteresis is 12 times that used to obtain the responses in Figures I.6 to I.8. The amount of hysteresis selected for the ×20 scaled-up version was 0.18% of the vehicle weight per metre of skirt. This is an extremely large value and is not likely feasible in a flexible skirt design.

I.5 Conclusions

Several important factors affecting the response of the nonlinear segmented skirt model have been determined. In particular, the choice of the footprint shape approximation has surprisingly large effects on the predicted vehicle static and dynamic behaviour. A fairly high degree of geometry detail is required to get accuracy within 10 to 20 percent for major vehicle response parameters, for example, pitch stiffness. Although cushion capacitance and duct inertia have almost no effect on pitch heave dynamics for the laboratory scale model the ×20 scaled-up simulations indicate large changes associated with these orders. These results suggest that in an uncompartmented air cushion the skirt materials normally used will not provide adequate damping for a large scale craft. Hence designers planning to build larger craft with this skirt system should give careful consideration towards ensuring that the craft has adequate damping.

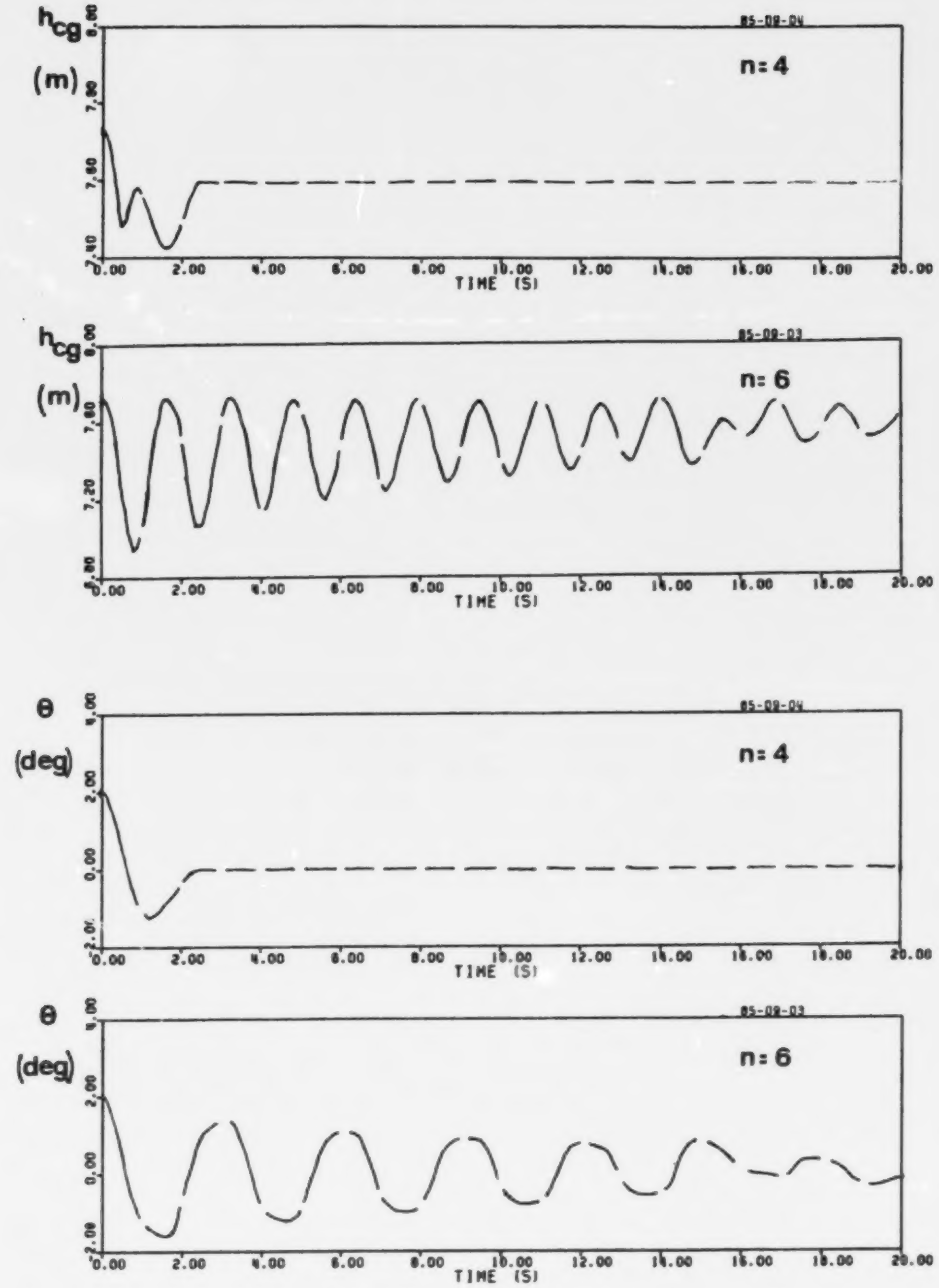

Figure I.9: Response of the Fourth and Sixth Order Models to a Two Degree Initial Condition Disturbance in Pitch - x20 Scale-up of Labrig Model

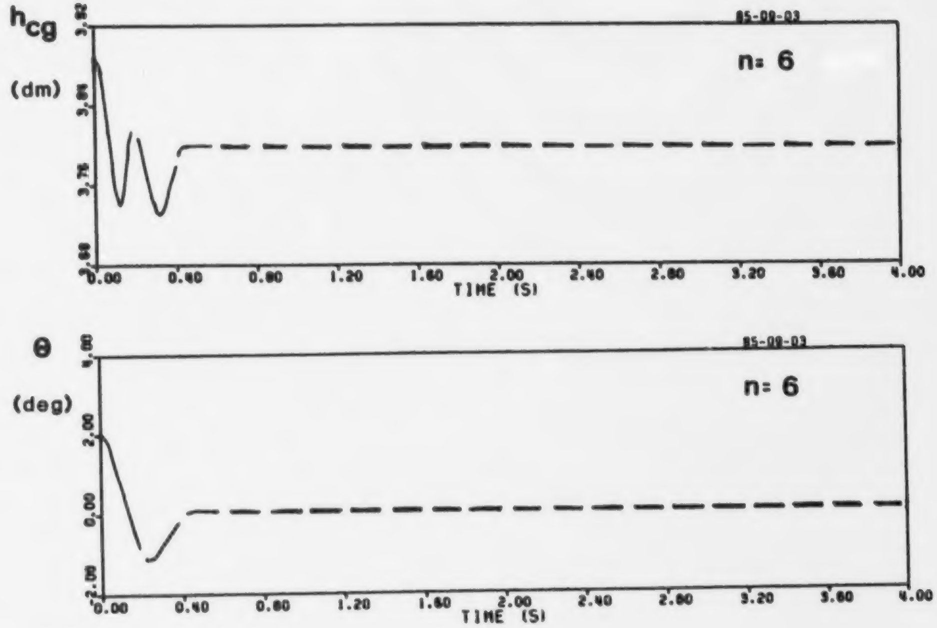

Figure I.10: Response of Labrig Model to a Two Degree Initial Condition Disturbance in Pitch - Damping is Scaled from the x20 Scale-up Response

REFERENCES - APPENDIX I

I.1 See Appendix E.

I.2 Sullivan, P. A., Hinchey, M. J., et al, "Research into Air Cushion Stability: 1979 Report", Transportation Development Centre, Transport Canada, Montreal, Report No. TP3109E, Jan. 1982.

I.3 Sullivan, P. A., Hartmann, P. V., Graham, T. A., "Application of System Identification Flight Analysis Techniques to the Pitch-Heave Dynamics of an Air Cushion Vehicle", Canadian Aeronautics and Space Journal, Vol. 29, No. 4, Dec. 1983, pp. 337-358.

I.4 Wylie, E. B., Streeter, V. L., Fluid Transients, McGraw-Hill, New York, 1978.

I.5 Sweet, L. M., Richardson, H. H., and Wormley, D. N., "Linearized Models, Stability Criteria and Experimental Verification for Plenum Air Cushions with Compressor-Duct Interactions", DOT-FRA-ORD & D74-40, Department of Transportation USA, May 1974.

I.6 Hinchey, M. J., "Heave Instabilities of Amphibious Air Cushion Suspension Systems", University of Toronto, Institute for Aerospace Studies Report No. 246, Nov. 1980.

I.7 Boghani, A. B., Captain, K. M., and Wormley, D. N., "Heave-Pitch-Roll Analysis and Testing of Air Cushion Landing Systems", National Aeronautics and Space Administration, Washington, Contractor Report CR-2917, 1978.

I.8 Doctors, L. J., "The Effect of Air Compressibility on the Nonlinear Motion of an Air Cushion Vehicle Over Waves", School of Mechanical and Industrial Engineering, University of New South Wales, Sydney, Report Nov/Arch 76/1, Jan. 1976.

I.9 Doctors, L. J., "Nonlinear Motion of an Air Cushion Vehicle Over Waves", Journal of Hydronautics, Vol. 9, No. 2, April 1975.

I.10 Swift, M. R., Lebel, D., "Heave Motion of Air Cushion Vehicles", Journal of Hydronautics, Vol. 12, No. 2, Apr. 1978, pp. 85-87.

I.11 See Appendix E.

I.12 See Appendix D.

APPENDIX J: GEOMETRIC FUNCTIONS USED IN THE ANALYSIS OF SEGMENTED SKIRT DYNAMICS (T. A. Graham)

NOMENCLATURE

The following is a list of the explicit expressions and definitions for the A_i, A_i' and A_i^p and other variables used in the following sections.

$$A_1 = H_{sp}\cos\theta + \frac{L_s}{2}\sin\theta - h$$

$$A_2 = H_{sp}\cos\theta - \frac{L_s}{2}\sin\theta - h$$

$$A_3 = \frac{L_s}{2}\cos\theta + H_{sp}\sin\theta$$

$$A_4 = \frac{L_s}{2}\cos\theta - H_{sp}\sin\theta$$

$$A_5 = B_s L_s \cos\theta(h - H_{sp}\cos\theta)$$

$$A_6 = \cot\theta + \cot(\beta-\theta), \text{ Case 2}$$

$$= \cos\theta + \sin\theta\cot(\beta-\theta), \text{ Case 3}$$

$$A_7 = \frac{1}{\sin^2(\beta-\theta)} - \frac{1}{\sin^2\theta}, \text{ Case 2}$$

$$= \frac{\sin^2\theta}{\sin^2(\beta-\theta)} - 1, \text{ Case 3}$$

$$A_8 = L_s\cos\theta + A_2\cot(\beta+\theta) + A_1\cot(\beta-\theta)$$

$$A_9 = B_s + 2(H_{sp}\cos\theta - h)\cot\beta$$

$$A_{10} = L_s\cos\theta + L_s\sin\theta\cot(\beta-\theta)$$

$$A_{11} = B_s + 2L_s \sin\theta \cot\beta$$

$$A_{12} = (A_8 A_9 A_{10} A_{11})^{1/2}$$

$$A_{13} = A_8 A_9 + A_{10} A_{11} + A_{12}$$

$$A_{14} = L_s{}^2\left(\frac{B_s}{2} + L_s \frac{\sin\theta \cot\beta}{3}\right)$$

$$A_{15} = 1 + \frac{A_{10} A_{11}}{2A_{12}}$$

$$A_{16} = A_9[\cot(\beta+\theta) + \cot(\beta-\theta)] + 2A_8 \cot\beta$$

$$A_{17} = A_4 \cot(\beta-\theta) + \frac{A_1}{\sin^2(\beta-\theta)}$$

$$A_{18} = L_s \sin\theta + A_3 \cot(\beta+\theta) + \frac{A_2}{\sin^2(\beta+\theta)}$$

$$A_{19} = A_9 + \frac{A_{12}}{2A_8}$$

$$A_{20} = A_{20A}\left(A_8 + \frac{A_{12}}{2A_9}\right)$$

$$A_{20A} = 2H_{sp} \sin\theta \cot\beta$$

$$A_{21} = A_{21A}\left(A_{11} + \frac{A_{12}}{2A_{10}}\right)$$

$$A_{21A} = L_s\left[\cos\theta \cot(\beta-\theta) + \frac{\sin\theta}{\sin^2\theta(\beta-\theta)} - \sin\theta\right]$$

$$A_{22} = A_{22A}\left(A_{10} + \frac{A_{12}}{2A_{11}}\right)$$

$$A_{22A} = 2L_s \cos\theta \cot\beta$$

$$A_{23} = L_s^{2}\cos\theta(B_s + L_s\sin\theta\ \cot\beta)$$

$$A_{24} = \frac{1}{2}\left[\frac{(A_{17} - A_{18})}{A_8} + \frac{A_{20A}}{A_9} + \frac{A_{21A}}{A_{10}} + \frac{A_{22A}}{A_{11}}\right]$$

$$A_6' = \cos\theta\ \cot(\beta-\theta) + \sin\theta\left(\frac{1}{\sin^2(\beta-\theta)} - 1\right)$$

$$A_7' = \frac{2\sin\theta}{\sin^2(\beta-\theta)}\left[\cos\theta + \sin\theta\ \cot(\beta-\theta)\right]$$

$$A_{14}' = \frac{1}{3} L_s^{3}\cos\theta\ \cot\beta$$

$$A_{17}' = 2\left[A_1\cot(\beta-\theta) + \frac{A_4}{\sin^2(\beta-\theta)} - (A_1 + h)\cot(\beta-\theta)\right]$$

$$A_{18}' = -\frac{2[A_3 + A_2\cot(\beta+\theta)]}{\sin^2(\beta+\theta)} + L_s\cos\theta + (A_2 + h)\cot(\beta+\theta)$$

$$A_{19}' = -A_{20A} + \frac{A_{12}}{2A_8}\left(A_{24} - \frac{(A_{17} - A_{18})}{A_8}\right)$$

$$A_{20}' = 2H_{sp}\cos\theta\ \cot\beta\left(A_8 + \frac{A_{12}}{2A_9}\right) + A_{20A}\left[A_{17} - A_{18} + \frac{A_{12}}{2A_9}\left(A_{24} + \frac{A_{20A}}{A_9}\right)\right]$$

$$A_{21}' = L_s\left(\frac{2}{\sin^2(\beta-\theta)} - 1\right)(\sin\theta\ \cot(\beta-\theta) + \cos\theta)\left(A_{11} + \frac{A_{12}}{2A_{10}}\right)$$

$$+ A_{21A}\left[A_{22A} + \frac{A_{12}}{2A_{10}}\left(A_{24} - \frac{A_{21A}}{A_{10}}\right)\right]$$

$$A_{22}' = -2L_s\sin\theta\ \cot\beta\left(A_{10} + \frac{A_{12}}{2A_{11}}\right) + A_{22A}\left[A_{21A} + \frac{A_{12}}{2A_{11}}\left(A_{24} - \frac{A_{22A}}{A_{11}}\right)\right]$$

$$A_{23}' = L_s^{3}\cos2\theta\ \cot\beta - L_s^{2} B_s\sin\theta$$

$$A_8^p = \left[\cos\theta - \frac{\sin\theta}{2}\left[\cot(\beta+\theta) - \cot(\beta-\theta)\right]\right] \frac{dL_s}{dp_c}$$

$$+ \cos\theta\left[\cot(\beta+\theta) - \cot(\beta-\theta)\right] \frac{dH_s}{dp_c} - \left(\frac{A_2}{\sin^2(\beta+\theta)} + \frac{A_1}{\sin^2(\beta-\theta)}\right) \frac{d\beta}{dp_c}$$

$$A_9^p = \frac{dB_s}{dp_c} + 2\cos\theta \cot\beta \frac{dH_s}{dp_c} - \frac{2(H_{sp}\cos\theta - h)}{\sin^2\beta} \frac{d\beta}{dp_c}$$

$$A_{10}^p = \left[\cos\theta + \sin\theta \cot(\beta-\theta)\right] \frac{dL_s}{dp_c} - \frac{L_s \sin\theta}{\sin^2(\beta-\theta)} \frac{d\beta}{dp_c}$$

$$A_{11}^p = \frac{dB_s}{dp_c} + 2\sin\theta \cot\beta \frac{dL_s}{dp_c} - 2L_s \frac{\sin\theta}{\sin^2\beta} \frac{d\beta}{dp_c}$$

B_s = width of skirt at lip

C_D = mass flow coefficient from cushion to atmosphere

C_0, C_1 = constants

$$dh_1 = \frac{-L_s}{2} \cos\theta - H_{SPL}\sin\theta$$

$$dh_2 = \frac{L_s}{2} \cos\theta - H_{SPL}\sin\theta$$

h = height of centre of mass above ground plane = $h_{CG} - h_G$

h_{CG} = height of centre of mass above datum

h_G = height of ground plane above datum

$$h_1 = H_{SPL}\cos\theta - \frac{L_s}{2} \sin\theta - h$$

$$h_2 = H_{SPL}\cos\theta + \frac{L_s}{2} \sin\theta - h$$

H_L = equivalent leak height

H_P = distance from plane through the top of skirt segments to the centre of mass (pivot if constrained)

$H_{sp} = H_S + H_P$

H_S = distance between parallel planes through skirt segment tops and tips

$H_{SPL} = H_S + H_P - H_L$

ℓ_1 = distance from bottom of skirt attachment to ground

ℓ_2 = distance from skirt knee to ground

L_s = length of skirt at lip

p_c = cushion pressure

R_s = radius of skirt corners at hem

u_d, u_n = variables used in calculating ϕ

v_d, v_n = variables used in calculating ϕ'

$$Z_{p_1} = -H_{SPL}\cos\theta + \frac{L_s}{2}\sin\theta$$

$$Z_{p_2} = -H_{SPL}\cos\theta - \frac{L_s}{2}\sin\theta$$

β = segment angle with ground in level flight

ζ = segment angle at knee

θ = net pitch angle = $\theta_C - \theta_G$

θ_C = pitch angle of cushion

θ_G = pitch angle of ground plane

λ = segment angle at tips

π = 3.14159...

ϕ = angle of upper corner intersection with ground, maximum = ϕ_{max}, see figure

ϕ' = angle of lower corner intersection with ground, maximum = ϕ'_{max}, see figure

Subscripts

o = undeformed value

Notation

For an arbitrary function f,

$$f_x(h, \theta, p_c) = \frac{\partial}{\partial x} f(h, \theta, p_c) \quad \text{where } x \varepsilon \{h, \theta, p_c\}$$

$fi(h, \theta, p_c)$ = ith component of $f(h, \theta, p_c)$ such that

$$\sum_i fi(h, \theta, p_c) = f(h, \theta, p_c)$$

$f_x i(h, \theta, p_c)$ = ith component of $f_x(h, \theta, p_c)$ such that

$$\sum_i f_x i(h, \theta, p_c) = f_x(h, \theta, p_c)$$

J.1 Introduction

The restoring forces and moments for pitch-heave motion of the segmented skirt system are mainly generated through ground contact and the subsequent changes in skirt geometry. A geometric theory for the static forces developed during contact with a flat plane ground was described in Section 3 of Ref. J.1. Good agreement was obtained for pitch and roll stiffness and it was shown that added detail of the geometry improved agreement between theory and experiment. The theory was also shown to be inadequate for the high roll or pitch condition when the ground plane intersects the segments above the knee region, Fig. J.1. Here it showed a large reduction in restoring moment which was not seen in the experiments. In addition the segments buckled before the knee region was encountered. The static model for the low-roll condition provided good approximations to the air escape or leak area, the support or footprint area, and the restoring moment as functions of the pitch or roll angle and heave height. This low-roll theory was used as a basis for the dynamic theory outlined here.

J.2 The Dynamic Skirt Model

The skirt is assumed to be a massless elastic membrane which deforms to lie flush with the ground surface in the event of ground contact. The skirt is assumed to maintain an equilibrium shape corresponding to the cushion pressure except for areas in contact with the ground. In dynamic motion of the air cushion, three regimes of skirt contact can occur. These are:

(i) The skirt is totally out of contact with the ground.

(ii) The skirt is in partial contact with the ground, i.e., the undeformed skirt lip plane and the ground plane intersect.

(iii) The skirt is in contact with the ground throughout its entire perimeter.

The three regimes are referred to as cases 1, 2 and 3 respectively and are shown in figures J.2, J.3 and J.4. The dynamics requires approximations for the leak area, footprint area, restoring moment, and the cushion volume. These will be functions of the segment geometry in the non-contact regime, the geometry of the ground surface, the net pitch or roll angle, θ, the vertical distance, h, between a datum on the vehicle and one on the ground, and changes in skirt geometry resulting from cushion pressure changes. The cushion geometry in the non-contacting regime is defined by the parameters L_S, B_S, H_S, R_S and β which are the skirt length at the lip, the skirt width at the lip, the height of the skirt from lip to segment top, the corner radius of the skirt lip, and the segment angle, respectively. These parameters are shown in Figures J.2 - J.4 and when the skirt is elastic they are functions of pressure so that the geometry functions given below all have an implicit dependence on pressure. The ground surface is assumed to

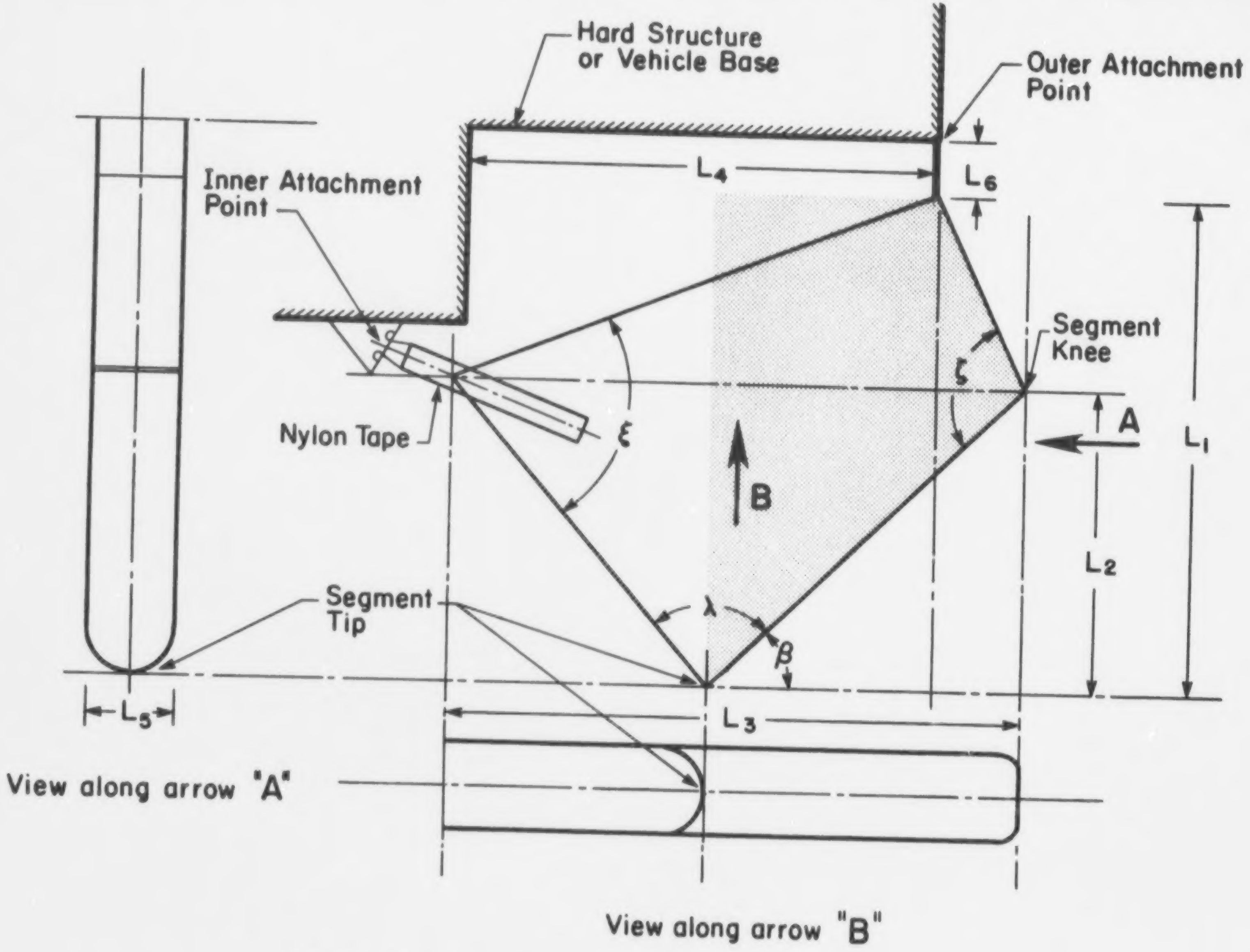
Hard Structure or Vehicle Base
Outer Attachment Point
L_4
L_6
Inner Attachment Point
Segment Knee
ζ
Nylon Tape
ε
A
L_1
B
L_2
Segment Tip
λ
β
L_5
L_3
View along arrow "A"
View along arrow "B"

Figure J.1 Segmented Skirt Finger Geometry.

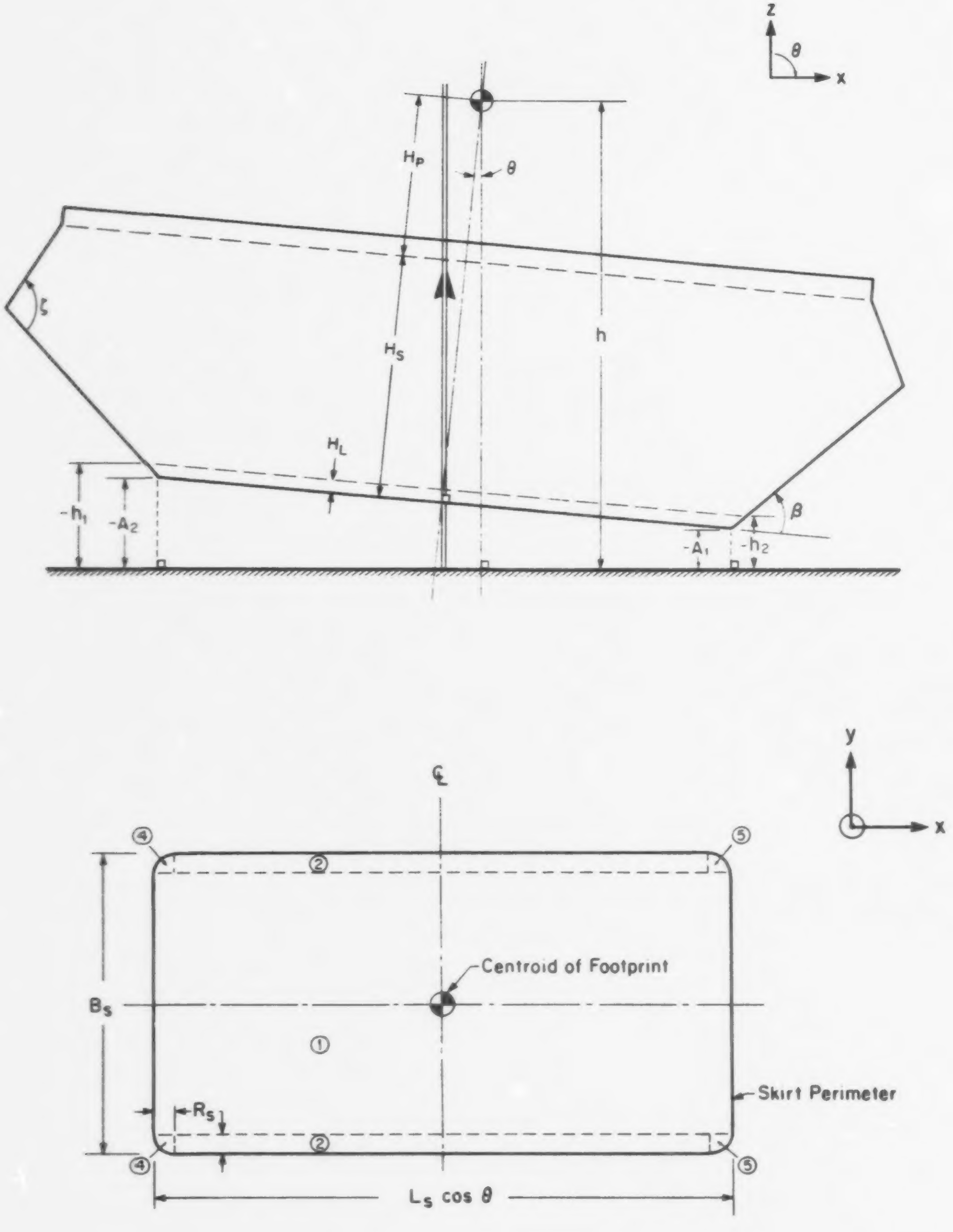
z
θ
x
H_P
θ
ζ
H_S
h
H_L
$-h_1$
$-A_2$
β
$-A_1$
$-h_2$
℄
y
x
④
⑤
②
Centroid of Footprint
B_S
①
Skirt Perimeter
R_S
②
④
⑤
$L_S \cos\theta$

Figure J.2 Noncontacting Skirt Geometry - Case 1.

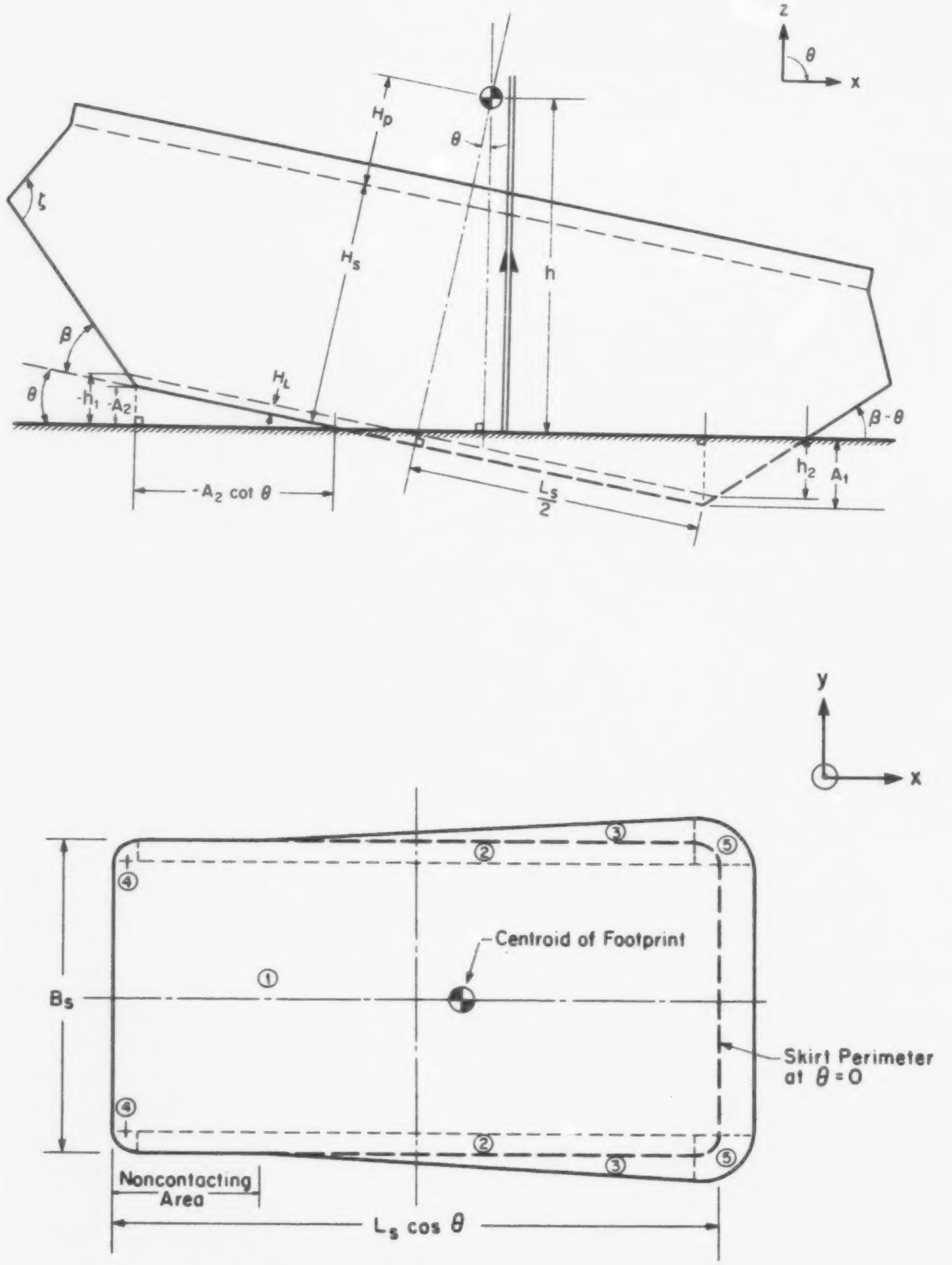
z
θ
x
H_p
θ
H_s
h
ζ
β
θ
-h_1
-A_2
H_L
β - θ
h_2
A_1
- A_2 cot θ
L_s/2
y
x
③
②
⑤
④
Centroid of Footprint
①
B_s
Skirt Perimeter at θ = 0
④
②
③
⑤
Noncontacting Area
L_s cos θ

Figure J.3 Partial Contact Skirt Geometry - Case 2.

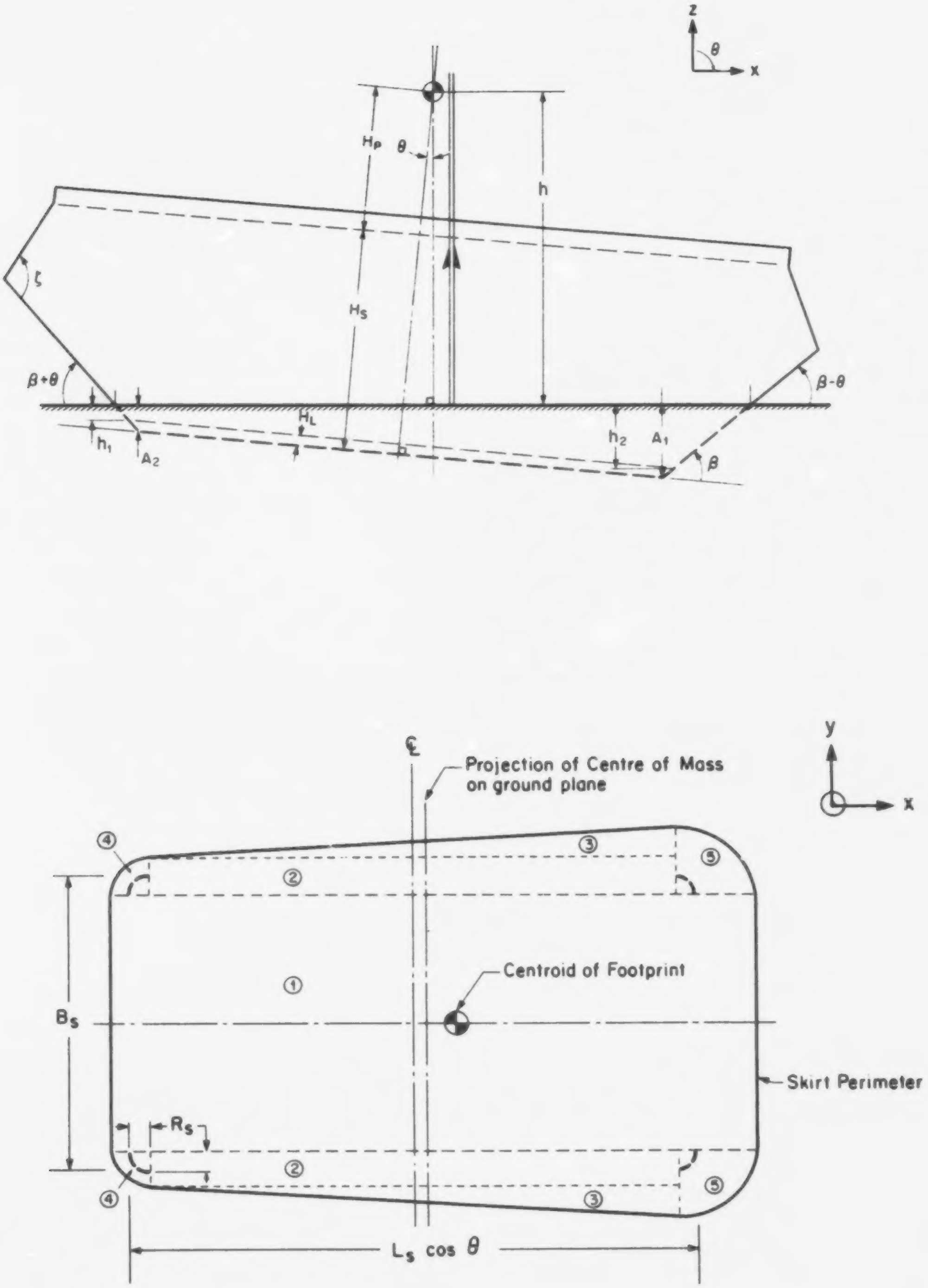
z
θ
x
H_P
θ
h
ζ
H_S
β+θ
β-θ
H_L
h_1
A_2
h_2
A_1
β
℄
Projection of Centre of Mass on ground plane
y
x
④
③
②
⑤
①
Centroid of Footprint
B_S
Skirt Perimeter
R_S
②
④
③
⑤
L_s cos θ

Figure J.4 Full Contact Skirt Geometry - Case 3.

be a plane which is free to move vertically and in rotation about an axis parallel to the vehicle axis of rotation. For pitch it is assumed that the vehicle rotates about an axis of longitudinal symmetry of the cushion which is displaced a distance H_p upward from the skirt top.

The geometry variables h, θ, and p_c are easily defined in terms of the vehicle state variables. In fact when the vehicle centre of gravity lies on the cushion longitudinal and lateral planes of symmetry and the ground remains fixed in a horizontal plane the state variables h_{cg}, θ_c and p_c correspond exactly with the geometry variables. The linearized dynamics use partial derivatives of the geometry approximations with respect to the state variables. These partial derivatives can be obtained simply from the derivatives given below and when the geometry variables and state variables coincide the derivatives also coincide.

All variables used in the development which follows are defined in the list of nomenclature. It has been assumed that the craft pivot point or centre of gravity lies in the lateral and longitudinal planes of symmetry of the cushion. In the development a sequence of variables $\{A_i\}$ are used in place of long repetitive algebraic structures in the basic parameters and geometry variables; these are summarized within the nomenclature list at the end of this appendix.

J.3 Leak Area - a_ℓ (h, θ, p_c)

J.3.1 General Comments on Leak Area

The exit flow area is composed of three components, a residual leak area that remains when the bottom of the cushion is completely shut off, the peripheral area between the segment tips, the ground plane, and the flow out of the cusped openings at the scalloped lower edge of the skirt. The latter is approximated by means of an "equivalent leak height" H_L based on the flow discharge coefficient and the cushion flow. This leak height is subtracted from the skirt height to give an equivalent skirt height, H_{SL}, for use in flow calculations. All functions assume $\theta > 0$ with values for $\theta < 0$ given by the symmetry conditions quoted. The three flow cases are as follows.

J.3.2 Case 1: $h > H_{SPL}\cos\theta - \frac{L_s}{2}\sin\theta$

$$a\ell(h,\ \theta,\ p_c) = 2\left[B_s + L_s\cos\theta + \frac{\pi}{\sqrt{2}}\ R_s\ \sqrt{1 + \cos^2\theta} - 2R_s(1 + \cos\theta)\right]$$

$$\times\ (h - H_{SPL}\cos\theta) + a\ell_{min} \qquad (J.1)$$

$$a\ell_h(h, \theta, p_c) = 2[B_s + L_s\cos\theta + \frac{\pi}{\sqrt{2}} R_s \sqrt{1 + \cos^2\theta} - 2R_s(1 + \cos\theta)] \tag{J.2}$$

$$\begin{aligned} a\ell_\theta(h, \theta, p_c) = {} & 2H_{SPL}\sin\theta[B_s + L_s\cos\theta + \frac{\pi}{\sqrt{2}} R_s \sqrt{1 + \cos^2\theta} \\ & - 2R_s(1 + \cos\theta)] + 2(h - H_{SPL}\cos\theta)[2R_s\sin\theta \\ & - L_s\sin\theta - \frac{\pi}{\sqrt{2}} R_s \frac{\sin\theta\cos\theta}{\sqrt{1 + \cos^2\theta}}] \end{aligned} \tag{J.3}$$

$$\begin{aligned} a\ell_{p_c}(h, \theta, p_c) = {} & -2[B_s + L_s\cos\theta + \frac{\pi}{\sqrt{2}} R_s \sqrt{1 + \cos^2\theta} - 2R_s(1 + \cos\theta)] \\ & \times \cos\theta \frac{dH_s}{dp_c} + 2(h - H_{SPL}\cos\theta)[\frac{dB_s}{dp_c} + \cos\theta \frac{dL_s}{dp_c} + (\frac{\pi}{\sqrt{2}} \sqrt{1 + \cos^2\theta} \\ & - 2(1 + \cos\theta)) \frac{dR_s}{dp_c}] \end{aligned} \tag{J.4}$$

J.3.3 Case 2: $-\frac{L_s}{2}\sin\theta + H_{SPL}\cos\theta < h < \frac{L_s}{2}\sin\theta + H_{SPL}\cos\theta$

J.3.3.1 Case 2: Perimeter Considerations

The flow gap at any point along the cushion is given by

$$\text{gap} = h - \frac{H_{SPL}}{\cos\theta} + x\sin\theta \tag{J.5}$$

where

$$-\frac{L_s}{2} + H_{SPL}\tan\theta < x < \frac{L_s}{2} + H_{SPL}\tan\theta.$$

The restrictions show that gap will equal zero at some point, x_o, where

$$x_o = \left(\frac{H_{SPL}}{\cos\theta} - h\right)\frac{1}{\sin\theta}$$

The shut-off assumption then stipulates that

$$\begin{aligned} \text{gap} &= 0, && -\frac{L_s}{2} + H_{SPL}\tan\theta < x < x_o \\ &= h - \frac{H_{SPL}}{\cos\theta} + x\sin\theta, && x_o < x < \frac{L_s}{2} + H_{SPL}\tan\theta \end{aligned} \qquad (J.6)$$

The ground plane may also intersect the skirt lip in the corner radius areas when case 2 conditions are satisfied. The appropriate perimeter must be calculated for the flow in these sections. This perimeter is defined by the angles ϕ and ϕ', shown in figure J.5, for the upper and lower ends of the cushion respectively and the equation

$$\text{Perimeter} = \frac{2\pi}{\sqrt{2}} R_s(1 + \cos^2\theta)^{1/2} \qquad (J.7)$$

which approximates the elliptic integral for the half ellipse. A proportional relation is used so that the perimeter on the upside is

$$\text{Perimeter} = \frac{2\phi}{\sqrt{2}} R_s(1 + \cos\theta)^{1/2} \qquad (J.8)$$

and on the downside is

$$\text{Perimeter} = \frac{2\phi'}{\sqrt{2}} R_s(1 + \cos\theta)^{1/2} \qquad (J.9)$$

where

$$\phi = \arctan\left[\frac{(-h_1(2R_s\sin\theta - h_1))^{1/2}}{\cos\theta(R_s\sin\theta + h_1)}\right] \qquad (J.10)$$

and

$$\phi' = \arctan\left[\frac{\cos\theta(R_s\sin\theta - h_2)}{(h_2(2R_s\sin\theta - h_2))^{1/2}}\right] \qquad (J.11)$$

The leak area for these corner sections is obtained by assuming that the gap over the perimeter is equal to the gap height at the middle of the side

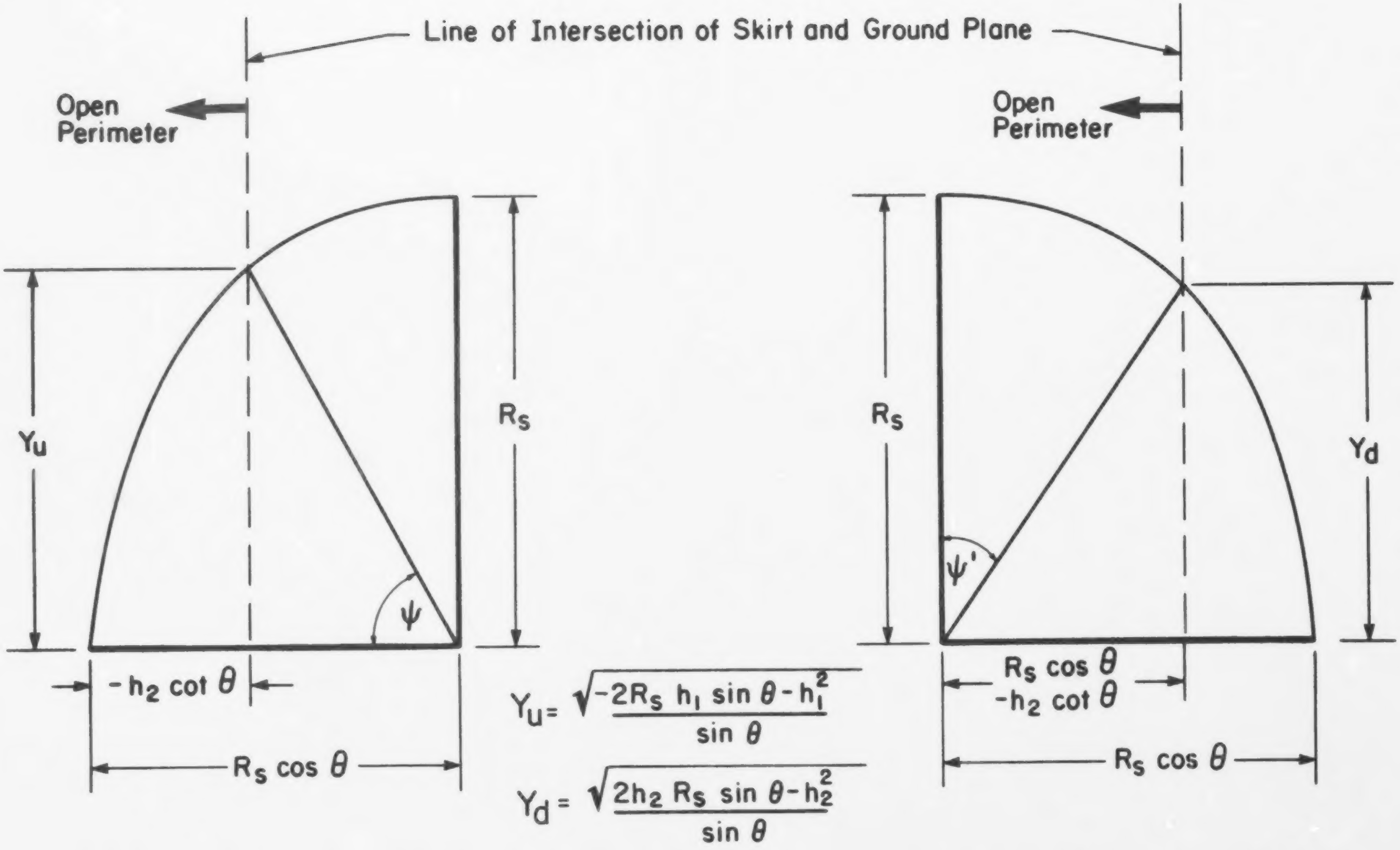
Line of Intersection of Skirt and Ground Plane
Open Perimeter
Open Perimeter
Y_u
R_s
ψ
$- h_2 \cot \theta$
$R_s \cos \theta$
R_s
ψ'
Y_d
$R_s \cos \theta$
$-h_2 \cot \theta$
$R_s \cos \theta$

$$Y_u = \sqrt{\frac{-2R_s h_1 \sin \theta - h_1^2}{\sin \theta}}$$

$$Y_d = \sqrt{\frac{2h_2 R_s \sin \theta - h_2^2}{\sin \theta}}$$

a) Intersection at Upper End

b) Intersection at Lower End

Figure J.5 Corner Intersection Angle Definitions.

projection of the corner opening. In the limit as ϕ, $\phi' \to \pi/2$ the denominators in equations J.10 and J.11 go to zero. To avoid numerical problems constants C and C_0 are chosen to allow ϕ_{max} and ϕ'_{max} near $\pi/2$ but avoid the division by zero. Case 2 is then divided into three sections:

$$\text{(a)} \qquad -h_1 < C_1 R_s \sin\theta$$

$$\text{(b)} \qquad -h_1 > C_1 R_s \sin\theta \quad \text{and} \quad h_2 > R_s \sin\theta \qquad \text{(J.12)}$$

and

$$\text{(c)} \qquad C_0 R_s \sin\theta \le h_1 < R_s \sin\theta$$

J.3.3.2 Leak area

The leak area is given as

$$\text{(a)}\ a\ell(h, \theta, p_c) = -h_1\left(B_s - 2R_s + \frac{\phi R_s}{\sqrt{2}}\sqrt{1 + \cos^2\theta}\right) + a\ell_{min} \qquad \text{(J.13)}$$

$$\text{(b)}\ a\ell(h, \theta, p_c) = -\frac{2\phi_{max}}{\sqrt{2}} R_s\sqrt{1 + \cos^2\theta}\left(h_1 + \frac{C_1 R_s \sin\theta}{2}\right)$$

$$- h_1(B_s - 2R_s) + (h_1 + C_1 R_s \sin\theta)^2 \cot\theta + a\ell_{min} \qquad \text{(J.14)}$$

$$\text{(c)}\ a\ell(h, \theta, p_c) = -\frac{2\phi_{max}}{\sqrt{2}} R_s\sqrt{1 + \cos^2\theta}\left(h_1 + \frac{C_1 R_s \sin\theta}{2}\right) - (B_s - 2R_s)h_1$$

$$+ \left(L_s - (1 + C_1)R_s\right)\left[(1 - C_1)R_s \sin\theta - 2(H_{SPL}\cos\theta - h)\right]\cos\theta$$

$$+ \frac{\phi' R_s\sqrt{1 + \cos^2\theta}}{\sqrt{2}}(R_s \sin\theta - h_2) + a\ell_{min} \qquad \text{(J.15)}$$

J.3.3.3 Heave derivatives

$$\text{(a)}\quad a\ell_h(h,\theta,p_c) = B_s - 2R_s + \frac{\phi R_s}{\sqrt{2}}\sqrt{1+\cos^2\theta} - \frac{h_1 R_s\sqrt{1+\cos^2\theta}}{\sqrt{2}}\,\phi_h \qquad (J.16)$$

where

$$\phi_h = \frac{u_d{}^2 + u_n{}^2\cos^2\theta}{(u_d{}^2 + u_n{}^2)u_n\cos\theta}, \qquad u_d = \cos\theta(R_s\sin\theta + h_1),$$

$$u_n = [-h_1(2R_s\sin\theta + h_1)]^{1/2}$$

$$\text{(b)}\quad a\ell_h(h,\theta,p_c) = B_s - 2R_s + \frac{2\phi_{max}R_s}{\sqrt{2}}\sqrt{1+\cos^2\theta} - 2(h + C_1R_s\sin\theta)\cot\theta \qquad (J.17)$$

$$\text{(c)}\quad a\ell_h(h,\theta,p_c) = B_s - 2R_s + \frac{2\phi_{max}R_s}{\sqrt{2}}\sqrt{1+\cos^2\theta} + 2(L_s - (1 + C_1)R_s)\cos\theta$$

$$+ \frac{R_s\sqrt{1+\cos^2\theta}}{\sqrt{2}}\,(\phi' + (R_s\sin\theta - h_2)\phi_h') \qquad (J.18)$$

where

$$\phi_h' = \frac{1}{v_n{}^2 + v_d{}^2}\left(\frac{-v_n}{v_d}(h_2 - R_s\sin\theta) + v_d\cos\theta\right)$$

$$v_d = [h_2(2R_s\sin\theta - h_2)]^{1/2}, \qquad v_n = \cos\theta(R_s\sin\theta - h_2)$$

J.3.3.4 Pitch derivatives:

$$(a)\ a\ell_\theta(h,\ \theta,\ p_c) = -\ dh_1\left(B_s - 2R_s + \frac{\phi R_s\sqrt{1 + \cos^2\theta}}{\sqrt{2}}\right)$$

$$-\ h_1\ \frac{R_s\sqrt{1 + \cos^2\theta}}{\sqrt{2}}\left(\phi_\theta - \frac{\phi\sin\theta\cos\theta}{1 + \cos^2\theta}\right) \qquad (J.19)$$

where

$$\phi_\theta = \frac{1}{u_d{}^2 + u_n{}^2}\left[-\ \frac{u_d}{u_n}\left(R_s\sin\theta dh_1 + R_s\cos\theta h_1 + dh_1h_1\right)\right.$$

$$\left. +\ u_n(h_1\sin\theta - dh_1\cos\theta - R_s\cos2\theta)\right]$$

$$u_d = \cos\theta(R_s\sin\theta + h_1), \qquad u_n = \left(-h_1(2R_s\sin\theta + h_1)\right)^{1/2}$$

$$(b)\ a\ell_\theta(h,\ \theta,\ p_c) = -dh_1(B_s - 2R_s)$$

$$-\ \frac{R_s\sqrt{1 + \cos^2\theta}}{\sqrt{2}}\left[h_1\phi_{max_\theta} + \phi_{max}\left(2dh_1 + C_1R_s\cos\theta\right.\right.$$

$$\left.\left. -\ 2(h_1 + C_1R_s\sin\theta)\ \frac{\sin\theta\cos\theta}{1 + \cos^2\theta}\right)\right]$$

$$+\ 2(h_1 + C_1R_s\sin\theta)(dh_1 + C_1R_s\cos\theta)\cot\theta - \frac{(h_1 + C_1R_s\sin\theta)^2}{\sin^2\theta} \qquad (J.20)$$

where

$$\phi_{max_\theta} = \frac{(1 - C_1)^2\sin\theta}{(1 - C_1)^2\cos^2\theta + C_1(2 - C_1)}$$

(c) $a\ell_\theta(h, \theta, p_c) = -dh_1(B_s - 2R_s)$

$$- \frac{R_s\sqrt{1 + \cos^2\theta}}{\sqrt{2}} \Big[h_1\phi_{max_\theta} + \phi_{max}(2dh_1 + C_1R_s\cos\theta$$

$$- 2(h_1 + C_1R_s\sin\theta)\ \frac{\sin\theta\cos\theta}{1 + \cos^2\theta}) \Big]$$

$$+ (L_s - (1 + C_1)R_s)[(1 - C_1)R_s\cos 2\theta + 2H_{SPL}\sin 2\theta - 2h\sin\theta]$$

$$+ \frac{R_s\sqrt{1 + \cos^2\theta}}{\sqrt{2}} \Big[(\frac{\phi'\sin 2\theta}{2(1 + \cos^2\theta)} + \phi'_\theta)(R_s\sin\theta - h_2)$$

$$+ \phi'(R_s\cos\theta - dh_2)\Big] \qquad (J.21)$$

where ϕ_{max_θ} is the same as in equation J.20.

J.3.3.5 Pressure derivatives:

$$\text{(a) } a\ell_{p_c}(h, \theta, p_c) = - (\cos\theta\ \frac{dH_s}{dp_c} - \frac{\sin\theta}{2}\ \frac{dL_s}{dp_c})\ (B_s - 2R_s + \frac{\phi\sqrt{1 + \cos^2\theta}}{\sqrt{2}}\ R_s)$$

$$- h_1 \left[\frac{dB_s}{dp_c} + (\frac{\phi\sqrt{1 + \cos^2\theta}}{\sqrt{2}} - 2)\ \frac{dR_s}{dp_c} + \frac{R_s\sqrt{1 + \cos^2\theta}}{\sqrt{2}}\ \frac{d\phi}{dp_c} \right] \qquad (J.22)$$

where

$$\frac{d\phi}{dp_c} = \frac{u_d^2}{u_d^2 + u_n^2}\left[\left(\cos\theta\,\frac{dH_s}{dp_c} - \frac{\sin\theta}{2}\,\frac{dL_s}{dp_c}\right)\left(\frac{R_s\sin\theta}{u_d u_n} - \frac{u_n}{u_d^2}\cos\theta\right) - \frac{h_1\sin\theta}{u_d u_n}\,\frac{dR_s}{dp_c}\right]$$

and u_d and u_n are as in equation J.16.

$$\text{(b)}\quad a\ell_{p_c}(h,\,\theta,\,p_c) = -2\left[\left(\frac{\phi_{max}\sqrt{1+\cos^2\theta}}{\sqrt{2}} - \frac{C_1\cos\theta}{2}\right)(h_1 + C_1R_s\sin\theta) - h_1\right]$$

$$\times\,\frac{dR_s}{dp_c} - \left(\cos\theta\,\frac{dH_s}{dp_c} - \frac{\sin\theta}{2}\,\frac{dL_s}{dp_c}\right)\left[B_s - 2R_s + 2\phi_{max}\,\frac{R_s\sqrt{1+\cos^2\theta}}{\sqrt{2}}\right.$$

$$\left.-\,\cot\theta(h_1 + C_1R_s\sin\theta)\right] - h_1\,\frac{dB_s}{dp_c} \qquad \text{(J.23)}$$

$$\text{(c)}\quad a\ell_{p_c}(h,\,\theta,\,p_c) = -2\left[\frac{\phi_{max}\sqrt{1+\cos^2\theta}}{\sqrt{2}}\,(h_1 + C_1R_s\sin\theta) - h_1\right]\frac{dR_s}{dp_c}$$

$$-\,h_1\,\frac{dB_s}{dp_c} - \left(B_s - 2R_s + \frac{2\phi_{max}\sqrt{1+\cos^2\theta}}{\sqrt{2}}\right)\left(\cos\theta\,\frac{dH_s}{dp_c} - \frac{\sin\theta}{2}\,\frac{dL_s}{dp_c}\right)$$

$$+\,\cos\theta\left[\{(1 - C_1)R_s\sin\theta - 2(H_{SPL}\cos\theta - h)\}\,\frac{dL_s}{dp_c}\right.$$

$$+\,\{2(1 + C_1)(H_{SPL}\cos\theta - h) + (1 - C_1)L_s\sin\theta\}\,\frac{dR_s}{dp_c}$$

$$\left.-\,2(L_s + (1 + C_1)R_s)\cos\theta\,\frac{dH_s}{dp_c}\right]$$

Continued

$$+ \frac{R_s\sqrt{1 + \cos^2\theta}}{\sqrt{2}} \Big[(R_s\sin\theta - h_2) \frac{d\phi'}{dp_c} + \phi'(2\sin\theta - \frac{h_2}{R_s}) \frac{dR_s}{dp_c}$$

$$- \phi'(\cos\theta \frac{dH_s}{dp_c} + \frac{\sin\theta}{2} \frac{dL_s}{dp_c})\Big] \qquad (J.24)$$

where

$$\frac{d\phi'}{dp_c} = \frac{v_d}{v_n^2 + v_d^2} \Big[\sin\theta(\cos\theta - \frac{h_2 v_n}{v_d^2}) \frac{dR_s}{dp_c}$$

$$- (\cos\theta + \frac{v_n}{v_d^2} (R_s\sin\theta - h_2))(\cos\theta \frac{dH_s}{dp_c} + \frac{\sin\theta}{2} \frac{dL_s}{dp_c})\Big]$$

and v_d and v_n are as in equation J.18.

J.3.4 Case 3: $h < \frac{-L_s}{2} \sin\theta + H_{SPL}\cos\theta$

$$a\ell(h, \theta, p_c) = a\ell_{min} \qquad (J.25)$$

$$a\ell_h(h, \theta, p_c) = 0 \qquad (J.26)$$

$$a\ell_\theta(h, \theta, p_c) = 0 \qquad (J.27)$$

$$a\ell_{p_c}(h, \theta, p_c) = 0 \qquad (J.28)$$

This case corresponds to the nominally shut-off condition.

J.3.5 Symmetry Conditions

The following symmetry conditions apply for all leak area cases:

$$a\ell(h, {}^{-}\theta, p_c) = a\ell(h, {}^{+}\theta, p_c), \qquad a\ell_h(h, {}^{-}\theta, p_c) = a\ell_h(h, {}^{+}\theta, p_c),$$

$$a\ell_\theta(h, {}^{-}\theta, p_c) = -a\ell_\theta(h, {}^{+}\theta, p_c), \text{ and } \quad a\ell_{p_c}(h, {}^{-}\theta, p_c) = a\ell_{p_c}(h, {}^{+}\theta, p_c),$$

J.4 Footprint Area - $af(h, \theta, p_c)$

J.4.1 General Commments on Footprint Area

As with the leak area three cases apply. The first occurs when the segment tips are all out of contact with the ground, the second when only some of the segment tips are out of contact with the ground and the third when all segments contact the ground. The footprint area has been divided into several sections (see figures J.2-J.4) to clarify the moment calculations presented in the following section. All functions assume $\theta > 0$ with values for $\theta < 0$ given by the symmetry conditions quoted.

J.4.2 Case 1: $A_1 < 0$

$$af(h, \theta, p_c) = \left[L_sB_s - 4R_s{}^2(1 - \tfrac{\pi}{4})\right] \cos\theta \qquad (J.29)$$

$$af_h(h, \theta, p_c) = 0 \qquad (J.30)$$

$$af_\theta(h, \theta, p_c) = -\left[L_sB_s - 4R_s{}^2(1 - \tfrac{\pi}{4})\right] \sin\theta \qquad (J.31)$$

$$af_{p_c}(h, \theta, p_c) = \cos\theta \left[B_s \frac{dL_s}{dp_c} + L_s \frac{dB_s}{dp_c} - 8R_s(1 - \tfrac{\pi}{4}) \frac{dR_s}{dp_c}\right] \qquad (J.32)$$

Symmetry conditions:

$$af(h, -\theta, p_c) = af(h, +\theta, p_c), \quad af_\theta(h, -\theta, p_c) = -af_\theta(h, +\theta, p_c)$$

$$af_{p_c}(h, -\theta, p_c) = af_{p_c}(h, \theta, p_c)$$

J.4.3 Case 2: $A_2 < 0 < A_1$

J.4.3.1 Footprint area

$af1(h, \theta, p_c) = (B_s - 2R_s)(L_s\cos\theta + A_1\cot(\beta-\theta))$ - central rectangle

$af2(h, \theta, p_c) = 2R_s(L_s - 2R_s)\cos\theta$ - rectangular sides

$af3(h, \theta, p_c) = \frac{\pi}{2} R_s{}^2 \cos\theta$ - upper end elliptical

$af4(h, \theta, p_c) = (A_1 - R_s\sin\theta)^2\cot\beta \cot\theta$ - triangular sides

$= 0 \quad \text{if } |A_1| < |R_s\sin\theta|$

$af5(h, \theta, p_c) = \frac{\pi}{2}(R_s + (A_1 - R_s\sin\theta)\cot\beta)(R_s\cos\theta + A_1\cot(\beta-\theta))$

- lower end elliptical

$$af(h, \theta, p_c) = \sum_{i=1}^{5} afi(h, \theta, p_c) \qquad (J.33)$$

Symmetry condition: $afi(h, -\theta, p_c) = afi(h, +\theta, p_c), \quad i = 1,...5$

J.4.3.2 Heave derivatives:

$af_h1(h, \theta, p_c) = -(B_s - 2R_s)\cot(\beta-\theta)$

$af_h2(h, \theta, p_c) = 0$

$af_h3(h, \theta, p_c) = 0$

$$af_h4(h,\ \theta,\ p_c) = -2(A_1 - R_s\sin\theta)\cot\beta\cot\theta$$

$$af_h5(h,\ \theta,\ p_c) = -\frac{\pi}{2}\left[(R_s\cos\theta + A_1\cot(\beta-\theta))\cot\beta\right.$$

$$\left. + (R_s + (A_1 - R_s\sin\theta)\cot\beta)\cot(\beta-\theta)\right]$$

$$af_h(h,\ \theta,\ p_c) = \sum_{i=1}^{5} af_h i(h,\ \theta,\ p_c) \qquad (J.34)$$

Symmetry condition: $af_h i(h,\ {}^{-}\theta,\ p_c) = af_h i(h,\ {}^{+}\theta,\ p_c)$, $i = 1,\ldots 5$

J.4.3.3 Pitch derivatives

$$af_\theta 1(h,\ \theta,\ p_c) = (B_s - 2R_s)\left(\frac{A_1}{\sin^2(\beta-\theta)} + A_4\cos(\beta-\theta) - L_s\sin\theta\right)$$

$$af_\theta 2(h,\ \theta,\ p_c) = -2R_s(L_s - 2R_s)\sin\theta$$

$$af_\theta 3(h,\ \theta,\ p_c) = -\frac{\pi}{2}R_s{}^2\sin\theta$$

$$af_\theta 4(h,\ \theta,\ p_c) = -(A_1 - R_s\sin\theta)^2\,\frac{\cot\beta}{\sin^2\theta}$$

$$+ 2(A_1 - R_s\sin\theta)(A_4 - R_s\cos\theta)\cot\beta\cot\theta$$

$$= 0 \quad \text{if} \quad A_1 < R_s\sin\theta$$

$$af_\theta 5(h,\ \theta,\ p_c) = \frac{\pi}{2}\Big[(A_4 - R_s\cos\theta)(R_s\cos\theta + A_1\cot(\beta-\theta))\cot\beta$$

Continued

$$+ \left(R_s + (A_1 - R_s\sin\theta)\cot\beta\right)\left(A_4\cot(\beta-\theta) + \frac{A_1}{\sin^2(\beta-\theta)} - R_s\sin\theta\right)\Bigg]$$

$$af_\theta(h,\ \theta,\ p_c) = \sum_{i=1}^{5} af_\theta i(h,\ \theta,\ p_c) \qquad (J.35)$$

Symmetry condition: $af_\theta i(h_1,\ {}^-\theta,\ p_c) = -af_\theta i(h,\ {}^+\theta,\ p_c)$

J.4.3.4 Pressure derivatives

$$af_{p_c}1(h,\ \theta,\ p_c) = (B_s - 2R_s)\left[\cos\theta\frac{dL_s}{dp_c} + \cot(\beta-\theta)\left(\frac{\sin\theta}{2}\frac{dL_s}{dp_c} + \cos\theta\frac{dH_s}{dp_c}\right) - \frac{A_1}{\sin^2(\beta-\theta)}\frac{d\beta}{dp_c}\right] + \left(A_1\cot(\beta-\theta) + L_s\cos\theta\right)\left(\frac{dB_s}{dp_c} - 2\frac{dR_s}{dp_c}\right)$$

$$af_{p_c}2(h,\ \theta,\ p_c) = 2\cos\theta\left[(L_s - 4R_s)\frac{dR_s}{dp_c} + R_s\frac{dL_s}{dp_c}\right]$$

$$af_{p_c}3(h,\ \theta,\ p_c) = \pi R_s\cos\theta\frac{dR_s}{dp_c}$$

$$af_{p_c}4(h,\ \theta,\ p_c) = 2(A_1 - R_s\sin\theta)\cot\beta\,\cot\theta\left(\frac{\sin\theta}{2}\frac{dL_s}{dp_c} + \cos\theta\frac{dH_s}{dp_c} - \sin\theta\frac{dR_s}{dp_c}\right) - (A_1 - R_s\sin\theta)^2\frac{\cot\theta}{\sin^2\beta}\frac{d\beta}{dp_c}$$

$$= 0 \quad \text{if} \quad A_1 < R_s \sin\theta$$

$$\begin{aligned}
af_{p_c}5(h,\ \theta,\ p_c) = \frac{\pi}{2} \Big[& (R_s + (A_1 - R_s \sin\theta)\cot\beta)\{\cos\theta \frac{dR_s}{dp_c} \\
& + \cot(\beta-\theta)(\frac{\sin\theta}{2} \frac{dL_s}{dp_c} + \cos\theta \frac{dH_s}{dp_c}) - (\frac{A_1}{\sin^2(\beta-\theta)} \frac{d\beta}{dp_c})\} \\
& + (A_1 \cot(\beta-\theta) + R_s \cos\theta)\{\frac{\sin\theta}{2} \cot\beta \frac{dL_s}{dp_c} \\
& - (A_1 - R_s \sin\theta) \frac{1}{\sin^2\beta} \frac{d\beta}{dp_c} + \cot\beta \cos\theta \frac{dH_s}{dp_c} + (1 - \sin\theta\cot\beta) \frac{dR_s}{dp_c}\} \Big]
\end{aligned}$$

$$af_{p_c}(h,\ \theta,\ p_c) = \sum_{i=1}^{5} af_{p_c} i(h,\ \theta,\ p_c) \qquad \text{(J.36)}$$

Symmetry condition: $af_{p_c} i(h,\ {}^{-}\theta,\ p_c) = af_{p_c} i(h,\ {}^{+}\theta,\ p_c)$

J.4.4 Case 3: $A_2 > 0$

J.4.4.1 Footprint area

$af1(h,\ \theta,\ p_c) = (B_s - 2R_s)[L_s \cos\theta + A_2 \cot(\beta+\theta) + A_1 \cot(\beta-\theta)]$ - central rectangle

$af2(h,\ \theta,\ p_c) = 2(L_s - 2R_s)\cos\theta[R_s + (A_2 + R_s \sin\theta)\cot\beta]$ - rectangular sides

$af3(h,\ \theta,\ p_c) = (L_s - 2R_s)^2 \cos\theta \sin\theta \cot\beta$ - triangular sides

$$af4(h,\ \theta,\ p_c) = \frac{\pi}{2}\,[R_s + (A_2 + R_s\sin\theta)\cot\beta][R_s\cos\theta + A_2\cot(\beta+\theta)]$$

- elliptical upper

$$af5(h,\ \theta,\ p_c) = \frac{\pi}{2}\,[R_s\cos\theta + A_1\cot(\beta-\theta)][R_s + (A_1 - R_s\sin\theta)\cot\beta]$$

- elliptical lower

$$af(h,\ \theta,\ p_c) = \sum_{i=1}^{5} afi(h,\ \theta,\ p_c) \qquad (J.37)$$

Symmetry condition: $afi(h,\ {}^{-}\theta,\ p_c) = afi(h,\ {}^{+}\theta,\ p_c),\ i = 1,\ldots,5$

J.4.4.2 Heave derivatives

$$af_h1(h,\ \theta,\ p_c) = -(B_s - 2R_s)[\cot(\beta+\theta) + \cot(\beta-\theta)]$$

$$af_h2(h,\ \theta,\ p_c) = -2(L_s - 2R_s)\cos\theta\ \cot\beta$$

$$af_h3(h,\ \theta,\ p_c) = 0$$

$$af_h4(h,\ \theta,\ p_c) = -\frac{\pi}{2}\Big[(R_s\cos\theta + A_2\cot(\beta+\theta))\cot\beta$$

$$+ [R_s + (A_2 + R_s\sin\theta)\cot\beta]\cot(\beta+\theta)\Big]$$

$$af_h5(h,\ \theta,\ p_c) = -\frac{\pi}{2}\Big[(R_s\cos\theta + A_1\cot(\beta-\theta))\cot\beta$$

$$+ [R_s + (A_1 - R_s\sin\theta)\cot\beta]\cot(\beta-\theta)\Big]$$

$$af_h(h,\ \theta,\ p_c) = \sum_{i=1}^{5} af_hi(h,\ \theta,\ p_c) \qquad (J.38)$$

Symmetry condition: $af_h i(h, {}^{-}\theta, p_c) = af_h i(h, {}^{+}\theta, p_c)$, $i = 1,\ldots,5$

J.4.4.3 Pitch derivatives

$$af_\theta 1(h, \theta, p_c) = (B_s - 2R_s)(A_4\cot(\beta-\theta) + \frac{A_1}{\sin^2(\beta-\theta)} - A_3\cot(\beta+\theta)$$

$$- \frac{A_2}{\sin^2(\beta+\theta)} - L_s\sin\theta)$$

$$af_\theta 2(h, \theta, p_c) = 2(L_s - 2R_s)[R_s(\cos 2\theta \cot\beta - \sin\theta)$$

$$- (A_2\sin\theta + A_3\cos\theta)\cot\beta]$$

$$af_\theta 3(h, \theta, p_c) = (L_s - 2R_s)^2\cos 2\theta \cot\beta$$

$$af_\theta 4(h, \theta, p_c) = \frac{\pi}{2}[-(R_s + (A_2 + R_s\sin\theta)\cot\beta)\{R_s\sin\theta + A_3\cot(\beta+\theta)$$

$$+ \frac{A_2}{\sin^2(\beta+\theta)}\} + (R_s\cos\theta - A_3)(R_s\cos\theta + A_2\cot(\beta+\theta))\cot\beta]$$

$$af_\theta 5(h, \theta, p_c) = \frac{\pi}{2}[(A_4\cot(\beta-\theta) + \frac{A_1}{\sin^2(\beta-\theta)}$$

$$- R_s\sin\theta)(R_s + (A_1 - R_s\sin\theta)\cot\beta)$$

$$+ (R_s\cos\theta + A_1\cot(\beta-\theta))(A_4 - R_s\cos\theta)\cot\beta]$$

$$af_{\theta}(h,\ \theta,\ p_c) = \sum_{i=1}^{5} af_{\theta}i(h,\ \theta,\ p_c) \qquad (J.39)$$

Symmetry condition: $af_{\theta}i(h,\ {}^{-}\theta,\ p_c) = -af_{\theta}i(h,\ {}^{+}\theta,\ p_c),\ i = 1,\ldots,5$

J.4.4.4 Pressure Derivatives

$$\begin{aligned} af_{p_c}1(h,\ \theta,\ p_c) = {} & (L_s\cos\theta + A_2\cot(\beta+\theta) + A_1\cot(\beta-\theta))\left(\frac{dB_s}{dp_c} - 2\,\frac{dR_s}{dp_c}\right) \\ & + (B_s - 2R_s)\Big[\left(\cos\theta - \frac{\sin\theta}{2}\,\{\cot(\beta+\theta) - \cot(\beta-\theta)\}\right)\frac{dL_s}{dp_c} \\ & + \cos\theta\{\cot(\beta+\theta) + \cot(\beta-\theta)\}\,\frac{dH_s}{dp_c} - \left(\frac{A_2}{\sin^2(\beta+\theta)} + \frac{A_1}{\sin^2(\beta-\theta)}\right)\frac{d\beta}{dp_c}\Big] \end{aligned}$$

$$\begin{aligned} af_{p_c}2(h,\ \theta,\ p_c) = {} & 2\cos\theta\Big[\{R_s + (A_2 + R_s\sin\theta)\cot\beta\}\left(\frac{dL_s}{dp_c} - 2\,\frac{dR_s}{dp_c}\right) \\ & + (L_s - 2R_s)\Big\{(1 + \sin\theta\cot\beta)\,\frac{dR_s}{dp_c} + \cot\beta\left(\cos\theta\,\frac{dH_s}{dp_c} - \frac{\sin\theta}{2}\,\frac{dL_s}{dp_c}\right) \\ & - (A_2 + R_s\sin\theta)\,\frac{1}{\sin^2\beta}\,\frac{d\beta}{dp_c}\Big\}\Big] \end{aligned}$$

$$\begin{aligned} af_{p_c}3(h,\ \theta,\ p_c) = {} & (L_s - 2R_s)\cos\theta\sin\theta\,\Bigg[2\cot\beta\left(\frac{dL_s}{dp_c} - 2\,\frac{dR_s}{dp_c}\right) \\ & - (L_s - 2R_s)\,\frac{1}{\sin^2\beta}\,\frac{d\beta}{dp_c}\Bigg] \end{aligned}$$

$$
\begin{aligned}
af_{p_c}4(h,\ \theta,\ p_c) = \frac{\pi}{2}\Bigg[& [R_s + (A_2 + R_s\sin\theta)\cot\beta]\Big\{\cos\theta\,\frac{dR_s}{dp_c} \\
& + \cot(\beta+\theta)\Big(\cos\theta\,\frac{dH_s}{dp_c} - \frac{\sin\theta}{2}\,\frac{dL_s}{dp_c}\Big) - \frac{A_2}{\sin^2(\beta+\theta)}\,\frac{d\beta}{dp_c}\Big\} \\
& + \{R_s\cos\theta + A_2\cot(\beta+\theta)\}\Big[(1 + \sin\theta\,\cot\beta)\,\frac{dR_s}{dp_c} + \cot\beta\Big\{\cos\theta\,\frac{dH_s}{dp_c} \\
& - \frac{\sin\theta}{2}\,\frac{dL_s}{dp_c}\Big\} - \frac{(A_2 + R_s\sin\theta)}{\sin^2\beta}\,\frac{d\beta}{dp_c}\Big]\Bigg]
\end{aligned}
$$

$$
\begin{aligned}
af_{p_c}5(h,\ \theta,\ p_c) = \frac{\pi}{2}\Bigg[& [R_s + (A_1 - R_s\sin\theta)\cot\beta]\Big\{\cos\theta\,\frac{dR_s}{dp_c} \\
& + \cot(\beta-\theta)\Big(\cos\theta\,\frac{dH_s}{dp_c} + \frac{\sin\theta}{2}\,\frac{dL_s}{dp_c}\Big) - \frac{A_1}{\sin^2(\beta-\theta)}\frac{d\beta}{dp_c}\Big\} \\
& + [R_s\cos\theta + A_1\cot(\beta-\theta)]\Big\{(1 - \sin\theta\,\cot\beta)\,\frac{dR_s}{dp_c} \\
& + \cot\beta\Big(\cos\theta\,\frac{dH_s}{dp_c} + \frac{\sin\theta}{2}\,\frac{dL_s}{dp_c}\Big) - \frac{(A_1 - R_s\sin\theta)}{\sin^2\beta}\,\frac{d\beta}{dp_c}\Big\}\Bigg]
\end{aligned}
$$

$$
af_{p_c}(h,\ \theta,\ p_c) = \sum_{i=1}^{5} af_{p_c}i(h,\ \theta,\ p_c) \qquad (J.40)
$$

Symmetry condition: $af_{p_c}i(h, {}^{-}\theta, p_c) = af_{p_c}i(h, {}^{+}\theta, p_c)$

J.5 Restoring Moment

J.5.1 General Comments on Restoring Moment

The resultant moment produced by the cushion deformation is composed of shifts in the centre of pressure position caused by skirt-ground contact, moments resulting from forces transmitted through skirt material, and a much smaller portion which is caused by unbalanced momentum flux out of the cushion. The latter, although small, is important as it ensures static stability when the skirt does not touch the ground. Moments resulting from skirt forces require different assumptions and are discussed in the section on Skirt Hysteresis. The moment from the centre of pressure shift is calculated using the footprint divided as in the previous section. The restoring moment can be written as follows:

$$M_p = p_c \sum_{i=1}^{5} afi(h, \theta, p_c)XMPi(h, \theta, p_c) \qquad (J.41)$$

$$+ \text{ Momentum Flux Terms } + \text{ Skirt Force Moments}$$

Only the momentum flux terms and the various moment arms to the area centroids, the XMPi, are given in this section. The derivatives of the $afi(h, \theta, p_c)$ will be used to simplify presentation.

J.5.2 Case 1: $A_1 < 0$

$$M(h, \theta, p_c) = [H_{sp}af(h, \theta, p_c)\sin\theta$$

$$- 2C_DB_s(h_1\{Z_{p_1} + (1 - \frac{C_D}{2})h_1\} - h_2\{Z_{p_2} + (1 - \frac{C_D}{2})h_2\})]p_c \qquad (J.42)$$

$$M_h(h, \theta, p_c) = 2C_DB_sp_c[Z_{p_1} + (2 - C_D)h_1 - Z_{p_2} - (2 - C_D)h_2] \qquad (J.43)$$

$$M_\theta(h, \theta, p_c) = H_{sp}p_c[af_\theta(h, \theta, p_c)\sin\theta + af(h, \theta, p_c)\cos\theta]$$

$$- 2C_DB_sp_c[dh_1(Z_{p_1} + (1 - C_D)h_1) - dh_2(Z_{p_2} + (1 - C_D)h_2)] \qquad (J.44)$$

$$M_{p_c}(h,\ \theta,\ p_c) = \frac{M(h,\ \theta,\ p_c)}{p_c} + p_c[af(h,\ \theta,\ p_c)\sin\theta\ \frac{dH_s}{dp_c}$$

$$+ H_{sp}\sin\theta\ af_{p_c}(h,\ \theta,\ p_c) - 2C_D(h_1\{Z_{p_1} + (1 - \frac{C_D}{2})h_1\}$$

$$- h_2\{Z_{p_2} + (1 - \frac{C_D}{2})h_2\})\ \frac{dB_s}{dp_c}$$

$$- 2C_DB_s\{(Z_{p_1} + (1 - C_D)h_1)(\cos\theta\ \frac{dH_s}{dp_c} - \frac{\sin\theta}{2}\ \frac{dL_s}{dp_c})$$

$$- (Z_{p_2} + (1 - C_D)h_2)(\cos\theta\ \frac{dH_s}{dp_c} + \frac{\sin\theta}{2}\ \frac{dL_s}{dp_c})\}] \qquad (J.45)$$

Symmetry conditions:

$M(h,\ ^-\theta,\ p_c) = -M(h,\ ^+\theta,\ p_c)$, $\quad M_h(h,\ ^-\theta,\ p_c) = -M_h(h,\ ^+\theta,\ p_c)$,

$M_\theta(h,\ ^-\theta,\ p_c) = M_\theta(h,\ ^+\theta,\ p_c)$, $\quad M_{p_c}(h,\ ^-\theta,\ p_c) = -M_{p_c}(h,\ ^+\theta,\ p_c)$

J.5.3 Case 2: $A_2 < 0 < A_1$

J.5.3.1 Moment arms and moment

$$XMP1(h,\ \theta,\ p_c) = H_{sp}\sin\theta - \frac{A_1}{2}\cot(\beta-\theta)$$

$$XMP2(h,\ \theta,\ p_c) = H_{sp}\sin\theta$$

$$XMP3(h,\ \theta,\ p_c) = H_{sp}\sin\theta + (\frac{L_s}{2} - R_s + \frac{4R_s}{3\pi})\cos\theta$$

$$XMP4(h,\ \theta,\ p_c) = (H_{sp} - h\cos\theta)\ \frac{1}{\sin\theta} - \frac{2}{3}\ (A_1 - R_s\sin\theta)\cot\theta$$

$$XMP5(h,\ \theta,\ p_c) = H_{sp}\sin\theta - (\frac{L_s}{2} - R_s)\cos\theta - \frac{4}{3\pi}\,(R_s\cos\theta + A_1\cot(\beta-\theta))$$

$$XMP6(h,\ \theta,\ p_c) = -h_1(Z_{p_1} + (1 - \frac{C_D}{2})h_1) + XMP6A$$

where

$$XMP6A = 0 \qquad \text{if } h_2 > 0$$

$$= h_2[Zp_2 + (1 - \frac{C_D}{2})h_2] \qquad \text{if } h_2 < 0$$

$$M(h,\ \theta,\ p_c) = p_c[\sum_{i=1}^{5} XMPi(h,\ \theta,\ p_c)afi(h,\ \theta,\ p_c) + 2C_DB_sXMP6] \quad (J.46)$$

Symmetry condition: $XMPi(h,\ {}^{-}\theta,\ p_c) = -XMPi(h,\ {}^{+}\theta,\ p_c)$

J.5.3.2 Heave derivatives

$$XMP_h1(h,\ \theta,\ p_c) = \frac{\cot}{2}\,(\beta-\theta)$$

$$XMP_h2(h,\ \theta,\ p_c) = 0$$

$$XMP_h3(h,\ \theta,\ p_c) = 0$$

$$XMP_h4(h,\ \theta,\ p_c) = -\frac{\cot\theta}{3}$$

$$XMP_h5(h,\ \theta,\ p_c) = \frac{4}{3\pi}\cot(\beta-\theta)$$

$$XMP_h6(h,\ \theta,\ p_c) = Z_{p_1} + (2 - C_D)h_1 + XMP_h6A$$

where

$$XMP_h6A = 0 \qquad \text{if} \quad h_2 > 0$$

$$= -Z_{p_2} - (2 - C_D)h_2 \qquad \text{if} \quad h_2 < 0$$

$$M_h(h,\ \theta,\ p_c) = p_c \left[\sum_{i=1}^{5} \{af_hi(h,\ \theta,\ p_c)XMPi(h,\ \theta,\ p_c)\right.$$

$$+ \, afi(h,\, \theta,\, p_c) XMP_h i(h,\, \theta,\, p_c)\} + 2C_D B_s XMP_h 6 \Big] \qquad \text{(J.47)}$$

Symmetry condition: $XMP_h i(h,\, {}^{-}\theta,\, p_c) = -XMP_h i(h,\, {}^{+}\theta,\, p_c)$

J.5.3.3 Pitch derivatives

$$XMP_\theta 1(h,\, \theta,\, p_c) = H_{sp}\cos\theta - \frac{1}{2}\left(A_4\cot(\beta-\theta) + \frac{A_1}{\sin^2(\beta-\theta)}\right)$$

$$XMP_\theta 2(h,\, \theta,\, p_c) = H_{sp}\cos\theta$$

$$XMP_\theta 3(h,\, \theta,\, p_c) = H_{sp}\cos\theta - \left(\frac{L_s}{2} - R_s + \frac{4}{3\pi} R_s\right)\sin\theta$$

$$XMP_\theta 4(h,\, \theta,\, p_c) = \frac{h}{\sin^2\theta} - \frac{H_{sp}\cos\theta}{\sin^2\theta} + \frac{2}{3}\,\frac{(A_1 - R_s\sin\theta)}{\sin^2\theta}$$

$$- \frac{2}{3}(A_4 - R_s\cos\theta)\cot\theta$$

$$XMP_\theta 5(h,\, \theta,\, p_c) = H_{sp}\cos\theta + \left(\frac{L_s}{2} - R_s\right)\sin\theta$$

$$- \frac{4}{3\pi}\left(A_4\cot(\beta-\theta) + \frac{A_1}{\sin^2(\beta-\theta)} - R_s\sin\theta\right)$$

$$XMP_\theta 6(h,\, \theta,\, p_c) = -dh_1(Z_{p_1} + h_1(1 - C_D)) + XMP_\theta 6A$$

where

$$XMP_\theta 6A = 0 \qquad \text{if} \quad h_2 > 0$$

$$= dh_2[Z_{p_2} + (1 - C_D)h_2] \qquad \text{if} \quad h_2 < 0$$

$$\begin{aligned} M_\theta(h, \theta, p_c) = p_c \Bigg[\sum_{i=1}^{5} &(af_\theta i(h, \theta, p_c) XMPi(h, \theta, p_c) \\ &+ afi(h, \theta, p_c) XMP_\theta i(h, \theta, p_c)) + 2C_D B_s XMP_\theta 6 \Bigg] \end{aligned} \qquad (J.48)$$

Symmetry condition: $XMP_\theta i(h, {}^-\theta, p_c) = XMP_\theta i(h, {}^+\theta, p_c)$

J.5.3.4 Pressure derivatives

$$\begin{aligned} XMP_{p_c}1(h, \theta, p_c) = &\left(\sin\theta - \frac{\cos\theta\cot(\beta-\theta)}{2}\right) \frac{dH_s}{dp_c} - \frac{\sin\theta\cot(\beta-\theta)}{4} \frac{dL_s}{dp_c} \\ &+ \frac{A_1}{2\sin^2(\beta-\theta)} \frac{d\beta}{dp_c} \end{aligned}$$

$$XMP_{p_c}2(h, \theta, p_c) = \sin\theta \frac{dH_s}{dp_c}$$

$$XMP_{p_c}3(h, \theta, p_c) = \sin\theta \frac{dH_s}{dp_c} + \cos\theta\left(\frac{1}{2} \frac{dL_s}{dp_c} + \left(\frac{4}{3\pi} - 1\right) \frac{dR_s}{dp_c}\right)$$

$$XMP_{p_c}4(h, \theta, p_c) = \frac{1}{3}\left(\frac{1}{\sin\theta} + 2\sin\theta\right) \frac{dH_s}{dp_c} - \frac{\cos\theta}{3} \frac{dL_s}{dp_c} + \frac{2}{3}\cos\theta \frac{dR_s}{dp_c}$$

$$\begin{aligned} XMP_{p_c}5(h, \theta, p_c) = &\left(\sin\theta - \frac{4}{3\pi}\cos\theta\cot(\beta-\theta)\right) \frac{dH_s}{dp_c} + \cos\theta\left(1 - \frac{4}{3\pi}\right) \frac{dR_s}{dp_c} \\ &- \frac{1}{2}\left(\cos\theta + \frac{4}{3\pi}\sin\theta\cot(\beta-\theta)\right) \frac{dL_s}{dp_c} + \frac{4}{3\pi} \frac{A_1}{\sin^2(\beta-\theta)} \frac{d\beta}{dp_c} \end{aligned}$$

$$XMP_{p_c}6(h, \theta, p_c) = -\left(Z_{p_1} + (1 - C_D)h_1\right)\left(\cos\theta \frac{dH_s}{dp_c} - \frac{\sin\theta}{2} \frac{dL_s}{dp_c}\right) + XMP_{p_c}6A$$

where

$$XMP_{p_c}6A = 0 \qquad \text{if } h_2 > 0$$

$$= [Z_{p_2} + (1 - C_D)h_2]\left(\cos\theta \frac{dH_s}{dp_c} + \frac{\sin\theta}{2}\frac{dL_s}{dp_c}\right)$$

$$\text{if } h_2 < 0$$

$$M_{p_c}(h, \theta, p_c) = \frac{M(h, \theta, p_c)}{p_c} + \left[\sum_{i=1}^{5} \{af_{p_c}i(h, \theta, p_c)XMPi(h, \theta, p_c)\right.$$

$$\left. + afi(h, \theta, p_c)XMP_{p_c}i(h, \theta, p_c)\} + 2C_D\{B_s XMP_{p_c}6 + XMP6 \frac{dB_s}{dp_c}\}\right] p_c \quad (J.49)$$

Symmetry condition: $XMP_{p_c}i(h, {}^{-}\theta, p_c) = -XMP_{p_c}i(h, {}^{+}\theta, p_c)$

J.5.4 Case 3: $A_2 > 0$

J.5.4.1 Moment arms and moment

$$XMP1(h, \theta, p_c) = H_{sp}\sin\theta + \frac{1}{2}\left(A_2\cot(\beta+\theta) - A_1\cot(\beta-\theta)\right)$$

$$XMP2(h, \theta, p_c) = H_{sp}\sin\theta$$

$$XMP3(h, \theta, p_c) = H_{sp}\sin\theta - \frac{1}{3}\left(\frac{L_s}{2} - R_s\right)\cos\theta$$

$$XMP4(h, \theta, p_c) = H_{sp}\sin\theta + \left(\frac{L_s}{2} - R_s\right)\cos\theta + \frac{4}{3\pi}\left(R_s\cos\theta + A_2\cot(\beta+\theta)\right)$$

$$XMP5(h, \theta, p_c) = H_{sp}\sin\theta - \left(\frac{L_s}{2} - R_s\right)\cos\theta - \frac{4}{3\pi}\left(R_s\cos\theta + A_1\cot(\beta-\theta)\right)$$

$$XMP6(h, \theta, p_c) = -h_1(Z_{p_1} + (1 - \frac{C_D}{2})h_1) \qquad \text{if } h_1 < 0,\ h_2 > 0$$

$$= -h_1(Z_{p_1} + (1 - \frac{C_D}{2})h_1) + h_2(Z_{p_2} + (1 - \frac{C_D}{2})h_2) \text{ if } h_1 < h_2 < 0$$

$$M(h, \theta, p_c) = p_c \left[\sum_{i=1}^{5} XMPi(h, \theta, p_c) afi(h, \theta, p_c) + 2C_D B_s XMP6 \right] \quad (J.50)$$

Symmetry condition: $XMPi(h, {}^-\theta, p_c) = -XMPi(h, {}^+\theta, p_c)$

J.5.4.2 Heave derivatives

$$XMP_h 1(h, \theta, p_c) = \frac{1}{2} (\cot(\beta-\theta) - \cot(\beta+\theta))$$

$$XMP_h 2(h, \theta, p_c) = 0$$

$$XMP_h 3(h, \theta, p_c) = 0$$

$$XMP_h 4(h, \theta, p_c) = - \frac{4}{3\pi} \cot(\beta+\theta)$$

$$XMP_h 5(h, \theta, p_c) = \frac{4}{3\pi} \cot(\beta-\theta)$$

$$XMP_h 6(h, \theta, p_c) = 0, \qquad \text{if } h_1, h_2 > 0$$

$$= -Z_{p_1} - (2 - C_D)h_1, \qquad \text{if } h_1 < 0,\ h_2 > 0$$

$$= -Z_{p_1} - (2 - C_D)(h_1 - h_2) + Z_{p_2} \qquad \text{if } h_1 < h_2 < 0$$

$$M_h(h, \theta, p_c) = p_c \left[\sum_{i=1}^{5} \{XMP_h i(h, \theta, p_c) afi(h, \theta, p_c) + XMPi(h, \theta, p_c) af_h i(h, \theta, p_c)\} + 2C_D B_s XMP_h 6 \right] \quad (J.51)$$

Symmetry condition: $XMP_h i(h, {}^-\theta, p_c) = -XMP_h i(h, {}^+\theta, p_c)$

J.5.4.3 Pitch derivatives

$$XMP_\theta 1(h,\ \theta,\ p_c) = H_{sp}\cos\theta - \frac{1}{2}\{A_3\cot(\beta+\theta) + \frac{A_2}{\sin^2(\beta+\theta)}$$

$$+ A_4\cot(\beta-\theta) + \frac{A_1}{\sin^2(\beta-\theta)}\}$$

$$XMP_\theta 2(h,\ \theta,\ p_c) = H_{sp}\cos\theta$$

$$XMP_\theta 3(h,\ \theta,\ p_c) = H_{sp}\cos\theta + \frac{1}{3}(\frac{L_s}{2} - R_s)\sin\theta$$

$$XMP_\theta 4(h,\ \theta,\ p_c) = H_{sp}\cos\theta - (\frac{L_s}{2} - R_s)\sin\theta$$

$$- \frac{4}{3\pi}(R_s\sin\theta + A_3\cot(\beta+\theta) + \frac{A_2}{\sin^2(\beta+\theta)})$$

$$XMP_\theta 5(h,\ \theta,\ p_c) = H_{sp}\cos\theta + (\frac{L_s}{2} - R_s)\sin\theta$$

$$+ \frac{4}{3\pi}(R_s\sin\theta - A_4\cot(\beta-\theta) - \frac{A_1}{\sin^2(\beta-\theta)})$$

$$XMP_\theta 6(h,\ \theta,\ p_c) = 0, \qquad \text{if } h_1,\ h_2 > 0$$

$$= -dh_1(Z_{p_1} + h_1(1-C_D)), \qquad \text{if } h_1 < 0,\ h_2 > 0$$

$$= -dh_1(Z_{p_1} + h_1(1-C_D)) + dh_2(Z_{p_2} + (1-C_D)h_2), \qquad \text{if } h_1 < h_2 < 0$$

$$M_\theta(h,\ \theta,\ p_c) = p_c \left[\sum_{i=1}^{5} \{XMP_\theta i(h,\ \theta,\ p_c)afi(h,\ \theta,\ p_c) \right.$$

$$+ \mathrm{XMPi}(h,\ \theta,\ p_c)\mathrm{af}_\theta i(h,\ \theta,\ p_c)\} + 2C_D B_s \mathrm{XMP}_\theta 6(h,\ \theta,\ p_c)\Big] \qquad (J.52)$$

Symmetry condition: $\mathrm{XMP}_\theta i(h,\ {}^-\theta,\ p_c) = \mathrm{XMP}_\theta i(h,\ {}^+\theta,\ p_c)$

J.5.4.4 Pressure derivatives

$$\mathrm{XMP}_{p_c}1(h,\ \theta,\ p_c) = \left[\frac{\cos\theta}{2}\left(\cot(\beta+\theta) - \cot(\beta-\theta)\right) + \sin\theta\right]\frac{dH_s}{dp_c}$$

$$- \frac{\sin\theta}{4}\left\{\cot(\beta+\theta) + \cot(\beta-\theta)\right\}\frac{dL_s}{dp_c} + \frac{1}{2}\left\{\frac{A_1}{\sin^2(\beta-\theta)} - \frac{A_2}{\sin^2(\beta+\theta)}\right\}\frac{d\beta}{dp_c}$$

$$\mathrm{XMP}_{p_c}2(h,\ \theta,\ p_c) = \sin\theta\,\frac{dH_s}{dp_c}$$

$$\mathrm{XMP}_{p_c}3(h,\ \theta,\ p_c) = \sin\theta\,\frac{dH_s}{dp_c} - \frac{\cos\theta}{3}\left(\frac{1}{2}\frac{dL_s}{dp_c} - \frac{dR_s}{dp_c}\right)$$

$$\mathrm{XMP}_{p_c}4(h,\ \theta,\ p_c) = \left(\sin\theta + \frac{4\cos\theta\,\cot(\beta+\theta)}{3\pi}\right)\frac{dH_s}{dp_c}$$

$$+ \frac{1}{2}\left(\cos\theta - \frac{4\sin\theta\,\cot(\beta+\theta)}{3\pi}\right)\frac{dL_s}{dp_c}$$

$$- \cos\theta\left(1 - \frac{4}{3\pi}\right)\frac{dR_s}{dp_c} - \frac{4}{3\pi}\,\frac{A_2}{\sin^2(\beta+\theta)}\,\frac{d\beta}{dp_c}$$

$$\mathrm{XMP}_{p_c}5(h,\ \theta,\ p_c) = \left(\sin\theta - \frac{4\cos\theta\,\cot(\beta-\theta)}{3\pi}\right)\frac{dH_s}{dp_c}$$

$$- \frac{1}{2}\left(\cos\theta - \frac{4\sin\theta\,\cot(\beta-\theta)}{3\pi}\right)\frac{dL_s}{dp_c} + \cos\theta\left(1 - \frac{4}{3\pi}\right)\frac{dR_s}{dp_c} + \frac{4}{3\pi}\,\frac{A_1}{\sin^2(\beta-\theta)}\,\frac{d\beta}{dp_c}$$

$$\mathrm{XMP}_{p_c}6(h,\ \theta,\ p_c) = 0, \qquad \text{if } h_1,\ h_2 > 0$$

$$= -\left(\cos\theta\,\frac{dH_s}{dp_c} - \frac{\sin\theta}{2}\,\frac{dL_s}{dp_c}\right)\left(Z_{p_1} + (1-C_D)h_1\right), \text{if } h_1 < 0,\ h_2 > 0$$

$$\begin{aligned} = &-\left(\cos\theta\,\frac{dH_s}{dp_c} - \frac{\sin\theta}{2}\,\frac{dL_s}{dp_c}\right)\left\{Z_{p_1} + (1-C_D)h_1\right\} \qquad \text{if } h_1 < h_2 < 0 \\ &+ \left(\cos\theta\,\frac{dH_s}{dp_c} + \frac{\sin\theta}{2}\,\frac{dL_s}{dp_c}\right)\left(Z_{p_2} + (1-C_D)h_2\right) \end{aligned}$$

$$\begin{aligned} M_{p_c}(h,\ \theta,\ p_c) = \frac{M(h,\ \theta,\ p_c)}{p_c} + p_c \Bigg[&\sum_{i=1}^{5} \{\mathrm{XMP}_{p_c}i(h,\ \theta,\ p_c)\mathrm{af}i(h,\ \theta,\ p_c) \\ &+ \mathrm{XMP}i(h,\ \theta,\ p_c)\mathrm{af}_{p_c}i(h,\ \theta,\ p_c)\} + 2C_D\mathrm{XMP}6(h,\ \theta,\ p_c)\,\frac{dB_s}{dp_c} \\ &+ 2C_D B_s \mathrm{XMP}_{p_c}6(h,\ \theta,\ p_c)\Bigg] \end{aligned} \qquad (J.53)$$

Symmetry condition: $\mathrm{XMP}_{p_c}i(h,\ {}^{-}\theta,\ p_c) = -\mathrm{XMP}_{p_c}i(h,\ {}^{+}\theta,\ p_c)$

J.6 Cushion Volume

J.6.1 Assumptions Used to Calculate Cushion Volume

The cushion volume is approximated using a triangular footprint as shown in Figures J.6 and J.7. The volume is composed of two parts: a "dead" volume which is the volume enclosed by the skirt when all segment tips are just touching the ground surface, and an "active" volume which includes additional volume for the air gap between the skirt and ground and a subtracted volume corresponding to that part of the "dead" volume which would lie below the ground plane if the skirt did not deform on contact with the ground. The dead volume is calculated assuming that the volume consists of two tubes, one of volume equal to the footprint area times skirt height, the other a tube with cross-sectional area defined by the segment edges, a vertical plane through the segment tips, and the hard structure as shown in Figure J.1. This tube has a length equal to that of the straight side and end sections plus that of a circle with radius equal to the mean of the tip radius and the knee radius.

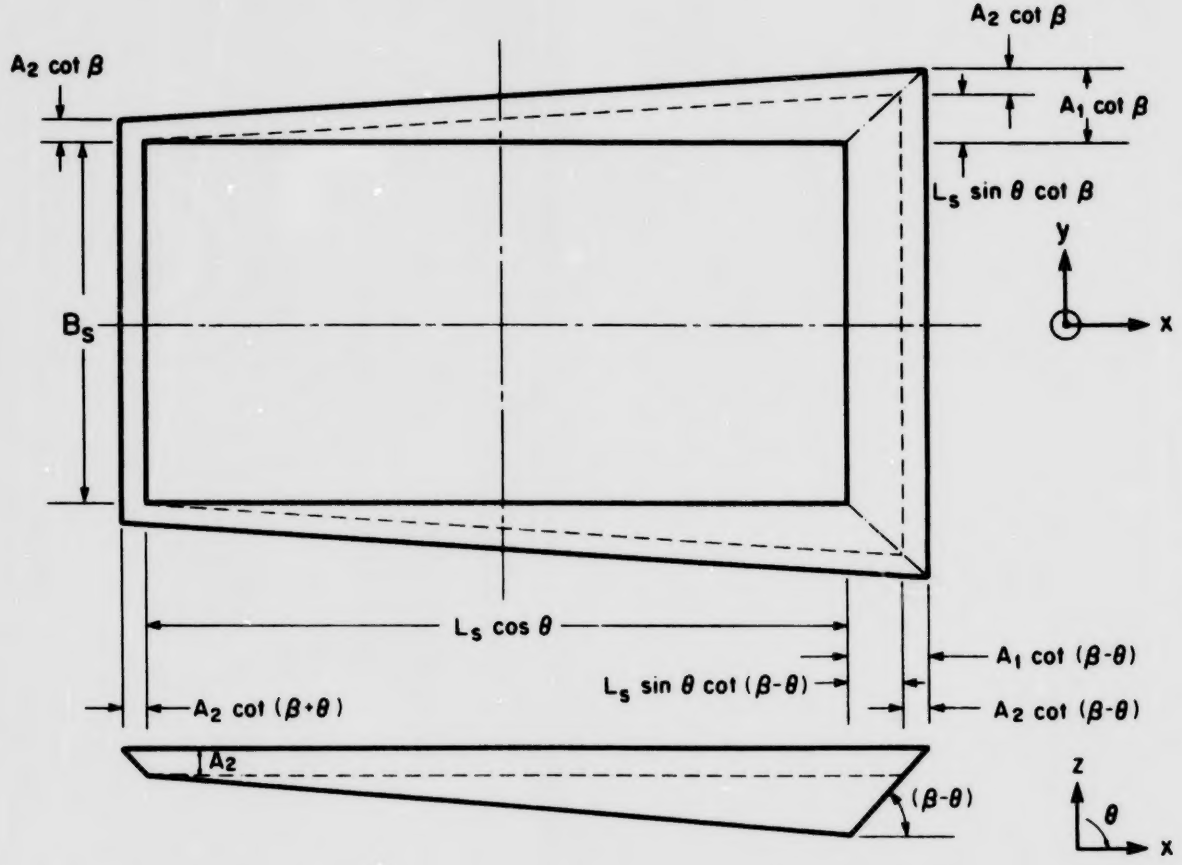
$A_2 \cot \beta$
$A_2 \cot \beta$
$A_1 \cot \beta$
$L_s \sin \theta \cot \beta$
y
x
B_s
$L_s \cos \theta$
$A_1 \cot (\beta - \theta)$
$L_s \sin \theta \cot (\beta - \theta)$
$A_2 \cot (\beta + \theta)$
$A_2 \cot (\beta - \theta)$
A_2
$(\beta - \theta)$
z
θ
x

Figure J.6 Triangular Footprint Geometry in Noncontacting and Complete Contact Cases.

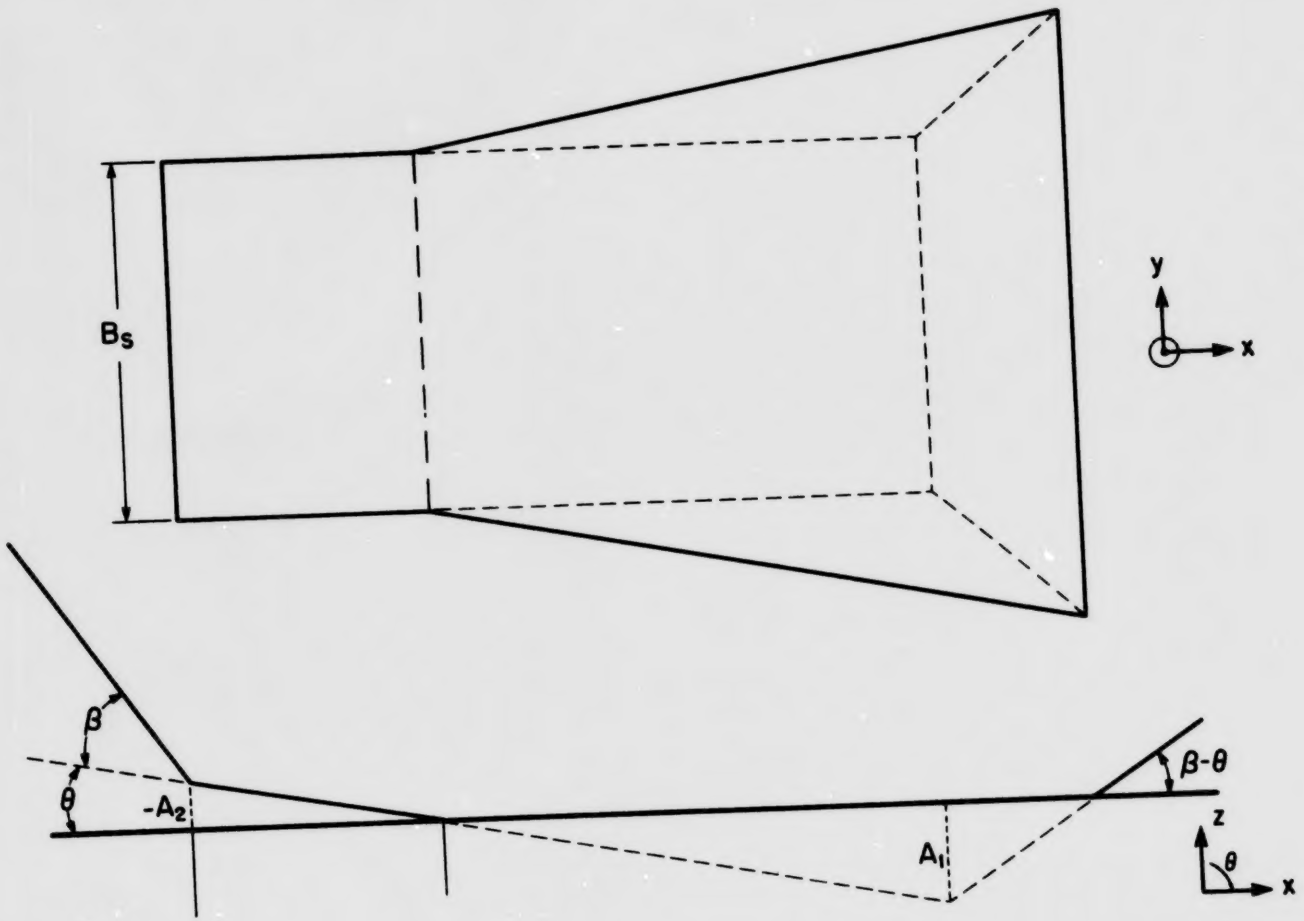
Bs
y
x
β
θ
-A₂
A₁
β-θ
z
θ
x

Figure J.7 Triangular Footprint Geometry in Partial Contact.

J.6.2 "Dead" Volume

$$V_{co}(p_c) = H_sL_sB_s - R_s{}^2(4 - \pi)H_s + [\ell_1\ell_2\cot\beta - \frac{1}{2}\,\ell_2{}^2\cot\beta$$

$$- \frac{1}{2}\,(\ell_1 - \ell_2)^2\tan(\pi-\zeta+\beta_0)]\{2(L_s + B_s - 4R_s) + 2\pi(R_s + \frac{\ell_2}{2}\cot\beta)\} \qquad (J.54)$$

where ℓ_1 and ℓ_2 are assumed to depend on H_s as $\ell_1 = \ell_{10} - H_{so} + H_s$ and $\ell_2 = \ell_{20} - H_{so} + H_s$.

$$\frac{\partial V_{co}(p_c)}{\partial H_s} = L_sB_s - R_s{}^2(4-\pi) + \{\text{as in } V_{co}(p_c)\}[(\ell_1 + \ell_2)\cot\beta$$

$$- \ell_2\cot\beta - (\ell_1 - \ell_2)\tan(\pi-\zeta+\beta_0)]$$

$$+ [\text{as in } V_{co}(p_c)]\ \pi\tan(\frac{\pi}{2} - \beta)$$

$$\frac{\partial V_{co}}{\partial L_s} = H_sB_s + 2[\text{as in } V_{co}(p_c)]$$

$$\frac{\partial V_{co}}{\partial B_s} = L_sH_s + 2[\text{as in } V_{co}(p_c)]$$

$$\frac{\partial V_{co}}{\partial \beta} = - \{\text{as in } V_{co}(p_c)\}[\ell_1\ell_2 - \frac{\ell_2{}^2}{2}]\ \frac{1}{\sin^2\beta}$$

$$- [\text{as in } V_{co}(p_c)]\{\frac{\pi\ell_2}{\sin^2\beta}\}$$

$$\frac{\partial V_{co}}{\partial R_s} = -2R_s(4-\pi)H_s + [\text{as in } V_{co}(p_c)](2\pi-8)$$

$$V_{co_{p_c}}(p_c) = \frac{\partial V_{co}}{\partial H_s}\frac{dH_s}{dp_c} + \frac{\partial V_{co}}{\partial L_s}\frac{dL_s}{dp_c} + \frac{\partial V_{co}}{\partial B_s}\frac{dB_s}{dp_c} + \frac{\partial V_{co}}{\partial \beta}\frac{d\beta}{dp_c} + \frac{\partial V_{co}}{dR_s}\frac{dR_s}{dp_c} \tag{J.55}$$

J.6.3 Total Volume Including "Active" and "Dead" Volumes

J.6.3.1 Case 1: $A_1 < 0$

$$V_c(h, \theta, p_c) = V_{co} + A_5 \tag{J.56}$$

$$V_{c_h}(h, \theta, p_c) = B_s L_s \cos\theta \tag{J.57}$$

$$V_{c_\theta}(h, \theta, p_c) = B_s L_s \sin\theta(2H_{sp}\cos\theta - h) \tag{J.58}$$

$$V_{c_{\theta\theta}}(h, \theta, p_c) = 2B_s L_s H_{sp}\cos 2\theta - B_s L_s h\cos\theta \tag{J.59}$$

$$V_{c_{p_c}}(h, \theta, p_c) = V_{co_{p_c}}(h, \theta, p_c) + \cos\theta(h - H_{sp}\cos\theta)(B_s \frac{dL_s}{dp_c} + L_s \frac{dB_s}{dp_c})$$

$$- B_s L_s \cos^2\theta \frac{dH_s}{dp_c} \tag{J.60}$$

J.6.3.2 Case 2: $A_2 < 0 < A_1$

$$V_c(h, \theta, p_c) = V_{co}(p_c) + \frac{B_s}{2} A_2{}^2\cot\theta - A_6(\frac{B_s}{2} A_1{}^2 + \frac{\cot\beta}{3} A_1{}^3) \tag{J.61}$$

$$V_{c_h}(h, \theta, p_c) = -B_s A_2 \cot\theta + A_6(B_s A_1 + \cot\beta\ A_1{}^2) \tag{J.62}$$

$$V_{c_\theta}(h, \theta, p_c) = -B_s(A_2 A_3 \cot\theta + \frac{1}{2}\ \frac{A_2{}^2}{\sin^2\theta}) - A_1{}^2 A_7(\frac{B_s}{2} + \frac{A_1}{3}\cot\beta)$$

$$- A_1 A_4 A_6(B_s + A_1\cot\beta) \tag{J.63}$$

$$V_{c_{\theta\theta}}(h, \theta, p_c) = B_s\left[(A_3{}^2 - A_2{}^2 - A_2 h)\cot\theta + (2A_2 A_3 + A_2{}^2\cot\theta)\frac{1}{\sin^2\theta}\right]$$

Continued

$$- 2A_1^2\left(\frac{B_s}{2} + \frac{A_1\cot\beta}{3}\right)\left(\frac{\cot\theta}{\sin^2\theta} + \frac{\cot(\beta-\theta)}{\sin^2(\beta-\theta)}\right)$$

$$- (B_s + A_1\cot\beta)\{2A_1A_4A_7 - (A_1^2 + A_1h - A_4^2)A_6\} - A_1A_4^2A_6\cot\beta \tag{J.64}$$

$$V_{c_{p_c}}(h, \theta, p_c) = V_{co_{p_c}}(p_c) + A_1^2\left[\left(\frac{B_s}{2} + \frac{A_1\cot\beta}{3}\right)\frac{\sin\theta}{\sin^2(\beta-\theta)} + \frac{A_6A_1}{3\sin^2\beta}\right]\frac{d\beta}{dp_c}$$

$$+ \frac{1}{2}(A_2^2\cot\theta - A_1^2A_6)\frac{dB_s}{dp_c} + B_sA_2\cot\theta\left(\cos\theta\frac{dH_s}{dp_c} - \frac{\sin\theta}{2}\frac{dL_s}{dp_c}\right)$$

$$- A_1A_6(B_s + A_1\cot\beta)\left(\cos\theta\frac{dH_s}{dp_c} + \frac{\sin\theta}{2}\frac{dL_s}{dp_c}\right) \tag{J.65}$$

J.6.3.3 Case 3: $A_2 > 0$

The volume is divided into three components, the "dead" volume, the volume of the pyramid frustum formed by the ground plane and a plane parallel to it but A_2 units lower, and the volume of the pyramidal section which represents the maximum of volume calculated in Case 2.

$$V_c(h, \theta, p_c) = V_{co} - \frac{A_2A_{13}}{3} - A_6A_{14}\sin\theta \tag{J.66}$$

$$V_{c_h}(h, \theta, p_c) = \frac{1}{3}(A_{13} + A_2A_{15}A_{16}) \tag{J.67}$$

$$V_{c_\theta}(h, \theta, p_c) = \frac{A_3A_{13}}{3} - \frac{A_2}{3}[(A_{17} - A_{18})A_{19} - A_{20} + A_{21} + A_{22}]$$

$$- A_7A_{14} - A_6A_{23} \tag{J.68}$$

$$V_{c_{\theta\theta}}(h, \theta, p_c) = \frac{(A_2 + h)A_{13}}{3} + \frac{2A_3}{3}[(A_{17} - A_{18})A_{19} - A_{20} + A_{21} + A_{22}]$$

$$- \frac{A_2}{3}[(A'_{17} - A'_{18})A_{19} + (A_{17} - A_{18})A'_{19} - A'_{20} + A'_{21} + A'_{22}]$$

$$- A'_7A_{14} - A_7A'_{14} - A_6A'_{23} - A'_6A'_{23} \tag{J.69}$$

$$V_{c_{p_c}}(h,\ \theta,\ p_c) = V_{co_{p_c}}(p_c) - \frac{A_{13}}{3}\left(\cos\theta\,\frac{dH_s}{dp_c} - \frac{\sin\theta}{2}\,\frac{dL_s}{dp_c}\right)$$

$$+ A_{14}\,\frac{\sin^2\theta}{\sin^2(\beta-\theta)}\,\frac{d\beta}{dp_c}$$

$$- A_6\sin\theta\left[L_s(B_s + L_s\sin\theta\cot\beta)\,\frac{dL_s}{dp_c} + \frac{L_s^2}{2}\,\frac{dB_s}{dp_c} - \frac{L_s^3\sin\theta}{3\sin^2\beta}\,\frac{d\beta}{dp_c}\right]$$

$$- \frac{A_2}{3}\left[A_8^p A_9 + A_8 A_9^p + A_{10}^p A_{11} + A_{10}A_{11}^p + \frac{A_{12}}{2}\left(\frac{A_8^p}{A_8} + \frac{A_9^p}{A_9} + \frac{A_{10}^p}{A_{10}} + \frac{A_{11}^p}{A_{11}}\right)\right] \tag{J.70}$$

J.6.4 Symmetry Conditions

In all cases the following symmetry conditions apply:

$$V_c(h,\ {}^-\theta,\ p_c) = V_c(h,\ {}^+\theta,\ p_c), \qquad V_{c_h}(h,\ {}^-\theta,\ p_c) = V_{c_h}(h,\ {}^+\theta,\ p_c),$$

$$V_{c_\theta}(h,\ {}^-\theta,\ p_c) = -V_{c_\theta}(h,\ {}^+\theta,\ p_c), \qquad V_{c_{\theta\theta}}(h,\ {}^-\theta,\ p_c) = V_{c_{\theta\theta}}(h,\ {}^+\theta,\ p_c)$$

and

$$V_{c_{p_c}}(h,\ {}^-\theta,\ p_c) = V_{c_{p_c}}(h,\ {}^+\theta,\ p_c)$$

J.7 Skirt Hysteresis

When the skirt is in contact with the ground additional forces are generated which give rise to the hysteresis which is a characteristic of pitch and heave stiffness curves [J.1, J.2]. This hysteresis arises from two sources, the friction between the skirt and the ground surface and from the internal forces generated by the bending of the skirt material during ground contact. At present suitable theories to estimate the contributions to heave and pitch have not been developed. This important aspect of the pitch-heave dynamics is currently a subject of ongoing work.

REFERENCES - APPENDIX J

J.1. Sullivan, P. A., et al, "Research Into Air Cushion Stability - 1979 Report", Transportation Development Centre, Transport Canada, Montreal, Report TP3109E, January 1982.

J.2. See Appendix E.

APPENDIX K: MEASUREMENT OF SKIRT CONTACT FORCES IN A SINGLE CELL

(N. H. Milligan and P. A. Sullivan)

K.1 Introduction

Measurement of static stiffness of various flexible skirt cushion models in roll and pitch at UTIAS have persistently shown the existence of hysteresis giving a reduced restoring moment when the vehicle is returning to its equilibrium position [K1, K2, K3]. Three mechanisms have been suggested: (i) for some multicell geometries, buckling of the cells when rolled or pitched, leading to failure of the cushion seal and subsequent loss of lift and restoring moment, (ii) sliding friction between skirt and ground, and (iii) the ability of some types of skirt material to carry small but significant forces when being forced by vehicle motion towards the ground, but which are absent or greatly reduced when the skirt is moving away from the ground. Appendix E reviews the evidence obtained from UTIAS tests which leads to these suggestions. We believe that, of the three, the third mechanism is the most likely to be encountered in ACV model testing because, unlike mechanisms (i) and (ii), it is not related to specific skirt geometries, and because it appears to be related to the viscoelastic or stress-relaxation properties of certain elastomers used in model skirts.

Investigations of the dynamics of cushion systems at UTIAS in which type (iii) hysteresis was known to be present have strongly suggested that it can have a major effect on the dynamics. Indeed the investigations described in Ref. K.3, which used the uncompartmented, segmented skirt that is the subject of the present contract, indicated that all the hysteresis appeared as damping. Nevertheless, we have generally been uncertain about its significance at full scale, and consequently have not investigated it in any detail. During the tenure of the present contract, measurements on TDC's icebreaker bow, the 270 tonne ACIB, described in Appendix E, indicated that significant contact forces existed which could be the source of a type (iii) hysteresis. Consequently, since it can have major implications both for mathematical modelling of cushion dynamics, and for scaling of skirt material for model tests, we considered that a detailed investigation was needed, and certainly fell within the terms of reference of the present Contract.

In a complete investigation of this phenomenon one would begin with suitable simple material tests, such as the uniaxial dynamic tension and stress relaxation tests described in Appendix B, and then use an appropriate structural analysis to predict the history of the forces of skirtground contact. However, given the complexity of the typical flexible skirt geometry, and given the nonlinear and anisotropic properties of the elastomer coated fabric used as skirt material, it is evident that such a fundamental approach is a formidable task. Consequently, we adopted two simpler approaches, initially essentially empirical, but subsequently involving some theoretical support. The first approach was not successful, but the second has proved more fruitful.

K.2 Initial Test Proposal

The aim of the first project was to obtain confirmation of inferences drawn from analysis of flight test data obtained from the UTIAS Circular

Track test vehicle, namely, that all the observed static hysteresis appeared as damping in the dynamics [K.3]. The configuration chosen for this purpose is shown in Figure K.1. It consists of a single conical cell constrained to move in pure heave. The bottom of the cell remains continuously in contact with the ground, while hovergap action is obtained by use of a special valve. This arrangement has two advantages: it eliminates the nonlinear valving effect of segment geometry on the cushion air escape process discussed in Appendix Q, and it maximizes the effect of the contact forces on the dynamics. We planned to measure the contact force hysteresis in a simple static experiment similar to that used on TDC's ACIB (see Appendix E), then use this measured force as empirical input data to a theory. This is the conceptual equivalent to using a measured coefficient of sliding friction in an analytical dynamic investigation, and although it completely avoids consideration of the structural aspect, is a useful first step. The theoretical predictions of the dynamics of the model in Figure K.1 were to be compared with an experiment.

The model skirt material that has been used for these and subsequent tests is extruded polyethylene film. Although this material is not suitable for skirts on practical vehicles, it has three advantages for the present work. Firstly, it is known to exhibit substantial hysteresis, secondly, it is readily available in a range of thicknesses, and thirdly, it has reasonably linear and isotropic structural properties. This last advantage facilitates development of theoretical analyses, and thus should give a much clearer indication of the role of material thickness in generating contact forces than would various elastomer-fabric combinations having both different thicknesses and fabric weights.

We initially planned to test the model in the Sphere Facility. Although this imposed the severe constraint of limiting measurements to responses to initial condition disturbances nevertheless, in the absence of an adequate model of the dynamics of the fan used in the Heave Table Facility, and in view of the success of the work described in Appendices B and C, we deemed this appropriate. Upon successful completion of both the present experiment and the work on the valving effect of segment geometry on cushion air escape described in Appendix Q, a similar investigation of a segmented skirt model was to be undertaken.

Preliminary static measurements on the model of Figure K.1 implied the existence of a much more significant dependence of contact forces on time than had been hitherto supposed. This led to the redesign of the experiment to measure the contact forces, and this is discussed in the next section.

K.3 Apparatus Developed for Measuring Contact Forces

The apparatus finally developed to measure the contact forces is depicted in Figure K.2. A single conical cell is again used, but the model is installed in the servo-hydraulic heave table facility to allow investigation of stress-relaxation and frequency dependent effects. The model is fixed, and the air pressure inside the cell is maintained by the facility fan. The required equilibrium pressure is obtained by adjusting the fan speed, and to minimize pressure fluctuations induced by table motion air is allowed to escape from orifices in a plenum chamber which is structurally uncoupled form the cell being tested.

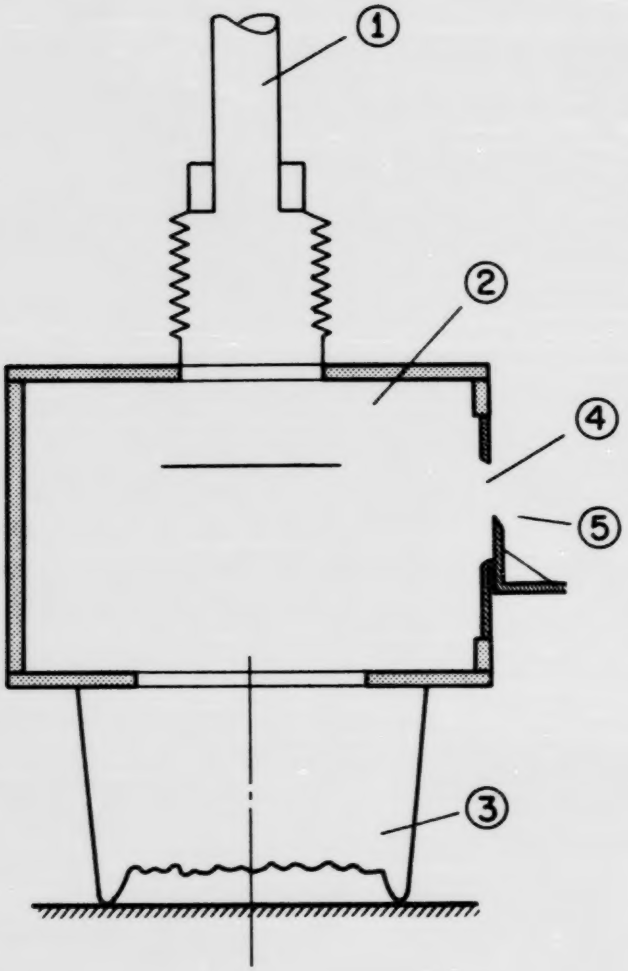

Figure K.1 Configuration used in preliminary tests. Air is fed from the UTIAS Sphere by a duct, 1, into a plenum box, 2, which is free to heave. A cone of the test material, 3, attached to and pressurized by the box remains continuously in contact with the ground-board. Air cushion action is simulated by the slot, 4, in the plenum box and the knife-edge, 5, attached to the ground.

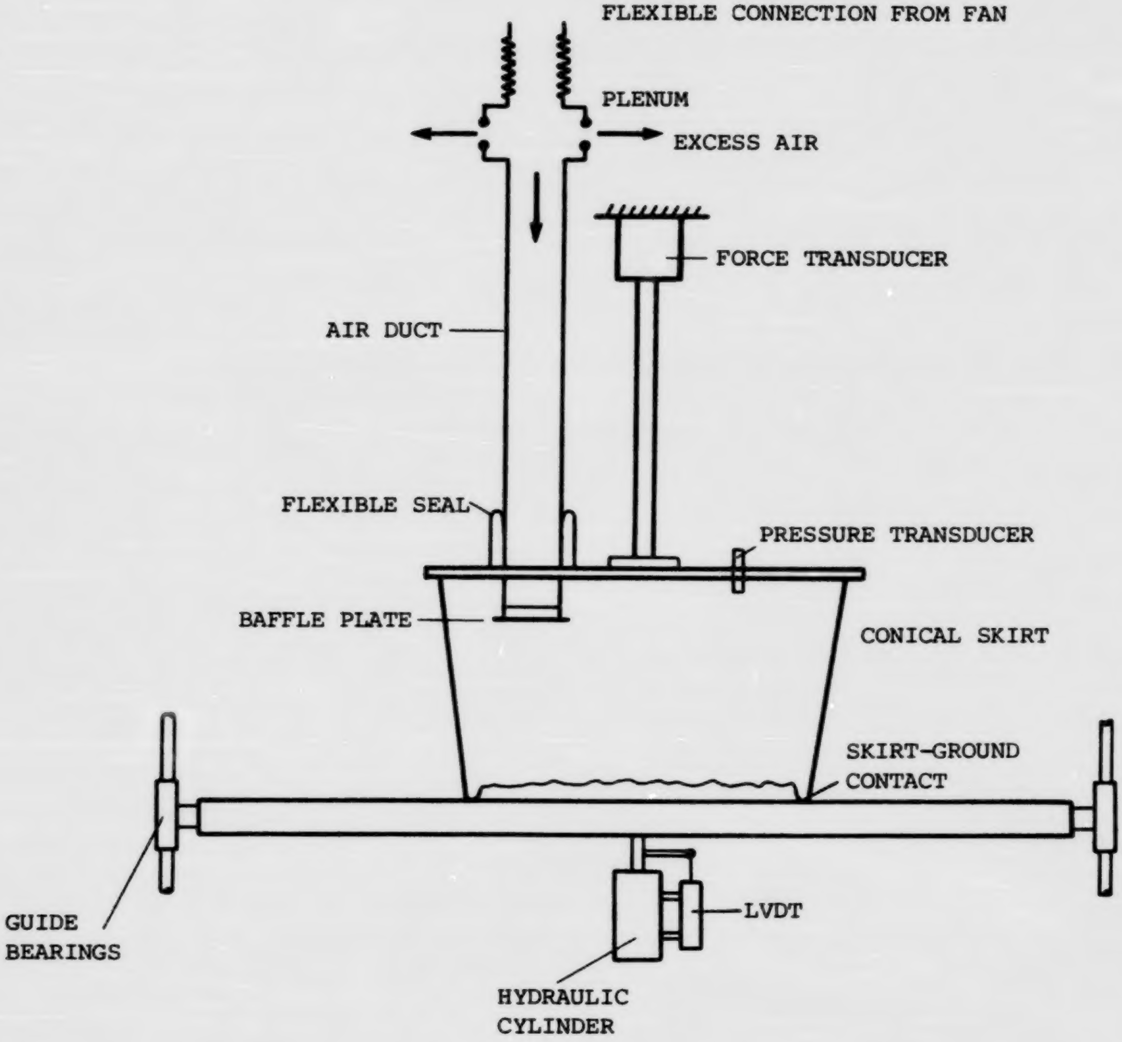
FLEXIBLE CONNECTION FROM FAN
PLENUM
EXCESS AIR
FORCE TRANSDUCER
AIR DUCT
FLEXIBLE SEAL
PRESSURE TRANSDUCER
BAFFLE PLATE
CONICAL SKIRT
SKIRT-GROUND CONTACT
GUIDE BEARINGS
LVDT
HYDRAULIC CYLINDER

Figure K.2 Apparatus finally developed for measuring contact forces.

With the table executing the desired motion, which is typically an oscillation of a known frequency and amplitude, the histories of the outputs of the transducers measuring table motion, total force and cell pressure are recorded by a microprocessor-based digital data acquisition system, the main elements of which are depicted in Figure K.3. When compared with the old system, which is essentially the ultraviolet strip chart recorder shown in Figure K.3, the new system has enabled a large improvement both in the speed of data acquisition and analysis, and in the qualilty of the data itself. Indeed, certain experiments which were barely feasible, such as that described in Appendix H, are now straightforward to execute.

K.4 Preliminary Results

Figures K.4 and K.5 give typical preliminary results. The contact force at any instant is computed by subtracting from the measured total force the computed cushion pressure force. The pressure force is computed using cell footprint areas calculated from the uninflated cone geometry. Measurements of footprint area at three table heights indicated that, except for the thinnest material used in the tests, the effect of hoop deformation appeared to be undetectable and that errors in estimating the area are less than 1%. This can cause a significant error in the measurement of the contact force, perhaps as much as 10% in any given experiment; however, it is a systematic error and does not affect computed differences of contact force due to stress relaxation effects.

The data in Figures K.4 and K.5 were obtained at table frequencies of 0.01 Hz and 3.77 Hz respectively, and with the skirt in contact with the table for only part of the cycle. The reference height for the displacement is the mean height of the oscillating table. Both sets of data show hysteresis in the force associated with skirt-table contact, with the force being larger when the table is moving upward, as originally inferred. The build-up of contact force as the table moves upward occurs over a distance of about 1.5 mm for both sets of data. This occurs partly because it is very difficult to trim the material to be at a uniform height above the table. However, even if the bottom of the cell is perfectly parallel to the table, it is expected that the contact force increases continuously from the point of initial contact and reaches a maximum when the slope of the bottom edge is horizontal and parallel to the table; this is depicted in Figure K.6. The coincidence of the data obtained during both upward and downward motion for that portion of the cycle when the skirt is out of contact with the table is a useful indication that no phase distortion is introduced by the anti-aliasing analog filters and that any dynamic hoop extension effects on cushion footprint area that could be caused by the viscoelastic properties of the skirt material are negligible. The non-zero value of force computed for the out-of-contact portion of the cycle is caused by an offset force introduced by guy-wires to support the model.

K.5 Discussion and Conclusion

The existence of significant hysteresis in the contact force at frequencies as low as 0.01 Hz confirm the inferences about the role of this force made from the earlier static tests described in Refs. K.1-K.3. However, the data obtained at 3.77 Hz also indicates that there may be

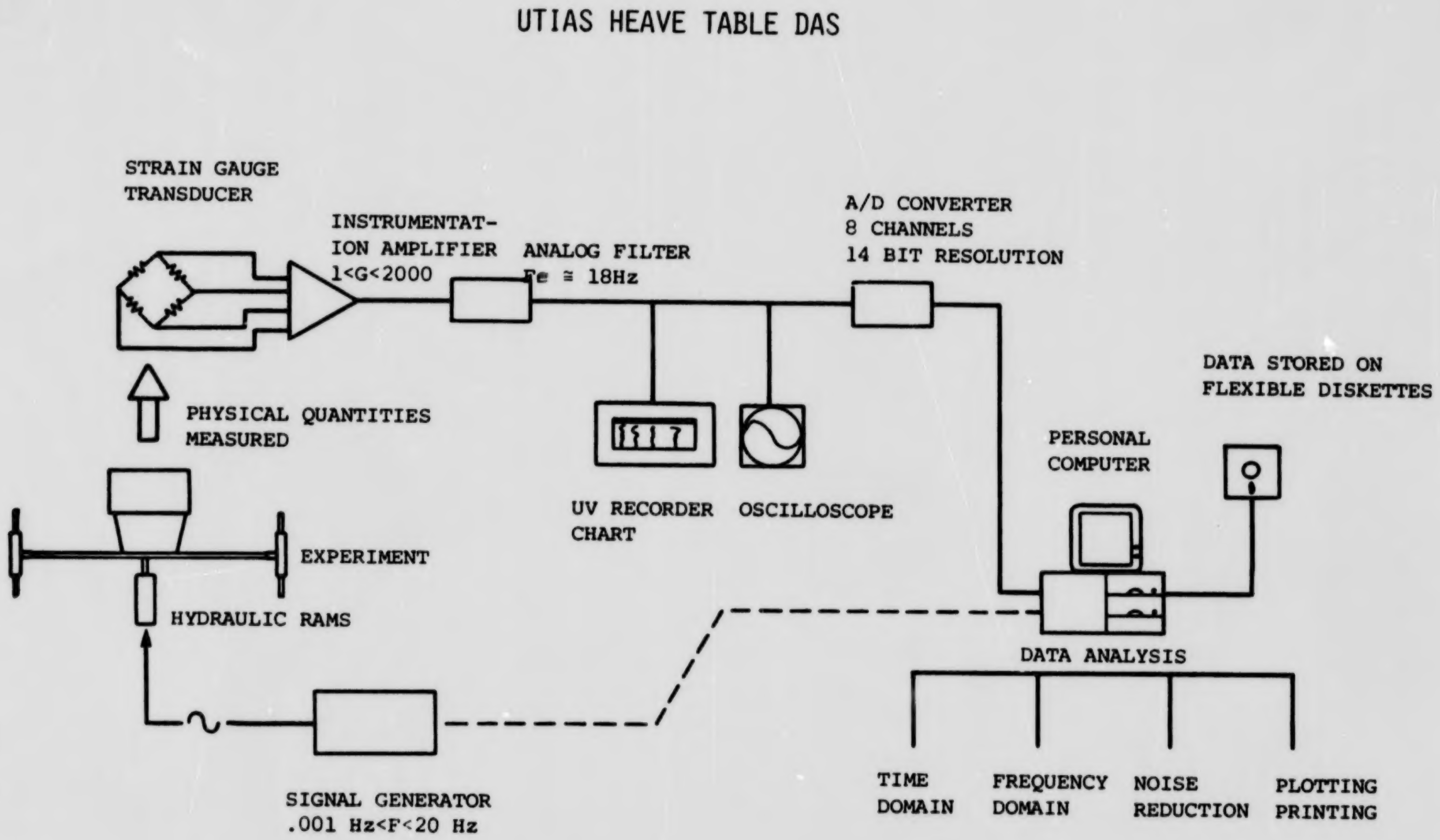
UTIAS HEAVE TABLE DAS
STRAIN GAUGE TRANSDUCER
INSTRUMENTATION AMPLIFIER 1<G<2000
ANALOG FILTER Fc ≅ 18Hz
A/D CONVERTER 8 CHANNELS 14 BIT RESOLUTION
DATA STORED ON FLEXIBLE DISKETTES
PHYSICAL QUANTITIES MEASURED
UV RECORDER CHART
OSCILLOSCOPE
PERSONAL COMPUTER
EXPERIMENT
HYDRAULIC RAMS
DATA ANALYSIS
SIGNAL GENERATOR .001 Hz<F<20 Hz
TIME DOMAIN
FREQUENCY DOMAIN
NOISE REDUCTION
PLOTTING PRINTING

Figure K.3 Micro-computer based digital-data acquisition system used in the tests.

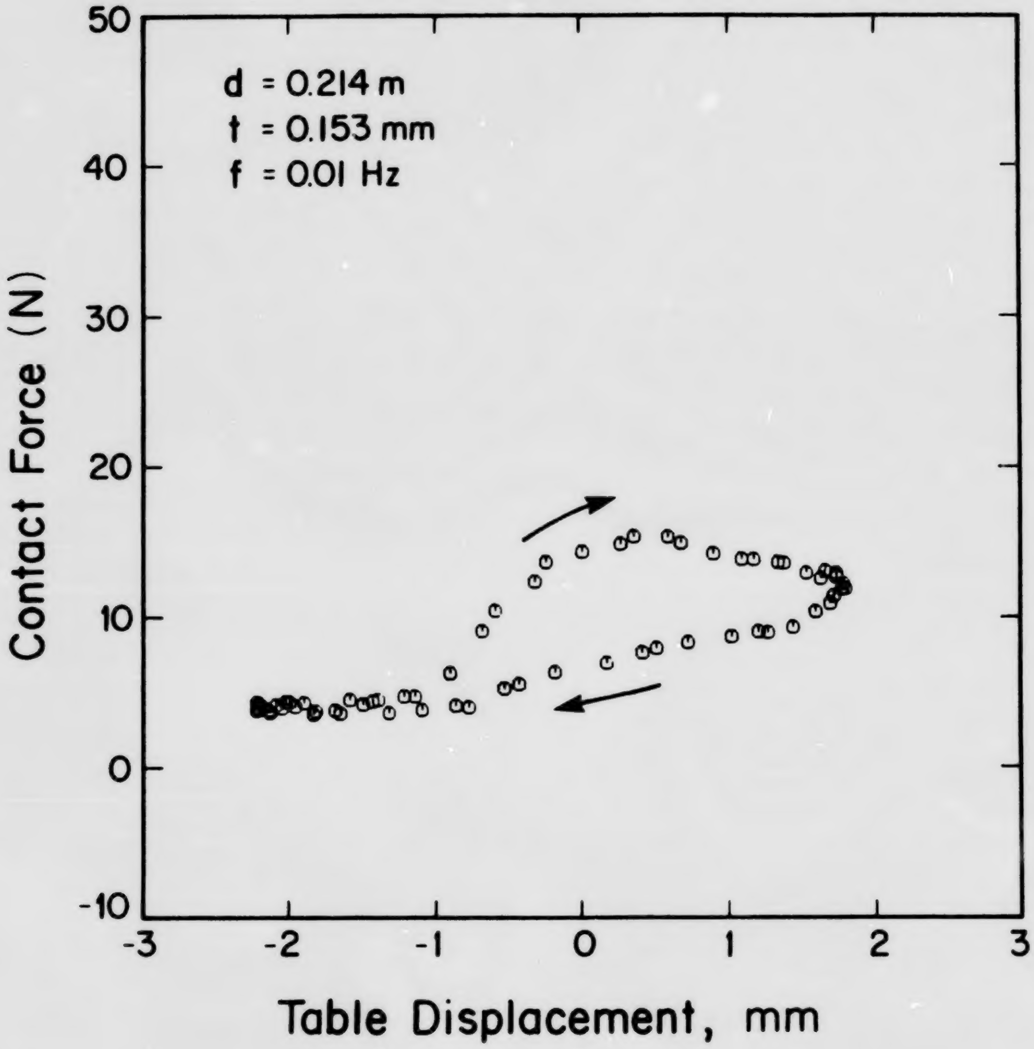

Figure K.4 Measured skirt contact forces as a function of table displacement at a table frequency of 0.01 Hz.

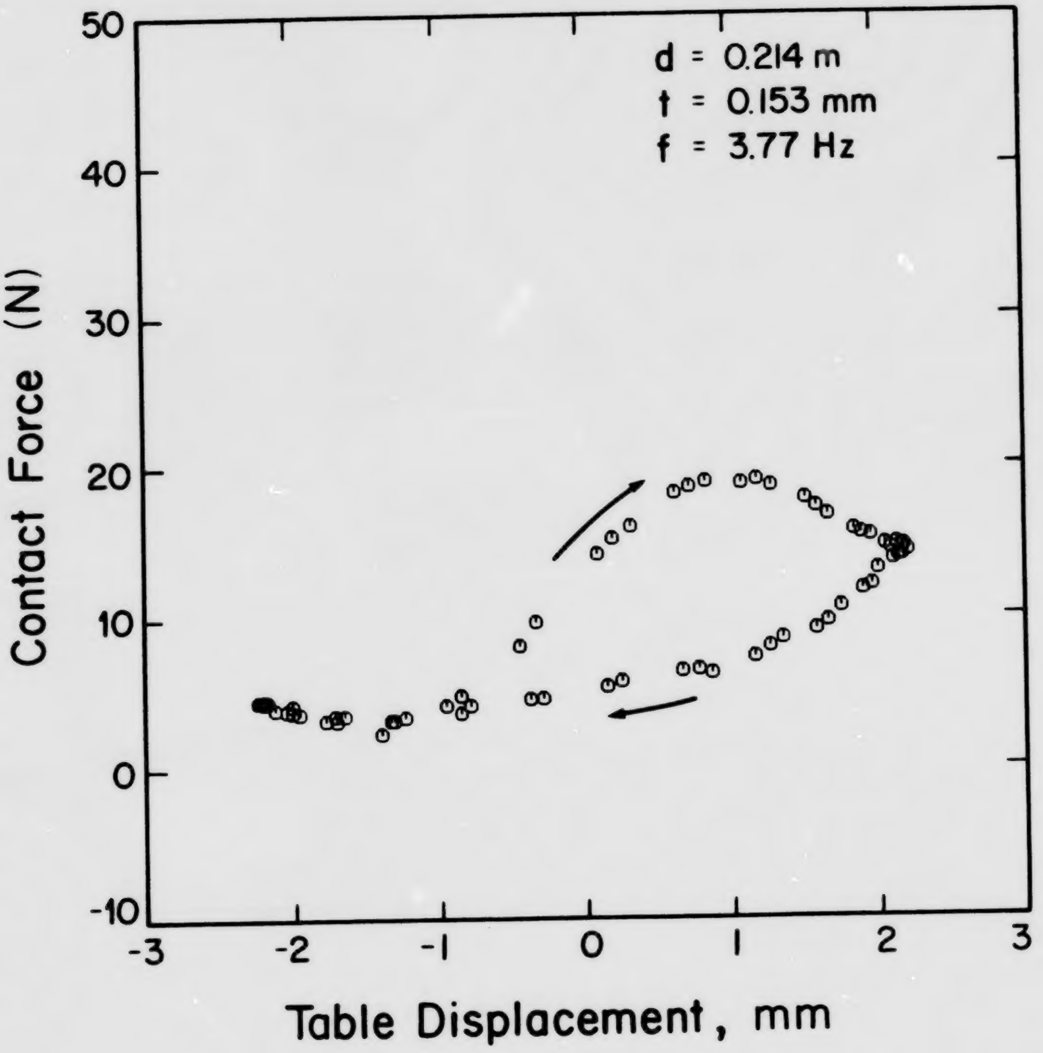

Figure K.5 Measured skirt contact forces as a function of table displacement at a table frequency of 3.77 Hz.

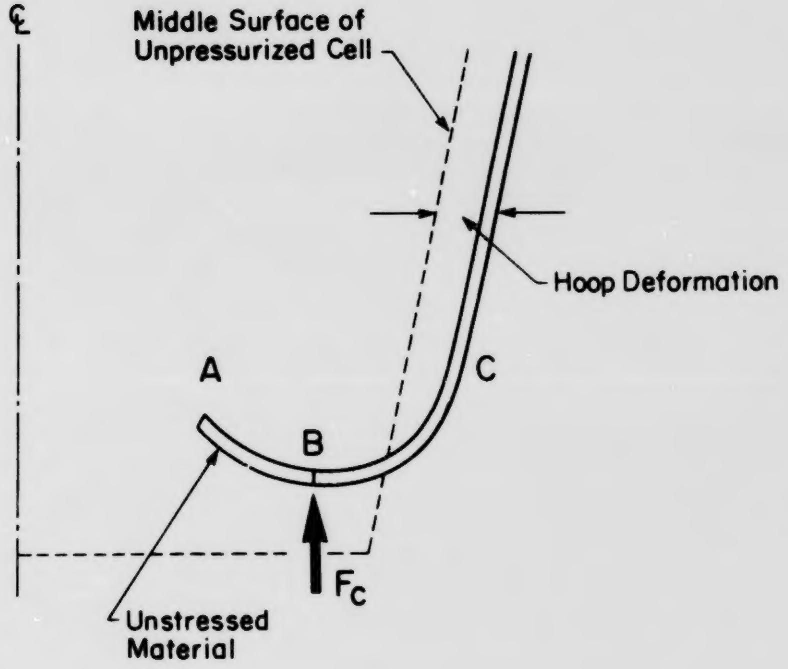
℄
Middle Surface of Unpressurized Cell
Hoop Deformation
A
B
C
F_c
Unstressed Material

Figure K.6 Illustrating development of contact force. As depicted the force F_c has reached a maximum, starting from zero when the particle of the cone A just touches the table. Observation suggests that when the point of contact has moved to particle B the portion AB is unstressed.

significant frequency dependence, with the effective damping being higher than that which would be inferred from a static test.

The overall conclusion is that a reliable technique for measuring contact force hysteresis has been developed, but the task of detailed investigation is far from complete. To facilitate interpretation of these tests, the apparatus depicted in Figure K.7 is being used to obtain flexural rigidity data; the data obtained thus far in general correlates well with the contact force measurements. Also a theory for the elastic component of the force is being developed. Note that the required result cannot be obtained simply by using any of the available analyses for the loading of conical shells. All of these are based on infinitesimal deformation theory, which assumes that the curvatures and slopes of the middle surface of the loaded shell can be approximated by those of the unloaded shell. As Figure K.6 shows, this is clearly not the case in the region of skirt-ground contact. We must resort to finite deflection theory.

Finally it is anticipated that, on successful completion of this work, the heave dynamics of the model depicted in Figure K.1 will be investigated. It is also anticipated that successful completion of the work on the dynamic response of the Heave Table Fan described in Appendix H will enable us to use this facility, with confidence. This is important because the Sphere facility cannot readily investigate frequency-dependent effects.

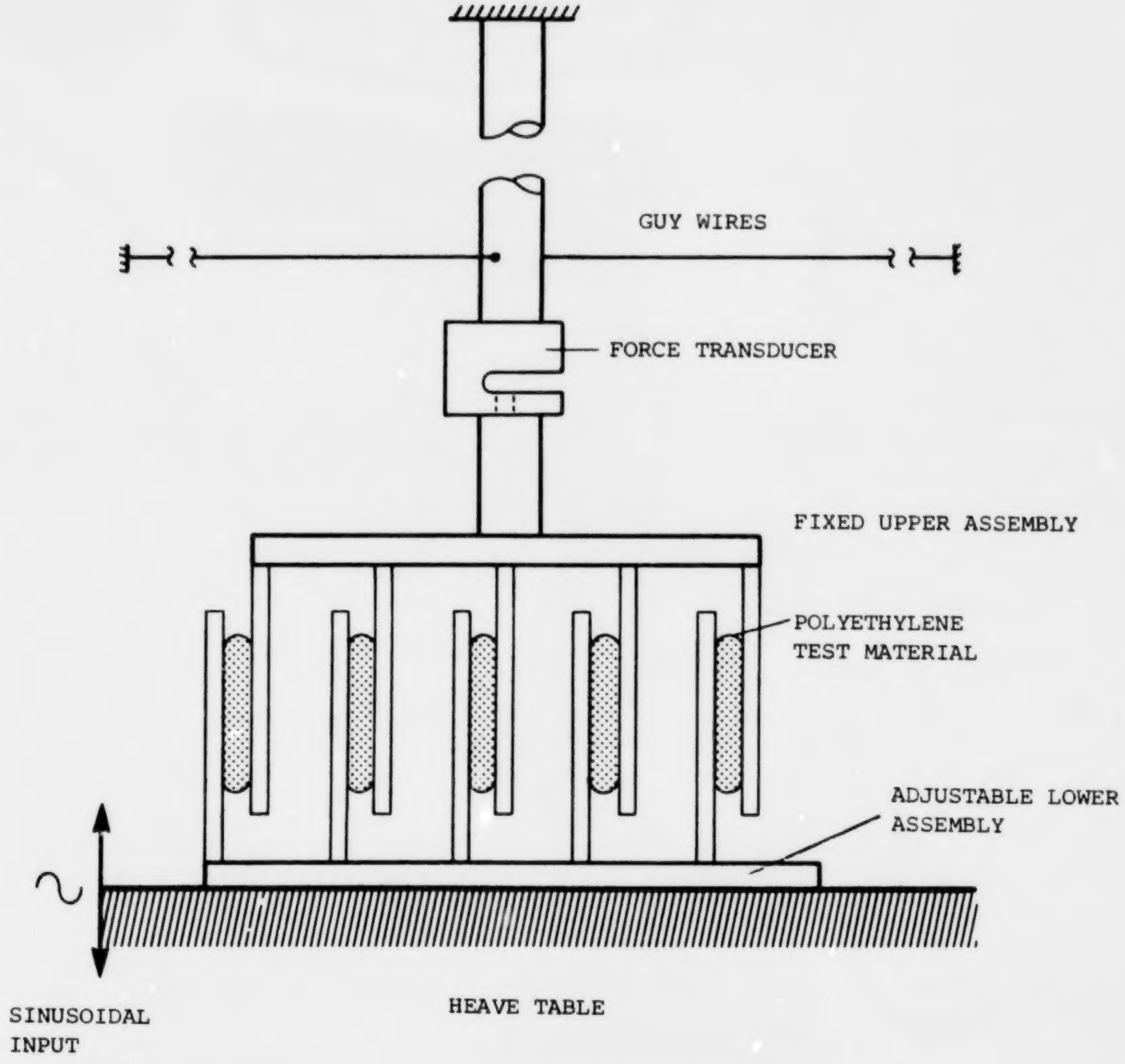
GUY WIRES
FORCE TRANSDUCER
FIXED UPPER ASSEMBLY
POLYETHYLENE TEST MATERIAL
ADJUSTABLE LOWER ASSEMBLY
SINUSOIDAL INPUT
HEAVE TABLE

Figure K.7 Apparatus used in dynamic flexural rigidity tests. Loops of test material are rolled between the fingers of the upper and lower assemblies.

REFERENCES - APPENDIX K

K.1 Sullivan, P. A., Hinchey, M. J., and Delaney, R. G., "An Investigation of the Roll Stiffness Characteristics of Three Flexible Skirted Air Cushion Systems", University of Toronto, Institute for Aerospace Studies, Toronto, Canada, Report No. 213, March 1977.

K.2 Sullivan, P. A., Hinchey, M. J., Murra, I., and Parravano, J., "Research on the Stability of Air Cushion Systems", University of Toronto, Institute for Aerospace Studies, Toronto, Canada, Report No. 238, Nov. 1979.

K.3 Sullivan, P. A., Hinchey, M. J., Hartmann, P. V., Dupuis, A., Green, G., and Graham, T., "Research into Air Cushion Stability: 1979 Report", Transportation Development Centre, Transport Canada, Montreal, Report TP-3109-E, Jan. 1982.

APPENDIX L: DEVELOPMENT OF SYSTEM IDENTIFICATION TECHNIQUES FOR THE ANALYSIS OF ACV FLIGHT TEST DATA (T. A. Graham and M. J. Hinchey)

L.1 Introduction

The previous contract report, [L.1], contains results from the first attempt to apply parameter estimation techniques to ACV flight test data obtained on the circular track vehicle. Parameter estimation is one way of interpreting the large amounts of data produced in experiments on multivariable systems, i.e., systems with several state variables, and it is a part of the system identification - parameter estimation process. This process is illustrated in Figure L.1; although it can be broken down further, the process consists of three major parts: the parameter estimation process shown within the dashed line, the experiment or input, and the model selection-validation process. For research into vehicle dynamics the purpose of system identification is to select a mathematical model of the system which will give acceptable predictions for all inputs of interest and permit interpretation of the resulting parameter estimates within the known physical framework of the system. The selection of a class of models, i.e. the choice of mathematical formulation of the physical framework, from which a particular one is selected is therefore critical for research purposes. There are two elements to the parameter estimation process; the selection of a criterion or cost function derived from assumptions about the system model class and from assumptions about the noise, and the parameter adjustment process which is the attempt to minimize the criterion function for the given input data and model by changing the model parameters.

The results reported in reference L.1 used an initial disturbance input, a maximum likelihood estimation technique and a linear constant coefficient system model. The maximum likelihood estimation was implemented through a modified version of the FORTRAN program listed in reference L.2. The results obtained at that time were encouraging; the estimates of pitch stiffness and pitch damping were close to the values measured in static tests, and the time histories from the parameter estimation model and the experiment were qualitatively similar. There were, however, several problems with the implementation as it stood. In particular, it was very difficult to get the numerical parameter adjustment procedure to converge, and some of the other estimated parameters differed significantly from the values obtained in the static experiments. Furthermore, the experimental data showed an induced roll motion which complicated the interpretation of the experiments.

L.2 Approach Adopted in Present Work

A two pronged approach was employed to address the problems. First, as dicussed in Section 3.2, to eliminate the induced roll a new lift fan package was designed and built so that gyroscopic torques were eliminated. This also allowed a wider range of cushion flow conditions to be scaled, and simplified interpretation of unsteady flow conditions. Second, the existing linear parameter estimation programme was used with ACV data, first experimental and then simulated, to develop improvements in the estimation technique. The advantages of simulated data are that the original model coefficients are known and that any desired degree of noise from zero up can

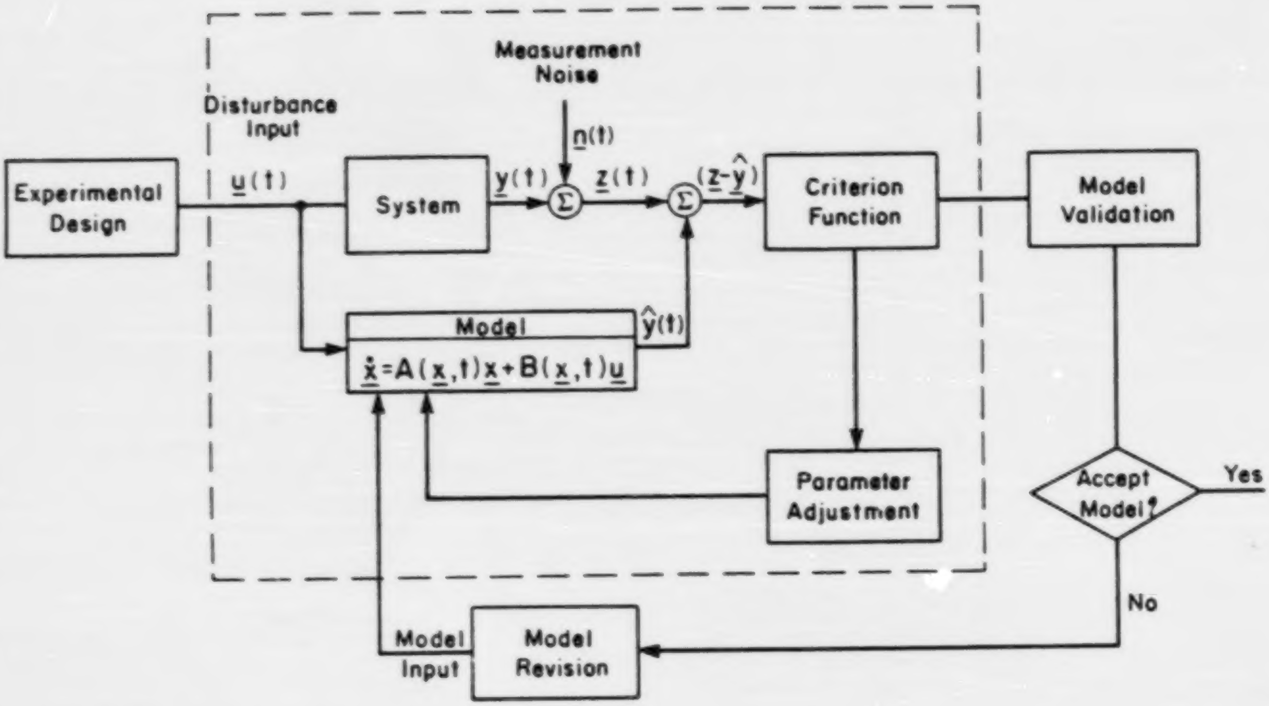
Measurement Noise
Disturbance Input
n(t)
Experimental Design
u(t)
System
y(t)
z(t)
(z-ŷ)
Criterion Function
Model Validation
Model
ŷ(t)
ẋ=A(x,t)x+B(x,t)u
Parameter Adjustment
Accept Model?
Yes
No
Model Input
Model Revision

Figure L.1 System identification - parameter identification concept. Standard state-space matrix notation is used.

be superimposed on the model response. Unfortunately, results comparable to those in ref. L.1 have proved difficult to obtain. Attempts to use the program with data from the circular track met with no success, in spite of promising results obtained with moderately noisy simulated data from aircraft dynamics. At this point nonlinear simulation programs based on simplified cushion geometries were developed. Instead of the static hysteresis linear viscous damping was used in the simulation to reduce the number of system nonlinearities. The simulations gave noiseless data to facilitate program debugging and evaluation. Acceptable results were obtained for a two conical cell cushion model subjected to a very small amplitude oscillation only if the cushion capacitance was neglected. Similarly the process converged for one case of very small amplitude oscillation with the HSL skirt model when the cushion capacitance was neglected. Subsequent attempts to use the simulations with even minor variations in the input disturbance met with no success.

Maine and Iliff, [L.3] have stated that

> "Probably the most difficult part of parameter estimation is to straddle the fine line between models too simple to adequately represent the system and too complicated to be identifiable. There is no conservative position on this issue; excesses in either direction can be fatal."

Many of the problems in our first attempts resulted from using a model that was at once too simple and too complex. The model was too simple in that it used a linear constant coefficient model for the dynamics; as discussed in Appendix I the nonlinearities of hysteresis, of the footprint area function, and of the flow area function are strong, and the latter two in particular produce large state dependent changes in the linear dynamics coefficients of the vehicle. The model was too complex in that, as originally used, it included 5 orders for the dynamics, 2 for pitch, 2 for heave, and 1 for the pneumatic capacitance. The success, albeit marginal, of the parameter estimation when capacitance was not included indicated that it might not be important in the dynamics of the circular track vehicle. Thus the parameter estimation problem could be simplified by eliminating the capacitive order and thereby removing the associated parameters.

The next phase of the project was to determine the nature of the parameter nonlinearities and whether or not the capacitance is important for vehicle dynamics in the range of operating conditions of interest. Ideally the capacitance question could be resolved from flight test data, but current criteria for evaluating the system order [L.4 to L.12], have not been developed to the point where practical application is straightforward, and in any case a large amount of computer time would be required to implement and develop them. Additionally, the estimation of hysteresis parameters is also very computationally intensive. At present the best techniques involve random search techniques, [L.13], and are not adapted to multivariable systems. Consequently an alternative approach was adopted. That approach is to develop fully validated dynamics models, which can then be used to develop parameter estimation techniques. To that end models of the dynamics of the circular track vehicle were synthesized. The models incorporate an extension of the detailed geometric theory, [L.1], for the HSL skirt and are for different system orders. This approach has the benefit that orders due to capacitance, and/or, inertia of the air in the fan ducting can be switched on and off and the outputs for different order systems compared for different input disturbances. In addition the geometric theory can be used to determine the forms of the nonlinearities in the dynamic system parameters.

At the present time the geometric theory functions giving the HSL skirt dynamics parameters have been developed. They are presented in Appendix J. The dynamics theory for a cushion with the HSL skirt has also been developed. Some preliminary results of the dynamics with an inelastic skirt are given in Appendix I. These and others not presented there indicate that the duct inertia and the capacitance are not important for initial condition type disturbances in pitch for vehicles the size of the 2m x 4m planform circular track vehicle, or the 1.2m x 2.4m laboratory model.

REFERENCES - APPENDIX L

L.1 Sullivan, P. A., et al, "Research into Air Cushion Stability: 1979 Report", Transportation Development Centre, Transport Canada, Montreal, TP 3109, Jan. 1982.

L.2 Taylor, L. W. and Iliff, K. W., "Systems Identification Using a Modified Newton-Raphson Method - A Fortran Program", National Aeronautics and Space Administration TN D-6374, May 1972.

L.3 Maine, R. E. and Iliff, K. W., "Identification of Dynamic Systems - Theory and Formulation", National Aeronautics and Space Administration Reference Publication 1138, Feb. 1985.

L.4 Akaike, Hirotugu, "Canonical Correlation Analysis of Time Series and the Use of an Information Criterion", System Identification: Advances and Case Studies, Edited by Raman K. Mehra and Dimitri G. Lainiotov, Academic Press, 1976.

L.5 Rissanen, J., "Minimax Entropy Estimation of Models for Vector Processes", System Identification: Advances and Case Studies, Edited by Raman K. Mehra and Dimitri G. Lainiotov, Academic Press, 1976.

L.6 Shibata, Ritei, "Selection of the Order of an Autoregressive Model by Akaike's Information Criterion", Biometrica, Vol. 63, No. 1, 1976, pp. 117-126.

L.7 Rissanen, J., "Modeling by Shortest Data Description", Automatica, Vol. 14, 1978, pp. 465-471.

L.8 Rissanan, J., "Consistent Order-Estimates of Autoregressive Processes by Shortest Description of Data", Analysis and Optimization of Stochastic Systems, University of Oxford, 1978.

L.9 Rissanan, J., "Shortest Data Description of Order Estimates in ARMA-Processes", International Symposium on Systems Optimization and Analysis, No. 14, Rocquencourt, Dec. 11-13, 1978. Edited by A. V. Balakrishnan, M. Thona, A. Bensoussan, J. L. Lions.

L.10 Schwarz, Gideon, "Estimating the Dimension of a Model", The Annals of Statistics, Vol. 6, No. 2, 1978, pp. 461-464.

L.11 Fine, Terrence, Hwang, William, "Consistent Estimation of System Order", IEEE Transactions on Automatic Control, Vol. AC24, No. 3, 1979, pp. 387-402.

L.12 Hannan, E. J., "The Estimation of the Order of an ARMA Process", The Annals of Statistics, Vol. 8, No. 5, 1980, pp. 1071-1081.

L.13 Andronikan, A., Bekey, G. A., and Masri, S. F., "Identification of Nonlinear Hysteretic Systems Using Random Search", Sixth IFAC Symposium on Identification and System Parameter Estimation Preprints, Arlington, VA, June 7-11, 1982.

APPENDIX M: ON THE ROLE OF PNEUMATIC CAPACITANCE IN ACV DYNAMICS AND ITS MODELLING (P. A. Sullivan and T. A. Graham)

NOMENCLATURE

Roman

C_c	cushion capacitance = $V_c/\gamma P_a$ for a fixed cushion volume
C_{Fi}	coefficients in fan law
g	acceleration due to gravity
h	height of vehicle centre of gravity above datum
h_c	height of cushion volume
h_w	disturbance height
L	reference length of craft, usually overall length
ℓ_w	disturbance wavelength
M	mass of craft
P_a	absolute atmospheric pressure
p_c	cushion gauge pressure
Q	volume flux
R	whirling arm radius
S_a	cushion support area
t	time
T	atmospheric temperature
U	forward speed of vehicle
V_c	volume of cushion
W	vehicle weight

Greek

γ	ratio of specific heats of air
λ	scale ratio = L_m/L_f
ϕ	angle subtended by model at centre of whirling arm facility

ρ_a	atmospheric density
θ	pitch angle of model

Subscripts

f	full scale
m	model scale

M.1 Introduction

Although analytical investigations of ACV dynamics have been pursued for over two decades it seems that the role played by the air compressibility in the basic cushion volume, which for low cushion pressures is modelled as a pneumatic capacitance, is unclear or controversial. For example, although its key role in destabilizing heave dynamics was pointed out by Ribich and Richardson in 1968 [M.1], as recently as 1984 it was omitted from a nonlinear analysis of the effect of ducting on cushion dynamics by Matsuo and Matsuo [M.2], on the grounds "the cushion pressure is small", and by Swift and Lebel [M.3] because "of the large leakage of ACV's". Doctors [M.4], in a numerical investigation of the nonlinear pitch-heave dynamics of a two-chamber model moving over waves concluded that significant compressibility effects occurred only at the higher wave encounter frequencies. He quoted results for craft as long as 40 m. More recently, at UTIAS, a detailed analytical model of the pitch-heave dynamics of the uncompartmented segmented skirt that is the subject of the present Contract [Appendix I] has indicated that it is not significant for a 2.44 m long model but certainly is for a vehicle twenty times as long (see Figures I.8 and I.9). Yet this analysis showed that this particular cushion configuration is subject to a combined pitch-heave instability which occurs when the cushion capacitance is omitted.

For analytical purposes, a safe approach might be to retain it, but this philosophy has two problems. The first is that it can create computationally stiff systems and cause attendant numerical difficulties. In an attempt to use response matching system identification procedures in the analysis of ACV flight data obtained from a 1000 kg model, retention of capacitance created serious convergence difficulties [M.4]. Also in general ACV dynamics can be very nonlinear and quite complex, so that even for numerical simulations, simplification is highly desirable. Unfortunately, nothing appears to be available in the open literature which can be used as a guide or criterion for assessing the importance of capacitance in particular cases.

A related question, the subject of this Appendix, is: if important, how can capacitance be scaled for model test? Therein lies a difficulty which appears to have been first noticed by Lavis, Bartholomew and Jones [M.5], who noted that if λ is the ratio of model size to full scale size, then scaling requires the model capacitance to be smaller by the ratio λ^2. If no special allowance is made and the model cushion volume is geometrically similar to that of the full scale vehicle, the cushion volume will be smaller in proportion to λ^3, so that the model capacitance given by $C_c = V_c/\gamma P_a$ will be too small by the ratio λ. Lavis et al [M.5] advocated testing in a wind tunnel in which the atmospheric pressure can be controlled to compensate for this effect. The problem of scaling capacitance has also been discussed by Richardson [M.6] who used a "physical" argument based on the "aeroelasticity triangle" first proposed by Collar [M.7] to show that, by altering the effective acceleration due to gravity, capacitance could be scaled. This he proposed to achieve by using a whirling arm facility.

In Section M.2 we develop scaling requirements by using the Pi-theorem of dimensional analysis. This reproduces the results obtained by Richardson [M.6] but indicates that the suggestion of Lavis et al will not work. In Section M.3, the implications for scaling model tests are discussed, and a solution is suggested.

M.2 Conditions for Scaling of Pneumatic Capacitance

The approach adopted here is a variation of that described by Mantle [M.8]. To be as specific as possible, consider the problem investigated in Appendix I, the pitch-heave dynamics of an uncompartmented, segmented skirt cushion operating over a rigid surface. To derive basic scaling requirements for a laboratory model, assume for simplicity that the vehicle is forced to move over solid waves of length ℓ_w and height h_w, and that the skirt is an inelastic massless membrane. Then inspection of the differential equations shows that the pitch angle θ and heave height h depend on the following variables:

$$\theta,\ h = f(t;\ L,\ W,\ g,\ \rho_a,\ C_c,\ U,\ \ell_w,\ h_w,\ C_{F0},\ C_{F1},\ C_{F2},\ \ldots) \qquad (M.1)$$

In this equation, t is the independent variable, and the remaining quantities are parameters. Now for scaling a physical model test the list given in equation M.1 almost certainly excludes important parameters such as those controlling skirt flexibility and unsteady fan response. However, as with all scaling arguments based on the Pi-theorem, omission of important parameters does not invalidate scaling requirements deduced from equation M.1, it merely means that other constraints may have to be met.

Following the usual Pi-theorem argument, choose three parameters having independent dimensions as reference quantities. Mantle chooses ρ_a, L and V as reference quantities, but here because we wish to consider the case of zero forward motion, we choose ρ_a, L and W. Note that the vehicle mass M cannot be used since, with D{ } denoting "dimensions of", $D\{M\} = D\{\rho L^3\}$. Then the Pi-theorem guarantees that equation M.1 can be replaced by

$$\theta,\ \bar{h} = (\bar{t};\ \bar{g},\ \bar{C}_c,\ \bar{V},\ \bar{\lambda}_w,\ \bar{h}_w,\ \bar{C}_{F0},\ \bar{C}_{F1},\ \bar{C}_{F2},\ \ldots) \qquad (M.2)$$

where the bar indicates a dimensionless equivalent, that is, for example $\bar{g} = g/(\rho_a^{\alpha} L^{\beta} W^{\gamma})$, where the exponents α, β, γ are chosen to make $D\{g\} = D\{\rho_a^{\alpha} L^{\beta} W^{\gamma}\}$. According to the Pi-theorem, the dynamics of a full scale vehicle can be predicted from a geometrically similar small scale model if the model test parameters are chosen to make the nondimensional quantities in (M.2) the same as those for the full scale vehicle. For the present discussion, the key groups are:

(i) gravity scaling:

$$\bar{g} = \frac{\rho_a g L^3}{W} \tag{M.3}$$

(ii) capacitance scaling:

$$\bar{C}_c = \frac{C_c W}{L^5} \tag{M.4}$$

(iii) forward speed scaling:

$$\bar{U} = UL(\rho_a/W)^{1/2} \tag{M.5}$$

Note that condition (M.3) is equivalent to the cushion density parameter $\bar{p}_c = p_c/(\rho_a gL)$ used by Mantle [M.8] since $W = p_c S_a$ and $S_a \propto L^2$. Also condition (M.5) is effectively the Froude scaling requirement; this is demonstrated below.

To explore the consequences of these constraints suppose that, in addition to specifying model size, the test facility can control both g and ρ_a. Then with the subscripts "f" indicating full scale vehicle and "m" the test model, scaling requires

$$\frac{W_m}{\rho_{am} g_m L_m{}^3} = \frac{W_f}{\rho_{af} g_f L_f{}^3} \tag{M.6}$$

$$\frac{C_{cm} W_m}{L_m{}^5} = \frac{C_{cf} W_f}{L_f{}^5} \tag{M.7}$$

$$U_m L_m (\rho_{am}/W_m)^{1/2} = U_f L_f (\rho_{af}/W_f)^{1/2} \tag{M.8}$$

Hence gravity scaling requires the weight of the test model to be such that

$$\frac{W_m}{W_f} = \frac{\rho_{am} g_m}{\rho_{af} g_f} \lambda^3 \tag{M.9}$$

The capacitance of the model cushion must then satisfy

$$\frac{C_{cm}}{C_{cf}} = \frac{W_f}{W_m} \lambda^5 = \frac{\rho_{af} g_f}{\rho_{am} g_m} \lambda^2 \tag{M.10}$$

if both W and C_c are to be simultaneously scaled. Finally, equations (M.8) and (M.9), when combined, give the condition on the model velocity

$$\frac{U_m}{U_f} = \left(\frac{g_m}{g_f} \lambda\right)^{1/2} \tag{M.11}$$

which is the usual Froude scaling for the ratio of inertial to gravitational forces.

It should be noted that the scaling rules embodied in equations (M.9) to (M.11), are independent of the choice of variables used as reference quantities. This is guaranteed by the Pi-theorem, but to convince the skeptic, use the vehicle mass M, its reference scale length L, and the acceleration due to gravity g as reference quantities; then equation (M.2) is replaced by

$$\theta,\ h^* = f(t^*;\ \rho^*,\ C_c^*,\ U^*,\ \lambda_w^*,\ h_w^*,\ C_{F0}^*,\ \ldots) \tag{M.12}$$

where the asterisk indicates a second set of nondimensional quantities. Then we have, for the quantities of interest, ρ^*, C_c^*, U^*

$$\rho^* = \frac{\rho L^3}{M} = \frac{\rho g L^3}{W} = \bar{g} \tag{M.13}$$

$$C_c^* = \frac{C_c M g}{L^5} = \bar{C}_c \tag{M.14}$$

$$U^* = \frac{U}{\sqrt{Lg}} = \bar{U}(W/\rho g L^3)^{1/2} = \frac{\bar{U}}{\bar{g}} \tag{M.15}$$

from which it is obvious that the same scaling rules are derived.

To explore the consequences of these rules consider first the straightforward case for which ρ and g are the same at model and full scale. The equation (M.9) gives $W_m \propto L_m{}^3$ and, since the cushion footprint area $S_{am} \propto L_m{}^2$, the cushion pressure p_c for the model must satisfy $p_{cm} \propto L_m$. According to equation (M.10), $C_{cm} \propto L_m{}^2$ but since, in a geometrically scaled model $C_c \propto V_c \propto L_m{}^3$, a fundamental contradiction exists. This is the difficulty first pointed out by Lavis et al [M.5]. Its implications can be illustrated by the following argument. In a model, the region corresponding to the payload-carrying part of the full scale vehicle does not usually serve any specific purpose, so that it might be used as additional volume for capacitance. Since $V_c = h_c S_a$, and h_c is an effective or average cushion depth, and since $S_a \propto L^2$, then capacitance scaling amounts to the requirement that $h_{cm} = h_{cf}$.

The existence of mutually contradictory scaling requirements deduced from arguments based solely on dimensional considerations is a well known problem in facing model testing; perhaps the best known example is the requirements of Froude and Reynolds number for towing tank tests of ship models, the first requiring $U_m \propto L_m^{1/2}$ and the second $U_m \propto L_m^{-1}$. As in the ship testing case, it signals the need for a deeper understanding of the physics in order to develop satisfactory model testing procedures.

The conclusion that the capacitance scaling problem cannot be resolved by altering the atmospheric density follows immediately from equation (M.10) and the definition of C_c:

$$\frac{C_{cm}}{C_{cf}} = \frac{V_{cm}}{\rho_{am}RT_{am}} \cdot \frac{\rho_{af}RT_{af}}{V_{cf}} = \frac{\rho_{af}g_f}{\rho_{am}g_m}\lambda^2 \qquad (M.16)$$

or

$$\frac{V_{cm}}{V_{cf}} = \frac{g_f}{g_m} \cdot \frac{T_{am}}{T_{af}}\lambda^2 \qquad (M.17)$$

Since in most experiments $T_{am} = T_{af}$ approximately, equation (M.17) indicates that simply altering atmospheric pressure or density does not alleviate the capacitance scaling problem. We make no attempt to reconcile this conclusion with the recommendation of Lavis et al [M.5], since they gave no argument to justify their claim.

This discussion is concluded by observing that the suggestions of Richardson [M.6] are confirmed. Consider ρ_a fixed, but g variable. Then for a geometrically scaled cushion volume with $C_c \propto \lambda^3$ from equation (M.10),

$$\frac{C_{cm}}{C_{cf}} = \lambda^3 = \frac{g_f}{g_m}\lambda^2\frac{L_m{}^2}{L_f{}^2} \quad \text{or} \quad \frac{g_m}{g_f} = \lambda^{-1} \qquad (M.18)$$

Then equation (M.11) combined with (M.18) gives

$$\frac{U_m}{U_f} = 1 \qquad (M.19)$$

which is the scaling requirement proposed by Richardson.

M.3 Implications for Model Testing

Scaling capacitance by using a whirling arm facility has a severe limitation. It is pointed out by Richardson [M.6] that, if the effective gravity is provided by rotating the model on an arm of radius R, then with $g_m = U_m{}^2/R$,

$$Fr_m \triangleq \frac{U_m}{\sqrt{L_m g_m}} = (R/L_m)^{1/2} = \phi_m^{-1/2} \tag{M.20}$$

where ϕ_m is the angle subtended by the model at the centre of the arm. This places a lower limit on test speed. Richardson suggests $\phi = 30°$ is a practical maximum, which requires $Fr = 1.38$ as a lower limit. For a vehicle such as the Bell Aerospace Voyageur, $L_f = 23.3$ m, so that this imposes a minimum equivalent full scale speed $U_f = 17.8$ m/sec or 39.7 mph; this vehicle has a quoted normal maximum service speed of 42 mph. For a low speed platform such as the 24.7 m ACIB, the minimum speed is 40.8 mph; obviously one can rule out the use of a whirling arm for all but a very restricted range of conditions, and other methods of scaling capacitance have to be sought.

As suggested above, the most straightforward way to achieve this goal might be to add extra volume in the unused portions of the superstructure of the model. For a large model such as the UTIAS Circular Track Test Vehicle, this might be a feasible approach. Thus Voyageur has a maximum overall height to the top of its payload of about 4.5 m and a cushion depth of about 1.22 m. Hence with $h_{cm} = h_{cf}$, $\lambda = 3.67$, and this corresponds to a model length of 6.35 m; at the upper limit of what could be tested on the 43 m diameter UTIAS Facility.

Another solution might be to incorporate pressure-dependent cushion volume, perhaps by carefully selecting the flexibility of the model skirts themselves, or by incorporating a specially designed flexible volume. Recall that a mathematical model of cushion dynamics always includes a cushion flow conservation equation of the form

$$C_c \frac{dp_c}{dt} + \frac{dV_c}{dt} = Q_c - Q_a \tag{M.21}$$

In this equation, the second term accounts for the air stored by virtue of changes in cushion volume, and this volume change is caused by both vehicle motion and skirt deformation under the action of p_c. That is, for the case in Appendix I, $V_c = V_c(h, \alpha, p_c)$ so that

$$\frac{dV_c}{dt} = \frac{\partial V_c}{\partial h}\dot{h} + \frac{\partial V_c}{\partial \alpha}\dot{\alpha} + \frac{\partial V_c}{\partial p_c}\dot{p}_c \tag{M.22}$$

Hence equation (M.22) can be rearranged to give

$$(C_c + \frac{\partial V_c}{\partial p_c})\dot{p}_c + \frac{\partial V_c}{\partial \alpha}\dot{\alpha} + \frac{\partial V_c}{\partial h}\dot{h} = Q_c - Q_c \qquad (M.23)$$

where $C_{CE} = C_c + \partial V_c/\partial p_c$ is an equivalent capacitance. It is the term C_{CE} which can be adjusted to scale capacitance by incorporating a flexible volume.

Obviously a major consideration is that the inertia of any flexible or moving elements in this device be so low that the response to pressure fluctuations is essentially quasistatic. One possible way to achieve this is to use a cylinder of the lightweight elastomer-fabric materials that are used to model skirts. However, the tests described in Appendix B show that these materials can have highly nonlinear and frequency-dependent stiffness properties, so that care would have to be exercised to ensure that, for the frequencies and pressure fluctuations of interest, the errors introduced were below acceptable levels. A second approach might be to use a bellows system in which the extension is controlled by helical or other mechanical springs. Since such springs can be designed to have linear stiffness properties over a wide range of deflections, the uncertainties associated with the use of the elastic properties of elastomer-fabrics would be eliminated, but care would have to be taken to ensure that the inertia is small enough to meet the quasistatic response requirement.

Examples of scaling capacitance to the UTIAS Circular Track Facility are now presented for the Bell Voyageur and the ACIB. The practical minimum weight of the track test vehicle in its present configuration is about 900 kg. For a Voyageur with planform dimensions of 23.3 m by 11.2 m and fully loaded at 52 tonnes, equation (M.9) gives $\lambda = 0.259$ and model planform dimensions of 6.02 m × 2.90 m. This is significantly larger than the current planform dimensions of 4.08 m × 2.03 m, but is nevertheless feasible. The capacitance of Voyageur is estimated to be about 2.14×10^{-3} m^3/Pa, which according to equation (M.10) is equivalent to 1.43×10^{-4} m^3/Pa for $\lambda = 0.259$. The capacitance available from the scaled cushion volume is about 3.761×10^{-5} m^3/Pa. The extra capacitance can be supplied by a bellows having a total cross-sectional area of 2.4 m^2 and a total spring stiffness of 548 N/cm. Assuming that this stiffness is divided amongst a large number of springs and that the moving piston is made from a lightweight composite material sandwich panel, a total mass of the moving parts of the bellows of 2 kg is feasible. Thus the natural frequency of such a system is about 26.3 Hz. To avoid phase distortion, one would probably limit maximum model test frequencies to about one half of this, which means for testing a Voyageur model at 9.55 m/sec (21.4 mph), which corresponds to a full scale speed of 18.8 m/s (42 mph), a frequency limit of 13 Hz corresponds to ℓ_w no shorter than 12% of craft length. If the extra capacitance was to be attained by using a cylinder of the 0.12 mm thick urethane coated nylon fabric used for the tests described in Appendix B, then the uniaxial tension test data of table B.1 indicates that a diameter and length of about 1.5 m and 0.73 m respectively would be required.

For the 24.7 m × 24.7 m planform ACIB operating at its minimum weight of 175 tonnes, equation (M.9) indicates that for a model mass of 900 kg the planform dimensions would be 4.26 m × 4.26 m. The capacitance of the ACIB is estimated to be 5.94×10^{-3} m^3/Pa, and when scaled to the above model size, the required capacitance is 1.76×10^{-4} m^3/Pa. The capacitance available from the basic model volume is about 3.27×10^{-5} m^3/Pa, so that the extra to be supplied by the bellows requires $A_p = 0.8$ m^2 and the total spring stiffness of 44.6 N/cm. For a panel weight of 0.75 kg, the natural frequency of the system is 12.3 Hz. Assuming a maximum full scale speed of 10 knots or 5.15 m/sec, which scales to 2.13 m/sec for the Circular track model, and maximum desirable frequencies of 6 Hz, disturbances having ℓ_w down to 8% of model length could be investigated. The bellows travel Δw required for the two cases described above are 11 cm and 105 cm respectively, and if $A_p = 1.6$ m^2 then $\Delta w = 5$ cm and 53 cm.

A key requirement is that the device must have enough variable volume to accommodate the pressure fluctuations generated by vehicle motion. The simulations given in Appendix I can be used to obtain an estimate of the amount required. For the bellows system, the total panel movement Δw required is

$$\Delta w = \Delta V_p / A_p = \frac{1}{A_p} \int \frac{\partial V_c}{\partial p_c} \frac{dp_c}{dt}\, dt = \frac{1}{A_p} \frac{\partial V_c}{\partial p_c} \quad \Delta p_c \qquad (M.24)$$

where V_p and A_p are bellows volume and cross-sectional area respectively. The integral is taken over that part of a cycle for which $\dot{p}_c$ does not change sign. Assuming a pitch-heave resonse to an initial condition disturbance, the model in Appendix I predicts that the maximum Δp is about 0.6 kPa for a vehicle having M = 900 kg and a 4 m by 2 m planform. If the Voyageur scale model experiences a smilar fluctuation then, with $A_p = 1.2$ m^2 the total travel Δw required is 5.0 cm, and for $A_p = 2.4$ m^2, $\Delta w = 2.5$ cm. A more severe test would be a heave oscillation involving skirt-ground contact leading to flow shut-off. Appendix C shows that pressures may peak at values as high as 6.5 p_{ce}, in which case for $A_p = 1.2$ m^2, $\Delta w = 43$ cm and for $A_p = 2.4$ m^2, $\Delta w = 22$ cm. These are probably too large to be acceptable in practice.

M.4 Concluding Remarks

The main thrust of the present discussion is that, of the three proposals for scaling cushion capacitance ACV testing discussed here, only a facility of the type and size of the UTIAS Circular Track has any realistic prospect of scaling cushion capacitance at representative operating conditions. Of course the question as to whether scaling of cushion capacitance is actually required still seems to be undecided, and perhaps an important step in developing adequate procedures for scale model ACV tests should be the clarification of that question.

REFERENCES - APPENDIX M

M.1 Ribich, W. A. and Richardson, H. H. "Dynamic Analysis of Heave Motion for a Transport Vehicle Fluid Suspension", Dept. of Mechanical Engineering, Massachusetts Institute of Technology, Boston, Report DSR-76110-3, Jan. 1967.

M.2 Matsuo, H. and Matsuo, K., "A Nonlinear Analysis of the Cushion Stability of Slowly Oscillating ACV's", Journal of Aircraft, Vol. 21, No. 7, Jul. 1984, pp. 539-541.

M.3 Swift, M. R. and Lebel, D., "Heave Motion of Air Cushion Vehicles", Journal of Hydronautics, Vol. 12, No. 2, Apr. 1978, pp. 85-87.

M.4 Doctors, L. J., "Effect of Air Compressibility on the Nonlinear Motion of an Air Cushion Vehicle Over Waves", School of Mechanical and Industrial Engineering, University of New South Wales, Sydney, Report Nav/Arch 76/1, Jan. 1976.

M.5 Lavis, D. R., Bartholomew and Jones, J. C., "Response of Air Cushion Vehicles to Random Seaways and the Inherent Distortion in Scale Models", Journal of Hydronautics, Vol. 8, No. 3, Jul. 1979, pp. 83-94.

M.6 Richardson, J. R., "A Scaling Technique for Hovercraft Models", Hovercraft Unit, National Physical Laboratory, G. B. Rept. No. 13, Jul. 1970.

M.7 Collar, A. R., "The Expanding Domain of Aeroelasticity", Journal of the Royal Aeronautical Society, Vol. 50, Aug. 1946, pp. 616-636.

M.8 Mantle, P., "Air Cushion Craft Development", U.S. Navy, David W. Taylor Naval Ship Research and Development Center, Bethesda, Report DTNSRDC-80/012, Jan. 1980, pp. 61-65.

APPENDIX N: RESPONSE FUNCTIONS IN THE LIMIT OF ZERO FREQUENCY FOR OVERWATER STABILITY ANALYSIS (M. J. Hinchey)

N.1 Introduction

In the limit of zero frequency, the frequency response functons developed in Appendix F should show the water-surface to respond quasi-statically to cushion pressure variations. This fact is used below to check the water surface-pressure interaction model.

N.2 Spatially Averaged Deflection

The response function is

$$\frac{\overline{\Delta\eta(i\omega)}}{\Delta p(i\omega)} = N(i\omega) = A + Bi \tag{N.1}$$

where

$$A = \frac{2}{\rho_W g\,\nu b}\left[\frac{1}{2\pi}\left[C_e + \mathrm{Ln}(2\nu b) + g(2\nu b)\right] - \sin\nu b\,\cos\nu b\right] \tag{N.2.1}$$

and

$$B = \frac{2}{\rho_W g\,\nu b}\sin^2\nu b \tag{N.2.2}$$

In the limit as ω tends to 0, ν tends to 0. So B reduces to

$$B = \frac{2}{\rho_W g\,\nu b}(\nu b)^2 = \frac{2}{\rho_W g}\,\nu b = 0 \tag{N.3}$$

Also, in the limit as ω tends to 0, $g(2\nu b)$ reduces to (see [N.1])

$$-\left(C_e + \mathrm{Ln}(2\nu b) - \frac{\pi}{2}\sin 2\nu b\right) \tag{N.4}$$

So A reduces to

$$A = \frac{+2}{\rho_W g\,\nu b}\left[-\sin\nu b\,\cos\nu b + \frac{\sin 2\nu b}{4}\right] = \frac{-1}{\rho_W g}$$

Thus

$$\frac{\overline{\Delta\eta(io)}}{\Delta p(io)} = -\frac{1}{\rho_W g} \tag{N.5}$$

which is the expected result.

N.3 Deflection at Lip

The response function is

$$\frac{\Delta\eta_{lip}(i\omega)}{\Delta p(i\omega)} = M(i\omega) = X + Yi \qquad (N.6)$$

where

$$X = -\frac{1}{\pi\rho_w g}\{3\pi - 2si(\nu b) - 4f(\nu b)\cos\nu b - 4\pi\sin^2\nu b$$

$$- 2\sin(2\nu b)[Ci(2\nu b) - Ci(\nu b)] + 2\cos(2\nu b)[si(2\nu b) - si(\nu b)]\} \qquad (N.7.1)$$

and

$$Y = \frac{4}{\rho_w g}\sin\nu b\cos\nu b \qquad (N.7.2)$$

In the limit as ω tends to 0, Y reduces to

$$Y = \frac{4}{\rho_w g}\nu b = 0 \qquad (N.8)$$

Also in the limit as ω tends to zero [N.1]

$$si(\nu b) \text{ tends to } -\frac{\pi}{2}$$

$$f(\nu b) \text{ to } [C_e + Ln(\nu b)]\nu b + \frac{\pi}{2} = \frac{\pi}{2}$$

$$[Ci(2\nu b) - Ci(\nu b)] \text{ to } Ln(2\nu b) - Ln(\nu b) = Ln(2)$$

$$[si(2\nu b) - si(\nu b)] \text{ to } 0 \qquad (N.9)$$

So X reduces to

$$X = -\frac{1}{\pi\rho_w g}[3\pi + \pi - 2\pi - 0 - 0 + 0]$$
$$= -\frac{2}{\rho_w g} \qquad (N.10)$$

Thus

$$\frac{\Delta\eta_{1ip}(i0)}{\Delta p(i0)} = -\frac{2}{\rho_w g} \qquad (N.11)$$

which is the expected result.

N.4 Sine and Cosine Integral Functions of Ref. N.1

$$f(z) = Ci(z)\sin z - si(z)\cos z$$

$$g(z) = -Ci(z)\cos z - si(z)\sin z$$

$$si(t) = Si(t) - \frac{\pi}{2}$$

$$Si(z) = \sum_{n=0}^{\infty} \frac{(-1)^n z^{2n+1}}{(2n+1)(2n+1)!}$$

$$Ci(z) = C_e + Lnz + \sum_{n=1}^{\infty} \frac{(-1)^n z^{2n}}{3n(2n)!}$$

REFERENCES - APPENDIX N

N.1 Abramowitz, M., and Stegun, I., Handbook of Mathematical Functions with Formulas, Graphs, and Mathematical Tables, Dover, New York, 1972.

APPENDIX 0: PRESSURE-WATER SURFACE INTERACTION COMPUTED BY LAMB (M. J. Hinchey)

0.1 Pressure-Water Surface Interaction

For the pressure oscillation

$$\Delta p = \frac{P}{2b} e^{i\omega t} \qquad |x| < b$$

Lamb gives

$$g\rho_w \Delta\eta = -\frac{P}{b} e^{i(\omega t - \kappa b)} \cos\kappa x + \frac{\kappa P e^{i\omega t}}{\pi b} \int_0^\infty \frac{e^{-mb}\cosh(mx)}{m^2 + \kappa^2} dm \qquad (0.1)$$

where

$$\kappa = \frac{\omega^2}{g} \qquad (0.2)$$

This becomes

$$\frac{\Delta\eta}{\Delta p} = \frac{-2e^{i\kappa b}}{g\rho_w} \cos\kappa x + \frac{2\kappa}{\pi g\rho_w} \int_0^\infty \frac{e^{-mb}\cosh(mx)}{m^2 + \kappa^2} dm \qquad (0.3)$$

Note that this is symmetric with respect to x.

0.2 Spatially Averaged Deflection

By definition, this is

$$\overline{\Delta\eta} = \frac{1}{2b} \int_{-b}^{+b} \Delta\eta dx \qquad (0.4)$$

or, using Equation (0.3),

$$\frac{\overline{\Delta\eta}}{\Delta p} = -\frac{2(\cos\kappa b - i\sin\kappa b)}{bg\rho_w} \frac{\sin\kappa b}{\kappa} + \frac{\kappa}{b\pi g\rho_w} \int_{-b}^{+b} \int_0^\infty \frac{e^{-mb}}{m^2 + \kappa^2} \cosh(mx) dm dx \qquad (0.5)$$

where

$$\int_{-b}^{+b} \cosh(mx)dx = \frac{2\sinh(mb)}{m} \qquad (0.6)$$

and

$$\sinh(mb) = \frac{e^{mb} - e^{-mb}}{2} \tag{0.7}$$

This gives

$$\frac{\overline{\Delta\eta}}{\Delta p} = - \frac{2(\cos\kappa b - i\sin\kappa b)}{bg\rho_w}\,\frac{\sin\kappa b}{\kappa} + \frac{2\kappa}{b\pi g\rho_w}\int_0^\infty \frac{e^{-mb}\,\frac{\sinh(mb)}{m}}{m^2 + \kappa^2}\,dm \tag{0.8}$$

0.3 Water Deflection at Lip

By definition, this is

$$\Delta\eta_{x=+b} + \Delta\eta_{x=-b} \tag{0.9}$$

or, using Equation (0.3)

$$\frac{\Delta\eta_{lip}}{\Delta p} = - \frac{4(\cos\kappa b - i\sin\kappa b)}{g\rho_w}\cos\kappa b + \frac{4\kappa}{\pi g\rho_w}\int_0^\infty \frac{e^{-mb}\,\frac{\cosh(mb)}{m}}{m^2 + \kappa^2}\,dm \tag{0.10}$$

where

$$\cosh(mb) = \frac{e^{mb} + e^{-mb}}{2} \tag{0.11}$$

0.4 Quasi-Static Limiting Cases: Spatially Averaged Deflection

In the limit as ω tends to 0 and b tends to 0, Equation (0.8) reduces to

$$\frac{\overline{\Delta\eta}}{\Delta p} = - \frac{2\cos\kappa b\sin\kappa b}{g\rho_w\kappa b} + \frac{2\kappa}{b\pi g\rho_w}\int_0^\infty \frac{e^{-mb}\,\frac{\sinh(mb)}{m}}{m^2 + \kappa^2}\,dm$$

$$= - \frac{2\kappa b}{g\rho_w\kappa b} + \frac{2\kappa}{\pi g\rho_w}\int_0^\infty \frac{dm}{m^2 + \kappa^2}$$

$$= - \frac{2}{g\rho_w} + \frac{2\kappa}{\pi g\rho_w}\,\frac{\pi}{2\kappa}$$

$$= - \frac{1}{g\rho_w} \tag{0.12}$$

0.5 Water Deflection at Lip

In the limit as ω tends to 0 and b tends to 0, Equation (0.10) reduces to

$$\frac{\Delta\eta_{lip}}{\Delta p} = -\frac{4\cos^2\kappa b}{g\rho_w} + \frac{4\kappa}{\pi g\rho_w}\int_o^\infty \frac{e^{-2mb}\cosh(mb)}{m^2+\kappa^2}\,dm$$

$$= -\frac{4}{g\rho_w} + \frac{4\kappa}{\pi g\rho_w}\left[\int_o^\infty \frac{dm}{2(m^2+\kappa^2)} + \int_o^\infty \frac{e^{-2mb}}{2(m^2+\kappa^2)}\,dm\right]$$

$$= -\frac{4}{g\rho_w} + \frac{4\kappa}{\pi g\rho_w}\left[\frac{\pi}{4\kappa} + \frac{\pi}{4\kappa}\right]$$

$$= -\frac{2}{g\rho_w} \qquad (0.13)$$

APPENDIX P. PRELIMINARY INVESTIGATION OF SEGMENT-WATER SURFACE INTERACTIONS

(M. J. Hinchey, P. A. Sullivan and C. Walsh)

NOMENCLATURE

Roman

$A(k)$, $B(k)$, $C(k)$	quantities in dispersion relationship
g	acceleration due to gravity
H_a	initial air gap before air flow is turned on
h_a	air gap when air is flowing
h_w	water depth when air is flowing
k	wave number = $2\pi/\lambda$
p_a	atmospheric pressure
p_s	suction pressure
Q	volume flux per unit width
T	surface tension of air-water interface
U_a	mean air gap velocity
x, y	coordinates defined in Figure P.4

Greek

λ	wavelength of disturbance
ρ_a	air density
ρ_w	water density
ω	radian frequency of disturbance

P.1 Introduction

During attempts to measure a discharge coefficient for air escaping under flexible skirt segments partially immersed in water, as part of the work on overwater stability described in Appendix F, it was observed that the segments would almost always oscillate. This oscillation occurred at a frequency of about 5 Hz, and observation of the process by using a motion picture camera showed that it was associated with an instability of the interface between the air escaping under the segments and the surrounding water. The apparatus used for these observations is depicted in Figure P.1. Three segments were mounted in a small water tank 1.25 m long, 0.45 m high and 0.18 m wide. Figure P.2 is a sequence of motion picture photographs taken at approximately 64 frames/sec. These clearly show the air-water interface instability, which commences at or near the bottom tip of the segments, propagates in the direction of the air flow, and grows rapidly enough to cause contact between the segment and the water wave. This process is violent enough to cause a vertical motion of the entire segment.

This phenomenon suggested the existence of a second source of the instability observed by Fowler [P.1]. The present Appendix describes an exploratory investigation into the phenomenon. For analytical simplicity, only the highly simplified geometry depicted in Figure P.3 is investigated.

Considerable theoretical and experimental work has been done on wind generated water surface instabilities. Early theoretical work assumed irrotational or potential air and water flows [P.2, P.3]. The more recent studies have dealt with the effects of viscosity and are based on Orr-Sommerfeld type equations [P.4, P.5]. The major effects of viscosity are to cause the air flow to induce a highly sheared surface drift in the water near its surface and to introduce a critical viscous layer in the interior of the air flow which can be very destabilizing [P.6, P.7]. As yet, we do not know if viscosity is needed for adequate modelling of the present problem. However, an inviscid analysis is the simplest that demonstrates a dynamic instability and it seems appropriate to examine this as a candidate mechanism.

P.2 Analysis

The stability analysis applied here is the well-known Kelvin-Helmholtz problem for the dynamic instability at an interface between two coflowing inviscid incompressible fluids. For this analysis, as depicted in Figure P.4, the channel is assumed to be infinitely long in the flow direction, and the details are given in [P.2]. In addition to the inviscid assumption the flow is assumed to be irrotational and the unperturbed streams are assumed to be uniform in the y-direction. The analysis considers the behaviour of a small perturbation in the form of a single sinusoid. For example the velocity potential perturbation is assumed to have the form

$$\phi(x, y, t) = \mathrm{Re}\left\{\psi(y)e^{i(\omega t-kx)}\right\} \qquad (P.1)$$

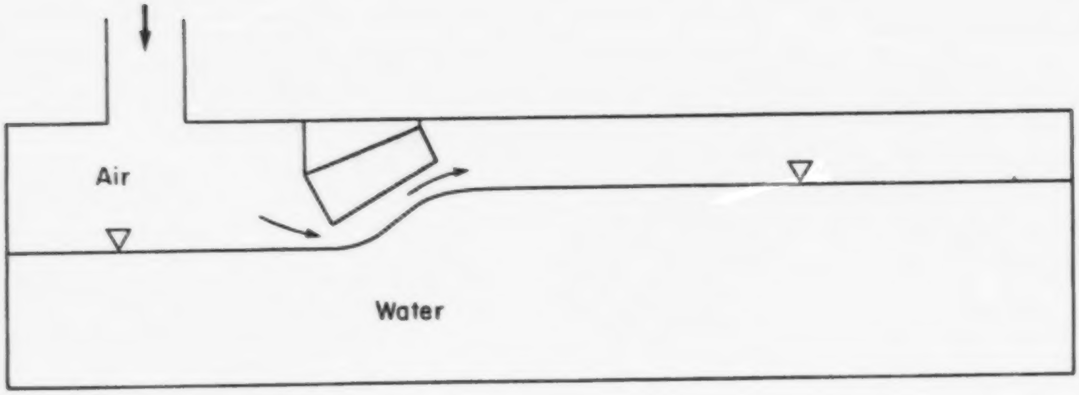

Figure P.1 Diagram of water tank used to observe oscillation of segments.

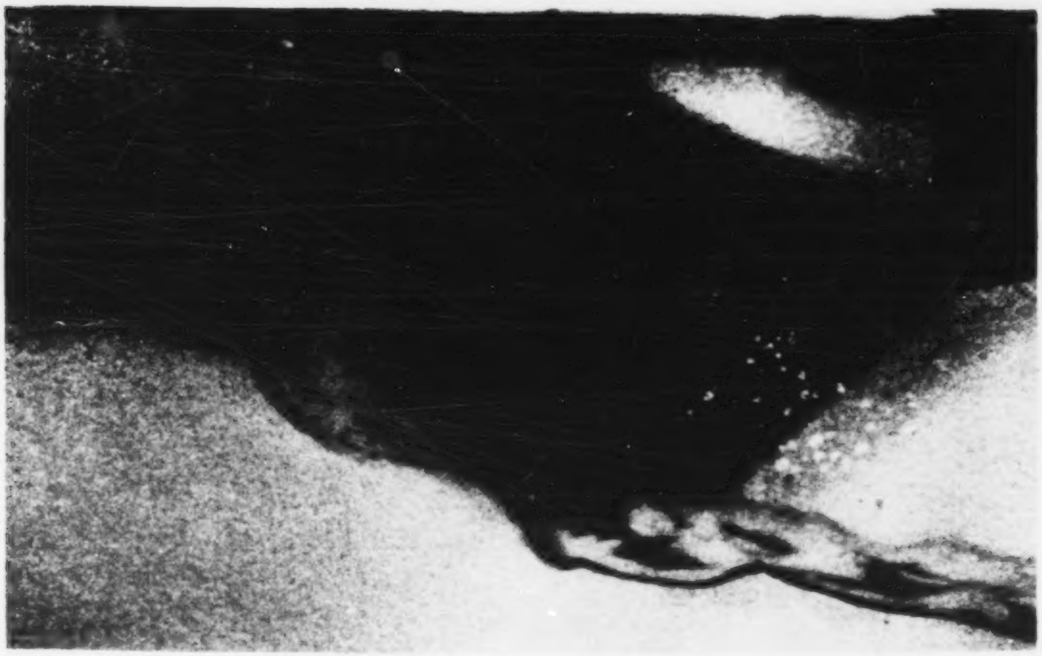

Figure P.2 (a)

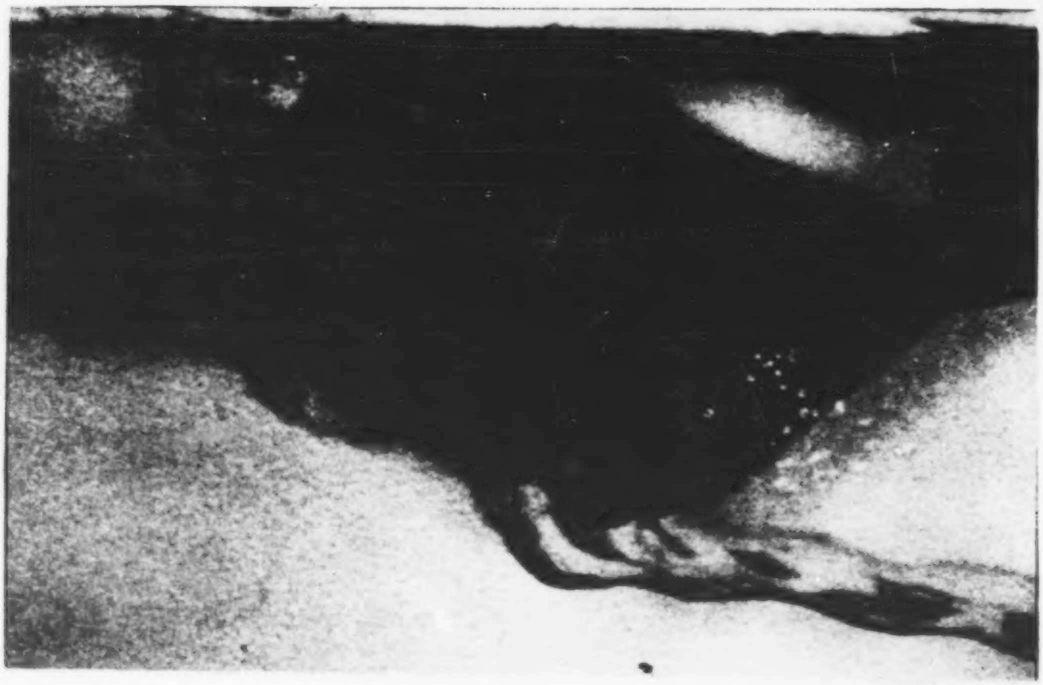

Figure P.2(b)

Figure P.2(a)-(d) Sequence of photographs taken by motion picture camera of air-water surface instability.

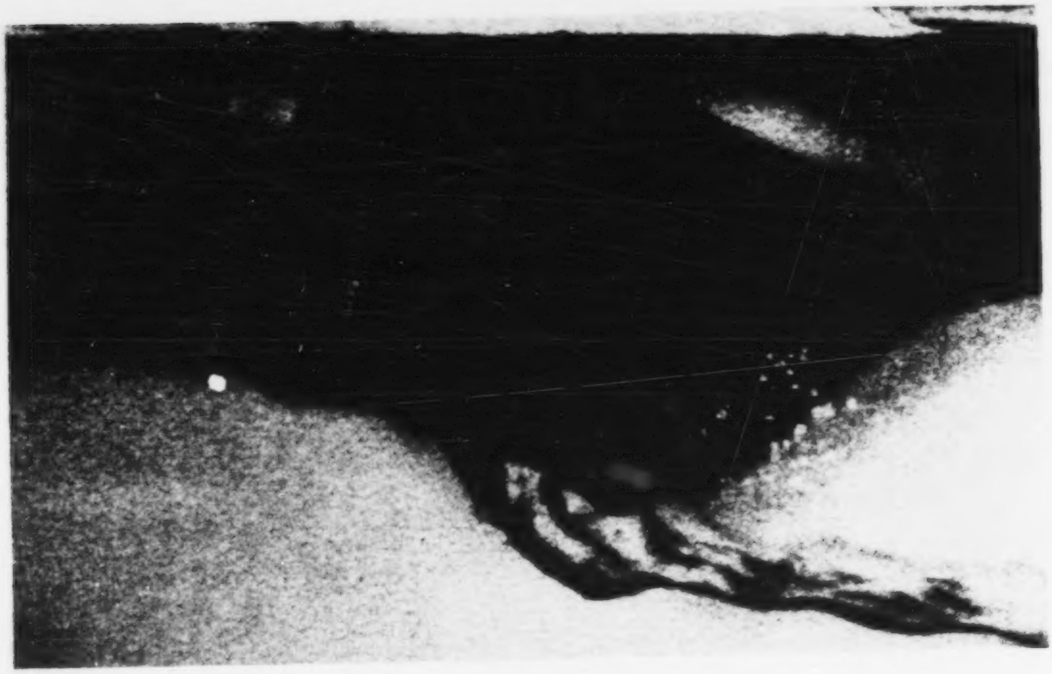

Figure P.2(c)

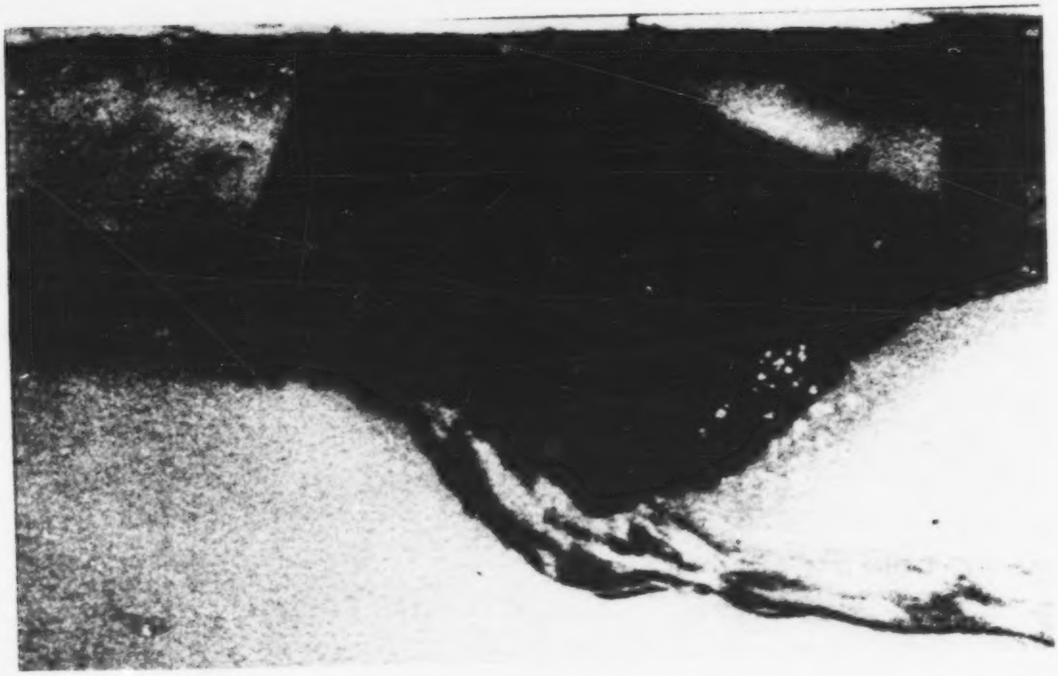

Figure P.2(d)

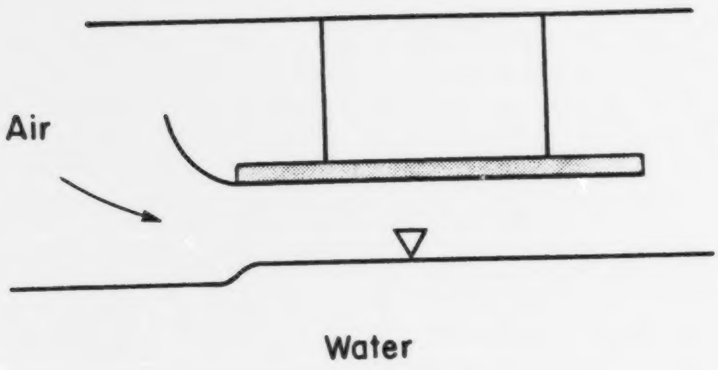

Figure P.3 Simplified experimental model

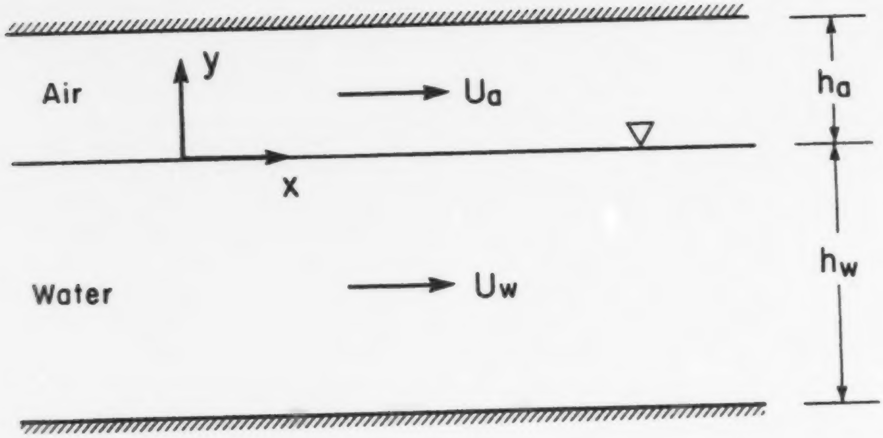
y
Air
U_a
x
Water
U_w
h_a
h_w

Figure P.4 Geometry used in analysis.

In this expression, ω is the radian frequency and k the wave number, given by $k = 2\pi/\lambda$. With a corresponding expression for the pressure perturbations, substitute these into Laplace's equation, the interface conditions of continuity of pressure and normal component of velocity, and the upper and lower boundary conditions of zero normal component of velocity to obtain, after appropriate algebra, an expression for ω as a function of k. This is the "dispersion relationship" for this problem, and it has the form

$$\omega(k) = -\frac{B \pm (B^2 - 4AC)^{1/2}}{2A} \tag{P.2}$$

where A, B, C are functions of k and the parameters in the problem. For $U_w = 0$, which is the case of interest here

$$A(k) = \frac{\rho_a}{k \tanh kh_a} + \frac{\rho_w}{k \tanh kh_w} \tag{P.3.1}$$

$$B(k) = \frac{-2\rho_a U_a}{\tanh kh_a} \tag{P.3.2}$$

$$C(k) = \rho_a g - \rho_w g^* + \frac{\rho_a U_a{}^2 k}{\tanh kh_a} \tag{P.3.3}$$

where ρ_a and ρ_w are the air density and water density respectively, k is the wave number, ω is its frequency, h_a and h_w are the air channel and water channel depths respectively, g is the acceleration due to gravity and

$$g^* = g + \frac{k^2 T}{\rho_w} \tag{P.4}$$

where T is the local surface tension at the water surface.

The functional forms for A, B and C, equations P.3, show that for any given k, as U_a increases from zero, B^2-4AC is at first positive so that two real values of ω exist, with the lesser ω corresponding to waves tending upstream. Eventually, as U_a increases a critical value U_{ac} is reached at which B^2-4AC becomes negative and the two roots of the dispersion relationship form a complex conjugate pair $\omega_r \pm \omega_i$ where w_r and ω_i are both positive. The assumed functional form (P.1) then becomes,

$$\phi = \mathrm{Re}\{\psi(y)e^{-\omega_i t}\, e^{i(\omega_r t-kx)}\}$$

$$\phi = \mathrm{Re}\{\psi(y)e^{+\omega_i t}\, e^{i(\omega_r t-kx)}\} \qquad \text{(P.5)}$$

The second of these corresponds to a wave that is growing in time and is therefore unstable. This corresponds to

$$U_{ac}^2(k) = \frac{1}{k}\{\frac{\tanh kh_w}{\rho_w} + \frac{\tanh kh_a}{\rho_a}\}(g^*\rho_w - g\rho_a) \qquad \text{(P.6)}$$

Equation (P.6) is known as the "flutter boundary" for U_a as a function of k and signals the onset of instability at a given k. In general equation (P.6) will have a particular value of k for which U_{ac} is a minimum, so that a most critical wave number usually exists.

Another critical speed U_{ao} is the so-called "stasis speed" thought to have significance in relation to a flow limitation phenomenon discussed below. This is the condition $U_{ao}(k)$ at which the upstream tending waves associated with one of the roots of the dispersion relation (P.2) begin to be swept downstream. This corresponds to $C(k) = 0$ which gives

$$U_{ao}^2 = \frac{1}{k}\frac{\tanh kh_a}{\rho_a}(g^*\rho_w - g\rho_a) \qquad \text{(P.7)}$$

Comparison of equations (P.6) and (P.7) shows that since $k > 0$, $U_{ao} < U_{ac}$.

Consider now the experimental apparatus depicted in Figure P.5, which was used in some of the experiments. Air is drawn into the tank from atmosphere at pressure p_a by a suction pressure p_s. Initially the gap between the plate and water surface is H_a. As p_s decreases the air is accelerated into the gap between the plate and water surface. For the portion of the channel at which the water surface is parallel to the plate, according to Bernoulli's law

$$U_a = [2(p_a - p_s)/\rho]^{1/2} \qquad \text{(P.8)}$$

However since $p_s < p_a$ the water surface under the plate rises and the gap decreases to $h_a < H_a$. With no water motion the pressure distribution in the water is hydrostatic, and

$$\rho_w g(H_a - h_a) = (p_a - p_s) \qquad \text{(P.9)}$$

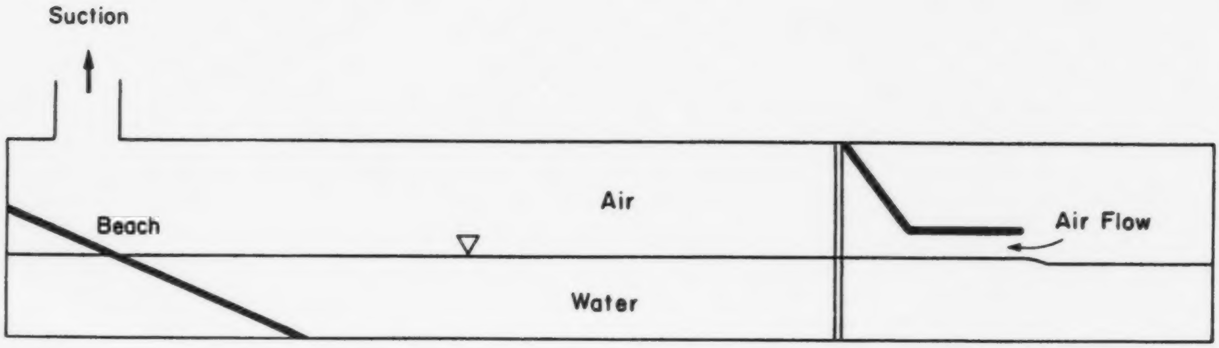
Suction
Air
Beach
Air Flow
Water

Figure P.5 Suction water tank used in experiments.

The volume flux that is obtained from these opposing tendencies of increasing U_a and decreasing h_a is given by

$$Q = (2(p_a - p_s)/\rho_a)^{1/2}[H - (p_a - p_s)/(\rho_w g)] \qquad (P.10)$$

Differentiation of this result with respect to p_s shows that there is a value of p_s or U_a for which no further increase in Q can occur and Q_a becomes independent of any further decrease in p_s. This occurs when $h_a = 2/3\ H_a$ and

$$U_a^2 \overset{\Delta}{=} U_{as}^2 = \frac{\rho_w}{\rho_a} g h_a \qquad (P.11)$$

This flow limitation is analogous to gasdynamic choking of a convergent-divergent nozzle. In the long wave limit, $k \to 0$, and with the assumption that $\rho_w >> \rho_a$, equation (P.6) reduces to (P.11). Thus equation the static speed is related to flow limitation.

Figure P.6 gives plots of equations (P.6), (P.7) and (P.11) for two cases: (i) fluid depths held constant, and (ii) allowed to vary as a result of the pressure variation that occurs during an experiment. The static boundary is indistinguishable from the flutter boundary, and the latter has a most critical k of about 15. For the depths varying case the critical velocity is significantly lower than that corresponding to flow limitation according to the static theory.

P.3 Experimental Models

To study experimentally an approximation to the simplified geometry, the segments in the small water tank were replaced by a flat plate as shown in Figure P.3. A rounded entrance section was installed to prevent a possible flow separation or vena contracta effect. However, results obtained without it were basically the same as those obtained with it. The plate was also given a very small inclination to ensure that waves which did form would appear just downstream of the entrance. Some experiments were also performed using the tank shown schematically in Figure P.5. This second tank is approximately 230 cm long, 38 cm high, and 7.5 cm wide. This is much longer; also the air is sucked under the plate from atmosphere and not blown under to atmosphere. In both series of experiments the air flow Q was measured using an ASME standard orifice plate. The flow speed U at any given longitudinal position was assumed to be given by

$$V = \frac{Q}{A} \qquad (P.12)$$

where A, the flow area, was taken to be equal to the tank width times the local air gap.

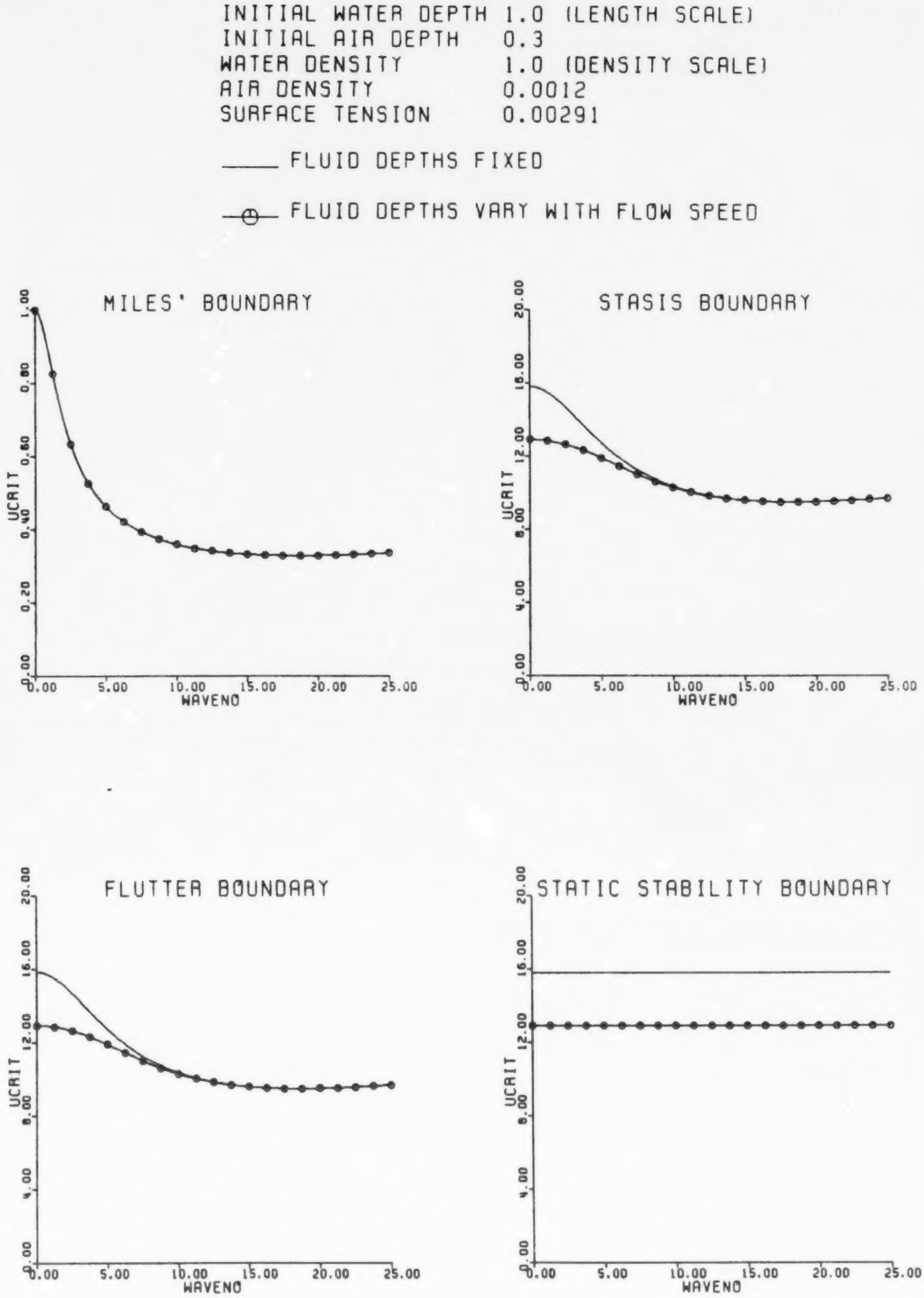

Figure P.6 Critical velocity as a function of wave number for representative geometry.

P.4 Results and Discussion

Stability results obtained from the two water tanks are presented in Figures P.7 and P.8. Those in Figure P.7 were obtained using the small tank while those in Figure P.9 were obtained using the suction tank. For a range of entrance gaps the air flow was increased until waves formed. The continuous curve in each figure is the flutter boundary while the dashed line is the static stability boundary. With the small tank, data could not be obtained for entrance gaps greater than 1.7 cm. For these gaps the air flow became turbulent just downstream of the entrance, the water surface became ruffled and the onset of wave generation was difficult to detect. This was not a problem for the suction tank where the air was sucked from atmosphere and thus relatively free of turbulence. Figure P.9 shows two photographs of the waves generated.

Experiments with an adjustable angle plate in the suction water tank showed that as the angle was increased instability with a well defined harmonic in time tended to disappear. The free surface tended to break up close to the edge of the plate and spray was formed. At moderate angles, for example around 45°, harmonic instability was still present. However, at 90° only a faint harmonic could be detected. The flow in the latter case appeared to be dominated by spray. These results suggest that water surface instabilities would be a problem for segment skirt systems but not for multicell tapered cone systems.

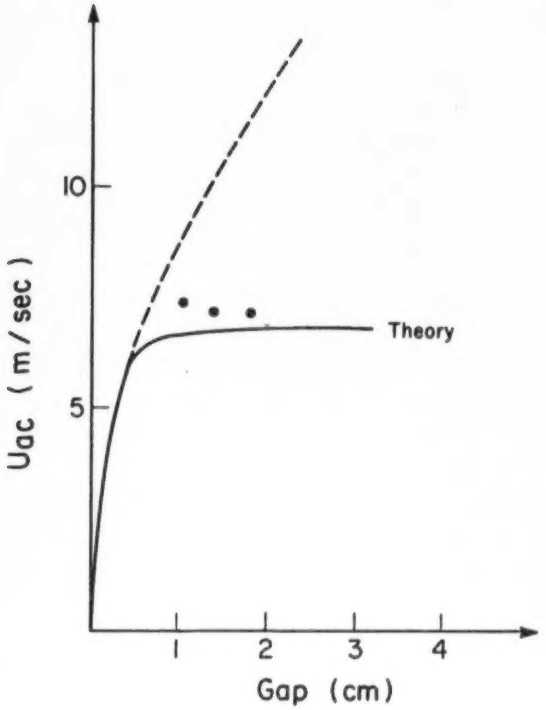

Figure P.7 Stability measurements from first water tank in which pressurized air is blown over the water.

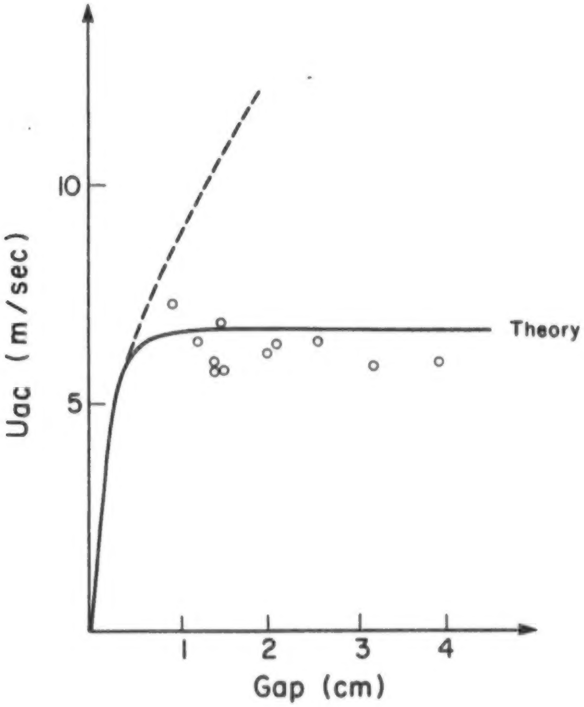

Figure P.8 Stability results from second water tank in which turbulence-free air is sucked over water surface.

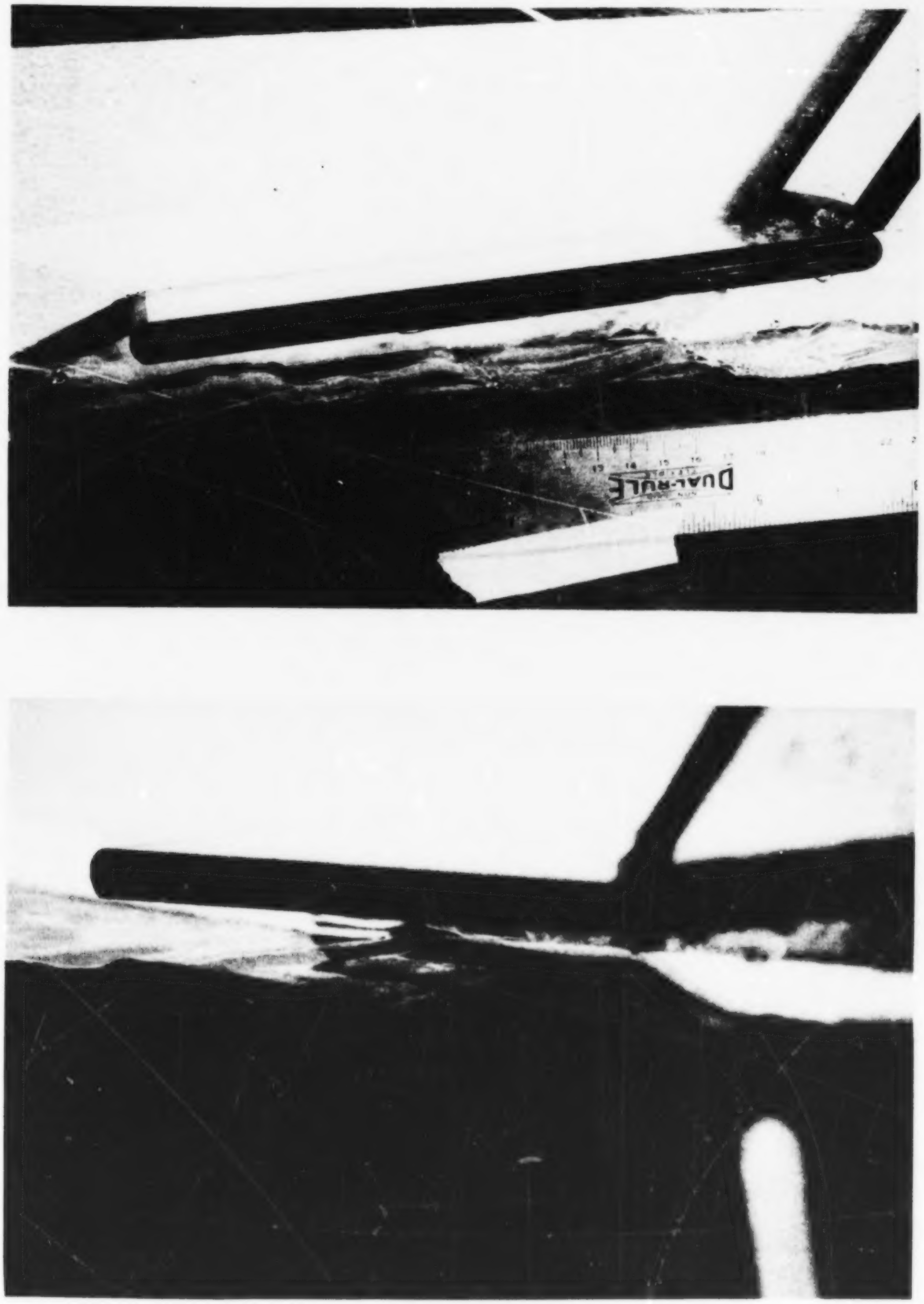

Figure P.9 Two photographs of instabilities observed in second water tank. In both cases the air flow is from left to right, and one can observe the increase in water height caused by the air pressure reduction at the entrance associated with its acceleration into the channel. In the upper photograph the instability occurs shortly after the channel entrance, and in the second the wave is further downstream.

REFERENCES - APPENDIX P

P.1 Fowler, H. S., "An Experiment on the Heave Oscillation of a Light Air Cushion Vehicle Over Water", Canadian Aeronautics and Space Journal, Vol. 26, No. 2, 1980, 92-96.

P.2 Lamb, H., Hydrodynamics, Dover, New York, 1945. See Arts. 267, 268.

P.3 Lighthill, M. J., Waves in Fluids, Cambridge University Press, Cambridge, 1978.

P.4 Miles, J. H., "On the Generation of Surface Waves by Shear Flows", Journal of Fluid Mechanics, Vol. 3, No. 2, 1957, pp. 185-204.

P.5 Valenzuela, G. R., "The Growth of Gravity-Capillary Waves in a Coupled Shear Flow", Journal of Fluid Mechanics, Vol. 76, No. 2, 1976, pp. 229-250.

P.6 Wu, J., "Laboratory Studies of Wind-Wave Interactions", Journal of Fluid Mechanics, Vol. 34, No. 1, 1968, pp. 91-111.

P.7 Wu, J., "Wind-Induced Currents", Journal of Fluid Mechanics, Vol. 68, No. 1, pp. 49-70.

APPENDIX Q: EFFECT OF SEGMENT GEOMETRY ON HEAVE DYNAMICS AND STABILITY

(P. A.Sullivan and J. E. Byrne)

NOMENCLATURE

Roman

A_b	area of base of vehicle
A_e	effective exit flow area
a_i, b_i	coefficients in flow function determined by regression
C_h	nondimensional equivalent hovergap
C_{QC}	$Q_e(\rho/2WA_b)^{1/2}$
C_{PC}	P_{ce}/P_a
h	cushion height
h_e	equivalent hovergap
L_p	peripheral length of base of vehicle, or cushion footprint
P_a	absolute atmospheric pressure
P_{ce}	cushion pressure at equilibrium
Q_e	flow through cushion

Greek

ρ	atmospheric air density

Q.1 Introduction

When an uncompartmented, segmented skirt is hovering at zero pitch and roll angle, in order to achieve static stability the bottom tips of the segments contact the ground. This implies that, for a certain range of vehicle heights, the cushion air escapes to atmosphere through gaps between the segments which are approximately triangular in shape. Hence, whereas for cushion geometries such as the conical cell used in the investigations described in Appendices B and C, the cushion exit flow area is linearly dependent on vehicle height, for segmented skirts the dependence on height is nonlinear. As the work described in Appendix C suggests, this nonlinearity might be expected to have large effects on dynamics. The purpose of the work described here is to explore this question.

The approach to the problem was basically the same as that used in the investigation of skirt material effects on the heave stability of a conical cell described in Appendix B. Measurements of the effect of cushion height h and cushion pressure p_c on cushion flow rates Q_e were obtained from the segmented skirt installed on the 2.44m × 1.22m planform cushion dynamics model. This data was then used to specify coefficients in an empirical formula for $Q_e = f(h, p_c)$, the so-called "flow function". The flow function was then incorporated into a mathematical model of the heave dynamics of a single plenum chamber fed by a duct from a constant pressure air source. Thus the mathematical model is identical to that used for the investigations of Appendix C with the exception that a different cushion exit flow relationship is used. The aim of the analysis was to examine both the linear stability characteristics and the limit cycle behaviour of unstable motion, with a view to obtaining an experimental confirmation in the UTIAS Sphere Facility, as was done for the work described in Appendices B and C. The skirt material used in the tests was the 0.10 mm thick urethane coated nylon fabric known to be free of static hysteresis (see Figure E.9).

Q.2 Determination of Segment Flow Function

Now the air escape process is believed to be orifice-like so that, if A_e is the effective or equivalent total flow area, one would expect

$$Q_e = A_e(h)\ (2p_{ce}/\rho)^{1/2} \tag{Q.1}$$

where A_e is a nonlinear function of h. In practice small skirt deformations due to variations in p_{ce} are expected so that $A_e = A_e(h, p_c)$. With L_p defined as a reference length of the cushion footprint, Equation (Q.1) can be rewritten in the nondimensional form

$$C_h \triangleq Q_e/[L_p h(2p_{ce}/\rho)^{1/2}] = h_e/h \tag{Q.2}$$

where h_e is an equivalent hovergap. Hence C_h is an equivalent nondimensional hovergap.

Figure Q.1 gives measured values of C_h obtained from the 2.44m × 1.22m planform model as a function of p_c for various values of h. To obtain this data the model was levelled with respect to the table over which it was hovering, and then locked to this height. The heights of reference points on the four corners of the model above the table were measured with a vernier height gauge, and the cushion height was taken to be the average of these four. Also, since the peripheral length of the cushion footprint is difficult to measure precisely, the peripheral length of the vehicle base, 7.32m, was used for L_p. The data shows that, for any given h, as p_c increases from zero, C_H at first decreases rapidly, but at a very low value of p_c it then begins to increase very slowly. Hence over the range of pressures of interest there is a weak, linear dependence on p_c. This confirms that the flow is essentially orifice-like. Note also that at h = 0.26721m, with the segments completely on the ground, there is a leakage flow which is perhaps as much as 20% of that corresponding to the segment tips just touching. This is attributed to leakage between the segments, particularly near their upper attachment points. The existence of this leakage does not, however, create a problem for analysis of the dynamics, since it is automatically included in the effective A_e. Finally it is thought that the rapid decrease in C_h near $p_c = 0$ is associated with deployment of the segments as they are first inflated, and thus merits no further consideration.

Figure Q.2 gives the dependence of C_h on h for four reference values of p_c, obtained from Figure Q.2 by interpolation, and extrapolation of the linear part in the case of $p_c = 0$. As expected, as h increases the dependence is highly nonlinear, until the tips of the segments leave the ground. The data in Figure Q.2 shows that the cushion height increases by about 12.2 mm as the segments make the transition from fully contacting to just touching. From Figure Q.1, at $p_c = 0.373$ kPa, C_h increases from 0.0056 to 0.0194. This corresponds to an increase in equivalent hovergap from 1.44 mm to 5.49 mm. Assuming that $h_e = 1.44$ mm accounts for the effect of air leaks between segments for all values of cushion height, and with the perimeter of the footprint estimated to be 5.848m, when the segments are just touching the ground the flow through the triangular areas between the segment bottom and ground corresponds to $\Delta h_e = 5.06$ mm and an effective discharge coefficient of about 0.41. Thus one effect of the segments on the flow and dynamics can be viewed as reduction in the effective discharge coefficient C_d.

For the investigations of the dynamics, the data of Figure Q.1 was modelled by a quadratic in cushion height and a linear dependence on p_c; that is the flow Q_a escaping to atmosphere was computed from

$$Q_a = L_p h(2p_c/\rho)^{1/2} \left[(a_0 + a_1 h + a_2 h^2)(1 + b_1 p_c)\right] \qquad (Q.3)$$

where the coefficients a_0, a_1, a_2, b_1 were obtained by standard regression techniques.

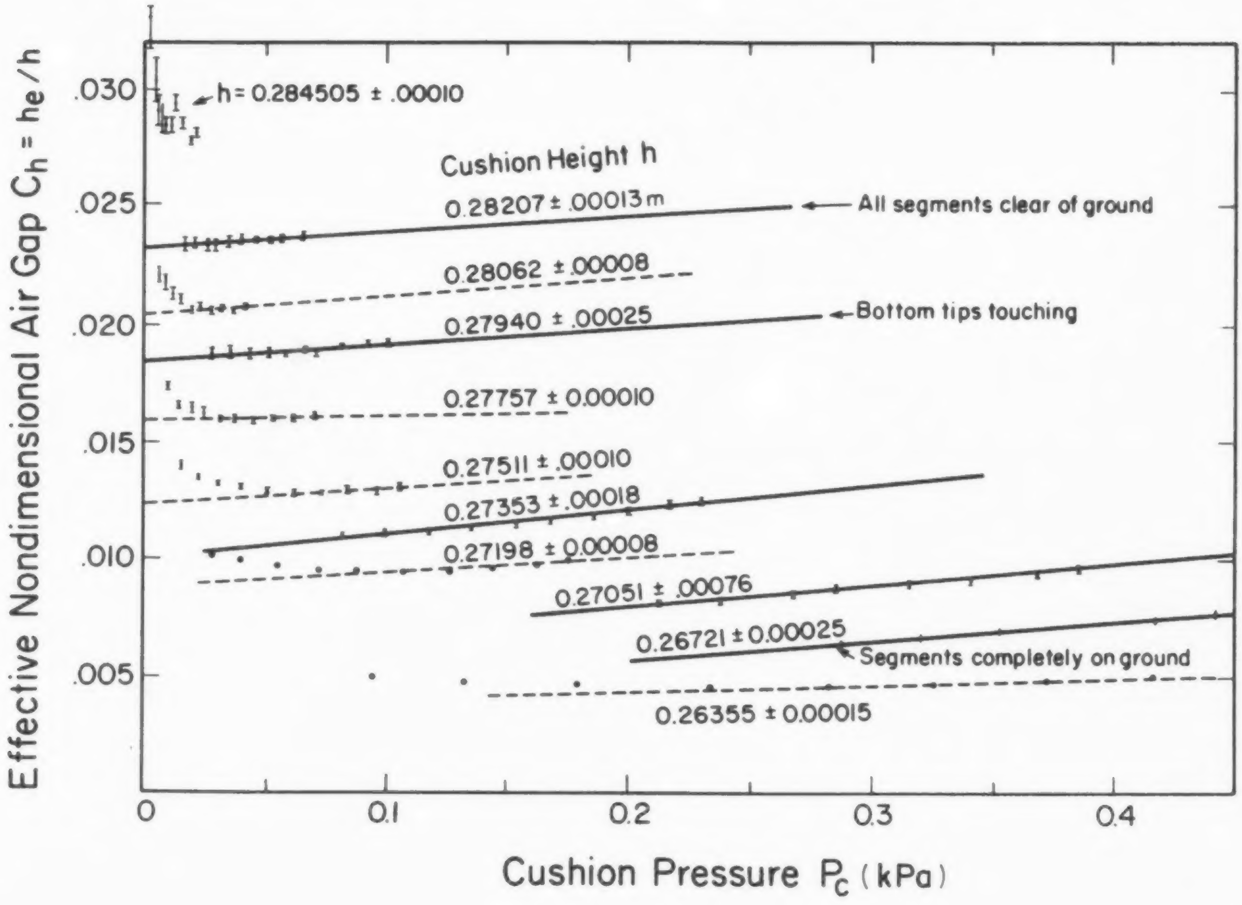

Figure Q.1 Effect of cushion pressure on effective air gap at various cushion heights.

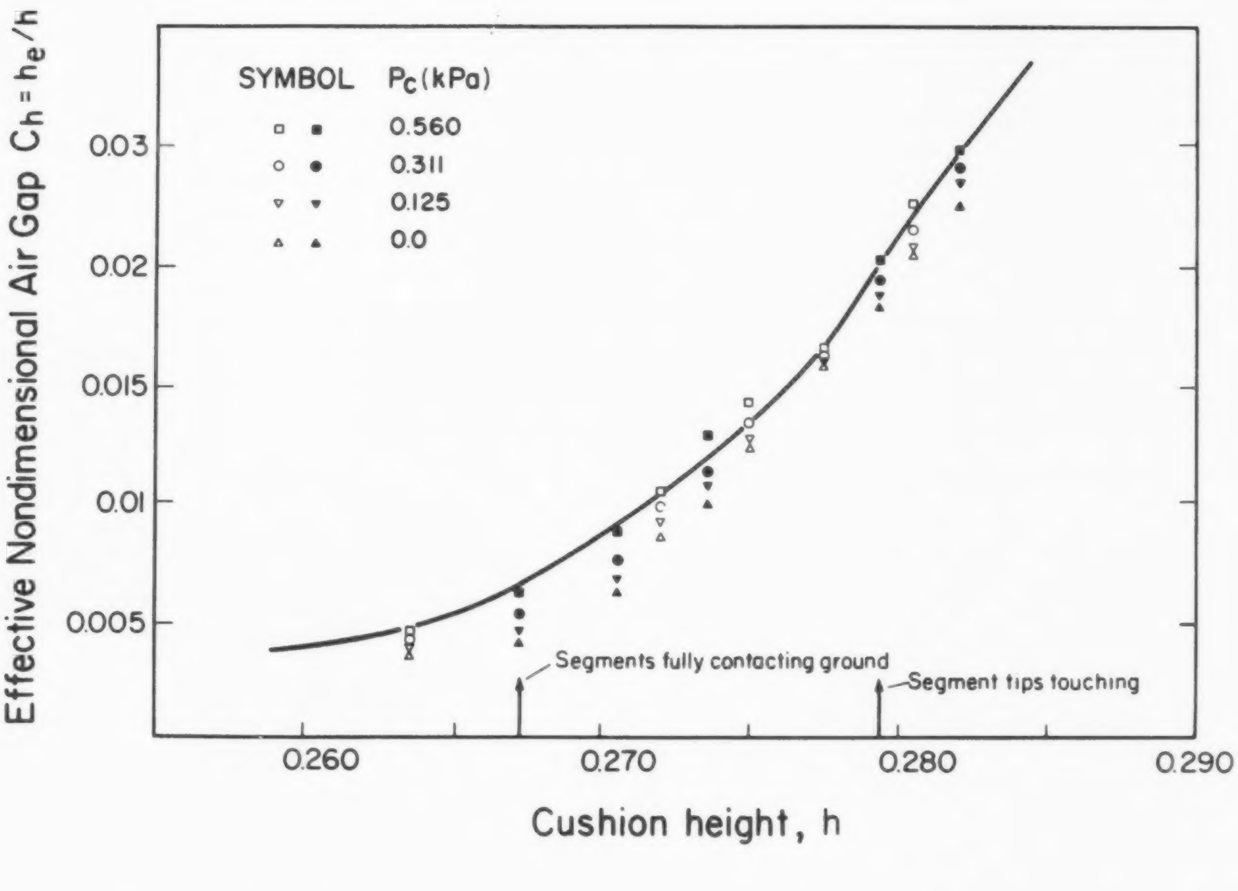

Figure Q.2 Effect of cushion height on effective air gap at various cushion pressures.

Q.3 Investigations of the Dynamics

Owing to lack of availability of suitable personnel, only a linear stability analysis was performed. The equations used in the analysis are those of Appendix C, Equations (C.1) and (C.4) to (C.8) with Equations (C.6) and (C.7) replaced by (Q.3). Linear stability boundaries were obtained by standard techniques.

Typical stability boundaries in terms of nondimensional cushion pressure, $C_{pc} = p_{ce}/p_a$, and nondimensional cushion flow $C_{QC} = Q_e[\rho_a/2WA_b]^{1/2}$ are given in Figure Q.3. Boundaries are given for the two duct lengths used in the Sphere Facility, and the boundaries for a rigid skirt having the same basic cushion volume are included for reference. Figure Q.4 gives the computed effect of discharge coefficient on the stability of a rigid cell for reference. At any given operating pressure p_c and equilibrium flow Q_e, the major effect of the segments is a large stabilization relative to the rigid skirt case, since the boundaries have been moved significantly to the left. The data in Figure Q.4 suggests that this stabilization may be a discharge coefficient effect. However the segmented skirt boundaries in Figure Q.3 appear to have become very insensitive to duct length, in contract to the rigid skirt data. Furthermore they display a feature not present in the rigid skirt behaviour. It has been shown [Q.1] that for a rigid skirt duct-plenum system the region of instability extends down to zero p_c. Namely, for a cushion hovering at a fixed weight and hence a fixed p_{ce}, as Q_e is lowered there is always a region of dynamic instability. In contrast, the computed boundaries for the segmented skirt imply that for C_{pc} below about 0.012 the cushion is stable down to zero Q_e. This is the opposite of an effect predicted and observed in the investigation of Appendix B but no explanation for it has to date been elicited.

Q.4 Discussion and Conclusion

A circular planform model was constructed for the Sphere Facility using segments from the model used to obtain the flow function data. A partial confirmation of the prediction of Figure Q.3 was obtained in that, for the maximum values of C_{pc} available at time, about 0.015, the model was found to be completely stable. Work on this model has been in abeyance, again owing to lack of suitable personnel.

Two main conclusions can be drawn. The first is that the flow function measurements have demonstrated that by simple modifications of the usual cushion exit flow law it is possible to incorporate their effect into dynamics analyses. The second is that the limited data presented here suggests that they can have a major effect on the dynamics.

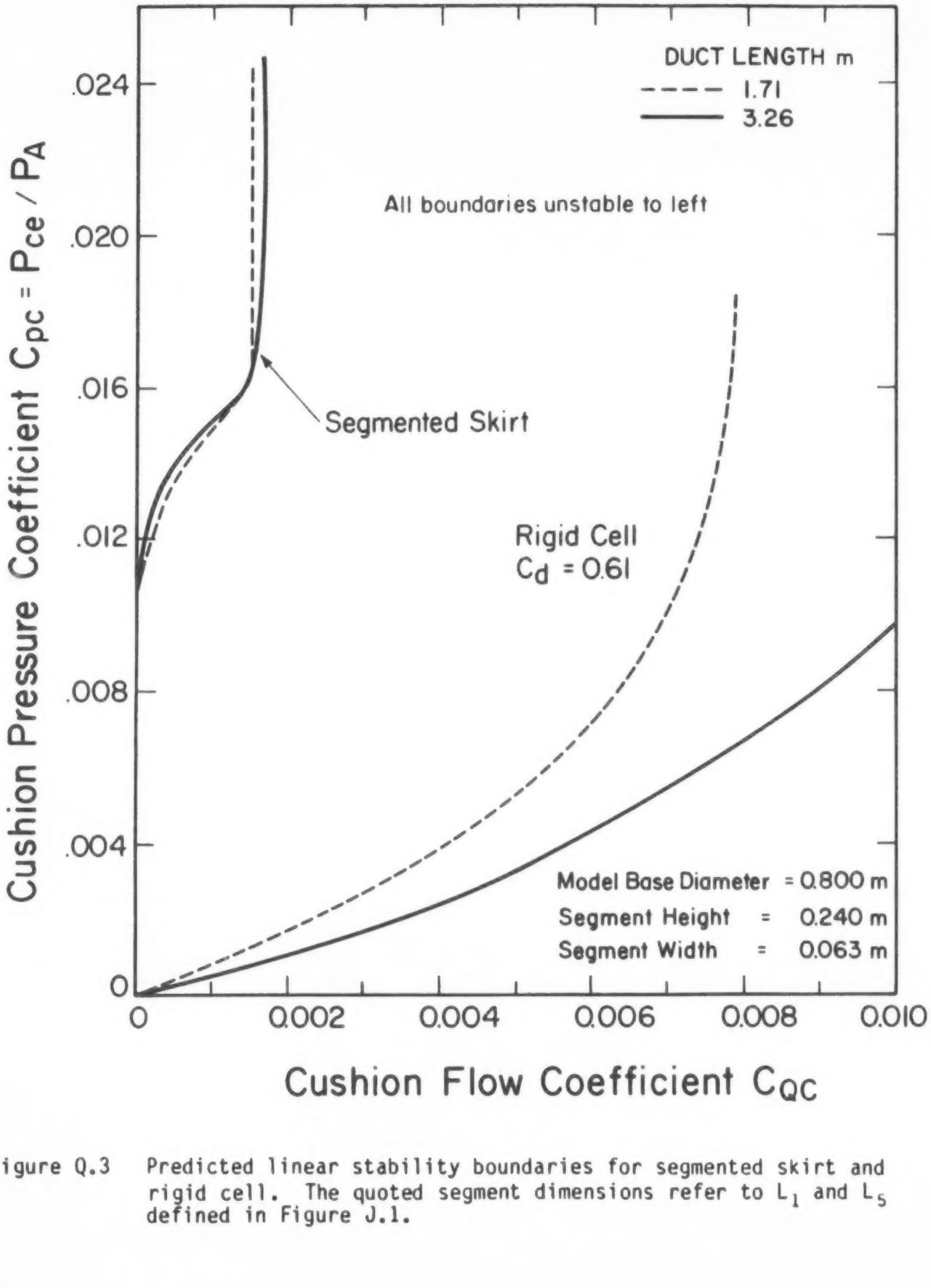

Figure Q.3 Predicted linear stability boundaries for segmented skirt and rigid cell. The quoted segment dimensions refer to L_1 and L_5 defined in Figure J.1.

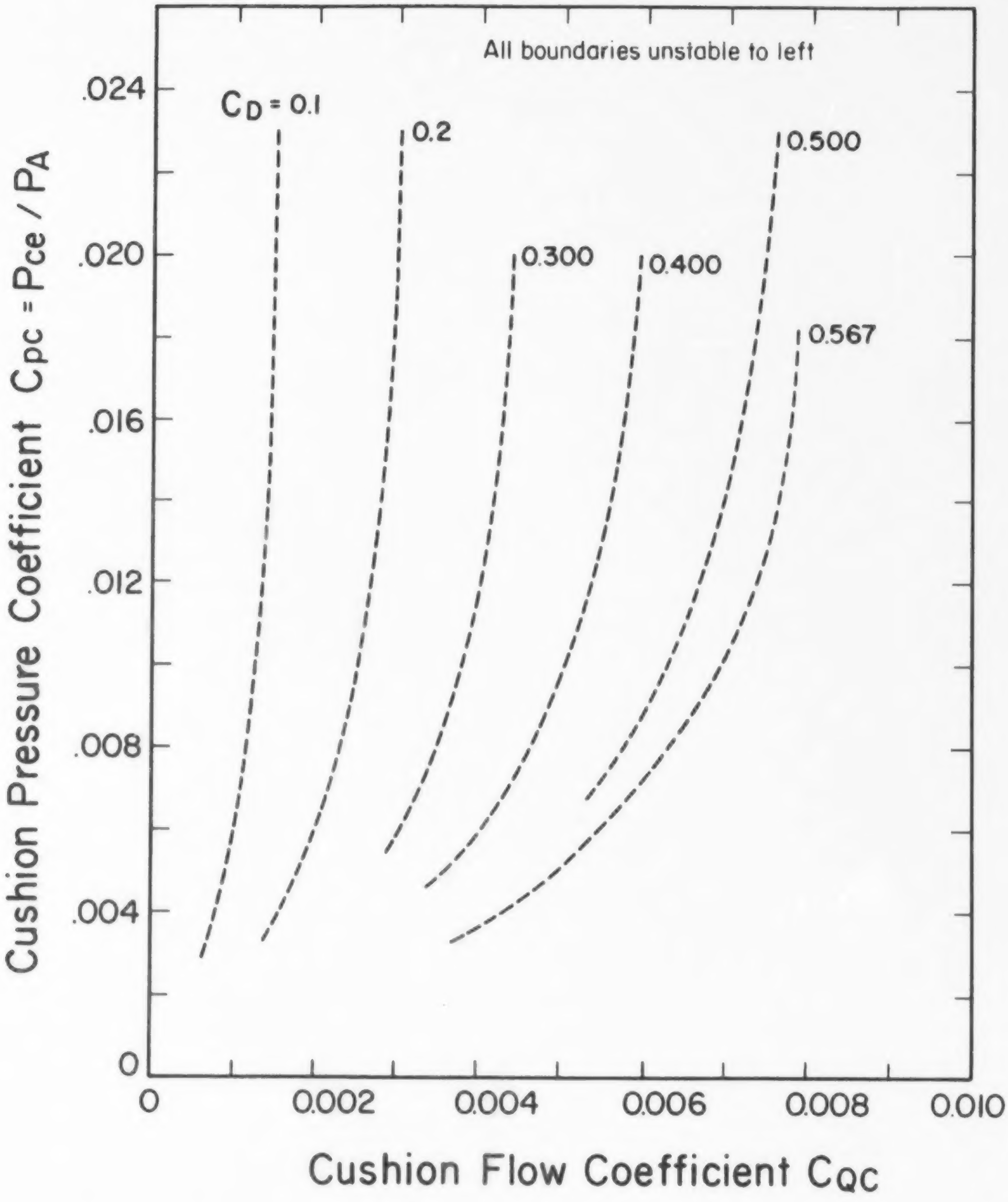

Figure Q.4 Effect of exit flow discharge coefficient on stability of a rigid plenum chamber.